



ABSTRACTBAND

106.

JAHRESTAGUNG DER DEUTSCHEN GESELLSCHAFT FÜR PATHOLOGIE

Leipzig
1. bis 3. Juni
2023

**Pathologie –
mehr als das Auge sieht!**
**Pathology –
more than meets the eye!**



www.pathologie-jahrestagung.de



Institut für Pathologie
und Neuropathologie
Universitätsklinikum
Tübingen

Abstractband



106. Jahrestagung der Deutschen Gesellschaft für Pathologie e.V. 1. – 3. Juni 2023, Leipzig

„Pathology – more than meets the eye!“

Schwerpunkte der Jahrestagung

- Hämatopathologie
- Multiparametrische Zell- und Gewebeanalyse
- Intraoperative Gewebesensorik
- Pathologie und Interdisziplinarität
- Aus- und Weiterbildung
- Gemeinsame Sitzungen mit anderen Fachgesellschaften
- AG Sitzungen zu allen Teilbereichen der Pathologie

Vorsitzender der Gesellschaft

Prof. Dr. med. Gustavo Baretton, Dresden

Tagungspräsident

Prof. Dr. med. Falko Fend

Herausgeberin, Lektorat und Copyright

Deutsche Gesellschaft für Pathologie e.V.
Geschäftsstelle
Robert-Koch-Platz 9
10115 Berlin
geschaeftsstelle@pathologie-dgp.de

Tagungsorganisation

Kongress- und Kulturmanagement GmbH (KUKM)
dgp2022@kukm.de

Klicken Sie auf den Beitragstitel, um direkt zum ausgewählten Abstract zu gelangen.

Inhaltsverzeichnis

Keynote: The classification of lymphomas	14
The classification of lymphomas.....	14
Keynote: The origins and evolution of follicular lymphoma	14
The origins and evolution of Follicular Lymphoma.....	14
DGP01 Klassifikation myeloischer Neoplasien I: Fortschritte und offene Fragen.....	15
Current classification of myeloproliferative neoplasms	15
The role of flow cytometry in the classification of myeloid disorders.....	15
DNA methylation profiling in blastic plasmacytoid dendritic cell neoplasm	16
Comparative gene expression profiling reliably separates extramedullary AML (eAML) and blastic plasmacytoid dendritic cell neoplasm (BPDCN)	17
Robust and explainable AI-aided evaluation of leukocytes morphology for leukemia diagnostics.....	18
The bone marrow microenvironment in hemophagocytic lymphohistiocytosis.....	18
DGP02 Classification of myeloid neoplasia II: progress and controversies	19
The current classification of acute leukemias	19
DGP03 Freie Vorträge I - Hämatopathologie	19
Molecular profiling of EBV associated diffuse large B cell lymphoma.....	19
B-cell clonality assessment using a Next Generation Sequencing Approach	20
A roadmap to Richter Syndrome: Boolean network modeling to elucidate regulatory mechanisms and personalized therapeutic options	21
A pilot study on the epigenome-wide methylation analysis of diffuse large B-cell lymphoma	22
DGP04 Digitale Pathologie	23
AI in pathology : There is more than meets the eye	23
Automatic, non-teachmark based coregistration of mass spectrometry images and hematoxylin and eosin stained microscopy images	23
Repeatable study of the PD-L1 CPS in Triple-negative breast cancer based on the AI-assisted model.....	24
Clinical-grade tumor detection and tissue segmentation in colorectal specimens using artificial intelligence tool.....	26
Application of artificial intelligence (AI) in counting of eosinophil granulocytes in gastrointestinal biopsies	27
Artificial intelligence for tumor detection and histological regression grading in oesophageal adenocarcinomas: an algorithm development and validation study	28
Development and international multi-center validation of AI tool for kidney tumor detection and subtyping.....	28
DGP05 Classification of Lymphoma I : progress and open questions	29
What is new in the classification of peripheral T-cell lymphomas?	29
Classification of Histiocytoses and dendritic cell neoplasms	30
DGP06 Single-Cell and Spatially Resolved NGS	30
A single-cell multi-omic and spatial atlas of nodal B cell lymphomas uncovers further levels of intratumor heterogeneity.....	30
Investigating immune and non-immune cell interactions in IDH2-mutant sinonasal undifferentiated carcinoma by FFPE-based single nucleus RNA sequencing	30
Clonal dynamics of chemoradioresistance evolution and metastatic progression in rectal cancer.....	31

Genome-wide DNA methylation-based machine-learning algorithms differentiate intrahepatic cholangiocarcinoma from intrahepatic metastases of pancreatic ductal adenocarcinoma	32
Dedifferentiated Chondrosarcoma: Correlation of Whole Exome Sequencing Data with Histopathology and Immunohistochemical Analysis.	33
Cancer-associated fibroblasts influence the immune response and disease outcome in NSCLC, thereby facilitating resistance to immune checkpoint blockade.	34
DGP08 Hot topics in hematopathology - gemeinsam mit der EA4HP	35
HHV8-negative/ EBV-negative primary effusion-based lymphomas	35
TFH lymphoma and associated clonal hematopoiesis.....	35
DGP09 Proteomik und Metabolomik	36
SpiderMass Ambient Ionization Mass spectrometry: A novel mini-invasive in vivo technology for intraoperative in man diagnostics	36
Proteomic Analyses of the Urothelial Cancer Landscape Reveal Highly Distinct Prognostic and Predictive Subtypes	36
Proteomic subtypes of intrahepatic cholangiocarcinoma are significantly linked to patient's time-to-recurrence	38
Differentiation of esophageal inflammatory diseases by using tandem mass spectrometry (LC-MS/MS)	39
DGP10 Sino-German Colorectal Cancer Session	40
AMER1 deficiency promotes the distant metastasis of colorectal cancer by inhibiting SLC7A11- and FTL-mediated ferroptosis	40
Validation of Prognostic Effect and Molecular Characterization of Stroma AReactive Invasion Front Areas (SARIFA) as Promising Biomarker in Colorectal Cancer	40
Experimental Evaluation of the Impact of Microenvironmental Factors on Tumor Immunity in Colorectal Cancer.....	41
Specific intracellular retention of circSKA3 promotes colorectal cancer metastasis by attenuating ubiquitination and degradation of SLUG	42
Analysis of the functional role of Acyl-CoA Synthetase Long Chain Family Member 5 (ACSL5) in human colorectal carcinoma	42
pT3 colorectal cancer revisited: a multicentric study on the histological depth of invasion in more than 1000 pT3 carcinomas - Proposal for a new pT3a/pT3b subclassification .	43
DGP11 Classification of Lymphoma II : progress and open questions	43
Classification of aggressive B-cell lymphomas - perspective from ICC	43
DGP12 Multiparametric tissue analysis I	44
A DNA toolbox for spatial biology from imaging to sequencing	44
Integrative modeling of multiplex imaging data identifies a spatial immune signature of oral squamous cell carcinoma histological grade	45
Extensive spatial characterization of the tumour-microenvironment in a large bicentric clinical non-small cell lung cancer cohort and correlation with clinical and pathological parameters	46
High-resolution multiplex spinning disk confocal immunofluorescence of tumor tissues as a tool to simultaneously extract spatial morphological and protein expression information at the subcellular level	47
Highly Multiplexed Microscopy of the Bone Marrow Microenvironment during Leukemic Progression in Mice	47
JUN-mediated mechanisms and therapeutic implications in fibrotic diseases of the lung and the skin	48
DGP13 Freie Vorträge II - Gemischte Themen.....	49
Omicron matters – an autopsy study	49
The tetraspanin CD63 contributes to human idiopathic pulmonary fibrosis and mouse lung fibrosis and regulates the focal adhesion kinase pathway	49

Construction of renal carcinoma classification digital pathological repository	50
Subcellular localisation patterns of ANXA4 influence migratory modes in ccRCC	50
Mesosopic 3D Analysis of the Microarchitecture of the Human Liver	51
A RhoA – YAP/TAZ – ARHGAP29 mechano-signaling axis sustains the glomerular filtration barrier in health and disease	52
Multiparametric classification of bladder cancer using immunohistochemistry and targeted sequencing	52
Membranous NECTIN-4 expression frequently decreases during metastatic spread of urothelial carcinoma and is associated with enfortumab vedotin resistance	53
Associations of TACSTD2/TROP2 and NECTIN-4/NECTIN-4 with molecular subtypes, PD-L1 expression and FGFR3 mutational status in two advanced urothelial bladder cancer cohorts	54
DGP14 Hämatologische Neoplasien in Kindern	55
GPOH-HD/EuroNet-PHL Study Center: Morphology - Genetics -Clinic	55
Myelodysplastic syndrome and inherited bone marrow failure in childhood	55
Whole Exome Sequencing of circulating tumor DNA of paediatric Hodgkin Lymphoma patients	55
Post mortem germline genetic testing – proclamation for an undervalued procedure with preventive power for relatives at risk	56
DGP15 Multiparametric tissue imaging II	57
4D strategical diagnostics in the lymph node	57
Dissecting antitumoral mechanisms of a virus-based immunotherapy in melanoma using highly multiplexed tissue imaging and machine learning	58
Characterizing intratumor heterogeneity and the tumor microenvironment of colorectal cancer and intrahepatic cholangiocarcinomas by MALDI imaging	58
DGP17 Gemeinsame Sitzung DRG und DGP I : State-of-the-art CT und MRT	
Untersuchungstechniken in Korrelation zur Pathologie	59
Correlation of Pathology and multiparametric MagneticResonance Imaging	60
Synchrotron-based three-dimensional imaging: new opportunities in correlative histotomography of solid tumors	60
An artificial intelligence solution for evaluation of prostate needle core biopsy specimens: impact in a non-specialist setting	60
3D Reconstruction of Prostate Carcinoma	61
Bedside US-guided minimal invasive multiorgan autopsy of COVID-19 deceased: a proof of concept study at the ICU.	62
DGP18 Freie Vorträge III - Hämatopathologie	63
Molecular Subtyping of Diffuse Large B-Cell-Lymphoma Using Panel-Sequencing	63
In-depth genomic profiling of Follicular Lymphoma	64
CDK6 protein expression is associated with disease progression and treatment resistance in multiple myeloma	64
Molecular alterations of primary refractory diffuse large B-cell lymphoma/high grade B- cell lymphoma with MYC- and BCL2- rearrangement and MYC- and BCL6- rearrangement as potential targets for personalized therapy	65
Mutational landscape of gastrointestinal T-cell lymphoma from Latin America	66
Comparative molecular characterization of primary extramedullary plasmacytoma and extramedullary manifestations of multiple myeloma	67
DGP20 Gemeinsame Sitzung DRG und DGP II: KI in Radiologie und Pathologie	67
AI in applied clinical radiology	67
The fatal trajectory: beyond Covid-19	68
Colorectal cancer screening aided by AI	68
DGP21 Molecular diagnostics in hematological neoplasms	69
Liquid biopsy in lymphoma	69

DGP22 Sensortechniken zur Gewebeanalyse, AI in der Pathologie (mit DGCH)	69
Methods, applications and future perspectives of intraoperative tissue identification	69
Multisensory intraoperative tissue recognition - how we teach medical technology 'fine sense'	69
Stimulated Raman Histology for evaluation of oral squamous cell carcinoma	70
Sectioning-free H&E imaging with a mobile multiphoton microscope	70
DGP23 Freie Vorträge IV - Multiparametrische Gewebeanalyse.....	73
Multiomic spatial phenotyping of a partial immunotherapy response in head and neck cancer.....	73
Optimized Preanalytics for Deep Proteomic Profiling of FFPE Tissue.....	73
Kinetics of Proteome Alterations in Human Autopsy Tissues in Relation to Time After Death.....	75
NGS analysis of pancreatic neck margin as ancillary tool for the detection of microscopic incomplete resections	75
TelePi: An affordable telepathology microscope camera system anyone can build and use.....	76
The tissue microenvironment and the loss of TP53 induce the expression of the embryological transcription factor SIX1 in ductal pancreatic adenocarcinomas	78
Normics: Improved Omics Data Normalization for Explorative Biomarker Studies	78
µCT-based Identification of Relevant Tissue Structures in Paraffin Blocks	79
DGP24 Freie Vorträge V - Uro- und Tumorpathologie	81
Fast track carcinogenesis in Lynch syndrome by a "two in one hit" mechanism	81
Correlation of histopathological hallmarks with survival data in squamous cell carcinomas of the bladder – development of a novel multiparametric grading system. .	81
PSPC1 interacts with KDM5C and is a Prognostic Biomarker in Prostate Cancer	82
Lymphoepithelioma-Like Carcinoma of the Bladder (LELC-B) – analysis of tumor and immune cells.....	82
Updating germ cell tumor pathogenesis -The ability of seminomas for FOXA2-driven extra-embryonic differentiation.....	83
Updating germ cell tumor pathogenesis -The ability of seminomas for FOXA2-driven extra-embryonic differentiation	83
Role of Cell-ECM interactions in renal tubular epithelial cells in the context of progressive chronic kidney disease (CKD).....	84
AG01 Hämatopathologie	84
The genetics of extranodal marginal zone lymphoma of MALT	84
Primary Bone Diffuse Large B-cell Lymphoma (PB-DLBCL) – a distinct lymphoma entity	85
Characteristics of primary cutaneous diffuse large B-cell lymphoma, leg-type in respect to features of systemic DLBCL and testicular DLBCL.	86
The small and large cell variants of nodal marginal B-cell lymphomas present with various growth patterns associated with different KI-67 indexes	86
A pilot study on dissecting the methylomes of diffuse large B-cell lymphomas of primary CNS and NOS types.....	87
Mutational profiles and established risk factors differ between elderly and younger patients with diffuse large B-cell lymphoma.....	88
AG02 Gastroenteropathologie I.....	89
Esophageal adenocarcinoma: understanding the molecular basis of differential treatment response.....	89
The new prognostic biomarker Stroma Areactive Invasion Front Areas (SARIFA) is based on an interaction between tumor cells with tumor promoting adipocytes potentially caused by an altered immune response in gastric cancer	89
Post-neoadjuvant assessment of tumour budding according to ITBCC subgroups delivers stage- and regression-grade independent prognostic information in intestinal-	

type gastric adenocarcinoma.....	90
Urokinase-type plasminogen activator receptor (uPAR) cooperates with mutated KRAS in regulating cellular plasticity and gemcitabine response in pancreatic adenocarcinomas	91
Shedded particles of the larval stage of E.multilocularis and E. granulosus increase NK cells in the germinal center of human lymph nodes.....	91
Identifying and Characterizing Essential Genes in the Presence or Absence of HIF1a in Hepatocellular Carcinoma	92
Tumor-Immune-Interaction and Senescence-associated Molecules in Colorectal Carcinoma	93
AG02 Gastroenteropathologie II.....	94
Loss of SATB2 occurs more frequently than CDX2 in colorectal carcinoma and identifies particularly aggressive cancer in high risk subgroups	94
PPAR γ activation promotes the proliferation of colorectal cancer cell lines and enhances the apoptotic effect of 5-Fluorouracil.	94
TPX2 expression as negative predictor of gemcitabine efficacy in pancreatic cancer ...	95
Bacterial Lipopolysaccharide as a Negative Predictor of AdjuvantGemcitabine Efficacy in Pancreatic Cancer	95
Establishment of a 3D ex vivo Culture of Pancreatic Cancer Tumor Fragments for Drug Testing.....	96
Enhancer of Zeste Homolog 2 (EZH2) Is a Marker of High-Grade Neuroendocrine Neoplasia in Gastroenteropancreatic and Pulmonary Tract	97
Postoperative Pancreatic Fistula Prediction Using Digital Pathology Based Analyses at the Parenchymal Resection Margin of the Pancreas – Results from the Randomized Multicenter RECO-PANC trial	97
AG03 Uro-pathologie I	98
Germ cell tumour-related somatic-type malignancies: Characterizing the mutational burden, DNA methylation landscape and proteome to identify the tissue-of-origin, mechanisms of therapy resistance and druggable targets	98
Organoid models for the prediction of therapy response on tyrosine kinase inhibitors in clear cell renal cell carcinoma.....	99
The role of carbohydrate responsive element binding protein (ChREBP) in nephrocarcinogenesis.....	99
Characterization of the transcription factor GATA6 in urinary bladder carcinoma	100
Proposal for a novel histologic grading approach for muscle-invasive urothelial bladder cancer correlating with disease aggressiveness and patient outcomes	100
Proteomic analysis of non-muscle invasive and muscle invasive bladder cancer highlights distinct subgroups.....	101
AG03 Uro-pathologie II	102
Testicular Cancer: New Developments, Molecular Pathology and Current Research Keynote	102
Molecular investigation for optimization the diagnosis, prognosis und therapy of prostate cancer (Habilitation).....	103
Tumour architecture and emergence of strong genetic alterations are bottlenecks for clonal evolution in primary prostate cancer.....	103
AG04 Gynäko- und Mammopathologie I	104
DNA Methylation-based Profiling of Rare Mesenchymal Tumors of the Uterus Identifies Distinct Signatures of GREB1- and KAT6B-rearranged Neoplasms.....	104
Indoleamine 2,3- Dioxygenase and PD-L1 Expression in High-Grade Serous Carcinoma of the Female Genital Tract – Favorable Prognostic (Co-)Effect in a Reclassified Large Clinical Cohort	105
Optimizing the FOLR1 RxDx Immunohistochemical Companion Diagnostic Kit for	

Eligibility Testing for Novel Antibody-Drug Conjugate Elahere (Mirvetuximab/Soravtansine) for Ovarian Carcinoma Treatment	105
Claudin 18.2 expression in histological subtypes of matched ovarian cancer primaries and metastases	106
STK11 mutated adnexal tumor	107
An integrated approach to the diagnosis of mesenchymal tumors of the uterus.....	107
AG04 Gynäko- und Mammopathologie II	108
A novel organoid system that mimics usual ductal hyperplasia (UDH) and mammary ductal carcinoma in situ (DCIS) suggests that DCIS-related myoepithelial cells are premalignant and form an integral part of intraductal breast lesions	108
A pilot study on the epigenomic characterization of luminal A and luminal B breast cancer.....	109
Correlation between neutrophil-to-lymphocyte ratio and pathological response to neoadjuvant therapy in triple negative breast cancer	109
Histological assessment of treatment response during thermo-radiotherapy of recurrent breast cancer – a longitudinal study	110
Software-assisted evaluation of immunophenotypic variation regarding D2-40, CD31 and Prox1 in sinus endothelium in sentinel lymph nodes of invasive breast carcinoma including prognostic impact	110
The HER2DX genomic test for HER2+ breast cancer	111
AG05 Kinder- und Fetalpathologie	111
Lymphocytic myocarditis - an underestimated diagnosis concerning babies and older children?	111
Autopsies of fetocids with congenital heart malformations- a single center study in Germany.....	112
Tissue shrinkage of resected specimens in Hirschsprungs disease: Why paediatric surgeons think the bowel specimen was longer than indicated in the pathology report.	113
AG06 Thoraxpathologie	113
Phosphoproteomic Analysis Identifies TYRO3 as a Mediator of Sunitinib Resistance in Metastatic Thymomas.....	113
Histological, immunohistological and molecular characterization of congenital pulmonary airway malformation (CPAM).....	114
Deciphering molecular mechanisms of chemoresistance in SCLC.....	115
CD63 serves as a don't-eat-me-signal in lung adenocarcinomas and steers macrophages towards the immunosuppressive M2 phenotype	115
Tumor intrinsic PD-L1 exerts an oncogenic function through activation of the Wnt/ β -catenin pathway in human non-small cell lung cancer.....	116
Epidemiology of Thymoma and Thymus Cancer in the United States and Germany, 1999-2019	116
Lung Adenocarcinoma Promotion by Air Pollutants.....	117
AG07 Herz-, Gefäß-, Nieren- und Transplantationspathologie	118
Current diagnostic aspects in cardiac transplantation and rejection	118
Allorecognition and the spectrum of kidney transplant rejection	118
Electron microscopy and the renal transplant: helpful for more black and white diagnoses and less shades of grey?	118
Fluorescence Confocal Microscopy on Liver Specimens for Full Digitization of Transplant Pathology.....	119
AG08 Knochen-, Gelenk- und Weichgewebspathologie.....	119
A single-hit shortcut to tumorigenesis through epigenome remodeling and impaired differentiation in oncohistone-driven giant cell tumor of bone.....	119
Exploring the Role of RANKL and RUNX2 in Giant Cell Tumor of the Bone: A Study on	

GCTB Cell Lines in vitro	120
Analysis of 24 giant cell tumors of bone before and after denosumab therapy reveals complex time-dependent morphological changes.....	121
TIM3 qualifies as a potential immunotherapeutic target in high-risk soft tissue sarcomas	122
Biphenotypic sinonasal sarcomas harbor characteristic gene fusions involving PAX3 and show a distinct DNA methylation profile.....	124
CIC-rearranged sarcomas – A diagnostic challenge.	125
AG09 Zytopathologie/Fortbildung	126
Gynaecological cytology as an essential component in the prevention of cervical carcinoma-Squamous and glandular changes:Glandular lesions	126
AG10 Kopf-Hals-Pathologie	126
Predicting clinically relevant genetic alterations from conventional histopathological slides of thyroid carcinoma using vision transformers	126
Clinico-pathological characterization of sinonasal adenoid cystic carcinoma reveals high prevalence of MYB-NFIB gene fusion and prognostic factors	127
The concept of “differentiated” dysplasia in oral potential malignant disorders and its translation to daily practice	127
TRIM21 Expression as a Prognostic Biomarker for Progression-free Survival in HNSCC.....	129
CMTM6-Status in Head & Neck Squamous Cell Cancer Predicts Survival and Response to Radiochemotherapy.....	129
AG11 Dermatopathologie.....	130
Cutaneous B-cell infiltration: diagnostic algorithms, differential diagnosis and pitfalls.	130
From digital workflow to AI assisted diagnosis	130
Loss BRCA-associated Protein 1 (BAP1) expression in uveal melanoma is associated with morphological features of dedifferentiation and adverse prognosis	131
Expression of PRAME in Melanoma in situ versus dysplastic nevi: Immunohistochemical Study.....	132
An immunohistochemical analysis of Basal Cell Carcinoma from 50 patients under the age of 40.....	132
AG12 Geschichte und Ethik der Pathologie	133
Concept of disease and interdisciplinarity - are comparative sciences still reasonable?.....	133
Zoonosen bei einheimischen, wildlebenden Säugetieren	134
History of postgraduate specialisation	134
AG13 Informatik, digitale Pathologie und Biobanking I	135
Interactive AI training with minimal annotations.....	135
Predicting simplified consensus molecular classes in muscle-invasive bladder cancer (MIBC) with deep learning (DL)	135
An Open Source Library for Anonymization of Whole Slide Images.....	137
Enhancing Accuracy and Transferability using CNN Ensembles.....	137
Digital transformation of the histopathological routine laboratory - Do´s & don´t s	138
AG13 Informatik, digitale Pathologie und Biobanking II	138
How disruptive is Digital for (Continuing) Medical Education in Pathology	138
Artificial Intelligence for pathology-based biomarkers in oncology.....	139
A multi-center study: artificial intelligence assisted prediction of lymph node status in breast cancer.....	139
Knowledge Graphs in (Nephro-)pathology for decision tree extraction.....	142
AG 13 DACH-Symposium der AG Informatik, Digitale Pathologie und Biobanking	143
Digital Pathology in Austria.....	143
National digital pathology projects in Switzerland: an update	143

Getting the most out of Digital Pathology for AI development.....	144
DIA / AI in Pathology Diagnostics – the Swiss view.....	144
How to harvest features from a pathologist viewing a WSI for development of AI- Algorithms.....	145
MarrowQuant2.0, a move toward computational bone marrow pathology?	145
AG14 Molekularpathologie I.....	146
MLH1 promotor methylation – comparison of different testing strategies and optimization of cut-off values for distinguishing hereditary and sporadic cancer origin	146
A pilot study on the epigenomic profiling of homologous recombination deficient (HRD) high-grade serous carcinoma of the ovaries.....	146
Deletions with Microhomologies - Patterns of DNA Double-Strand Break Repair - an in- silico Analysis of the Mutational Landscape of TCGA	147
Comparison of five different assays for the detection and genotyping of human papillomavirus in cervical liquid-based cytology and formalin fixed paraffin embedded tissue	148
Homologous recombination deficiency (HRD) assessment by targeted next generation sequencing using the OncoPrint Comprehensive Assay Plus and the determination of the Genomic Instability Metric (GIM) in ovarian cancer	148
QuIP EQA scheme for the molecular pathological detection of theHRD status in ovarian cancer 2023.....	149
AG14 Molekularpathologie II.....	150
Comprehensive transcriptomic analysis of prostate cancer lung metastases.....	150
Aberrant fucosylation sustains the NOTCH and EGFR/NF-kB pathways and is a negative prognostic factor in human intrahepatic cholangiocarcinoma.....	150
eIF4A1 as an Actionable Target with Prognostic Value in Human Hepatocellular Carcinoma	151
Integrated epigenome-wide methylation analysis of EGFR amplified Glioblastoma	152
Single Nucleus RNA Sequencing of Gastric Normal and Tumor Tissue after Neoadjuvant Treatment enables the examination of tumoral heterogeneity	152
AG14 Molekularpathologie III.....	153
A European newcomer's experience with NGS-based proficiency testing offered by College of American Pathologists.....	153
Specific T-cell receptor beta rearrangements of gluten-triggered circulating CD8 ⁺ T-cells are significantly enriched in duodenal celiac disease specimen	153
Analysis, interpretation and structured interactive reporting of a large NGS-panel and Whole Exome Sequencing in molecular pathology diagnostics.....	154
Low-input WES using compromised tumor specimens – A challenge for routine molecular diagnostics	155
DGP07 Junges Forum I - How to do.....	155
How to: Bone Marrow Examination	155
How to: Multiparametric tissue analysis.....	156
P01 Postersitzung AG Hämatopathologie	156
Tissue-equivalents of lymphoid clonal haematopoiesis of indeterminate potential (L- CHIP): Potential precursor lesions of lymphoma	156
Case report: Follicular Dendritic Sarcoma in a cervical lymph node mimicking metastasis of anaplastic thyroid carcinoma.	157
Immune escape mechanisms in myeloid sarcomas	158
Time dependent changes of the (immune-)phenotype upon JAK2 inhibition in JAK2 V617F mutated cell lines	158
PTP1BD6 und PTP1BD2-4 – Functional analyses of the oncogenic variants of PTP1B.....	159
Supporting routine bone marrow diagnostics with NGS-based analyses	160

Digital pathology - workflow for quantification of bone marrow characteristics in reactive and neoplastic histological sections.....	160
P02 Postersitzung AG Gastroenteropathologie I.....	161
Morphological subtypes of low grade intraepithelial neoplasia in patients with and without ulcerative colitis: reproducibility, frequency and clinical relevance	161
Morphological subtypes of low grade intraepithelial neoplasia in patients with ulcerative colitis: Frequency and prognostic value.....	162
Microsatellite instability and sex-specific differences of survival in gastric cancer after neoadjuvant chemotherapy without and with taxane	163
Inflammatory pseudopolyps: a possible infrequent manifestation in neurofibromatosis type I.....	163
Abdominal tuberculosis (Tbc) with perforation of the small intestine	164
Tumorbiological behaviour and metastatic spread in lower gastrointestinal tract cancer – correlation with gene expression patterns	165
Coincidence of three carcinomas (Ca) of the gastrointestinal (GI) tract at different segments	165
P02 Postersitzung AG Gastroenteropathologie II.....	166
Squamous esophageal carcinoma of the young adult	166
Immunohistochemical positivity of Nup153 is associated with neuroendocrine differentiation	167
Intratumoral heterogeneity in poorly cohesive gastric cancer correlates with clinicopathological features.....	168
Tumor area infiltration and absolute tumor cell numbers in endoscopic biopsies of therapy-naive upper GI tract carcinomas – implications for predictive biomarker testing.....	168
Significant tumor regression after neoadjuvant chemotherapy in gastric cancer, but poor survival of the patient? - Role of MHC class I alterations.....	169
Analysis of SH2D4A promoter activity reveals positive regulation by inflammatory cytokines via transcription factor KLF4.	169
Does gastric cancer show gender-specific differences in the perioperative management, early postoperative and longterm oncosurgical outcome - results of a prospective multicentre observational study	170
Esophageal carcinomas with "fetal cell-like differentiation" - rare but therapeutically relevant.....	171
P02 Postersitzung AG Gastroenteropathologie III.....	172
Impact of the underlying diagnosis comparing chronic pancreatitis ("Pan") vs. pancreatic head carcinoma ("Ca") onto the early postoperative outcome after pylorus-preserving pancreatic head resection (PPPHR) according to Traverso-Longmire	172
Metastatic pancreatic ductal adenocarcinoma as a mimicker of lepidic non-small cell lung cancer – an exemplary case of a broad oncological autopsy program	172
Sarcoma as rare differential diagnosis of a pancreatic tumor lesion.....	174
Mid-term finding after pancreatic trauma mimics pancreatic tumor lesion	175
N-cadherin helps discriminate primary liver carcinomas from liver metastases of an extrahepatic primary	176
Expression of CDH6 in Cholangiocarcinogenesis and its Diagnostic Relevance in High-Grade Biliary Intraepithelial Neoplasia.....	176
Proteome-based characterization of Exportin-1 directed therapy in liver cancer	177
IgG4-positive plasma cells in Echinococcus multilocularis affected liver tissue are significantly increased as compared to autoimmune hepatobiliary diseases	177
The Value of fine needle aspiration cytology (FNAC) in determining the histogenesis of liver nodules	178

P03 Postersitzung Uropathologie I.....	179
EpCAM Tumor Specificity and Proteoform Patterns in Urothelial Cancer.....	179
Reverse transcriptases of endogenous retroviruses and LINE1 synthesize RNA:DNA hybrids induce inflammation in muscle invasive bladder cancer.....	179
TACSTD2 (Trop2) Expression on the urothelial Carcinoma (UC): Immunohistochemical Study	180
Surrogate Immune Marker Analysis for Simplified Molecular Classification in Upper Tract Urothelial Carcinoma.....	180
The ETS transcription factor ELF3 regulates the matrisome of invasive bladder carcinoma via SERPINB2.....	181
CKLF-like MARVEL Transmembrane Domain Containing Protein 6 and Programmed Cell Death Ligand 1 as Prognostic Biomarkers in Upper Tract Urothelial Carcinoma ..	182
Evaluation of immunohistochemical markers for neuroendocrine carcinomas of the bladder and prostate.....	183
ICAM-1 as a potential predictive marker for immune checkpoint inhibitor response in bladder cancer.....	183
P03 Postersitzung Uropathologie II.....	184
The human telomerase reverse transcriptase (hTert) single nucleotide polymorphisms (SNPs) rs2736100 and rs2853669 are not associated to tumor characteristics in renal cell carcinoma (RCC).....	184
Diagnostic and prognostic aspects of intratumoral morphological heterogeneity in clear cell renal cell carcinoma	185
No evidence for recurrent, functional mutations in exon 9 of the GPS1 gene in penile squamous cell carcinoma	185
Retrospective proteomics-analysis for the identification of tumour-resident protein markers for personalized risk and therapy stratification in prostate cancer patients	186
Recommendations of macroscopic examination after nephrectomy for cases with autosomal dominant polycystic kidney disease (ADPKD): Back to basics	187
Diagnostic pitfall of a urogenital condition with simple solution by conventional histopathological techniques and ultrastructure: Old is gold	187
TROP2 is a possible target but not a prognostic biomarker in prostate cancer	188
BRD9 inhibition as potential treatment option for testicular germ cell tumors	189
P04 Postersitzung AG Gynäkopathologie und Mammopathologie	190
HPV-genotyping versus conventional cervical cytology as a screening method to detect dysplastic cervical epithelial changes	190
Molecular subtyping of breast cancer by Ki67 in the era of artificial intelligence	190
Sclerosing stromal tumor of the ovary: clinicopathological and immunohistochemical characteristics of eight cases.....	191
p16 ^{INK4a} immunohistochemistry as a diagnostic marker in endometrial stromal sarcomas	192
Giant cell tumor of the uterus.....	192
HPV test improves CIN 3 detection in the 2020 launched German cervical cancer screening programme.....	193
Molecular classification of vulval cancer: Comparing pre-surgical biopsy and surgical specimen of radical vulvectomy from the same patients	194
TROP-2 expression in vulval carcinoma - as a possible target for the treatment approach with antibody drug conjugates (ADC)	194
P05 Gemischte Postersitzung II	195
Mogamulizumab-associated rash (MAR) of the scalp in a patient with follicular Mycosis fungoides.....	195
Hypoxia and Ezrin Expression in Primary Melanoma Have High Prognostic Relevance	196

Acute myocardial infarction caused by anomalous left coronary artery in a 3-year-old boy with repaired tetralogy of Fallot	197
Congenital infantile fibrosarcoma with fatal perinatal complications - a case report	198
An exceptionally rare case of Fetal Lung Interstitial Tumor (FLIT)?	199
Late pregnancy infection with <i>Listeria monocytogenes</i> with fatal fetal outcome	199
P06 Postersitzung Thoraxpathologie	200
“Super Survivor” after Lung Transplantation – Protective Role of Macrophages?	200
miR-338-3p and miR-126-3p expression is associated with tumour differentiation in primary squamous cell carcinomas of the lung	200
Tumor microenvironment patterns in pulmonary carcinoids	202
Indolyl-chalcone derivatives induce pleural mesothelioma cell apoptosis through aberrant tubulin polymerization and deregulation of microtubule-associated proteins	202
Genomic profiling of histomorphologic subtypes reveals distinct molecular patterns in NSCLC	203
Hepatoid differentiated Adenocarcinoma in the Lung: Primary or Metastasis? – Two examples of a rare differential diagnosis.	203
Inhibition of paracrine signaling by cancer-associated fibroblasts leads to depletion of malignant pleural mesothelioma cells in vitro.	204
P07 Gemischte Postersitzung I	206
Lasso-based feature selection identifies active relaxation as the most informative left ventricular parameter for proteomic perturbations during myocardial remodeling and reverse-remodeling	206
Comparative analysis of the mitochondrial population surrounding the intercalated discs in heart diseases – an ultrastructural study	207
Post-mortem diagnosis of lethal microscopic polyangiitis in a 41-year-old male with arthralgia and hemoptysis. A case report.	207
Interstitial vasculitis associates with severe kidney injury independent of ANCA-associated glomerulonephritis	208
The role of Insulin-like Growth Factor-1 and Bone Morphogenetic Protein-7 in the pathophysiology of non-unions – an in vitro study on the differentiation of human mesenchymal stem cells and possible therapeutic perspectives	209
Rare case of an isolated Echinococcus cyst within the iliopsoas muscle	209
Nectin-4 is widely expressed in Head and Neck Squamous Cell Carcinoma	210
P13 Postersitzung AG Informatik, digitale Pathologie und Biobanking I	211
Segmentation of renal microvasculature and detection of cell types in glomeruli using convolutional neural networks (CNNs)	211
Automated segmentation of tubuli and peritubular capillaries in kidney tissue using Convolutional Neural Networks (CNNs)	211
Polarized light scanner for digital pathology	212
Separate classification of central and peripheral regions of HE-stained colorectal carcinomas for clinical outcome	213
Spatial distribution and determinants of <i>Helicobacter pylori</i> cases in the Rhine-Main area - A spatial ecological study.	214
Prediction of molecular subtypes in muscle invasive bladder cancer (MIBC) based on histopathological images	214
Deep learning-based classification of pancreatobiliary differentiated carcinomas in the liver	215
P13 Postersitzung AG Informatik, digitale Pathologie und Biobanking II	215
Quality Control: a Closer Look at How Training and Test Data Influence CNN Performance	215
Prediction of progression free survival in non muscle invasive bladder cancer (NMIBC) based on histopathological images	216

ProteoGenDB: A Fast Proteogenomic Pipeline for Identifying Sequence Variants in Proteomics Data	216
Explainable artificial intelligence providing better comprehensibility for artificial intelligence using the example of prostate cancer – Preliminary results.....	217
Neural Network Assisted Pathology for Labeling Tumors in Whole-Slide-Images of Glioblastoma.....	218
Optimization of workflows in pathological diagnostics through the interlink of AutoHotkey with a laboratory information system	219
Artificial intelligence-based assessment of Ki67 concordance and prognosis in breast cancer: Update from the automated Ki67 scoring guideline of the International Ki67 Working Group	219
Comparative analysis of morphological parameters of breast cancer NST with immunophenotypical parameters using Artificial Intelligence (AI).....	222
P14 Postersitzung Molekularpathologie I	222
Biomarker analysis from Phase 1/2 study of tusamitamab ravtansine (SAR408701) in patients with advanced non-small cell lung cancer (NSCLC)	222
Prognostic Relevance Of Q787Q EGFR Polymorphism In Adenocarcinomas Of The Lung.....	223
Comparative bioinformatic analysis of KRAS, STK11 and KEAP1 (co-)mutations in Non-Small Cell Lung Cancer with a special focus on KRAS G12C	224
Acyl-coA synthetase long chain 5 (ACSL5) inhibits tumor cell growth and serves as a diagnostic marker in non-small cell lung cancer	224
Investigating the role of oncogenic mutation BRAF-V600E in the diet-associated ChREBP knock-out mice Hepatocarcinoma development.....	225
Genetic alterations with potential impact on PD-(L)1 targeted treatment in various cancer entities – Biobank research project of the INFINITY registry	226
Immune cell profiles in solid tumors and correlation to PD-L1 and tumor mutational burden	227
Analytic validation of EasyPGX ready NTRK Fusion – A CE-IVD approved one step real-time multiplex RT-PCR assay for the fast track detection of clinically relevant NTRK1,2,3 genetic rearrangements	227
Analytic validation of EasyPGX ready PIK3CA – A CE-IVD approved one step real-time multiplex RT-PCR assay for the fast track detection of PIK3CA mutations	228
Analytic validation of EasyPGX ready ALK/ROS1/RET/MET – A CE-IVD approved one step real-time multiplex RT-PCR assay for the fast track detection of clinically relevant ALK, ROS1, RET, MET genetic rearrangements.....	229
P14 Postersitzung Molekularpathologie II	229
Clonal and „intrinsic“ heterogeneity of somatic variants in microsatellite-stable colorectal carcinomas and their metastases	229
The role of mitochondrial DNA alterations and mTOR signalling in pancreatic neuroendocrine tumors (panNETs)	230
Whole-exome sequencing of five mixed neuroendocrine-non-neuroendocrine neoplasms of the gastrointestinal tract	231
Analysis of miRNA Expression in Dedifferentiated Chondrosarcoma.....	231
Proteogenomic landscape of non-small cell lung cancer.....	233
N-Glycan in-situ Characterization of Small Blue Round Cell Tumors	234
Gene Expression Profiling of Uveal Melanoma revealed Immunogenic Phenotypes in Primary Tumors as well as in Metastases	234
Analysis and annotation of next generation sequencing data with the database Cancer Genome Interpreter-Clinics.....	235
Integrating proteomics into diagnostic molecular pathology reports for molecular tumor board decisions	236

Analytic validation of OncoDEEP – A comprehensive genomic profiling NGS panel for mutational and clinical biomarker analysis in routine cancer patient diagnostics.....	237
P.InterPath. Postersitzung Pathologie und Interdisziplinarität.....	237
Pathology Cancer Dashboard: Development of a pathology-centered online application for epidemiologically guided differential diagnosis	237
Shortage of vascular surgery specialists as of other medical specialists in Germany - alarming aspects and a possible multidisciplinary effective approach for its improvement.....	238
Joining Forces for Better Treatment: The Power of Multidisciplinary Limb Board Meetings with Live Microscopy	239
$\alpha\beta6$ -integrin expression in different cancer entities: new insights for theranostics.....	239
Correlation of pathological and microbiological findings in non-neoplastic vitrectomy specimens: a single-center retrospective study	240
Individualized targeted treatment in a case of a rare TFG-ROS1 fusion positive inflammatory myofibroblastic tumor (IMT).....	241
Thrombospondin 3 affects lineage commitment in primary liver cancer	242
Diagnostic challenge on liver biopsy: AFP-positive carcinoma of the esophagogastric junction with MET Exon 14 Skipping mutation.....	242
Correlation of imaging and (histo)pathological evaluation in the diagnosis of hepatocellular carcinoma in liver explants	243
Theranostic Imaging of SSTR expression in iodine-refractory thyroid carcinoma.....	244
Proteomic signatures of recurrent and non-recurrent primary tumors in the head and neck area to differentiate patient conditions highlighting age and smoking specific alterations	244
P.Multipar. Postersitzung Multiparametrische Zell- und Gewebeanalyse	245
Comprehensive characterization of virus and inflammation distribution in human Borna virus encephalitis	246
Influence of vaccination status and virus variant on the immunological events in fatal SARS-CoV-2 infections	246
Development of novel oligonucleotide sequences to increase the multiplexing capacity of the CODEX platform.....	247
Diagnosis of a sialidosis case using tissue-based liquid chromatography-tandem mass spectrometry (LC-MS/MS)	248
Digital Spatial Profiling: Pre-analytical effect of EDTA and target sequence annotation.	248
Multivariate modelling of mid-infrared spectra of colorectal cancer	249
Shotgun proteomics of breast carcinoma pathological subtypes	249
Autorenindex.....	249

Amount of abstracts: 331

Date of export: May 24, 2023

Keynote: The classification of lymphomas

KN03

The classification of lymphomas

E. Campo

University of Barcelona, Institut d'Investigacions Biomèdiques August Pi I Sunyer (IDIBAPS), Barcelona, Spain

The classification of the hematological neoplasms in the last 25 years has been generated through iterative international efforts to achieve broad consensus among hematopathologists, geneticists, molecular scientists, and clinicians. In the last years significant knowledge has been generated in lymphoid neoplasms with a relevant impact of genomic studies. The 2022 International Consensus Classification (ICC) has been prepared following the same successful process used for the third, fourth and updated fourth editions of the World Health Organization Classification of Hematologic Neoplasms coordinated by a steering committee approved by the Executive Committees of the European association for Haematopathology and the Society of Hematopathology. The topics which needed an update were initially prepared by different working groups and subsequently presented and discussed in clinical advisory committee (CAC) meeting with the participation of a large group of pathologists, clinicians and scientists who all approved the classification after reaching consensus in all topics. The definition, recommended studies, and criteria for the diagnosis of many entities have been extensively refined. Some categories considered provisional have been upgraded to definite entities. Terminology for some diseases has been revised to adapt nomenclature to the current knowledge of their biology, but these modifications were restricted to well-justified situations. Major findings from recent genomic studies have impacted the conceptual framework and diagnostic criteria for many disease entities. Simultaneously, the International Agency for Cancer Research (IARC) of the WHO has generated a new edition of the classification of these neoplasms. The similarities and differences will be presented.

Keynote: The origins and evolution of follicular lymphoma

KN05

The origins and evolution of Follicular Lymphoma

B. Nadel

INSERM U1104, CNRS UMR7280, Aix Marseille Université UM2, Centre d'Immunologie de Marseille-Luminy, Marseille, France

Follicular lymphoma (FL) is the most common indolent non-Hodgkin lymphoma. FL is characterized by translocations involving t(14;18)(q32;q21) translocations, detectable in nearly 90% of tumors driving overexpression of the anti-apoptotic protein BCL2. Yet, ~70% of healthy carry t(14;18)+ cells in blood and tissues. Although circulating t(14;18) at high frequencies predicts an increased risk, the vast majority of individuals with detectable translocations will never develop FL. Likewise, while overexpression of BCL2 is seen in potential nodal precursor lesions such as *in situ* follicular neoplasia (ISFN), fewer than 5% of such patients develop FL. *BCL2* translocations are therefore critical but not sufficient for FL development, and additional genetic alterations are likely required for lymphomagenesis. FL samples paired in space or time often show limited mutational concordance, suggesting that FL evolves and persists from a reservoir of precursor cells bearing early variants. The existence of distant circulating FL precursors has been directly confirmed in studies of clonally related lymphomas in transplant donor-recipient pairs. Sequencing studies of FL tumors have identified recurrent and clonally dominant lesions as potential early events, including mutation of chromatin modifying genes (*KMT2D*, *CREBBP*, *EZH2*, *EP300*, ..). Together, these observations suggest that even clones present years before diagnosis may contain committed cancer precursor cells (CPC). However, there has been no direct systematic characterization of FL precursor mutations in pre-diagnostic samples, and little is known about the hierarchy and timing of somatic aberrations preceding FL diagnosis. Because CPC are expected to be rare cells, detecting such variants presents a great technical challenge. Using ultra-deep targeted genotyping (CAPP-Seq), we screened t(14;18)-positive pre-diagnostic blood samples from healthy individuals who later developed FL. We provide direct evidence for the combination of *BCL2* translocation with *CREBBP* KAT domain mutations as characteristic committed precursor lesions of FL. Such pre-diagnostic mutations are detectable years before clinical diagnosis and may therefore help discriminating individuals at risk for lymphoma development.

FCM data and may help to streamline existing antibody panels.

Literaturangaben:

- [1] Arber DA, Orazi A, Hasserjian RP et al, (2022), International consensus classification of myeloid neoplasms and acute leukemias: Integrating morphologic, clinical, and genomic data., *Blood*, 140; 1200-1228
- [2] Khoury JD, Solary E, Abla O et al. , (2022), The 5th edition of the world health organization classification of haematolymphoid tumours: Myeoid and histiocytic/dendritic neoplasms., *Leukemia*, 36; 1703-1719
- [3] Kern W, van de Loosdrecht A., (2023), Flow cytometry in the diagnosis of myelodysplastic syndromes, *Cytometry B Clin Cytom* 2023, 104;10-11
- [4] van der Velden VHJ, Preijers F, Johansson U et al, (2023), Flow cytometric analysis of myelodysplasia: Pre-analytical and technical issues-recommendations from the european leukemianet, *Cytometry B Clin Cytom* , 104; 15-26
- [5] Porwit A, Rajab A, (2015), Flow cytometry immunophenotyping in integrated diagnostics of patients with newly diagnosed cytopenia: One tube 10-color 14-antibody screening panel and 3-tube extensive panel for detection of mds-related features. , *Int J Lab Hematol*, 37; 133-143
- [6] van Dongen JJ, Lhermitte L, Bottcher S et al, (2012), Euroflow antibody panels for standardized n-dimensional flow cytometric immunophenotyping of normal, reactive and malignant leukocytes, *Leukemia*, 26; 1908-1975
- [7] Patnaik MM, Timm MM, Vallapureddy R et al, (2017), Flow cytometry based monocyte subset analysis accurately distinguishes chronic myelomonocytic leukemia from myeloproliferative neoplasms with associated monocytosis. , *Blood Cancer J*, 7; 584

DGP01.03

DNA methylation profiling in blastic plasmacytoid dendritic cell neoplasm

P. Lohneis¹, J. Schwarting^{1,2,3}, H. M. Witte^{2,3,4}, A. Künstner^{2,5,6}, V. Bernard¹, S. Stölting¹, N. von Bubnoff^{2,3}, E. M. Murga Penas⁷, H. Merz¹, H. Busch^{2,5,6}, N. Gebauer^{2,3}, A. Feller¹

¹Hämatopathologie Lübeck, Lübeck, Germany, ²Universitätsklinik Schleswig-Holstein, Campus Lübeck, University Cancer Center Schleswig-Holstein, Lübeck, Germany, ³Universitätsklinik Schleswig-Holstein, Campus Lübeck, Klinik für Hämatologie und Onkologie, Lübeck, Germany, ⁴Bundeswehrkrankenhaus Ulm, Klinik für Hämatologie und Onkologie, Ulm, Germany, ⁵Universität zu Lübeck, Group for Medical Systems Biology, Lübeck, Germany, ⁶Universität zu Lübeck, Institut für Kardiogenetik, Lübeck, Germany, ⁷Universitätsklinik Schleswig-Holstein, Campus Kiel, Institut für Humangenetik, Kiel, Germany

Questions/Background

Die blastäre Neoplasie plasmazytoider dendritischer Zellen (BPDCN) ist eine schwer zu behandelnde, seltene und aggressive Neoplasie. In einer kürzlich durchgeführten Multiomics-Analyse hat unsere Arbeitsgruppe die Mutations- und Transkriptionslandschaft von BPDCN charakterisiert [1]. Neben dem erwarteten klassischen pDC-Subtyp wurde dabei ein Common(c)DC-angereicherter Subtyp identifiziert, der vorwiegend bei älteren Patienten auftritt, weniger Mutationen aufweist und einen schlechteren Verlauf hat. In beiden Subtypen konnten genomische Aberrationen epigenetischer Regulatoren nachgewiesen werden. Die epigenetische Landschaft von BPDCN ist jedoch noch weitgehend uncharakterisiert.

Methods

Die genomweiten DNA-Methylierungsmuster wurden in BPDCN von 51 Patienten mit dem Illumina MethylationEPIC BeadChip untersucht und mit den bereits bekannten Whole Exome Sequencing /RNA-seq-Daten aus denselben Proben korreliert.

Results

Durch ein unsupervised clustering der 420 am stärksten differentiell methylierten Cytosin-Guanin-Dinukleotid (CpG)-Stellen konnte die Kohorte in vier Cluster unterteilt werden. Cluster 2 setzt sich dabei ausschließlich aus atypischen, mit cDC-Signaturen angereicherten C2-BPDCN-Fällen mit SRSF2- oder DNMT3A-Mutationen zusammen. Cluster vier zeigt eine starke C1-BPDCN-Dominanz und typische C1-Treibermutationen, darunter EP300, ARID2 und NF1. Insgesamt beobachteten wir bei der C2-BPDCN eine stärkere Methylierung mit einer Regulierung mehrerer Onkogene und Tumorsuppressorgene wie NOTCH4 und MAP3K13 und eine Regulation von Entzündungs-assoziierten Genen wie TLR9, IL10RA und IL2RA.

Conclusion

Unsere aktuellen Ergebnisse legen nahe, dass die genomweiten DNA-Methylierungslevel die klinisch und genomisch unterschiedlichen Subtypen der BPDCN rekapitulieren und möglicherweise dazu beitragen, diese zu formen.

Literaturangaben:

DGP01.04

Comparative gene expression profiling reliably separates extramedullary AML (eAML) and blastic plasmacytoid dendritic cell neoplasm (BPDCN)

T.-C. Schade¹, D. Nann¹, G. Ott², K. Kurz², A. Rosenwald³, A. Zamo³, W. Klapper⁴, I. Oschlies⁴, H. Stein⁵, A. Feller⁶, S. Cogliatti⁷, S. Dirrhofer⁸, S. Forchhammer⁹, J. Weller¹⁰, P. Sander¹, A. Rau¹, F. Otto¹, E. Kohler¹, F. Mihalik¹, R. Braun¹, J.-P. Geppert¹¹, A. Chott¹², J. Slotta-Huspenina¹³, I. Bonzheim¹, L. Quintanilla-Martinez de Fend¹, F. Fend¹

¹Institute of Pathology, University Hospital Tuebingen, Tuebingen, Germany, ²Department of Clinical Pathology, Robert-Bosch-Krankenhaus, Stuttgart, Germany, ³Institute of Pathology, Wuerzburg University, Wuerzburg, Germany, ⁴Institute of Pathology, University Hospital Schleswig-Holstein, Kiel, Germany, ⁵Pathodiagnostics Berlin MVZ, Reference Center for Hematopathology Berlin, Berlin, Germany, ⁶Institute of Hematopathology, Luebeck, Luebeck, Germany, ⁷Institute of Pathology, Kanton Hospital St. Gallen, St. Gallen, Switzerland, ⁸Institute of Medical Genetics and Pathology, University Hospital Basel, Basel, Switzerland, ⁹Department of Dermatology, University Hospital Tuebingen, Tuebingen, Germany, ¹⁰Department of Hematology, University Hospital Tuebingen, Tuebingen, Germany, ¹¹Institute of Pathology and Dermatohistology Tuebingen, Tuebingen, Germany, ¹²Institute of Pathology and Microbiology, Clinic Ottakring, Vienna, Austria, ¹³Institute of Pathology, Technical University of Munich, Munich, Germany

Questions/Background

Extramedullary AML (eAML)/myeloid sarcoma and blastic plasmacytoid dendritic cell neoplasm (BPDCN) are rare hematologic malignancies presenting in extramedullary sites such as skin, lymph node and central nervous system. Due to overlapping clinical and immunophenotypic features, differentiation of these two entities can be difficult. Aim of our study was to perform comparative gene expression profiling (GEP) of a multi-institutional series of eAML and BPDCN to identify altered biological pathways, as well as differences and similarities in their transcriptome.

Methods

FFPE BPDCN samples were collected from hematopathology reference centers in Germany, Switzerland and Austria. eAML cases were obtained from Tübingen and TU Munich. All cases were stained for CD123, CD56, TCL1 and TCF4. GEP of eAML and BPDCN was performed using EdgeSeq Oncology Biomarker panel comprising 2549 genes, followed by Ion Torrent sequencing. Differential gene expression analysis was performed using DESeq2 (p-adj. <0.05 and fold change >1.5).

Results

GEP of 21 eAML and 14 BPDCN cases identified 45 differentially expressed genes. All cases clustered with their respective entity with the exception of one eAML case. *LYZ* (78x), *DEFB1* (51x), *PRL* (24), *IDO1* (15x), *DACH1* (12x), *CCL23* (10x), *XCR1* (7x), *ITGB2* (7x), *CACNA1H* (7x) and *SPI1* (6x) emerged as top upregulated genes in eAML vs. BPDCN. BPDCN showed upregulation of *TCL1A* (306x), *PTCRA* (119x), *PFKFB2* (23x), *CDH1* (18x), *IRF7* (16x), *RASD1* (15x), *GNG7* (12x), *CLIC3* (11x), *TLR7* (8x), and *TNFRSF21* (8x). Interestingly, the single eAML case clustering with BPDCN showed upregulation of *TCL1* and *PTCRA*, as well as other genes upregulated in BPDCN group. Immunohistochemically, this case was unremarkable (weak CD123, negative for CD56 and TCL1).

Conclusion

GEP of eAML and BPDCN identified 45 differentially expressed genes and allowed a robust separation of these two entities. *TCL1A*, *PTCRA*, *CDH1*, *IRF7* and *TLR7* are well-known pDC-specific markers, while most upregulated genes in eAML, including *LYZ* (lysozyme) and *DEFB1* (defensin β), are associated with neutrophil and monocyte lineage. Since separation of eAML and BPDCN by immunophenotyping can be challenging due to frequent expression of CD56 and CD123 in both entities, GEP provides a robust, additional diagnostic tool. *TCL1A* and *PTCRA*, which were highly upregulated in all BPDCN cases compared to eAML, could serve as key diagnostic genes for this discrimination.

This study was financially supported by Stemline.

Robust and explainable AI-aided evaluation of leukocytes morphology for leukemia diagnostics.

C. Matek^{1,2}, C. Marr²

¹Pathologisches Institut Universitätsklinikum Erlangen, Erlangen, Germany, ²Institute of AI for Health / Hemholtz Zentrum München, München, Germany

Questions/Background

Cytomorphologic evaluation of peripheral blood and bone marrow samples remains a cornerstone of the diagnostic workflow of leukemia evaluation. As in the past 150 years, cytomorphologic evaluation and quantification is still today performed by human examiners under the light microscope. In the past few years, a number of increasingly refined methods for cell classification based on artificial intelligence (AI) methods have been developed.

Methods

The present work shows applications of modern deep learning-based methods for developing robust algorithms for leukocyte classification to support morphologic leukemia diagnostics. Development of these methods is based on the availability of large, well-annotated databases of single cells digitized at high imaging quality. We present two large, publically available databases of leukocytes which form the basis for a successful application of deep learning-techniques.

Additionally, end-to-end learning systems typically do not offer a transparent human-interpretable explanation for their classification decisions, which is often referred to as a "black box" property. We apply several explainability methods to check the decisions of the algorithms and render them more transparent to the human user.

Furthermore, developed algorithms are tested for stability using image data from different labs, preanalytic workflows and scanner platforms. We show how robustness and stability methods can be used to make the systems developed usable to a wider range of data from diverse sources.

Results

Deep learning-based methods achieve a high level of classification accuracy for both single cells and disease entities and attain human-level performance for some tasks. While limited data availability remains a challenge, they can be stabilised against a number of practically important inter-domain variations and image corruptions.

Conclusion

Deep learning-based methods promise to emerge as a fast, robust and quantitatively accurate diagnostic support system for leukocyte cytomorphology. Challenges remain in the high quality requirements on scanning systems. A promising next step will be integration with histology data which includes the tissue context.

The bone marrow microenvironment in hemophagocytic lymphohistiocytosis

T. Menter¹, M. Trebo^{2,3}, J. Fauser^{2,3}, L. Horvath^{2,3}, A. Pircher^{2,3}, B. Posch^{2,3}, M. Medinger⁴, S. Soppe^{2,3}, D. Wolf^{2,3}, A. Tzankov¹

¹Institut für Pathologie, Basel, Switzerland, ²Medizinische Universität Innsbruck, Innsbruck, Austria, ³Comprehensive Cancer Center Innsbruck (CCCI) and Tyrolean Cancer Research Institute (TKFI), Innsbruck, Austria, ⁴Universitätsspital Basel, Hämatologie, Basel, Switzerland

Question/Background

Hemophagocytic lymphohistiocytosis (HLH) is a severe, potentially life threatening disease resulting in an uncontrolled activation of macrophages. HLH has various etiologies and in many cases a distinct genetic predisposition. However, the role of crucial immune regulators and checkpoints have not been completely elucidated yet.

Methods

In this study, we analyzed bone marrow trephine biopsies of 37 clinically well-documented patients with confirmed HLH according to current standards (at least 5/8 HLH-defining symptoms and HLH-score >150) by immunohistochemistry for selected immune checkpoints. 11 bone marrow biopsies of healthy individuals were used as a control cohort.

Results

Causes for HLH were categorized as genetic, autoinflammatory, infectious, neoplastic and a combination of infectious and neoplastic. The age of the patients significantly differed between subgroups with a median

age of 28 years in the genetic, and a median age of 60 years in the neoplasia-associated subgroup. In the HLH cohort, we found positive correlations between the number of PDL1-positive cells and those expressing LILBR1 (Leukocyte Immunoglobulin Like Receptor B1), which is an important gatekeeper in regard to the stimulation of the immune system, while PD1 and PDL1 only correlated in the control group indicating disturbances in cellular signaling in HLH ($p=0.709$, $p=0.015$; $p=0.674$, $p=0.023$ respectively). SIRP α (Signal Regulatory Protein α), which interacts with CD47 and thus inhibits macrophage function, was significantly less prevalent in the HLH group compared to the control group (19/37 vs 1/11, $p=0.013$). Presence of CD40-positive cells positively correlated with increased amounts of PDL1 and CD47-positive cells ($p=0.743$ and 0.506 , respectively, $p<0.001$, each). Epstein-Barr-virus (EBV) positive cells could only be detected in male patients (9/24 vs. 0/13, $p=0.011$), but this did not affect the expression of the proteins investigated.

Conclusion

Our investigations provide insights into expression of immune checkpoints in HLH patients. We could show that homeostasis of several pathways gets disrupted. Further characterization of the impact of SIRP α , a potentially druggable target, is needed to find a way to regain control on the disturbed immunologic microenvironment in HLH.

DGP02 Classification of myeloid neoplasia II: progress and controversies

DGP02.02

The current classification of acute leukemias

T. Haferlach

MLL Münchner Leukämielabor GmbH, München, Germany

In recent decades, the classifications for acute leukemia have changed dramatically, becoming much more complex, but also more specific and gaining extremely great clinical importance. This applies both: to the classification and diagnosis as well as to the findings for the measurement of measurable residual disease (MRD). Even more, we see far-reaching information on the prognosis of the individual leukemia and especially on the specific therapy. All this together, regardless of whether we classify according to WHO or ICC, places the highest demands on the laboratories involved, the hematologists in their therapy recommendations and in the communication with the patients, as well as on the compliance of the patients. Undisputedly, typical methods continue to be of central importance. This applies to cytomorphology as well as to histology. In addition, immunochemistry and immunohistology play an important role. Classical chromosomal banding analysis continues to be a central component of any diagnosis in acute leukemia. However, most of the findings, changes and especially disease-defining criteria have been provided by molecular methods over the past 20 years. Today, diagnosis of acute leukemias is inconceivable without the use of panel sequencing. Genetic relevance can be extracted immediately, in all aspects of prognosis, therapy decision and therapy management.

It must therefore be our central task to use these diagnostic possibilities to operate on our patients needs promptly, correctly and with the most far-reaching therapeutic recommendations possible. It is the most important task of every scientist and doctor to set exactly this as a goal. It is no longer a question of what we have to do and not really only a question of how we have to do it, but only a question of why we have to do so. Why are these the methods further needed to diagnose acute leukemias. If we look from this direction, it does not make a big difference whether we call it according to WHO or ICC at the end, the patient must stand in the center.

DGP03 Freie Vorträge I - Hämatopathologie

DGP03.01

Molecular profiling of EBV associated diffuse large B cell lymphoma

I. Anagnostopoulos¹, F. Frontzek², A. Staiger^{3,4}, R. Wullenkord², M. Grau², M. Zapuklyak², K. Kurz⁵, H. Horn^{3,4}, T. Erdmann², F. Fend⁶, J. Richter⁷, W. Klapper⁷, P. Lenz⁸, S. Hailfinger², M. Trautmann⁹, W. Hartmann⁹, L. Quintanilla-Martinez⁶, A. Rosenwald¹⁰, G. Lenz², G. Ott^{3,4}

¹Universität Würzburg, Institut für Pathologie, Würzburg, Germany, ²Universität Münster, Medizinische Klinik A, Münster, Germany, ³Robert-Bosch-Krankenhaus, Institut für Klinische Pathologie, Stuttgart, Germany, ⁴Dr. Margarete Fischer Bosch Institut für Klinische Pharmakologie, Stuttgart, Germany, ⁵Robert-Bosch-Krankenhaus, Institut für Klinische Pathologie, Stuttgart, Germany, ⁶Eberhard-Karls-Universität, Institut für Pathologie und Neuropathologie, Tübingen, Germany, ⁷Christian-Albrechts-Universität, Sektion für Hämatopathologie, Institut für Pathologie, Kiel, Germany, ⁸Universität Marburg, Institut für Physik, Marburg, Germany, ⁹Universität Münster, Gerhard-Domagk-Institut für Pathologie, Münster, Germany, ¹⁰Universität Würzburg, Institut für Pathologie, Würzburg, Germany

Questions/Background

Epstein-Barr virus (EBV) associated diffuse large B cell lymphoma (DLBCL) represents a rare aggressive lymphoma subtype. As the specific molecular characteristics and the precise role of EBV in pathogenesis of this lymphoma remain elusive, we performed a comprehensive molecular analysis.

Methods

We investigated 60 primary EBV+ DLBCL using targeted sequencing of cancer candidate genes. Genome-wide determination of recurrent somatic copy number alterations was performed in 46 cases. For determination of cell-of-origin the NanoString Lymphoma subtyping test was employed. To assign samples to previously described genetic DLBCL subtypes the LymphGen 2.0 classifier was applied. For determination of PD-L1 expression antibody clone SP142 was used.

Results

Targeted sequencing identified recurrent mutations activating the *JAK-STAT* in 30% and *NOTCH* pathways in 22% of the cases analyzed. 52% of the cases were affected by mutations of genes encoding for chromatin modifiers, while 11% of the cases had mutations in genes contributing to immune evasion. Amplifications of 9p24.1 comprising *PD-L1/-L2* and *JAK2* were identified in 20% of the cases. PD-L1 expression was present in most cases with *PD-L1* amplification. By applying the LymphGen classifier 2.0 <20% of the cases could be assigned to one of the established molecular DLBCL subtypes.

Conclusion

The observed genetic abnormalities in EBV+ DLBCL strongly differ from DLBCL not other specified (NOS) supporting the notion that it represents a distinct entity. EBV infection may be responsible in inducing NF- κ B and enhancing JAK-STAT signaling in these cases. Our findings enable further functional studies exploring the therapeutic potential of targeting detected aberrations to improve outcome.

DGP03.02

B-cell clonality assessment using a Next Generation Sequencing Approach

T. Menter, I. Bratic-Hench, I. Alborelli, S. Dirnhofer, M. Manzo, A. Tzankov
Institut für Pathologie, Basel, Switzerland

Questions/Background

Assessing B-cell clonality is an important task in haematopathology and a helpful tool in routine diagnostics. PCR-based fragment-length analysis (e.g. based on BIOMED-2 primers) has been a useful method for several decades. Currently, first assays using high throughput sequencing (HTS, also called NGS) have become available.

Methods

To assess robustness and applicability of these novel assays, we compared the results for B-cell clonality via PCR and NGS (Oncomine™ BCR Pan-Clonality Assay, ThermoFisher) in 25 cases, including a variety of B-cell lymphomas and reactive lesions. Blood samples (n=3) and formalin fixed and paraffin embedded (FFPE) tissue blocks (n=22) were used. By NGS, both the ratios of top clone frequencies of IgH, Ig Kappa and Ig Lambda to the background clone frequency were assessed as well as so called light- and heavy chain “lineages” taking into account ongoing somatic hypermutation in lymphoma cells. Evaluation was performed according to the recommendations of the manufacturer and as previously published (J Mol Diagn. 2019 Mar;21(2):330-342).

Results

In 9/13 cases diagnosed as “clonal” and 9/12 cases diagnosed as “polyclonal” by PCR, NGS analysis was concordant. In four cases, the “clonal” result by PCR could not be confirmed by NGS analyzing IgH only, however, taking into account the light chains, clonality could be demonstrated in two of these specimens.

The two specimens in which clonality could not be detected by NGS were a marginal zone lymphoma of the skin and a primary cutaneous follicle center lymphoma. One specific case included infiltrates of a lymphoplasmacytic lymphoma and chronic lymphocytic B-cell leukemia (so called “composite lymphoma”). By NGS, two distinct clones reflecting the tumor amount of both lymphomas were found, while PCR did not detect two distinct clones. In three probes signed out as polyclonal by PCR analyzing IgH, clonality could be proven by NGS by assessing the light chains, which is in line with the neoplastic nature of the clonotypic cells as such B-cell would have been sorted out during B-cell development.

Conclusion

We could demonstrate that assessing clonality by NGS is a useful adjunct in lymphoma diagnostics. Analyzing both heavy chains and light chains increases sensitivity, yet it seems that especially in cutaneous B-cells lymphomas, it remains difficult. Further work will address the issue of whether the presence of distinct clones or rather the so called “lineages” detected should be considered as diagnostic parameter.

DGP03.03

A roadmap to Richter Syndrome: Boolean network modeling to elucidate regulatory mechanisms and personalized therapeutic options

J. Maier^{1,2}, N. Ikonomi², S. D. Werle², J. Schwab², R. Marienfeld¹, S. Stilgenbauer³, P. Möller¹, H. A. Kestler²

¹Ulm University Hospital, Institute of Pathology, Ulm, Germany, ²Ulm University, Institute of Medical Systems Biology, Ulm, Germany,

³Ulm University Hospital, Comprehensive Cancer Center Ulm, Ulm, Germany

Questions/Background

Chronic lymphocytic leukemia (CLL) is an indolent B-cell neoplasm which, in 5-10% of cases, will undergo malignant transformation into an aggressive B-cell lymphoma, termed Richter syndrome (RS). The mechanistic understanding of RS is currently a central issue affected by the scarce availability of wet laboratory models. On these grounds, we studied RS development from a systems biology perspective by applying a dynamic modeling approach, namely Boolean networks.

Methods

We used Boolean network modeling to simulate large molecular crosstalks over time on a qualitative level. Stable long-term behaviors of the system then represent biological phenotypes.

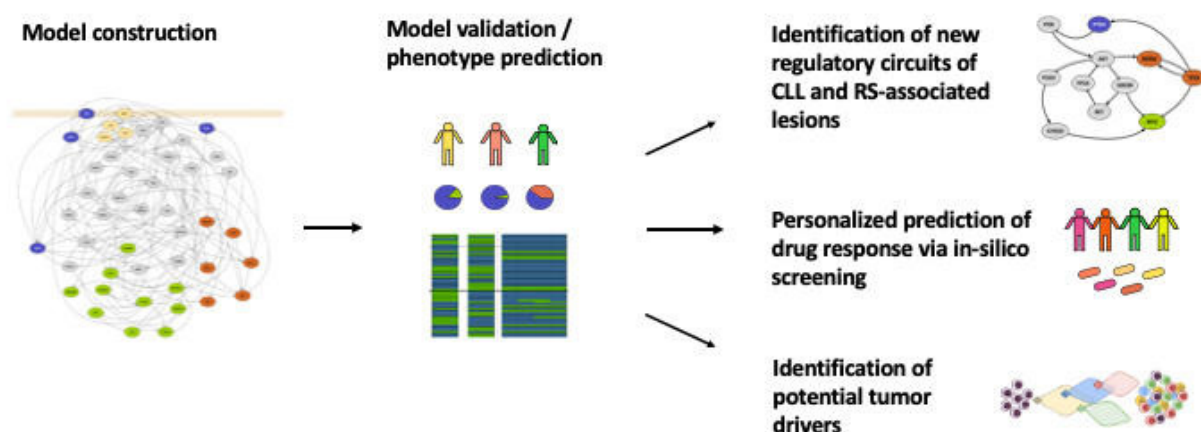
We also established a FFPE (formalin-fixed paraffine-embedded) tissue patient cohort of CLL and RS cases to challenge hypotheses generated by our *in-silico* predictions in human tissue sections.

Results

We established a large *in-silico* model of the CLL signaling network to recapitulate the main crosstalks involved in disease development. To validate our model, we conducted dynamic simulations of indolent CLL and RS-associated lesions and matched the resulting stable states to known behaviors of the tumors. Simulation of the unperturbed CLL model as well as RS-like phenotypes could correctly predict the experimentally observed phenotypical traits in terms of proliferation, cell survival, and gene specific activities. By studying *in-silico* cascades from BCR stimulated starting conditions to stable states of the systems we were able to highlight new players in the mechanisms underlying RS. Finally, we applied our system to tumor driver prediction as well as to the prediction of personalized therapeutic target identification via an exhaustive *in-silico* screening under different mutational conditions. We obtained a circumscribed set of target combinations to be effective dependent on the underlying hypothesized RS mechanism. This result is even more relevant considering that the experimental testing of all possible compounds within our model and their combinations would imply a drug screening of almost 5000 experiments per mutational condition.

Conclusion

We believe our approach could bridge the gap between RS phenotypical observations and underlying regulatory pathways, thus integrating and supporting experimental strategies.



Dynamic modeling of Richter Syndrome using Boolean networks: workflow from model construction to in-silico predictions.

DGP03.04

A pilot study on the epigenome-wide methylation analysis of diffuse large B-cell lymphoma

T. Kraus, D. Hölzl, K. Sotlar

Uniklinikum Salzburg, Universitätsinstitut für Pathologie, Salzburg, Austria

Questions/Background

Diffuse large B-cell lymphoma (DLBCL) are the most frequent type of non-Hodgkin lymphoma and account for approximately 30% to 40% of newly diagnosed lymphomas. Thereby, DLBCL is an inhomogeneous group of tumours both morphologically and clinically. Since some patients benefit from more aggressive therapy, it is important to identify these lymphomas early in the course of the disease. Thereby, Hans et al. found that DLBCL can be distinguished into prognostic subgroups of germinal center B-cell like (GCB) lymphomas and activated B-cell-like (ABC) lymphomas. Differentiation can be performed by applying distinct immunohistochemical markers, e.g. CD10, BCL-6, and MUM1. The aim of this study is to analyse the epigenomic landscape of DLBCL by DNA-methylation profiling and to identify differentially methylated genes and pathways in DLBCL of GCB and ABC subtypes.

Methods

In this pilot study, we performed epigenome-wide methylation analysis of 6 DLBCLs, including 3 of GCB and 3 of ABC subtype. Using the Illumina Infinium EPIC bead chip array we interrogated more than 850,000 methylation sensitive CpGs sites in parallel. Computational analysis was performed to identify differentially methylated genes. Gene ontology analysis was processed to reveal altered pathways.

Results

We found that DLBCL of GCB and ABC type show distinct alterations of the epigenomic landscape. We found distinct differentially methylated CpGs in GCB and ABC subtypes of DLBCLs. Thereby, 59% of CpGs were hypermethylated and 41% were hypomethylated in GCB DLBCL compared with ABC DLBCL. Analysis of genomic distribution showed that 17% were located in gene tiling regions, 2% in promoter regions, 1% in gene regions, and 3% in CpG island regions. 77% were located in other genomic locations. Interestingly, we found miRNAs loci among top differentially methylated gene regions.

Conclusion

In summary, in this pilot study, we performed an integrated epigenome-wide analysis of DLBCL of GCB and ABC subtypes and found distinct alterations of the DNA-methylation landscape depending on DLBCL subtype, possibly resulting in differentially expressed miRNAs between DLBCL subtypes.

DGP04 Digitale Pathologie

DGP04.01

AI in pathology : There is more than meets the eye

G. Litjens

Radboud UMC, Nijmegen, The Netherlands

Artificial intelligence is transforming many areas of daily life but is also having a significant impact on medicine. Although most common in specialties that have been digital for a long time, such as radiology, pathology is catching up rapidly. Several certified commercial products are already on the market, which have shown encouraging results in supporting pathologists in their daily routine, such as for Gleason grading of prostate biopsies or recognition of metastases in sentinel lymph nodes. However, these applications scratch the surface of the possibilities of artificial intelligence in digital pathology. In this talk, I will show that artificial intelligence can also enable a new way of doing pathology diagnostics, from unprecedented quantification capabilities to discovering new prognostic features that can improve patient care. Specifically, I will show lymphoma and breast and prostate cancer examples from my research group and connect those to the developments in the field. Furthermore, I will highlight several ways artificial intelligence can augment pathologists in practice and why artificial intelligence should not be considered a risk to the profession but a powerful new tool that can usher pathology into the future.

DGP04.03

Automatic, non-teachmark based coregistration of mass spectrometry images and hematoxylin and eosin stained microscopy images

S. S. Lakkimsetty¹, A. Weber², K. A. Bemis¹, M. Werner^{2,3}, M. Föll², O. Vitek¹, P. Bronsert^{2,3,4}

¹Northeastern University, Khoury College of Computer Sciences, Boston, United States of America, ²University of Freiburg, Medical Center, Institute for Surgical Pathology, Freiburg, Germany, ³University of Freiburg, Medical Center, Tumorbank Comprehensive Cancer Center Freiburg, Freiburg, Germany, ⁴University of Freiburg, Medical Center, Core Facility for Histopathology and Digital Pathology, Freiburg, Germany

Questions/Background

Pathologists usually identify cancerous regions on stained tissue slices based on morphological features. Mass spectrometry (MS) imaging techniques allow a spatially resolved identification of molecules and provide insights into molecular features of different tissues. To identify pathologically relevant regions on mass spectrometry images, an alignment of microscopy images and mass spectrometry images is needed.

Methods

Here we describe the automatic coregistration of hematoxylin and eosin stained microscopy images with mass spectrometry images obtained from a MALDI mass spectrometer. The processing of the MS images involves peak picking, peak alignment, peak filtering and peak binning. The obtained m/z features are clustered with the spatial shrunken centroids algorithm and the top 30 m/z features contributing most to the clusters are kept. Subsequently, the 30 m/z features are reduced to 3 m/z features via t-SNE. As input to the coregistration algorithm, grayscale MS images are taken. The tissue margins of both modalities are manually traced to eliminate the background. The resolution of the microscopy images are scaled down to match the resolution of the MS images. The microscopy images are as well converted into single-channel grayscale images. Cropping and padding of the microscopy images ensures a similar margin between tissue and image margin of both modalities. Coregistration can be performed in R and is exemplified on a colorectal cancer data set obtained by MALDI mass spectrometry.

Results

Qualitative assessment of the coregistration between microscopy and mass spectrometry images shows a good alignment of structural characteristics. The quantitative assessment via metrics such as Dice coefficient, normalized cross-correlation or displacement field Jacobian determinant shows in most cases an increase after coregistration.

Conclusion

Qualitative and quantitative assessments show a proper coregistration of microscopy and mass spectrometry images without the need for manually establishing teachmarks. Nevertheless, the general problem of assessing coregistration techniques still holds. Further research regarding the clinical relevance of the

established metrics is needed.

DGP04.04

Repeatable study of the PD-L1 CPS in Triple-negative breast cancer based on the AI-assisted model

J. Li, X. Wang, Y. Liu, J. Ying

The Fourth Hospital of Hebei Medical University, Department of Pathology, Shijiazhuang, China

Questions/Background

With the application of immunotherapies in TNBC, the consistency and accuracy of the interpretation in PD-L1 (DAKO 22C3) combined positive score (CPS) are more important than ever. However, pathologists have great variability in interpretation, we need to establish an objective and effective methods which is easy to repeat.

Methods

In this study, we established a deep learning-based artificial intelligence-assisted (AI-assisted) model, using cell detection and region segmentation algorithm.

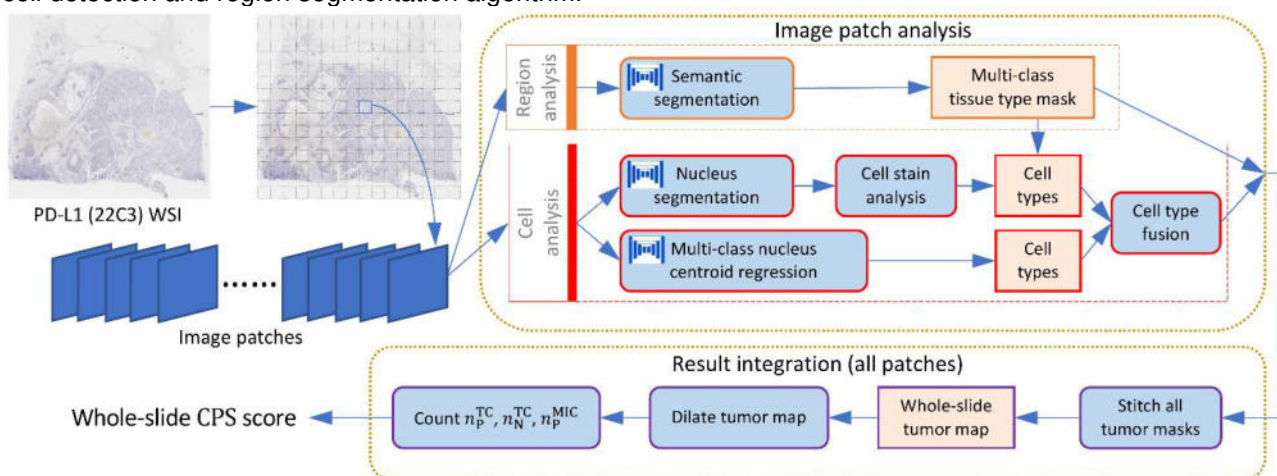


Figure1. The interpretation results and system diagram of PD-L1 CPS by AI-assisted model

Three rounds of ring studies (RSs) were conducted. 12 pathologists of different level evaluate the CPS of PD-L1 (DAKO 22C3) in TNBC patients by visual assessment and AI-assisted model.

Results

In the visual assessment, the interpretation results of PD-L1 (DAKO 22C3) CPS in different level pathologists have significant differences ($P < 0.05$), and the consistency of all the pathologists interpretation results was weak. Moreover, the internal consistency of all pathologists in the visual assessment is moderate, in which the repeatability of junior pathologists is the worst, the ICC value is 0.664 (95%CI:0.564-0.762). Through AI-assisted interpretation, the ICC value increased to 0.883 (95%CI:0.836-0.922) which improved the consistency of the interpretation results.

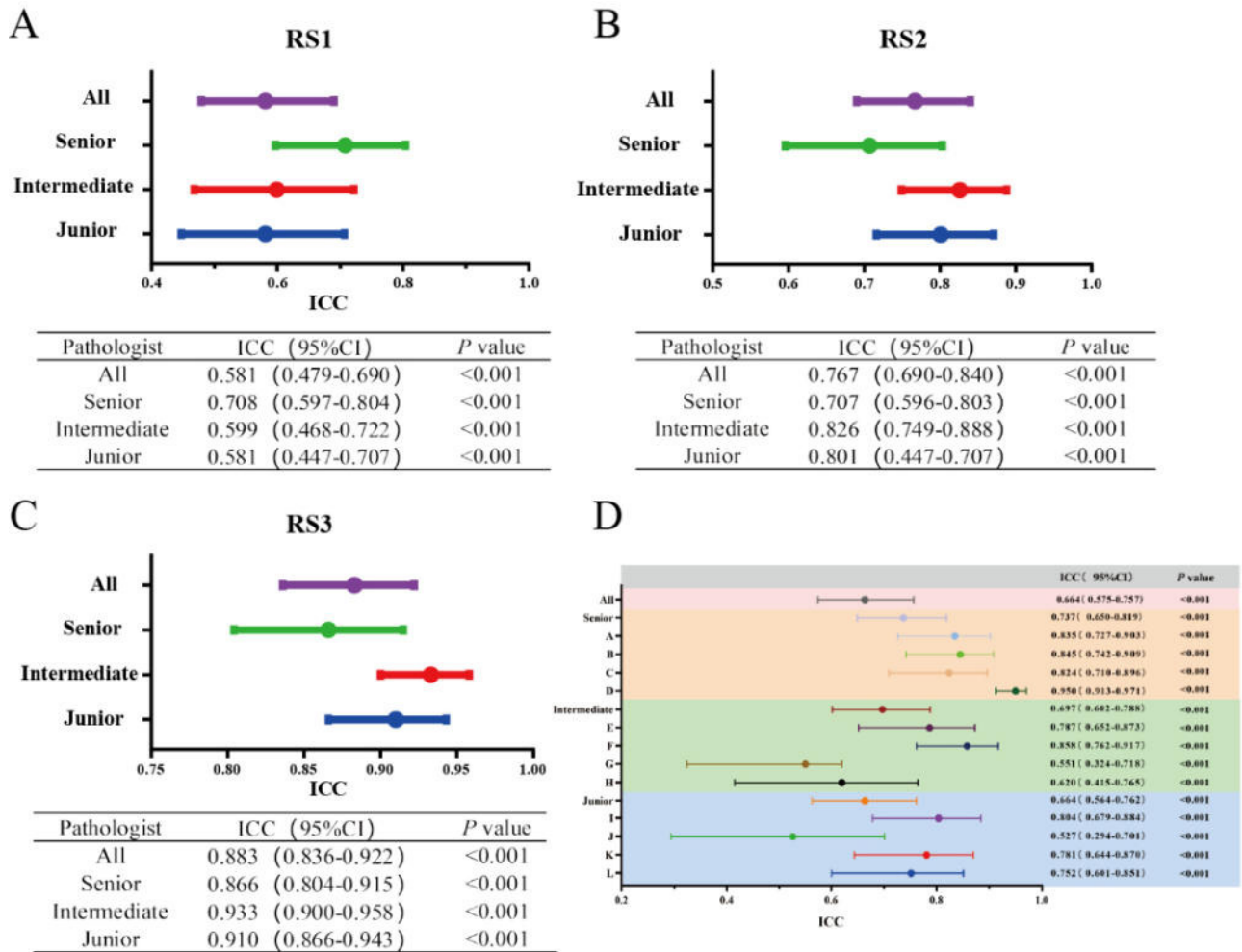


Figure2. The consistency and repeatability of the interpretation results. (A)-(C) The consistency of the PD-L1 CPS interpretation among the different level of pathologists in three ring studies. (D) The repeatability of the interpretation results between 12 pathologists in RS1 and RS2.

In addition, through AI-assisted interpretation, the repeatability and accuracy of the interpretation results has been further upgraded. At the same time, the acceptance of AI results by junior pathologists are high.

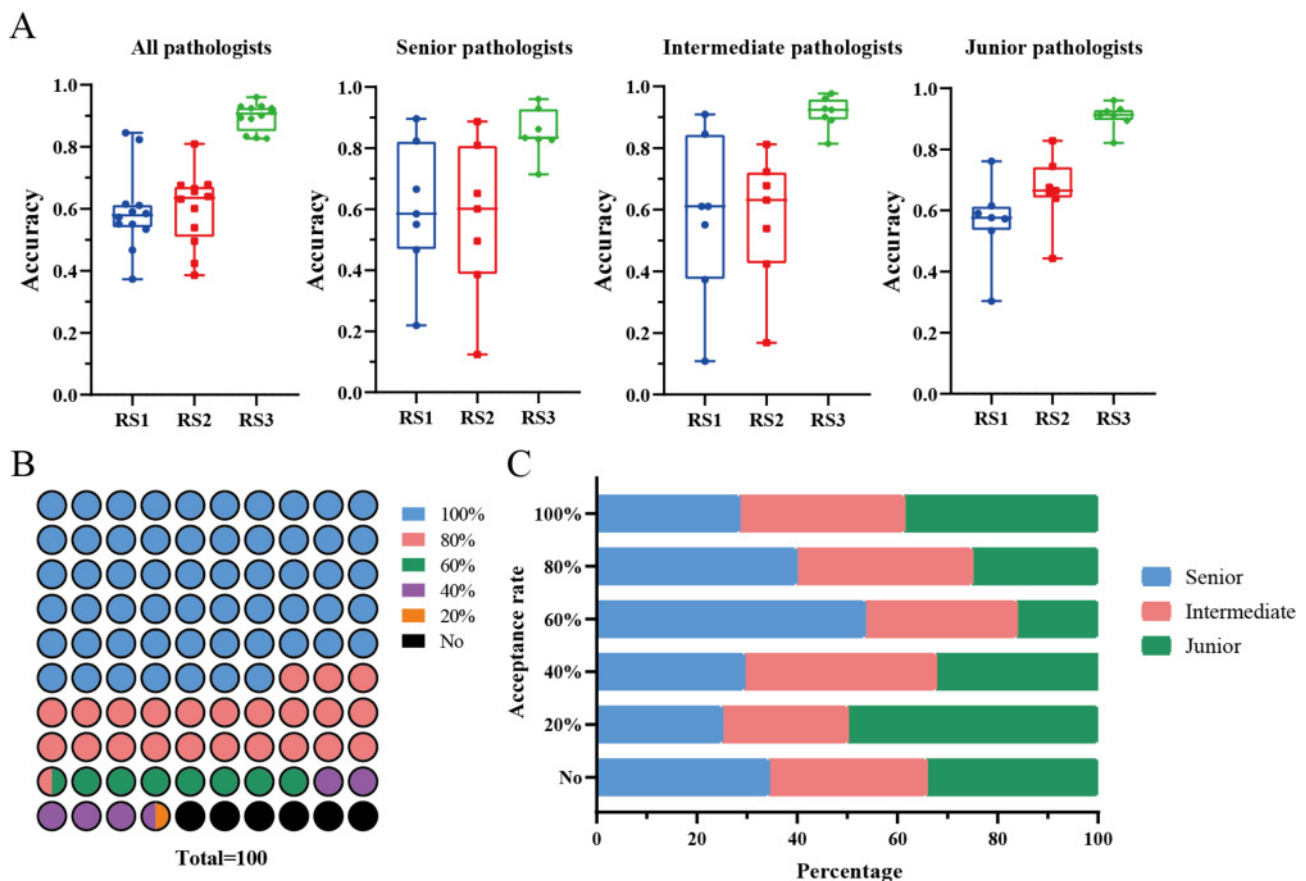


Figure3. Accuracies and acceptance rates of different experienced pathologists. (A) Boxplots of scoring accuracies for pathologists in different levels. (B) Acceptance rates of all pathologists in total 50 slides. (C) Percent stacked column chart of different levels of pathologists with AI score acceptance.

Conclusion

With the help of the AI-assisted diagnostic model, different levels of all the pathologists have achieved excellent consistency and repeatability in the interpretation of PD-L1 (DAKO 22C3) CPS. Moreover, the level of interpretation has been sought the rapid enhancement. It can be seen that AI-assisted diagnostic model provides a good approach to strengthen the consistency and repeatability in clinical practice.

DGP04.05

Clinical-grade tumor detection and tissue segmentation in colorectal specimens using artificial intelligence tool

J. Griem¹, M.-L. Eich¹, S. Schallenberg², A. Pryalukhin³, A. Bychkov⁴, J. Fukuoka⁵, V. Zayats⁶, W. Hulla³, J. Munkhdelger⁴, A. Seper⁷, T. Tsvetkov¹, A. Mukhopadhyay⁸, M. Fuchs⁸, A. Sanner⁸, J. Stieber⁸, N. Babendererde⁸, B. Schömig-Markiefka¹, S. Klein¹, R. Büttner¹, A. Quaas¹, Y. Tolkach¹

¹University Hospital Cologne, Cologne, Germany, ²University Hospital Charité, Berlin, Germany, ³State Hospital Wiener Neustadt, Wiener Neustadt, Austria, ⁴Kameda Medical Center, Kamogawa, Japan, ⁵Nagasaki University Hospital, Nagasaki, Japan, ⁶Laboratory for Medical Artificial Intelligence, Moscow, Russian Federation, ⁷Danube Private University, Wien, Austria, ⁸Technical University Darmstadt, Darmstadt, Germany

Questions/Background

Digital pathology adoption allows for applying computational algorithms to routine pathology tasks. Our study aimed to develop a clinical-grade AI tool for precise multi-class tissue segmentation in colorectal specimens (resections and biopsies) and clinically validate the tool for tumor detection in biopsy specimens.

Methods

The training dataset included 241 precisely manually annotated whole slide images from multiple institutes. The algorithm was trained for semantic segmentation of 11 tissue classes with an additional module for biopsy whole slide image classification. Six case cohorts from 5 pathology departments (four countries) were used for formal and clinical validation, digitized by four different scanning systems.

Results

The developed algorithm shows high precision of segmentation of different tissue classes in colorectal specimens with composite multi-class Dice score of up to 0.895 and pixel-wise tumor detection specificity and sensitivity of up to 0.958 and 0.987, correspondingly. In the clinical validation study on multiple external cohorts, the AI tool reached sensitivity 1.0 and specificity of up to 0.969 for tumor detection in biopsy whole-slide images. The AI tool analyzes most biopsy cases in < 1 min allowing effective integration into clinical routine.

Conclusion

We developed and extensively validated a highly accurate, clinical-grade tool for assistive diagnostic processing of colorectal specimens. This study is also a foundation for a SemiCOL computational challenge. We open-source multiple manually annotated and weakly-labeled test datasets, representing an enormous contribution to the colorectal cancer computational pathology field.

DGP04.06

Application of artificial intelligence (AI) in counting of eosinophil granulocytes in gastrointestinal biopsies

K. Petrovay-Cselényi¹, A. M. Balogh¹, A. Pesti², Z. Bedőházi³, A. Biricz³, É. Kocsmár², E. Kontsek², A. Kiss², P. Pollner⁴, Á. Cseh¹, G. Lotz²

¹Semmelweis University, Department of Pediatrics, Budapest, Hungary, ²Semmelweis University, Department of Pathology, Forensic and Insurance Medicine, Budapest, Hungary, ³Eötvös Loránd University, Department of Physics of Complex Systems, Budapest, Hungary, ⁴Hungarian Academy of Sciences, MTA-ELTE Statistical and Biological Physics Research Group, Budapest, Hungary

Questions/Background

Inflammation in the gastrointestinal tract, characterised by accumulation of eosinophilic granulocytes, may be a reactive phenomenon due to known pathological conditions or may be a primary disease. The primary form is known as eosinophilic gastrointestinal disorders (EGID). The pathological diagnosis of EGIDs is difficult because there is no consensus on the number of eosinophils that can be considered as pathological in different parts of the gastrointestinal (GI) tract and it can be difficult to exclude secondary causes. At present, eosinophilic esophagitis is the most characterized EGID, while other EGIDs are in the focus of scientific research. Our aim was to train artificial intelligence (AI) to determine the number of eosinophilic granulocytes in the GI tract.

Methods

GI biopsy slides of 15 patients diagnosed with tissue eosinophilia and 6 children diagnosed with non-eosinophilic disease at the Department of Pediatrics, Semmelweis University were digitized using a 3DHISTECH PANNORAMIC 1000 scanner in the Department of Pathology, Forensic and Insurance Medicine. The scanned sections were uploaded to Cytomine analytical application using OpenSlide software package. We annotated 30-50 eosinophilic granulocytes of different appearance per specimen on 50 slides randomly selected in Cytomine, representing different sections of the GI tract, and applied artificial intelligence training based on the YOLOv5 object recognition algorithm. A further learning cycle was performed to correct recognition errors. The two rounds of training included a total of 17 934 images.

Results

The AI detection Precision value was 95, meaning that 95 out of 100 detected eosinophils were actually recognized as eosinophil granulocytes by the human investigators. The Recall value was 90, meaning that AI was able to detect 90 eosinophils out of 100 eosinophil granulocytes annotated by human investigators. The group of patients with a history of tissue eosinophilia in at least one GI site had a significantly higher density of eosinophils in the entire length of the colon (3,924 [2,808-7,1127] in the control group and 14,310 [9,668-25,333] in the tissue eosinophilia patient population (p=0.013)).

Conclusion

The application of our AI-assisted eosinophil granulocyte counting on a larger GI biopsy digital slide archive may subsequently allow the determination of pathological eosinophil counts in different sections of the GI tract, thus contributing to the refinement of diagnostic criteria for EGIDs.

Artificial intelligence for tumor detection and histological regression grading in oesophageal adenocarcinomas: an algorithm development and validation study

Y. Tolkach¹, L. M. Wolgast¹, A. Damanakis¹, A. Pryalukhin², S. Schallenberg³, W. Hulla², M.-L. Eich¹, A. Mukhopadhyay⁴, M. Fuchs⁴, S. Klein¹, W. Schröder¹, C. Bruns¹, F. Gebauer¹, R. Büttner¹, B. Schömig-Markiefka¹, **A. Quaas¹**

¹University Hospital Cologne, Cologne, Germany, ²State Hospital Wiener Neustadt, Wiener Neustadt, Austria, ³University Hospital Charité, Berlin, Germany, ⁴Technical University Darmstadt, Darmstadt, Germany

Questions/Background

Oesophageal adenocarcinoma/adenocarcinoma of oesophagogastric junction (OESA) is one of the most common malignant tumors. Most patients receive neoadjuvant therapy before complete tumor resection. Histological evaluation includes the identification of residual tumor tissue in addition to areas of the regressive tumor, resulting in clinically relevant regression scoring. We developed an AI tool for tumor detection and tumor regression grading in OESA surgical specimens.

Methods

One training cohort and four independent test cohorts were used. Training cohorts and test cohort cases were extensively manually annotated for 11 tissue classes. A convolutional neural network (InceptionResNetV2) was trained for model development using a supervised principle. Clinical validation included processing of the whole resection cases by pathologists with and without AI assistance.

Results

High accuracy was achieved for both tumor (AUROC 0.997-0.998, 95%CI range 0.994-0.998 for external test cohorts) and regression tissue (AUROC 0.955-0.991, 95%CI range 0.945-0.991) detection (patch-level accuracy). Image normalization techniques improved detection of regression tissue. By validating the concordance of the AI tool against a group of pathologists (n=12), substantial agreement was observed (agreement 63.6%, quadratic kappa 0.749) at case level. The AI-based regression grading triggered true reclassification in seven cases (six cases with small tumor regions that were initially missed by pathologists). During prospective evaluation the hybrid approach of combining the AI tool as assistance increased the interobserver agreement among pathologists (agreement 85-95%) and substantially reduced diagnostic time per case (54% less time per case). The prognostic significance of the regular, AI-based grading was higher than that of pathologists. Two additional quantitative parameters: absolute volume of residual tumor and estimated pre-therapeutic tumor volume provided additional prognostic value as compared to conventional grading.

Conclusion

This study shows immediate and substantial benefits of AI-assisted diagnostics of OESA resection specimens, given as a hybrid approach is more accurate and less time-consuming.

Development and international multi-center validation of AI tool for kidney tumor detection and subtyping

M.-L. Eich¹, A. Pryalukhin², M. Sitova³, P. Lazarev³, M. Smirnov³, S. Schallenberg⁴, A. Bychkov⁵, W. Hulla², J. Fukuoka⁶, A. Seper⁷, A. Quaas¹, G. Netto⁸, R. Büttner¹, Y. Tolkach¹

¹University Hospital Cologne, Cologne, Germany, ²State Hospital Wiener Neustadt, Wiener Neustadt, Austria, ³Saint-Petersburg State Pediatric Medical University, Saint-Petersburg, Russian Federation, ⁴University Hospital Charité, Berlin, Germany, ⁵Kameda Medical Center, Kamogawa, Japan, ⁶Nagasaki University Hospital, Nagasaki, Japan, ⁷Danube Private University, Wien, Austria, ⁸University of Alabama, Birmingham, United States of America

Questions/Background

Digital pathology allows for automatization and objectivization of many pathology tasks. In this study, we create a deep learning-based tool for detection of epithelial renal tumors in histological sections (hematoxylin&eosin) and their subtyping.

Methods

A large training dataset of >700 digitized histological slides from patients with RCC and benign kidney tumors (1 slide / patient) with detailed manual annotations for 12 classes (9 benign and 3 tumor classes) was used for algorithm training. High-precision semantic segmentation networks were trained based on UNet++ architecture for two different tasks - tumor and multiple other tissue classes detection, and tumor subtyping

into clear-cell RCC, papillary RCC, chromophobe RCC, oncocytoma, or "other". Multiple large validation cohorts of patient cases were used for formal validation (algorithm precision of multi-tissue segmentation) and clinical validation (subtyping). These stem from 6 different departments from four countries and embrace > 1000 cases, representative of different subtypes, different pathology lab and digitization practices.

Results

Extensive data augmentation without stain normalization was sufficient to achieve high accuracies in most cases, given a large, well-annotated training dataset. High accuracy was achieved in test datasets ("never-seen" cases) for tumor tissue detection (Dice score 0.941-0.963). High levels of sensitivity and specificity for ccRCC, pRCC, and chrRCC, oncocytomas subtypes (>0.950, >0.960, respectively), as well as "other" subtypes were reached comparable with a ground truth provided by experts. The out-of-distribution situation detection implemented in the AI tool, e.g. in case uncommon morphology or "other" subtype, is a common sense mechanism, that allows AI tool to inform pathologists about necessity of additional stainings or external consultation.

Conclusion

Clinical-grade levels of accuracy were achieved for the developed AI-tool for kidney tumor detection and subtyping. The principle of work allows for easy integration into diagnostic routine, and out-of-distribution detection mechanism provides important diagnostic signals in case of non-standard situations (e.g., uncommon morphology or rare subtype).

DGP05 Classification of Lymphoma I : progress and open questions

DGP05.03

What is new in the classification of peripheral T-cell lymphomas?

L. de Leval

Centre Hospitalier Universitaire Vaudois (CHUV), Institut für Pathologie, Lausanne, Switzerland

Neoplasms of mature NK or T cells (PTCLs) are rare but diverse. In 2022, two classifications of lymphoid neoplasms were developed: the International Consensus Classification (ICC) and the 5th edition of the WHO classification (WHO5) < font size="1" >. Both are updates of the 2017 WHO classification. Advances in molecular and genomic profiling of PTCLs have translated into changes which overall reflect similar conceptual shifts in both proposals.

Among EBV+ lymphoproliferative disorders (LPDs) of childhood, hydroa vacciniforme LPD replaces hydroa vacciniforme-like LPD. Chronic active EBV disease replaces chronic active EBV infection, to denote a pathologic condition, confirmed by pathogenic mutations in some patients. Primary nodal EBV+ T-cell or NK cell lymphomas, formerly a subtype of PTCL, NOS, are now a separate entity. The three aggressive types of primary intestinal T-cell lymphomas (enteropathy-associated T-cell lymphoma (EATL), monomorphic epitheliotropic intestinal T-cell lymphoma and intestinal T-cell lymphoma, NOS) are unchanged. Type II refractory celiac disease has been added as an entity in the ICC, as this represents an "in situ" neoplasm precursor to EATL. "Indolent T- cell LPD of the gastrointestinal tract" is confirmed in the ICC with the addition of "clonal" to emphasize its neoplastic nature, and is modified to "indolent T-cell lymphoma" in WHO5. Both proposals have created a new category for indolent gastrointestinal LPD from NK cells. In 2017, the developing concept that follicular helper derivation represents a unifying feature of a large group of nodal CD4+ PTCLs, led to create an umbrella term "nodal T-cell lymphoma of T follicular helper origin". Since then, this notion has been reinforced by shared molecular and genetic features, and clinical data suggest that this grouping might be relevant to treatment decisions. Therefore the ICC considers one single disease entity, follicular helper T-cell lymphoma, comprising three subtypes, angioimmunoblastic, follicular and NOS. WHO5 considers a family of three related entities of nodal T-follicular helper cell lymphomas. Four entities of anaplastic large cell lymphomas are recognized, ALK+, ALK-, primary cutaneous and breast implant-associated. In addition, the ICC recommends genomic testing for *DUSP22* in ALK- cases. < font size="1" > PTCL, NOS, remains a diagnosis of exclusion, with currently too little evidence to validate clinically relevant phenotypic or molecular PTCL-GATA3 and PTCL-TBX21 subgroups.

DGP05.04

Classification of Histiocytoses and dendritic cell neoplasms

J.-F. Emile

Hôpital Ambroise Paré & Versailles SQY University, Paris-Saclay University, Pathology Department & BECCOH research unit, Boulogne, France

Histiocytosis is characterized by tissue infiltration by cells of macrophage or dendritic cell (DC) lineages. It corresponds to a heterogeneous group of diseases, including Langerhans cell histiocytosis (LCH), Erdheim Chester disease (ECD), Rosai-Dorfman-Destombes disease (RDD) and juvenile xanthogranuloma (JXG), most of which have recently been shown to be neoplasm of myeloid origin. They should be distinguished from other causes of macrophage accumulation, such as storage of intrinsic or extrinsic components, or tumors with a stroma very rich in histiocytes.

Diagnosis is based on histology, immunohistochemistry, molecular biology, clinic and radiology. The panel of antibodies for diagnosis includes CD163, PU.1, CD1a, CD207 (Langerin) and S100. Other markers such as CD4, CD14, CD68, OCT-2 may be helpful. Most cases harbor a somatic genetic alteration activating the MAP kinase cell signaling pathway. BRAFV600E is the most frequent, affecting half of LCH or ECD, but other mutations can involve *BRAF*, *MAP2K1*, *NRAS*, *KRAS* or *CSF1*, and fusion can involve *BRAF*, *ALK* or *NTRK1*.

Three main classifications have been proposed: WHO's (5th in press for Hematology and for skin), ICC (Campo et al. Blood 2022) and Histiocyte Society classification (Emile et al. Blood 2016). They are similar for the most frequent diseases (LCH, ECD, RDD), but differ substantially for [Malignant histiocytosis / histiocyte or DC sarcoma] and for histiocytoses of the skin.

DGP06 Single-Cell and Spatially Resolved NGS

DGP06.01

A single-cell multi-omic and spatial atlas of nodal B cell lymphomas uncovers further levels of intratumor heterogeneity

S. Dietrich

Universitätsklinikum Düsseldorf, Klinik für Hämatologie, Onkologie und Klinische Immunologie, Düsseldorf, Germany

The lymph node tumor microenvironment (TME) plays an essential role for pathogenesis of B-cell non-Hodgkin's lymphoma (B-NHL). T-cells represent an important component of the TME and have been identified as an attractive therapeutic target but a detailed characterization of T-cell signatures across nodal B-NHL entities is missing. We aimed to create an in-depth T-cell reference map of B-NHL and employed single-cell RNA- and T-cell receptor sequencing alongside quantification of surface proteins, flow cytometry and multiplexed immunofluorescence on 101 lymph nodes from healthy controls, and patients with diffuse large B-cell, mantle cell, follicular, or marginal zone lymphoma. This multimodal resource revealed quantitative and spatial aberrations of the T-cell microenvironment across and within investigated B-NHL entities which were linked to lymphoma grading or survival. Our resource illustrates how T-cell signatures can be traced in routine lymphoma biopsies and exemplifies how these signatures could be used to improve the understanding of lymphoma biology and prognosis.

DGP06.02

Investigating immune and non-immune cell interactions in IDH2-mutant sinonasal undifferentiated carcinoma by FFPE-based single nucleus RNA sequencing

A. Mock¹, Y. Zhdanovich¹, C. Geisenberger¹, D. Capper², F. Klauschen¹, P. Jurmeister¹

¹Pathologisches Institut der Universität München (LMU), München, Germany, ²Charité - Universitätsmedizin Berlin, Institut für Neuropathologie, Berlin, Germany

Questions/Background

Sinonasal undifferentiated carcinoma (SNUC) is a rare and aggressive tumor entity and the prognosis for

patients remains poor despite an extensive trimodal therapy (chemotherapy, surgery, radiotherapy). Beyond epigenetic profiles and recurrent genetic alterations, little is known about oncogenic pathways, intratumoral heterogeneity and the microenvironment in these cancers. In this project, we aim to identify novel biology-informed therapeutic rationales for IDH2-mutant SNUCs by deeply characterizing the immune and non-immune cell interactions with single nucleus RNA sequencing (snRNA-seq).

Methods

Six SNUCs harboring an *IDH2* mutation were retrospectively identified. FFPE blocks were up to 5 years old. Two 50 µm thick FFPE slices were used for every sample. Slices were deparaffinized and permeabilized before further library preparation with the Fixed RNA Profiling protocol (10x Genomics). Samples were multiplexed and submitted to Illumina sequencing. Raw data were demultiplexed, aligned and gene expression counted using the Cell Ranger analysis pipeline (10x Genomics). Data normalization, scaling and further transformations were performed using the *Seurat* R package. Non-tumor cell types were assigned by multimodal reference mapping using reference data from the Single-Cell Atlas of Human Healthy Airways. Tumor cells were identified by inference of copy number alterations. Pathway activity inference was performed using the *progeny* R package.

Results

Quality control analyses revealed a high fraction of confidently mapped reads (>60%) in all but one sample (5/6; 83%). This sample was excluded from further analysis. The average number of cells identified per sample was 7875 (range: 6068-11586) with an average of 12192 reads per cell (range: 8826-15416). These numbers are in line with published single-cell RNA sequencing data from fresh or frozen cancer tissue. Cell type annotation revealed a similar tumor microenvironment composition across samples, primarily consisting of fibroblasts, macrophages, natural killer cells and T cells. Inferred copy number profiles identified different tumor clones between and within samples. Pathway activity analysis indicates PI3K, TNFα and MAPK signaling as recurrent oncogenic dependencies.

Conclusion

snRNA-seq unlocks FFPE archives of pathology institutes for a deep phenotypic characterization of rare cancers such as SNUCs. Further integrated bioinformatic analyses will help formulate novel therapeutic rationales for this deadly cancer.

DGP06.03

Clonal dynamics of chemoradioresistance evolution and metastatic progression in rectal cancer

D. Hirsch¹, K. Heselmeyer-Haddad², J. Lieberich^{2,3}, Y. Ceribas³, M. Kelly⁴, K. Talsania⁵, Y. Zhao⁵, T. Gaiser⁶, T. Ried²

¹Universität Regensburg, Pathologie, Regensburg, Germany, ²National Institutes of Health, Genetics Branch, Bethesda, United States of America, ³Universitätsmedizin Mannheim, Institut für Pathologie, Mannheim, Germany, ⁴National Institutes of Health, Single Cell Analysis Facility, Bethesda, United States of America, ⁵National Institutes of Health, Frederick National Laboratory for Cancer Research, Frederick, United States of America, ⁶Institut für angewandte Pathologie, Speyer, Germany

Questions/Background

The standard treatment for locally advanced rectal cancer is chemoradiotherapy followed by surgery. However, patient response to neoadjuvant chemoradiotherapy is highly heterogeneous, ranging from complete tumor regression to no response. Over the course of disease, up to 40% of patients suffer from local relapse or the development of metachronous metastatic disease, compromising survival. It is not yet known how treatment resistance and disease progression in these patients evolve – whether from the selective outgrowth of pre-existing resistant clones during treatment or through the acquisition of additional, resistance conferring genomic alterations.

Methods

We aimed to delineate the genomic evolution and clonal architecture underlying treatment resistance and metastatic progression in rectal cancer based on a cohort of 45 patients with different degrees of response, from which 103 tumor samples were collected longitudinally over the course of treatment and metastatic progression. Tumor diagnosis and treatment response assessment are routinely based on the histopathologic evaluation of formalin-fixed paraffin-embedded (FFPE) patient tissues. We have developed a protocol for dissociation of FFPE tissue into single cells. These FFPE derived single cell suspensions were immunolabeled, flow-sorted and analyzed by whole exome sequencing of pure tumor and stromal cell populations, single cell sequencing and multiplex interphase fluorescence in situ hybridization.

Results

Across patients, different degrees of genomic complexity and clonal heterogeneity were observed. Major tumor clones were characterized by mutations in known colorectal cancer driver genes such as *APC*, *KRAS*

and *TP53* along with copy number gains of *EGFR*, *MYC*, *CDX2* and *ZNF217* and losses of *SMAD4* and *TP53*. Chemoradioresistance appeared to be mainly driven by adaptive selection of pre-existing genomic alterations. Yet in some patients *de novo* clones were detected post treatment. Clonal karyotypes remained largely stable throughout treatment, however, favoring clones with *TP53* loss post therapy.

Conclusion

In conclusion, clonal dynamics in response to neoadjuvant chemoradiotherapy were characterized by patterns of clonal extinction or persistence with adaptive evolution as a function of the patient's individual response. Furthermore, our data show the feasibility of high-resolution clonal reconstruction from whole exome sequencing and single cell data obtained from cells isolated from FFPE tissue.

DGP06.04

Genome-wide DNA methylation-based machine-learning algorithms differentiate intrahepatic cholangiocarcinoma from intrahepatic metastases of pancreatic ductal adenocarcinoma

M. P. Dragomir¹, T. G. Calina², E. Perez³, S. Schallenberg¹, T. Albrecht⁴, I. Koch¹, P. Wolkenstein⁵, B. Goeppert⁶, G. A. Calin⁷, S. Roessler⁴, C. Sers¹, D. Horst¹, F. Roßner¹, D. Capper³

¹Charité – Universitätsmedizin Berlin, Corporate Member of Freie Universität Berlin, Humboldt-Universität zu Berlin and Berlin Institute of Health, Institute of Pathology, Berlin, Germany, ²TGC Ventures UG, TGC Ventures UG, Berlin, Germany, ³Charité – Universitätsmedizin Berlin, Corporate Member of Freie Universität Berlin, Humboldt-Universität zu Berlin and Berlin Institute of Health, Department of Neuropathology, Berlin, Germany, ⁴Heidelberg University Hospital, Institute of Pathology and Liver Cancer Center Heidelberg, Heidelberg, Germany, ⁵German Cancer Consortium (DKTK), Partner Site Berlin, and German Cancer Research Center (DKFZ), DKTK Berlin, Berlin, Germany, ⁶RKH Klinikum Ludwigsburg, Institute of Pathology and Neuropathology, Ludwigsburg, Germany, ⁷MD Anderson Cancer Center, Department of Translational Molecular Pathology, Houston, United States of America

Questions/Background

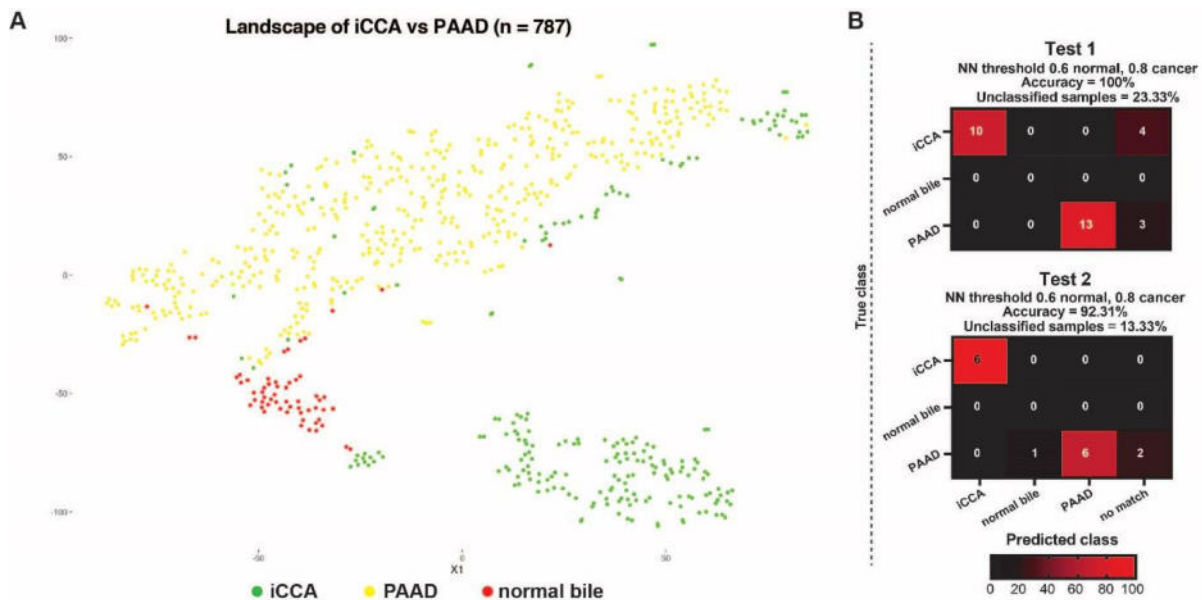
A newly diagnosed intrahepatic cholangiocarcinoma (iCCA) is resected and afterwards treated with adjuvant chemotherapy, on the other hand a liver metastases from a pancreatic ductal adenocarcinoma (PAAD) is not treated surgically and is managed with palliative chemotherapy. These two malignancies have a similar morphology, immunohistochemistry profile, and share the same driver mutations making differential diagnosis even after applying current molecular pathology tools difficult. We considered that genome-wide DNA-methylation can be used to develop machine-learning tools that can aid in performing this task.

Methods

We collected genome-wide DNA-methylation profiles for iCCA, PAAD, and normal bile tissue from multiple repositories from all over the world. We built a landscape of pancreato-biliary tumors to characterize methylation classes. We divided this data set into a reference and a validation cohort. We trained a support vector machine, a random forest, and a neural network model using the reference cohort. We tested the diagnostic tools on the validation cohort and on two additional in house cohorts: one consisting of surgical resections and a second consisting of core biopsies and intraoperative biopsies.

Results

We defined one homogenous PAAD methylation group, and two iCCA subgroups, matching the already known small bile duct type and large bile duct type iCCAs. On the validation cohort (n = 388) our random forest classifier showed an accuracy of 96.5%, the support vector machine classifier 95.62%, and the neural network reached the highest accuracy of 97.68%. In order to exclude other potential tumor entities, we added to our classifiers two different thresholds, one for carcinomas (0.8), and one for normal bile tissue (0.6) and reached an accuracy of 100% for neural network superior to random forest (99.71%) or support vector machine (96.52%). We tested our neural network classifier on two in-house sets, obtaining an accuracy of 100% for primary surgical resections and 92.3% for core and intraoperative biopsies.



A. Landscape of iCCA vs PAAD. B. Classification results.

Conclusion

We showed that a DNA-methylation based classifier can be a helpful and valuable tool in the diagnosis process of differentiating between an iCCA, liver metastasis of a PAAD, and normal bile tissue.

DGP06.05

Dedifferentiated Chondrosarcoma: Correlation of Whole Exome Sequencing Data with Histopathology and Immunohistochemical Analysis.

J. Schreier¹, A. Roessner¹, S. R. Ullmann¹, F. Karras¹, D. Schanze², S. Franke¹, D. Jechorek¹

¹Otto von Guericke Universität, Institut für Pathologie, Magdeburg, Germany, ²Otto-von-Guericke-Universität Magdeburg, Institut für Humangenetik, Magdeburg, Germany

Questions/Background

Dedifferentiated chondrosarcomas (DDCS) are mesenchymal bone tumors, typically characterized by two distinct areas. Histologically the highly differentiated tumor compartment differs considerably from the dedifferentiated part, resembling pleomorphic sarcoma. Since the molecular pathogenesis of DDCS is still unclear, our study aims to improve understanding of the molecular mechanisms underlying the development and progression of DDCS and help identify genetic differences between both parts[1].

Therefore whole exome sequencing (WES) of paired highly and poorly differentiated tissue samples was performed and compared with immunohistochemistry.

Methods

After histological classification and immunohistochemical staining with Ki67, p53, CDK4, Cyclin D1, p16 and H3k27me2[2], DNA was extracted from formalin-fixed, paraffin-embedded tissue samples. Afterwards the DNA was quantified and subjected to quality control measurements. WES analysis was performed on 10 paired tumor samples.

Results

Our molecular investigation of DDCS revealed significant mutations in driver genes and several pathways implicated in tumorigenesis. In line with recent publications, we have found IDH1/2 mutations in both tissue components of several DDCS samples, as well as alterations in the COL2A1 gene. Mutations of TP53 and TP53BP1 were identified in both parts as well. In addition to known drivers, a diverse range of alterations in APOB, ATRX, BRCA, GLI1/2, SOX9, and HSPs were detected.

Notable alterations in the dedifferentiated components affected traditional pathways associated with cell cycle regulation and differentiation like MAPK/ERK, next to genes involved in chromatin remodeling and histone modification. Mutations in metalloproteinases, Wnt/ β -catenin and cell differentiation signaling indicate molecular interference in cell fate determination, proliferation, and development. Interestingly alterations found in adenosin signaling point to dysregulation of tumor immunity.

Conclusion

The detection of IDH1/2 mutations in both tissue components emphasizes a monoclonal origin of DDCS.

Moreover, our findings confirm an established pattern of mutations in driver genes like CDKN2A, BRCA and

KIT. Further exploration of broad mutations in dedifferentiated components in pathways affecting not only cell cycle control, transcription regulation and proliferation, but tumor immunity could lead to new approaches in targeted therapies as well as specific immunotherapy.
Literaturangaben:

- [1] Lucas, C.-H. G., Grenert, J. P., & Horvai, A., (2020), Targeted Next-Generation Sequencing Identifies Molecular and Genetic Events in Dedifferentiated Chondrosarcoma. , Archives of Pathology & Laboratory Medicine. , <https://doi.org/10.5858/arpa.2020-0379-oa>, 2023-03-05
- [2] Gong, L. H., Su, Y. Bin, Zhang, W., Liu, W. F., Dong, R. F., Sun, X. Q., Zhang, M., & Ding, Y., (2021), Dedifferentiated Central Chondrosarcoma: A Clinical, Histopathological, and Immunohistochemical Analysis of 57 Cases. , Frontiers in Medicine, <https://doi.org/10.3389/fmed.2021.746909>

DGP06.06

Cancer-associated fibroblasts influence the immune response and disease outcome in NSCLC, thereby facilitating resistance to immune checkpoint blockade.

M. Wessolly^{1,2}, M. Asskali¹, M. Wiesweg^{2,3}, S. Stephan-Falkenau⁴, J. Kollmeier⁵, T. Mairinger⁴, C. Taube⁶, J. Wohlschläger⁷, S. Borchert^{1,2,8}, F. Mairinger^{1,2,8}

¹Universitätsklinikum Essen, Institut für Pathologie, Essen, Germany, ²Deutsches Konsortium für Translationale Krebsforschung (DKTK), Partnerstandorte Universitätsklinken Essen und Düsseldorf, Essen und Düsseldorf, Germany, ³Universitätsklinikum Essen, Innere Klinik (Tumorforschung), Essen, Germany, ⁴Helios Klinikum Emil von Behring, Fachbereich Gewebsdiagnostik/Pathologie, Berlin, Germany, ⁵Helios Klinikum Emil von Behring, Lungenklinik Heckeshorn, Berlin, Germany, ⁶Ruhrlandklinik, Westdeutsches Lungenzentrum, Klinik für Pneumologie, Essen, Germany, ⁷Diakonissenkrankenhaus Flensburg, Institut für Pathologie, Flensburg, Germany, ⁸Ruhrlandklinik, Westdeutsches Lungenzentrum, Institut für Pathologie, Essen, Germany

Question/Background

As the tumour microenvironment (TME) gained scientific attention over the past years, cancer-associated fibroblasts (CAFs) have been identified as key players in it. Since CAFs are driving forces for cancer progression, angiogenesis, and therapy resistance, they are considered an attractive target for therapy. Various pathways are regulated by CAFs, thus depicting additional potential targets for therapeutic intervention. The aim of this study is to enlighten the influence of CAFs on the tumour and TME, thereby uncovering the interaction/communication between the different components within the TME and with the tumour itself. Another focus lays on the mixture of different immune cells, their activity and phenotype. Furthermore, the immunosuppressive and -supportative effects are of special interest, as well as response to immune checkpoint blockade (ICB) in NSCLC.

Methods

83 patient-derived FFPE blocks from ICB treated samples diagnosed with NSCLC were used for this project. To examine the biological processes involved, RNA was isolated and a digital gene expression analysis was performed using the NanoString nCounter technology. Furthermore, two tissue microarrays (TMA) were created. On those, spatial digital gene expression analysis for tumour cells, infiltrating immune cells and the TME was performed using the GeoMx Digital Spatial Profiling technology. The TMA sections were also used for immunohistochemistry (IHC) analysis and were therefore stained and later evaluated via microscopy and an analysis software program called "QuPath". Lastly, data were pooled for exploratory data analysis.

Results

CAF infiltration was identified by FAP expression and observed in more than 50% of the evaluated samples. 64% of the FAP+ specimens had an overall strong immune infiltration. CAFs had a profound effect on the biology and the immune phenotype of the tumour. GSEA demonstrated that signaling pathways associated with immune response were enriched in tissues with low infiltration by FAP+ CAFs. Several immune cell markers were enriched in immune cell infiltrates and TME. FAP+ samples displayed significant amounts of infiltrating CD3-, CD8- and CD20-positive immune cells. Additionally, significant correlations between CAF infiltration and progression under ICB were unveiled.

Conclusion

Our results confirm a significant impact of CAFs on the immune response together with an influence on disease outcome. From this, we can infer that CAFs play a crucial role in ICB resistance.

DGP08 Hot topics in hematopathology - gemeinsam mit der EA4HP

DGP08.02

HHV8-negative/ EBV-negative primary effusion-based lymphomas

A. Di Napoli¹, L. Soma², S. Dirnhofer³

¹Sapienza University - Sant'Andrea University Hospital, Department of Clinical and Molecular Medicine, Roma, Italy, ²City of Hope National Medical Center, Department of Pathology, Duarte, CA, United States of America, ³University Hospital Basel, Institute of Medical Genetics and Pathology, Basel, Switzerland

Effusion-based (EB) lymphomas not associated with infection by Kaposi sarcoma herpes virus/human herpes virus 8 (KSHV/HHV8) are B-cell neoplasms presenting as serous effusions in the pleural (most of the cases), pericardial or peritoneal cavity in the absence of lymphadenopathy or mass lesions. These have been reported more commonly in Asian countries, in HIV-negative, elderly patients, and in fluid overload conditions such as chronic heart failure, renal insufficiency, protein losing enteropathy or liver failure/cirrhosis. The WHO-4R-classification mentioned to avoid misclassification of HHV8-negative EB-lymphomas as primary effusion lymphomas (PEL), which are HHV8+ and frequently EBV+, occur mostly in immunocompromised patients and show a dismal prognosis. The HHV8-negative EB-lymphomas have now been grouped in the new B-cell lymphoma entity "fluid overload-associated large B-cell lymphoma (FO-LBCL)" in the WHO-5R, and as the provisional entity "HHV8 and EBV negative primary effusion based lymphoma (HHV8negEBVneg-PEBL)" in the International Consensus Classification (ICC). Pathological features in both classifications include a centroblastic, immunoblastic, or anaplastic morphology, however, the ICC requires EBV-negativity and notes that most of these lymphomas express at least one B-cell marker, whereas the WHO-5R comprises cases with plasmablastic immunophenotype and EBV infection. Further reporting and assessment of these cases are warranted to refine diagnostic criteria of lymphomas in this unique setting.

DGP08.03

TFH lymphoma and associated clonal hematopoiesis

D. Nann

Universitätsklinikum Tübingen, Institut für Pathologie, Tübingen, Germany

T-follicular helper (TFH) cell lymphoma (TFHL) is a lymphoma of mature T cells with phenotypic characteristics and gene expression signature of TFH cells. The current 5th edition of the WHO classification defines three different entities in this group (angioimmunoblastic-type, follicular-type, NOS), whereas the ICC classification considers a single entity with three subtypes. The lymphoma harbors recurrent mutations of *RHOA*^{G17V}, *IDH2*^{R172}, *TET2* and *DNMT3A*. Whereas *RHOA*^{G17V} and *IDH2*^{R172} are almost exclusively found in this entity, *TET2* and *DNMT3A* mutations occur in a broad variety of hematological neoplasms and are the most frequently affected genes in clonal hematopoiesis (CH). CH in humans shows a progression rate to overt hematologic neoplasia of about 0.5 to 1% per year, depending on clone size, number of mutations and affected genes. In 2018, the first case was described in which a lymphoid (TFHL) and myeloid (AML) neoplasm arose from a common mutated progenitor cell with shared mutations and additional private mutations. In recent years, further studies showed in up to 70% of patients with TFHL the occurrence of identical mutations of *TET2* and/or *DNMT3A* in the myeloid cells, irrespective of bone marrow involvement, indicating a prominent role of CH in the pathogenesis of TFHL. In up to 18%, these patients show also additional synchronous or metachronous overt myeloid neoplasms, often with private myelodysplastic-type mutations, most often myelodysplastic syndrome, chronic myelomonocytic leukemia and acute myeloid leukemia. Recently, there is also evidence for two distinct lymphoid neoplasms arising from CH. The CH mutations can be already detected in the BM up to twelve years before development of an overt lymphoma. TFH lymphoma cases with antecedent or concomitant hematologic neoplasm often show high variant allelic frequencies of *TET2* and often more than one mutation, suggesting a role for surveillance in these patients.

DGP09 Proteomik und Metabolomik

DGP09.02

SpiderMass Ambient Ionization Mass spectrometry: A novel mini-invasive in vivo technology for intraoperative in man diagnostics

I. Fournier

Université de Lille, Laboratoire PRISM, Villeneuve d'Ascq Cedex, France

Despite important technological advances over the last decades, real-time diagnostic clearly remains a challenge. Yet the gold standard for oncology surgery remains the intraoperative pathology examination of the tissues excised by the surgeon. However, to keep the surgery in a reasonable timing this limits the exam to some pieces of tissues. Therefore, gathering and processing molecular data in real-time would enable shifting the pathology exam in the body for precision surgery. In this respect, Ambient Ionization Mass Spectrometry (AIMS) has paved the way for novel applications and have demonstrated a great potential for health applications. Dedicated AIMS such as SpiderMass technology can even be performed *in vivo*, advancing clinical applications to in-man use with to target *in vivo* intraoperative analysis for surgical decision making. The SpiderMass is based on a laser microprobe which uses resonant excitation of tissue water to promote mini-invasive micro-sampling. It is designed so that the mass instrument is standing remotely from the laser microprobe and the patient. Thus, SpiderMass enables remote mini-invasive *in vivo* analysis, safe and painless for the patient using 2.94 μm IR excitation leading to real-time molecular signature of the tissues. The technology can be used to distinguish cancer from normal cells, histological regions, or cancer types and grades uniquely by using the collected molecular fingerprints as barcoding and training the system thanks to machine learning. During the surgery, the generated data are then used to interrogate in real-time the classification models and provide instant feedback. We have been conducting a proof-of-concept study to assess the performances of the technology from dog sarcoma and demonstrated the high sensitivity and accuracy of the system for sarcoma grading and typing. The SpiderMass prototype was showcased in the veterinary surgery room on dog patients for bench *ex vivo* intraoperative analysis and *in vivo* assessment within the course of the surgery. We have also shown the possibility to use the technology from FFPE tissue sections providing access to retrospective studies. Additionally, the system was further developed to enable imaging of regions of interest, moving to automatic recognition of each pixel by real interrogation of built databases and opening the way to constructing molecular digital twins.

DGP09.04

Proteomic Analyses of the Urothelial Cancer Landscape Reveal Highly Distinct Prognostic and Predictive Subtypes

F. F. Dreßler^{1,2}, F. Diedrichs¹, D. Sabtan¹, S. Hinrichs², C. Krisp³, B. Michael², P. Mackedanz², M. Schlottfeldt², M. Hennig⁴, D. Schöb⁵, A. Miernik⁵, H. Schlüter⁶, U. Wetterauer⁵, R. Zubarev^{7,8}, S. Perner^{2,9}, P. Wolf^{5,10}, Á. Végvári⁸

¹Charité - Universitätsmedizin Berlin, Institut für Pathologie, Berlin, Germany, ²Universität zu Lübeck und UKSH Campus Lübeck, Institut für Pathologie, Lübeck, Germany, ³Universitätsklinikum Hamburg-Eppendorf, Institut für Klinische Chemie und Labormedizin, AG Massenspektrometrie und Proteomics, Hamburg, Germany, ⁴Universität zu Lübeck und UKSH Campus Lübeck, Klinik für Urologie, Lübeck, Germany, ⁵Universitätsklinikum Freiburg, Klinik für Urologie, Freiburg, Germany, ⁶Universitätsklinikum Hamburg-Eppendorf, Institut für Klinische Chemie und Labormedizin, AG Massenspektrometrie und Proteomicsstitut für Pathologie, Hamburg, Germany, ⁷Karolinska Institutet and SciLifeLab, Stockholm, Sweden, ⁸Karolinska Institutet, Division of Physiological Chemistry I, Department of Medical Biochemistry and Biophysics, Stockholm, Sweden, ⁹Pathologie des Forschungszentrum Borstel, Leibniz Lungenzentrum, Borstel, Germany, ¹⁰Universität Freiburg, Freiburg, Germany

Questions/Background

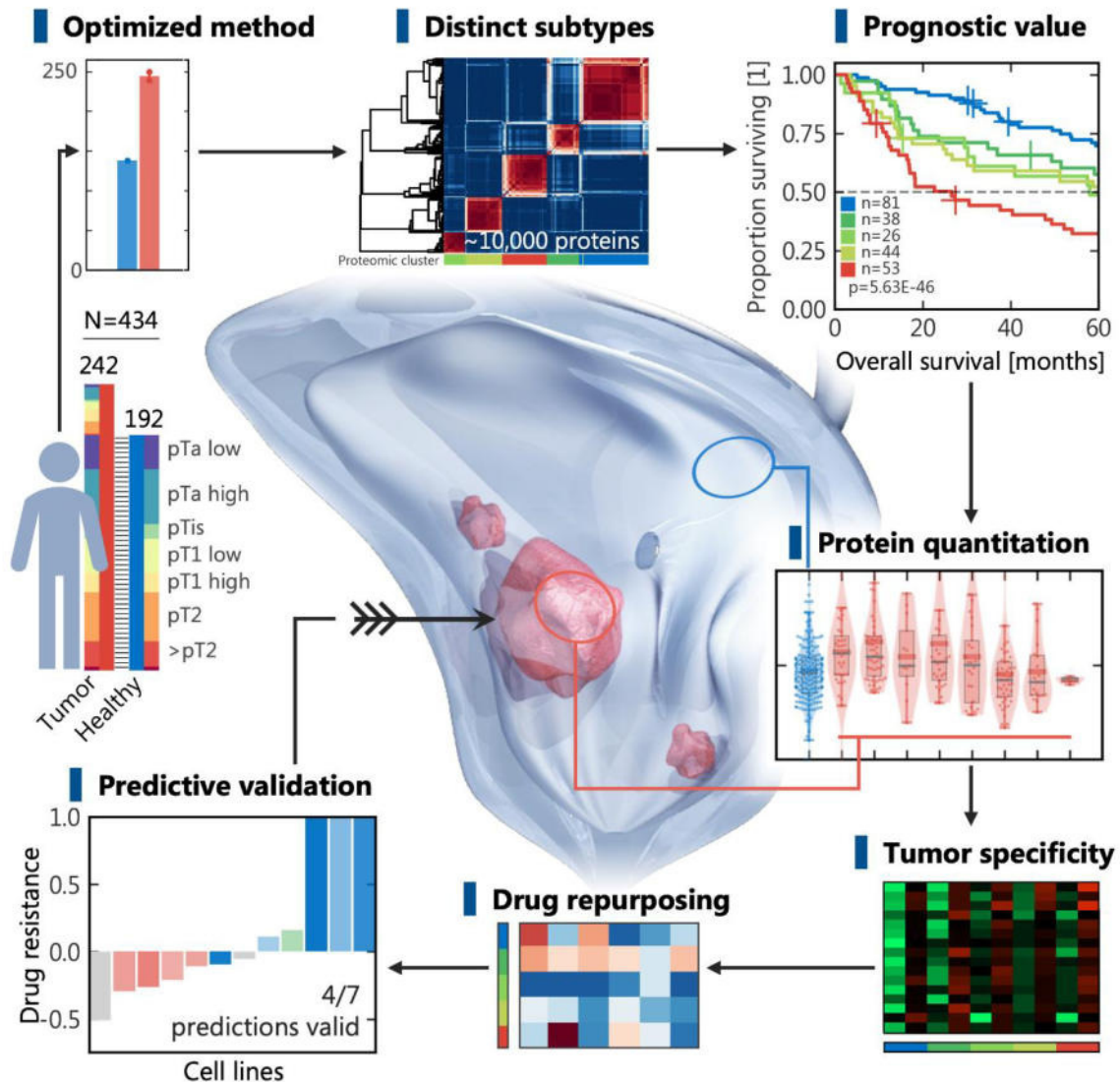
Urothelial cancer (UC) is a challenging disease with a wide tumor-biological spectrum. Most molecular classifications cover only muscle-invasive bladder cancer and are transcriptome-based, relating only indirectly to the therapeutically relevant and more stable protein level. Also, the advent of new targeted therapies requires quantitative data about the tumor specificity of their target proteins. We turned to the proteome to address these questions.

Methods

We performed deep proteomic profiling of a comprehensive cohort by optimized tandem mass tag-labelled liquid chromatography-coupled tandem mass spectrometry. Data acquisition was validated internally with immunoblotting and externally by bioinformatic reclassification within existing, filtered transcriptomic data. After bioinformatics, the top cluster defining proteins were quantified immunohistochemically under real-world conditions. Protein profiles were individualized and separately evaluated with drug repurposing libraries. Cell

viability assays were performed for a panel of twelve UC cell lines to validate these predictions in vitro.

Results



Graphical abstract

We analyzed 434 samples with 242 tumors and 192 paired normal mucosae, covering all stages of UC from pTa to >pT2. 9542 proteins were quantified and revealed five distinct proteomic subtypes. These were validated internally and externally, showing relevant survival stratification also in the TCGA dataset. The proteomic subtypes were independent from pathological groups with relevant stratification of progression-free and overall survival (low vs. high-risk: median 103 vs. 27 months). Tumor specificity of all proteins was highly heterogeneous across stages and subtypes. As an example, the therapeutic target NECTIN4 was generally overexpressed only in non-muscle-invasive UC. Drug repurposing revealed several new candidate drugs, each specific to different proteomic subtypes. In vitro data showed increased sensitivity by subtype in line with four out of seven representative predictions.

Conclusion

Proteomic subtypes add independent prognostic information and carry predictive value for several newly identified adjuvant drug candidates. The actual tumor specificity of biomarkers and drug targets is highly dependent on stage and subtype and calls for patient-specific individualized testing.

Proteomic subtypes of intrahepatic cholangiocarcinoma are significantly linked to patient's time-to-recurrence

T. Werner^{1,2,3}, K. L. Budau¹, M. Cosenza Contreras^{1,4}, F. Hause¹, K. Kurowski¹, N. Pinter¹, J. Schöler⁵, M. Werner¹, C. Sigel⁶, L. Tang⁶, P. Bronsert¹, O. Schilling^{1,7}

¹Institut für Klinische Pathologie, Universitätsklinikum Freiburg, Freiburg, Germany, ²Fakultät für Biologie, Universität Freiburg, Freiburg, Germany, ³Spemann Graduate School of Biology and Medicine (SGBM), Universität Freiburg, Freiburg, Germany, ⁴MeInBio Graduate School, Universität Freiburg, Freiburg, Germany, ⁵Discovery Sciences, Oncotest, Charles River, Freiburg, Germany, ⁶Department of Pathology, Memorial Sloan Kettering Cancer Center, New York, United States of America, ⁷German Cancer Consortium (DKTK) and German Cancer Research Center (DKFZ), Heidelberg, Germany

Questions/Background

Intrahepatic cholangiocarcinoma (ICC) is still insufficiently described on the molecular and proteomic level. Although ICCs frequently recur after initial surgery, only few tools are available to predict highly individual times-to-recurrence (TTR). In our study, we aimed to characterize protein expression profiles of primary ICC to derive putative markers for TTR.

Methods

After microdissection, tumor- and tumor-adjacent, non-malignant (TANM) tissues from 80 patients were measured via liquid-chromatography mass-spectrometry (LC-MS/MS) in data independent acquisition mode (DIA).

Results

On average, we quantified more than 2300 proteins per sample. As expected, tumor and TANM tissues displayed clearly segregated proteomes. In a hierarchical clustering analysis of tumor samples, we observe two proteome subgroups: cluster 1, which was enriched with extracellular matrix (ECM) components, and cluster 2, which showed increased expression of RNA- and protein turnover machinery. An investigation of semi-tryptic protein cleavage sites also revealed significantly increased proteolytic activity within cluster 1. When compared to cluster 1, patients grouped in cluster 2 showed significantly shorter TTRs. TANM tissue clusters and biology did not match to the identified tumor clusters. Additionally, we applied Cox proportional hazards model in a second, independent analysis to detect proteins whose expression correlates with TTR distribution. Gene set enrichment of thus identified hits uncovered similar biological motifs as in the clustering approach to determine the TTR.

To further examine the emerging role of tumor-stroma interactions, we investigated 9 independent xenografts of ICCs in mice. In an unsupervised, principal component analysis based on this multi-species proteomic approach, we also observed ECM proteins in association with infiltrating stroma, while tumors were enriched for proteins involved in splicing, translation, and metabolism of RNA.

Conclusion

Overall, recurrence-free survival in our cohort is shaped by the overexpression of either ECM components or synthesis and metabolism of RNA and proteins. The importance of tumor-stroma interactions in this context is highlighted by a xenograft mouse model and deserves further investigation.

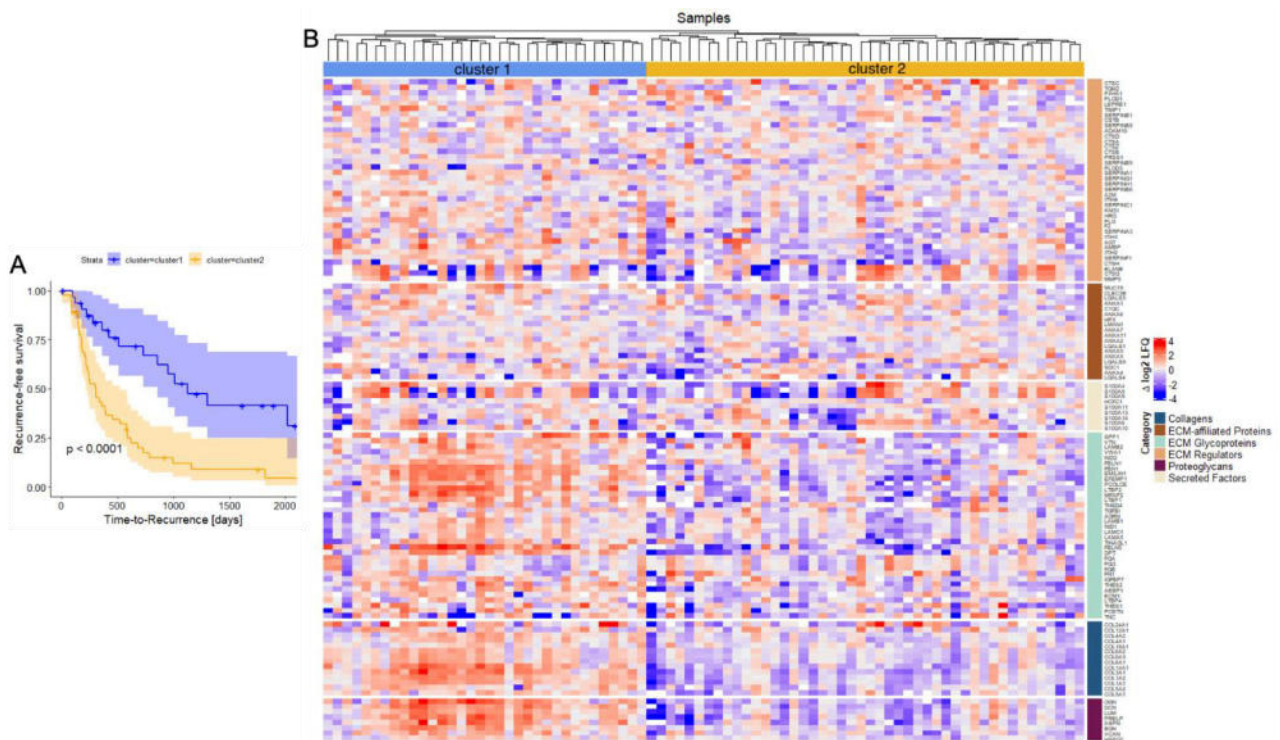


Figure 1 A) Kaplan-Meier plot of TTR distribution. B) Heatmap of detected matrixosomal proteins.

DGP09.06

Differentiation of esophageal inflammatory diseases by using tandem mass spectrometry (LC-MS/MS)

S. Mattern¹, V. Hollfoth¹, P. Riemenschneider¹, J. Luibrand¹, A. Dickemann¹, K. Singer¹, M. Franz-Wachtel², B. Macek², F. Fend¹, N. Malek³, S. Fusco³, J. Henes⁴, S. Singer¹

¹Universitätsklinikum Tübingen, Allgemeine und Molekulare Pathologie und Pathologische Anatomie, Tübingen, Germany, ²Eberhard Karls Universität Tübingen, Interfakultäres Institut für Zellbiologie (IFIZ) - Proteom Centrum, Tübingen, Germany, ³Universitätsklinikum Tübingen, Medizinische Klinik, Innere Medizin I - Gastroenterologie, Gastrointestinale Onkologie, Hepatologie, Infektiologie und Geriatrie, Tübingen, Germany, ⁴Universitätsklinikum Tübingen, Medizinische Klinik, Innere Medizin II - Hämatologie, Onkologie, klinische Immunologie und Rheumatologie, Tübingen, Germany

Questions/Background

Gastroesophageal reflux disease (GERD) is the most common cause of esophageal inflammation. However, other differential diagnoses such as eosinophilic esophagitis (EoE) and Crohn's disease (CD), among others, need to be considered. Due to partially overlapping histomorphological features the correct diagnosis can be challenging in particular settings. Here, we tested if FFPE proteomics can be used as an adjunct to conventional histology to increase diagnostic precision and to gain further insights into disease relevant alterations.

Methods

We analyzed and compared paraffin-fixed paraffin-embedded (FFPE) routine diagnostic esophageal biopsy specimen (N >30, including GERD, CD, EoE as well as "normal" esophagus control samples) by using liquid chromatography with tandem mass spectrometry (LC-MS/MS). Enrichment and network analyses using the STRING-Database and hierarchical cluster analyses using Morpheus (Broad Institute) were performed.

Results

By FFPE LC-MS/MS we could detect > 4000 protein groups from which several proteomic signatures could be derived. These signatures allowed clear discrimination between GERD, EoE, CD and even led to a revised diagnosis of particular cases. Proteomic changes included, for instance, high abundance of CD44 and CD9 as markers for activated eosinophilic granulocytes in EoE and alterations of the proteasome/inflammasome in CD.

Conclusion

In combination with conventional histology FFPE LC-MS/MS is a powerful tool to increase the precision in diagnosing esophageal inflammatory diseases (with implication for improved therapy and patient

management) and allows deeper insights in disease relevant changes.

DGP10 Sino-German Colorectal Cancer Session

DGP10.01

AMER1 deficiency promotes the distant metastasis of colorectal cancer by inhibiting SLC7A11- and FTL-mediated ferroptosis

S. Lei¹, M. Lai², H. Zhang¹

¹Zhejiang University School of Medicine, Department of Pathology & Pathophysiology, Hangzhou, China, ²Zhejiang University School of Medicine, Department of Pathology & Pathophysiology, Hangzhou, China

Aims

Ferroptosis, as a novel type of regulated cell death (RCD), has been implicated in cancer initiation and progression. However, the crosstalk between ferroptosis and cancer metastasis remains unclear. We aim to characterize the functional role of the high-frequency truncating mutation rate of AMER1 in the crosstalk between ferroptosis and cancer metastasis.

Methods & Results

We performed a comprehensive analysis of exome sequencing data from matched colorectal cancer primary sites and liver metastatic foci, and identified the tumor suppressor gene AMER1, which has a high rate of truncating mutation in colorectal cancer, that is strongly linked to synchronous hepatic metastasis. The RNA-seq data showed significant downregulation of reactive oxygen species (ROS) and the ferroptosis signaling pathway in AMER1-deficient cells. AMER1 deletion induced CRC cells ferroptosis resistance *in vitro*; *in vivo*, AMER1-deficient CRC cells formed more distant metastases than AMER1-naïve CRC cells, which mainly invaded lymph nodes. Interestingly, liproxstatin-1, an inhibitor of ferroptosis, effectively increased the hematogenous transfer of AMER1-naïve cells. Furthermore, the intracellular labile free iron content, cystine uptake levels and lipid levels corresponding to iron metabolism, GSH synthesis and lipid metabolism were tested. There was an increase in intracellular cystine levels as well as a decrease in the pool of labile free iron due to the inhibition of ubiquitination-mediated degradation of SLC7A11 and FTL by AMER1 deletion. AMER1 functions as a scaffold protein to interact with SLC7A11 and FTL and further to recruit β -TrCP1 and β -TrCP2 as a way to promote ubiquitination and degradation of SLC7A11 and FTL. The interaction site of AMER1 with SLC7A11 and FTL was just located within the conserved sequence region, and mutations in this region caused resistance to ferroptosis.

Conclusions

AMER1 mediates the crosstalk between ferroptosis and cancer metastasis by regulating the ubiquitination-mediated degradation of SLC7A11 and FTL. AMER1 deficiency increases the survival of CRC cells in the blood and promotes the distant metastasis of CRC, which provides a unique window of opportunity for treating metastatic CRC patients with AMER1 mutations with strategies that facilitate resensitization to ferroptosis.

DGP10.02

Validation of Prognostic Effect and Molecular Characterization of Stroma AReactive Invasion Front Areas (SARIFA) as Promising Biomarker in Colorectal Cancer

N. G. Reitsam¹, C. M. L. Löffler², H. S. Muti², B. Grosser¹, J. N. Kather^{2,3,4}, B. Märkl¹

¹Pathology, Faculty of Medicine, University of Augsburg, Augsburg, Germany, ²Else Kroener Fresenius Center for Digital Health, Medical Faculty Carl Gustav Carus, Technical University Dresden, Dresden, Germany, ³Department of Medicine 1, University Hospital and Faculty of Medicine Carl Gustav Carus, Technical University Dresden, Dresden, Germany, ⁴Pathology and Data Analytics, Leeds Institute of Medical Research at St James's, University of Leeds, Leeds, United Kingdom

Questions/Background

Recently, our research group has established Stroma AReactive Invasion Front Areas (SARIFA), defined as the direct contact between tumor cells and fat cells at the tumor invasion front, as an independent negative prognostic predictor for colon and gastric cancer patients. SARIFA is a hematoxylin & eosin (HE) based biomarker associated with a worse outcome, likely based on immunologic alterations combined with a tumor-promoting tumor-adipocyte interaction. Our aim was to further validate the prognostic potential and molecular background of SARIFAs in colorectal cancer (CRC).

Methods

Overall, 627 colorectal cancer cases of The-Cancer-Genome-Atlas (TCGA) cohorts COAD and READ were

initially screened, of which 215 cases could ultimately be classified with diagnostic whole slide images available through <https://portal.gdc.cancer.gov>. Clinical and molecular data (TCGA_PanCancerAtlas) of 207 classified cases could be retrieved of and were partly analyzed within <http://www.cbioportal.org/>. Additionally, we trained a deep-learning (DL) algorithm to predict SARIFA status directly from histological slides.

Results

72 (33.5%) of all analyzed cases were SARIFA-positive CRCs. SARIFA-positive CRC patients showed a statistically significant decreased overall survival and disease-specific survival, and a dramatically reduced progression free survival throughout all T stages and even when only considering T3/T4 CRCs (log rank, each p-value at least < 0.05). In the molecular characterization analysis, we observed variations at both mRNA as well as protein level, particularly an upregulation of Annexin A1 (ANXA1), an important anti-inflammatory protein. However, (so far) no relevant SARIFA-dependent differences have been found with regard to the most important driver mutations, microsatellite status, fraction genome altered, mutation count and/or tumor mutational burden. Lastly, we show that SARIFA status can be predicted by DL methods with a solid performance (AUC: 0.80) – currently only trained on this cohort.

Conclusion

Based on the TCGA cohorts COAD and READ, we could verify the prognostic potential of SARIFA in CRC. Our data further suggests the causal relevance of immunologic mechanisms in this context as SARIFA-positive CRCs seem not be characterized by distinct genomic changes. In this external validation study, SARIFA again proves to be a highly prognostic and potentially predictive HE-based biomarker in CRC, which is not only easy to assess but also may be classified automatically in the future.

DGP10.04

Experimental Evaluation of the Impact of Microenvironmental Factors on Tumor Immunity in Colorectal Cancer

P. K. Ziegler¹, A. Laycock¹, F. R. Greten², P. J. Wild¹

¹Dr. Senckenbergisches Institut für Pathologie, Frankfurt am Main, Germany, ²Georg-Speyer-Haus, Institut für Tumorbologie und experimentelle Therapie, Frankfurt, Germany

Question/Background

Despite considerable progress in preventive strategies, colorectal cancer remains one of the most common causes of tumor-related death in the western world and, especially in metastatic or recurrent carcinomas, therapeutic options are limited. Tumor neoantigens are recognized the Achilles heel of cancer cells displaying their distorted genomic base to the immune system. Neoantigens arise from i.e. mutated proteins and can act as inducers of anti-tumor immunity. In general, a high number of mutated proteins ("tumor mutational burden", TMB) acts as positive predictive feature of immune-checkpoint inhibitor therapy, however, up to 50% of cancers with high TMB or MSI lack T cell infiltration for unknown reasons.

Methods

In order to study antigen-presentation by tumor cells we make use of an orthotopic tumor transplantation model combined with the expression of ovalbumin, a well-characterized model antigen widely used in immunological studies. Murine intestinal organoids have been modulated to reflect mutations frequently found in human CRC, namely *APC*, *TP53*, *KRAS*, *TGFBR2*, (termed APTK) and with additional *AKT*-activation (termed APTAK). In previous studies we have determined tumors arising from APTK-organoids to reflect the conventional molecular subtype (CMS2) of CRC while APTKA-organoids give rise to "mesenchymal" (CMS4) tumors. Following orthotopic transplantation into the rectum of MHC-matched recipient mice these organoids rapidly engraft, form tumor masses and frequently metastasize into draining lymph nodes and the liver.

Results

We establish a novel model system for the analysis of antigen-presentation by tumor cells *in vitro* and *in vivo*. The model antigen ovalbumin has been characterized to give rise to specific MHC-I and -II restricted antigens, which can be detected using transgenic T cells or tetramers. Organoids are being transplanted into mouse rectum and tumor formation is monitored by endoscopy and examined by histology, IHC and flow cytometry. *In vitro* antigen-specific T cells response can be assessed using a co-culture system of ovalbumin-expressing tumor organoids and antigen-specific T cells.

Conclusion

Tumor antigen presentation is crucial for tumor suppressive effects by the adaptive immune system. Here, we establish a versatile transplantation model of murine intestinal organoids that reflects key characteristics of human CRC to quantify the immunological consequences of genetic alterations, microenvironmental factors or therapy related changes.

DGP10.04

Specific intracellular retention of circSKA3 promotes colorectal cancer metastasis by attenuating ubiquitination and degradation of SLUG

J. Deng¹, S. Liao², F. Liu³, H. Zhang²

¹Department of Pathology and Women's Hospital, Zhejiang University School of Medicine, Research Unit of Intelligence Classification of Tumor Pathology and Precision Therapy, Chinese Academy of Medical Sciences, Hangzhou, China, ²Department of Pathology, Zhejiang University School of Medicine, Research Unit of Intelligence Classification of Tumor Pathology and Precision Therapy, Chinese Academy of Medical Sciences, Hangzhou, China, ³Department of Colorectal Surgery, The First Affiliated Hospital, College of Medicine, Zhejiang University, Hangzhou, China

Aims: Our previous study demonstrated that tumor-suppressor circular RNAs (circRNAs) can be secreted outside of colorectal cancer (CRC) cells by exosomes. However, it remains unknown whether tumor-driving circRNAs can be specifically retained in cells to facilitate tumor metastasis.

Methods: Via circRNA-seq and analysis of circRNAs in serum samples from CRC patients, we found that circSKA3 was significantly upregulated in CRC tissues but downregulated in serum samples. First, we identified specific motifs that mediated circSKA3 retention in CRC cells. Then, we investigated the biological role of circSKA3 in promoting CRC progression *in vitro* and *in vivo*. Furthermore, circularization elements and key functional regulatory elements were identified with truncated vectors. Finally, antisense oligonucleotides (ASOs) targeting the specific motif of circSKA3 were synthesized for CRC therapy.

Results: CircSKA3 promoted CRC progression *in vitro* and *in vivo* and was retained in CRC cells via a specific cellmotif element. Interestingly, the cellmotif element was also the site of the circSKA3–SLUG interaction, which inhibited SLUG ubiquitination degradation and promoted CRC epithelial–mesenchymal transition (EMT). Moreover, FUS was identified as a key circularization regulator of circSKA3. Finally, the ASOs targeting circularization and cellmotif elements repressed circSKA3 expression, abolished the SLUG–circSKA3 interaction, and further inhibited CRC EMT and metastasis *in vitro* and *in vivo*.

Conclusions: CRC cells might retain circSKA3 in the cytoplasm through a specific cellmotif, and intracellular circSKA3 can block SLUG ubiquitination degradation and promote CRC metastasis. Furthermore, our specific ASOs targeting the key circularization element and functional motif of circSKA3 will be a novel antitumor strategy.

DGP10.06

Analysis of the functional role of Acyl-CoA Synthetase Long Chain Family Member 5 (ACSL5) in human colorectal carcinoma

M. Nenkov¹, Y. Ma¹, J. M. Murrieta-Coxa², M. Schmidt³, O. Huber³, Y. Chen¹, N. Gaßler¹

¹Section Pathology of the Institute of Forensic Medicine, Jena University Hospital, Jena, Germany, ²Placenta-Labor, Jena University Hospital, Jena, Germany, ³Institute of Biochemistry II, Jena University Hospital, Jena, Germany

Questions/Background

Dysregulated metabolic pathways in CRC (colorectal carcinoma), have been frequently observed, resulting in abnormal glycolysis, glutaminolysis and lipid synthesis. Lipid metabolic reprogramming, especially abnormal fatty acid metabolic pathways including long chain fatty acids (LCFAs) activation by the enzymes called long-chain acyl-CoA synthetases (ACSLs) has been reported to drive tumor development and progression, correlating with poor prognosis in CRC patients. ACSL5, one of the ACSLs family member is highly expressed in the intestinal mucosa. So far, little is known about the impacts of different isoforms of ACSL5 in CRC development and progression, since the previous studies mostly focused on exploring the role of the short isoform of ACSL5 (isoform b). The aim of our study was to assess the expression and the prognostic value of ACSL5 in CRC. Additionally, we aimed to do functional analysis and activity of three isoforms of ACSL5 in different colon cancer cell lines.

Methods

Establishment of “gain-of-function” cell models, CRC cell lines (SW480 and LoVo) with no/very low endogenous expression level of ACSL5 have been chosen for the establishment of the ‘Gain Function’ cell models by stable transfection with three expression vectors of ACSL5 representing isoforms a, b (without exon 1) and x1 (isoform a with exon 20 deletion). Primary human colorectal carcinoma (clinical samples)-based experiments: Analysis of protein expression of ACSL5 in primary CRC samples by immunohistochemistry on tissue microarray (TMA).

Results

Our data showed that ACSL5 was highly expressed in the majority of primary CRC patient samples (77 out of 126; 61%), and high expression of ACSL5 was significantly negatively associated with the survival rate. We found that ACSL5 expression was significantly correlated to the expression of p53 in case of the low grade tumors. ACSL5 stable transfected cell lines showed higher ACSLs activity accompanied by increased Wnt/ β catenin signaling and consequently increased cell migration and invasion. ACSL5 promoted the resistance to the XAV939 induced apoptosis. Furthermore, exosomes secreted by SW480-ACSL5 isoform b showed decreased level of microRNA-19a-3p.

Conclusion

To conclude, ACSL5 exerts an oncogenic function in SW480 cell through activation of Wnt/ β catenin signaling, along with an increased ACSLs activity

DGP10.08

pT3 colorectal cancer revisited: a multicentric study on the histological depth of invasion in more than 1000 pT3 carcinomas - Proposal for a new pT3a/pT3b subclassification

S. Förtsch¹, C. Lang-Schwarz², M. Eckstein³, C. Geppert³, M. Schmitt⁴, B. Konukiewicz⁵, T. Groll⁶, F. Schick Tanz⁶, J. Engel⁷, M. Gleitsmann⁴, C. C. Westhoff⁴, N. Frickel⁴, A.-S. Litmeyer⁴, A. Grass⁴, P. Jank⁴, S. Lange⁸, M. Tschurtschenthaler⁸, D. Wilhelm⁹, W. Roth¹, M. Vieth², C. Denkert⁴, W. Weichert⁶, I. Nagtegaal¹⁰, **M. Jesinghaus⁴**

¹Universitätsmedizin Mainz, Institut für Pathologie, Mainz, Germany, ²Universitätsklinikum Erlangen, Klinikum Bayreuth, Institut für Pathologie, Bayreuth, Germany, ³Universitätsklinikum Erlangen, Institut für Pathologie, Erlangen, Germany, ⁴Universitätsklinikum Gießen und Marburg, Institut für Pathologie, Marburg, Germany, ⁵Universitätsklinikum Schleswig-Holstein, Institut für Pathologie, Germany, ⁶Technische Universität München, Institut für Pathologie, München, Germany, ⁷Ludwig-Maximilians Universität München, Institut für medizinische Informationsverarbeitung, Biometrie und Epidemiologie, München, Germany, ⁸Technische Universität München, II Medizinische Klinik, Klinikum rechts der Isar, München, Germany, ⁹Technische Universität München, Chirurgische Klinik, Klinikum rechts der Isar, München, Germany, ¹⁰RadboudUMC, Institut für Pathologie, Nijmegen, The Netherlands

Questions/Background

Pathological TNM staging (pTNM) is the strongest prognosticator in colorectal carcinoma (CRC) and the foundation of its post-operative clinical management. Tumours that invade pericolic/perirectal adipose tissue generally fall into the pT3 category without further subdivision.

Methods

The histological depth of invasion into the pericolic/perirectal fat was digitally and conventionally measured in a training cohort of 950 CRCs (Munich). We biostatistically calculated the optimal cut-off to stratify pT3 CRCs into novel pT3a (≤ 3 mm)/pT3b (>3 mm) subgroups, which were then validated in two independent cohorts (447 CRCs, Bayreuth/542 CRCs, Mainz).

Results

Compared to pT3a tumours, pT3b CRCs showed significantly worse disease-specific survival, including in pN0 vs pN+ and colonic vs. rectal cancers (DSS: $P < 0.001$, respectively, pooled analysis of all cohorts). Furthermore, the pT3a/pT3b subclassification remained an independent predictor of survival in multivariate analyses (e.g. DSS: $P < 0.001$, hazard ratio: 4.41 for pT3b, pooled analysis of all cohorts). While pT2/pT3a CRCs showed similar survival characteristics, pT3b cancers remained a distinct subgroup with dismal survival.

Conclusion

The delineation of pT3a/pT3b subcategories of CRC based on the histological depth of adipose tissue invasion adds valuable prognostic information to the current pT3 classification and implementation into current staging practices of CRC should be considered.

DGP11 Classification of Lymphoma II : progress and open questions

DGP11.04

Classification of aggressive B-cell lymphomas - perspective from ICC

S. Dirnhofer

The International Consensus Classification (ICC) of lymphoid malignancies contains different changes. These include updated names of entities, sharpened diagnostic criteria, upgrades from provisional to definite entities and definition of new entities.

The definition of the most common aggressive B-cell lymphoma, **diffuse large B-cell lymphoma (DLBCL), NOS**, remains unchanged, and the ICC strongly encourages subtyping into germinal center B-like (GCB) or the activated B-like (ABC or non-GCB) DLBCL. It is recommended to deemphasize the importance of DLBCL expressing both MYC and BCL2 by immunohistochemistry (so-called “double-protein expressors”, DPE) and of DLBCL expressing CD5 because the adverse prognosis is weak and they do not reflect true biological groups. Recent comprehensive molecular profiling from large multi-platform studies showed 5–7 molecular subgroups with overlapping features and association with COO subgroup. At the moment, about 30 - 35% of DLBCL are not classifiable with the current molecular methods but it is expected that that transition to a molecular genetic classification will be feasible in the near future.

DLBCL, NOS, should be separated from specific types of large B-cell lymphomas. **Large B-cell lymphoma with IRF4 rearrangement** has been upgraded to a definite entity in both classifications but in the ICC it is listed within the group of follicular lymphomas (FL) because of its frequent follicular growth pattern and excellent prognosis.

The 2017 WHO classification recognized a provisional entity called Burkitt-like lymphoma with 11q aberration. Recent molecular studies have shown that these tumors are closer to GCB-DLBCL than Burkitt lymphoma. Therefore, the ICC changed the term to “*Large cell B-cell lymphoma with 11q aberration*” and maintains it as a provisional entity.

High-grade B-cell lymphomas with MYC and BCL2 rearrangements which are defined genetically and form a molecularly distinct group are now listed as a definite entity. This is in contrast to the more heterogeneous group of *high-grade B-cell lymphomas with MYC and BCL6 rearrangements* that are recognized as a provisional entity in the ICC.

The ICC recognizes **HHV-8 and EBV-negative primary effusion-based lymphoma** as a new provisional entity characterized by unifying features including presentation in elderly patients, medical conditions leading to fluid overload and HIV-negativity. Most cases show a favorable prognosis and some patients may have spontaneous regression.

DGP12 Multiparametric tissue analysis I

DGP12.01

A DNA toolbox for spatial biology from imaging to sequencing

S. Saka

European Molecular Biology Laboratory (EMBL), Genome Biology, Heidelberg, Germany

DNA is not only a fundamental constituent of cells, but has also great capacity for information storage. We leverage the predictability of DNA hybridization kinetics and orthogonality of DNA sequences to utilize DNA oligos as tagging and barcoding tools for improving the major limitations of *in situ* visualization of molecules. We have previously developed multiplexed imaging approaches such as SABER-FISH and Immuno-SABER that utilize DNA barcoding and a flexible *in situ* signal amplification system for efficient visualisation of many protein, DNA or RNA targets in cells and tissues. More recently, we started to leverage DNA barcoding for a new spatial transcriptomics approach, **Light-Seq**, which directly integrates fluorescence imaging and whole-transcriptome next-generation sequencing of the same cells in fixed biological samples. Light-Seq combines spatially-targeted, rapid photocrosslinking of DNA barcodes onto cDNAs *in situ* with a novel one-step DNA stitching reaction to create pooled, spatially-indexed sequencing libraries. This light-directed barcoding enables imaging-based *in situ* selection of multiple cell populations in intact fixed tissue samples for full transcriptome sequencing based on location, morphology, or protein stains, without cellular dissociation. Applying Light-Seq to mouse retinal sections, we recovered thousands of differentially enriched transcripts from three adjacent cellular layers and discovered new biomarkers for a very rare neuronal subtype, dopaminergic amacrine cells, from only 4-8 individual cells per section. Light-Seq provides an accessible workflow to combine *in situ* imaging and protein staining with next-generation sequencing of the same cells, leaving the sample intact for further analysis post-sequencing. We are using these methods to directly link multi-dimensional and high-resolution cellular phenotypes (including morphology, protein markers, spatial organization) to transcriptomic profiles for diverse sample types.

Integrative modeling of multiplex imaging data identifies a spatial immune signature of oral squamous cell carcinoma histological grade

J. Einhaus^{1,2}, D. Gaudilliere³, J. Hedou², D. Feyaerts², M. G. Ozawa⁴, M. Sato², E. A. Ganio², A. S. Tsai², I. A. Stelzer², K. C. Bruckman³, T. A. Bonham², M. Diop², L. Ferreira⁵, X. Han⁵, C. M. Schürch¹, B. Gaudilliere²

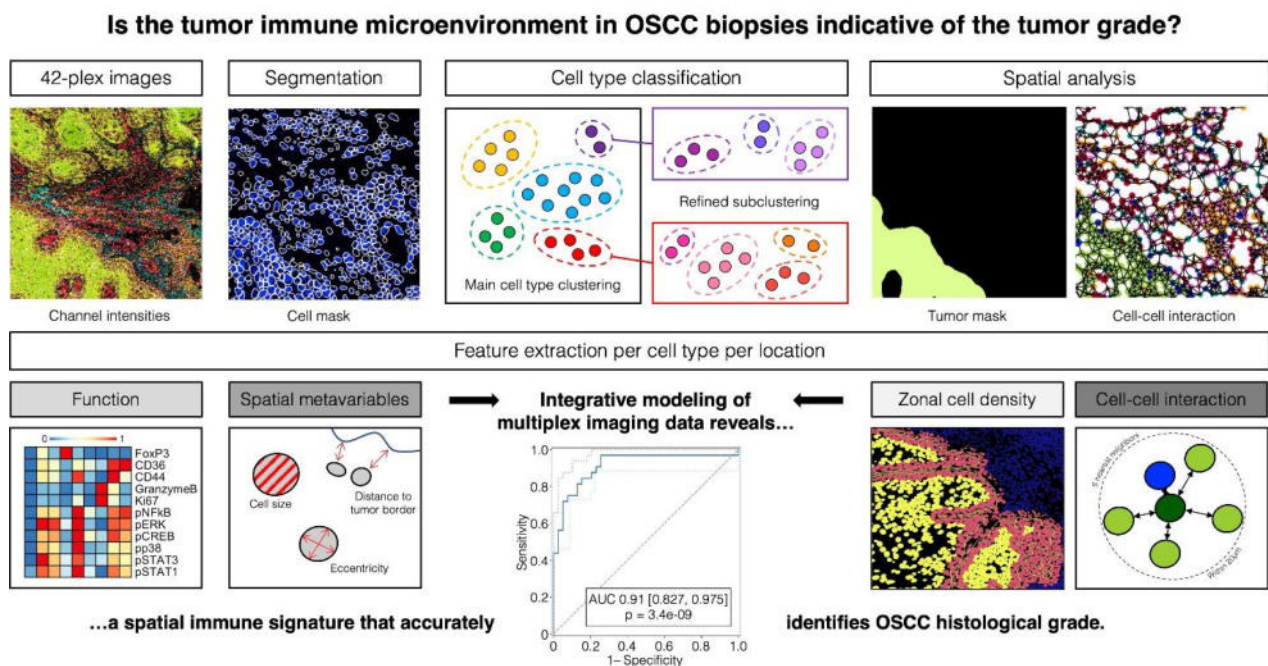
¹Universität Tübingen, Abteilung für Pathologie und Neuropathologie, Tübingen, Germany, ²Stanford University, Department of Anesthesiology, Perioperative and Pain Medicine, Palo Alto, United States of America, ³Stanford University, Department of Surgery, Palo Alto, United States of America, ⁴Stanford University, Department of Pathology, Palo Alto, United States of America, ⁵University of the Pacific, Arthur Dugoni School of Dentistry, San Francisco, United States of America

Questions/Background

Oral squamous cell carcinoma (OSCC) is a prevalent and highly aggressive neoplasm. Despite existing evidence-based treatment protocols, the prognosis of OSCC remains poor. Prognostic biomarkers are critically needed to identify patients at risk for recurrence and can point to novel targets for immune modifying therapies. To this end, recent advances in multiplex imaging analysis of tumors and the surrounding immune microenvironment provide unprecedented opportunities for biomarker discovery in cancer outcomes studies. However, multivariate analysis approaches that allow an integrative biological assessment are underdeveloped.

Methods

We applied multiplex imaging mass cytometry to analyze the tumor immune microenvironment in 24 OSCC biopsies and comprehensively characterized the signaling activity, abundance, and distribution of immune cells adjacent to and within the tumor invasive front.



Integrative modeling of multiplex imaging data reveals a spatial immune signature that accurately identifies OSCC histological grade

Results

Application of an integrative machine-learning pipeline that combines multivariate predictive modeling with reliable feature selection accurately classified tumors by histological grade (AUC of 0.913, $p = 2.753e-09$), a surrogate marker of lymph node metastasis and recurrence. Spatial standardization of cell type abundance, functional activity, cell size and distribution, as well as cell-cell interaction within biologically relevant zones (tumor core, tumor front, stroma) allowed the assembly of a multi-feature class dataset. Using stacked generalization and stability selection, our predictive model achieved excellent predictive performance and allowed for integrative, biological interpretation of the most relevant features. Indicative of higher-grade tumors were increased densities of myeloid cells, specifically M1 macrophages; elevated activation (NFkB

signaling), cytotoxicity (Granzyme B), and proliferation (Ki67) marker expression in stromal granulocytes; and tumor proximity to blood vessel cells.

Conclusion

The analysis allowed for distillation of the multiplex imaging dataset down to sentinel functional and spatial correlates of OSCC grades, providing a multivariate statistical framework for the discovery of prognostic biomarkers of long-term clinical outcomes in patients with OSCC.

DGP12.04

Extensive spatial characterization of the tumour-microenvironment in a large bicentric clinical non-small cell lung cancer cohort and correlation with clinical and pathological parameters

S. Schallenberg¹, G. Dernbach^{1,2}, S. Ruane², C. Böhm², L. Ruff², K. Standvoss², S. Ghosh², M. Dragomir^{1,3,4}, R. Fritz¹, I. Koch¹, C. Friedrich^{1,5}, S. Merkelbach-Bruse⁶, A. Quaas⁶, N. Frost⁷, K. Boschung⁸, W. Randerath⁸, G. Schlachtenberger⁹, M. Heldwein⁹, U. Keilholz^{3,10}, A. Vasaturo¹¹, K. Hekmat⁹, J.-C. Rückert¹², R. Büttner⁶, D. Horst¹, M. Alber¹³, F. Klauschen

¹Institute of Pathology, Charité – Universitätsmedizin Berlin, corporate member of Freie Universität Berlin, Humboldt-Universität zu Berlin and Berlin Institute of Health, Berlin, Germany, ²Aignostics GmbH, Berlin, Germany, ³German Cancer Consortium (DKTK), Partner Site Berlin, and German Cancer Research Center (DKFZ), Heidelberg, Germany, ⁴Berlin Institute of Health (BIH), Berlin, Germany, ⁵Max-Delbrück-Center for Molecular Medicine in the Helmholtz Association (MDC), Proteomics Platform, Berlin, Germany, ⁶Institute of Pathology, University Hospital Cologne, Köln, Germany, ⁷Department of Infectious Diseases and Respiratory Medicine, Charité – Universitätsmedizin Berlin, corporate member of Freie Universität Berlin, Humboldt-Universität zu Berlin and Berlin Institute of Health, Berlin, Germany, ⁸Bethanien Hospital, Clinic of Pneumology and Allergology, Center for Sleep Medicine and Respiratory Care, Institute of Pneumology at the University of Cologne, Solingen, Germany, ⁹Department of Cardiothoracic Surgery, University Hospital Cologne, Köln, Germany, ¹⁰Charité Comprehensive Cancer Center, Charité – Universitätsmedizin Berlin, corporate member of Freie Universität Berlin, Humboldt-Universität zu Berlin and Berlin Institute of Health, Berlin, Germany, ¹¹Ultivue, München, Germany, ¹²Department of General, Visceral, Vascular and Thoracic Surgery, Charité-Universitätsmedizin Berlin, Berlin, Germany, ¹³Institute of Pathology, Charité – Universitätsmedizin Berlin, corporate member of Freie Universität Berlin, Humboldt-Universität zu Berlin and Berlin Institute of Health

Questions/Background

Lung cancer is the leading cause of cancer death with an estimated 1.8 million deaths worldwide in 2020. Non-small cell lung cancer (NSCLC) represents about 80% of all lung cancer cases. The tumor microenvironment (TME) influences both clinical outcome and response to therapy. The location and composition of the different immune cells within tumors relates to their function and activity. Therefore, we developed an AI-driven image analysis approach that combines histomorphological and multiplex immunofluorescence data for an automated, cell-level characterization of the TME of NSCLC to predict clinical outcome and detect biomarkers of response to existing treatments.

Methods

In this bicentric study, we collected formalin-fixed paraffin embedded (FFPE) tissue and clinicopathological data from 1168 patients with resected stage I-IV NSCLCs from Charité and University Hospital Cologne. For tissue microarray (TMA) construction, four 1.5 mm tissue cores were punched from each tumor from high-purity tumor regions. 2 µm sections were stained with a 12-plex immunofluorescence panel (IF) followed by hematoxylin and eosin (H&E). All stains were scanned and co-registered at single cell accuracy. Deep learning models were developed to detect the different tumor regions: carcinoma, stroma, and necrosis from H&E, and 21 different cell subtypes from IF and H&E. The outputs from these models were then combined into spatial readouts characterizing the TME and correlated with clinical data.

Results

The tissue segmentation model achieved a macro averaged F1-score of 92%. Cell classification models quantified 21 different cell subtypes, determined cell positions and explored cell compositions. Our cell-classifier achieves a balanced accuracy of >90% on the tasks of (A) differentiating between PD-L1 positive carcinoma, PD-L1 negative carcinoma and other cells; and (B) separating regulatory T-cells (TREG), cytotoxic T-cells, and B-cells respectively from other cells. The correlation of spatial readouts with clinical data showed e.g., that a high density of TREG in the tumor stroma indicated a worse disease-free survival.

Conclusion

Our large real-world cohort and the AI-approach presented enable a broad exploration of the TME in NSCLC at single-cell resolution. It illustrates the utility of cell-based spatial analyses and highlights how AI can

improve our understanding of TME features that underlie clinical outcome and treatment response.

DGP12.05

High-resolution multiplex spinning disk confocal immunofluorescence of tumor tissues as a tool to simultaneously extract spatial morphological and protein expression information at the subcellular level

D. Papić¹, N. Pikki¹, J. Kluge¹, I. Koch¹, S. Ugliano², D. Horst¹, K. Bozek², **S. Florian**¹

¹Charité - Universitätsmedizin Berlin, Institut für Pathologie, Berlin, Germany, ²University and University Hospital Cologne, Center for Molecular Medicine Cologne, Köln, Germany

Questions/Background

The recent rise of spatial omics technologies is based on the insight that cell function cannot be fully understood if supracellular tissue architecture is not taken into account. The study of tissue architecture has always been one of the fundamental pillars of anatomic pathology. The second pillar, however, the study of cellular and subcellular morphology to predict tumor cell behavior, has so far not seen wide adoption in spatial omics technologies.

This is also the case with multiplex antibody tissue staining technologies: they enable the identification of small complex cell subpopulations defined through multiple protein markers in their original in situ context. Most larger studies in this area so far, however, treat each cell as a datapoint defined only through its tissue position and the staining intensity of the numerous measured markers, an approach that could be described as spatial flow cytometry. The morphological information at the single cell level, cell or nuclear shape and subcellular protein localization are largely neglected, mainly due to limitations in image resolution and image acquisition speed.

Methods

Here, we combine of a cyclic multiplex immunostaining protocol [1] with high-speed spinning disk confocal image acquisition from tumor tissues using water immersion objectives. Thus, we achieve sufficient speed and resolution to enable the simultaneous study of protein localization and morphology at the subcellular level as well as supracellular tissue architecture, preserving the full richness of information used in diagnostic pathology, combined with quantification of protein expression levels of up to 30 markers, exploiting the traditional advantages of flow cytometry. Highly accurate identification of nuclei for downstream segmentation is achieved using Deep Learning based segmentation.

Results

To illustrate the potential of this pipeline, we will present preliminary examples from a high-throughput project designed to reveal new therapeutic biomarkers in triple negative breast cancer (TNBC) through multiplex imaging of tumor samples obtained from 110 patients at diagnosis (biopsy), surgery (after neoadjuvant chemotherapy) and from relapsed tumors or metastases if applicable.

Conclusion

This approach will reveal so far inaccessible properties of malignant tumors and could facilitate the development of new biomarkers and generate new insights into tumor biology.

Literaturangaben:

[1] Lin, J. R. et al., Sorger, P. K. , (2018), Highly multiplexed immunofluorescence imaging of human tissues and tumors using t-CyCIF and conventional optical microscopes, *Elife*, e31657, 7

DGP12.06

Highly Multiplexed Microscopy of the Bone Marrow Microenvironment during Leukemic Progression in Mice

L. Li¹, G. Ivison², Y. Goltsev³, G. Nolan³, A. Mayer², C. Schürch¹

¹Department of Pathology and Neuropathology, University Hospital and Comprehensive Cancer Center Tübingen, Tübingen, Germany,

²Enable Medicine, Menlo Park, California, United States of America, ³Department of Pathology, Stanford University School of Medicine, Stanford, California, United States of America

Question/Background

The bone marrow microenvironment (BMME) crucially regulates normal hematopoiesis. In leukemias, the BMME is remodeled by leukemic cells that induce a dysfunctional, pro-leukemogenic niche, and the interplay of leukemic cells with their niche is critical for leukemia initiation and progression. Therefore, characterizing the BMME at the spatially resolved single-cell level using highly multiplexed microscopy will improve our mechanistic understanding of leukemic progression and endogenous antitumoral immunity, and may reveal novel targets for immunotherapy.

Methods

We generated a chronic myeloid leukemia (CML)-like disease in non-irradiated mice. Femoral bones were harvested from 3 mice each at 0 (control), 7, 14 and 21 days after leukemia onset and were investigated by CO-Detection by indEXing (CODEX) using a 53-marker antibody panel to identify different cell types, functional states and cellular neighborhoods in the BMME.

Results

We identified more than two million spatially resolved cells, including megakaryocytes, erythroid subsets, myeloid subsets, lymphoid subsets, vascular and stromal subsets, , hematopoietic stem/progenitor cells, as well as leukemic cell subsets. During leukemic progression, we observed a significant rearrangement of the BMME. Besides the expected growth of the leukemic clone, we found a massive increase in vascular cell types, whereas B cells were significantly reduced. A non-tumor neutrophil progenitor population significantly increased during leukemic progression. CD71, the transferrin receptor, was strongly up-regulated on tumor cells in advanced leukemia, suggesting a potential role for iron metabolism in malignant progression. Furthermore, in advanced-stage CML, PD-L1 was not only expressed by leukemic cells but also by non-malignant myeloid cells, such as macrophages. Computational analysis revealed 15 cellular neighborhoods, several of which contained PD-1+ T cell subsets. Specifically, PD-1+ CD8+ T cells were associated mostly with tumor cells in a so-called “tumor niche”, whereas PD-1+ CD4+ T cells and PD-1-negative T cells were not primarily spatially associated with tumor cells but were contained in the “immunovascular niche”.

Conclusion

Deeply characterizing the BMME by highly multiplexed microscopy will give new insights into the cellular composition and cell-cell interactions during leukemic progression and will likely lead to the discovery of novel mechanisms by which hematopoiesis and leukemias are regulated by their microenvironment.

DGP12.07

JUN-mediated mechanisms and therapeutic implications in fibrotic diseases of the lung and the skin

T. Lerbs¹, L. Cui², T. Chai³, C. Muscat², L. Chung⁴, R. Brown², K. Rieger², T. Shibata⁵, G. Wernig²

¹Universitätsklinikum Bonn, Pathologie, Bonn, Germany, ²Stanford School of Medicine, Pathology, Stanford, United States of America,

³Stanford School of Medicine, Institute for Stem Cell Biology and Regenerative Medicine, Stanford, United States of America, ⁴Stanford School of Medicine, Division of Immunology and Rheumatology, Stanford, United States of America, ⁵Stanford School of Medicine, Stanford, United States of America

Questions/Background

Idiopathic pulmonary fibrosis (IPF) and scleroderma are fibrotic diseases that share morphological, pathogenic, and clinical features. They are characterized by a dysfunctional immune system and lack efficient therapies. The transcription factor JUN exhibits pro-oncogenic functions, and upregulates the macrophage immune checkpoint CD47. This study explored whether JUN is a joint driver of IPF and scleroderma, and whether an immune checkpoint blockade (ICB) could be a therapy for both diseases.

Methods

To explore whether IPF and scleroderma express JUN, we measured the expression of JUN in fresh IPF tissue via Cytof, and in scleroderma via immunofluorescence (IF). We established primary fibroblast cultures from both diseases and measured the chromatin accessibility of JUN via ATAC-seq. We additionally explored through ATAC-seq whether deleting JUN via CRISPR-Cas9 reduced the chromatin accessibility of the immune checkpoints CD47 and PDL1 and the cytokine IL6. Then, we used a syngeneic JUN-driven skin fibrosis mouse model for an in-depth analysis via histology, IF, flow cytometry, and qPCR. We complemented these analyses with a niche-independent adaptive transfer model. Finally, we tested in a prophylactic and therapeutic setting whether treating mice with a CD47/IL6 blockade prevented and reversed skin fibrosis, and we validated the efficiency of a ICB in a bleomycin lung fibrosis model.

Results

Both IPF and scleroderma expressed JUN, and macrophages and T cells in IPF were converted into immunosuppressive phenotypes. Deleting JUN reduced the chromatin accessibility of CD47, PDL1, and IL6

in fibroblasts from both diseases. Inducing JUN in the syngeneic skin fibrosis model caused robust fibrosis that was mediated by an initial and hedgehog-dependent expansion of CD26+ dermal fibroblasts. On the single cellular level, JUN increased proliferation and mediated increased self-renewal to fibroblasts. JUN upregulated CD47 in the syngeneic model and blocking CD47 increased the phagocytosis of fibroblasts in vitro. Finally, the combined blockade of CD47 and IL6 not only prevented but also reversed skin fibrosis; a finding validated in the bleomycin lung model, in which the combined blockade of CD47, PDL1, and IL6 prevented lung fibrosis.

Conclusion

These results show that JUN is a joint driver of IPF and scleroderma that disturbs the regular immunity and upregulates the immune checkpoints CD47 and PDL1. In addition, this study shows the therapeutic potential of a ICB for both fibrotic diseases.

DGP13 Freie Vorträge II - Gemischte Themen

DGP13.01

Omicron matters – an autopsy study

C. Schwab¹, U. Merle², P. Schirmacher^{1,3}, T. Longerich¹

¹Universitätsklinikum Heidelberg, Pathologisches Institut, Heidelberg, Germany, ²Universitätsklinikum Heidelberg, Klinik für Gastroenterologie, Heidelberg, Germany, ³Deutsches Zentrum für Infektionsforschung, Standort Heidelberg, Heidelberg, Germany

Questions/Background

Even after more than two years Robert-Koch-Institutes' statistic does not discriminate whether death was related to coronavirus disease 2019 (COVID-19) or coincidences a non-fatal SARS-CoV-2 infection. This study addresses this question based on an autopsic approach with emphasis on virus variants.

Methods

Boa_Image_Frameised autopsies were performed on decedents with proven SARS-CoV-2 infection (n=117). Date were recorded in the COVID-19 autopsy and biomaterial registry Baden Wuerttemberg. Clinicopathological integration of findings was performed to define the cause of death. Lung damage was semiquantitatively assessed for the exudative, proliferating and fibrosing stage of COVID-19, respectively.

Results

The typical sequence of COVID-19-related lung injury was detectable in a variant independent fashion. Compared to precedent variants the lung injury was significantly less common, less severe and was less often the main cause of death in cases infected by Omicron variants (p<0.05). Following either booster vaccination or reinfection COVID-19 was not the main cause of death in any patient.

Conclusion

Autopsy registers are currently the only reliable data source for answering the question who died due to or independent of COVID-19. Compared to precedent variants, infection with an Omicron variant is rarely the cause of death as it affects the lungs less frequently and causes less severe lung disease. These findings should be considered when discussing strategies for future management of pandemics.

DGP13.02

The tetraspanin CD63 contributes to human idiopathic pulmonary fibrosis and mouse lung fibrosis and regulates the focal adhesion kinase pathway

E. Dingendorf¹, L. Cui², M. Stoffel¹, D. Kittel¹, G. Kristiansen¹, G. Wernig^{2,3}, T. Lerbs¹

¹Institut für Pathologie, Universitätsklinikum Bonn, Bonn, Germany, ²Stanford School of Medicine, Department of Pathology, Stanford, CA, United States of America, ³Stanford School of Medicine, Institute for Stem Cell Biology and Regenerative Medicine, Stanford, CA, United States of America

Questions/Background

Idiopathic pulmonary fibrosis (IPF) is a detrimental lung fibrosis with a poor prognosis. Underlying mechanisms are only partly understood and effective therapies are lacking. In this context, we used an explorative approach via mass spectrometry to identify therapeutic targets. Thereby, we identified an increased expression of the tetraspanin CD63, which is commonly found on intra- and extracellular membranes and laterally associates with other plasma membrane proteins like integrins. In this context, this study explored the role of CD63 in IPF and evaluated its potential as a therapeutic target.

Methods

We analyzed the expression of CD63 in fresh IPF tissue via mass spectrometry and validated the results in archived patient samples through immunofluorescence. We generated primary fibroblasts from IPF tissue and normal lung tissue and measured the expression of CD63 via immunofluorescence and flow cytometry. Next, we deleted CD63 in lung fibroblasts through CRISPR-Cas9 and analyzed changes in the proteome via mass spectrometry. Thereafter, we explored whether pro-inflammatory cytokines regulated the intra- and extracellular CD63 expression. Finally, we quantified the CD63 expression in fibroblasts and epithelial cells in a JUN driven lung fibrosis model.

Results

Mass spectrometry and IF stains showed an increase of CD63 in IPF patient samples and primary fibroblast cultures from IPF lungs expressed more CD63 than primary fibroblasts from normal lungs. Deleting CD63 reduced the signaling of the pro-fibrotic focal adhesion kinase (FAK) pathway and adding pro-inflammatory cytokines to primary fibroblasts increased the intracellular expression of CD63. Finally, inducing JUN in the JUN driven lung fibrosis model increased the expression of CD63 both in fibroblasts and in epithelial cells.

Conclusion

This study shows that the expression of CD63 is increased both in human IPF and mouse lung fibrosis. CD63 additionally stimulates pro-fibrotic signaling in lung fibroblasts; a finding that suggests that CD63 could be therapeutically targeted.

DGP13.03

Construction of renal carcinoma classification digital pathological repository

Q. Sun¹, H. Lan², W. Zhong³, J. Zhou³, D. Zhang¹, X. Teng³, M. Lai¹

¹Zhejiang University School of Medicine, Department of Pathology & Pathophysiology, Hangzhou, China, ²Zhejiang Normal University, Yiwu, China, ³The First Affiliated Hospital, Zhejiang University School of Medicine, Hangzhou, China

Aims: Digital pathology has brought new opportunities for remote pathological consultation and joint consultation owing to its convenient storage, management, browsing and transmission. The proposal of whole slide image (WSI) makes up for the view limitations of microscope and achieves panoramic imaging while ensuring resolution. However, the storage of WSIs requires a huge amount of storage equipment, which also causes great limitations for the training of large models under the background of big data. We hope to build new data storage specifications based on the example of renal cell carcinoma (RCC) to streamline the storage consumption, so as to provide help for the later application of artificial intelligence in medical real scenarios.

Methods: We combined the WSIs of 819 RCC in TCGA database, 122 RCC patients in our laboratory, and 500 RCC patients in the First Affiliated Hospital of Zhejiang University. Based on above data, we first constructed a standard template for data combing to facilitate data collection in the early stage and all WSIs were annotated by pathologists. Then, we used R and python language to create an automated WSI preprocessing software, including image privacy removal, image cropping, color standardization, annotation information migration. In addition, other clinical information of renal cancer, including pathological classification, malignant grade and basic information of patients, were corresponding to each other.

Results: We cropped all WSIs into patches with the size of 256*256 pixels. All patches were divided into carcinoma regions, para-cancer normal regions and other regions. Finally, millions of standardized pathological patches were obtained, and mature image classification models were introduced to accurately classify the subtypes of kidney cancer.

Conclusions: We constructed a standard digital pathological patch library of kidney cancer, and built an accurate image classification platform based on AI model to provide more accurate auxiliary diagnosis for the classification of kidney cancer classification.

DGP13.04

Subcellular localisation patterns of ANXA4 influence migratory modes in ccRCC

M. Wess¹, A. Kössinger¹, M. Rogg¹, K. Gräwe¹, A. Sammarco¹, M. Werner¹, M. Grabbert², O. Schilling¹, C. Schell¹

¹Institute for Surgical Pathology, Medical Center - University of Freiburg, Faculty of Medicine, University of Freiburg, Freiburg, Germany,

²Department of Surgery – Clinic for Urology, Faculty of Medicine, Medical Center – University of Freiburg, Freiburg, Germany

Questions/Background

The central genetic hallmark feature of clear cell renal cell carcinoma (ccRCC) is the frequent and early loss of function of VHL. The subsequent accumulation of HIF1a leads to a pseudohypoxic signalling state that affects cellular and extracellular-matrix (ECM) protein composition. Based on proteomic studies we have identified a highly significant accumulation of the phospholipid binding protein ANXA4 in ccRCC tumours.

Here, we aimed to characterise the functional impact of ANXA4 on tumour progression and underlying mechanisms.

Methods

Proteomics were used to reveal VHL-dependent protein expression in ccRCC cell lines (A498, 786-O) and CRISPR/Cas9-modified human proximal tubular epithelial cells (hRPTECs). For candidate proteins, an analysis of TCGA and cancer proteomics datasets was performed. Further functional analysis was conducted using overexpression and shRNA-mediated knockdown approaches (assessment of proliferation, migration and localisation studies).

Results

Proteomic analysis revealed differential regulation of ECM-related proteins with ANXA4 being significantly upregulated. Immunofluorescence studies displayed distinct subcellular localisation patterns of ANXA4 (nuclear and membrane localisation) depending on environmental factors such as membrane stress and cell density. Surprisingly, neither overexpression nor knockdown of ANXA4 altered cell growth, collective cell migration and drug sensitivity. However, knockdown of ANXA4 increased the capability of cancer cells for a confined space migratory mode. In line with these observations subcellular classification of ccRCC specimens revealed decreased nuclear localisation patterns in metastatic ccRCCs (compared to non-metastatic primary tumors).

Conclusion

The ECM-related protein ANXA4 has no direct effect on basic parameters such as proliferation or collective cell migration. However, ANXA4 downregulation supported confined space migration of ccRCC cells indicating a more invasive and potential metastatic behaviour. Reduced ANXA4 nuclear localisation in cells with low ANXA4 abundance and corresponding nuclear localisation patterns in primary (non-) metastatic tumours, suggest a central role of the ANXA4 downregulation in metastasis mediated by altered ANXA4 subcellular localisation. We hypothesise that this mechanosensitive mechanism of ANXA4 translocation modulates nuclear membrane stiffness and integrity. This in turn may facilitate nuclear remodelling to adapt to confined migration.

DGP13.05

Mesoscopic 3D Analysis of the Microarchitecture of the Human Liver

S. Bobe¹, F. Kiefer²

¹Universitätsklinikum Münster, Gerhard-Domagk-Institut für Pathologie, Münster, Germany, ²Universitätsklinikum Münster, European Institute for Molecular Imaging, Münster, Germany

Questions/Background

The microscopic and macroscopic architecture of the liver ensures its complex functionality. Presently diagnostic routines for hepatic disorders include macroscopic ultrasound, MR or CT imaging and microscopic histologic examination of biopsies in paraffine sections. Technical limitations of the resolution and specificity of macroscopic imaging modalities, as well as tissue loss in processing of liver biopsies for microscopic imaging lead to a lack of information in the mesoscale, which covers three dimensions spanning several millimeters corresponding to the size of whole biopsies. The volumetric mesoscale representation however is mandatory for complete understanding of branching patterns and orientation of multicellular hepatic structures like vasculature and bile ducts.

Aim of this study was to establish three-dimensional mesoscopic imaging of liver biopsies in order to uncover the structure of bile ducts[1] and lymph vessels[2] in human specimens and the mouse model.

Methods

Optical volumetric imaging of the liver is complicated by light scattering and absorption. To overcome this challenge, a whole mount staining approach was followed by delipidation and refractory index matching to obtain optically cleared transparent tissue specimens. Light sheet fluorescence microscopy and optical projection tomography were applied and compared to visualize and 3D-reconstruct portal structures.

Results

Light sheet fluorescence microscopy and optical projection tomography successfully 3D-reconstructed hepatic structures in the scale of several millimeters and analyzed bile ducts and vascular structures in the full tissue context with cellular resolution. Light sheet fluorescent microscopy revealed morphological characteristics of ductular reaction patterns in humans as non-continuously growing biliary network and allowed the first volumetric visualization of the lymphatic vasculature in the murine liver.

Conclusion

Mesoscopic imaging methods thereby qualified as promising tool to foster deeper understanding of three-dimensional pathological processes in the liver.

Literaturangaben:

- [1] Kong C, Bobe S, Pilger C, Lachetta M, Øie CI, Kirschnick N, Mönkemöller V, Hübner W, Förster C, Schüttelz M, Kiefer F, Huser T, Schulte am Esch J, (2021), Multiscale and Multimodal Optical Imaging of the Ultrastructure of Human Liver Biopsies, *Frontiers in Physiology* , 12: 637136, <https://doi.org/10.3389/fphys.2021.637136>
- [2] Redder E, Kirschnick N, Bobe S, Hägerling R, Hansmeier NR, Kiefer F , (2021), Vegfr3-tdTomato, a reporter mouse for microscopic visualization of lymphatic vessel by multiple modalities, *PloS One*, 16(9): e0249256, <https://doi.org/10.1371/journal.pone.0249256>

DGP13.06

A RhoA – YAP/TAZ – ARHGAP29 mechano-signaling axis sustains the glomerular filtration barrier in health and disease

M. Rogg¹, J. I. Maier¹, A. Sammarco¹, C. Van Wymersch¹, M. Werner¹, O. Schilling^{1,2}, C. Schell^{1,2}

¹Institute of Surgical Pathology, Faculty of Medicine, Medical Center - University of Freiburg, Freiburg, Germany, ²Freiburg Institute for Advanced Studies (FRIAS), University of Freiburg, Freiburg, Germany

Question/Background

Podocytopathy (podocyte disease) is a central factor in the development of chronic kidney disease. Increased mechanosignaling and dysregulation of small RhoGTPases in podocytes are well-known factors promoting the progression of glomerular disease. However, the intricate interplay of RhoGAPs and RhoGEFs modulating small GTPase signaling is incompletely understood in the context of podocyte physiology. Comprehensive dissection of these signaling networks might help in the identification of potential therapeutic targets and definition of disease entities.

Methods

We mapped small RhoGTPase signaling networks analyzing transcriptome and proteome data of murine podocytes. In vitro knockdown and expression studies were conducted in human immortalized podocytes. RNA sequencing, immunofluorescence, western blot and RhoGTPase activity measurements were employed. Candidate proteins were further analyzed in biopsy specimens from human glomerular disease.

Results

ARHGAP29 was identified as a novel RhoGTPase activating protein (RhoGAP) for RhoA in podocytes. RNA sequencing analysis revealed YAP/TAZ signaling and integrin adhesion dependent expression of *ARHGAP29* in podocytes. ARHGAP29 localized to podocyte protrusions in vitro and in vivo. Knockdown of *ARHGAP29* caused elevated RhoA activation, defective formation of cell protrusions and increased maturation of integrin adhesion complexes. Inverse effects were caused by forced expression of *ARHGAP29*. Moreover, ARHGAP29 expression was elevated in early stages of human podocyte disease.

Conclusion

Increased expression of ARHGAP29 might help to mitigate consequences of increased mechanotransduction and subsequent RhoA – actomyosin – YAP/TAZ activation as frequently observed in podocyte disease. Our results implicate that ARHGAP29 represents a so far not described negative feedback loop for elevated RhoA signaling in podocytes in health and disease.

DGP13.07

Multiparametric classification of bladder cancer using immunohistochemistry and targeted sequencing

I. A. Montes Mojarro¹, M. Granai¹, S. Hassas¹, S. Staehle¹, L. Schwaibold¹, S. Walz², L. M. Serna Higuera³, I. Bonzheim¹, A. Stenzl², H. Bösmüller¹, F. Fend¹

¹University Hospital Tübingen, Eberhard-Karls-University, Institute of Pathology and Neuropathology and Comprehensive Cancer Center Tübingen, Tübingen, Germany, ²University Hospital Tübingen, Eberhard-Karls-University, Department of Urology, Tübingen, Germany, ³University Hospital Tübingen, Eberhard-Karls-University, Department of Clinical Epidemiology and Applied Biostatistics, Tübingen, Germany

Questions/Background

Cancer classifications combining different types of tissue-based parameters have emerged as an important tool for tumor stratification. They provide a strong correlation with clinical behaviour and offer biological insight for neoplasms difficult to classify reproducibly. In bladder cancer (BC), diagnosis and grading of invasive and non-invasive urothelial tumors according to the current WHO classification poses challenges to pathologists in terms of reproducibility that has implications for clinical management [1].

Methods

The main objective of this work is to develop a multiparametric classification which considers histology, phenotype and molecular signature of bladder cancer. To this end, we applied immunohistochemistry (p53, FGFR3, HER2, Cyclin D1, MIB-1, CK5/6 and p40) targeted sequencing (*TP53*, *FGFR3*, *ERCC2*, *PIK3CA*,

PTEN and *STAG2*) and/or fluorescence in situ hybridization (HER2 and FGFR3) to a cohort of 45 non-muscle invasive urothelial carcinoma (NMIBC) and a second cohort of 132 muscle invasive BC (MIBC).

Results

Cases of NMIBC were reviewed and diagnosed as follows: papillary urothelial neoplasia of low malignant potential (PUN-LMP $n = 8$), non-invasive low grade-papillary urothelial carcinoma (LG-PUC, $n = 23$), and high grade (HG-PUC, $n = 14$). Overall, proliferation index and mitotic count assessed with MIB-1 and P-HH3 staining, respectively correlated with grading and clinical behavior. In addition, targeted sequencing confirmed frequent *FGFR3* mutations in non-invasive papillary tumors and identified mutations in *TP53* as high-risk. Combination of high MIB-1 and mitotic count, *FGFR3* WT and *TP53* mutation was identified as predictors of poor prognosis in NMIBC.

MIBC cases were subdivided according to their papillary ($n=51$) or non-papillary ($n=77$) morphology and luminal or basal profile according to CK5/6, and p40 expression. The overexpression of FGFR3 and HER2 (IHC score: 2++ or 3++) in 14% (18/128) and 62% (80/128) of these cases, respectively, highlighted these markers not only as prognostic tools but also as potential therapeutic targets. A detailed analysis of the prognostic relevance of our multiparametric approach for MIBC will be presented.

Conclusion

Integration of morphological, immunophenotypical and selected molecular parameters allows an improved risk stratification of urothelial carcinoma and may aid in clinical decision making.

This study was supported by the DFG (GRK 2543).

Literaturangaben:

[1] Netto GJ, Amin MB, Berney DM, Compérat EM, Gill AJ, Hartmann A, Menon S, Raspollini MR, Rubin MA, Srigley JR, Hoon Tan P, Tickoo SK, Tsuzuki T, Turajlic S, Cree I, Moch H. , (2022), The 2022 World Health Organization Classification of Tumors of the Urinary System and Male Genital Organs-Part B: Prostate and Urinary Tract Tumors. , Eur Urol., 469-482., 82(5), doi: 10.1016/j.eururo.2022.07.002.

DGP13.08

Membranous NECTIN-4 expression frequently decreases during metastatic spread of urothelial carcinoma and is associated with enfortumab vedotin resistance

N. Klümper¹, D. Ralser², J. Ellinger¹, F. Roghmann³, J. Albrecht¹, E. Below⁴, D. Sikic⁵, J. Breyer⁶, C. Bolenz⁷, F. Zengerling⁸, P. Erben⁹, K. Schwamborn¹⁰, R. Wirtz¹¹, T. Horn¹², D. Nagy¹³, M. Toma¹³, G. Kristiansen¹³, T. Büttner¹, O. Hahn¹⁴, V. Grünwald¹⁵, C. Darr¹⁵, E. Erne¹⁶, S. Rausch¹⁶, K. Schlack¹⁷, M. Abbas¹⁸, S. Zschäbitz¹⁹, C. Schwab²⁰, A. Mustea², P. Adam²¹, A. Manseck²², B. Wullich²³, M. Ritter¹

¹Department of Urology and Pediatric Urology, University Medical Center Bonn (UKB), Bonn, Germany, ²Department of Gynaecology and Gynaecological Oncology, University Medical Center Bonn (UKB), Bonn, Germany, ³Department of Urology, Marien Hospital, Ruhr-University Bochum, Bochum, Germany, ⁴Institute of Experimental Oncology, University Medical Center Bonn (UKB), Bonn, Germany, ⁵Department of Urology and Pediatric Urology, University Hospital Erlangen, Friedrich-Alexander-Universität Erlangen-Nürnberg, Erlangen, Germany, ⁶Department of Urology, University of Regensburg, Caritas St. Josef Hospital, Regensburg, Germany, ⁷Department of Urology and Pediatric Urology, University Hospital Ulm, University of Ulm, Erlangen, Germany, ⁸Department of Urology and Pediatric Urology, University Hospital Ulm, University of Ulm, Ulm, Germany, ⁹Department of Urology, University Hospital Mannheim, University of Heidelberg, Mannheim, Germany, ¹⁰Institute of Pathology, Technical University Munich, Munich, München, Germany, ¹¹Stratifyer, Köln, Germany, ¹²Department of Urology, Technical University Munich, München, Germany, ¹³Institute of Pathology, University Medical Center Bonn (UKB), Bonn, Germany, ¹⁴Department of Urology, University Medical Center Göttingen, Göttingen, Germany, ¹⁵Clinic for Internal Medicine (Tumor Research) and Clinic for Urology, Interdisciplinary Genitourinary Oncology at the West-German Cancer Center, Essen University Hospital, Essen, Germany, ¹⁶Department of Urology, Eberhard Karls University, Tübingen, Tübingen, Germany, ¹⁷Department of Urology, University Hospital Muenster, Münster, Germany, ¹⁸Department of Pathology, University Hospital Muenster, Münster, Germany, ¹⁹Department of Medical Oncology, National Center for Tumor Disease (NCT), University Hospital, Heidelberg, Germany, ²⁰Institute of Pathology, University of Heidelberg, Heidelberg, Germany, ²¹Pathologie Ingolstadt, Ingolstadt, Germany, ²²Department of Urology, Klinikum Ingolstadt, Ingolstadt, Germany, ²³Department of Urology and Pediatric Urology, University Hospital Erlangen, Erlangen, Germany

Questions/Background

The antibody-drug conjugate enfortumab vedotin (EV) releases a cytotoxic agent into tumor cells via binding to the membrane receptor NECTIN-4. EV has been recently approved for patients with metastatic urothelial carcinoma (mUC) without prior assessment of the tumor receptor status as ubiquitous NECTIN-4 expression is assumed.

Objective: To determine the prevalence of membranous NECTIN-4 protein expression, which represents the

biological prerequisite for EV binding, in primary tumors (PRIM) and patient-matched distant metastases (MET) as it has not yet been systematically studied and may be relevant for EV response.

Methods

Membranous NECTIN-4 protein expression was measured (H-score) by immunohistochemistry (IHC) in PRIM and corresponding MET ($N=137$) and in a multicenter EV-treated cohort ($N=39$). Progression-free survival (PFS) after initiation of EV treatment was assessed for the NECTIN-4 negative/weak (H-score 0-99) versus moderate/strong (H-score 100-300) subgroup. The specificity of the NECTIN-4 IHC staining protocol was validated by establishing CRISPR-Cas9-induced polyclonal NECTIN-4 knockouts in HT1376 cells using two independent sgRNAs. Resistance of HT1376 cells to EV by NECTIN-4 loss was confirmed using low-density colony formation assays.

Results

In our cohort, membranous NECTIN-4 expression significantly decreased during metastatic spread (Wilcoxon matched pairs $P<0.0001$, median H-score=40, interquartile range (IQR): 0-140), with 39.4% of MET lacking membranous NECTIN-4 expression. In our multicenter EV cohort, absence or weak membranous NECTIN-4 expression (35.9% of cohort) was associated with a significantly shortened PFS on EV (Logrank $P<0.0001$).

Conclusion

Membranous NECTIN-4 expression is frequently decreased or absent in mUC tissue. Of note, the data of our multicenter EV cohort indicates that clinical benefit of EV strongly depends on membranous NECTIN-4 expression. Thus, our results argue for a critical reconsideration of the current practice and suggest that the NECTIN-4 receptor status should be determined (ideally in a metastatic/progressive lesion) before initiation of EV therapy.

DGP13.09

Associations of TACSTD2/TROP2 and NECTIN-4/NECTIN-4 with molecular subtypes, PD-L1 expression and FGFR3 mutational status in two advanced urothelial bladder cancer cohorts

V. Bahlinger¹, A. Branz¹, P. L. Strissel¹, R. Strick², F. Lange¹, C. I. Geppert¹, N. Klümper³, M. Hölzl⁴, S. Wach⁵, H. Taubert⁵, D. Sikic⁵, B. Wullich⁵, M. Angeloni¹, F. Ferrazzi¹, L. Diehl⁶, M. Kovalenko⁶, E. Elboudwarej⁶, J. M. Jürgensmeier⁶, A. Hartmann¹, M. Eckstein¹

¹Institute of Pathology, University Hospital Erlangen, Erlangen, Germany, ²Laboratory for Molecular Medicine, Department of Gynecology and Obstetrics, University Hospital Erlangen, Erlangen, Germany, ³Department of Urology, University Medical Center Bonn (UKB), Bonn, Germany, ⁴Institute of Experimental Oncology, University Medical Center Bonn (UKB), Bonn, Germany, ⁵Department of Urology, University Hospital Erlangen, Erlangen, Germany, ⁶Gilead Sciences, San Francisco, United States of America

Questions/Background

Treatment options for advanced urothelial carcinoma (aUC) have rapidly evolved in recent years. Besides immunomodulative therapeutic options like anti-PD-(L)1 inhibitors and inhibitors targeting *FGFR* alterations, two new antibody-drug conjugates (ADC), sacituzumab govitecan (SG) and enfortumab vedotin (EV), have been approved for treatment. However, little is known about relations of specific aUC properties and the membranous expression of TROP2 and NECTIN-4, which represent the targets for the SG and EV. In addition, how these ADCs can be implemented in treatment options and what are the relation to other biomarkers must be investigated to improve precision medicine in aUC. To characterize associations of *TACSTD2/TROP2* and *NECTIN-4/NECTIN-4* protein and gene expression with morphomolecular and clinico-pathological characteristics of aUC in two large independent cohorts.

Methods

The TCGA BLCA ($n=405$) and the CCC-EMN ($n=247$) cohorts were retrospectively analyzed. RNA and protein expression of *TACSTD2/TROP2* and *NECTIN-4/NECTIN-4* were measured and correlated with clinico-pathological characteristics, molecular subtypes, *FGFR3* alterations and PD-L1 expression.

Results

TROP2/TACSTD2 and *NECTIN-4/NECTIN-4* are highly expressed at protein and transcript level in aUC, and their expression status did not correlate with patient survival in two independent cohorts. *NECTIN-4/NECTIN-4* expression was significantly higher in luminal tumors and reduced in squamous aUCs. NECTIN-4 was absent in 10.6% of samples, and 18.4% of samples had low expression (H-Score < 15). TROP2 negativity rate equalled 6.5%. *TACSTD2* and *NECTIN-4* expression was reduced in neuroendocrine-like and/or protein-analyzed double negative tumors. TROP2 and NECTIN-4 negative tumors (protein level) included

one sarcomatoid and four neuroendocrine aUC. *FGFR3* alterations and PD-L1 expression on tumor and immune cells did not associate with TROP2 or NECTIN-4 expression.

Conclusion

TACSTD2/TROP2 and *NECTIN-4/NECTIN-4* are widely expressed in aUC independent of *FGFR3* alterations or PD-L1 expression, thus representing a suitable target for ADC treatment in the majority of aUC. Expression loss associated with aggressive morphomolecular aUC subtypes, i.e. neuroendocrine(-like) and sarcomatoid aUC.

DGP14 Hämatologische Neoplasien in Kindern

DGP14.01

GPOH-HD/EuroNet-PHL Study Center: Morphology - Genetics -Clinic

A. Bräuninger¹, S. Gattenlöhner², D. Körholz³

¹Universitätsklinikum Gießen, Institut für Pathologie, Gießen, Germany, ²Universitätsklinikum Giessen, Institut für Pathologie, Giessen, Germany, ³Universitätsklinikum Giessen, Pädiatrische Hämatologie und Onkologie, Giessen, Germany

Hodgkin Lymphome (HL) repräsentieren ca. 15% der Malignome bei Kindern und Jugendlichen. Mit aktuellen multimodalen Chemo- und Radiotherapien werden 5-Jahres Überlebensraten von 95% erreicht. Trotzdem sind nach wie vor 10%-15% der Patienten von primärer Therapieresistenz oder Rezidiven und ein erheblicher Anteil von Spätfolgen der Therapie - Sekundär Malignomen, Schädigungen des kardiovaskulären Systems, reduzierte Fruchtbarkeit – betroffen. Deshalb müssen neben weiteren Verbesserungen bei der Therapie vor allem Marker identifiziert werden, die von Therapiebeginn an Patienten adaptierte Therapien ermöglichen.

In der Präsentation gehen wir auf beide Aspekte, Verfahren zur besseren Patienten Stratifikation und Verbesserungen bei der Therapie, ein. Wir stellen vor wie mittels digitaler Pathologie und neuronalen Netzwerken überprüft wird, ob ein Klassifikationssystem für nodulär Lymphozyten-prädominante HL bei Kindern und Jugendlichen prognostische Relevanz hat. Außerdem gehen wir auf die Möglichkeiten ein, die der Nachweis und die Untersuchung zirkulierender Tumor DNA (Liquid Biopsy) eröffnen. Schließlich werden die Verbesserungen der Therapie Resultate im Rahmen der EuroNet Studien sowie aktuelle Studien vorgestellt.

DGP14.02

Myelodysplastic syndrome and inherited bone marrow failure in childhood

M. Rudelius

Pathology LMU, München, Germany

Myelodysplastische Syndrome (MDS) im Kindesalter unterscheiden sich in der Histomorphologie und den molekularen Veränderungen erheblich von den MDS im Erwachsenenalter. Während bei Erwachsenen das Knochenmark meist hyperzellulär ist, sind über 80% der kindlichen MDS hypoplastisch mit multilineärer Dysplasie der trilineären Hämatopoese. Somatische Mutationen epigenetischer Regulatoren treten bei Kindern selten auf, häufiger sind Monosomie 7 oder eine vorbestehende Keimbahn-Prädisposition wie die GATA2-Defizienz oder das SAMD9/SAMD9L Syndrom. Diese frühen Formen des MDS manifestieren sich häufig in der Form einer refraktären Zytopenie des Kindesalters (RCC), welche ein charakteristisches morphologisches Muster zeigt. In der aktuellen internationalen Konsensus Klassifikation (ICC) und der Neuauflage der WHO wurden die Keimbahnmutationen in drei Hauptkategorien (1) assoziiert mit konstitutioneller Störung, (2) assoziiert mit Thrombozytopenie/dysfunktion und (3) Pathologie in mehreren Organsystemen untergliedert.

Insgesamt ist zur korrekten Diagnostik und Therapie des MDS im Kindesalter ein multidisziplinäres Vorgehen mit einem hohen Stellenwert der Histomorphologie essentiell.

DGP14.03

Whole Exome Sequencing of circulating tumor DNA of paediatric Hodgkin

Lymphoma patients

T. Jox¹, M. Dörrbecker², D. Körholz³, C. Mauz-Körholz³, S. Gattenlöhner¹, M. Bartkuhn², A. Bräuninger¹

¹Justus Liebig University and UKGM, Institute of Pathology, Gießen, Germany, ²Justus Liebig University and UKGM, Biomedical Informatics and Systems Medicine, Gießen, Germany, ³Justus Liebig University and UKGM, Department of paediatric Haematology and Oncology, Gießen, Germany

Questions/Background

Paediatric Hodgkin lymphoma (pHL) is one of the most common cancers in children and adolescents. The pathogenic mechanisms are largely unknown. Although treatment with actual therapy schemes is usually successful, 5-10% of pHLs show an insufficient response and harsh therapy often leads to secondary neoplasia and other health issues later in the lives of pHL patients.

Goals:

- 1) Identification of driver mutations to gain insights into the pathogenesis of pHL.
- 2) Identification of mutation patterns related to the different therapy responses to detect diagnostic markers for better therapy stratification.

Methods

We have previously shown that circulating cell free DNA (ccfDNA) from blood plasma of pHL patients is a suitable source to detect somatic mutations of pHL (Desch et al. 2019). Based on these findings we have established a protocol for performing whole exome sequencing (WES) with ccfDNA and applied it, together with targeted NGS for regions frequently affected by aberrant somatic hypermutation (ASH), to ccfDNA from pre-therapy blood samples of 110 pHL patients. WES of gDNA from blood cells was performed to distinguish somatic from germline mutations. Furthermore, a bioinformatics pipeline focussed on the distinction of background noise from low frequency variants was designed.

Results

We identified several recurrently mutated genes in pHLs in addition to those already known to contribute to pHL pathogenesis. Numbers of mutations in regions known to be targeted by ASH were significantly correlated with the number of somatic mutations in protein coding regions. Furthermore, signature of AID, a cytidine deaminase which is involved in somatic hypermutation and aging specific mutational signatures were enriched among the coding mutations, in line with an origin of paediatric Hodgkin-Reed/Sternberg cells from proliferating germinal centre B cells. Recently, it has been shown for several tumor entities, that length of ctDNA fragments are often shorter than ccfDNA fragments from non-tumor cells. We demonstrated that in pHL a significant fraction of ccfDNA is shorter than in healthy donors and that mutations are enriched in this shorter fraction. In addition, we found an enrichment of mutated genes from several HL specific pathways in cases with insufficient therapy response.

Conclusion

Using ccfDNA and WES we discovered several novel recurrently mutated genes, identified relevant mutational signatures and showed that mutations are significantly enriched in shorter ccfDNA fragments.

DGP14.04

Post mortem germline genetic testing – proclamation for an undervalued procedure with preventive power for relatives at risk

A.-C. Berking¹, A. Reitz², M. Richter³, B. Auber¹, M. Klitsch⁴, T. Ripberger¹, E. Gradhand², A. K. Bergmann¹

¹Medizinische Hochschule Hannover, Institut für Humangenetik, Hannover, Germany, ²Dr. Senckenbergisches Institut für Pathologie, Universitätsklinikum Frankfurt, Frankfurt, Germany, ³Kinder- und Jugendkrankenhaus auf der Bult, Neonatologie, Hannover, Germany,

⁴Medizinische Hochschule Hannover, Institut für Rechtsmedizin, Hannover, Germany

Introduction

Post mortem germline genetic testing can clarify the cause of death in unexplained cases by means of molecular genetic analyses (e.g. immunodeficiencies, neurological-, syndromic- or cardiovascular disorders), which cannot be determined by clinical autopsy only. It does not replace the clinical autopsy, but provides a valuable complementary procedure.

According to the German Federal Statistical Office, in 2020 2,081 persons under the age of 45 and 84 children died from unknown causes in Germany. The number of unreported cases is probably much higher. If an unknown cause of death is due to a genetic disease, the medical consequences and clinical implications are significant for biological relatives.

Methods

We examined 21 recent cases of unexplained death in children. In 17 patients genetic germline analysis was performed via array-CGH/next generation sequencing. Practical workflows and efficiency were reviewed in

terms of tissue preservation, cost coverage, genetic analyses and counselling.

Results

We identified a (likely) pathogenic variant in six patients (35%) explaining their death. The variants were associated with a wide range of genetic disorders: Ehlers-Danlos syndrome - vascular type, acute necrotizing encephalopathy, familial hemophagocytic lymphohistiocytosis, duplication 8q syndrome, epileptic encephalopathy. A variant of unknown significance was found in seven additional patients.

In the present cases, workflow and efficiency differed greatly. Proposals for improving post mortem germline genetic testing workflows were found in the literature, but no general recommendations, incorporating different disease entities and multiple clinical disciplines are established.

Conclusion

Our series and international studies demonstrate that post mortem germline genetic testing is able to identify causal genetic variants in around 30% of unexplained deaths. Yet our study and systematic literature review indicate that an interdisciplinary guideline is needed, addressing issues such as indication, relative's consent, post mortem tissue preservation, genetic counselling and cost coverage.

Therefore, we developed an interdisciplinary workflow to facilitate and ensure the performance of post mortem germline genetic testing – from the relative's consent to post-mortem tissue preservation and genetic counselling. This workflow offers not only improvements in patient care but also the opportunity to expand clinical and genetic disease knowledge.

DGP15 Multiparametric tissue imaging II

DGP15.02

4D strategic diagnostics in the lymph node

M.-L. Hansmann

Helios Universitätsklinikum Wuppertal, Institut für Pathologie und Molekularpathologie, Wuppertal, Germany

Die Lymphknotendiagnostik beruht primär auf einer mikroskopischen/histologischen Beurteilung des lymphatischen Gewebes. Wichtige diagnostische Parameter sind Kern- und Chromatin-Strukturen lymphatischer, sowie auch retikulärer Zellen. Darüber hinaus lässt sich das Immunsystem anhand dickerer Schnitte mit Hilfe von fluoreszierenden Farbstoffen, Antikörpern und konfokalen Lasern auch im 3D darstellen. Mit Computerprogrammen können die Zelloberflächen und deren Netzwerke sichtbar gemacht werden. Statt mit Flächen in 2D-Darstellungen kann man nun mit Volumina rechnen.

In lebenden Schnitten von lymphatischem Gewebe wurden zudem 4D-Techniken etabliert, die das Immunsystem in Zeit und Raum abbilden. Somit wird es möglich Immunreaktionen, wie auch maligne Lymphome, des Menschen in ihren zeitlichen Abläufen zu analysieren und auch maschinelle Lernmethoden einzusetzen.

Erste Analysen ergaben, dass T-Zellen in der Regel höhere Geschwindigkeiten erreichen als B-Lymphozyten. Auch Zellkontakte lassen sich im 3D/4D wesentlich exakter definieren, als in konventionellen 2D-Schnitten. Von besonderer Bedeutung erwiesen sich die Kontaktzeiten zwischen reaktiven Zellen, sowie auch Tumorzellen, in unterschiedlichen malignen Lymphomen. So erscheinen die Art der Zellbewegungen, wie auch die Kontaktzeiten, typisch für bestimmte Lymphomtypen. Dies zeigen Daten aus einer ersten Studie humaner Hodgkin- und Non-Hodgkin-Lymphome im 4D. Zudem wird maschinelles Lernen bei der Analyse von Movies reaktiven lymphatischen Gewebes eingesetzt. Die Filme geben Aufschluss über die Bewegung der verschiedenen Zellarten im Rahmen unterschiedlicher Immunreaktionen. Die vorgestellten Technologien und Untersuchungen versprechen neue Einblicke in die Entstehung, Biologie, Ausbreitung und Strategie maligner Lymphome. Zudem erlauben 4D-Technologien die Testung moderner Therapien einschließlich CAR-T-Zellen.

Literaturangaben:

[1] Scharf S, Ackermann J, Bender L, Wurzel P, Schäfer H, Hansmann ML, Koch I, (2023), Holistic View on the Structure of Immune Response: Petri Net Model, Biomedicines, doi: 10.3390/biomedicines11020452

[2] Hartmann S, Scharf S, Steiner Y, Loth AG, Donnadiou E, Flinner N, Poeschel V, Angel S, Bewarder M, Bein J, Brunnberg U, Bozzato A, Schick B, Stilgenbauer S, Bohle RM, Thurner L, Hansmann ML, (2021), Landscape of 4D Cell Interaction in Hodgkin and Non-Hodgkin Lymphomas, Cancers (Basel), doi: 10.3390/cancers13205208

[3] Wagner P, Strodthoff N, Wurzel P, Marban A, Scharf S, Schäfer H, Seegerer P, Loth A, Hartmann S, Klauschen F, Müller KR, Samek W, Hansmann ML, (2022), New definitions of human lymphoid and follicular cell entities in lymphatic tissue by machine learning,

DGP15.03

Dissecting antitumoral mechanisms of a virus-based immunotherapy in melanoma using highly multiplexed tissue imaging and machine learning

A. Makky¹, M.-T. Purde², Y. A. Palmowski¹, A. Rochwarger¹, S. Schmidt³, F. Hartmann², D. Bomze², F. Berner², B. Ludewig², H. Lauterbach³, K. Orlinger³, J. Cupovic², S. S. Ring^{2,4}, L. Flatz^{2,5,6}, C. M. Schürch¹

¹University Hospital and Comprehensive Cancer Center Tübingen, Department of Pathology and Neuropathology, Tübingen, Germany,

²Kantonsspital St. Gallen, Institute of Immunobiology, St. Gallen, Switzerland, ³Hookipa Pharma, Vienna, Austria, ⁴TU München, TranslaTUM, Munich, Germany, ⁵Kantonsspital St. Gallen, Department of Dermatology, St. Gallen, Switzerland, ⁶University Hospital Tübingen, Department of Dermatology, Tübingen, Germany

Questions/Background

Immunotherapy is a powerful therapeutic modality for metastatic melanoma due to the strong immunogenicity of these tumors. The immunotherapy mechanism relies on the recognition of melanoma-associated antigens (MAAs), which are presented to T cells by activated dendritic cells. T cell cytotoxicity leads to tumor cell death, releasing more MAAs, which reinforces the killing cycle. However, immunotherapies stimulating this cycle still face several barriers, such as an immunosuppressive tumor microenvironment (TME) and T cell tolerance to MAAs. Here, we applied CODEX highly multiplexed microscopy to dissect vaccination-induced immune responses in the TME at single-cell resolution in a melanoma mouse model treated with a virus-based vaccination immunotherapy.

Methods

Melanoma-bearing mice were immunized with propagating or non-propagating virus based vectors carrying the MAA TRP2, along with adoptive transfer of TRP2-specific CD8 T cells. Subcutaneous tumors were harvested, and fresh-frozen tissue sections were subjected to CODEX using a 50+ marker antibody panel. Image processing, cell segmentation, cell type identification, clustering and higher order data analysis were performed using supervised and unsupervised computational pipelines and machine learning algorithms.

Results

Mice vaccinated with propagating vector showed an immune response that controlled tumor growth compared to control mice vaccinated with non-propagating vector. We imaged 520,000 spatially resolved single cells, which were clustered into 20 cell types. We identified immune-tumor cell interactions and cellular neighborhoods that were associated with antitumoral immunity and built precise maps of the TME architecture in situ. These analyses showed that immunization with the propagation-competent vector induced deep tumor infiltration by antigen-specific CD8 T cells.

Conclusion

The virus propagation competence overcomes tolerance for TRP2, a self-antigen, leading to tumor cell killing and resulting in prolonged survival. The integration of CODEX and machine learning revealed the cell-cell interactions in the TME and the crosstalk between cellular neighborhoods that mediated the immune response. The combination of propagating vector with adoptive T cell transfer showed potential for complete tumor rejection, providing a foundation for next-generation immunotherapies.

DGP15.04

Characterizing intratumor heterogeneity and the tumor microenvironment of colorectal cancer and intrahepatic cholangiocarcinomas by MALDI imaging

M. Föll¹, L. Moritz¹, B. Barta¹, L. Meyer¹, M. Stillger¹, J. Thiery¹, A. Weber¹, N. Meier¹, B. Vollmer-Kary¹, P. Holzner², F. Takács³, H. Füllgraf¹, A. Jud², S. Fichtner-Feigl², P. Hönscheid⁴, M. Werner¹, O. Schilling¹, P. Bronsert¹

¹Medical Center – University of Freiburg, Institute for Surgical Pathology, Freiburg, Germany, ²Medical Center – University of Freiburg, Department of General and Visceral Surgery, Freiburg, Germany, ³Semmelweis University, Department of Pathology and Experimental Cancer Research, Budapest, Hungary, ⁴University Hospital Carl Gustav Carus, Institute Pathology, Freiburg, Germany

Question/Background

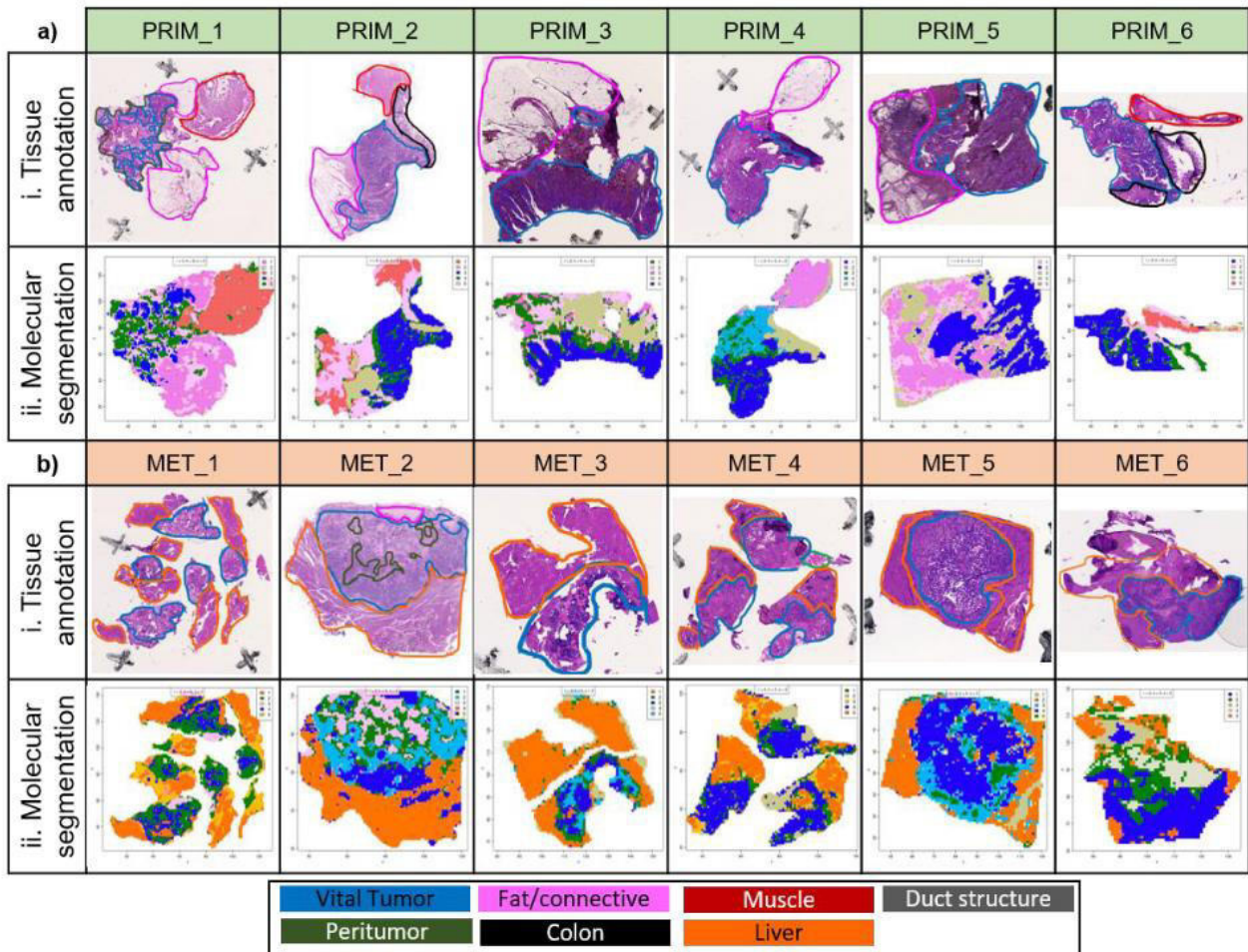
Colorectal cancer (CRC) and intrahepatic cholangiocarcinomas (iCCA) are surrounded by a complex tumor microenvironment, while the tumor cells show intratumor heterogeneity. Both characteristics play a crucial role in therapy response and resistance. They can be investigated by MALDI imaging, which is a mass spectrometry based technique that generates distribution profiles of biomolecules such as proteins and metabolites directly from thin tissue sections of formalin-fixed and paraffin-embedded (FFPE) tissues archived at pathologies.

Methods

We have performed tryptic peptide MALDI imaging of six primary colorectal cancers and patient matched metastases and of >400 tissue cores from 70 iCCA patients.

Results

In CRC tissues proteomic segments resembled tissue morphology



Tissue morphologies of CRC primary tumor and liver metastasis tissues differ in their spatial proteomic composition. a) Primary tumor and b) liver metastasis tissues. i. Tissue annotations in H&E images. ii. MALDI imaging proteomic segments show organized tissue architecture, which resemble the annotated tissue types shown in i.

and we found annexin A4 and prelamin A/C to be specific for vital tumor areas. Liver metastases of colorectal cancer showed higher heterogeneity between patients than primary tumors. iCCA tissues showed pronounced inter- and intra tumor heterogeneity and correlation with clinicopathological parameters are still ongoing. Additionally, we have set up 120 iCCA organotypic tissue slice cultures from fresh patient tumor tissues to generate a new iCCA preclinical model that allows functional follow up of our results and in the future also drug distribution and response studies. Histomorphological evaluation of the tissue slices cultured for five days showed a mixed picture, while culturing for 10 or more days reduced the number of tumor cells and increased activated fibroblasts.

Conclusion

MALDI imaging enables new insights into the spatio-molecular heterogeneity of the tumor and its microenvironment in CRC and iCCA. Once the culturing conditions are optimized, iCCA OTSC set the foundation for a new patient-derived preclinical iCCA model.

DGP17 Gemeinsame Sitzung DRG und DGP I : State-of-the-art CT und MRT Untersuchungstechniken in Korrelation zur Pathologie

DGP17.01

Correlation of Pathology and multiparametric MagneticResonance Imaging

G. Kristiansen

Universitätsklinikum Bonn, Institut für Pathologie, Bonn, Germany

Die präzise Beurteilung des Tumorstatus und der Ausbreitung des Prostatakarzinoms ist von entscheidender Bedeutung für die Behandlungsplanung und das therapeutische Management. In den letzten Jahren haben sich multiparametrische Magnetresonanztomographie (mpMRT) -basierte Bildgebungstechniken als vielversprechend für die nicht-invasive Evaluierung des Prostatakarzinoms etabliert.

Die PROMIS-Studie (Prostate MR Imaging Study) untersuchte die diagnostische Genauigkeit der mpMRT bei der Identifizierung klinisch signifikanter Prostatakarzinome im Vergleich zur transrektalen Ultraschall-gesteuerten Biopsie. Die Ergebnisse zeigten, dass die mpMRT eine höhere Sensitivität und spezifischere Erkennung von signifikanten Tumoren aufweist, was zu einer Reduzierung unnötiger Biopsien führen kann. Die MRI-first-Strategie wurde in der gleichnamigen Studie untersucht, um die Rolle der mpMRT als primäres diagnostisches Werkzeug vor einer Biopsie zu bewerten. Die Studie ergab, dass die Anwendung der MRI-first-Strategie zu einer signifikanten Reduktion unnötiger Biopsien führte, während die Erkennung klinisch signifikanter Tumoren verbessert wurde.

Die PRECISION-Studie (Prostate Evaluation for Clinically Important Disease: Sampling Using Image Guidance or Not?) untersuchte die Auswirkungen der mpMRT-gesteuerten Biopsie im Vergleich zur standardmäßigen transrektalen Ultraschall-gesteuerten Biopsie auf die Identifizierung klinisch signifikanter Tumoren. Die Studie zeigte, dass die mpMRT-gesteuerte Biopsie eine höhere Erkennungsrate von klinisch signifikanten Tumoren aufweist und eine geringere Rate an nicht signifikanten Tumoren im Vergleich zur standardmäßigen Biopsie aufweist.

Zusammenfassend zeigen diese wichtigen Studien zur Korrelation von Pathologie und mpMRT beim Prostatakarzinom, dass die mpMRT eine vielversprechende nicht-invasive Bildgebungstechnik ist, um klinisch signifikante Tumoren zu identifizieren und unnötige Biopsien zu reduzieren. Die Anwendung der MRI-first-Strategie und mpMRT-gesteuerten Biopsien könnte zu einer verbesserten Diagnose und einem optimierten therapeutischen Management des Prostatakarzinoms führen. Weitere Forschung ist jedoch erforderlich, um die langfristigen klinischen Auswirkungen dieser Ansätze zu bestätigen und die optimale Integration der mpMRT in den diagnostischen und therapeutischen Prozess zu definieren.

DGP17.03

Synchrotron-based three-dimensional imaging: new opportunities in correlative histotomography of solid tumors.

M. Ackermann

Helios Universitätsklinikum Wuppertal, Institut für Pathologie und Molekularpathologie, Wuppertal, Institut für Pathologie und Molekularpa, Germany

Synchrotronstrahlung gilt als die brillianteste und hellste Röntgenstrahlung der Welt und hat in den letzten Jahrzehnten eine enorme Weiterentwicklung in ihrem Anwendungsbereich erfahren. Die neue hierarchische Phasenkontrast-Tomografie (HiP-CT) nutzt die hellste Synchrotron-Strahlenquelle der Welt an der ESRF (European Synchrotron Radiation Facility) in Grenoble. Die Auflösung der konventionellen Computertomografie (CT) ist auch im klinischen Alltag auf wenige Millimeter beschränkt. Das HiP-CT erreicht hierbei Auflösungen unter einem Mikrometer und ermöglicht somit eine dreidimensionale Gewebeauflösung wie ein konventionelles zweidimensionales Lichtmikroskop. Weiterhin lassen sich über Phasenkontrast-Computertomografie ebenfalls paraffineingebettete Gewebeproben bis in den Submikronbereich zerstörungsfrei analysieren und im Nachgang molekular aufarbeiten.

DGP17.04

An artificial intelligence solution for evaluation of prostate needle core biopsy specimens: impact in a non-specialist setting

G. Niedobitek¹, G. Schmitz¹, M. Fella¹, A. Oliveira¹, J. Köllermann², J. Theunissen³, M. Vecsler³

¹Sana Klinikum Lichtenberg, Institut für Pathologie, Berlin, Germany, ²Dr. Senckenbergisches Institut für Pathologie, Universitätsklinikum Frankfurt, Frankfurt, Germany, ³Ibex Medical Analytics, Tel Aviv, Israel

Questions/Background

The increasing availability of whole slide scanners has facilitated the establishment of virtual microscopy as a diagnostic tool in histopathology. This has enabled the analysis of virtual slides by artificial intelligence (AI) algorithms and there is an increasing number of such tools available by now. Reliable diagnosis and grading

of prostate cancer in needle core biopsy (NCB) specimens is difficult and may yield conflicting results even among expert pathologists. In 2021, we have introduced a commercially available AI algorithm (Galen Prostate, Ibex Medical Analytics, Tel Aviv, Israel) for analysing prostate NCB specimens into our workflow. Here, we report on the results of using this algorithm in a second read workflow.

Methods

249 cases of prostate NCBs with a total of 2.085 tissue cores were retrieved from the archives of the Institute of Pathology, Sana Klinikum Lichtenberg, Berlin. These included 167 cases (67%) with a diagnosis of carcinoma and 82 benign cases (33%). Slides were scanned and images were processed by the Galen Prostate AI. Clinically relevant alerts generated by the AI were reviewed by an expert prostate pathologist (JK) and immunohistochemical (IHC) stains for 34βE12 and AMACR were performed as required.

Results

Of 82 cases initially diagnosed as benign, AI analysis yielded 13 alerts indicating that cancer may have been missed by the reporting pathologists. Immunohistochemistry and examination by an expert prostate pathologist yielded diagnoses of cancer in 1 case, 3 cases were diagnosed as atypical small acinary proliferation (ASAP), and 8 cases were considered benign. In 2 of the latter, tissue contaminants gave rise to AI cancer alerts. Among the 167 prostate cancer cases, 2 "Gleason higher than 3+3 alerts" were raised resulting in revised grades of both cases to 3+4. An in depth analysis of the results of these 167 cases at the single slide level revealed no "false positive" cancer diagnoses by the original reporting pathologists.

Conclusion

Our results suggest that introduction of the Galen Prostate AI solution provides an added level of security in the diagnosis and grading of prostate cancer. It reduces the need for second opinions as well as for immunohistochemical stains. By detecting clinically relevant mistakes, it increases patient safety in a non-specialist setting.

DGP17.05

3D Reconstruction of Prostate Carcinoma

T. Bisson, R. Carvalho, I. Dogan O, N. Zerbe, S. Elezkurtaj

Charité - Universitätsmedizin Berlin, Institut für Pathologie, Berlin, Germany

Questions/Background

Pathologists are able to get an idea of the three-dimensional extent of the tumors found in prostatectomy specimens during microscopic examinations. While this is not always relevant to diagnostics, it can be useful in a variety of contexts. There are already a number of publications describing the correlation of histological diagnostics of the prostate with MRI, for example. In another context, a 3D representation of the tumor can provide helpful feedback to the physicians or may be used in education or for statistical analysis.

Methods

We have developed an algorithm to virtually slice a 3D surface model according to the sectioning of the prostate specimen, resulting in a set of reference polygons approximating the real tissue slides. The 3D model itself may originate from various sources, such as a segmented MRI or a 3D scanner. It is also conceivable to use a generic 3D model of a prostate that is adapted to the dimensions of the prostatectomy specimen. Afterwards, the contours of the WSI of the prostate are registered to the sliced 3D model and the previously annotated tumor regions are transformed. Subsequently, the volume is reconstructed, which can be done either by blocks for each tumor region individually or by implicit surfaces for the entirety of the tumor regions.

Results

The sectioning of the prostatectomy specimen can be transferred to any 3D model of the prostate. However, since only information from the documentation is taken, deviating cutting angles and axes cannot be taken into account. We were able to show that the tumor regions of the WSIs can be transformed into the sliced 3D model, so that the 3D propagation of the tumor can already be visualized. Furthermore, the shape of the tumor can be approximated by volume reconstruction, but since the actual size of the tumor can only be estimated from the diagnostic specimens, no exact reference can be used to evaluate the accuracy of the reconstruction.

Conclusion

Our described method for the reconstruction of prostate carcinomas can be employed in a variety of ways. It can be used, for instance, to evaluate PI-RADS findings or to provide feedback to the operating surgeon. It can even be integrated into laboratory processes, adding 3D reconstruction to the reports or extracting information from the distribution and extent. In order to optimize the process, more sophisticated registration procedures and volume reconstruction techniques could be investigated.

Bedside US-guided minimal invasive multiorgan autopsy of COVID-19 deceased: a proof of concept study at the ICU.

T. Lahmer¹, K. Stock², S. Rasch¹, S. Porubsky³, S. Jeske⁴, C. Schustetter⁵, U. Protzer⁴, U. Heemann², R. Schmid¹, W. Weichert⁶, G. Weirich⁶, J. Slotta-Huspenina⁶

¹Technische Universität München, Department of Internal Medicine II, Klinikum Rechts der Isar, München, Germany, ²Technische Universität München, Department of Nephrology, Klinikum Rechts der Isar, München, Germany, ³Johannes Gutenberg-Universität Mainz, Institute of Pathology, Mainz, Germany, ⁴Technische Universität München, Institute of Virology, München, Germany, ⁵Technische Universität München, Institute of Pathology, München, Germany, ⁶Technische Universität München, Institute of Pathology, TUM School of Medicine, München, Germany

Questions/Background

Economic restrictions and workforce cuts have continually challenged conventional autopsies. Recently, the COVID-19 pandemic added tissue quality and safety requirements for the investigation of this disease launching efforts for upgrading autopsy strategies. Here, we pitched an interdisciplinary bedside multiorgan tissue procurement for COVID-19 casualties of intensive care units. We evaluated organizational feasibility, time efficiency, procedures' safety, tissue quality, diagnostic potential.

Methods

The study was carried out at an intensive care unit of the Klinikum rechts der Isar of the Technical University of Munich (TUM). Inclusion criteria were SARS-CoV-2 infection and next of kin consent. Ultrasound (US) examination and US-guided tissue procurement was done by an interdisciplinary team. Biopsies were formalin-fixed and paraffin-embedded (FFPE) and assessed for quality (vitality and length) and diagnosis. The procedure's efficiency was monitored by time recording of each step, safety issues by swabbing personal protective equipment and devices used for the detection of viral contamination. The study was approved by the ethics committee of the TUM (Ref. 225/20S) and funded by BMBF (FKZ 01KX2021).

Results

Five COVID-19 deceased were included. The mean time from a patient's death to starting the procedure at the ICU 162 minutes (129-210). US-examination required 13 minutes (5-16), tissue procurement 54 minutes (44-75). 318 biopsies were obtained (Ø 62 per deceased) from: lungs, liver, spleen, pancreas, kidneys, left heart, a. abdominalis, parotid gland, conjunctival mucosa, lacrimal gland, skin, and bone marrow. Hit rate was 96,4% and the mean biopsy length 11 mm (4-25). Biopsies contained well-preserved tissue without signs of autolysis by light microscopy. The typical findings of COVID-19 were found in all cases. Concerning safety, 54/55 swabs were negative for SARS-CoV-2. In one case, viral RNA was detected on the ultrasound transducer at low level (Fig.).



Sonographer

- 1: Right glove, palm
- 2: Left glove, palm
- 3: Lower arm, inside
- 4: Plastic apron, level of chest

Pathologist

- 5: Right glove, palm
- 6: Left glove, palm

Devices

- 7: Screen
- 8: Keyboard
- 9: Transducer
- 10: Ultrasound gel bottle (n.s)
- 11: Sample handling table (n.s.)

Swab collection localisations, n.s.: not shown

Conclusion

Interdisciplinary bedside tissue sampling is an efficient and safe method to obtain high-quality tissues for diagnostics and research purposes, and qualifies as an alternative to conventional autopsy. This procedure offers a yet unappreciated potential to surpass the limitations of research in postmortems.

DGP18 Freie Vorträge III - Hämatopathologie

DGP18.02

Molecular Subtyping of Diffuse Large B-Cell-Lymphoma Using Panel-Sequencing

F. Hagedorn¹, N. Fuhr¹, T. H. Dang¹, A. Mottok¹, T. Weber¹, M. Rummel², A. Bräuninger¹, S. Gattenlöhner¹, R. Schmitz¹

¹Institute of Pathology, Justus-Liebig-University, Giessen, Germany, ²Hematology, Department of Internal Medicine, Justus-Liebig-University, Giessen, Germany

Questions/Background

Diffuse large B-cell-lymphoma (DLBCL) is the most common type of B-cell non-Hodgkin lymphoma in adults. Several technical developments have enabled the subclassification of DLBCL into distinct molecular subgroups using gene-expression profiling and next-generation sequencing. However, the heterogeneity of existing assays and algorithms has hampered broad implementation and use in clinical practice. Therefore, our aim was to develop a simplified and optimized model for DLBCL subclassification to be used in clinical routine.

Methods

We studied more than 200 formalin-fixed, paraffin-embedded DLBCL specimens using hybrid capture based high throughput panel-sequencing, including genes that are frequently mutated in this disease. Identified variants were used to define the cell-of-origin (COO) and to determine the genetic subgroups of DLBCL. For COO classification we refined a modelling algorithm relying on Bayes' theorem that was initially developed by Scherer et al., 2016. Results were compared with other gene expression-based classifiers of DLBCL. Classification of genetic subgroups was performed using the LymphGen Classifier described by Wright et al., 2020.

Results

Our panel-based high throughput sequencing analysis was able to determine the COO and genetic subgroups of the DLBCL samples analysed. Compared to other methods of molecular subclassification, our technique shows a high degree of overlap to the standard methods currently used in clinical routine.

Conclusion

Panel-based high throughput sequencing is well suited for molecular subclassification of DLBCL. It is simple, cost-effective, highly reproducible, accurate and objective. We believe, that in the near future a molecular classification will be routinely applied to identify those patients with a high-risk genetic profile while others can be protected from unnecessary therapy toxicity.

DGP18.03

In-depth genomic profiling of Follicular Lymphoma

S. Kalmbach^{1,2,3}, M. Grau⁴, M. Zapukhlyak⁴, E. Leich⁵, V. Jurinovic⁶, E. Hoster⁶, A. M. Staiger^{1,2,3}, K. S. Kurz¹, O. Weigert^{7,8,9}, E. Gaitzsch^{7,8,9}, V. Passerini^{7,8,9}, M. Engelhard¹⁰, K. Herfarth¹¹, K. Beiske¹², F. Micci¹³, H.-W. Bernd¹⁴, A. C. Feller¹⁴, W. Klapper¹⁵, H. Stein¹⁶, M.-L. Hansmann¹⁷, S. Hartmann¹⁷, H. Holte¹², G. Lenz¹⁸, A. Rosenwald, G. Ott, H. Horn

¹Department of Clinical Pathology, Robert-Bosch-Krankenhaus, Stuttgart, Germany, ²Dr. Margarete Fischer-Bosch Institute of Clinical Pharmacology, Stuttgart, Germany, ³University of Tübingen, Tübingen, Germany, ⁴Department of Medicine A, Department of Hematology, Oncology and Pneumology, University Hospital Münster, Münster, Germany, ⁵Institute of Pathology, University of Würzburg and Comprehensive Cancer Center (CCC) Mainfranken, Würzburg, Germany, ⁶Institute for Medical Information Processing, Biometry, and Epidemiology, Ludwig-Maximilians-University Munich, München, Germany, ⁷Department of Medicine III, Ludwig-Maximilians-University Hospital Munich, München, Germany, ⁸Laboratory for Experimental Leukemia and Lymphoma Research (ELLF), German Cancer Consortium (DKTK), Munich, München, Germany, ⁹German Cancer Research Cancer (DKFZ), Heidelberg, Germany, ¹⁰Department for Radiotherapy, University Hospital of Essen, Essen, Germany, ¹¹Department of Radiation Oncology, University of Heidelberg, Heidelberg, Germany, ¹²Department of Oncology, Oslo University Hospital, Oslo, Norway, ¹³Section for Cancer Cytogenetics, Oslo University Hospital, Oslo, Norway, ¹⁴Hematopathology Lübeck, Lübeck, Germany, ¹⁵Institute of Pathology, Hematopathology Section and Lymph Node Registry, University Hospital Schleswig-Holstein, Campus Kiel, Kiel, Germany, ¹⁶Pathodiagnostik Berlin, Berlin, Germany, ¹⁷Institute of Pathology, University Hospital Frankfurt, Frankfurt, Germany, ¹⁸Department of Medicine A, Department of Hematology, Oncology and Pneumology, University Hospital Münster, #||

Questions/Background

Follicular lymphoma (FL) is mainly diagnosed in systemic clinical stages III and IV (sFL, 85%). In contrast, localized FL (IFL) comprising clinical stages I and II occur in only 15%. Existing biological data of IFL indicated molecular differences between IFL and sFL, although few data are available for IFL until now. Therefore, this study aimed at a global genomic characterization of large cohorts of IFL and sFL.

Methods

147 IFL and 122 sFL were available for somatic copy number analysis (SCNA). 140 IFL and 24 sFL were used for whole exome sequencing (WES). For SCNA profiling the OncoScan CNV Assay was used. WES was performed on an Illumina HiSeq platform. Downstream effects were assessed by analyzing gene and protein expression of target genes by RT-PCR and immunohistochemistry in tumor samples and immunoblotting in representative B-cell lymphoma cell lines.

Results

In general, similar SCNA profiles of IFL and sFL were observed. However, significant differences between IFL and sFL were detected for frequencies of chromosomal gains in 18q (14% IFL vs. 36% sFL; $p=0.00034$) and X (16% IFL vs. 39% sFL; $p=0.0002$). Moreover, novel frequently affected regions were detected in IFL and sFL, including gains in 6p21, 11q24 and 17q and losses in 8p11. Applying the GISTIC algorithm, novel significantly aberrant genes were identified in regions known to be frequently gained, e.g. *FCRL5* in 1q23 and *IKZF1* in 7p12. Gene expression analysis confirmed higher levels for the target genes *FCRL5*, *IKZF1* and *ETS-1* in the regions of gain (1q23, 7p12 and 11q24, respectively), as well as decreased GE of *ADAM32* (8p11-loss). Protein expression of target genes (*FCRL5*, *IKZF1* and *ETS-1*) was enhanced in cell lines and tumor samples harboring gains in the respective locus.

The mutational landscape of IFL and sFL was highly similar, including typical genetic lesions of FL (e.g. *CREBBP*, *KMT2D*, *TNFRSF14*, *EZH2*). However, *ARID1A* showed significantly higher mutation frequencies in sFL compared to IFL (29% vs 6%, $p=0.0001$). Additionally, different mutation patterns were found for *CREBBP* and *KMT2D* in IFL and sFL with splice site mutations predominantly occurring in IFL.

Conclusion

Although the molecular landscape of IFL and sFL was quite similar, some novel candidate genes were detected that perspective could serve as therapeutic targets or biomarkers. Further investigation is needed to elucidate differential mutational patterns in IFL and sFL.

DGP18.04

CDK6 protein expression is associated with disease progression and treatment resistance in multiple myeloma

T. Barth^{TF1}, J. Steinhart¹, M. Kull², J. Krönke³, P. Möller¹

¹Universität Ulm, Pathologie, Ulm, Germany, ²Universität Ulm, Innere Medizin III, Ulm, Germany, ³Charite Berlin, Hämatologie, Berlin, Germany

Questions/Background

Multiple myeloma (MM) is a genetically and clinically heterogenous malignancy of plasma cells. Despite the improvement of outcome after introduction of new drugs MM remains an incurable disease since virtually all patients become treatment resistant. Cyclin-dependent kinase 6 (CDK6) is an important cell cycle regulator

that is activated in many types of cancer and has been associated with drug resistance in MM. However, the association of CDK6 expression with disease stage, genetic alterations, and outcome, has not been systematically investigated in large patient cohorts.

Methods

Here, we analyzed CDK6 protein expression using immunohistochemistry in 203 formalin-fixed paraffine-embedded (FFPE) tissue samples from patients with MM (n=142), solitary plasmacytoma (n=4) and without hematologic malignancy (n=4).

Results

We found that 61.5% of all MM specimens express CDK6 at various levels. CDK6 expression increased with progression of disease with median 0% CDK6 positive plasma cells (range 0-15%) in MGUS to 30% (range 0-100%) in newly diagnosed MM up to 70% (range 0-100%) in relapsed cases. The highest CDK6 expression (72.5%, range 0-100%) was observed in extramedullary myeloma, a highly aggressive and treatment-resistant manifestation of MM. Analyses of serial samples from same patients revealed that CDK6 expression significantly increased in lenalidomide-treated patients and not in those who had no lenalidomide therapy. Further, we observed that patients who underwent lenalidomide-comprising induction therapy had a significantly shorter progression-free survival when their samples were CDK6 positive.

Conclusion

These data support that CDK6 protein expression is a marker for aggressive and drug-resistant disease and describe a potential drug target in MM.

DGP18.06

Molecular alterations of primary refractory diffuse large B-cell lymphoma/high grade B-cell lymphoma with MYC- and BCL2- rearrangement and MYC- and BCL6- rearrangement as potential targets for personalized therapy.

P. Lohneis¹, H. M. Witte^{2,3,4}, A. Fährlich^{4,5,6}, J. Riedel^{2,4}, A. Küstner^{4,5,6}, J. Ketzer^{2,4,7}, N. von Bubnoff^{2,4}, H. Merz¹, N. Gebauer^{2,4}, H. Busch^{4,5,6}, A. Feller¹

¹Hämatopathologie Lübeck, Lübeck, Germany, ²Universitätsklinik Schleswig-Holstein, Campus Lübeck, Klinik für Hämatologie und Onkologie, Lübeck, Germany, ³Bundeswehrkrankenhaus Ulm, Klinik für Hämatologie und Onkologie, Ulm, Germany, ⁴Universitätsklinik Schleswig-Holstein, Campus Lübeck, University Cancer Center Schleswig-Holstein, Lübeck, Germany, ⁵Universität zu Lübeck, Group for Medical Systems Biology, Lübeck, Germany, ⁶Universität zu Lübeck, Institut für Kardiogenetik, Lübeck, Germany, ⁷Universitätsklinik Schleswig-Holstein, Campus Lübeck, Klinik für Kinder- und Jugendmedizin, Lübeck, Germany

Questions/Background

Die etablierten Immunochemotherapie-Regime führen bei diffusen großzelligen B-Zell-Lymphomen/ high grade B-Zell-Lymphomen mit MYC- und BCL2- bzw. MYC- und BCL6-Rearrangements (DLBCL/HGBL-MYC/BCL2/BCL6) zu relativ hohen Rückfallraten oder primär refraktären Erkrankungen.

Es gibt zunehmend Belege für den klinischen Nutzen von molekularen Tumorboards (MTBs) für Patienten mit soliden Tumoren in einem fortgeschrittenen Erkrankungsstadium. Maligne hämatologische Neoplasien sind in den MTBs eher unterrepräsentiert. Wir haben in einem MTB-ähnlichen Ansatz versucht, personalisierte Behandlungsansätze für DLBCL/HGBL-MYC/BCL2/BCL6 aufgrund unserer bereits publizierten molekularen Daten [1] zu identifizieren.

Methods

In dieser Proof-of-Concept-Studie wenden wir einen MTB-ähnlichen Ansatz bei primär refraktären DLBCL/HGBL-MYC/BCL2/BCL6-Patienten (n=19) auf der Grundlage unserer zuvor veröffentlichten Whole Exome Sequencing (WES)-Daten an. Für die Annotation der genomischen Veränderungen wurde die für die klinische Routinediagnostik zertifizierte institutionelle MTB-Pipeline (University Cancer Center Schleswig-Holstein: UCCSH) verwendet. Es wurde eine konsekutive Datenbankrecherche und Annotation nach etablierten Evidenzstufen für immunologisch und molekular stratifizierte Therapien durchgeführt.

Results

Wir haben 14 DLBCL/HGBL-MYC/BCL2 und 5 DLBCL/HGBL-MYC/BCL6 eingeschlossen. In 16 der 19 untersuchten Lymphome konnten wir personalisierte Behandlungsansätze mit einer NCT/DKTK-Evidenzstufe von m2A oder höher identifizieren. Wir haben 14 Mutationen in Chromatin-Modifikatoren bzw. epigenetischen Modifikatoren wie EZH2 oder IDH1 detektiert, die als mögliche therapeutische Ziele eingestuft wurden. Darüber hinaus wies ein Fall BRCAness auf, die eine Therapie mit einem PARP-Inhibitor

nahelegt. Jedes empfohlene Therapeutikum war entweder von der FDA und/oder der EMA zugelassen oder zumindest für ein beschleunigtes Zulassungsverfahren der FDA/EMA vorgesehen.

Conclusion

In der Mehrzahl der primär refraktären HGBL-DH/TH-Fälle konnten wir durch den Einsatz eines "virtuellen" MTB-Ansatzes potenzielle personalisierte Behandlungsansätze für DLBCL/HGBL-MYC/BCL2/BCL6 identifizieren. Unsere Ergebnisse unterstreichen das Potenzial der molekularen Pathologie bei dieser schwer zu behandelnden Entität in einem frühen Stadium der Behandlungssequenz.

Literaturangaben:

[1] Künstner, A. et al., (2022), Mutational landscape of high-grade B-cell lymphoma with MYC-, BCL2 and/or BCL6 rearrangements characterized by whole-exome sequencing, *Haematologica*

DGP18.07

Mutational landscape of gastrointestinal T-cell lymphoma from Latin America

I. A. Montes Mojarro¹, A. Rau¹, J. Delgado², A. F. Ramirez-Ibarguen³, M. Guerrero⁴, S. Casavilca Zambrano⁴, G. Cualco⁵, M. V. Ortega⁵, E. A. Krowicki⁶, B. Rojas Mena⁷, H. García Rivello⁸, J. P. Santino⁸, A. Vijnovich-Barón⁹, M. F. Metrebian¹⁰, M. Narbaitz¹⁰, C. Barrionuevo⁴, C. Lome Maldonado³, I. Bonzheim¹, F. Fend¹, L. Quintanilla-Martinez¹

¹University Hospital Tübingen, Eberhard-Karls-University, Institute of Pathology and Neuropathology and Comprehensive Cancer Center Tübingen, Tübingen, Germany, ²Instituto Nacional de Ciencias Médicas y Nutrición Dr. Salvador Zubirán, Department of Pathology, Mexico city, Mexico, ³Instituto Nacional de Cancerología, Department of Pathology, Mexico city, Mexico, ⁴Instituto Nacional de Enfermedades Neoplásicas, Department of Pathology, Lima, Peru, ⁵Diagnostic SRL, Montevideo, Uruguay, ⁶Dr. Cosme Argerich General Hospital, Buenos Aires, Argentina, ⁷Hospital Calderón Guardia, Department of Pathology, San Jose, Costa Rica, ⁸Hospital Italiano de Buenos Aires, Department of Pathology, Buenos Aires, Argentina, ⁹Centro de Patología y Citología (CEPACIT), Buenos Aires, Argentina, ¹⁰Instituto de Investigaciones Hematológicas, Academia Nacional de Medicina, Department of Pathology, Buenos Aires, Argentina

Questions/Background

Primary gastrointestinal T-cell lymphomas (GI-TCL) are rare, usually aggressive non-Hodgkin lymphomas. Studies in Asian and European populations have described their main biological, molecular and clinical features [1]. However, corresponding data from Latin America are missing.

Methods

We studied 40 cases of primary GI-TCL from 10 different centers in Latin America. All cases were examined by H&E, immunohistochemistry (CD3, CD4, CD8, CD5, Beta F-1, TCR delta, CD103, CD30, CD56) and EBERs ISH. 29 cases with sufficient DNA quality were sequenced using an NGS custom AmpliSeq panel including *STAT3*, *STAT5B*, *JAK1*, *JAK3*, *TP53*, *SETD2*, *KMT2D*, *DDX3X*, *RHOA*, *PIK3CD*, *ARID1A*, *CCR4*, *FYN*, *CARD11*, *TET2*, *TNFAIP3*, *BCOR*, *PLCG1*, *VAV1*, *DNMT3A*. To validate pathogenic *SETD2* mutations, immunohistochemistry for H3K36me3 was performed.

Results

Enteropathy-associated T-cell lymphoma (EATL) was the most frequent diagnosis in 16/40 cases, followed by monomorphic intestinal epitheliotropic T-cell lymphoma (MEITL, 9/40) and extranodal NK/T-cell lymphoma, nasal type (ENKTCL, 9/40). Indolent T-cell lymphoproliferative disorder of the gastrointestinal tract (IT-LPD) and intestinal T-cell lymphoma not otherwise specified (ITCL-NOS) were rare, two cases of each. The remaining two cases remained unclassified. Interestingly, cases of EATL were common in Argentinians, while ENKTCL was prevalent in Mexicans. All EATL cases showed a CD4/CD8/CD5+ phenotype, with CD30 positivity in 12/16 and CD103 positivity in 8/16, whereas half of the MEITL cases showed a CD8/CD56/TCR $\gamma\delta$ + immunophenotype. EATL mutational signature was characterized by recurrent *JAK1-3/STAT3* mutations (7/13), followed by *DDX3X* (4/13) and *TP53* (4/13). *DDX3X* and *TET2/TNFAIP3* mutations were frequent and concurrent in 4/13 cases, probably indicating a history of refractory celiac disease type II. *SETD2* mutations were exclusive to MEITL and confirmed by lack of H3K36 trimethylation by immunohistochemistry. ENKTCL cases show frequent mutations in the *JAK3/STAT3* pathway (3/9) and in *DDX3X* (2/9). ITLPD-GIT cases lacked mutations in the examined genes.

Conclusion

GI-TCL in Latin America show a mutational signature comparable to European and Asian series. The distribution of the different entities in Latin America reflects the variable proportion of ethnic Native Americans in the population. We confirmed that lack of H3K36me3 expression correlates with *SETD2* alterations, being a useful tool in the diagnosis of MEITL.

Literaturangaben:

[1] Jaffe ES, (2020), T-cell and NK-cell neoplasms of the gastrointestinal tract - recurrent themes, but clinical and biological distinctions exist., *Haematologica.*, 1760-1762., 105(7), doi: 10.3324/haematol.2020.252924.

DGP18.08

Comparative molecular characterization of primary extramedullary plasmacytoma and extramedullary manifestations of multiple myeloma

A.-L. Wilhelmi, A. Vogelsberg, F. Otto, B. Mankel, I. Bonzheim, F. Fend

Institute of Pathology and Neuropathology, University Hospital and Comprehensive Cancer Center Tuebingen, Tuebingen, Germany

Questions/Background

Multiple myeloma (MM) is one of the most common hematologic neoplasms. Extramedullary manifestations of MM (EMM) often appear in advanced stages with a poor prognosis. Primary extramedullary plasmacytoma (EMP) must be distinguished from EMM as it represents a localized clonal plasma cell proliferation without apparent BM involvement or other hallmarks of MM. Despite morphological and phenotypical similarities, EMP has a much better prognosis. The genetic profile of EMP is largely unknown. The aim of this study is to compare the mutational profiles of EMP and EMM to decipher the basis for their different clinical behavior.

Methods

We searched for formalin-fixed, paraffin-embedded cases diagnosed as EMP or EMM in the archives of the Institute of Pathology of Tuebingen University Hospital. In addition to the standard workup, all samples were immunostained for MIB-1, CD56, Cyclin D1, P53, and MYC. Fluorescence in situ hybridization (FISH) was performed to investigate hyperdiploidy, immunoglobulin heavy chain (IGH) translocations, as well as 1q, 1p, and 17p13 (*TP53*) alterations. Next Generation Sequencing (NGS) was used to analyze 89 genes relevant to the oncogenesis of MM.

Results

A total of 30 cases was identified, including 14 EMM and 16 EMP. FISH analysis of 24 samples demonstrated alterations of the IGH locus including translocation in seven EMP and six EMM samples. Hyperdiploidy, defined as gains of at least two of the three investigated chromosomes 5, 9, and 15, was found in five EMP and nine EMM. Additionally, five EMM and two EMP had gains of 1q and 1p, suggesting polysomy of chromosome 1. Regarding secondary genetic events, two EMP and one EMM showed a 1q gain and 1p loss, while isolated gains of 1q were found in two EMM. A 17p13 deletion was detected in two EMM and none of the EMP lesions, whereas three EMP and two EMP showed gains of chromosome 17. Preliminary NGS data showed lower average mutation counts (mean 1,12) in EMP lesions compared to EMM (mean 1,75) per case. EMM showed mutations in genes typically associated with progressed MM including *KRAS*, *NRAS*, *RB1*, and *TP53*, which were absent in EMP.

Conclusion

Consistent with its more indolent course, our data suggest that EMP shows a different and less complex spectrum of genetic alterations compared to EMM, which typically carries mutations associated with advanced disease. These features could potentially be used to predict the clinical course in cases where the distinction between EMP and EMM is difficult.

DGP20 Gemeinsame Sitzung DRG und DGP II: KI in Radiologie und Pathologie

DGP20.02

AI in applied clinical radiology.

D. Truhn

Universitätsklinikum Aachen, Klinik für Diagnostische und Interventionelle Radiologie, Aachen, Germany

With the advent of ever more powerful AI tools, their application in clinical routine comes within reach. In this

lecture, a short overview over the potential applications and limitations of such tools in radiology will be given and an outlook will be provided of how AI might enable clinical radiologists and clinicians to become more efficient.

DGP20.03

The fatal trajectory: beyond Covid-19

D. Jonigk

Uniklinik der RWTH Aachen, Institut für Pathologie, Aachen, Germany

COVID-19 has been associated with a range of illness severity, ranging from minimal symptoms to life-threatening multisystem organ failure. The severe forms of COVID-19 appear to be associated with an angiocentric or vascular phase of the disease. The mosaic radiographic appearance of COVID-19 lungs reflects the secondary lobule — the lung anatomic compartment that is the watershed of the pulmonary and bronchial circulation. The length of hospitalization is associated with increased intussusceptive angiogenesis. This is associated with enhanced angiogenic, and fibrotic gene expression demonstrated by molecular profiling and metabolomic analysis. Increased plasma fibrosis markers correlate with their pulmonary tissue transcript levels and predicted disease severity. Plasma analysis confirm distinct fibrosis biomarkers (TSP2, GDF15, IGFBP7, Pro-C3) that predicted the fatal trajectory in COVID-19. Irreversible tissue ischemia induces fibrotic changes in the lung that are associated with long-haul COVID-19 alterations and clinical symptoms.

In all this, COVID-19 can serve as a template for the holistic and three-dimensional analysis of parenchyma remodeling. Further investigations should be conducted to elucidate the involvement of the secondary pulmonary lobules in concert with alterations of ventilation–perfusion mismatch and increased alveolar ventilation/perfusion ratio heterogeneities in alveolar dead space, not only of COVID-19 patients, but in other respiratory diseases.

DGP20.04

Colorectal cancer screening aided by AI

A. Kiss¹, E. Kontsek¹, A. Pesti¹, B. Sulyok², A. Olar², I. Csabai², P. Pollner³

¹Semmelweis University, Department of Pathology, Forensic and Insurance Medicine, Budapest, Hungary, ²Eötvös Lorand University, Department of Physics of Complex System, Budapest, Hungary, ³Hungarian Academy of Sciences, MTA-ELTE Statistical and Biological Physics Research Group, Budapest, Hungary

Questions/Background

Hungary has the highest rates of colorectal cancer morbidity and mortality worldwide, which prompted the initiation of a national screening program in 2018 to reduce the mortality of the disease. The program involves conducting colonoscopies on patients who test positive for fecal occult blood. To expedite the process and reduce the number of unnecessary biopsies, a machine learning-based algorithm is being developed to pre-filter cases that are likely to be true negatives. This algorithm will use artificial intelligence (AI) approaches on large datasets.

Methods

A total of 2,300 colorectal biopsies were obtained from the archive of the Department of Pathology, Forensic and Insurance Medicine Semmelweis University. The slides were scanned using a P1000 digital slide scanner manufactured by 3DHitech.. A 40x magnification objective was used for scanning. A Convolutional Neural Network (CNN) was trained on 2000 slides, and 300 slides were set aside for testing. The annotations were done in three stages: global, textual annotation for general diagnosis, local, textual annotation for specific tissue parts, and graphical, pixel-level annotation for local tissue parts.

Results

For the categorical conditions (*negative*, *non-neoplastic lesion*, *adenoma*, *CRC*) the confusion matrix shows that the model can accurately separate *CRC* and *adenoma* samples from each other and from the samples without *neoplasia*. Out of the 217 adenomas were 187 rightly classified by AI, however, 20 cases were regarded as non-neoplastic lesions and 10 cases as CRCs. All CRCs except one (listed as non-neoplastic lesion) were classified correctly by AI. However, the separation of the *negative* and the *non-neoplastic lesion* samples are less sufficient, 32 negative cases were classified as non-neoplastic lesion by the neural network. Altogether, the separation of *negative* samples from the *non-neoplastic lesions* have limited importance during colorectal cancer screening.

Conclusion

Incorporating a decision support module into the digital pathology software infrastructure could help reduce the workload on pathologists and would allow doctors to focus on the more complex cases and provide necessary supervision to the AI when needed. The fact, that the model predicts probabilities, enables the possibility of selecting a probability threshold, which can trade sensitivity for specificity based on the need.

DGP21 Molecular diagnostics in hematological neoplasms

DGP21.01

Liquid biopsy in lymphoma

D. Rossi

Institute of Southern Switzerland, Bellinzona, Switzerland

The rapid evolution of genomic technologies over the last years has led to the development of different methods for the detection, measurement and analysis of tumor cell-free DNA fragments (ctDNA) which are shed into body fluids by neoplastic cells and circulate at a low concentration in plasma and cerebrospinal fluid. In cancer patients, the proportion of tumor-derived cfDNA is defined as circulating tumor DNA. This analysis is also known as liquid biopsy. Liquid biopsy is a minimally invasive and highly versatile biomarker that overcomes fundamental limitations of imaging scans and tissue biopsies and may aid clinical decision-making in lymphoma. For this reason, this tool may have several clinical applications in terms of diagnosis, prognosis, and monitoring of minimal residual disease. However, there are still methodological issues that need to be resolved and further studies are needed to standardize its use and establish clinical utility. We highlight the key established principles regarding the liquid biopsy in lymphoma and emphasize the important research questions and future directions. We discuss some of the controversies around this method and its potential clinical applications.

DGP22 Sensortechniken zur Gewebeanalyse, AI in der Pathologie (mit DGCH)

DGP22.01

Methods, applications and future perspectives of intraoperative tissue identification

M. Enderle

Erbe Elektromedizin GmbH, Tübingen, Germany

In the last century there was an intensive development of technologies for intraoperative tissue identification and differentiation. The applications are manifold with a core purpose to identify target structures while preserving adjacent tissue thereby following a general paradigm of minimal-invasive medicine. Particularly in oncology, a further asset of these technologies is the identification or classification of neoplastic tissue to support and improve therapy, e.g. in breast cancer surgery.

Many technologies under consideration make use of the different physical characteristics of treated tissues, such as induced fluorescence, optical coherence or electrical impedance.

Recent developments are focusing on moving from *ex-vivo* to *in-situ* and from asynchronous to real-time assistance of the clinicians as for example by means of optical emission spectroscopy. Refinements of existing and creation of new methods will include AI tools to make them more powerful while reducing the inter-operator variability in operative interventions. This talk will address several aspects of the usage and suitability of these technologies for intraoperative, therapy-supporting application.

DGP22.02

Multisensory intraoperative tissue recognition - how we teach medical technology 'fine sense'

M. Weiß

Universitätsklinikum Tübingen, Universitäts-Frauenklinik, Tübingen, Germany

Novel surgical techniques are being developed with the goal of reducing invasiveness, complications, and treatment duration while maximizing treatment effectiveness. Reliable identification of target structures and surrounding tissue is crucial to achieve these objectives. However, there are significant advancements in pre- and postoperative diagnostics for distinguishing between benign and malignant tissue structures - like advanced imaging systems for precise guidance in preoperative decision-making – reliable technologies for intraoperative tissue identification are still missing. Consequently, additional information would be provided to assist surgeons in making critical decisions between resection and tissue preservation. This is also the goal of a recently installed DFG graduate college 2543 of the Universities within the Interuniversity Center for Medical Technologies Stuttgart - Tübingen (IZST).

Multisensory intraoperative tissue recognition may include the integration of data from multiple sensors to ensure reliable tissue identification including optical tissue properties as well as spectroscopic, electrical, and mechanical parameters of the tissue. This talk is focused on first practical experiences in-vitro and in-vivo with different technologies based on Raman spectroscopy, Hyperspectral imaging, and image processing algorithms.

By combining novel multimodal sensor systems with artificial intelligence and machine learning techniques, there is great potential for new procedures to differentiate between tissues beyond what individual sensor data can provide. These methods may complement the gold standard of intraoperative tissue identification, namely frozen section diagnostics.

DGP22.03

Stimulated Raman Histology for evaluation of oral squamous cell carcinoma

D. Steybe¹, P. Poxleitner¹, S. Timme², M. Metzger¹, P. Voss¹, K. Kurowski², J. Strähle³, J. Beck³, M. Werner², R. Schmelzeisen¹, **P. Bronsert²**

¹Department of Oral and Maxillofacial Surgery, Freiburg im Breisgau, Germany, ²Institute for Surgical Pathology, Freiburg im Breisgau, Germany, ³Department of Neurosurgery, Freiburg im Breisgau, Germany

Questions/Background

Intraoperative histopathological differentiation between neoplastic and non-neoplastic tissue is of high relevance in surgical treatment of oral cancer. The aim of the present study was to evaluate Stimulated Raman Histology (SRH) with conventional H&E stained frozen sections.

Methods

80 tissue samples were obtained from 8 OSCC patients. Using conventional H&E stained frozen sections and SRH, these samples were analyzed for the presence of neoplastic tissue and for further sub-classification of non-neoplastic tissue into normal mucosa, connective tissue, muscle tissue, adipose tissue, salivary gland tissue, lymphatic tissue and inflammatory cells.

Results

38 out of 80 samples were classified as OSCC. Regarding the differentiation between neoplastic and non-neoplastic tissue, high agreement between H&E and SRH and high accuracy of SRH were demonstrated. Considering the sub classification of non-neoplastic tissues, SRH performance was dependent on the type of tissue.

Conclusion

The presented data demonstrate the capability of SRH to differentiate between neoplastic and non-neoplastic tissues in oral cancer patients; thus, this technology has the potential to be applied for intraoperative evaluation of surgical margins. However, further prospective studies and guidelines for interpretation of SRH images from the head and neck region are required.

DGP22.04

Sectioning-free H&E imaging with a mobile multiphoton microscope

M. Strauch¹, J. P. Kolb¹, C. Rose², N. Merg³, J. Hundt³, C. Kümpers⁴, S. Perner⁵, S. Karpf⁶, R. Huber^{1,6}

¹Medizinisches Laserzentrum Lübeck GmbH, Lübeck, Germany, ²Dermahistologisches Einsendelabor Lübeck, Lübeck, Germany, ³Universität zu Lübeck, Lübecker Institut für Experimentelle Dermatologie (LIED), Lübeck, Germany, ⁴Universitätsklinikum Schleswig-Holstein (UKSH), Institut für Pathologie, Lübeck, Germany, ⁵MVZ HPH Institut für Pathologie und Hämatopathologie GmbH, Hamburg, Germany, ⁶Universität zu Lübeck, Institut für Biomedizinische Optik, Lübeck, Germany

Questions/Background

Recent advances in multiphoton fluorescence laser technology have led to a widening range of possible applications in the histological examination of bulk tissue[1][2][3][4]. Histological images can be obtained

from bulk tissue without the need for freezing or a microtome. Different stains have been evaluated depending on the laser technology, but the classic stains haematoxylin and eosin have been difficult to observe using fluorescence microscopy. We optimised a special laser system to see if we could use the classic H&E stains, which are cheap and readily available.

Methods

We are developing a proof-of-principle prototype of a mobile microscope for imaging bulk tissue directly in the operating room. The tissue is examined as soon as it is removed from the patient, quickly stained with H&E and then placed directly into the microscope. The microscope scans the tissue and produces a digital H&E image. The image can then be interpreted by a pathologist directly on the instrument's screen or remotely. So far, most of the tissue samples, we investigated, have been porcine organs, but we have started to look at some first human samples originating from brain, lung, and skin surgery.

Results

We developed a 6-minute H&E staining protocol that stains the surface and superficial layers of a biopsy. By changing the orientation of the sample, it can be examined from different directions. The sectioning capability of the microscopy technique, as indicated in Figure 1, is inferior to paraffin sections but shows good overall agreement with frozen sections.

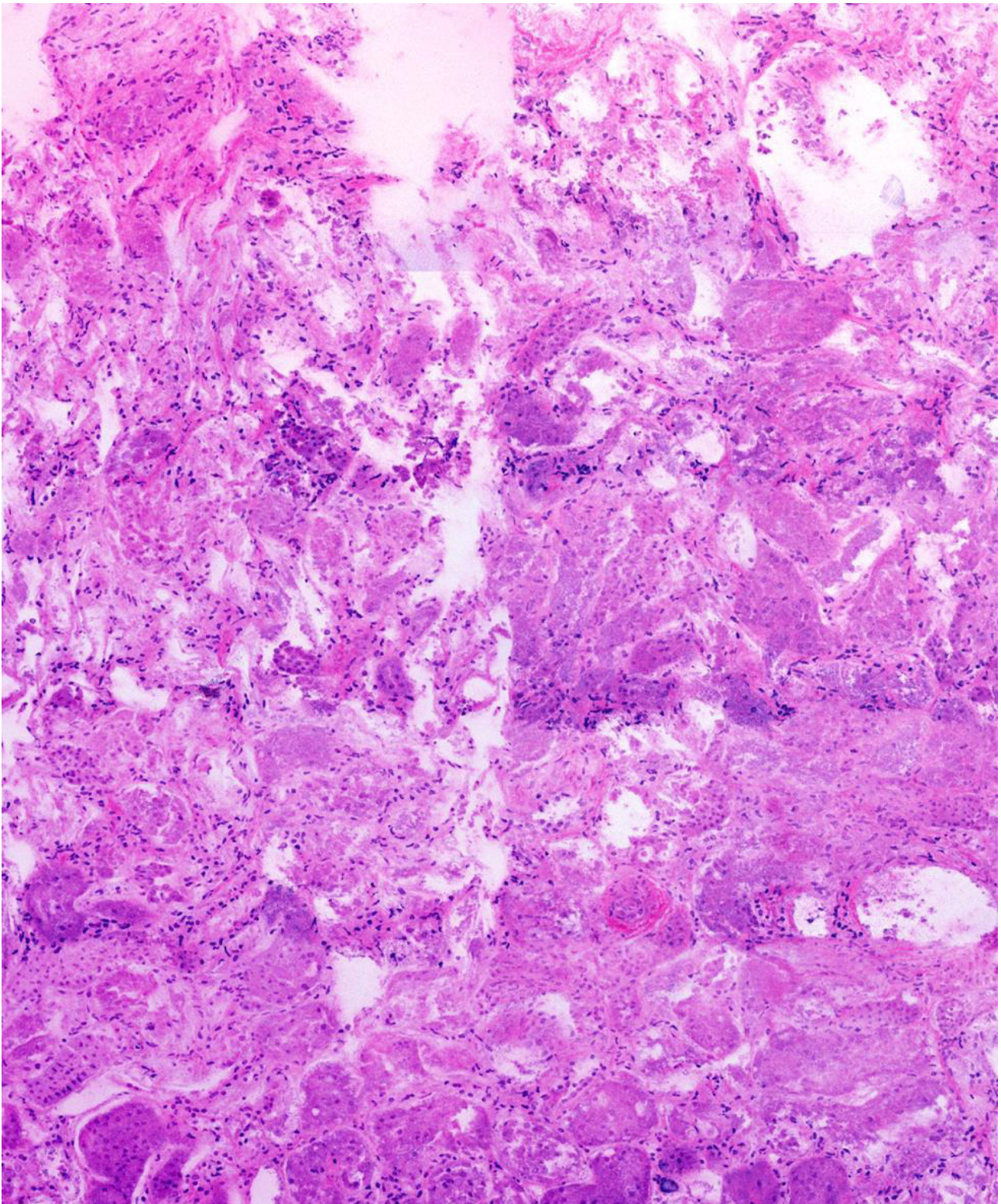


Figure 1: The image region shows an example of a 1.6mm x 2mm of a bulk piece of H&E-stained porcine kidney (~2mm thick). The virtual section shown is recorded ~20µm below the surface of the tissue.

Conclusion

We have created digital H&E images of fresh, bulk H&E-stained tissue without the need for sectioning. The images are therefore free of freezing and sectioning artifacts and can therefore be used for tissue that is generally difficult or impossible to study with frozen sections. The digital images can be sent directly to the pathologist or displayed in the operating theatre, eliminating transport time, a major cause of surgical delays in most hospitals. This reduces the time needed to evaluate biopsies during surgery to 15-30 minutes, depending on the size and number of biopsies.

Literaturangaben:

- [1] Helmchen, F., Denk, W., (2005), Deep tissue two-photon microscopy, *Nat Methods*, 2(12):932-940, <https://doi.org/10.1038/nmeth818>
- [2] Tao YK, Shen D, Sheikine Y, et al., (2014), Assessment of breast pathologies using nonlinear microscopy, *PNAS*, 111(43):15304-15309, <https://doi.org/10.1073/pnas.1416955111>
- [3] Cahill LC, Giacomelli MG, Yoshitake T, et al., (2017), Rapid virtual hematoxylin and eosin histology of breast tissue specimens using a compact fluorescence nonlinear microscope, *Lab Invest*, 98(1):150-160, <https://doi.org/10.1038/labinvest.2017.116>
- [4] Cahill LC, Wu Y, Yoshitake T, et al., (2020), Nonlinear microscopy for detection of prostate cancer: analysis of sensitivity and specificity in radical prostatectomies, *Mod Pathol*, 33(5):916-923, <https://doi.org/10.1038/s41379-019-0408-4>

DGP23 Freie Vorträge IV - Multiparametrische Gewebeanalyse

DGP23.01

Multiomic spatial phenotyping of a partial immunotherapy response in head and neck cancer

S. Seidel¹, J. Monkman², K. O'Byrne³, B. Hughes⁴, N. Jahveri¹, N. Ma¹, B. Ben Cheikh¹, O. Braubach¹, A. Kulasinghe²

¹Akoya Biosciences, Marlborough, MA, United States of America, ²The University of Queensland, Brisbane, Queensland, Australia, ³The Princess Alexandra Hospital, Brisbane, Queensland, Australia, ⁴The Royal Brisbane Women's Hospital, Brisbane, Queensland, Australia

Questions/Background

Immune check point inhibitors (ICI) comprise promising treatments for mucosal head and neck squamous cell cancer (HNSCC). Emerging successes with anti-PD-1/PD-L1 ICI therapy have led to durable responses and prolonged survival but currently available diagnostic biomarkers have limited value, leading to poor stratification of patients prior to treatment regimens. New predictive biomarkers are thus needed to guide patient selection for highly targeted ICI therapies. The tumor microenvironment (TME) composition and cellular architecture is key to understanding immune responsive and resistant phenotypes and is the subject of this study.

Methods

We used single-cell, multiomic spatial phenotyping to characterise the TME of metastatic/recurrent HNSCC tumors from a cohort of n=40 patients treated with Pembrolizumab / Nivolumab. The discovery cohort consisted of patients who had complete vs. partial vs. stable vs. progressive responses to ICI therapy. We first analyzed tissues using an ultrahigh-plex antibody panel (100+antibodies), imaged with the PhenocyclerFusion platform (Akoya Biosciences). We then conducted additional whole-slide spatial biology experiments with a mixed protein / RNA detection panel to obtain multiomic spatial signatures that could offer cues as to which treatment matches best with certain outcome groups.

Results

Our study identified stromal, immune, and metabolic tissue signatures associated with resistance to immunotherapy. Immune profiling data identified defined tumor areas of high and low immune infiltration and these correlated well with differences in metabolic activity. Furthermore, RNA-based molecular profiling allowed us to map distinct chemokine environments within dissimilar tumor regions and to identify potential drivers of immune infiltration vs. exclusion.

Conclusion

Our study demonstrates the power of unbiased multiomic spatial phenotyping with whole-slide imaging to identify biomarkers associated with response to ICI therapy in HNSCC.

DGP23.02

Optimized Preanalytics for Deep Proteomic Profiling of FFPE Tissue

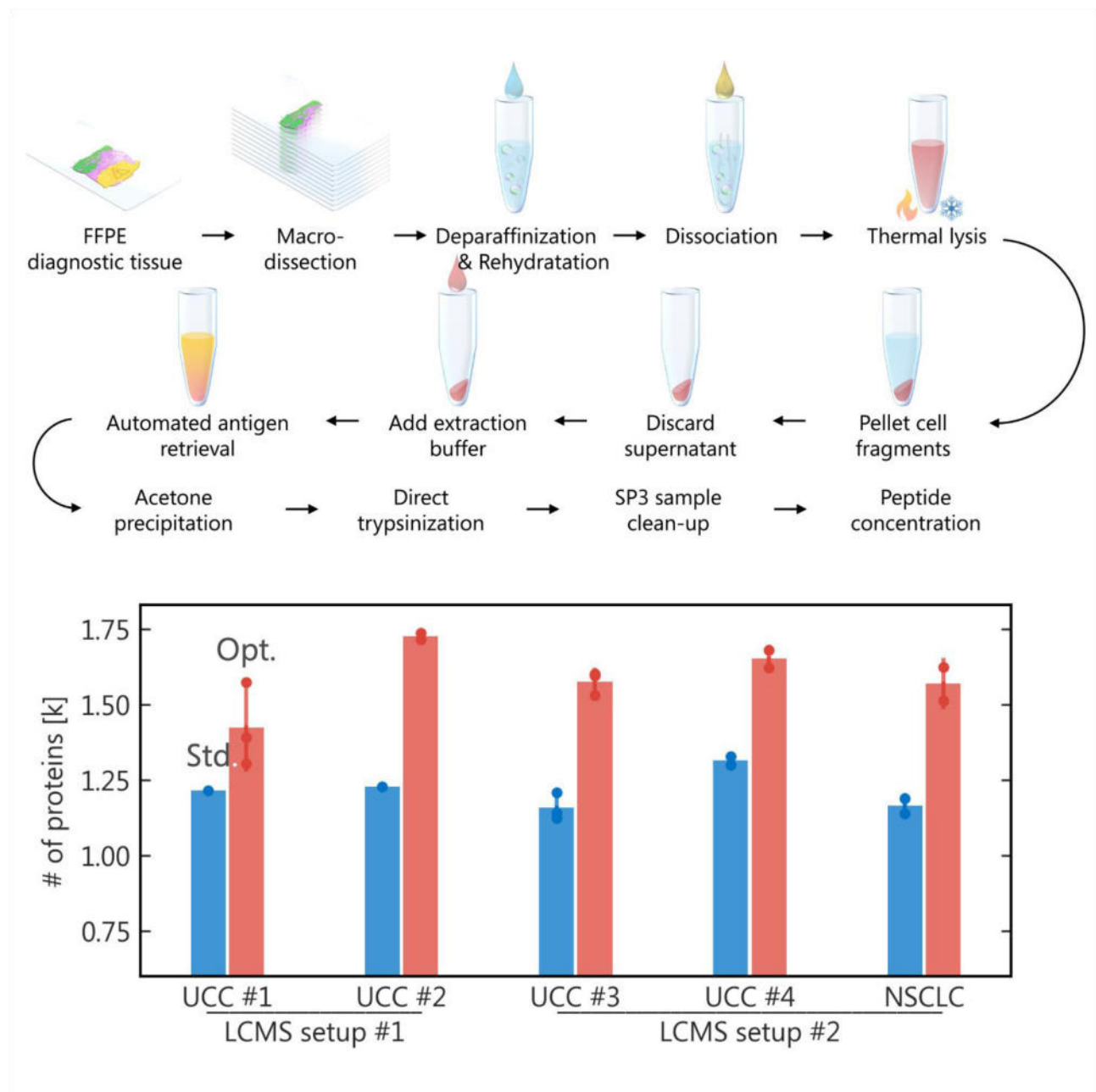
F. F. Dreßler^{1,2}, C. Krisp³, S. Hinrichs², B. Michael², P. Mackedanz², M. Schlottfeldt², H. Schlüter⁴, S. Perner^{2,5}, R. Zubarev^{6,7}, P. Wolf^{8,9}, Á. Végvári⁷

¹Charité - Universitätsmedizin Berlin, Institut für Pathologie, Berlin, Germany, ²Universität zu Lübeck und UKSH Campus Lübeck, Institut für Pathologie, Lübeck, Germany, ³Universitätsklinikum Hamburg-Eppendorf, Institut für Klinische Chemie und Labormedizin, AG Massenspektrometrie und Proteomics, Hamburg, Germany, ⁴Universitätsklinikum Hamburg-Eppendorf, Institut für Klinische Chemie und Labormedizin, AG Massenspektrometrie und Proteomics, Institut für Pathologie, Hamburg, Germany, ⁵Pathologie des Forschungszentrum Borstel, Leibniz Lungenzentrum, Borstel, Germany, ⁶Karolinska Institutet and SciLifeLab, Stockholm, Sweden, ⁷Karolinska Institutet, Division of Physiological Chemistry I, Department of Medical Biochemistry and Biophysics, Stockholm, Sweden, ⁸Universitätsklinikum Freiburg, Klinik für Urologie, Freiburg, Germany, ⁹Universität Freiburg, Freiburg, Germany

Questions/Background

Liquid chromatography-coupled tandem mass spectrometry (LC-MS/MS) is the current gold standard technique for proteomic analyses. In complex biological, i.e. clinical samples, it is negatively affected by quantitative imbalances within the sample. These are caused by highly abundant proteins such as smooth muscle or extracellular matrix (ECM) proteins. Membrane proteins, key players in oncogenic signal transduction and metastatic processes, are even less accessible due to their reduced solubility, co-localization with structural and ECM proteins, and the geometric abundance imbalance (cytosolic proteins covering the cell volume exceed cell surface proteins by a dimension).

Methods



Graphical abstract

We applied standard membrane-enrichment assays to FFPE tissue. To overcome their severe limitations, we developed a novel extraction protocol. We enzymatically and mechanically disassembled the ECM (freeing the cell surface) and thermally disrupted the cells to produce cell fragments. FFPE samples are chemically glued together by the fixative, yielding pieces of cell membrane and organelles with attached cytosolic proteins. We pelleted these fragments, solubilized proteins, and included both solubilized proteins and fragments with residual (membrane) proteins in direct trypsinization. We compared our protocol to standard direct trypsinization on three different LC-MS/MS setups.

Results

Boa_Image_Frame assays failed for FFPE specimens, mostly due to sample loss. Using the example of four urothelial cancer and one non-small cell lung cancer specimen, we tested our protocol in label-free, single-

run, short-gradient experiments. Our protocol raised the number of all identified proteins by mean 30 %, with an over proportional increase in membrane proteins. Using tandem mass tag-labelled samples, we could confirm a specific increase of membrane protein abundances. Selecting highly specific enzymes, we could decrease unspecific protein degradation by more than half, down to regular levels.

Conclusion

Our optimized protocol increased analysis depth and the number of identified membrane proteins, which are highly relevant for targeted therapies.

DGP23.03

Kinetics of Proteome Alterations in Human Autopsy Tissues in Relation to Time After Death

É. Kocsmár¹, M. Schmid², M. Cosenza-Contreras², I. Kocsmár¹, M. Föll², L. Krey², B. A. Barta², G. Rácz¹, A. Kiss¹, M. Werner², O. Schilling², P. Bronsert², G. Lotz¹

¹Semmelweis University, Department of Pathology, Forensic and Insurance Medicine, Budapest, Hungary, ²University Medical Center, Institute of Surgical Pathology, Freiburg, Germany

Questions/Background

Protein expression is a key tool in both routine histological diagnostics and tissue-based research studies. Despite its widespread use, the extent of its applicability in post-mortem settings remains poorly understood. On the other hand, tissue samples obtained during autopsy can provide unique insights into advanced disease stages, particularly in cancer research.

In this study, our objectives were threefold: (i) to determine the maximum post-mortem interval (PMI) that permits accurate characterization of protein expression patterns, (ii) to examine organ-specific variations in protein degradation, and (iii) to assess whether certain proteins exhibit distinct degradation kinetics.

Methods

The proteome of human tissue samples obtained from routine autopsies was analyzed using liquid chromatography-tandem mass spectrometry (LC-MS/MS) to investigate the effect of post-mortem interval (PMI) on protein degradation. Tissue samples were collected from lungs, kidneys, and livers of deceased patients with different PMIs (6, 12, 18, 24, 48, 72, and 96 hours) with lack of specific diseases affecting the investigated organs.

Results

For kidney and liver, significant degradation of proteins became evident at 48 hours. For lung, the proteome composition was fairly unchanged at 48 h, and significant protein degradation was only detectable at 72 h, suggesting that degradation kinetics appear to be organ-specific. Our functional analyses suggest that proteins with similar post-mortem kinetics may not necessarily be grouped into groups with the same biological function. In the kidney, however, the over-representation of protein families with analogous structural motifs suggests that common structural features may contribute to the similarity in post-mortem dynamics of these proteins.

Conclusion

Our study shows that a longer post-mortem period can have a significant impact on proteome decomposition, but sampling within 24 h generally provides adequate proteome preservation, as degradation is within acceptable limits even in organs with faster autolysis. Understanding the biology behind the PMI-dependent changes of the proteome offers breathtaking opportunities for diagnostic and therapeutic improvements and paves the way for reliable protein-based diagnostics on human autopsy tissue samples.

DGP23.05

NGS analysis of pancreatic neck margin as ancillary tool for the detection of microscopic incomplete resections

B. Pawlowski, L. Häberle, F. Opitz, A. Yavas, W. Göring, I. Esposito

Institut für Pathologie, UKD Düsseldorf, Düsseldorf, Germany

Questions/Background

Pancreatic ductal adenocarcinoma (PDAC) is an aggressive tumor with dismal prognosis. High recurrence rates are in part related to incomplete resections. Therefore, histopathologic frozen section analysis of the pancreatic neck margin is usually performed during pancreatic surgery. The increasing availability of fast-track molecular analyses could render them suitable for application in intraoperative diagnostics. The aim of this study is to investigate whether additional molecular analyses of the pancreatic neck margin is superior to histopathological examination alone.

Methods

Formalin-fixed paraffin-embedded pancreatic neck margin specimens originally diagnosed as free of cancer obtained from patients who had undergone partial pancreatoduodenectomy for PDAC were retrospectively collected (n=32). Additionally, swabs of fresh pancreatic neck margins from frozen section examination were prospectively collected (n=32). All were subjected to next generation sequencing using the Cancer HotSpot Panel v2 (ThermoFisher Scientific, Waltham, USA). PDAC tissue from the central tumor area of the resected specimen was analyzed for reference.

Results

Pathogenic *KRAS* or *TP53* mutations were found in 13 margins (41%) in the retrospective cohort; in 11 cases (85%) mutations were concordant with those found in the tumor. In all cases, mutations were related to the presence of a neoplastic lesion, such as low-grade PanIN (n=10), cancer colonization of ductal structures (n=2) or high-grade intraductal papillary mucinous neoplasia (n=1) in the margin at histopathologic re-evaluation.

In the prospective cohort, 29 margins (91%) were tumor free at frozen section analysis. *KRAS* or *TP53* mutations were found in 16 originally tumor free margins (55%); however, only 9 mutations (41%) in the margin were concordant with those found in tumor tissue. Here, 14 mutation-positive cases of originally tumor free margins (88%) could be explained by the presence of precursor lesions, such as low-grade PanIN (n=10) and low-grade intraductal papillary mucinous neoplasia (n=1) or of invasive cancer (n=3) at histopathologic re-evaluation.

Conclusion

Molecular analysis of resection margin by next generation sequencing is an effective diagnostic method to screen pancreatic neck margins for the presence of precursor lesions or PDAC. However, the possibility of false-positive results questions its applicability in routine diagnostic procedures.

DGP23.06

TelePi: An affordable telepathology microscope camera system anyone can build and use

A. Youssef, A. Rosenwald, M. T. Rosenfeldt

University of Würzburg, Institute of Pathology, Würzburg, Germany

Questions/Background

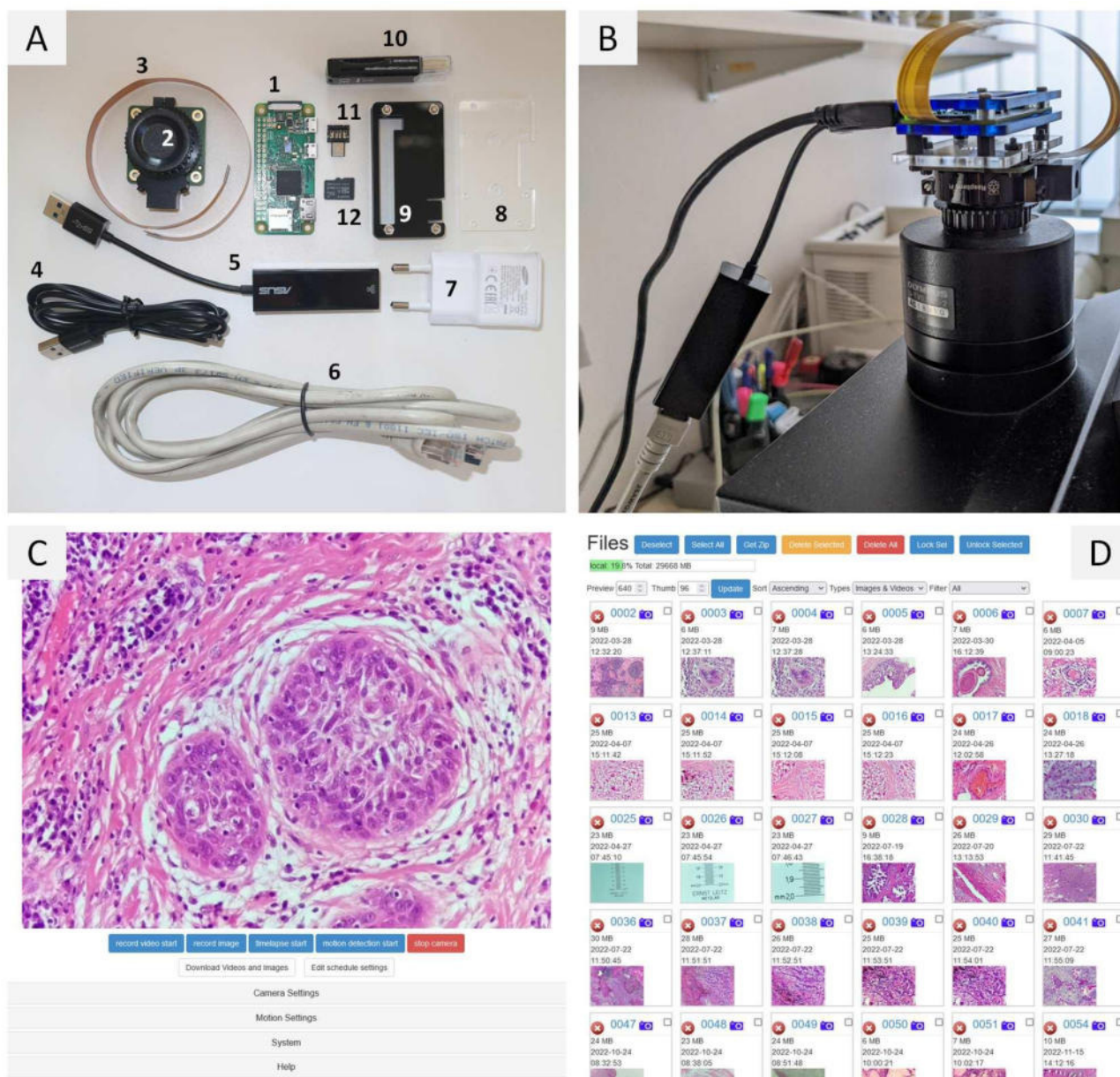
Telepathology facilitates histological diagnoses through sharing expertise between pathologists, with added benefits in terms of teaching and potential research collaborations [Ref1]. However, the upfront acquisition costs and ongoing service contracts are often prohibitive especially in low-resource settings [Ref2], [Ref4], where telepathology would especially be of paramount importance due to a frequent paucity of trained pathologists [Ref3].

Methods

We have constructed a telepathology camera system (TelePi) with a budget of < 120 € using the Raspberry Pi Zero and its High-Quality Camera Module. These readily available, off-the-shelf parts are mounted to a standard microscope and paired with open-source software on a Linux operating system. The system requires no additional hardware parts, maintenance costs or service contracts, has a small footprint and can be moved and shared across several microscopes, and is independent from other operating systems.

Results

TelePi uses a responsive and high-resolution web-based live stream which allows remote consultation between two locations. TelePi can serve as a telepathology system for remote diagnostics of frozen sections. Additionally, it can be used as a standard microscope camera and be paired with the open-source image analysis package, Fiji. This allows for example stitching of multiple images taken at high resolution into one large image that exceeds the field of view of the chosen objective. The quality of the TelePi system compared favorable to commercially available telepathology systems that exceed its cost by more than 125-fold. Additionally, images are of publication quality equal to that of a whole slide scanner which costs 800 times more.



Overview of TelePi. A) Required components for the hardware assembly. B) Assembled and running TelePi. C) The RPi Web Cam Interface showing a live image. D) Image and video download interface.

Conclusion

In summary, TelePi is an affordable, versatile and inexpensive camera system that potentially enables telepathology in low-resource settings without sacrificing image quality.

Literaturangaben:

- [Ref1] Weinstein, R. S.; Graham, A. R.; Richter, L. C.; Barker, G. P.; Krupinski, E. A.; Lopez, A. M.; Erps, K. A.; Bhattacharyya, A. K.; Yagi, Y.; Gilbertson, J. R., (2009), Overview of telepathology, virtual microscopy, and whole slide imaging: prospects for the future, *Hum Pathol*, 1057--69, 8, <https://pubmed.ncbi.nlm.nih.gov/19552937/>
- [Ref2] Orah, N.; Rotimi, O., (2019), Telepathology in Low Resource African Settings, *Front Public Health*, 264, <https://www.ncbi.nlm.nih.gov/pubmed/31572705>
- [Ref3] Stauch, G.; Raoufi, R.; Sediqi, A.; Dalquen, P.; Fritz, P.; Aichmuller, C.; Aichmuller-Ratnaparkhe, M.; Hubler, M., (2022), [Experiences with telepathology in northern Afghanistan : A 10-year success story], *Pathologie (Heidelb)*, 303-310, 4, <https://www.ncbi.nlm.nih.gov/pubmed/35238979>
- [Ref4] van Zyl, C.; Badenhorst, M.; Hanekom, S.; Heine, M., Unravelling 'low-resource settings': a systematic scoping review with qualitative content analysis, *BMJ Glob Health*, 6, <https://www.ncbi.nlm.nih.gov/pubmed/34083239>

The tissue microenvironment and the loss of TP53 induce the expression of the embryological transcription factor SIX1 in ductal pancreatic adenocarcinomas

M. Stoffel, E. Dingendorf, D. Kittel, G. Kristiansen, T. Lerbs
Institut für Pathologie, Universitätsklinikum Bonn, Bonn, Germany

Questions/Background

In our previous studies, we have shown that ductal pancreatic adenocarcinomas (PDAC) re-express the embryological transcription factor SIX1, and that SIX1 induces an epithelial-mesenchymal transition and cancer stem cell-phenotype in PDAC cell lines in vitro and in vivo. During its progression, PDAC typically show a loss in tumor suppressors like *TP53* and *SMAD4* and a desmoplastic stroma response with abundant anti-inflammatory M2 macrophages. This study explored whether the tissue microenvironment and losses in tumor suppressors regulate the expression of SIX1.

Methods

We deleted *TP53* and *SMAD4* via CRISPR-Cas9 in MIA Paca-2 cells and confirmed the successful deletion via flow cytometry and western blotting. We then measured the expression of *SIX1* on the gene regulatory and protein level via a luciferase reporter assay and flow cytometry. To test whether cytokines regulate *SIX1*, we additionally added TGF- β . Finally, we generated primary fibroblast cultures from patient samples and differentiated M2 macrophages from the peripheral blood, and co-incubated both with MIA Paca-2 cells, to explore whether cells of the tissue microenvironment alter the expression of SIX1. Each time, we measured the expression of SIX1 both on the gene regulatory level and the protein level via a SIX1 reporter assay and flow cytometry.

Results

Deleting *TP53* and *SMAD4* had opposite effects on the expression of *SIX1* on the gene regulatory and the protein level. While the loss of *SMAD4* decreased the promoter activity and protein expression of *SIX1*, the loss of *TP53* increased both; an increase that was further bolstered by adding TGF- β . In contrast, adding TGF- β to wild-type cells did not alter the expression of *SIX1*. In accordance with these results, both fibroblasts and M2 macrophages increased the expression of SIX1.

Conclusion

We show that typical changes in PDAC like the loss of *TP53* and the desmoplastic tissue microenvironment with its abundant M2 macrophages jointly upregulate *SIX1*. These findings suggest that SIX1 with its pro-tumorigenic functions is a potential therapeutic target for PDAC.

Normics: Improved Omics Data Normalization for Explorative Biomarker Studies

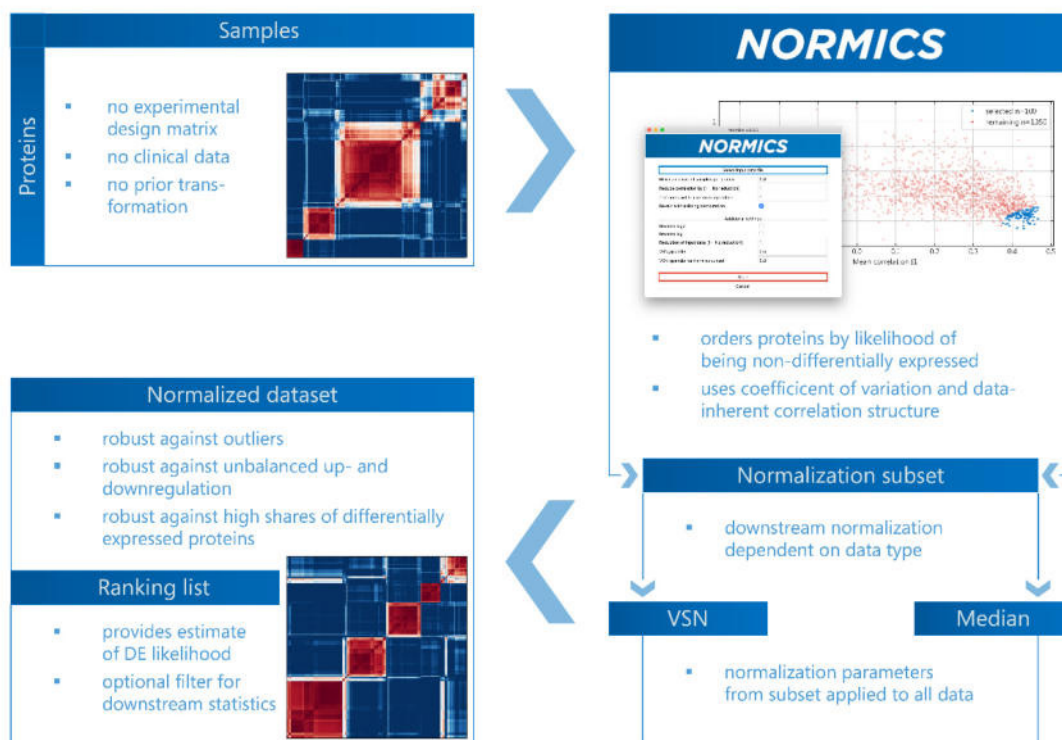
F. F. Dreßler^{1,2}

¹Charité - Universitätsmedizin Berlin, Institut für Pathologie, Berlin, Germany, ²Universität zu Lübeck und UKSH Campus Lübeck, Institut für Pathologie, Lübeck, Germany

Questions/Background

Several algorithms for the normalization of omics data are currently available, each based on a priori assumptions. Among these is the extent to which differential expression (DE) can be handled. This factor is unknown in explorative biomarker screens, yet highly relevant when the samples are biologically diverse - e.g., when different tumors or tumor stages are investigated or when tumor specificity is to be quantified by comparison to healthy tissue. At the same time, the increasing depth of omics analyses often requires the selection of subsets with a high probability of being DE to obtain meaningful results in downstream bioinformatical analyses.

Methods



Graphical abstract

Based on the relationship of technical variation and (true) biological DE of an unknown share of proteins, we propose the "Normics" algorithm: Proteins are ranked based on their expression level-corrected variance and the mean correlation with all other proteins. The latter serves as a novel indicator of the non-DE likelihood of a protein in a given dataset. Subsequent normalization is based on a subset of non-DE proteins only. No a priori information such as batch, clinical, or replicate group is necessary.

Results

Simulation data demonstrated robust and superior performance across a wide range of stochastically chosen parameters. Five publicly available spike-in and biologically variant datasets were reliably and quantitatively accurately normalized by Normics with improved performance compared to standard variance stabilization as well as median, quantile, and LOESS normalizations. In complex biological datasets Normics correctly determined proteins as being DE that had been cross-validated by an independent transcriptome analysis of the same samples. In both complex datasets Normics identified the most DE proteins. Cluster identification and separation of own proteomic cohort data was improved when based on Normics-selected DE proteins.

Conclusion

We demonstrate that combining variance analysis and data-inherent correlation structure to identify non-DE proteins improves data normalization. Boa_Image_Frame normalization algorithms can be consolidated against high shares of (one-sided) biological regulation. The statistical power of downstream analyses can be increased by focusing on Normics-selected subsets of high DE likelihood.

DGP23.09

μCT-based Identification of Relevant Tissue Structures in Paraffin Blocks

V. Stehl¹, M. Al Kallaa¹, A. Harbecke¹, J. Chen², M. Wiczorek², M. Thalwaththe Gedara³, S. Moser³, V. Heusinger-Heß³, M. Seidl¹

¹Institut für Pathologie, Universitätsklinikum Düsseldorf, Institut für Pathologie, Düsseldorf, Germany, ²ImFusion GmbH, München, Germany, ³Fraunhofer Ernst-Mach-Institut, Efringen-Kirchen, Germany

Questions/Background

In Germany 500,000 people are diagnosed with cancer every year. A key role is played by the approximately

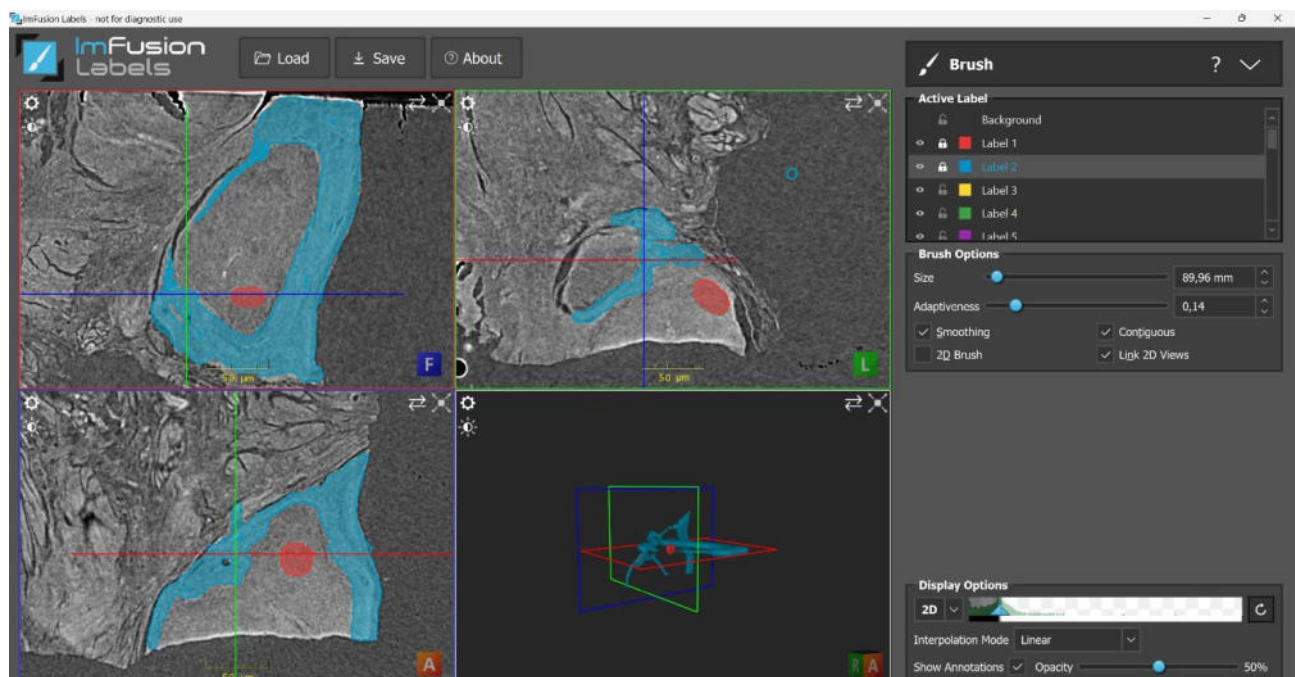
1,600 pathologists who analyze about 40 million tissue samples each year. The diagnosis is established from few histological tissue sections selected from the total sample based on experience. On our way to ideally virtual histology, label-free, non-destructive μ CT imaging can give insight into the tissue still left in the FFPE block to identify yet hidden relevant structures, allowing more precise sectioning in the first step. We therefore **aim** to visualize structures of at least 10 μ m resolution together with larger structures of 1-2 mm, which allow to guide the technician during the sectioning process at the microtome to the relevant part of the FFPE block.

Methods

The method was developed on tonsils, which display squamous epithelium and germinal centers used as test structures to be identified. Annotation was performed using the software provided by our collaborators, which was adapted for our application. To the date, our focus is on phase-contrast μ CT imaging and "simple" absorption μ CT.

Results

In the phase contrast μ CT data, we investigated structures like capillaries, glands (10-25 μ m), muscle fibers, squamous epithelium (25-100 μ m) and germinal centers (500+ μ m). The shape of larger structures is visualized to be identified on the cutting surface of the FFPE block.



Phase-contrast- μ CT scan of FFPE tonsil tissue annotated with the ImFusion Suite. Germinal center labeled in red, squamous epithelium labeled in blue. The scale bar shows a scale of 50 μ m, respectively.

Conclusion

Phase-contrast μ CT images provide a comprehensive way to place the whole sample in the pathological context. With software-based analysis, structures in the tissue can be identified, morphometrically analyzed and reidentified at the microtome. The method will be further developed and transferred to paired samples of head and neck tumors and their lymph node (micro)metastasis.

The experiments are part of the collaboration project HORUS (BMBF 13GW0571D). Collaborating institutions: ImFusion GmbH, Munich; DORNER Health IT Solutions, Muellheim; Fraunhofer EMI, Efringen-Kirchen; Institute for Surgical Pathology, Medical Center-University of Freiburg; Institute of Pathology, Heinrich Heine University and University Hospital of Duesseldorf.

DGP24 Freie Vorträge V - Uro- und Tumorpathologie

DGP24.01

Fast track carcinogenesis in Lynch syndrome by a "two in one hit" mechanism

H. Bläker

University Clinic Leipzig, Pathologie, Leipzig, Germany

Questions/Background

Heterozygote, onkogene Mutationen im β -Catenin Gen (*CTNNB1*) reichen im Kolorektum nicht für eine Tumorentstehung aus, eine weitere stabilisierende Mutation ist notwendig. Diese besteht zu 75% in einer Dopplung der Mutante durch homologe Rekombination. *CTNNB1* Mutationen sind bei kolorektalen Karzinomen daher selten, eine Ausnahme sind Karzinome von Patienten mit *MLH1* Keimbahnmutation, hier finden sich in 50% *CTNNB1* Mutationen. *CTNNB1* und *MLH1* liegen in enger Nachbarschaft auf Chromosom 3p. Wir haben die Hypothese aufgestellt, dass eine bei Gene überspannende homologe Rekombination gleichzeitig *MLH1* inaktiviert und *CTNNB1* aktiviert.

Methods

Zur Frage, ob heterozygote Mutationen in *CTNNB1* bereits in nicht dysplastischer Kolonschleimhaut nachweisbar sind, wurden 100 sporadische Adenome mittels Pyrosequenzierung und NGS auf *CTNNB1* Mutationen und single nucleotide polymorphismen (SNP) zwischen und in *MLH1* und *CTNNB1* auf homologe Rekombination untersucht.

21 *CTNNB1* mutierte Kolorektale Karzinome von Lynch Syndrom Patienten wurden auf eine homologe Rekombination untersucht, 6 von diesen mittels whole exome sequencing (WES).

Results

7 von 100 Adenomen zeigten eine *CTNNB1* Mutation, in vier Fällen war die Mutation homozygot, In zwei der letzteren Fälle zeigte sich eine heterozygote Mutation in der das Adenom umgebenden, nicht dysplastischen Schleimhaut.

19 von 21 *MLH1* assoziierten Lynch-Karzinomen zeigten in der SNP-Analyse eine kontinuierliche, *CTNNB1* und *MLH1* einschließende, homologe Rekombination auf 3p. In der WES Analyse stellte sich eine beide Gene einschließende homologe Rekombination dar, die bis an das Ende des Chromosom 3p reichte.

Conclusion

Ein homologes Rekombinationsgeschehen führt bei Patienten mit *MLH1* Keimbahnmutation in Kolon-Zellen mit einer initial nicht für die Tumorgenese relevanten, heterozygoten *CTNNB1* Mutation simultan zu einer Inaktivierung der DNA-Reparatur und zu einer onkogenen Aktivierung von β -Catenin (two in one hit). Der Mechanismus besteht in einer mitotischen Rekombination bei Crossing over und ist physiologisch.

DGP24.02

Correlation of histopathological hallmarks with survival data in squamous cell carcinomas of the bladder – development of a novel multiparametric grading system.

M.-S. Bösherz, M. Jung, M. Rose, D. D. Jonigk, N. T. Gaisa

Institute of Pathology, University Hospital RWTH Aachen, Aachen, Germany

Questions/Background

Primary squamous cell carcinoma (SCC) of the bladder is a rare subtype of bladder cancer and shows various morphologies and grades. While grading systems for squamous cell carcinomas of other sites, such as head and neck SCC, have been refined in recent years, to date no common grading system has been established for primary SCC of the bladder. This study aims to provide comprehensive insights to the relevance of different histopathological parameters for prognosis and grading in bladder SCC.

Methods

In a cohort of 114 patients with primary bladder SCC and mixed SCC and urothelial carcinoma, we evaluated distinct histopathological aspects, namely growth (solid, ulcerative, polypous) and infiltration (trabecular, heterogeneous, nodular, infiltrative) pattern, keratinization, necrosis, and lymphocytic infiltration (TILs), and correlated the resulting scores with recurrence-free (RFS) and overall survival (OS).

Results

Kaplan Meier analyses revealed a significant impact of necrosis on both RFS and OS: The median OS of tumors with necrosis >50% was 8 months compared to those with low necrosis proportions (>0-10%; median OS: 128 months). A cox regression model considering pathological T- and N-status showed that necrosis was an independent prognostic factor affecting Hazard Ratio (HR) by 1.63 ($p < 0.01$). For infiltration and histological growth patterns as well as keratinization no prognostic impact could be delineated. Extensive TILs correlated with longer RFS and OS, but as a singular parameter no significant association was shown in a multivariate analysis.

Conclusion

Since - besides necrosis - several histological parameters such as keratinization, infiltration and growth pattern have no prognostic impact as singular factors, we propose a more complex multiparametric scoring approach for grading of bladder SCC in order to enhance prognostic impact. This data underlines the importance of histopathological hallmarks for prognosis, and we hope this study contributes to the establishment of a common grading system for primary bladder SCC.

DGP24.03

PSPC1 interacts with KDM5C and is a Prognostic Biomarker in Prostate Cancer

A.-L. Lemster¹, A. Weingart¹, J. Bottner¹, S. Perner², V. Sailer¹, A. Offermann¹, J. Kirfel¹

¹Institute of Pathology, University Hospital Schleswig-Holstein, Campus Luebeck, Luebeck, Germany, ²MVZ HPH Institute of Pathology and Hematology GmbH, Hamburg, Germany

Questions/Background

In Prostate Cancer (PCa), prognosis assessment with current clinical prognostic factors remains difficult for some patients, and sensitivity for detecting aggressive tumours is limited. Many patients receiving androgen deprivation therapy develop (metastatic) castration-resistant PCa (CRPC), which is still considered incurable. Therefore, new biomarkers and therapeutic strategies for PCa and CRPC are urgently needed. Epigenetic aberrations, including histone modifications, are key factors in prostate carcinogenesis and have been shown to trigger PCa metastasis. We previously demonstrated, that the histone lysine demethylase KDM5C is overexpressed in PCa and that this is associated with a reduced biochemical recurrence-free survival in patients after prostatectomy. We could also show that KDM5C plays an important role in cell migration and invasion through the modulation of the epithelial-mesenchymal transition (EMT) signalling pathways. Histone-modifying enzymes are often assembled together in complexes with multiple subunits that allow the coordinated action of distinct activities to efficiently regulate chromatin remodeling. To understand the global function of KDM5C in PCa, we aimed to identify proteins that interact with KDM5C and investigate their expression in PCa.

Methods

We used Tandem Affinity Purification (TAP) technology to isolate TAP-tagged KDM5C proteins along with the associated proteins from PC3 cell lysates. The eluate was then analyzed by nanoflow liquid chromatography/tandem mass spectrometry (nanoLC-MS/MS) to identify the proteins. To investigate the expression of PSPC1 and to study the correlation with KDM5C in PCa, immunohistochemistry was performed using PSPC1 and KDM5C antibodies on ~750 PCa tissue samples. Western blotting was used to analyse the expression of PSPC1 in PCa cell lines.

Results

We found that KDM5C interacts with several proteins in the PC3 cell line, including PSPC1. Interestingly, many of these proteins have been reported to be associated with the development of PCa. We also detected a correlation between the expression of KDM5C and PSPC1 in PCa tissue. The expression of PSPC1 was upregulated in primary and metastatic PCa and was linked to a later tumor stage. Overexpression of PSPC1 was associated with a poor biochemical recurrence-free survival in PCa patients.

Conclusion

PSPC1 interacts with KDM5C, an EMT promoting factor in PCa, and like KDM5C, PSPC1 is a promising predictive marker for treatment failure in PCa.

DGP24.04

Lymphoepithelioma-Like Carcinoma of the Bladder (LELC-B) – analysis of tumor and immune cells

L. Weers¹, F. Koll², A. Weigert³, J. Köllermann¹, C. Döring¹, T. Szarvas⁴, K. W. Schmid⁵, F. Chun², P. Wild¹, H. Reis¹

¹Goethe-Universität Frankfurt, Dr. Senckenbergisches Institut für Pathologie, Frankfurt am Main, Germany, ²Universitätsklinikum Frankfurt, Goethe-Universität, Klinik für Urologie, Frankfurt am Main, Germany, ³Goethe-Universität Frankfurt, Institut für Biochemie I - Pathobiochemie, Frankfurt, Germany, ⁴Universitätsklinikum Essen, Klinik für Urologie, Essen, Germany, ⁵Universität Duisburg-Essen, Pathologie Universitätsklinikum Essen, Essen, Germany

Questions/Background

Lymphoepithelioma-like urothelial carcinoma of the bladder (LELC-B) is a rare histologic subtype of urothelial carcinoma characterized by syncytial growth and strong immune cell infiltrates. Improved response rates to immune checkpoint inhibitor (ICI) therapies have been described. However, the risk factors for the development of LELC-B and the causes of immune cell infiltrates are unknown. We performed molecular, clinicopathologic, and morphologic characterization of this histologic subtype.

Methods

We identified 11 muscle-invasive bladder cancers with pure and mixed LELC-B. We analyzed PD-L1 expression, mismatch repair proteins (MMR) by immunohistochemistry (IHC), and Epstein-Barr coding region (EBER) by in situ hybridization (ISH). Multiplex immunofluorescence (IF) of tumor microenvironment (TME) (PD-L1, PanCK, aSMA, vimentin, CD45, Ki67) and T cells (CD4, CD3, PD1, CD163, CD8, FoxP3) were used to quantify and characterize cell populations. Transcriptomic signatures were compared with cases with the usual histological subtype (NOS). We calculated tumor mutational burden (TMB) and characterized mutational profiles using whole-exome DNA sequencing (WES) data.

Results

All cases were highly positive for PD-L1, MMR-proficient, and negative for EBER-ISH. Immune cell infiltrates were characterized by CD8 T cells. High PD-1/PD-L1 expression on immune and tumor cells was confirmed by multiplex IF and algorithm-based cell type quantification. Immune cell signaling pathways were upregulated in LELC-B compared with NOS cases. All LELC-B cases showed high TMB.

Conclusion

The high mutational burden of the tumor may explain the immunogenicity of LELC-B, leading to upregulation of PD-1/PD-L1 and making ICI a promising treatment option. We plan to investigate neoantigens and mutational signatures to identify mechanisms of pathogenesis.

DGP24.05

Updating germ cell tumor pathogenesis -The ability of seminomas for FOXA2-driven extra-embryonic differentiation

F. Bremmer¹, L. Lubk¹, P. Ströbel¹, D. Nettersheim²

¹Universitätsmedizin Göttingen, Institut für Pathologie, Göttingen, Germany, ²Heinrich Heine University Düsseldorf, Department of Urology, Urological Research Laboratory, Translational UroOncology, Düsseldorf, Germany

Questions/Background

Do seminomas may have a greater developmental potential as assumed and are they able to undergo extra-embryonic differentiation into yolk sack tumours?

Methods

To confirm the hypothesis of seminoma to YST differentiation, we stained 382 seminomas for FOXA2, Glypican-3, AFP, Gata-3, CDX-2, SOX-2, SOX-17 and OCT3/4 by immunohistochemistry. In addition, we performed OCT3/4/FOXA2 double staining to visualize the yolk sac tumor cells next to the OCT3/4 positive seminoma cells. Furthermore, we screened the TCGA GCT cohort (n = 149) for mutation, DNA methylation and expression of FOXA2.

Results

We found 5,49 % (21 of 382) to be FOXA2⁺. The immunohistochemical double staining with OCT3/4 and FOXA2 shows the single-cell FOXA2-positive yolk sac tumour cells (OCT3/4 negative) and the OCT3/4-positive seminoma cells (FOXA2 negative). In addition, SOX2 negativity and SOX17 positivity (and OCT3/4-) confirmed absence of embryonic carcinomas in these cells and the presence of seminoma cells around the FOXA2⁺ cells, suggesting that YST cells developed from seminoma cells, since it is unlikely that all EC cells differentiated solely into YST or disappeared. On analysis of the TCGA-cohort we identified 9 out of 60 (15 %) seminomas (PRAME⁺, SOX2⁻) with low to moderate FOXA2 expression, which might represent seminomas with YST differentiation. Of note, FOXA2 is quite unmutated in GCT (0.7 %, 1 amplification), but samples with the highest FOXA2 expression showed high DNA methylation in a CpG dinucleotide (cg10003443) located upstream the FOXA2 coding sequence. Next, we correlated FOXA2⁺ seminomas to the corresponding serum AFP levels and GPC3 immunohistochemistry status. None of the FOXA2⁺ seminoma showed elevated serum AFP levels and no AFP or GPC3 positivity on immunohistochemical analysis, suggesting that FOXA2 induction precedes AFP and GPC3 production / expression and is a far

more sensitive biomarker than AFP or GPC3, which obviously are first detectable at a higher tumor burden. This is in line with our hypothesis of FOXA2 being the initial driver of YST formation.

Conclusion

In summary, seminomas harbor a greater developmental potential as assumed and are able to undergo extra-embryonic differentiation (YST, CC) independent of EC formation. FOXA2 functions as a sensitive new biomarker to detect occult YST elements in seminoma patients and should be implemented into pathological routine.

DGP24.06

Role of Cell-ECM interactions in renal tubular epithelial cells in the context of progressive chronic kidney disease (CKD)

A. Merz¹, M. Rogg¹, M. Wess¹, A. Paolini², A. Sammarco¹, G. Walz², M. Werner¹, C. Schell¹

¹Universitätsklinikum Freiburg, Institut für Klinische Pathologie, Freiburg, Germany, ²Universitätsklinikum Freiburg, Department of Medicine IV, Freiburg im Breisgau, Germany

Questions/Background

Chronic kidney disease (CKD) is mainly defined by interstitial fibrosis of the renal parenchyma and progressive atrophy of proximal tubules (PT). The latter is characterized by pronounced thickening and multilamellation of the tubular basement membrane, whereas fibrosis is promoted by accumulation of extracellular matrix (ECM) translating into increased matrix rigidity. The role of mechanotransduction as well as the corresponding signaling programs activated in this context remain elusive. ECM composition and mechanical forces are sensed and translated into the cell by the integrin adhesion complex (IAC). Here, we aimed to elucidate the functional role of the ILK-Pinch-Parvin (IPP) complex as an essential part of the IAC in PT damage response and CKD.

Methods

Morphological assessment of Ischaemia-Reperfusion injury (IRI) mouse model was performed. Transcriptome studies of human proximal tubular epithelial cells (hRPTECs) under pro-fibrotic conditions were analyzed. CRISPR/Cas9 genome editing was employed to generate knockout cell lines of the IPP complex (ILK, PARVA as well as PARVA/PARVB double KO).

Results

TGF β treatment (resembling pro-fibrotic conditions) resulted in a partial epithelial-to-mesenchymal transition (EMT) state of hRPTECs. Transcriptome analysis demonstrated an altered regulation of several matrisome and adhesome genes, including members of the IPP complex. Similar alterations were observed in PTs of IRI mice. Further characterization using IPP KO cell lines revealed an altered cytoskeleton, cell morphology and total number of IACs, as well as an altered distribution of the latter. Interestingly, PARVA/PARVB double KOs lacked the ability to form a proper cytoskeleton, resulting in a significant reduction in cell area and IACs. Further genetic perturbation studies demonstrated the strong interdependence of individual IPP-complex members for stabilization and regulation of IACs.

Conclusion

We have established a simplified model to investigate processes of partial EMT in hRPTECs resembling hallmark features of tubular remodeling in CKD. In vivo, transcriptome and functional data indicate a central role of the IPP-complex in orchestrating cell-matrix interactions as an underlying theme of tubular atrophy.

AG01 Hämatopathologie

AG01.01

The genetics of extranodal marginal zone lymphoma of MALT

M.-Q. Du

University of Cambridge, Department of Pathology, Cambridge, United Kingdom

MALT lymphoma invariably arises from a background of chronic microbial infection and/or autoimmune disorder at diverse sites, which are caused by different aetiologies. The chronic infection and/or

autoimmunity cause prolonged immune responses, triggering Darwinian evolution of autoreactive B-cells, their clonal expansion and eventual malignant transformation following acquisition of genetic changes. Apart from chronic BCR signalling, T-cell helps also play a critical role in the lymphoma development as exemplified in the gastric form. The acquired genetic changes, such as t(11;18)(q21;q21) / *BIRC3* (*API2*::*MALT1*, t(14;18)(q32;q21)/*IGH*::*MALT1*, t(1;14)(p22;q32)/*IGH*::*BCL10* and *TNFAIP3* (A20) inactivation by deletion and/or mutation, vary considerably at different sites of MALT lymphoma, but commonly target the canonical and non-canonical NF- κ B pathways downstream of BCR/TLR and CD40/BAFFR respectively. More recent studies show that thyroid MALT lymphomas harbour frequent and concurrent inactivating mutations in *TET2*, *CD274* (*PD-L1*) and *TNFRSF14*, and their inactivation may dysregulate co-inhibitory interactions between neoplastic B and T-helper cells, indirectly promoting their co-stimulations. While in salivary gland MALT lymphoma, *GPR34* is frequently activated by mutation or to a less extent t(X;14)(p11;q32)/*IGH*::*GPR34*, and importantly its signalling is likely maintained independent of its genetic changes through paracrine stimulation mediated by lymphoepithelial lesions. In addition, there are recurrent mutations in other GPCRs, such as CCR6, where the chemokine receptor signalling is activated by ligands produced by the inflamed epithelia, linking the innate immune responses to lymphoma genesis. In summary, the development of MALT lymphoma is driven by oncogenic cooperation between chronic immunological stimulations (both innate and acquired immune responses) and somatic genetic changes, but involves different aetiologies hence different players at various sites.

AG01.02

Primary Bone Diffuse Large B-cell Lymphoma (PB-DLBCL) – a distinct lymphoma entity

V.-S. Ivanova¹, T. Menter¹, J. Davies², S. Dirnhofer¹, A. Tzankov¹

¹University Hospital Basel, University of Basel, Pathology, Institute of Medical Genetics and Pathology, Basel, Switzerland, ²University of Leeds, Leeds Institute for Data Analytics, Leeds, United Kingdom

Questions/Background

Primary bone lymphoma (PBL) is rare, accounting for 1–2% of all lymphomas. Patients present with one or more bone (typically metadiaphyseal) lesions, without significant lymph node or other extranodal involvement. It mainly comprises diffuse large B-cell lymphomas (DLBCL). Dismayingly, PBL has been left out of all current lymphoma classification systems precluding it from being recognised as a separate lymphoma entity/subentity. Herein, in the narrow sense of primary bone DLBCL (PB-DLBCL), we define and highlight its distinctive clinical presentation, morphology, phenotype, gene expression profile (GEP) and molecular genetics.

Methods

We collected 27 cases (10 female, 17 male, age range 22–93, mean age 63) and investigated the expression of CD10, CD20, BCL2, BCL6, MUM1, and MYC by immunohistochemistry (IHC), performed gDNA sequencing with a customised lymphoma panel, covering 172 genes, and carried out FISH to evaluate *MYC*, *BCL2* and *BCL6* translocations. We also attempted to genetically subclassify cases in terms of DLBCL subtype by using the overt two-step classifier and LymphGen. Finally, we performed GEP for cell-of-origin subtyping and *in-silico* comparison to uncover up- and down-regulated genes as opposed to other DLBCL.

Results

By applying the Hans algorithm, 22 cases (81%) were GCB and only 5 – non-GCB. FISH showed 2 *BCL2*, 3 *BCL6* and 1 *MYC* rearranged instances. One case each had *MYC* and *BCL2*, and 1 *BCL2* and *BCL6* rearrangements. DNA sequencing highlighted *TP53* (n=7), *B2M* (n=5), *EZH2* (n=5), *KMT2D* (n=5), *TNFRSF14* (n=4) and *SGK1* (n=4) as the most frequently mutated genes in PB-DLBCL. The two-step classifier subclassified 12 out of 24 cases as EZB (n=8), ST2 (n=3) and MCD (n=1), while LymphGen was not able to subclassify any due to a lack of defining features. All 19 cases that passed quality control for GEP were classified as GCB, and 1 was molecular high-grade. The top 10 up-regulated genes in PB-DLBCL were: *MAP2K7*, *HLA-DRA*, *UBE4A*, *MAF*, *LRMP*, *PAFAH1B2*, *NF2*, *GRB2*, *CFLAR*, *MAFB*, whereas the top 10 down-regulated were: *NREP*, *BAK1*, *CRIP1*, *CSTF1*, *PCSK7*, *TRPM2*, *TNFSF4*, *CKS1B*, *CD19*, *CDK16*.

Conclusion

We provide compelling molecular evidence that PB-DLBCL is a specific entity. Apart from its distinctive clinical and morphologic presentation, almost all cases are GCB by IHC and all by GEP. PB-DLBCL mutational profile is similar to the one of follicular lymphoma (FL), but its GEP and frequency of *BCL2* rearrangements are unequivocally different from nodal GCB-DLBCL and FL.

Characteristics of primary cutaneous diffuse large B-cell lymphoma, leg-type in respect to features of systemic DLBCL and testicular DLBCL.

J. Richter¹, L. Knemöller¹, K. Koch¹, U. Wehkamp², M. Wobser³, J. Haag⁴, W. Klapper¹, I. Oschlies¹

¹University Hospital Schleswig-Holstein, Campus Kiel, Department of Pathology, Hematopathology Section, Kiel, Germany, ²University Hospital Schleswig-Holstein, Campus Kiel, Department of Dermatology, Venerology and Allergology, Kiel, Germany, ³University Hospitals Würzburg, Department of Dermatology, Venerology and Allergology, Würzburg, Germany, ⁴University Hospital Schleswig-Holstein, Campus Kiel, Department of Pathology, Kiel, Germany

Questions/Background

Primary cutaneous diffuse large B-cell lymphoma (DLBCL), leg-type (PCDLBCL) is distinguished from systemic DLBCL due to its clinical, histopathological and molecular characteristics. It affects elderly adults with female predominance and preferential involvement of the skin of the lower extremities. Compared to systemic DLBCL, PCDLBCL seems a more homogenous entity with obvious predominance of an activated (ABC)/non-germinal-centre-(nonGCB) B-cell phenotype and highly recurrent mutations including *MYD88* and *CD79B* mutation. Recent cytogenetic data on PCDLBCL provided divergent results.

The aim of our study was to characterize phenotypic and molecular features of PCDLBCLs, in comparison to systemic nodal/extranodal DLBCL (systDLBCL) and the testicular DLBCL (testDLBCL), the latter as an example for a lymphoma affecting an immunoprivileged site.

Methods

We identified a total of 131 PCDLBCLs in the files of the Hematopathology Section in Kiel. Clinical data were retrieved at diagnosis or retrospectively. Samples were analyzed using Immunohistochemistry (IHC; CD10, BCL2, BCL6, Cyclin D1 and MUM1), in situ hybridization (EBER), Fluorescence in situ hybridization (FISH; *MYC*, *BCL6*, *BCL2* and *IGH*) and *MYD88* and *CD79B* hotspot mutation analyses by Pyrosequencing. The results were compared to systDLBCL and testDLBCL cohorts. Furthermore, 18 PCDLBCL, 17 systDLBCL (nonGCB) and 8 testDLBCL were selected for gene expression profiling using a comprehensive oligo-based Transcriptome Panel (HTG molecular Diagnostics, Tuscon, USA).

Results

Our data indicate that PCDLBCL frequently harbor mutations affecting *MYD88* and *CD79B* (58% (58/100) and 32% (32/99), respectively). The majority of PCDLBCL displayed a nonGCB cell of origin (COO) phenotype (88%, 68/77). By FISH, 18% (15/85) carried chromosomal breaks affecting *MYC*, 13% (7/55) breaks in *BCL6*, 3% (2/65) breaks in *BCL2*, and 25% (12/49) breaks in *IGH*. A "double hit" was observed in 2/55 (4%) of samples. COO and chromosomal breaks did not differ between PCDLBCL arising on the leg ("leg type") compared to other sites.

Conclusion

Preliminary results on gene expression data suggest a high similarity between the three analyzed lymphoma subtypes (PCDLBCL, systDLBCL (nonGCB) and testDLBCL). Further analyses focusing on differentially expressed genes and known deregulated signaling pathways in DLBCLs are ongoing.

The small and large cell variants of nodal marginal B-cell lymphomas present with various growth patterns associated with different Ki-67 indexes

F. Spada, P. Möller, T. F. E. Barth

Universitätsklinikum Ulm, Pathologie, Ulm, Germany

Questions/Background

Nodal marginal zone B-cell lymphoma (NMZL) is an indolent tumour characterized by a small cell morphology (sc-NMZL); a blastic, large cell variant of it has been described (lc-NMZL). The lack of specific markers is a major concern in the diagnosis of NMZL. Primary nodal DLBCL is the main differential diagnosis for the blastic variant of NMZL.

Methods

We analysed the growth patterns of 34 sc-NMZL and 35 lc-NMZL. The patterns published by others are:

diffuse, nodular, perifollicular, and interfollicular. We measured proliferation by the Ki-67 and included immunohistochemistry for bcl2, bcl6, Mum1, CD10, CD23, CD5, and IgD. We tested new immunohistochemical markers reported in literature as possible markers for NMZBL, such as IRTA1, MNDA and T-BET on a group of 30 sc-NMZBL, 16 lc-NMZBL and 19 primaries nodal DLBCL.

Results

We detected the described growth patterns both in the sc and in lc-NMZBL in the following percentages: 9% perifollicular, 12% interfollicular, 50% nodular, 6% diffuse and a 24% displaying a coexistence of more than one pattern for sc-NMZBL; 13% perifollicular, 13% interfollicular, 16% nodular, 16% diffuse and a 55% mixed for lc-NMZBL. Further, we detected an additional pattern that we described as sclerosing in two samples, one in small cell and one in large cell group. We found a significant association ($p < 0.005$) between the diffuse growth pattern (or the presence of a diffuse component in the sample) and higher KI-67 index. Large cell samples have a generally higher proliferation rate than small cell samples ranging from 20 to 80 percent while small cell lymphomas showed a <5 to 20% range. However, this distinction is not free from exceptions since we observed a minority of lymphomas with a small cell morphology and a high KI-67 index and *vice versa* low proliferative lymphomas with blastic cell morphology. For the IHC stainings of IRTA1, MNDA and T-bet, the positivity rate was not discriminative since these markers were detected also in DLBCLs.

Conclusion

We have observed an unexpected complexity of growth patterns in small cell and blastic variant of NMZBL. Interestingly, the different, partly overlapping growth patterns and the association with proliferation seems to suggest a progression, from the perifollicular to the diffuse pattern.

**Cases were also contributed by Prof. Dr. A. Feller, Prof. Dr. F. Fend, Prof. Dr. M. Hansmann, Prof. Dr. W. Klapper, Prof. Dr. G. Ott, Prof. Dr. A. Rosenwald, Prof. Dr. H. Stein, Prof. Dr. H. Wacker.*

AG01.05

A pilot study on dissecting the methylomes of diffuse large B-cell lymphomas of primary CNS and NOS types

T. Kraus, D. Hölzl, K. Sotlar

Uniklinikum Salzburg, Universitätsinstitut für Pathologie, Salzburg, Austria

Questions/Background

Primary diffuse large B-cell lymphomas of the central nervous system (CNS-DLBCLs) are rare tumors accounting for 2-3% of all brain tumors. Furthermore, primary CN-DLBCLs account for 4-6% of all extranodal DLBCLs. In the western world, there is an annual incidence of 0.5 cases per 100,000 population. In 65%, CNS-DLBCLs are solitary brain lesions, 38% are located in the cerebral hemispheres. Approximately 60-80% of CNS-DLBCLs are of non-germinal center B-cell-like (non-GCB according to Hans et al.) subtype. Till today, the etiological factors leading to CNS-DLBCL still remain unknown. The aim of this pilot study is to identify differentially methylated genes and pathways of CNS-DLBCL compared with non-CNS DLBCLs, of NOS (not otherwise specified) subtypes.

Methods

In this study, we performed epigenome-wide methylation analysis on 6 DLBCL cases, i.e. 3 CNS-DLBCLs and 3 DLBCL, NOSs. Applying the Illumina Infinium EPIC bead chip array we interrogated more than 850,000 methylation sensitive CpGs sites in parallel. Computational analyses were performed to identify differentially methylated genes. Gene ontology analysis was processes to reveal altered pathways.

Results

We found that CNS-DLBCL and DLBCL, NOS show distinct epigenomic alterations of the DNA methylation landscape. Focussing on gene regions, 457 gene regions were significantly differentially methylated with methylation differences of at least 10 % and p-values of less than 0.05 applying t-test. Interestingly, we found 7 miRNAs, 11 snoRNAs and 9 lncRNAs among top hits.

Conclusion

In summary, in this pilot study, we found significantly differentially methylated gene regions in CNS-DLBCLs compared with DLBCL, NOS, this may enable to molecularly differentiate between primary CNS-DLBCLs and DLBCLs, NOS, with brain involvement.

Mutational profiles and established risk factors differ between elderly and younger patients with diffuse large B-cell lymphoma

K. S. Kurz¹, M. Kreuz², M. Ziepert², A. M. Staiger^{1,3}, T. F. Barth⁴, H.-W. Bernd⁵, A. C. Feller⁵, W. Klapper⁶, H. Stein⁷, M.-L. Hansmann⁸, P. Möller⁴, N. Schmitz⁹, L. Trümper¹⁰, M. Loeffler¹¹, A. Rosenwald¹², G. Ott¹, **H. Horn**^{1,3}

¹Robert-Bosch-Krankenhaus, Abteilung für Klinische Pathologie, Stuttgart, Germany, ²Institute for Medical Informatics, Statistics, and Epidemiology, Universität Leipzig, Leipzig, Germany, ³Dr. Margarete Fischer-Bosch-Institute of Clinical Pharmacology, Stuttgart and University of Tübingen, Stuttgart, Germany, ⁴Institute of Pathology, Universitätsklinikum Ulm, Ulm, Germany, ⁵Hämatopathologie Lübeck, Lübeck, Germany, ⁶Institute of Pathology, Hematopathology Section and Lymph Node Registry, Universitätsklinikum Schleswig-Holstein, Campus Kiel, Kiel, Germany, ⁷Pathodiagnostik, Berlin, Berlin, Germany, ⁸Institute of Pathology and Molecular Pathology, Helios Universitätsklinikum Wuppertal, Wuppertal, Germany, ⁹Department of Internal Medicine, Hematology and Oncology, Universitätsklinikum Münster, Münster, Germany, ¹⁰Department of Hematology and Oncology, Georg-August Universität, Göttingen, Göttingen, Germany, ¹¹Institute for Medical Informatics, Statistics, and Epidemiology, Universität Leipzig, Leipzig, Germany, ¹²Institute of Pathology, Universität Würzburg, Würzburg, Germany

Questions/Background

Although it is well-known that age is a prominent factor for the survival of patients diagnosed with lymphoma, biological differences between younger and elderly patients with diffuse large B-cell lymphoma (DLBCL) have only rarely been investigated. Correlation of molecular findings with treatment response might enable optimization of risk stratification and treatment.

Methods

For re-evaluation of established and newly analyzed biomarkers, data from cohorts of elderly patients (≥ 60 y, $n=772$) and younger patients (18-60y, $n=119$) treated within clinical trials of the German Lymphoma Alliance (GLA, formerly DSHNHL) were included. *BCL2* and *MYC* expression, dual expression of both, *BCL2*- and/or *MYC*-translocation, as well as ABC subtype were re-analyzed.^{1,2} Treatment response was categorized into patients with complete remission (CR) and refractory (ref) or relapsed (rel) patients (ref/rel). For a targeted resequencing approach, 287 elderly and 90 younger patients were included.

Results

The expression of biomarkers in tumors between patients achieving CR and ref/rel patients differed significantly in both younger and elderly patients. In elderly patients, enhanced *BCL2* expression ($p=0.0414$) and enrichment of ABC subtype ($p<0.001$) was observed in ref/rel DLBCL. In contrast, in tumors from ref/rel patients the percentage of *BCL2* breaks and protein expression was significantly enhanced ($p=0.0004$ and $p=0.0324$, respectively). Moreover, ref/rel patients had a significant higher proportion of tumors with dual expressor phenotype compared to CR patients ($p=0.0410$).

The frequency of observed mutations differed between patients cohorts with *TP53* (20%), *MYD88* (18%) and *CREBBP* (17%) mutations most commonly observed in elderly patients, while *TNFAIP3* (61%), *EP300* (58%) and *CREBBP* (58%) were most frequently mutated in younger patients. While *TP53* was of prognostic impact in the cohort of elderly patients³ *TP53* mutations did not predict clinical outcome in younger patients. Of interest, mutations in *CREBBP* did not correlate with inferior outcome in elderly patients (EFS: $p=0.719$; PFS: $p=0.998$; OS: $p=0.939$), but OS was significantly shorter in younger patients with *CREBBP* mutations ($p=0.034$).

Conclusion

Younger and elderly patients with DLBCL obviously display different biological risk factors. Perspectively, this is of particular interest possibly enabling an adjustment of therapeutic interventions.

¹Horn et al. 2013 (PMID: 23335369)

²Staiger et al. 2017 (PMID: 28525305)

³Zenz et al. 2017 (PMID: 28614910)

AG02 Gastroenteropathologie I

AG02.01

Esophageal adenocarcinoma: understanding the molecular basis of differential treatment response

C. Jonas¹, N. Heramvand², T.-P. Yang², S. Hoppe¹, S. Neiß³, S.-H. Chon³, W. Schröder³, C. Bruns³, H. Schlößer³, R. Büttner¹, S. Merkelbach-Bruse¹, Y. Zhao³, H. Alakus³, A. Quaas¹, M. Peifer², A. M. Hillmer¹

¹Faculty of Medicine and University Hospital Cologne, Institute of Pathology, Cologne, Germany, ²Center for Molecular Medicine Cologne, Department for Translational Genomics, Cologne, Germany, ³Faculty of Medicine and University Hospital Cologne, Department of General, Visceral and Cancer Surgery, Cologne, Germany

Questions/Background

Therapy response in esophageal adenocarcinoma varies dramatically, ranging from primary resistance to major (<10 % remaining vital tumor) or even complete response.

Methods

To investigate the molecular nature of resistance, we compared 10 major responders after treatment with their paired treatment naïve primary biopsy by whole exome- and RNA-sequencing.

Results

2/10 tumors showed extreme genomic differences between the pre- and post-therapy situation. We hypothesize that in these cases the resistant clones might be early slowly proliferating (sub-) clones, which therefore survived therapy. The loss of a *TP53* mutation (p.V172G) in one of these tumor samples supports this hypothesis as *TP53* mutations accumulate during tumorigenesis of EAC at a more progressed stage. Post-therapy tumors were characterized by upregulation of extracellular matrix (ECM) genes in part due to therapy-induced healing and lower tumor content. *MMP2*, *THY-1/CD90* and *POSTN*, markers for cancer associated fibroblasts, were highly expressed. By screening 600 EAC specimen for *MMP2* expression, we found a tendency for correlation between a high expression of *MMP2* and a worse prognosis in primary resected EAC patients. To determine the molecular characteristics of early relapse we analyzed 70 EAC tumor/normal pairs by whole exome and RNA-sequencing and compared three patient groups based on their therapy response. We also distinguished between long (> 2 years) and short term (< 2 years) survivors. Within the cohort, we observed *TP53* as the most frequently mutated cancer gene (60 %). Comparing the mutational landscape between long and short survivors, *FAT3* was more frequently mutated in short survivors ($p = 6.07E-03$). We detected nine microsatellite instable (MSI) tumors. Four of them had extremely high rates of instable markers. Interestingly, three of these four MSI extremes were complete responder. On the transcriptomic level, we could not observe significant differences neither between the response groups nor between survival rates.

Conclusion

Overall, we found evidence for a high level of intra tumor heterogeneity that likely contributes to the emergence of resistant clones, *FAT3* mutations associated with short survival and some extreme MSI tumors among complete responders. The data will help to understand the process of resistance and course of relapse and to identify biomarkers that distinguish different clinically relevant EAC subgroups and potentially provide new targets for intervention.

AG02.02

The new prognostic biomarker Stroma Areactive Invasion Front Areas (SARIFA) is based on an interaction between tumor cells with tumor promoting adipocytes potentially caused by an altered immune response in gastric cancer

B. Grosser¹, C. M. Heyer², J. Austgen¹, E. Sipos¹, N. G. Reitsam¹, A. Hauser², D. Vlasenko³, A. Probst⁴, M. Schlesner², B. Märkl¹

¹Pathology, Medical Faculty Augsburg, University of Augsburg, Augsburg, Germany, ²Institute of Biomedical Informatics, Data Mining and Data Analytics, Faculty of Applied Informatics, University Augsburg, Augsburg, Germany, ³General and Visceral Surgery, Faculty of Medicine, University of Augsburg, Augsburg, Germany, ⁴Gastroenterology, Faculty of Medicine, University of Augsburg, Augsburg,

Questions/Background

Recently, we presented the new histomorphological negative prognostic biomarker Stroma AReactive Invasion Front Areas (SARIFA) in gastric cancer, defined as the direct contact between tumor cells and fat cells. Previous analyses have indicated an interaction of tumor cells with tumor-promoting adipocytes potentially caused by an altered immune reaction as an underlying process.

The aim of this study was to further elucidate the underlying genomic, transcriptional and immunological mechanisms of the SARIFA phenomenon.

Methods

SARIFA was classified on H&E-stained tissue sections of a local series of adenocarcinomas of the stomach and the gastroesophageal junction (n = 60). SARIFA status was assessed in the TCGA STAD cohort (n = 191) and genomic and transcriptomic data were analyzed in regard to SARIFA-status. Further, a spatially resolved transcriptome analysis in the stroma and in macrophages at the invasion front was conducted. Expression of interleukins was investigated using RNA-scope.

Results

In the TCGA STAD cohort no genomic differences regarding the SARIFA status could be found, whereas the gene expression analyses showed an upregulation of FABP4 in SARIFA positive tumors and the transcriptional regulation of white adipocyte differentiation, triglyceride metabolism and katabolism were upregulated in pathway analyses. In the spatially resolved transcriptome analysis of SARIFA-positive tumors FABP4 and the transcriptional regulation of white adipocyte differentiation was upregulated in macrophages. Additionally, a significantly lower expression of IL6 and TNFa was observed at the invasion front using RNA-scope.

Conclusion

SARIFA proves to be an extremely promising negative prognostic biomarker in gastric cancer implicating an interaction of tumor-cells with tumor promoting adipocytes with crucial changes of the tumor cell metabolism. SARIFA does not seem driven by tumor genetics but very likely by an altered immune response as a potential causative mechanism.

AG02.03

Post-neoadjuvant assessment of tumour budding according to ITBCC subgroups delivers stage- and regression-grade independent prognostic information in intestinal-type gastric adenocarcinoma

M. Jesinghaus¹, A.-L. Herz², M. Kohlruss², M. Silva², A. Grass¹, A. Novotny³, S. Lange⁴, K. Ott⁵, T. Schmidt⁶, M. Gaida⁷, A. Hapfelmeier⁸, C. Denkert¹, W. Weichert², G. Keller²

¹Universitätsklinikum Gießen und Marburg, Institut für Pathologie, Marburg, Germany, ²Technische Universität München, Institut für Pathologie, München, Germany, ³Technische Universität München, Klinik für Chirurgie, Klinikum rechts der Isar, München, Germany, ⁴Technische Universität München, II Medizinische Klinik, Klinikum rechts der Isar, München, Germany, ⁵Klinikum Rosenheim, Klinik für Chirurgie, München, Germany, ⁶Universitätsklinikum Köln, Klinik für Chirurgie, Köln, Germany, ⁷Universitätsmedizin Mainz, Institut für Pathologie, Mainz, Germany, ⁸Technische Universität München, Institut für AI und Informatik, München, Germany

Questions/Background

Tumour budding (TB) has been associated with adverse clinicopathological factors and poor survival in a plethora of therapy-naïve carcinoma entities including gastric adenocarcinoma (GC). As conventional histopathological grading is usually omitted in the post-neoadjuvant setting of GC, our study aimed to investigate the prognostic impact of TB in GCs resected after neoadjuvant therapy.

Methods

We evaluated TB according to the criteria from the International Tumour Budding Consensus Conference (ITBCC) in 167 post-neoadjuvant resections of intestinal-type GC and correlated the results with overall survival (OS) and clinicopathological parameters. GCs were categorised into Bd1 (0-4 buds, low TB), Bd2 (5-9 buds, intermediate TB), and Bd3 (≥10 buds, high TB).

Results

Carcinomas with intermediate and high TB were significantly enriched in higher ypTNM stages and strongly associated with reduced 5-year OS in univariable analyses (p < 0.001). In multivariable analyses including sex, age, resection status, UICC stage, and tumour regression grading, TB remained a stage-independent predictor of survival (p < 0.001, hazard ratio Bd2: 2.60, Bd3: 4.74).

Conclusion

The assessment of TB according to the ITBCC criteria provides valuable prognostic information in the post-neoadjuvant setting of intestinal-type GC and may be a considerable substitute for the conventional grading system in GCs after neoadjuvant therapy.

AG02.04

Urokinase-type plasminogen activator receptor (uPAR) cooperates with mutated KRAS in regulating cellular plasticity and gemcitabine response in pancreatic adenocarcinomas

L. Peng¹, Y. Li¹, S. Yao¹, H. Bohnenberger¹, J. Gaedcke², V. M. Baart³, C. F. Sier³, A. Neesse⁴, V. Ellenrieder⁴, H. Bohnenberger¹, F. Fuchs¹, J. Kitz¹, P. Ströbel¹, **S. Küffer¹**

¹Universitätsmedizin Göttingen, Institut für Pathologie, Göttingen, Germany, ²Universitätsmedizin Göttingen, Klinik für Allgemein-, Viszeral- und Kinderchirurgie, Göttingen, Germany, ³Leiden University Medical Center, Department of Surgery, Leiden, The Netherlands, ⁴Universitätsmedizin Göttingen, Klinik für Gastroenterologie, Göttingen, Germany

Questions/Background

Pancreatic ductal adenocarcinoma (PDAC) remains one of the most lethal cancers. Given the currently limited therapeutic options, the definition of molecular subgroups with the development of tailored therapies remains the most promising strategy. Patients with high-level gene amplification of urokinase plasminogen activator receptor (*uPAR/PLAUR*) have an inferior prognosis. We analyzed the uPAR function in PDAC to understand this understudied PDAC subgroup's biology better.

Methods

A total of 67 PDAC samples with clinical follow-up and TCGA gene expression data from 316 patients were used for prognostic correlations. Gene silencing by CRISPR/Cas9, as well as transfection of *uPAR* and mutated *KRAS*, were used in PDAC cell lines (AsPC-1, PANC-1, BxPC3) treated with gemcitabine to study the impact of these two molecules on cellular function and chemoresponse. HNF1A and KRT81 were surrogate markers for the exocrine-like and quasi-mesenchymal subgroup of PDAC, respectively.

Results

High levels of uPAR were correlated with significantly shorter survival in PDAC, especially in the subgroup of HNF1A-positive exocrine-like tumors. uPAR knockout by CRISPR/Cas9 resulted in activation of FAK, CDC42, and p38, upregulation of epithelial makers, decreased cell growth and motility, and resistance against gemcitabine that could be reversed by re-expression of uPAR. Silencing of *KRAS* in AsPC1 using siRNAs reduced uPAR levels significantly, and transfection of mutated *KRAS* in BxPC-3 cells rendered the cell more mesenchymal and increased sensitivity towards gemcitabine.

Conclusion

Activation of uPAR is a potent negative prognostic factor in PDAC. uPAR and KRAS cooperate in switching the tumor from a dormant epithelial to an active mesenchymal state, which likely explains the poor prognosis of PDAC with high uPAR. At the same time, the active mesenchymal state is more vulnerable to gemcitabine. Strategies targeting either KRAS or uPAR should consider this potential tumor-escape mechanism.

AG02.06

Shedded particles of the larval stage of E.multilocularis and E. granulosus increase NK cells in the germinal center of human lymph nodes

L. Schreiber, J. Nell, J. Grimm, L. Zhang, T. F. E. Barth, P. Möller
Institut für Pathologie, Universitätsklinikum Ulm, Ulm, Germany

Questions/Background

E. Granulosus and *E. multilocularis* are cestodes and the larval stage causes one of the most life-threatening zoonosis in humans known as cystic and alveolar Echinococcosis (CE and AE). Humans, as a false intermediate host, ingests the eggs and after penetration of the wall of the gastrointestinal tract the larval state forms multiple hepatic lesions called metacestodes. The disease seems to deviate the immune defense by yet not well understood mechanisms. We have shown that particles shed from the outer layer of the metacestode (so-called laminated layer) are found in the germinal centers of the regional lymph nodes ([1]). We have shown further that these particles, called small particles of *E. multilocularis* and *E. granulosus* (SPEMS and SPEGS, respectively) activate NK cells *in vitro*. This finding raises the question if this effect can be seen *in vivo*.

Methods

We used Cellprofiler™ to develop an image analysis program that identified germinal centers containing particles and quantified the number of NK cells within them, comparing these counts to those of germinal centers without particles. For each analyzed lymph node, two tissue sections were immunohistochemically stained, one with EmG3, a specific antibody targeting SPEMS and SPEGS, and the other with an antibody against CD57, a surface receptor on NK and T cells. The stains were scanned and matched using a computer software. To confirm the identification of NK cells, we performed double immunofluorescence staining. All in all, we analyzed 3 lymph nodes of patients with AE and 3 lymph nodes of patients with CE including 252 germinal centers.

Results

In the double immunofluorescence staining with CD3 and CD57, we confirmed the presence of CD57+/CD3- cells, therefore classified as NK cells. Statistical analyses revealed a significant increase in the number of NK cells in SPEM-/SPEG-positive lymph follicles compared to controls ($p=0,0010$; $p=0,00001$; respectively).

Conclusion

We were able to show a direct correlation between particles of the laminated layers and the expansion of natural killer (NK) cells in germinal centers of lymph nodes in samples of patients with AE and CE. These findings, together with our previous data, confirm an interaction between these particles and NK cells *in vivo*. NK cells play an important role in forming an effective immune response against echinococcosis. Therefore, the increase of NK cells in lymph nodes might play an important role in the immune evasion of Echinococcosis.

Literaturangaben:

[1] Thomas F. E. Barth., Tobias S. Herrmann, Dennis Tappe, Lorenz Stark, Beate Grüner, Klaus Buttenschoen, Andreas Hillenbrand, Markus Juchems, Doris Henne-Bruns, Petra Kern, Hanns M. Seitz, Peter Möller, Robert L. Rausch, Peter Kern, Peter Deplazes, (2012), Sensitive and Specific Immunohistochemical Diagnosis of Human Alveolar Echinococcosis with the Monoclonal Antibody Em2G11, PLOS, Neglected Tropical Disease, 6, <https://www.ncbi.nlm.nih.gov/pmc/articles/PMC3493387/pdf/pntd.0001877.pdf/?tool=EBI>

AG02.07

Identifying and Characterizing Essential Genes in the Presence or Absence of HIF1a in Hepatocellular Carcinoma

M. Zeller¹, T. Huth¹, E. C. Dreher¹, S. Lemke^{2,3,4,5}, D. Castven⁶, D. Ibberson⁷, E. Eiteneuer¹, S. Pusch^{8,9}, J. U. Marquardt⁶, S. Nahnsen^{2,5,10}, P. Schirmacher¹, S. Rössler¹

¹Institute of Pathology, Heidelberg University Hospital, Heidelberg, Germany, ²Quantitative Biology Center (QBiC), University of Tübingen, Tübingen, Germany, ³Department of Peptide-based Immunotherapy, University and University Hospital Tübingen, Tübingen, Germany, ⁴Institute for Cell Biology, Department of Immunology, University of Tübingen, Tübingen, Germany, ⁵Cluster of Excellence iFIT (EXC2180) "Image-Guided and Functionally Instructed Tumor Therapies", University of Tübingen, Tübingen, Germany, ⁶Department of Medicine I, University Medical Center Schleswig Holstein, Lübeck, Germany, ⁷Deep Sequencing Core Facility, CellNetworks Excellence Cluster, University of Heidelberg, Heidelberg, Germany, ⁸Institute of Pathology, University Hospital Heidelberg, Department of Neuropathology, Heidelberg, Germany, ⁹Clinical Cooperation Unit Neuropathology, German Cancer Research Center (DKFZ), Heidelberg, Germany, ¹⁰Biomedical Data Science, Department of Computer Science, University of Tübingen, Tübingen, Germany

Question/Background

Hepatocellular Carcinoma (HCC) is the most common type of liver cancer and poses many challenges due to therapy resistance. Expression and downstream signaling of the hypoxic transcription factor HIF1a have been suggested to contribute to HCC aggressiveness. The goal of this project was to use genome-wide CRISPR screening to identify genes essential in HCC cells with HIF1a activation.

Methods

We performed a lentiviral CRISPR-Cas9 screening in HLF cells to identify essential genes. Cells were treated with Dimethyloxalylglycin (DMOG) to emulate the hypoxic conditions typical in HCC by stabilizing HIF1a through the inhibition of its degradation. Genes were ranked by the decrease of essentiality-scores after DMOG treatment versus untreated conditions. Based on literature research, top ranked prospects were prioritized and two candidates were further investigated by CRISPR-Cas9 knockout (KO) or siRNA mediated knockdown (KD). Gene silencing was verified using Inference-of-CRISPR-Edits (ICE) Analysis, qPCR and Western blot. The candidates were functionally tested by colony formation, cell viability, transwell migration, scratch migration, cell adhesion and 3D sprouting assay. Two different HCC cell lines were used, HLF and HCC68.

Results

We identified non-erythrocytic spectrin beta V (SPTBN5), a cytoskeletal protein, and Calpain 2 (CAPN2), a cytosolic protease, as top candidates to be essential in HCC cells with HIF1a activation. Effective silencing of both candidates was obtained with two independent sgRNAs or with siRNA pools and validated in HLF and HCC68 cells. SPTBN5-KO/KD or CAPN2-KO/KD decreased both viability and colony formation and DMOG treatment strengthened this effect. Moreover, both KO and KD of CAPN2 or SPTBN5 reduced cell migration and adhesion efficiency of HLF and HCC68 cells, which decreased additionally when combined with DMOG treatment. Furthermore, CAPN2-KO in HLF lowered the aggressiveness and invasion of cells in a 3D matrix.

Conclusion

The data presented here suggest that the cytoskeleton-involved genes CAPN2 and SPTBN5 are required for viability, migration and aggressiveness of HCC cells in the presence of HIF1a. These results propose a link between certain cytoskeletal functions and hypoxia tolerance. Understanding this connection may provide insight into how HCC cells react to HIF1a signaling, potentially exposing vulnerabilities exploitable for the treatment of HCC in the future.

AG02.08

Tumor-Immune-Interaction and Senescence-associated Molecules in Colorectal Carcinoma

F. Kellers¹, A. Fernandez², B. Konukiewitz¹, M. Schindeldecker², K. Tagscherer², A. Heintz³, M. Jesinghaus⁴, W. Roth², S. Förtsch²

¹University Medical Center Schleswig-Holstein, Campus Kiel, Department of Pathology, Kiel, Germany, ²Universitätsmedizin Mainz, Institut für Pathologie, Mainz, Germany, ³Marienhaus Klinikum Mainz, Klinik für Allgemein- und Viszeralchirurgie, Mainz, Germany,

⁴Universitätsklinikum Gießen und Marburg, Institut für Pathologie, Marburg, Germany

Questions/Background

Cellular senescence permanently arrests the cell cycle of premalignant cells following protumorigenic stimuli, counteracting tumor progression.[1] Senescence induction leads to phenotypic and metabolic changes and alters the interaction with the cells' microenvironment. This mediates tumor-immunosurveillance but bears promalignant potential and may contribute to disease progression.[2] Investigating prognostic implications of senescence induction and assessment of senescence as therapeutic target in colorectal carcinoma (CRC) demand robust biomarkers. Our study[3] aims to investigate the prognostic potential of senescence markers and to understand the interaction of senescent tumor cells and immune cells.

Methods

Senescence was induced in CRC cell lines by low-dose-etoposide treatment and confirmed by Senescence-associated β -galactosidase (SA- β -GAL) staining and fluorescence activated cell sorting (FACS) analysis. We established co-cultures of senescent cells and various immune cell lines and conducted cell viability assays, electron microscopy and live cell imaging. Immunohistochemical markers were studied on a tissue microarray containing tumor tissue of n=598 CRC patients and evaluated using digital image analysis. Results were correlated with disease-specific survival (DSS) and progression-free survival (PFS).

Results

Expression of different senescent-associated markers correlates with in- or decreased DSS and PFS. Close proximity of p21+ senescent tumor cells and CD8+ immune cells correlates with increased DSS and PFS. In vitro, senescent cells were dose-dependently eliminated by immune cell lines TALL-104 and NK-92 cells (mimicking cytotoxic T cells and natural killer T cells), which is facilitated via direct cell-cell-contact and induction of apoptosis and granule exocytosis.

Conclusion

Depicting the initiation of this important anti-tumor-mechanism, markers of cellular senescence are of significant prognostic relevance in CRC. Our results moreover show the pleiotropic effect of senescence in vivo. Absence as well as exceeding expression of senescence markers is associated with a negative prognosis in CRC. The impact of cellular senescence depends on tumor microenvironment and immunosurveillance of senescent cells. Proximity analyses of senescent cells and tumor-infiltrating immune cells have significant prognostic relevance and reflect this.

Literaturangaben:

[1] Serrano M, Lin AW, McCurrach ME, Beach D, Lowe SW, (1997), Oncogenic ras provokes premature cell senescence associated with accumulation of p53 and p16INK4a, Cell, 593-602, 88(5)

[2] Coppe JP, Desprez PY, Krtolica A, Campisi J, (2010), The senescence-associated secretory phenotype: the dark side of tumor suppression, Annu Rev Pathol, 99-118, 5

[3] Kellers F, Fernandez A, Konukiewitz B, Schindeldecker M, Tagscherer KE, Heintz A, et al., (2022), Senescence-Associated Molecules and Tumor-Immune-Interactions as Prognostic Biomarkers in Colorectal Cancer, Front Med, Lausanne, 865230, 9

AG02 Gastroenteropathologie II

AG02.09

Loss of SATB2 occurs more frequently than CDX2 in colorectal carcinoma and identifies particularly aggressive cancer in high risk subgroups

M. Schmitt^{1,2}, M. Silva³, B. Konukewitz^{2,4}, C. Lang², K. Steiger², K. Halfter⁵, J. Engel⁵, P. Jank¹, N. Pfarr², D. Wilhelm⁶, S. Försch⁷, C. Denkert¹, M. Tschurtschenthaler⁸, W. Weichert^{2,9,10}, M. Jesinghaus^{1,2}

¹Universitätsklinikum Gießen-Marburg (UKGM), Institut für Pathologie, Marburg, Germany, ²Technische Universität München, Institut für Allgemeine Pathologie und Pathologische Anatomie, München, Germany, ³Technische Universität München, 2. Medizinische Klinik, München, Germany, ⁴Christian-Albrechts-Universität, Institut für Pathologie, Kiel, Germany, ⁵Ludwig-Maximilians-Universität, Institut für medizinische Informationsverarbeitung, Biometrie und Epidemiologie (IBE), Münchner Krebsregister, München, Germany, ⁶Klinikum rechts der Isar, Technische Universität München, Klinik und Poliklinik für Chirurgie, München, Germany, ⁷Universitätsmedizin der Johannes Gutenberg-Universität Mainz, Institut für Pathologie, Mainz, Germany, ⁸Klinikum rechts der Isar, Technische Universität München, Institut für Translationale Krebsforschung (TranslaTUM), 2. Medizinische Klinik, München, Germany, ⁹Deutsches Konsortium für Translationale Krebsforschung (DKTK), München, Germany, ¹⁰Bayerisches Zentrum für Krebsforschung (BZKF), München, Germany

Questions/Background

Special AT-rich sequence-binding protein 2 (SATB2) has emerged as an alternative immunohistochemical marker to CDX2 for colorectal differentiation. However, the distribution and prognostic relevance of SATB2 expression in colorectal carcinoma (CRC) have to be further elucidated.

Methods

SATB2 expression was analysed in 1039 CRCs and correlated with clinicopathological and morphological factors, CDX2 expression as well as survival parameters within the overall cohort and in clinicopathological subgroups.

Results

SATB2 loss was a strong prognosticator in univariate analyses of the overall cohort ($p < 0.001$ for all survival comparisons) and in numerous subcohorts including high-risk scenarios (UICC stage III/high tumour budding). SATB2 retained its prognostic relevance in multivariate analyses of these high-risk scenarios (e.g., UICC stage III: DSS: $p = 0.007$, HR: 1.95), but not in the overall cohort (DSS: $p = 0.1$, HR: 1.25). SATB2 loss was more frequent than CDX2 loss (22.2% vs. 10.2%, $p < 0.001$) and of higher prognostic relevance with only moderate overlap between SATB2/CDX2 expression groups.

Conclusion

SATB2 loss is able to identify especially aggressive CRCs in high-risk subgroups. While SATB2 is the prognostically superior immunohistochemical parameter compared to CDX2 in univariate analyses, it appears to be the less sensitive marker for colorectal differentiation as it is lost more frequently.

AG02.10

PPAR γ activation promotes the proliferation of colorectal cancer cell lines and enhances the apoptotic effect of 5-Fluorouracil.

L. Schöckel, C. Woischke, M. Günther, S. Ormanns, J. Neumann
Pathologisches Institut, Ludwig-Maximilians-Universität München, München, Germany

Questions/Background

Colorectal cancer (CRC) as well as diabetes mellitus (DM) represent one of the most relevant health problems of western industrialized nations.[1, 2] Peroxisome proliferator-activated receptor gamma (PPAR γ) belongs to the nuclear receptor family and is involved in the regulation of adipogenesis, lipid metabolism, insulin sensitivity, vascular homeostasis, and inflammation.[3] Moreover, PPAR γ agonists, so-called thiazolidinediones, are well established in DM type 2 therapy.[4] In addition, pro- and anti-tumour properties of PPAR γ have been described in the literature for various tumour entities.[3] Here we examined the influence of PPAR γ activation and inhibition on the cell viability of colorectal cancer cell lines and the chemotherapy sensitivity of 5-Fluorouracil (5-FU).

Methods

Proliferation and the chemotherapy sensitivity of 5-FU of colorectal cancer cell lines HT29 and SW403 were

detected depending on PPAR γ activity using the resazurin cell viability assay. PPAR γ activation was accomplished by treating the cells with rosiglitazone and pioglitazone. The inhibition of PPAR γ was investigated by administration of GW9662, a direct PPAR γ antagonist, and establishment of transient knockdown using siPools.

Results

The treatment with pioglitazone and rosiglitazone led to a significant, dose-dependent increase in proliferation rate. In accordance with this, the PPAR γ inhibition with GW9662 resulted in a significant decrease in proliferation rate. The transient knockdown of PPAR γ caused a cell viability reduction in the SW403 cell line. In addition, we observed a significant increase in chemotherapy sensitivity to 5-FU through the activation of PPAR γ .

Conclusion

In summary, the activation of PPAR γ leads to increased proliferation of colorectal cell lines and thus promotes tumour-progressive properties in CRC. The administration of PPAR γ agonists increases the 5-FU chemotherapy sensitivity. Therefore, establishing a combination therapy of both agents could potentially still be beneficial for patients with CRC. Randomized clinical trials remain necessary to verify the effect in vivo.

AG02.12

TPX2 expression as negative predictor of gemcitabine efficacy in pancreatic cancer

M. Günther¹, S. Surendran¹, M. Haas², V. Heinemann², M. von Bergwelt-Baildon², J. Engel³, J. Werner², S. Böck², **S. Ormanns**¹

¹Pathologisches Institut, Medizinische Fakultät, LMU München, München, Germany, ²LMU Klinikum München, München, Germany,

³Ludwig-Maximilians-Universität, Institute for Medical Information Processing, Biometry and Epidemiology, München, Germany

Questions/Background

Targeting protein for Xenopus kinesin-like protein 2 (TPX2) overexpression in human tumors is associated with increased malignancy. Its effect on gemcitabine-resistance in pancreatic ductal adenocarcinoma (PDAC) has not been studied yet.

Methods

The prognostic impact of TPX2 expression was examined in the tumor tissue of 139 patients with advanced PDAC (aPDAC) treated within the AIO-PK0104 trial or translational trials and of 400 resected PDAC (rPDAC) patients. The findings were validated using RNAseq data of 149 resected PDAC patients.

Results

In the aPDAC cohorts, 13.7 % of all samples showed high TPX2 expression, conferring significantly shorter progression-free survival (PFS, HR 5.25, p<0.001) and overall survival times (OS, HR 4.36, p<0.001) restricted to gemcitabine-based treated patients (n = 99). In the rPDAC cohort, 14.5% of all samples showed high TPX2 expression, conferring significantly shorter disease-free survival times (DFS, HR 2.56, p<0.001) and OS times (HR 1.56, p=0.04) restricted to patients treated with adjuvant gemcitabine. RNAseq data from the validation cohort confirmed the findings.

Conclusion

High TPX2 expression may serve as negative predictor of gemcitabine-based palliative and adjuvant chemotherapy in PDAC and could be used to inform clinical therapy decisions.

AG02.13

Bacterial Lipopolysaccharide as a Negative Predictor of Adjuvant Gemcitabine Efficacy in Pancreatic Cancer

M. Günther¹, L. Gil¹, S. Surendran¹, M. A. Palm¹, V. Heinemann², M. von Bergwelt-Baildon², J. Mayerle², J. Werner², J. Engel³, S. Böck², **S. Ormanns**¹

¹Pathologisches Institut, Medizinische Fakultät, LMU München, München, Germany, ²LMU Klinikum München, München, Germany,

³Ludwig-Maximilians-Universität, Institute for Medical Information Processing, Biometry and Epidemiology, München, Germany

Questions/Background

No predictive biomarker for adjuvant gemcitabine efficacy has been established yet. Recent pre-clinical and retrospective translational studies provided evidence that intratumoral bacteria may mediate gemcitabine resistance. The objective was to evaluate whether intratumoral bacterial lipopolysaccharide (LPS) detection

as surrogate marker for bacterial colonization is associated with outcome in resected pancreatic ductal adenocarcinoma (PDAC) patients treated with adjuvant gemcitabine chemotherapy (aGC).

Methods

Retrospective analysis of archival tumor tissue from 230 aGC patients compared to 146 patients receiving either no or non-gemcitabine-based adjuvant chemotherapy (naGC) after curative intent PDAC resection at an academic tertiary care center between 2000 and 2016. Disease free survival (DFS) and overall survival (OS) calculated from resection until clinically and / or radiologically apparent disease relapse or disease related death respectively.

Results

We detected LPS in 86 samples from 376 patients (197 men, 179 women; median [range] age 66, [41 - 83] years). LPS detection defined a specific tumor microbiome composition revealed by sequencing of the bacterial 16s-rRNA gene. In the 230 aGC patients, LPS detection was associated with worse DFS (8.3 vs 13.7 months, HR 1.75, 95% CI 1.22 - 2.49, $P = .002$) and OS (21.7 vs 28.5 months, HR 1.80, 95% CI, 1.23 - 2.57, $P = .001$), but not in the 146 naGC patients (DFS 5.6 vs 7.4 months, HR = 1.20, 95% CI 0.79 - 1.82, $P = .39$; OS 13.3 vs 18.7 months, $P = .06$, HR = 1.45, 95% CI 0.98 - 2.16). Multivariate analyses confirmed that LPS detection was associated with DFS independent of tumor differentiation, disease stage and R-status in the aGC cohort (HR 1.66, 95%CI 1.14 - 2.42, $P=.008$) but not in the naGC cohort

Conclusion

Intratumoral LPS detected by immunohistochemistry defines a specific tumor microbiome composition and may serve as negative predictor for adjuvant gemcitabine efficacy in resected PDAC. This finding indicates a potential role of microbiome modification to overcome bacteria-mediated chemotherapy resistance.

AG02.14

Establishment of a 3D ex vivo Culture of Pancreatic Cancer Tumor Fragments for Drug Testing

F. Caliskan, L. Häberle, F. Opitz, A. Yavas, I. Esposito

Institut für Pathologie, Universitätsklinikum Düsseldorf, Düsseldorf, Germany

Questions/Background

Pancreatic ductal adenocarcinoma is an aggressive cancer with an increasing incidence, limited therapy options and poor prognosis with a 5-year survival rate of only 11%. As a result, there is an urgent need for personalized therapeutic approaches in the context of precision medicine.

Methods

Tumor fragments (1-2 mm) obtained from 7-8 week old p48Cre^{tg}/+;LSL-KrasG12D/+;p53flox/flox, p48Cre^{tg}/+;LSL-KrasG12D/+;p53flox/flox;Tenascin C^{-/-} and p48Cre^{tg}/+;LSL-KrasG12D/+;p53flox/flox;Periostin^{-/-} mice (n=5 for each genotype) were cultivated on gelatin sponges for 21 days. After 3, 7, 10, 14 and 21 days of culture, the tumor fragments with sponges were fixed in formalin, embedded in paraffin, sectioned and stained with haematoxylin-eosin. Furthermore, immunohistochemistry was performed for Cytokeratin-19, Ki-67, cleaved Caspase-3, SOX-9, α -SMA, Tenascin C and Periostin for analysis of viability, 3D growth behaviour and assessment of the stromal reaction. In addition, drug testing was performed on 3 tumors of p48Cre^{tg}/+;LSL-KrasG12D/+;p53flox/flox mice. Therefore, cultures originated from one tumor were split into 3 groups maintaining a non-treated control culture, a low-dose (100 ng/ml) and a high-dose (500 ng/ml) Gemcitabine-treated culture. Gemcitabine was added to the medium every third day of culture for an overall culturing time of 21 days.

Results

Our results show that cultivated tumor fragments remain viable and retain their proliferative capacity for at least 21 days. In addition, they grow into the sponges and display an accompanying stromal reaction with expression of extracellular matrix proteins. Interestingly, on days 3 and 7, tumor growth is mostly localized at the external sides of the sponges, whereas at later time points (14 days) it proceeds into the deeper parts of the sponges. While apoptosis occurs in the central parts of tumor fragments due to lack of medium diffusion, the ingrowing fraction of cells keeps vital and proliferative. After application of Gemcitabine, increased apoptosis and reduced ingrowth into the sponge is observed in comparison to non-treated cultures.

Conclusion

In conclusion, pancreatic cancer tumor fragments represent a suitable *ex vivo* platform for drug testing with retained relevant biologic characteristics of the neoplastic tissue, such as invasive ability and accompanying stromal reaction.

Enhancer of Zeste Homolog 2 (EZH2) Is a Marker of High-Grade Neuroendocrine Neoplasia in Gastroenteropancreatic and Pulmonary Tract

S. Bremer¹, G. Bittner², O. Elakad², H. Dinter², J. Gaedcke³, A. König¹, A. Amanzada¹, V. Ellenrieder¹, A. Freiherr von Hammerstein-Equord⁴, P. Ströbel², **H. Bohnenberger²**

¹Universitätsmedizin Göttingen, Klinik für Gastroenterologie, Gastrointestinale Onkologie und Endokrinologie, Göttingen, Germany,

²Universitätsmedizin Göttingen, Institut für Pathologie, Göttingen, Germany, ³Universitätsmedizin Göttingen, Klinik für Allgemein-, Viszeral- und Kinderchirurgie, Göttingen, Germany, ⁴Universitätsmedizin Göttingen, Klinik für Herz-, Thorax- und Gefäßchirurgie, Göttingen, Germany

Questions/Background

Tumor grading is the most important prognostic predictor in patients with neuroendocrine neoplasms (NEN) and guides therapeutic management. NEN can be separated into well-differentiated and poorly differentiated types. The more aggressive NEN have been further separated into neuroendocrine tumors (NET-G3) with a better prognosis and neuroendocrine carcinomas (NEC) with a worse prognosis. NET G3 tumors were first described in the gastroenteropancreatic system, but have subsequently also been recognized in other organs, including the thymus. In the lung, the same concept seems to apply, and these tumors are currently called carcinoid tumors with elevated mitotic count/high proliferation index. Despite this distinction's tremendous clinical and therapeutic relevance, optimal diagnostic biomarkers are still lacking.

Methods

In this study, we analyzed the protein expression and prognostic impact of Enhancer of Zeste Homolog 2 (EZH2) in 219 tissue samples of gastroenteropancreatic (GEP-NEN) and pulmonary NEN (P-NEN). For further classification of our collection, we evaluated morphology, mitotic count, Ki67 index, and the expression of p53, RB, Chromogranin A (CgA), SSTR2A, DAXX, and ATRX in all included high-grade NEN.

Results

In our study, strong expression of Enhancer of Zeste Homolog 2 (EZH2) was virtually absent in well-differentiated G1 and G2 NEN, while G3 tumors showed a dichotomous expression with either very weak or very strong expression. In NEN G3, EZH2 overexpression alone could recapitulate the subclassification into NET G3 and NEC and was significantly and strongly associated with poor prognosis. Patients with low EZH2 expression presented with only slightly worse overall survival than patients with NEN G1/2 tumors. Interestingly, EZH2 seems to act independently of Polycomb Repressive Complex 2 (PRC2) in NEN.

Conclusion

In summary, our data clearly demonstrate that EZH2 expression is associated with high-grade NENs, can be used to discriminate NET G3 from NEC, and strongly predicts the survival of patients with NEN G3. Furthermore, EZH2 might be an attractive new therapeutic target in NEN, as inhibitors of EZH2 are already available and are currently being tested in various clinical studies.

Postoperative Pancreatic Fistula Prediction Using Digital Pathology Based Analyses at the Parenchymal Resection Margin of the Pancreas – Results from the Randomized Multicenter RECOPANC trial

A. Mályi¹, S. Timme², T. Keck³, M. Werner², U. Wellner³, P. Bronsert²

¹Institute of Translational Medicine, Semmelweis University, Budapest, Hungary, ²Institute for Surgical Pathology, Freiburg im Breisgau, Germany, ³Department of Surgery, University Medical Center Schleswig-Holstein, Campus Lübeck, Lübeck, Germany

Questions/Background

Artificial intelligence's (AI) role is growing in medical disciplines. Postoperative pancreatic fistula (POPF) represents the most dreaded post-operative complication within pancreatic surgery. Pancreatic tissue texture is acknowledged as one of the strongest predictors for POPF. No standard consensual objective reference has been defined to evaluate the pancreas composition, despite of the different methodological attempts. The presented study's aim was to objectify the pancreatic tissue composition by applying AI-assisted image analysis to correlate the mined histology data with all clinic-pathological parameters from the RECOPANC

study.

Methods

From 14 academic centers, 320 patients were included in the RECOPANC study. After several exclusionary steps, 134 patients' slides were enrolled for AI assisted digital analysis using QuPath. Tissue fields were defined for each slide by experienced pathologists. Machine learning was trained for the tissue compartments (acinary, fibrotic and fat tissue). All compartments were calculated according to their relative and absolute area. POPF was determined according to ISGPF 2005 definition. Patients were divided into No POPF / Grade A and Grade B/C groups.

Results

Relative fibrotic tissue area was revealed as a highly significant determinant for the prediction of clinically relevant POPF (CR-POPF). Compared with the palpatory assessment of the pancreatic texture, the AI assessed pathological amount of fibrotic tissue achieved significantly better predictive power and accuracy for the CR-POPF.

Conclusion

The present study is the first correlating AI-assisted quantified pancreatic tissue composition and POPF within a multicentric cohort. The findings propose an option to standardize POPF prediction through digital quantitative histopathological tissue composition analyses.

AG03 Uropathologie I

AG03.01

Germ cell tumour-related somatic-type malignancies: Characterizing the mutational burden, DNA methylation landscape and proteome to identify the tissue-of-origin, mechanisms of therapy resistance and druggable targets

F. Bremmer¹, P. Pongratanakul², M. Skowron², Y. Che³, A. Richter¹, S. Küffer¹, K. Reuter-Jessen¹, H. Bohnenberger¹, S. Pauls⁴, C. Kresbach⁵, U. Schüller⁵, K. Stühler⁴, P. Albers³, P. Ströbel¹, D. Nettersheim²

¹Universitätsmedizin Göttingen, Institut für Pathologie, Göttingen, Germany, ²Heinrich Heine University Düsseldorf, Department of Urology, Urological Research Laboratory, Translational UroOncology, Düsseldorf, Germany, ³Heinrich Heine University Düsseldorf, Department of Urology, Medical Faculty and University Hospital Düsseldorf, Heinrich Heine University Düsseldorf, Düsseldorf, Germany, ⁴Heinrich Heine University Düsseldorf, Molecular Proteomics Laboratory (MPL), Biological and Medical Research Centre (BMFZ), Düsseldorf, Germany, ⁵University Hospital Hamburg-Eppendorf, Institute of Neuropathology, Hamburg, Germany

Questions/Background

Germ cell tumors might undergo transformation into a somatic-type malignancy, resulting in a cell fate switch to tumours usually found in somatic tissues, such as sarcomas or carcinomas. These tumours are associated with a poor prognosis, however the molecular and epigenetic mechanisms triggering STM are still unclear. Furthermore the tissue-of-origin is still under debate and biomarkers are lacking.

Methods

To address these questions above, we analyzed a cohort of somatic-type malignancy on mutational, epigenetic and protein level using modern and high-throughput methods like TSO assays, 850k DNA methylation arrays and mass spectrometry. Before tumours were morphologically and immunohistochemically characterized.

Results

We show that based on DNA methylation and proteome data carcinoma-related STM more closely resemble yolk-sac tumors, while sarcoma-related STM resemble teratoma. STM harbor mutations in FGF signaling factors (FGF6/23, FGFR1/4) highlighting the corresponding pathway as a therapeutic target. Furthermore, STM utilize signaling pathways, like AKT, FGF, MAPK, and WNT to mediate molecular functions coping with oxidative stress, toxin transport, DNA helicase activity, apoptosis and the cell cycle. Collectively, these data might explain the high therapy resistance of STM. Finally, we identified putative novel biomarkers secreted by STM, like EFEMP1, MIF, and DNA methylation at specific CpG dinucleotides.

Conclusion

This study described molecular and (epi)genetic features of STM in detail in a unique cohort of patient material providing comprehensive mutation, proteome and DNA methylation data as starting point for future studies. For the first time, we show that on a molecular level carcinoma-related STM more closely resemble YST, while sarcoma-related STM resemble TER. Additionally, we identified common mutations as well as molecular and epigenetic mechanisms contributing to the therapy resistance of STM. Finally, we identified new STM biomarkers and therapeutic options to treat STM patients, which should be translated into clinical testing.

AG03.02

Organoid models for the prediction of therapy response on tyrosine kinase inhibitors in clear cell renal cell carcinoma

K. Baschun¹, L. K. Esser¹, K. Fuchs¹, A. Sahu², N. Klümper³, A. Buess², J. Ellinger³, M. Ritter³, G. Kristiansen¹, M. Hölzel⁴, M. I. Toma¹

¹University Hospital Bonn, Institute of Pathology, Bonn, Germany, ²University Hospital Bonn, Core Unit of Bioinformatics Analyses, Bonn, Germany, ³University Hospital Bonn, Department of Urology, Bonn, Germany, ⁴University Hospital Bonn, Institute of Experimental Oncology, Bonn, Germany

Question/Background

Renal cancer is one of the most common neoplasms of the urinary tract system, making up 96% of the malignant neoplasia of the kidney. Clear cell renal cell carcinoma is the most common subtype, with a metastasis risk of about 30-50%. The first line therapy of metastasized RCC comprise combinations of immunecheckpoint inhibitors and tyrosine kinase inhibitors depending on the patient's risk profile. The aim of this study was to predict the therapy response to TKI in organoid models.

Methods

32 patients undergoing a partial or radical nephrectomy between 2019 and 2020 at the Department of Urology, University Hospital Bonn, were included. We cultivated Air-Liquid Interface Patient Derived Organoids (ALI PDOs) from fresh tumor material. The organoids were treated with 10mM Cabozantinib for one or three weeks, while the control group remained untreated. We determined therapy response by quantifying necrotic areas after embedding the organoids. Bulk RNA 3' Seq of our primary tissues was performed and the results were correlated with the therapy response. Promising markers were stained by immunohistochemistry.

Results

We successfully cultivated 24 cases. All cases were treated for one week and 16 cases also for three weeks with Cabozantinib. A high therapy response (more than 66% necrotic areas) was noticed in 41.7% after one week of treatment and 56.2% after three weeks of treatment. RNA Seq revealed *TNFRSF12A* is significantly upregulated and *SEMA3D* is significantly downregulated in the cohort with a good therapy response. The analysis of the TCGA Kidney renal clear cell carcinoma (TCGA-KIRC) cohort revealed that the upregulation of *TNFRSF12A* and the downregulation of *SEMA3D* is significantly correlated with shorter survival times in renal cancer.

Conclusion

Organoids are a promising tool for therapy testing *in vitro* and identification of predictive biomarkers, which could potentially improve the therapy choices in renal cancer.

AG03.03

The role of carbohydrate responsive element binding protein (ChREBP) in nephrocarcinogenesis

K. Hansen, C. Burkert, M. Engeler, P. Vakeel, M. Yasser, F. Dombrowski, S. Ribback

Universitätsmedizin Greifswald, Institut für Pathologie, Greifswald, Germany

Questions/Background

The PI3K/AKT/mTOR pathway is frequently over-activated in renal cell carcinomas and is upregulated in diabetic nephropathy. The related transcription factor ChREBP mediates metabolic alterations such as upregulation of glycolysis and lipogenesis. Diabetic rats show glycogen-storing lesions in the distal tubules of the kidney that present morphologically as clear cell tubules (CCTs). Rat CCTs resemble glycogenotic tubules in humans, so-called Armanni-Ebstein-lesions (AEL). Previous studies from our group revealed a preneoplastic character of AELs and rat CCTs including activation of the PI3K/AKT/mTOR pathway and upregulation of ChREBP. Since a protooncogenic role of ChREBP has been proposed in hepatocellular carcinoma and other malignancies, we hypothesised that ChREBP may also act as a protooncogenic mediator in the kidney.

Methods

The aim of the present study was to investigate the role of ChREBP in diabetes-induced

nephrocarcinogenesis in mice. Diabetes was induced by Streptozotocin-injection in C57Bl/6J wildtype (WT) and ChREBP-KO mice. Mice were sacrificed at one week, four weeks, 3, 6 or 12 months. Kidney tissue of diabetic WT- and ChREBP-KO mice and non-diabetic WT- and ChREBP-KO controls was analysed with special reference to CCTs and kidney tumors using histology, immunohistochemistry and Western Blot analysis.

Results

CCTs were present in the proximal and distal tubules of diabetic WT as well as ChREBP-KO mice. Glycogen accumulation was detected by periodic acid Schiff reaction and confirmed by transmission electron microscopy (TEM). The amount of CCTs was higher and CCTs were more prominent in ChREBP-KO mice compared to diabetic WT mice. CCTs were not observed in non-diabetic animals. Proliferative activity in the kidney tubules was assessed by BrdU labeling index, which showed no difference between the two genotypes.

Advanced preneoplastic lesions and renal cell carcinomas were detected in diabetic WT and ChREBP-KO mice, but occurred earlier in diabetic ChREBP-KO mice. Surprisingly, also non-diabetic ChREBP-KO mice showed preneoplastic lesions and tumors of the kidney, contrasting normal kidneys of non-diabetic WT mice. Immunohistochemistry findings indicate an upregulation of the PI3K/AKT/mTOR pathway in tumors of non-diabetic ChREBP-KO mice.

Conclusion

These findings indicate an unexpected and to date unknown tumor suppressive function of ChREBP in the kidney. However, the mechanisms by which loss of ChREBP leads to kidney tumor formation remain to be understood.

AG03.04

Characterization of the transcription factor GATA6 in urinary bladder carcinoma

F. Fahrenschoen¹, M. Günther^{1,2}, R. Nawroth³, C. Stief⁴, G. B. Schulz⁴, D. Horst⁵, S. Ormanns^{1,2}

¹Pathologisches Institut, Medizinische Fakultät, LMU, München, Germany, ²DKTK Partner Site, Munich, Germany, ³Urologische Klinik und Poliklinik, Klinikum rechts der Isar, Technische Universität, München, Germany, ⁴Urologische Klinik und Poliklinik, LMU Klinikum, München, Germany, ⁵Pathologisches Institut, Charité-Universitätsmedizin, Berlin, Germany

Questions/Background

The transcription factor GATA6 plays pivotal roles in embryonic development and has been associated with differential traits in tumor biology, for instance GATA6 is associated with favorable prognosis in pancreatic cancer. In this project, we examined its effects on malignancy-associated disease characteristics in bladder cancer.

Methods

GATA6 expression was examined by immunohistochemistry in a cohort of 250 resected urothelial bladder cancer tumors. RNAseq expression data of 389 tumors from the TCGA cohort were employed as validation cohort. GATA6 expression was manipulated by siRNA-mediated gene knockdown and CRISPR/Cas9-mediated lentiviral gene knockout in GATA6-expressing bladder cancer cell lines as well as lentivirally mediated, doxycycline-inducible overexpression in GATA6-negative cell lines. The effects of the gene knockdown / knockout and its overexpression on malignancy-associated biological traits such as proliferation, migration, invasion, and chemotherapy-resistance were examined using corresponding assays. Finally, the effects on the transcriptome and potential associated signal transduction pathways were analyzed by western blot and RNA-sequencing to explain biological properties and possibly investigate new therapeutic approaches.

Results

In contrast to pancreatic cancer, high GATA6-expression was significantly associated with poor prognosis in bladder cancer in both the exploratory as well as the validation cohort. Interestingly, the manipulation of GATA6 *in vitro* displayed heterogeneous effects: Whereas GATA6-expression seemed to be associated with increased chemotherapy-resistance, its knockdown seemed to decrease cell proliferation. Interestingly, GATA6-expression seems to be associated to the expression of markers of epithelial-mesenchymal-transition such as fibronectin (FN-1) and FOXA1. The invasion and migration assays are currently ongoing.

Conclusion

GATA6-expression is associated with poor prognosis in bladder cancer and may be associated with epithelial-mesenchymal transition. Further research will elucidate its function in malignancy promoting traits such as proliferation, chemotherapy-resistance, migration and invasion.

AG03.05

Proposal for a novel histologic grading approach for muscle-invasive urothelial

bladder cancer correlating with disease aggressiveness and patient outcomes

M. Eckstein¹, C. Matek¹, P. Wild², H. Taubert³, S. Wach³, D. Sikic³, B. Wullich³, C. I. Geppert¹, E. Compérat⁴, A. Lopez-Beltran⁵, R. Montironi⁶, L. Cheng⁷, T. van der Kwast⁸, M. Colechia⁹, B. W. G. van Rhijn^{10,11}, M. Amin^{12,13}, G. J. Netto¹⁴, J. Lehmann^{15,16}, M. Stöckle¹⁷, K. Junker¹⁷, A. Hartmann¹, S. Bertz¹

¹Institute of Pathology, University Hospital, Friedrich-Alexander-University of Erlangen-Nuremberg, Erlangen, Germany, ²University Hospital Frankfurt & Frankfurt Cancer Institute (FCI)/ Goethe University Frankfurt, Dr. Senckenberg Institute of Pathology (SIP), Frankfurt, Germany, ³University Hospital Erlangen/ Friedrich-Alexander Universität Erlangen-Nürnberg (FAU), Department of Urology and Pediatric Urology, Erlangen, Germany, ⁴Medical University of Vienna, Department of Pathology, Vienna, Austria, ⁵Faculty of Medicine, Cordoba University, Unit of Anatomical Pathology, Cordoba, Spain, ⁶Polytechnic University of the Marche Region, Molecular Medicine and Cell Therapy Foundation, Ancona, Italy, ⁷Brown University Warren Alpert Medical School, and the Legorreta Cancer Center at Brown University, Department of Pathology and Laboratory Medicine, Providence, RI, United States of America, ⁸University Health Network, Laboratory Medicine Program, Princess Margaret Cancer Center, Toronto, Canada, ⁹Vita-Salute San Raffaele University, IRCCS San Raffaele Hospital and Scientific Institute, Milano, Italy, ¹⁰Netherlands Cancer Institute-Antoni van Leeuwenhoek Hospital, Department of Surgical Oncology (Urology), Amsterdam, The Netherlands, ¹¹University of Regensburg, Department of Urology, Caritas St. Josef Medical Center, Regensburg, Germany, ¹²USC Keck School of Medicine, Department of Urology, Los Angeles, CA, United States of America, ¹³University of Tennessee Health Science Center, Department of Pathology and Laboratory Medicine, Memphis, TN, United States of America, ¹⁴University of Alabama at Birmingham, Department of Pathology and Laboratory Medicine, Birmingham, AL, United States of America, ¹⁵Städtisches Krankenhaus Kiel, Department of Urology, Kiel, Germany, ¹⁶Urologische Gemeinschaftspraxis Prüner Gang, Kiel, Germany, ¹⁷Saarland University, Department of Urology and Pediatric Urology, Homburg/Saar, Germany

Questions/Background

Grading of muscle-invasive bladder cancer (MIBC) according to current World Health Organization (WHO) criteria is controversial due to its limited prognostic value. We developed a specific grading system for MIBC integrating histomorphologic phenotype, stromal tumor infiltrating lymphocytes (sTILs), tumor budding, growth and spreading patterns.

Methods

Tissue specimens and clinical data of 484 patients receiving cystectomy and lymphadenectomy with curative intent with or without adjuvant chemotherapy. Histomorphologic phenotypes, sTILs, tumor budding, growth and spreading patterns were evaluated and merged to four grade groups (GG). GGs were correlated with molecular subtypes, immune infiltration, immune checkpoint expression, extracellular matrix remodeling (ECM) and epithelial-mesenchymal transition (EMT) activity.

GGs were associated with overall, disease specific and progression-free survival (OS, DSS, PFS) in univariable and multivariable analyses. Association with biological features was analyzed with descriptive statistics.

Results

Integration of two histomorphologic tumor groups, three sTILs groups, three tumor budding groups and four growth/ spread patterns yielded four novel GGs that had high significance in univariable survival analysis (OS, DSS, PFS). GGs were also confirmed as independent prognostic predictors with the greatest effect in multivariable Cox regression analysis.

Correlation with molecular data showed a gradual transition from basal to luminal subtypes from GG1 to GG4, a gradual decrease in survival, immune infiltration and immune checkpoint activity, and a gradual increase in ECM remodeling and EMT activity.

Conclusion

We propose a novel, prognostically relevant, and biologically based grading system for MIBC in cystectomies and, slightly modified, for transurethral resection specimens, applicable to routine pathological sections.

AG03.06

Proteomic analysis of non-muscle invasive and muscle invasive bladder cancer highlights distinct subgroups

T.-L. J. Dinh^{1,2,3}, M. Cosenza-Contreras^{1,2,3}, M. Li^{1,4,5}, M. Zirngibl¹, N. Pinter¹, F. Hause¹, L. Pauli¹, F. Imberg¹, A. Huynh¹, M. Schmid¹, K. Kurowski¹, I. Glavinsky¹, M. Neuer¹, C. Van Wymersch¹, L. Bergmann¹, L. Braun¹, G. Espadas^{6,7}, J. Schüler⁸, T. Werner^{1,2,9}, E. Brombacher^{9,10,11}, E. Sabido⁶, C. Kreutz, M. Werner, M. Grabbert, P. Bronsert, C. Schell, O. Schilling

¹Institute for Surgical Pathology, Faculty of Medicine, University of Freiburg, Freiburg i. Br., Germany, ²Faculty of Biology, University of Freiburg, Freiburg i. Br., Germany, ³MelnBio Graduate School, University of Freiburg, Freiburg i. Br., Germany, ⁴Institute of Pharmaceutical Sciences, University of Freiburg, Freiburg i. Br., Germany, ⁵SFB 1479, Oncoescape, University of Freiburg, Freiburg i. Br., Germany, ⁶Proteomics Unit, Center for Genomic Regulations, Barcelona, Spain, ⁷University Pompeu Fabra, Barcelona, Spain, ⁸Charles River Laboratories Germany GmbH, Freiburg i. Br., Germany, ⁹Spemann Graduate School of Biology and Medicine, University of Freiburg, Freiburg i. Br., Germany, ¹⁰Institute of Medical Biometry and Statistics, Faculty of Medicine and Medical Center, University

Question/Background

Urothelial bladder cancer ranks among the top ten malignancies worldwide, with approximately 20% of cases presenting as a muscle-invasive entity with worse prognosis. Here, we give an update to our proteomic study on non-muscle invasive and muscle invasive bladder cancer (NMIBC/MIBC).

Methods

We used a cohort comprising treatment-naïve cases of both NMIBC (N=17) and MIBC (N=51), as well as neoadjuvant-treated MIBC patients (N=11). Protein was extracted from formalin-fixed, paraffin embedded (FFPE) samples after macrodissection and analyzed by data-independent acquisition (DIA), yielding an average proteome coverage of >6000 quantified proteins per sample.

Results

The proteomic differences between treatment-naïve and neoadjuvant-treated patients with MIBC were found to be insignificant. However, when comparing treatment-naïve MIBC to NMIBC, we observed an enriched proteomic signature of extracellular matrix (ECM) and immune response components in MIBC, along with a depletion of lipid metabolism and cell-cell adhesion. Using Immunohistochemistry (IHC), we showed that stromal FAP expression is higher in MIBC, indicative for the strong presence of cancer-associated fibroblasts.

Unsupervised clustering of NMIBC proteomes resulted in two clusters, which correlated with grade and featured prominent signatures of either cell adhesion or lipid/DNA metabolism.

Unsupervised analysis of treatment-naïve MIBC produced three distinct clusters with signatures of metabolism, immune-functionality, and ECM. These subgroups resembled transcriptomic consensus clusters previously reported in the literature (Kamoun et al., 2020), specifically luminal-papillary, basal/squamous, and stroma-rich.

Our semi-tryptic data analysis indicates increased endogenous proteolytic processing in MIBC, with upregulated expression of MMP-14. MMP-14 knockdown reduced T24 cell invasion and migration, consistent with previous in vitro studies. Using patient-unmatched transcriptomic data, we detected 1,378 SAAVs, including 53 oncogenic. MIBC had more deactivating TP53 mutations, while NMIBC had more activating FGFR3 mutations, aligning with previous genomic studies. Finally, proteomic analysis of a small patient-derived xenograft (PDX) cohort (N=8) revealed tumor-stromal protein correlation.

Conclusion

In conclusion, our study provides a comprehensive understanding of the proteomic biology of early and advanced bladder cancer, and we were able to identify clusters that resemble clinically relevant mRNA expression subtypes of MIBC.

AG03 Uropathologie II

AG03.07

Testicular Cancer: New Developments, Molecular Pathology and Current Research **Keynote**

A. Lopez Beltran

Córdoba University Medical School, Córdoba, Spain

The subdivision of germ cell tumors into the vast majority derived from germ cell neoplasia in situ and those unrelated has been retained by the 2022 WHO revision. Gonadoblastoma is now added to the noninvasive lesions derived from germ cell neoplasia in situ, due to the fact that it is composed of neoplastic germ cells set in a matrix of immature sex cord cells.

Although the term “seminoma” remains unchanged, it is recognized that in the testis and in any other organ, the terms dysgerminoma, seminoma, and germinoma are used for the same tumor with a similar appearance everywhere in the body. To this end, seminoma was placed in the “germinoma” family of tumors in the 2022 WHO revision, but greater unification of terminology would add desirable in the future. Other nomenclature changes include replacement of the term “Primitive neuroectodermal tumor” by “embryonic neuroectodermal tumor” to assist to separate these tumors clearly from Ewing sarcoma.

A teratoma with somatic-type malignancy is a teratoma that develops a distinct secondary component that resembles a somatic-type malignant neoplasm. Criteria for the diagnosis of “teratoma with somatic transformation” have been modified and it is now recommended to make all measurements in millimeters to gain accuracy and reproducibility. The size criterion has been changed to a 5-mm diameter in the 2022 WHO revision. It is also recommended to avoid the term teratoma with a secondary malignant component or

teratoma with malignant transformation; since it may lead to a misconception that testicular teratoma lacking any somatic-type malignancy are benign. Most examples of neuroendocrine tumors (formerly referred to as carcinoid) in the testis, are now classified as “prepubertal type testicular neuroendocrine tumor”.

Literaturangaben:

[doi:10.1016/j.eururo.2022.06.016] Moch, H. et al, (2022), The 2022 World Health Organization Classification of Tumours of the Urinary System and Male Genital Organs—Part A: Renal, Penile, and Testicular Tumours, *European Urology*, 4 5 8 – 4 6 8

AG03.08

Molecular investigation for optimization the diagnosis, prognosis und therapy of prostate cancer (Habilitation)

A. Offermann

Universitätsklinikum Schleswig-Holstein, Campus Lübeck, Institut für Pathologie, Lübeck, Germany

Questions/Background

Prostate cancer requires individual therapeutic management to avoid overtreatment of indolent disease but to ensure maximal therapy for patients with high risk and aggressive disease. This cumulative habilitation thesis includes translational and basic research studies on the development of diagnostic and prognostic biomarkers for prostate cancer, as well as on the identification of novel therapeutic targets for advanced disease.

Methods

A broad range of methods including histomorphology, immunohistochemistry, transcriptional profiling by RNA sequencing as well as cell culture experiments were used. RNA sequencing was performed using the Nanostring platform. In vitro studies were conducted on prostate cancer cell lines PC-3 und LNCaP. Functional experiments include proliferation, cell cycle and apoptosis assays.

Results

We validated the recently introduced novel prostate cancer grading on our own cohort. In two other studies we identified the signaling molecules CDK19 and TRIM24 as independent prognostic biomarkers, and CDK19 as diagnostic biomarker for the detection of the precursor lesion high-grade PIN. Identically to CDK19, MED15 belongs to the Mediator complex that we identified to be involved in the development of castration resistance and to be linked to PI3K signaling. In order to investigate the implication of posttranslational protein modification for prostate cancer bone metastasis, we performed a transcriptome analysis of all human tripartite family of proteins (TRIM) genes encoding the E3 ligases TRIM. Differentially expressed TRIM genes were linked to tumor related pathways as well as to oncogenes and tumor suppressor genes. In another study, we explored TRIM24 as an independent prognostic biomarker for prostate cancer.

Conclusion

As a summary, these studies collect data about prognostic markers for primary prostate cancer as well as molecular mechanisms which might contribute to prostate cancer progression. The main focus was to investigate members of the transcriptional regulator Mediator complex and the TRIM family of posttranslational modifiers. Assessment of CDK19 and TRIM24 support risk stratification of prostate cancer and serve as independent biomarkers. The transcription factor MED15 is implicated in the development of aggressive castration-resistant prostate cancer and might be a novel therapeutic target. Finally, the E3 ligases TRIM show divergent expression patterns in bone metastatic prostate cancer and are linked to oncogene-related pathways.

AG03.09

Tumour architecture and emergence of strong genetic alterations are bottlenecks for clonal evolution in primary prostate cancer

Y. Tolkach¹, R. Büttner¹, M. Peifer², M.-L. Eich¹, A. Bovier³, N. Abedpour², F. Kreten³

¹University Hospital Cologne, Cologne, Germany, ²University of Cologne, Cologne, Germany, ³University of Bonn, Bonn, Germany

Questions/Background

Prostate cancers (PCA) reveal high levels of intratumoural heterogeneity related to genomic tumour evolution through clonal acquisition of driver alterations. Intratumoural heterogeneity is a major obstacle for

selection of individualized therapies for patients.

Methods

In this study, we create a realistic mathematical model that reconstructs PCA growth from the time of the formation of the first malignant cell up to its evolution into a full-size PCA with superimposed processes of clonal evolution. We validate our findings in synthetic tumor through deep multiregional exome sequencing of 5 primary prostate cancers.

Results

We show that tumour architecture is a major bottleneck and warrants strong genomic driver alterations leading to divergent clonal evolution. Early consecutive acquisition of strong genetic alterations represents a proxy for the formation of aggressive tumours with limited number of clonal hierarchy patterns. A biopsy study of synthetic tumours shows tight spatial intermixing of dominant clones and delineates the importance of biopsy extent for adequate sampling. The patterns of clonal evolution received during mathematical modelling are evident in deep multiregional exome sequencing of primary tumors from five patients with prostate cancer.

Conclusion

Our model provides reasonable predictions of PCA genomic evolution close to the current state of evidence from patient samples, is flexible for integration of the emerging data, and can guide further clinical research.

AG04 Gynäko- und Mammopathologie I

AG04.01

DNA Methylation-based Profiling of Rare Mesenchymal Tumors of the Uterus Identifies Distinct Signatures of GREB1- and KAT6B-rearranged Neoplasms

F. Kommoss¹, D. Kolin², B. Howitt³, C. Parra-Herran², M. Nucci², B. Dickson⁴, J.-C. Lee⁵, A. Agaimy⁶, A. von Deimling⁷, C.-H. Lee⁸

¹Institute of Pathology, Heidelberg University Hospital, Heidelberg, Germany, ²Brigham and Womens Hospital, Boston, United States of America, ³Stanford University School of Medicine, Stanford, United States of America, ⁴Mount Sinai Hospital, Toronto, Canada,

⁵National Taiwan University Hospital, Taipei, Taiwan, ⁶University Hospital Erlangen, Erlangen, Germany, ⁷Institute of Neuropathology, Heidelberg University Hospital, Heidelberg, Germany, ⁸University of Alberta, Edmonton, Canada

Questions/Background

The last few years have witnessed the description of several “new” uterine sarcoma types, including rare tumors with novel gene-rearrangements. Here we analyze DNA methylation profiles in a cohort of uterine mesenchymal neoplasm with novel gene-rearrangements, in the context of established tumor types, to study their classification and gain insight into their biology.

Methods

We collected a multicenter cohort including uterine mesenchymal tumors with *KAT6B::KANSL1* gene fusion (n=9) and *GREB1*-rearrangement (n=9). Whole genome DNA-methylation analysis was performed using the Illumina Infinium MethylationEPIC 850k BeadChip kit. Data were analyzed by t-distributed stochastic neighbor embedding analysis (t-SNE).

Results

T-SNE analysis of array-based DNA methylation data together with a previously generated methylation data set including 8 samples of non-neoplastic muscle (control), 6 SMARCA4-deficient uterine sarcomas (SDUS), 18 low- (LGESS) and 31 high-grade endometrial stromal sarcomas (HGESS), 22 embryonal rhabdomyosarcomas (eRMS), 27 leiomyomas (LMO) and 37 leiomyosarcomas (LMS), as well as 15 uterine tumors resembling ovarian sex-cord tumors (UTROSCT) revealed multiple distinct methylation clusters. In detail, we identified a distinct cluster for UTROSCT (including 7 tumors with *ESR1::NCOA2/3* gene fusion), that clustered with *GREB1*-rearranged tumors. *KAT6B::KANSL1* tumors formed a distinct cluster, with few outliers distributed among other clusters. Interestingly, we observed two distinct clusters of smooth muscle tumors, both of which included LMO and LMS.

Conclusion

Our study shows that *GREB1*-rearranged tumors closely resemble conventional UTROSCT based on DNA methylation analysis. Mesenchymal tumors with *KAT6B::KANSL1* represent molecularly distinct tumor entities, however larger cohorts of these rare neoplasms will have to be analyzed to expand on our findings. Furthermore, our study identifies two novel DNA methylation clusters of uterine smooth muscle tumors, which warrants further investigation.

Indoleamine 2,3- Dioxygenase and PD-L1 Expression in High-Grade Serous Carcinoma of the Female Genital Tract – Favorable Prognostic (Co-)Effect in a Reclassified Large Clinical Cohort

N. Neudeck¹, A. Fischer¹, J. Pasternak², M. Grube², K. Greif¹, C. Beschoner¹, S. Brucker², D. Wallwiener², F. Fend¹, S. Kommoss², A. Staebler¹

¹Institut für Pathologie und Neuropathologie, Universitätsklinikum Tübingen, Tübingen, Germany, ²Universitäts-Frauenklinik, Universitätsklinikum Tübingen, Tübingen, Germany

Questions/Background

High-grade serous tubo-ovarian carcinoma (HGSC) is one of the most immunologically active tumor entities. Therefore, immunotherapeutic approaches move into focus for individualized therapies. In previous studies from our group, the immune regulator Indoleamine 2,3- Dioxygenase (IDO1), was identified as tumor associated antigen (TAA) in the HLA-ligandome, suggesting a combined function. Therefore, we analyzed IDO1 in a large cohort of HGSC and performed a multiparametric analysis with PD-L1, tumor infiltrating lymphocytes (TILs) and clinical parameters.

Methods

A consecutive series of 392 cases from the Womens' Hospital of the University Tuebingen from 2000 until 2016 was (re)-classified or confirmed as high-grade serous tubo-ovarian carcinoma. Tissue microarrays (TMAs) were constructed and analyzed for IDO1 expression on tumor cells and on TILs by immunohistochemistry, followed by integrated analyses with previous data on PD-L1, CD3⁺ and CD8⁺ TILs.

Results

In 98.7% of cases (n= 387/392), sufficient tissue for IDO1 expression was available. TILs in HGSC showed IDO positivity in 57% of cases, while 89.9% (n=348/387) of cases showed any positivity on tumor cells (>1% positive staining). Significantly improved median overall and disease-free survival was observed within a range of maximal IDO1 expression on TILs from >10-25% in hotspots (OS 1.549 days; p=0.007 vs. DFS 637 days; p=0.089). For IDO1 expression on tumor cells, also a range >10% was beneficial (OS 1.311 days; p<0.001 vs. DFS 535 days; p=0.016). The combination of PD-L1 and IDO1 expression on TILs showed best median OS results. However, IDO1 expression on TILs >25% leads to reverse effects with poorest median OS.

Conclusion

In conclusion, IDO1 expression on TILs with intermediate level has a positive effect on survival, which was even increased by PD-L1 and high numbers of TILs. However, high-level expression (>25%) resulted in poor overall survival. We hypothesize, that intermediate level IDO1 expression is associated with immunologically "hot" tumors, which are prognostically favorable. If the level of 25% positive TILs is crossed, the inhibitory effects will predominate over the immune response. Therefore, IDO1 expression has different effects on survival, depending on the level of expression and the interplay with other factors in the tumor microenvironment.

Optimizing the FOLR1 RxDx Immunohistochemical Companion Diagnostic Kit for Eligibility Testing for Novel Antibody-Drug Conjugate Elahere (Mirvetuximab/ Soravtansine) for Ovarian Carcinoma Treatment

A. Jungbluth, P. Ruh, E. Hernandez, D. Frosina, L. Ellenson

Memorial Sloan Kettering Cancer Center, Pathology, New York, United States of America

Questions/Background

Recently antibody-drug conjugate Elahere® (mirvetuximab/soravtansine) has been released for the treatment of epithelial ovarian carcinoma. Eligibility testing is performed by FOLR1 expression analysis based on FOLR1 RxDx diagnostic kit provided by Ventana-Roche. We repeatedly failed to achieve the positive control staining of normal Fallopian tube as outlined in the FOLR1 RxDx guidelines. Consequently, we tried to optimize FOLR1 RxDx immunostaining by modifying staining procedures.

Methods

FOLR1 RxDx kit is based on mAb FOLR1-2.1 ready-to-use/RTU preparation, a mandatory staining protocol employing the Ventana Benchmark Ultra stainer platform and reagents. FOLR1 RxDx instructions stipulate normal Fallopian tube as positive control tissue and specifying the required staining pattern of the Fallopian tube epithelium. An immunostained Fallopian tube sample-slide is also provided with the kit.

We tested several Ultra staining protocols by modifying primary incubation and/or antigen retrieval time. We also tested the FOLR1 RxDx kit on the Leica Bond-3 stainer platform employing Leica reagents except the primary antibody.

Results

The mandatory FOLR1RxDx staining protocol consists of a 32' primary incubation time and 64' AGR time (hipH buffer, CC1) and secondary detection system Optiview. Following kit instructions including, protocol, reagents, and equipment, we failed to achieve the required 'predominantly moderate circumferential membranous' immunostaining in various Fallopian tube specimens. Only marginal improvement could be achieved by varying primary incubation and AGR time. We then tested mAb FOLR1-2.1 on the Leica Bond-3 platform, which resulted in strong and consistent staining using a 30' incubation and 30' AGR time (hi pH buffer, ER2). Moreover, diluting the RTU preparation up to 1:5 still generated staining vastly superior to the FOLR1 RxDx protocol performed on the Ventana Ultra stainer. Similar results and differences were seen in various ovarian carcinoma samples.

Conclusion

FOLR1 expression typing is compulsory for Elahere therapy eligibility testing. However, employing the mandatory FOLR1 RxDx reagents, equipment, and protocol often results in weak staining. A significantly more consistent and stronger immunostaining can be achieved by employing FOLR1 RxDx on the Leica Bond-3 platform. Our analysis suggests that FOLR1 RxDx testing following current protocol and equipment recommendations could vastly underestimate the number of eligible patients.

AG04.04

Claudin 18.2 expression in histological subtypes of matched ovarian cancer primaries and metastases

P. Wagner¹, P. Gass², P. Pöschke², M. Eckstein¹, L. Gloßner¹, A. Hartmann¹, M. W. Beckmann², P. A. Fasching², M. Ruebner², R. Erber¹

¹Institute of Pathology, University Hospital Erlangen, Friedrich-Alexander-Universität Erlangen-Nürnberg (FAU), Comprehensive Cancer Center Erlangen-EMN, Erlangen, Germany, ²Department of Gynaecology and Obstetrics, University Hospital Erlangen, Friedrich-Alexander-Universität Erlangen-Nürnberg (FAU), Comprehensive Cancer Center Erlangen-EMN (CCC ER-EMN), Erlangen, Germany

Questions/Background

Claudins function as part of tight junctions. Physiologically, claudin 18 splice variant 2 (CLDN18.2) expression is restricted to the gastric epithelium, but it has also been detected in gastric, esophageal, pancreatic, ovarian, and lung cancer. Zolbetuximab, a chimeric IgG1 antibody targeting CLDN18.2 that has been shown to significantly prolong progression-free and overall survival in patients suffering from CLDN18.2-positive, HER2-negative locally advanced gastric cancer, is currently being studied in other advanced solid cancers in clinical trials. Interestingly, both metastatic gastrointestinal mucinous carcinomas from the upper gastrointestinal tract and mucinous primary ovarian carcinomas (MPOCs) were reported to express CLDN18.2 in up to 84%. However, little is known about CLDN18.2 expression in other histological subtypes of primary ovarian cancer (POC) and their matching metastases.

Methods

Using a cohort of all histological POC subtypes, we investigated the immunohistochemical (IHC) CLDN18.2 expression in both POCs (n=542) and matching metastatic tissue (OCM, n=388) plus 96 metastases without primary. To account for intratumoral CLDN18.2 heterogeneity, tissue microarrays comprised both the tumor center and periphery. IHC assessment was performed according to the phase III SPOTLIGHT study with CLDN18.2 positivity being defined as biomarker expression of $\geq 75\%$ in tumor cells with moderate-to-strong membranous staining.

Results

Overall, CLDN18.2 positivity was detected in 4% (21/521) of POC centers and 3.5% (18/305) of their peripheries. In MPOCs, CLDN18.2 positivity rates were 46% (18/39) in the tumor centers and 37.5% (15/40) in their peripheries. Positivity rates for the corresponding mucinous OCMs (MOCMs) were 33% (4/12, center) and 27% (3/11, periphery). In regard to CLDN18.2 positivity, intratumoral concordance rates were 62.5% (15/24) in POCs and 75% (3/4) in metastases. Interestingly, the expression patterns of primary and metastatic cells differed in 75% of the matched pairs. With no relevant expression in 99.5% of the nonmucinous tumors, CLDN18.2 positivity was almost exclusively seen in the mucinous subtype.

Conclusion

In ovarian cancer, CLDN18.2 positivity was, with rare exceptions, restricted to the mucinous subtype, and expression seemed to be pronounced at the primary site and the tumor center. Nevertheless, 33% of MOCMs presented with CLDN18.2 positivity. Hence, CLDN18.2 might be a promising target for personalized therapy in patients with advanced POMC.

AG04.05

STK11 mutated adnexal tumor

W. Solass

Universität Bern, Pathologie, Bern, Switzerland

Questions/Background

31-year-old woman with an incidentally detected mass in the left adnexal loge during a routine inspection. No prior history of disease and inconspicuous family history was documented. Transvaginal ultrasound and MRI confirmed a 6.5 cm large mass in the left adnexal loge with potential origin from the fallopian tube.

Methods

Macroscopy: A well-circumscribed nodular tumor in the peri-adnexal soft tissue (ligament) was seen and resected during laparoscopic resection. Additionally, three isolated nodules of the Douglas peritoneum and the peritoneum of the sacrouterine ligament were sent for histological analysis.

Histology: Heterogeneous growth pattern.

Immunohistochemistry was non-conclusive, showing a homogenous WT1 positivity, patchy PAX8 positivity, P53- Wildtype and only a moderate proliferation index of 10-20%. Wolffian- neoplasms and sex cord stromal tumors were excluded.

Results

Additional Next-generation sequencing was performed, which detected a STK11 mutation (c.734+1G>A 86.3%) and defined the entity of STK11 mutated adnexal tumor.

Conclusion

STK11 mutated adnexal tumor is an emerging entity in the WHO classification with only 22 published cases worldwide.

50% of these cases have an association with Peutz-Jeghers syndrome.

The clinical outcome is variable depending on the completeness of the surgical resection.

Metastasis and/or recurrence of disease is described in 80% of these 22 patients.

It is important to raise the awareness of this new entity among clinicians and pathologists.

AG04.06

An integrated approach to the diagnosis of mesenchymal tumors of the uterus

E. Oliva

Harvard Medical School, Dana-Farber/Harvard Cancer Center (DF/HCC), Boston, United States of America

Integration of morphology, immunohistochemistry and molecular findings is evolving our knowledge and thus the classification of mesenchymal tumors of the uterus. Even though smooth muscle tumors continue to be the most common, we struggle in the distinction between some leiomyoma variants and smooth muscle tumors of uncertain malignant potential from leiomyosarcomas (LMS). A new proposed algorithm to separate among these categories is based on alterations involving TP53, RB1, ATRX, PTEN, CDKN2A, or MDM2. Furthermore high-grade sarcomas with myogenic differentiation harboring hotspot PDGFRB mutations and others may closely mimic leiomyosarcoma. The spectrum of myxoid tumors has also expanded as besides myxoid LMS, the possibility of inflammatory myofibroblastic tumor and BCOR rearranged high-grade endometrial stromal sarcoma (HG-ESS) should be considered. A novel GLI-1 sarcoma associated with myxoid background has recently been described and other tumors involving the uterus can be myxoid including NTRK sarcomas. Thus, an immunohistochemical panel should include CD10, ER, PR, cyclinD1, BCOR, ALK, ROS, pan TRK and muscle markers (depending on the differential)(one should be aware of pitfalls) as well as molecular studies. Be aware that inflammatory myofibroblastic tumor is positive for most smooth muscle markers and may closely mimic a smooth muscle tumor in the primary or metastases and high-grade endometrial sarcoma with BCOR alterations may be positive for smooth muscle actin as well as panTRK. Furthermore, some myxoid leiomyosarcomas are known to have PLAG1 fusions and this may help if present in this diagnosis. When evaluating an epithelioid or epithelioid and spindle neoplasm in the uterus, the possibility of PEComa, uterine tumor resembling an ovarian sex cord tumor, and SMARCA4 deficient uterine sarcoma or even undifferentiated carcinoma should be considered in the differential diagnosis. Melanocytic, epithelial and sex cord markers as well as SMARCA4 (BRG1) should be added to the immunohistochemical panel. We know now that PEComas and LMS share some immunohistochemical and molecular features but it is important to diagnose PEComas as they can be treated with mTOR inhibitors. If the epithelioid cells are small and blue and are associated with brisk mitotic activity, the possibility of YWHAE high-grade endometrial stromal sarcoma should be considered. A subset of epithelioid leiomyosarcomas are

now shown to have PRG fusions.

AG04 Gynäko- und Mammopathologie II

AG04.07

A novel organoid system that mimics usual ductal hyperplasia (UDH) and mammary ductal carcinoma in situ (DCIS) suggests that DCIS-related myoepithelial cells are premalignant and form an integral part of intraductal breast lesions

J. Kluge, D. Papić, I. Koch, D. Horst, **S. Florian**

Charité - Universitätsmedizin Berlin, Institut für Pathologie, Berlin, Germany

Questions/Background

The transition from ductal carcinoma in situ (DCIS) to invasive cancer and how and when malignant cells acquire the ability to invade the stroma surrounding the duct is not fully understood. The currently leading hypothesis is that, to become invasive, the epithelial cells proliferating in the duct lumen need to penetrate the surrounding layer of myoepithelial cells. Supporting this hypothesis, it has been shown that myoepithelial cells actively capture and push back such cancerous intraductal cells, thus inhibiting the development of invasive cancer [1]. However, recent observations from patient samples using multiplexed imaging show that, paradoxically, DCIS with a partially disrupted myoepithelial cell layer has a lower likelihood of recurrence after surgery than lesions with an intact layer of myoepithelial cells [2].

Methods

We have developed a system of genetically related organoids that mimic usual ductal hyperplasia (UDH, [3]) and DCIS. They fully recapitulate the morphological criteria as well as patterns of marker expression of these premalignant entities.

Results

Interestingly, although in each case they are originally derived from a single cell clone, the organoids autonomously develop two cell populations: intraductal luminal proliferating cells and a single layer of surrounding peripheral myoepithelial cells. This suggests that DCIS might consist not only of one but two cell populations: luminal cells *and* myoepithelial cells that are derived from a common mutated bipotent stem cell. We will introduce our organoid system as well as evidence from previous research supporting the concept that myoepithelial cells surrounding DCIS can be part of the lesion and genetically related to the enclosed proliferating luminal cells.

Conclusion

According to this model, to develop breast cancer, it would not be sufficient for epithelial cells to acquire the ability to invade stroma. It would be equally important that myoepithelial cells, forming part of the lesion, would lose the ability to form an external myoepithelial cell layer. As a next step, to validate this hypothesis, we will isolate luminal and epithelial cells from DCIS through microdissection and compare their genetic profile to determine if they are clonally related.

Literaturangaben:

[1] Sirka, O. K. et al., Ewald, A. J., (2018), Myoepithelial cells are a dynamic barrier to epithelial dissemination, J Cell Biol, 3368-3381, 217(10)

[2] Risom, T. et al., Angelo, M. , (2022), Transition to invasive breast cancer is associated with progressive changes in the structure and composition of tumor stroma, Cell, 299-310.e18, 185(2)

[3] Florian, S. et al., Mitchison, T. J., (2019), A human organoid system that self-organizes to recapitulate growth and differentiation of a benign mammary tumor, PNAS, 11444-11453, 116(23)

A pilot study on the epigenomic characterization of luminal A and luminal B breast cancer

T. Kraus, J. Schwaiger, K. Sotlar

Uniklinikum Salzburg, Universitätsinstitut für Pathologie, Salzburg, Austria

Questions/Background

Breast cancer (BC) is the most frequent cancer in women worldwide. Thereby, therapy depends on the biological profile underlying breast cancer, e.g. estrogen receptor expression, progesterone receptor expression, Her2 status, tumour grade, proliferative activity. Furthermore, gene expression testing enables to allocate BCs to distinct molecular subtypes: Luminal A, luminal B, basal-like and Her2-enriched. Depending on the molecular subtype and the tumor proliferation (Ki67-index), BC patients receive individualized treatments. The aim of this study was to perform an epigenomic characterization of luminal A and luminal B cancers, the latter requiring adjuvant chemotherapy based on the usually much worse prognosis.

Methods

In this pilot study we performed epigenome-wide methylation analysis on 16 BCs with 8 cancers of luminal A and 8 cancer of luminal B subtype. Applying the Illumina Infinium EPIC bead chip array we were able to interrogate more than 850,000 methylation sensitive CpG sites in parallel. Computational analyses were performed to identify differentially methylated genes. Gene ontology analyses were processed to reveal altered pathways.

Results

We found that BCs of luminal A subtype showed 468 significantly differentially methylated gene regions compared with BCs of luminal B subtype. Thereby, 365 gene regions were hypermethylated and 103 gene regions were hypomethylated in luminal B cancers compared with luminal A cancers. Gene ontology (GO) analysis showed that chromatin silencing at rRNA pathway was the top hypomethylated pathway.

Conclusion

In summary, in this pilot study, we found significant differences in DNA methylation signatures between luminal A and luminal B breast cancers, possibly representing a new/additional tool for BC molecular subtyping and, thus, prognostication.

Correlation between neutrophil-to-lymphocyte ratio and pathological response to neoadjuvant therapy in triple negative breast cancer

M. Zhao, Y. Liu, J. Ying

The Fourth Hospital of Hebei Medical University, Department of Pathology, Shijiazhuang, China

Questions/Background

Immune response plays an important role in the treatment and prognosis evaluation of breast cancer. The aim of this study was to investigate the correlation between peripheral blood neutrophil to lymphocyte ratio (NLR) and response to neoadjuvant therapy (NAT) and patient prognosis.

Methods

A total of 126 patients with triple-negative breast cancer who received neoadjuvant therapy were enrolled in this study. PD-L1 (22C3), TILs, CD8+TIL and FOXP3+TIL were detected by immunohistochemistry in core needle biopsy specimens before NAT, and NLR was calculated. PD-L1(CPS) positivity was defined as ≥ 10 stained cells. The median of CD8+TIL and FOXP3+TIL interpretation results was used as the cut-off value to determine high or low expression levels. spearman rank correlation analysis was used to analyze the correlation between each index and pCR. Receiver operating characteristic (ROC) curve was used to evaluate the accuracy of NLR in predicting pCR, and Youden index was used to determine the high or low level of NLR.

Results

NLR was negatively correlated with TILs density and CD8+/FOXP3+ TIL density ratio (Spearman's Rho = -0.286, $p=0.023$; Spearman's Rho coefficient = -0.310, $p=0.013$). Patients with low NLR/high TILs density showed the highest pCR rate (23/24, 95%), while only 3/11 patients (21%) with high NLR/low TILs density achieved pCR. Patients with low NLR had the highest pCR rate in PD-L1 positive patients, while patients with high NLR had the lowest pCR rate in PD-L1 negative patients ($p = 0.001$). Multivariate analysis showed that high NLR was independently associated with pCR (HR = 3.106, 95%CI = 1.507-6.404, $p = 0.002$).

Conclusion

NLR may be a potential biomarker for predicting response to NAC in TNBC patients.

Histological assessment of treatment response during thermo-radiotherapy of recurrent breast cancer – a longitudinal study

P. Bronsert^{1,2}, T. S. Jelonnek³, K. Dreyling³, S. Timme-Bronsert^{1,2}, J.-O. Gebbers⁴, P. Vaupel^{2,3}, A.-L. Grosu^{2,3}, A. M. Lüchtenborg^{2,3}, A. R. Thomsen³

¹University of Freiburg - Medical Center, Department of Surgical Pathology, Freiburg, Germany, ²German Cancer Consortium (DKTK), Partner Site Freiburg, Freiburg, Germany, ³University of Freiburg - Medical Center, Department of Radiation Oncology, Freiburg, Germany, ⁴University of Berne, Institute of Pathology, Research Group AI, Berne, Switzerland

Questions/Background

Following curative treatment for breast cancer, non-resectable recurrences occur in 3-5% of cases and are often challenging to treat due to previous therapy. The combination of superficial hyperthermia and re-irradiation (HT+reRT) is a treatment option for recurrent breast cancer due to radiosensitizing effects of hyperthermia.

Our objective was the evaluation of histological treatment response in patients' tissue treated with HT+reRT.

Methods

20 prospective and 14 retrospective patients were enrolled in a non-randomized trial (local ethics committee approval: FR-ETK 201/19) to study therapy response and histological processes in patients tissue treated with HT+reRT. Superficial hyperthermia of 39-43°C was applied for 60 min with water-filtered infrared-A irradiation (wIRA) immediately followed by irradiation with 4 Gy/week in 5-6 consecutive weeks. Before start of treatment, during ongoing therapy (dose of 12 Gy) and at follow-up after 6 weeks, punch biopsies (2 mm diameter) were taken and processed for (immuno-)histochemistry. Histological regression was graded according to Miller-Payne, based on tumor cellularity. Epidermal thickness and minimal distance between epidermis and tumor cells were measured. Patient outcome was determined by clinical examination and photo documentation.

Results

Biopsies from 31 patients at doses of 0-24 Gy were analysed. 29 treated regions could be followed longitudinally, of which 68% showed decreased tumor cellularity. A marked or complete tumor regression (Miller-Payne score of 4 or 5) was found in 44% of data sets, 27% showed progression or no regression at the final data point. Tumor-free distance from skin was increased in 21 locations, with simultaneous reduction in cellularity in 15 locations. Epidermal thickness was reduced slightly during treatment. Histological observations corresponded to clinically assessed patient outcome.

Conclusion

Thermo-radiation treatment correlates with reduction of local tumor burden indicated by histological regression and increased tumor-free distance to skin. Interestingly, histological regression can often be observed already early during treatment whereas clinical response typically becomes evident after end of therapy. Our data indicate that patients may be subdivided into 3 groups: Patients with histological regression at (a) low or (b) higher doses and (c) non-responding patients. Identification of predictive markers for treatment response is subject of ongoing research.

Software-assisted evaluation of immunophenotypic variation regarding D2-40, CD31 and Prox1 in sinus endothelium in sentinel lymph nodes of invasive breast carcinoma including prognostic impact

J. Derben¹, M. Örum¹, C. Blasberg¹, A. Hattesoht¹, M. Kalder², C. Denkert¹, C. C. Westhoff¹

¹UKGM GmbH/ Philipps-Universität Marburg, Institut für Pathologie, Marburg, Germany, ²UKGM GmbH/ Philipps-Universität Marburg, Klinik für Frauenheilkunde und Geburtshilfe/ Brustzentrum Regio, Marburg, Germany

Questions/Background

Several studies have demonstrated the *de novo* formation of lymphatic vessels or the reorganization of lymphatic sinuses in tumor-draining lymph nodes, partly preceding the detection of lymphatic metastases. This "lymphovascular niche" is supposed to facilitate the survival of metastatic tumor cells. Recently, we have shown that a higher proportion of D2-40 stained subcapsular sinuses in sentinel lymph nodes (SLN) in breast cancer (BC) patients is significantly associated with worse overall survival (OS) and an independent prognostic parameter in multivariate analysis. This study aims at evaluating the observed immunophenotypic variations of sinus endothelium in SLN of BC in a larger cohort by software-assisted image analysis with respect to clinicopathological data and prognostic impact.

Methods

Suitable cases with SLN of invasive BC were identified in the Institute of Pathology and the corresponding clinical and histopathological data was extracted. Lymph nodes of 231 patients were stained for HE, D2-40, CD31 and Prox1. QuPath software was used for training on digitized slides and for assessing the immunohistochemical stained absolute area of endothelial cells of the subcapsular sinus. The Cutoff Finder web application was used for identification of the best cutoff for continuous parameters according to OS. Collected data was statistically evaluated for age, tumor size, TNM parameters, grading, tumor type, receptor/ HER2 status and OS.

Results

Absolute area of D2-40-/CD31-/Prox1-stained subcapsular endothelial cells (SEC) defined by QuPath-assisted evaluation showed a significant positive correlation with each other. With dichotomization according to the cutoffs identified by Cutoff Finder, a larger area of CD31-positive SEC was significantly associated with worse OS ($p = 0.001$). A larger area of D2-40 and Prox1 demonstrated a tendency towards worse OS. Larger area of D2-40-/CD31-/Prox1-stained SEC was an independent marker for worse OS in multivariate analysis. Smaller total area of subcapsular sinus correlated significantly with higher age and with worse OS in univariate analysis.

Conclusion

QuPath-assisted evaluation of immunophenotypic variations of subcapsular sinus endothelium in SLN essentially confirmed and extended our previous findings regarding D2-40, CD31 and Prox1. The concept of a lymphovascular niche remains to be further elucidated in the setting of clinical pathology, especially in the context of different cofactors such as activation status of the immune system.

AG04.12

The HER2DX genomic test for HER2+ breast cancer

A. Prat

University of Barcelona, Hospital Clinic Barcelona / IDIBAPS, Oncology Department, Barcelona, Spain

In this presentation, I will provide a comprehensive overview of the development and validation process of the HER2DX genomic assay, a cutting-edge diagnostic tool specifically designed for patients diagnosed with early-stage HER2-positive breast cancer. This innovative assay combines the expression analysis of 27 genes, including a B-cell gene signature, with relevant clinical data, offering three distinct types of information that are crucial for effective treatment decision-making.

One key aspect of the HER2DX assay is its inclusion of a B-cell gene signature. B-cell-related genes play a significant role in the immune response and tumor microenvironment in HER2-positive breast cancer. By incorporating this gene signature, the HER2DX assay provides valuable insights into the interaction between the tumor and the immune system, aiding in the understanding of the disease biology and potential response to treatment.

Furthermore, the HER2DX assay generates a risk-score by meticulously analyzing the genomic profile of the tumor, taking into account various genetic markers associated with HER2-positive breast cancer, including the B-cell gene signature. This risk-score provides valuable insights into the likelihood of disease progression and recurrence.

Additionally, the HER2DX assay incorporates a pCR (pathologic complete response) likelihood score, which evaluates the probability of achieving a complete eradication of cancer cells following neoadjuvant treatment. The HER2DX genomic assay has undergone extensive validation through multiple retrospective studies, encompassing a wide range of tumor samples. Moreover, it has been rigorously evaluated in prospective clinical trials, including notable studies like the APT trial. These validations have consistently demonstrated the robustness and reliability of the assay, affirming its clinical utility and efficacy in accurately assessing HER2-positive breast cancer.

Overall, the development and validation of the HER2DX genomic assay, including its incorporation of a B-cell gene signature, represent a significant advancement in the field of breast cancer diagnostics. By integrating genomic analysis, including immune-related gene expression, with clinical data, this innovative tool empowers clinicians with comprehensive and personalized information, facilitating optimal treatment decisions for patients with early-stage HER2-positive breast cancer.

AG05 Kinder- und Fetalpathologie

AG05.01

Lymphocytic myocarditis - an underestimated diagnosis concerning babies and

older children?

R. Dettmeyer

Institut für Rechtsmedizin Justus-Liebig-Universität Gießen, Giessen, Germany

Einleitung. Die Diagnose einer (post-)viralen lymphozytären Myokarditis basierte in der Vergangenheit auf den sog. Dallas-Kriterien. Deren Wert wird beeinträchtigt durch eine hohe Inter-Observer-Variabilität und dem sog. Sampling Error, beziehen sich die Dallas-Kriterien doch auf myokardiale Biopsien. Die spätere immunhistochemische Qualifizierung und Quantifizierung interstitieller intramyokardialer Lymphozyten und Makrophagen führte zur Etablierung von Normwerten für Proben vom Erwachsenenmyokard.

Lymphozytäre Myokarditis im Säuglings- und Kindesalter. Todesfälle als Folge einer viralen Myokarditis sind im Säuglingsalter selten. Bei älteren Kindern konnten gelegentlich letale virale Myokarditiden nachgewiesen werden. Im Säuglingsalter werden plötzliche natürliche Todesfälle in vielen Ländern am häufigsten dem Sudden Infant Death Syndrome (SIDS) zugeordnet. Per definitionem darf dies erst nach Ausschluss aller diagnostischen Möglichkeiten geschehen.

Konventionell-histologische Diagnostik. Bei in konventionell-histologischen Färbungen nur singulär fokal nachweisbaren lymphozytären Infiltraten ist deren Interpretation umstritten, die Zahl der untersuchten Proben ist von Bedeutung.

Immunhistochemie. Die immunhistochemische Qualifizierung und Quantifizierung interstitieller Lymphozyten und Makrophagen erlaubt die Angabe von Grenzwerten für die Diagnose einer Myokarditis im Säuglingsmyokard.

Molekulargenetik. In Abhängigkeit vom Verlauf der viralen Infektion kann die molekulargenetische Diagnostik zum Nachweis viralen Genoms im Myokard führen.

Ergebnis. Die stufenweise Ausschöpfung des Spektrums diagnostischer Optionen führt zu einem häufigeren Nachweis (post-)viraler Myokarditiden vor allem im Säuglingsalter. Vorrangig sind Enteroviren (Coxsackieviren) und Adenoviren nachweisbar, aber auch das Epstein-Barr-Virus und PVB-19 kommen vor.

AG05.03

Autopsies of fetocids with congenital heart malformations- a single center study in Germany

A. Reitz, S. Gretser, E. Gradhand

Dr. Senckenbergisches Institut für Pathologie, Frankfurt am Main, Germany

Question/Background

Even though congenital heart disease is common, the causes for these malformations are currently not entirely known. Researchers suspect a multifactorial disease etiology including a genetic component since first degree relatives of affected patients show an up to 3-fold increased risk of having a congenital heart disease themselves. In order to evaluate the respective diagnostic process, autopsy reports were checked for consistency between clinical and autopsy diagnoses and for the rate of performed genetic testing.

Methods

Reports of all fetal autopsies performed at the Department of Pathology, University Clinic Frankfurt am Main, Germany from 2018 to 03/2023 were screened for fetocides due to congenital heart malformations. Autopsy findings were compared to the clinical information provided by the obstetricians. If the autopsy findings completely confirmed the clinical diagnosis, they were grouped as 'consistent'. If there were additional findings that were previously unknown to clinicians or were not provided, they were grouped as 'consistent with information gain'. In case of discrepancies cases were grouped as 'not consistent'. As an indicator of how many times genetic testing of any kind was performed, we scanned all files of autopsy cases whether frozen autopsy material was referred for genetic testing.

Results

Out of all autopsies (n=186), 8 were sent in as fetocides due to congenital heart malformations. Almost all cases were 'consistent with information gain' (87,5%). Additional information mostly consisted of specifications on the heart malformation itself, but also included significant findings of other fetal organs and the placenta. One case showed complete correspondence (12,5%). None were grouped as 'not consistent'. In 25% of cases frozen fetal material was referred for genetic testing (compared to an overall rate in all autopsy cases of 5,6%).

Conclusion

Even though congenital heart malformations are common, autopsies on fetuses with these conditions are rarely performed in Germany. While the rate of genetic testing in those cases exceeds the overall rate of all performed autopsies, it could still be greatly improved in order to further our knowledge of disease etiologies. Furthermore, even if genetic testing is done, pathologists in Germany do not get a respective report which

makes it difficult to prepare a conclusive autopsy report. Clinical diagnoses and possible treatment for living relatives or future pregnancies therefore may remain superficial or incomplete.

AG05.04

Tissue shrinkage of resected specimens in Hirschsprungs disease: Why paediatric surgeons think the bowel specimen was longer than indicated in the pathology report.

S. Gretser¹, K. Weber², Y. Braun³, P. Harter⁴, U. Rolle³, J. McNally⁵, E. Gradhand⁶

¹Universitätsklinikum Frankfurt, Dr. Senckenbergisches Institut für Pathologie, Frankfurt am Main, Germany, ²Universitätsklinikum Frankfurt, Neurologisches Institut (Edinger Institute), Frankfurt am Main, Germany, ³Universitätsklinikum Frankfurt, Abteilung für pädiatrische Chirurgie und pädiatrische Urologie, Frankfurt am Main, Germany, ⁴Ludwig-Maximilians Universität, Zentrum Für Neuropathologie und Prionen Forschung, München, Germany, ⁵Universitätsklinikum Bristol and Weston, Abteilung für pädiatrische Chirurgie, Bristol, United Kingdom, ⁶Universitätsklinikum Frankfurt, Dr. Senckenbergisches Institut für Pathologie, Frankfurt am Main, Germany

Question/Background

Tissue shrinkage due to formalin fixation is a known phenomenon in some adult specimens but not studied in pediatric specimens especially for bowel specimens of HD patients. The objective of this study is to quantify the extent of HD specimens shrinkage from the time of the fresh specimens at the point of surgery up to formalin fixation.

Methods

Colorectal HD specimens from two different pathology institutes were measured at the time of surgery as well as at the time of cut-up, either fresh (Frankfurt cohort) or after formalin fixation (Bristol cohort) and statistically analyzed.

Results

In total, sixteen colorectal specimens were included. In the Bristol cohort, following formalin fixation, the specimens length decreased by 26.3% (n=8, p<0.001). In the Frankfurt cohort, without formalin fixation, the specimens shrank by an average of 16.9% (n=8, p=0.05). One specimen which was measured twice before formalin fixation initially shrank by 19% while it shrank additional 8% after formalin fixation.

Conclusion

This study is the first to describe the extent of postoperative tissue alteration / specimen shrinkage in HD specimens. The two different cohorts revealed that tissue shrinkage is mostly caused by tissue retraction/alteration after organ removal but also to a lesser extent by fixation with formalin. Surgeons and (neuro-)pathologists should be aware of the sizeable shrinking artifact to avoid unnecessary confusion.

AG06 Thoraxpathologie

AG06.01

Phosphoproteomic Analysis Identifies TYRO3 as a Mediator of Sunitinib Resistance in Metastatic Thymomas

S. Küffer¹, J. Grabowsky¹, S. Okada^{1,2}, N. Sojka¹, S. Welter³, A. von Hammerstein-Equord⁴, M. Hintertaner⁴, L. Cordes³, X. von Hahn¹, D. Müller¹, C. Sauer⁵, H. Bohnenberger¹, A. Marx^{1,5}, P. Ströbel¹

¹Universitätsmedizin Göttingen, Institut für Pathologie, Göttingen, Germany, ²Kyoto Prefectural University of Medicine, Department of Surgery, Graduate School of Medical Science, Kyoto, Japan, ³Lungenklinik Hemer, Thoraxchirurgie, Hemer, Germany, ⁴Universitätsmedizin Göttingen, Klinik für Thorax-, Herz- und Gefäßchirurgie, Göttingen, Germany, ⁵Universitätsmedizin Mannheim, Institut für Pathologie, Mannheim, Germany

Questions/Background

After initially responding to empiric radio-chemotherapy, most advanced thymomas (TH) and thymic carcinomas (TC) become refractory and require second-line therapy. The multi-target receptor tyrosine kinase (RTK) inhibitor, sunitinib, is one of the few options, especially in patients with thymic carcinomas, and has resulted in partial remissions and prolonged overall survival. However, sunitinib shows variable activity in thymomas, and not all patients benefit equally. A better understanding of its mode of action and the definition of predictive biomarkers would help select patients who profit most.

Methods

Six cell lines were treated with sunitinib in vitro. Cell viability was measured by MTS assay and used to define in vitro responders and non-responders. A quantitative real-time assay simultaneously measuring the phosphorylation of 144 tyrosine kinase substrates was used to correlate cell viability with alterations of the phospho-kinome, calculate a sunitinib response index (SRI), and impute upstream tyrosine kinases. Sunitinib was added to protein lysates of 29 malignant TH and TC. Lysates were analyzed with the same phosphorylation assay. The SRI tentatively classified cases into potential clinical responders and non-responders. In addition, the activation patterns of 44 RTKs were studied by phospho-RTK arrays in 37 TH and TC.

Results

SRI application separated thymic epithelial tumors (TET) in potential sunitinib responders and resistant cases. Upstream kinase prediction identified multiple RTKs potentially involved in sunitinib response, many of which were subsequently shown to be differentially overexpressed in TH and TC. Among these, TYRO3/Dtk stood out since it was exclusively present in metastatic TH. The function of TYRO3 as a mediator of sunitinib resistance was experimentally validated in vitro.

Conclusion

Using indirect and direct phosphoproteomic analyses to predict sunitinib response in malignant TET, we have shown that TH and TC express multiple important sunitinib target RTKs. Among these, TYRO3 was identified as a potent mediator of sunitinib resistance activity, specifically in metastatic TH. TYRO3 may thus be both a novel biomarker of sunitinib resistance and a potential therapeutic target in advanced thymomas and thymic carcinomas.

AG06.02

Histological, immunohistological and molecular characterization of congenital pulmonary airway malformation (CPAM)

M. von Laffert¹, S. Schweitzer¹, M. Lacher², O. Aubert², F. W. Hirsch³, D. Gräfe³, K. Hauptmann⁴, A. Arnold⁴, D. Horst⁴, M. Chirica⁵, F. Klauschen⁵, U. Obeck¹, M. Boeschen¹, M. Stiller⁶, H. Bläker⁶

¹Universitätsklinikum Leipzig, Institut für Pathologie, Leipzig, Germany, ²Klinik und Poliklinik für Kinderchirurgie, Leipzig, Germany,

³Institut für Kinderradiologie, Leipzig, Germany, ⁴Institut für Pathologie Charité, Berlin, Germany, ⁵Institut für Pathologie LMU, München, Germany, ⁶Universitätsklinikum Leipzig, Leipzig, Germany

Questions/Background

Congenital pulmonary airway malformation (CPAM) is a hamartomatous cystic lesion of the lung. The classification refers to Stocker with type I, II, III being the most common. Basis is the size of the cyst and its morphological nature. Another possible finding are foci of goblet cell hyperplasia (GCH). An underlining *KRAS*-mutation was described. Fakler and Hermelijn (each 2020) were the first presenting larger molecular studies. *KRAS* mutations were detected in all GCH (9/33 and 11/23 samples). The data concerning the occurrence of the mutation in the adjacent CPAM epithelia were conflicting. Hermelijn could detect *KRAS* mutations in both (GCH and non-mucinous lesional tissue). This was confirmed by Nelson et al. (2022) within the largest single-center study so far (89 patients; Stocker type I and/or III). The latter did not reflect type II lesions. Furthermore, a multicenter study encompassing immunohistochemistry (IHC) and molecular data reflecting mutations (DNA) and fusions (RNA) is still missing.

Methods

So far, we have collected 39 cases (21UKL-Leipzig, 10LMU Munich, 8Charité Berlin). The Stocker classification seems somewhat arbitrary. Thus, we reevaluated all samples according to size of cyst, composition of epithelium, cyst wall, presence of GCH. Then, we performed IHC (18 marker panel) with regards to cytokeratin expression, cell cycle, transcription factors (i.a. TTF1, PAX8, Napsin, Surfactant, CK5/6, CK7, CK20, p16, p53) and Next Generation Sequencing (NGS: 40 gene panel; 113 fusion panel).

Results

80% of the data are analysed so far. 31% of the samples were type1, 23% type 2, 43% showed mixed type pattern. 46% were Napsin positive, 41% CK20-positive. 23% showed *KRAS* mutations (7x*G12D*, 1x*G12V*, 1x *G12D/V* co-mutation). Mutations were detected in GCH and non-GCH cystic areas. One CCAM with *KRAS G12D* mutation showed a further *TP53* mutation.

Conclusion

Our preliminary data suggest that the arbitrary subdivision in type I+II seems not practicable, as hybrid lesions are dominating. A subclassification besides conventional histology, based on protein expression (as Napsin/CK 20) and molecular data (*KRAS*-status) seems to be more appropriate. To the best of our knowledge, we are the first reporting a *KRAS G12D/TP53* co-mutation and a CPAM harboring a *KRAS* double mutation (*G12D+V*). Our still ongoing and growing cohort tries to shed light on the evolution of this entity. Further steps focus the implementation of clinical (outcome) and radiological (prediction) data.

Deciphering molecular mechanisms of chemoresistance in SCLC

C. Kümpers¹, S. Marwitz², M. Jokic³, C. Heide³, A. Fähnrich⁴, I. Vlasic^{3,5}, F.-O. Paulsen³, T. Olchers⁶, M. Reck⁶, H. Busch⁴, T. Goldmann², S. Perner⁷, J. Kirfel³

¹Institute of Pathology University Hospital Schleswig-Holstein Campus Luebeck, Lübeck, Germany, Pathologie, Lübeck, Germany,

²Histology Research Center Borstel, Leibniz Lung Center, Borstel, Germany, Borstel, Germany, ³Institute of Pathology University Hospital Schleswig-Holstein Campus Luebeck, Lübeck, Germany, ⁴Institute of Experimental Dermatology, University of Lübeck, Lübeck, Germany, Lübeck, Germany, ⁵Laboratory for Protein Dynamics, Division of Molecular Medicine, Ruđer Bošković Institute, Zagreb, Croatia, Zagreb, Croatia, ⁶LungenClinic Grosshansdorf, Großhansdorf, Germany, Großhansdorf, Germany, ⁷Institute for Hematopathology, Hamburg, Germany, Hamburg, Germany

Questions/Background

Aim: SCLC is an aggressive form of lung cancer with a very poor prognosis and limited therapeutic options. Although SCLC initially responds well to platinum-based chemotherapy, it mostly recurs and at recurrent status, it most often shows resistance to therapy. This demonstrates the need for the identification of mechanisms underlying this resistance and derivation of novel therapeutic targets.

Methods

Methods: We identified SCLC patients (n=26) with paired samples of pre- and post-treatment tumors. We performed a whole-transcriptome analysis and identified the hallmark gene sets on significant differentially expressed genes between naïve and relapsed SCLC samples. Findings of the transcriptomic analysis were in part studied on the protein level by immunohistochemistry. Furthermore, it was analyzed which gene sets have an impact on the time-to-relapse.

Results

Results: We identified distinct transcriptomic profiles which differed significantly between pre-treatment and post-treatment SCLC. One striking difference consisted in the exclusion of immune pathways in the chemorelapsed SCLC. We identified the two gene sets "DNA Repair" and "KRAS Signaling Down" to have an impact on time-to-relapse. A high gene set score for "DNA Repair" was associated with a short time-to-relapse and reciprocally, a high score gene set score for "KRAS Signaling Down" was associated with a prolonged time to relapse in chemotherapy naïve samples.

Conclusion

Conclusion: This study gives invaluable insight into the key differences in transcriptomic profiles of pre-treatment and post-treatment SCLC. We could imagine that these findings might point out ways for the design of novel targeted therapy to improve the survival of SCLC patients.

CD63 serves as a don't-eat-me-signal in lung adenocarcinomas and steers macrophages towards the immunosuppressive M2 phenotype

E. Dingendorf¹, M. Stoffel¹, D. Kittel¹, G. Kristiansen¹, G. Wernig^{2,3}, T. Lerbs¹

¹Institut für Pathologie, Universitätsklinikum Bonn, Bonn, Germany, ²Stanford School of Medicine, Department of Pathology, Stanford, CA, United States of America, ³Stanford School of Medicine, Institute for Stem Cell Biology and Regenerative Medicine, Stanford, CA, United States of America

Questions/Background

Lung cancer is the primary cause of cancer-related mortality in Germany. Though new therapies, in particular immunotherapies and targeted therapies, allow long-time survival even in advanced stages, only a minority of patients benefits from them and tumors often grow resistant over time. A diversification of therapeutic approaches is necessary to allow patients to switch between therapies several times and to increase survival. The tetraspanin CD63 is commonly found on intra- and extracellular membranes, and correlates with a worse survival in lung adenocarcinomas. This study explored through which mechanisms CD63 drives lung adenocarcinomas and whether targeting CD63 offers therapeutic potential.

Methods

First, we quantified the expression of CD63 and the number of macrophages in fresh patient samples via spectral flow cytometry and validated these results via in situ-hybridization and immunohistochemistry. Thereafter, we deleted CD63 through CRISPR-Cas9 in three lung cancer cell lines (A549, H819, and LC19),

and tested whether CD63 drives proliferation in vitro and in an adoptive transfer model in vivo. Next, we used flow cytometry and a luciferase reporter assay to determine whether the expression of CD63 is regulated through cytokines. Thereafter, we explored whether the deletion of CD63 increases the phagocytosis of lung cancer cell lines through macrophages in vitro. Additionally, we used flow cytometry to test whether CD63 steers macrophages towards the immunosuppressive M2 phenotype.

Results

Lung adenocarcinomas showed an increased expression of CD63 in spectral flow cytometry and immunohistochemistry, and CD63 was correlated with a more intense macrophage infiltrate. Functionally, deleting CD63 reduced the proliferation of three lung cancer cell lines, both in vitro and in vivo. Adding pro-inflammatory cytokines to A549 cells increased the intracellular expression of CD63 but decreased its promoter activity. Deleting CD63 increased the macrophage-mediated phagocytosis of all three lung cancer cell lines, and blocking CD63 through an antibody steered macrophages towards the pro-inflammatory M1 phenotype.

Conclusion

This study demonstrates that CD63 exerts several pro-tumorigenic functions in lung adenocarcinomas. In particular, it protects lung cancer cells from phagocytosis and steers macrophages towards the immunosuppressive M2 phenotype. All together, these results suggest the potential of a targeted therapy against CD63.

AG06.05

Tumor intrinsic PD-L1 exerts an oncogenic function through activation of the Wnt/ β -catenin pathway in human non-small cell lung cancer

Y. Ma¹, R. Marinkova¹, M. Nenkova¹, L. Jin², O. Huber³, J. Sonnemann⁴, N. Peca¹, N. Gaßler¹, Y. Chen¹

¹Section Pathology of the Institute of Forensic Medicine, Jena University Hospital, Friedrich Schiller University, Jena, Germany,

²Zhejiang Provincial People's Hospital, Department of Hematology, Hangzhou, China, ³Institut of Biochemie II, Jena University Hospital, Friedrich Schiller University Jena, Jena, Germany, ⁴Children's Clinic, Jena University Hospital, Friedrich Schiller University Jena, Department of Pediatric Hematology and Oncology, Jena, Germany

Questions/Background

Programmed death-ligand 1 (PD-L1) strongly inhibits T cell activation, thereby aiding tumors in escaping the immune response. PD-L1 inhibitors have proven to be effective in treatment of different types of cancer including non-small cell lung cancer (NSCLC). Yet, the knowledge regarding the biological function of tumor cell intrinsic PD-L1 in lung cancer remains obscure.

Methods

In the present study, we used "gain-of-function" and "loss-of-function" strategies, as well as exosomal microRNA analysis, aiming to shed more light on the functional role of PD-L1 in NSCLC.

Results

We found that PD-L1 silencing resulted in decreased migratory and invasive ability of tumor cells, together with attenuated colony forming capacity. Ectopic expression of PD-L1 showed the opposite effects, along with increased activities of MAPK and Wnt/ β -catenin pathways, and upregulation of Wnt/ β -catenin target genes. Additionally, overexpression of PD-L1 was associated with dysregulated cellular and exosomal miRNAs involved in tumor progression and metastasis. In primary lung tumors, immunohistochemistry revealed that both PD1 and PD-L1 were highly expressed in lung squamous cell carcinoma (SCC), compared to adenocarcinoma ($p=0.045$ and $p=0.036$, respectively), and in SCC, PD1 expression was significantly associated with tumor grading ($p=0.016$).

Conclusion

Taken together, our data suggest that PD-L1 may exert an oncogenic function in NSCLC cells through activating Wnt/ β -catenin signaling, and it may act as a potential diagnostic marker for lung SCC.

AG06.06

Epidemiology of Thymoma and Thymus Cancer in the United States and Germany, 1999-2019

T. S. Gerber¹, S. Strobl¹, A. Marx², W. Roth¹, S. Porubsky¹

¹University Medical Center Mainz, Institute of Pathology, Mainz, Germany, ²University Medical Center, Institute of Pathology, Göttingen,

Questions/Background

Thymic epithelial tumors are a rare type of thoracic solid tumor that occurs most commonly in the anterior mediastinum. The WHO classification divides thymomas from thymic carcinomas, but epidemiological data are limited due to rarity and complexity, especially in Germany.

Methods

Cancer registry data was obtained from the National Cancer Institute's Surveillance, Epidemiology, and End Results (SEER) program and the Centre for Cancer Registry Data (Zentrum für Krebsregisterdaten, ZfKD). Using this data, we analyzed the entities occurring in the anterior mediastinum as well as the incidence, age, sex, frequency, and survival of the different thymus tumor subtypes. The incidence rate changes were calculated using joinpoint regression analysis.

Results

In patients younger than twenty years, 80% (US) and 67% (GER) of tumors are lymphomas and germ cell tumors, while in older patients 63% (US) and 64% (GER) are comprised of thymic epithelial tumors. In the US, there were 8,171 patients with epithelial tumors of the thymus, with a male-to-female ratio of 1.09, mean age of 59.48 years, and an incidence rate of 2.68 per million inhabitants per year at risk. In Germany, 3,081 patients were diagnosed, with a male-to-female ratio of 1.03, a mean age of 61.33 years, and an incidence rate of 3.06 per million inhabitants per year. In the regression model for the evaluation of the age-adjusted incidence rate of epithelial tumors of the thymus in the US, two joinpoints were identified in 2008 and 2011, but overall, the incidence rate remained relatively stable over time. The mean survival of patients with type AB thymomas was overall the most favorable, while patients with thymic carcinomas showed the poorest survival.

Conclusion

This is the first study to systematically investigate epidemiological characteristics of epithelial tumors of the thymus in Germany in a large cohort.

AG06.07

Lung Adenocarcinoma Promotion by Air Pollutants

W. Hill¹, E. Lim², C. Weeden², C. Lee², M. Augustine³, K. Chen⁴, F.-C. Kuan⁵, F. Marongiu⁶, E. Evans Jr⁶, D. Moore⁴, F. Rodrigues⁷, O. Pich², B. Bakker², H. Cha⁸, R. Myers⁹, F. v. Maldegem¹⁰, M. Lüchtenborg¹¹, E. Grönroos¹², J. Downward¹³, T. Jacks¹⁴, C. Carlsten¹⁵, I. Malanchi⁷, A. Hackshaw¹⁶, K. Litchfield¹⁷, W. Hill¹, J. DeGregori⁶, M. Jamal-Hanjani¹⁸, C. Swanton²

¹Cancer Evolution and Genome Instability lab, The Francis Crick Institute, London, United Kingdom, ²Cancer Evolution and Genome Instability lab, The Francis Crick Institute, London, United Kingdom, ³Cancer Research UK Lung Cancer Centre of Excellence, University College London Cancer Institute, London, UK, London, United Kingdom, ⁴Cancer Research UK Lung Cancer Centre of Excellence, University College London Cancer Institute, London, United Kingdom, ⁵Department of Hematology and Oncology, Chang Gung Memorial Hospital, Chiayi, Taiwan, ⁶Department of Biochemistry and Molecular Genetics, University of Colorado Anschutz Medical Campus, Aurora, United States of America, ⁷Tumour-Host Interaction Laboratory, The Francis Crick Institute, London, United Kingdom, ⁸Division of Hematology-Oncology, Department of Medicine, Samsung Medical Center, Sungkyunkwan University School of Medicine, Seoul, Republic of Korea (South Korea), ⁹BC Cancer Research Institute, University of British Columbia, Vancouver, Canada, ¹⁰Department of Molecular Cell Biology and Immunology, Amsterdam, The Netherlands, ¹¹National Disease Registration Service (NDRS), NHS England, Leeds, United Kingdom, ¹²Cancer Evolution and Genome Instability Laboratory, The Francis Crick Institute, London, United Kingdom, ¹³Oncogene Biology Laboratory, The Francis Crick Institute, London, United Kingdom, ¹⁴David H. Koch Institute for Integrative Cancer Research, Cambridge, United States of America, ¹⁵Department of Medicine, Division of Respiratory Medicine, Chan-Yeung Centre for Occupational and Environmental Respiratory Disease, Vancouver Coastal Health Research Institute, Vancouver, Canada, ¹⁶Cancer Research UK and UCL Cancer Trials Centre, London, United Kingdom, ¹⁷Tumour Immunogenomics and Immunosurveillance Laboratory, University College London Cancer Institute, London, United Kingdom, ¹⁸Cancer Metastasis Laboratory, University College London Cancer, London, United Kingdom

A complete understanding of how exposure to environmental substances promotes cancer formation is lacking. More than 70 years ago, tumorigenesis was proposed to occur in a two-step process: an initiating step that induces mutations in healthy cells, followed by a promoter step that triggers cancer development. Here we propose that environmental particulate matter measuring $\leq 2.5 \mu\text{m}$ ($\text{PM}_{2.5}$), known to be associated with lung cancer risk, promotes lung cancer by acting on cells that harbour pre-existing oncogenic mutations in healthy lung tissue. Focusing on EGFR-driven lung cancer, which is more common in never-smokers or light smokers, we found a significant association between $\text{PM}_{2.5}$ levels and the incidence of lung cancer for 32,957 EGFR-driven lung cancer cases in four within-country cohorts. Functional mouse models revealed that air pollutants cause an influx of macrophages into the lung and release of interleukin-1 β . This process results in a progenitor-like cell state within EGFR mutant lung alveolar type II epithelial cells that fuels tumorigenesis. Ultradeep mutational profiling of histologically normal lung tissue from 295 individuals across 3 clinical cohorts revealed oncogenic *EGFR* and *KRAS* driver mutations in 18% and 53% of healthy tissue

samples, respectively. These findings collectively support a tumour-promoting role for PM_{2.5} air pollutants and provide impetus for public health policy initiatives to address air pollution to reduce disease burden.

AG07 Herz-, Gefäß-, Nieren- und Transplantationspathologie

AG07.01

Current diagnostic aspects in cardiac transplantation and rejection

R. M. Bohle

Universitätsklinikum des Saarlands, Institut für Pathologie, Homburg/Saar, Germany

R. M. Bohle

Department of Pathology, Saarland University Medical Center, Homburg (Saar), Germany

Cardiac transplantation is one of the key therapies for end-stage chronic heart failure. If indicated, it is the only true "cure" for most of these patients. Meanwhile clinical indications and contraindications are well established. Medical care following transplantation focusses on immunosuppression, infection prevention and health maintenance.

The current pathomorphological analyses of the transplanted hearts aim at clinically indicated endomyocardial biopsies or surveillance biopsies for standardized grading of acute cellular rejection, antibody-mediated rejection or mixed type of rejection. Beyond chronic rejection and cardiac allograft vasculopathy can occur. The explanted heart should also be investigated in a standardized way. The histodiagnostic procedures include rapid protocols for formalin-fixed, paraffin-embedded endomyocardial biopsies, various immunostaining tests, i.e. for the typing of leukocytes, macrophages, endothelial cells, markers of complement activation and markers for the detection of opportunistic infections. Recently several non-invasive blood-sampling techniques have been introduced as tools identifying rejection and may be used for the monitoring of pediatric patients. Additionally digital pathology approaches were established to support the morphological diagnoses of acute and chronic graft failure as well as the diagnoses and prediction of cardiac allograft vasculopathy.

The most important diagnostic procedures are discussed with respect to new ISHLT guideline for the care of heart transplant recipients.

AG07.02

Alloreognition and the spectrum of kidney transplant rejection

J. Callemeyn

KU Leuven, Nephrology and Renal Transplantation Research Group, Leuven, Belgium

Detection of mismatched human leukocyte antigens by adaptive immune cells is considered as the main cause of transplant rejection, leading to either T-cell mediated rejection or antibody-mediated rejection. This canonical view guided the successful development of immunosuppressive therapies and shaped the diagnostic Banff classification for kidney transplant rejection that is used in clinics worldwide.

However, several observations have recently emerged that question this dichotomization between T-cell mediated rejection and antibody-mediated rejection, related to heterogeneity in the serology, histology, and prognosis of the rejection phenotypes. In parallel, novel insights were obtained concerning the dynamics of donor-specific anti-human leukocyte antigen antibodies, the immunogenicity of donor-recipient non-human leukocyte antigen mismatches, and the autoreactivity against self-antigens. Moreover, the potential of innate alloreognition was uncovered, as exemplified by natural killer cell-mediated microvascular inflammation through missing self, and by the emerging evidence on monocyte-driven alloreognition.

This talk will highlight the gaps in the current classification of rejection, provide an overview of the expanding insights into the mechanisms of alloreognition, and critically appraise how these could improve our understanding and clinical approach to kidney transplant rejection.

AG07.03

Electron microscopy and the renal transplant: helpful for more black and white

diagnoses and less shades of grey?

T. Menter

Institut für Pathologie, Basel, Switzerland

In diesem Vortrag wird die Bedeutung der Elektronenmikroskopie für die Diagnostik von Nierentransplantaten dargestellt.

Die Elektronenmikroskopie hat hierbei eine Bedeutung bei zwei verschiedenen Krankheitskomplexen: zum einen kann sie hilfreich sein, ein frühes Rezidiv der Erkrankung, die zum terminalen Nierenversagen geführt hat, nachzuweisen (z. B. Podozytopathie, Immunkomplexablagerungen, Amyloidose).

Daneben hat sie auch eine wichtige Funktion für den Nachweis einer humoralen Abstoßung. Mittels der Elektronenmikroskopie kann durch den Beleg der Veränderungen an Basalmembranen der peritubulären Kapillaren und der glomerulären Kapillarschlingen die Diagnose einer humoralen Abstoßung gestellt werden, frühe Formen der Transplantatglomerulopathie zeigen sich oft zuerst in der Elektronenmikroskopie, hierfür gibt es auch einen eigenen Bestandteil in der Banff-Klassifikation (cg1a).

Durch die Integration von Fallbeispielen aus der täglichen Routine wird die Anwendung elektronenmikroskopischer Befunde und deren Differentialdiagnosen demonstriert.

AG07.05

Fluorescence Confocal Microscopy on Liver Specimens for Full Digitization of Transplant Pathology

M. N. Kinzler¹, F. Schulze², A. Reitz², S. Gretser², P. Ziegler², O. Shmorhun², M. Friedrich-Rust¹, J. Bojunga¹, S. Zeuzem¹, A. A. Schnitzbauer³, W. O. Bechstein³, H. Reis², A. P. Barreiros⁴, P. J. Wild^{2,5,6}

¹Department of Internal Medicine I, University Hospital Frankfurt, Goethe University Frankfurt am Main, Germany, Frankfurt am Main, Germany, ²Dr. Senckenberg Institute of Pathology, University Hospital Frankfurt, Goethe University Frankfurt am Main, Germany, Frankfurt am Main, Germany, ³Department of General, Visceral, Transplant and Thoracic Surgery, University Hospital Frankfurt, Goethe University Frankfurt am Main, Germany, Frankfurt am Main, Germany, ⁴German Organ Procurement Organization (DSO), 60594 Frankfurt am Main, Germany, Frankfurt am Main, Germany, ⁵Frankfurt Institute for Advanced Studies (FIAS), Frankfurt am Main, Germany, Frankfurt am Main, Germany, ⁶Frankfurt Cancer Institute (FCI), University Hospital Frankfurt, Goethe University Frankfurt am Main, Germany, Frankfurt am Main, Germany

Questions/Background

Fluorescence confocal microscopy (FCM) is a rapidly evolving tool that provides real-time virtual hematoxylin-eosin (HE) images of native tissue. Data about the potential of FCM as an alternative to frozen sections for the evaluation of donor liver specimens are lacking so far. Aim of the current study was to determine the value of FCM in liver specimens according to the criteria of the German Society for Organ Procurement (DSO).

Methods

In this prospective study, conventional histology and FCM scans of 50 liver specimens (60% liver biopsies, 26% surgical specimens, 14% donor samples) were evaluated according to the DSO.

Results

Comparison of FCM scans and conventional frozen sections revealed almost perfect levels of agreement for cholangitis ($k=0.877$), fibrosis ($k=0.843$) and malignancy ($k=0.815$). Substantial levels of agreement could be obtained for macrovesicular steatosis ($k=0.775$), inflammation ($k=0.763$), necrosis ($k=0.643$) and steatohepatitis ($k=0.643$). Levels of agreement were moderate for microvesicular steatosis ($k=0.563$). Strength of agreement between frozen sections and FCM was superior to the comparison of conventional HE and FCM imaging

Conclusion

We introduce FCM as a potential alternative to frozen section that may represent a novel approach to liver transplant pathology where timely feedback is crucial, and the deployment of human resources is becoming increasingly difficult.

AG08 Knochen-, Gelenk- und Weichgewebspathologie

AG08.02

A single-hit shortcut to tumorigenesis through epigenome remodeling and impaired

differentiation in oncohistone-driven giant cell tumor of bone.

P. Lutsik^{1,2}, D. Mancarella², A. Baude², S. Oez², M. Ganslmeier², G. Oldfield², A. Kühn², C. Jiang³, Z. Huang⁴, B. Lenoir^{5,6}, J. Förster⁷, D. Jäger^{5,8}, I. Zörnig^{5,8}, F. Haller⁹, U. Toprak¹⁰, N. Halama^{5,6}, S. Haas¹¹, A. Riemer⁷, U. Oppermann³, M. Llamazares-Prada², A. Lindroth¹², J. Fellenberg¹³, C. Plass²

¹KU Leuven, Department of Oncology, Leuven, Belgium, ²German Cancer Research Center (DKFZ), Cancer Epigenomics, Heidelberg, Germany, ³Botnar Research Centre, University of Oxford, Nuffield Department of Orthopaedics, Rheumatology and Musculoskeletal Sciences, Oxford, United Kingdom, ⁴German Cancer Research Center (DKFZ), Applied Tumor Immunity, Heidelberg, Germany, ⁵German Cancer Research Center (DKFZ), Clinical Cooperation Unit „Applied Tumor Immunity“, Heidelberg, Germany, ⁶German Cancer Research Center (DKFZ), Translational Immunotherapy, Heidelberg, Germany, ⁷German Cancer Research Center (DKFZ), Immunotherapy and Immunoprevention, Molecular Vaccine Design, Heidelberg, Germany, ⁸National Center for Tumor Diseases and Heidelberg University Hospital, Medical Oncology, Heidelberg, Germany, ⁹University Hospital Erlangen, Friedrich-Alexander University Erlangen-Nürnberg, Institute of Pathology, Erlangen, Germany, ¹⁰German Cancer Research Center (DKFZ), Neuroblastoma Genomics, Heidelberg, Germany, ¹¹German Cancer Research Center (DKFZ), Stem Cells and Cancer, Heidelberg, Germany, ¹²National Cancer Center, Cancer Biomedical Science, Seoul, Republic of Korea (South Korea), ¹³Orthopedic University Hospital Heidelberg, Ruprecht-Karl University of Heidelberg, Department of Experimental Orthopedics, Heidelberg, Germany

Giant cell tumor of bone (GCTB) is a rare, locally aggressive and currently incurable bone neoplasm with infrequent metastasis (<5% of cases), affecting mostly adolescent and young adult patients [1]. GCTB lesions emerge due to the accumulation of excessive multi-nucleated osteoclasts (giant cells). Nonetheless, the GCTB neoplastic compartment is comprised by mesenchymal-type stromal cells. The exact cell-of-origin and events triggering its neoplastic transformation are enigmatic. Over 90% of GCTB cases carry a single hotspot mutation in *H3F3A*, most frequently leading to the G34W substitution in the replication-independent histone variant H3.3 [2]. We and others have demonstrated the absence of other recurrent genetic events, implying that the H3.3-G34W oncohistone is a sole disease driver with a striking capability to induce tumorigenesis in GCTB, mostly likely through an epigenetic regulation impairment in the uncharacterized cell-of-origin. Although possible mechanisms have been proposed [3,4], the details remain elusive. Through a sequence of genomic, transcriptomic and epigenomic analyses, we have earlier shown that GCTB stromal cells undergo a global epigenetic remodeling, most prominently characterized by the loss of DNA methylation and an apparent distortion of heterochromatin repression [5]. Since the epigenetic state in the GCTB cell-of-origin is uncharted, the interpretation of these alterations lacks an adequate reference. Thus, we conducted a detailed multiomic characterization of gene expression and chromatin states in GCTB patients, cell lines and non-cancerous mesenchymal stromal cells, subject to osteogenic differentiation. This analysis revealed a complex hierarchy of cell populations within the neoplastic compartment at various differentiation stages. Mapping GCTB patient cells to the exact stage is crucial to disentangling H3.3-G34W-driven and differentiation-related epigenetic changes, and will require sophisticated models for cancer cell-of-origin inference. Furthermore, GCTB features complex microenvironment dynamics, with subsets of patients with high immune cells infiltration. We could show that this is likely caused by (i) derepression of cryptic transcripts in normally heterochromatic gene-poor domains; (ii) potential immunogenicity of the processed oncohistone itself. These insights might lead to the development of novel management approaches, beyond the current standard of care of RANKL targeted therapy with denosumab.

Literaturangaben:

- [1] Ricardo Kalil in E. Santini-Araujo et al. (eds.), (2015), Tumors and Tumor-Like Lesions of Bone , Springer, London, Giant Cell Tumor of Bone, https://doi.org/10.1007/978-1-4471-6578-1_24
- [2] Behjati et al., Distinct H3F3A and H3F3B driver mutations define chondroblastoma and giant cell tumor of bone, Nature Genetics, 1479-1482, 45, <https://doi.org/10.1038/ng.2814>
- [3] Jain et al., (2020), Histone H3.3 G34 mutations promote aberrant PRC2 activity and drive tumor progression, Proceedings of the National Academy of Sciences of the United States of America, 27354-27364, 117(44), <https://doi.org/10.1073/pnas.2006076117>
- [4] Khazei et al., (2020), H3.3G34W promotes growth and impedes differentiation of osteoblast-like mesenchymal progenitors in Giant Cell Tumour of Bone, Cancer Discovery, 1968-1987, 10(12), <https://doi.org/10.1158/2159-8290.CD-20-0461>
- [5] Lutsik et al., (2020), Globally altered epigenetic landscape and delayed osteogenic differentiation in H3.3-G34W-mutant giant cell tumor of bone, Nature Communications, 5414, 11(1), <https://doi.org/10.1038/s41467-020-18955-y>

AG08.03

Exploring the Role of RANKL and RUNX2 in Giant Cell Tumor of the Bone: A Study on GCTB Cell Lines in vitro

G. Lutteri, K. Mellert, J. Nell, P. Möller, T. F. E. Barth
Universität Ulm, Institute of Pathology, Ulm, Germany

Questions/Background

The Giant Cell Tumor of the bone (GCTB) is an intermediate malignant, lytic bone tumor with an aggressive behavior. It commonly occurs in the epiphyseal or metaphyseal region of long bones. GCTBs appear to be decoupled from physiological stimuli. RANKL and RUNX2 are key factors of the bone homeostasis. Therefore, we focused our analysis on these molecules in an *in vitro* study.

Methods

We stimulated a GCTB cell line (GCT-4) in 12-Well plates with the active form of Vit.D3, Calcitriol (concentrations: 0nM, 0.05nM, 0.1nM, 0.5nM, 1nM, 10nM) and with a human fragment of Parathyroid hormone (concentrations: 15 pg/ml, 30pg/ml, 45 pg/ml, 65 pg/ml and 100pg/ml). To detect the expression of RANKL we used the ELISA technique. The same technique was used to follow the temporary course of the expression of RANKL in 2 primary cultures. One of the two cultures is particularly of interest because it displays a very rare mutation on the H3F3A gene, the G34V mutation.

RUNX2 expression was investigated in different established GCTB cell lines (GCT-3M, GCT-4, GCT-5) and normalized with the expression value in the HDLM-2 Hodgkin Lymphoma cell line known to express this protein. We measured the RUNX2 gene expression by qPCR with self-designed and optimized primers.

Results

We observed that the Calcitriol treatment caused an average decrease of around 60% in RANKL expression in the GCT-4 cell line after 7 days and of 50% after 14 days of stimulation. This effect is no longer evident after 21 days of stimulation. PTH stimulation on the same cell line led to a slight increase in RANKL expression, with an average rise of 12% within the physiological dose (15-65 pg/ml). We also detected RANKL in the medium at the first passage of the primary cultures in a range from 1.71 ng/ml up to 48.6 ng/ml.

RUNX2 expression, detected by qPCR, in GCTB cell lines was higher than HDLM-2 cell line. It was upregulated in response to PTH stimulation in GCT-4, especially by stimulating with 100pg/ml PTH (1.3-fold, compared with unstimulated cells).

Conclusion

The stimulation with Calcitriol of GCTB tumor cells showed an opposite trend on RANKL expression if compared with physiological conditions. On the other hand, PTH still has the potential to stimulate the expression of RANKL in the cell lines.

Further, we induced growth stimulating the GCT-4 cells with PTH. These results indicate that regulation of RANKL is partially decoupled from Calcitriol and PTH stimulation.

AG08.04

Analysis of 24 giant cell tumors of bone before and after denosumab therapy reveals complex time-dependent morphological changes

S. Arndt¹, W. Hartmann², A. Rókus³, B. Leinauer¹, A. von Baer⁴, M. Schultheiss⁴, J. Pablik⁵, H. Fritzsche⁶, C. Mogler⁷, D. Baumhoer⁸, K. Mellert¹, P. Möller¹, M. Szendrői³, G. Jundt⁸, T. F. Barth¹

¹Institut für Pathologie, Universitätsklinikum Ulm, Ulm, Germany, ²Sektion für Translationale Pathologie, Gerhard-Domagk-Institut für Pathologie, Universitätsklinikum Münster, Münster, Germany, ³Orthopädie und Institut für Pathologie, Semmelweis Universität, Budapest, Hungary, ⁴Klinik für Unfall-, Hand-, Plastische und Wiederherstellungschirurgie, Universitätsklinikum Ulm, Ulm, Germany, ⁵Institut für Pathologie, Universitätsklinikum Carl Gustav Carus, Dresden, Germany, ⁶UniversitätsCentrum für Orthopädie, Unfall- & Plastische Chirurgie, Universitätsklinikum Carl Gustav Carus, Dresden, Germany, ⁷Institut für Pathologie, Technische Universität München, München, Germany, ⁸Knochentumor-Referenzzentrum (KTRZ) am Institut für Pathologie, Universitätsspital Basel und Universität Basel, Basel, Switzerland

Questions/Background

Giant cell tumor of bone (GCTB) is an osteolytic tumor. *H3F3A*-mutated neoplastic stromal cells release RANKL, which leads to accumulation of osteoclastic giant cells. The treatment of choice is surgical curettage; alternatively, the anti-RANKL antibody denosumab is used. Many reports of patients treated with denosumab show major changes in GCTB histology, but no time correlation of therapy and morphological changes has been settled.

Methods

We collected tissue from 24 patients who received denosumab for varying time periods. All tissue sample were available in pairs (pre- and post-denosumab). The H.E.-stained slides were analyzed regarding morphological changes. To characterize the cells in detail, we added immunohistochemical staining for *H3F3A* mutation, RUNX2, and SATB2.

Results

Patients treated with denosumab showed dramatic changes in their tumor morphology. We detected a loss of giant cells, a decrease of *H3F3A*-mutated cells and a simultaneous increase in matrix formation. We observed two different types of matrix formation: first, a strand-like matrix formation with intermingled spindle-shaped cells, which was predominant in 10/24 tissue samples. Second, we observed osteoid formation with osteoblast-like round cells (predominant type in 11/24 patients). Two patients could not be assigned to either group because they expressed both types equally. The two groups of matrix formation could be further divided into the following patterns: Strand-like matrix formation: a) high cell density with incipient strand-like matrix formation b) scarring fibrosis with drastic decrease of vital cells. Osteoid neoformation: a) plump, disorganized osteoid b) osteoid in trabeculae. The various patterns were overlapping and independent of time course. The immunohistochemical staining for RUNX2 showed fewer positive cells in the post-denosumab samples (mean: 87% to 53%). SATB2 was reduced as well (mean 57% to 19%). In one patient, who received denosumab for 24 months, no *H3F3A*-mutated cells could be detected in the tissue.

Conclusion

We identified different patterns in denosumab-treated patients but were not able to match these patterns with the time course indicating that the tissue response to denosumab is heterogenous and so far, unpredictable. RUNX2 and SATB2 are markers of osteoblast differentiation. The decrease of these two markers might be a hint for a possible expansion of a RUNX2- and SATB2-negative population that warrants further characterization as a potential pool for malignant transformation.

AG08.05

TIM3 qualifies as a potential immunotherapeutic target in high-risk soft tissue sarcomas

L. M. Berclaz¹, A. Altendorf-Hofmann², L. H. Lindner¹, H. R. Dürr³, F. Klauschen⁴, T. Knösel⁴

¹Ludwig-Maximilians-Universität (LMU) University Hospital, Department of Internal Medicine III, Munich, Germany, ²Friedrich-Schiller-Universität Jena, Department of General, Visceral and Vascular Surgery, Jena, Germany, ³Ludwig-Maximilians-Universität (LMU) University Hospital, Musculoskeletal Oncology, Department of Orthopaedic Surgery, Physical Medicine and Rehabilitation, Munich, Germany, ⁴Ludwig-Maximilians-Universität (LMU), Institute of Pathology, Munich, Germany

Questions/Background

Expression of T cell immunoglobulin and mucin domain-containing protein 3 (TIM3), an immune checkpoint receptor on T cells, has been associated with dismal outcomes and advanced tumor stages in various solid tumors. Blockade of TIM3 in combination with other checkpoint inhibitors has demonstrated promising results in preclinical models and is currently under examination in several clinical trials. This study examines TIM3 expression in high-risk soft tissue sarcomas (HRSTS).

Methods

Tumor cell expression of TIM3 was analyzed on protein level in pre-treatment biopsies of patients with HRSTS. TIM3 expression was correlated with clinicopathological parameters including tumor-infiltrating lymphocyte (TIL) counts, programmed cell death 1 (PD-1) and programmed cell death ligand 1 (PDL-1) expression in a well-characterized cohort of patients with HRSTS. Rates of observed survival and cumulative 5-year tumor free survival dependent on the expression of TIM3 were analyzed.

Results

TIM3 expression was observed in 101 (56%) out of 179 pre-treatment biopsies of patients with HRSTS. Among other parameters, TIM3 expression was significantly more often seen in undifferentiated pleomorphic sarcomas (UPS) compared to other histological subtypes ($p < 0.001$), high TIL counts ($p < 0.001$), high PD-1 and PD-L1 expression ($p < 0.001$ and $p < 0.001$, respectively) (table 1). TIM3 expression did not have a prognostic impact on survival in patients with HRSTS (figure 1).

Factor	Strata	Total	TIM3 >0		p-value
		n	n	%	
Sex	Male	92	59	64	0.036
	Female	87	42	48	
Age at initial diagnosis (years)	<55	92	43	47	0.010
	≥55	87	58	67	
Histological subtype	UPS	59	44	75	<0.001
	Liposarcoma	31	11	35	
	Leiomyosarcoma	40	26	65	
	Other	49	20	41	
Tumor Location	Extremities	71	47	66	0.045
	Non-extremities	108	54	50	
FNCLCC Grade	Intermediate (G2)	89	46	52	0.229
	High (G3)	90	55	61	
Surgical margins	R0	69	48	70	0.011
	R1	83	41	49	
	R2	14	4	29	
	No resection	13	8	62	
Chemotherapy	Yes	134	80	60	0.164
	No	45	21	47	
Radiotherapy	Yes	30	16	53	0.535
	No	106	48	45	
	Missing	43			
Regional Hyperthermia (RHT)	Yes	139	86	62	0.007
	No	40	15	38	
TIL counts (cells/50HPF)	0-5	108	46	43	<0.001
	≥6	70	54	77	
	Missing	1			
PD-1 expression	0	61	18	30	<0.001
	≥0	77	46	60	
	Missing	41			
PD-L1 expression	0	139	66	47	<0.001
	≥0	34	31	91	

Table 1: Correlation of TIM3 expression with important clinicopathological parameters.

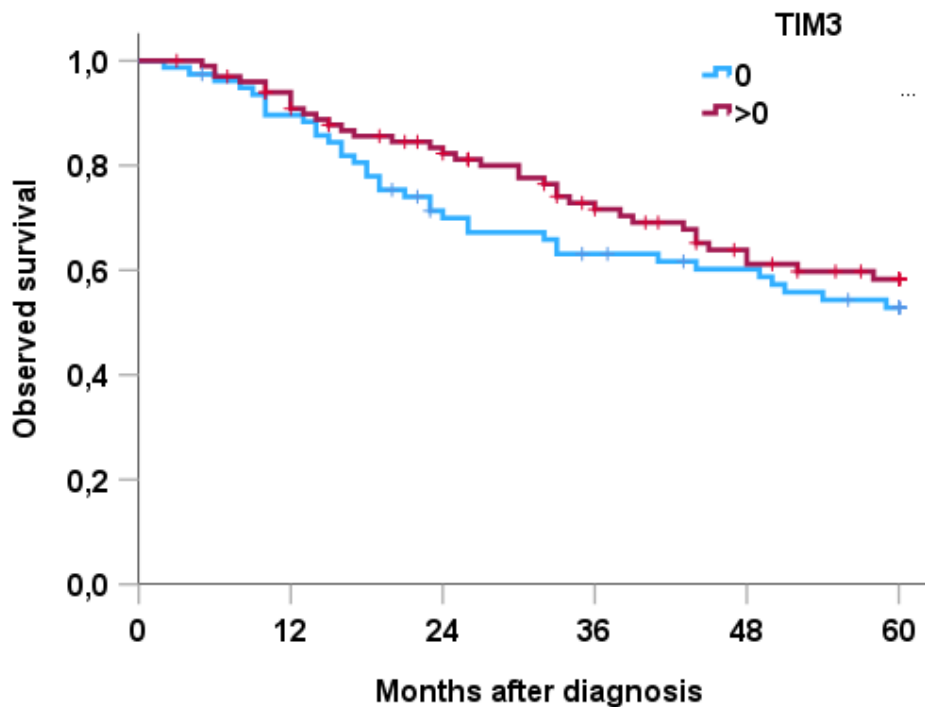


Figure 1: Observed survival according to TIM3 expression.

Conclusion

This is the first study to demonstrate significant tumor cell expression of TIM3 in specific subsets of patients with HRSTS. With only limited data on immunotherapy in sarcomas, TIM3 qualifies as a potential immunotherapeutic target in high-risk soft tissue sarcomas.

AG08.06

Biphenotypic sinonasal sarcomas harbor characteristic gene fusions involving PAX3 and show a distinct DNA methylation profile

G. Mechtersheimer¹, F. K. F. Kommos¹, M. Kirchner¹, A. Stenzinger¹, A. von Deimling², D. Reuss²

¹Institut für Pathologie, Universitätsklinikum Heidelberg, Allgemeine Pathologie und Pathologische Anatomie, Heidelberg, Germany,

²Institut für Pathologie, Universitätsklinikum Heidelberg, Neuropathologie, Heidelberg, Germany

Questions/Background

Biphenotypic sinonasal sarcoma (BSNS) is a rare, usually low-grade spindle cell sarcoma, which is characterized by a biphenotypic smooth muscle and neural differentiation, and usually harbors gene fusions involving PAX3. A minority of cases also exhibit focal morphological and/or immunohistochemical signs of skeletal muscle differentiation. Given the broad spectrum of differential diagnosis, which ranges from cellular schwannomas and solitary fibrous tumors to highly aggressive sarcomas such as synovial sarcoma, diagnosing BSNS represents a challenge. Here, we performed an in-depth analysis of a small series of BSNS.

Methods

A comprehensive morphological and immunophenotypic characterization and targeted RNA-based next-generation sequencing (NGS) for the identification of gene fusions, as well as genome-wide methylation analysis using the 850 k EPIC array was performed on four BSNS samples from three patients, including two samples of a repeatedly relapsed BSNS.

Results

All BSNS were composed of dense fascicles of relatively monotonous spindle cells, embedded in a collagenous and focally myxoid stroma. No image found for uniqueTag: Image01. The mitotic activity was low with none to one mitosis per 10 high power fields (hpf). No necrosis was detected. The fourth and fifth BSNS recurrence from one patient showed extensive rhabdomyosarcomatous overgrowth (> 70% of the tumor area) with up to 24 mitoses per hpf and plurifocal necrosis. Immunohistochemically, all BSNS cases

displayed co-expression of S100 protein and α -smooth muscle actin to a variable extend. Desmin and myogenin were diffusely positive in areas of rhabdomyosarcomatous differentiation in one case. RNA based NGS identified *PAX3::MAML3* gene fusions in all tumors. Unsupervised clustering of DNA methylation data, together with a reference cohort including spindle cell mimics and various subtypes of rhabdomyosarcoma, identified a distinct cluster for BSNS including the recurrent case with rhabdomyosarcomatous overgrowth.

Conclusion

BSNS are rare sarcomas usually with a low malignant potential, however, in rare cases may show high-grade transformation with rhabdomyosarcomatous overgrowth mimicking rhabdomyosarcoma. Molecular profiling such as RNA-based NGS or DNA methylation profiling may be helpful adjuncts in confirming a diagnosis of BSNS.

AG08.07

CIC-rearranged sarcomas – A diagnostic challenge.

E. Wardelmann¹, A. Kuntze¹, K. Falkenberg¹, L. Braun¹, A.-C. Puller¹, M. Schulte¹, B. Heitkötter¹, S. Elges¹, F. Müller¹, W. Hartmann², M. Trautmann²

¹Universitätsklinikum Münster, Gerhard-Domagk-Institut für Pathologie, Münster, Germany, ²Universitätsklinikum Münster, Abteilung für Translationale Pathologie, Gerhard-Domagk-Institut für Pathologie, Münster, Germany

Questions/Background

CIC-rearranged sarcomas belong to the category of undifferentiated small round cell sarcomas. They represent the second most common subtype after Ewing sarcoma. On the molecular level, they are characterized by *CIC* fusion genes, with the two most common fusion partners *DUX4* and *DUX4L*, the latter being a paralog of *DUX4*. In addition, more rare fusion gene variants exist. In this study, we aimed at subtyping our cases of *CIC*-rearranged sarcomas identified in our GIST- and Sarcoma Registry Münster by using targeted RNA sequencing to identify the fusion partners of *CIC*. Furthermore, we report on the frequency of false negative results when using RNA sequencing compared to fluorescence in situ hybridization (FISH) using *CIC*-break apart dual color probes.

Methods

We identified 37 cases of *CIC*-rearranged sarcomas. FISH analysis was performed on interphase nuclei of paraffin-embedded 3 μ m-sections with *CIC*-break apart dual color probes (cut-off > 15 aberrant signals among 100 nuclei). RNA was extracted from FFPE blocks, RNA sequencing was performed with the Illumina TruSight RNA Fusion Panel on a MiniSeq system (Illumina). Data was analyzed by Illumina's RNASeq Alignment BaseSpace app and the Arriba fusion-calling algorithm, both using the STAR aligner for read mapping.

Results

In our cohort, there were 19 males and 18 females. Mean age was 44.2 years (min 11y, max 85y), 20 cases were below 40 years of age. The most frequent location (n=36) was extremity followed by pelvis, abdomen, bone, neck, CNS, kidney and lung. All cases (n=32) expressed WT1 in the cytoplasm and additionally in the nuclei in 17 cases. CD99 expression was heterogeneous with 2 negative and 4 nearly negative cases. In 21 cases with available RNA sequencing data, 3 different fusion genes types were identified by Illumina's RNASeq Alignment BaseSpace app: *CIC::CITED1*, *LYPD6::CIC*, and *CIC::NUTM1*. These 3 cases were confirmed with the Arriba fusion-calling algorithm. In addition, Arriba identified 4 additional *CIC*-rearranged fusion genes: [*CIC::TEKTAP2/MIR3687*; *CIC::DUX4L9*], *CIC::DUX4L2*, *CIC::DUX4L4* [*HFM1::CIC*; *CIC::TEKTAP2/MIR3687*].

Conclusion

Identification of *CIC*-rearranged sarcomas remains challenging. Among 21 cases with proven FISH break-apart signals in the *CIC* gene locus, only 7 cases with *CIC* genomic rearrangements could be identified with RNASeq. In case of an undifferentiated sarcoma with unclear genomic alteration, *CIC*-FISH analysis should be performed upfront to avoid underdiagnosing *CIC*-rearranged sarcomas.

AG09 Zytopathologie/Fortbildung

AG09.02

Gynaecological cytology as an essential component in the prevention of cervical carcinoma-Squamous and glandular changes:Glandular lesions

I. Baltisser

Institut für histologische und zytologische Diagnostik AG, Aarau, Schweiz, Aarau, Switzerland

Adenocarcinomas constitute about 25% of all cervical cancer. With its heterogeneity and about 15% of non-HPV associated subtypes this tumour represents a substantial challenge in the prevention and the diagnosis of cervical carcinomas. Furthermore, it is often necessary to distinguish between true HPV negative cervical cancer and false HPV negative cases or an incorrect classification of non-cervical cancer. The aim of this study is a documentation of the importance of cytological examination of glandular cells in the context of already established HPV- Tests and the continuing increase of additive techniques. The following conclusions are based on a review of literature data and our own expertise.

The most benign glandular changes do not require any additional examinations. But advanced knowledge of the same issue is essential for the correct diagnosis of adenocarcinoma in situ (AIS) of the uterine cervix. The most common HPV associated AIS of usual type shows characteristic cytological criteria and can be additionally substantiated by p16/Ki67 positivity. The cytological diagnosis of invasive HPV associated adenocarcinoma is also possible, but occasionally a support with some immunohistochemical methods is necessary. The cytological diagnosis of HPV negative AIS is difficult, because the typical cellular changes are usually much less pronounced or even missing. However, the cytological identification of HPV negative adenocarcinoma and its precursors, with often very subtil glandular changes in a Pap smear, is currently the only option for an early detection of this aggressive and therapy resistant neoplasia. The definitive differentiation between an HPV negative adenocarcinoma of the uterine cervix and a non-cervical cancer is oftentimes not possible without the support of additional methods, especially immunohistochemical methods and additional molecular techniques.

Currently, in the age of immunohistochemical and molecular methods, which are inaccessible to some, the cytological examination of glandular cells is an important indicator for the setting of the correct prophylactic and diagnostic paths.

AG10 Kopf-Hals-Pathologie

AG10.01

Predicting clinically relevant genetic alterations from conventional histopathological slides of thyroid carcinoma using vision transformers

I. Marion¹, C. Mueller¹, C. Glasner¹, S. Schulz¹, A. Fernandez¹, W. Roth¹, S. Strobl¹, D.-C. Wagner¹, A. Schad¹, J. N. Kather², T. J. Musholt³, J. I. Staubitz³, N. Hartmann¹, S. Försch¹

¹Universitätsmedizin Mainz, Institut für Pathologie, Mainz, Germany, ²Else Kroener Fresenius Center for Digital Health, Technische Universität Dresden, Dresden, Germany, ³Universitätsmedizin Mainz, Klinik für Allgemein-, Viszeral- und Transplantationschirurgie, Mainz, Germany

Questions/Background

Thyroid carcinomas are the most common malignant tumors of the endocrine organs. Papillary thyroid carcinoma (PTC) makes up about 80% of these neoplasms. Classically, BRAF mutations occur in up to 50%, panRAS mutations in 10-15% and RET translocations in up to 35%. The detection of these alterations during routine pathological diagnosis is complex and expensive. Here, artificial intelligence (AI) could be used to predict genetic changes using conventional histopathological slides.

Methods

Two cohorts of PTC patients were used in this study. The first cohort included 484 patients from the TCGA consortium, the second cohort 150 patients from a Mainz collective. The BRAF, panRAS and RET status was determined for all patients. A new deep learning technique, called Vision Transformers, was trained on digitized H&E sections for the presence of these alterations. The TCGA cohort served as a training set and

the Mainz cohort as a real external test set. Subsequently, explainable AI methods were used to identify new morphological criteria associated with particular genetic changes.

Results

We could demonstrate that BRAF, panRAS and above all RET alterations can be predicted with good to excellent accuracy values. The performance of the training set was almost identical to that of the test set. Markup images enabled visualization directly within the digitized H&E sections. By analyzing the top level tiles, new, previously unknown morphological criteria associated with the genetic alterations could be identified.

Conclusion

The prediction of genetic alterations based on histopathological slides using AI has the potential to significantly improve the clinical management of PTC patients. Our models have achieved accuracies that could already be used for pre-screening for example. The use of the latest generation of AI algorithms offers numerous advantages - e.g. better performance with significantly less consumption of computational resources. The aim is to develop a faster and more cost-effective method compared to conventional mutation analyses. With the help of explainable AI methods, new morphological patterns associated with certain genetic alterations can also be identified.

(Promotion von I.M.)

AG10.02

Clinico-pathological characterization of sinonasal adenoid cystic carcinoma reveals high prevalence of MYB-NFIB gene fusion and prognostic factors

T. Mauthe^{1,2}, C. M. Meerwein¹, D. Holzmann¹, U. Held³, S. N. Freiberger^{2,4}, **N. J. Rupp^{2,4}**

¹Department of Otorhinolaryngology - Head and Neck Surgery, University Hospital Zurich, Zurich, Switzerland, ²Faculty of Medicine, University of Zurich, Zurich, Switzerland, ³Department of Biostatistics, Epidemiology, Biostatistics, and Prevention Institute, University of Zurich, Zurich, Switzerland, ⁴Department of Pathology and Molecular Pathology, University Hospital Zurich, Zurich, Switzerland

Questions/Background

Adenoid cystic carcinoma (AdCC) is a salivary gland neoplasm that infrequently appears in the sinonasal region. It is known for its usually slow yet aggressive growth, a tendency for perineural invasion, high recurrence rates, and poor long-term prognosis. The aim of this study was to evaluate the outcome and clinico-pathological parameters of sinonasal AdCC.

Methods

A retrospective analysis was conducted on all cases of AdCC affecting the nasal cavity or paranasal sinuses between 2000 and 2018 at the University Hospital Zurich. Data on presenting symptoms, anatomic site, diagnostics, first-line therapy, and follow-up were collected. Tumor material was examined for growth patterns, necrosis and perineural/lymphovascular invasion, as well as analyzed for molecular alterations (including *MYB/MYBL1* and *NOTCH1* gene alterations). Kaplan-Meier curves were generated to evaluate overall survival (OS) including analysis with the log-rank test.

Results

A total of n=14 patients were included. The mean age at presentation was 57.7 years. Sequencing revealed *MYB-NFIB* gene fusion in 11/12 analyzable cases. Factors associated with decreased survival were solid growth pattern ($p = 0.003$), histopathological high-grade transformation ($p < 0.001$), and tumor epicentre in the sphenoid sinus ($p < 0.001$).

Conclusion

Solid growth pattern, high-grade transformation, and sphenoid sinus invasion are negative prognostic factors in sinonasal AdCC. A high prevalence of *MYB-NFIB* gene fusion may help in the correct classification of diagnostically challenging (e.g. metatypical) cases.

AG10.03

The concept of “differentiated” dysplasia in oral potential malignant disorders and its translation to daily practice

A.-S. Becker¹, M. Holm¹, J. Liese², A. Zimpfer¹

¹Institut für Pathologie Universitätsmedizin Rostock, Rostock, Germany, ²Department of Oral, Maxillofacial and Plastic Surgery, University Medical Centre of Rostock, Germany, Rostock, Germany

Questions/Background

Oral squamous cell carcinoma is the most common malignancy of the oral cavity with various precancerous lesions including "classic" oral epithelial dysplasia as defined by WHO. Analogous to the vulva, the concept of HPV-independent precursor lesions being either TP53 wild-type or mutated has emerged as a second mechanism for malignant transformation of (potentially precancerous) squamous epithelium exhibiting certain histologic features termed "differentiated" dysplasia (difD). In difD, the risk of progression increases with aberrant CK13/17 expression. We analyze the frequency of difD and match its CK13/17 staining pattern with the results of prior oral brush cytology.

Methods

Oral biopsies diagnosed as simple hyperplasia or difD were retrieved from institutional archives. Classic dysplasia as well as (non-)invasive carcinomas were included as reference group. Morphology was revised and whole sections stained for p53, Ki67, CK13 and CK17. Brush cytology findings were obtained from clinical records.

Results

The cohort consisted of n=130 biopsies from n=107 patients (38% female; median age 57 years) including 27% simple hyperplasia, 37% difD, 16% low/moderate grade classic dysplasia, 8% high grade classic dysplasia/carcinoma in situ and 3% invasive cancers. Lichen planus, proliferative verrucous hyperplasia and hyperplastic candidiasis sum up to 9%. Concerning morphology, difD had the highest rate of confluent rete ridges and hypergranulosis. Compared to simple hyperplasia, CK13 loss/CK17 gain was significantly higher in difD. Focusing on difD, 75% showed aberrant keratin expression, 100% p53 wild type staining pattern and reactively increased Ki-67 labeling (Figure).

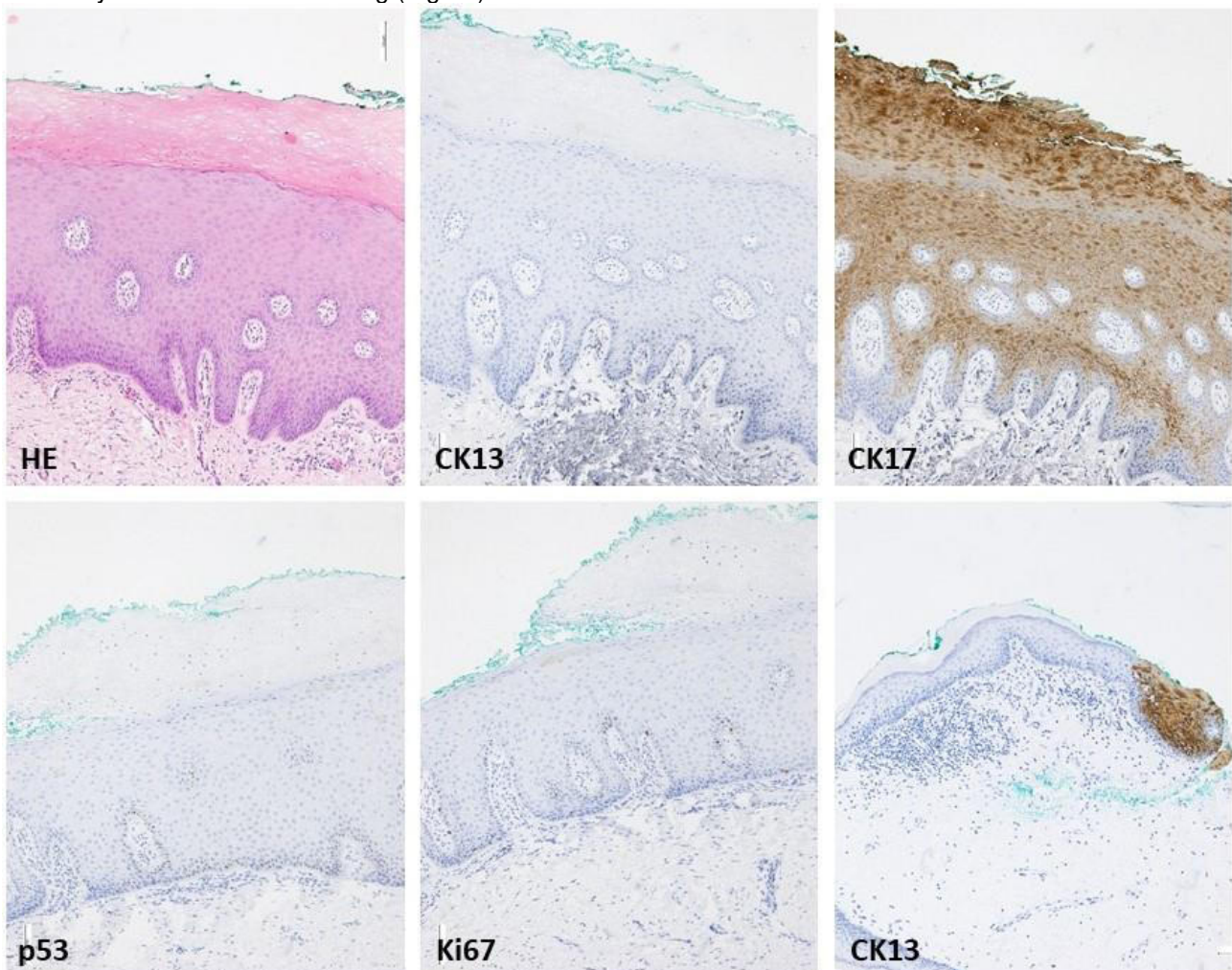


Figure legend: Aberrant CK13 loss and CK17 gain in simple hyperplasia, with p53 showing a wildtype pattern in the basal cell layer. All cases with available brush cytology prior to diagnosis of difD exhibited negative cytology results.

Conclusion

CK13 loss and CK17 gain were frequent events in our small cohort of difD. This simply assessable keratin-cocktail can help to identify patients a) with difD b) having a higher risk for malignant transformation, although features of malignancy might not be obvious by morphology. Synchronous oral brush cytology results were "negative for malignancy" in all difD samples. Like p53 and Ki67 immunohistochemistry,

cytology seems to be of no additional value, probably due to persistent epithelial maturation.

AG10.04

TRIM21 Expression as a Prognostic Biomarker for Progression-free Survival in HNSCC

A. von Bernuth¹, J. Ribbat-Idel¹, L. Klapper¹, T. Jagomast¹, J. Kirfel¹, D. Rades², A. Leichtle³, R. Pries³, K.-L. Bruchhage³, S. Perner^{1,4}, A. Offermann¹, V. Sailer¹, C. Idel³

¹Institut für Pathologie UKSH Campus Lübeck, Lübeck, Germany, ²Klinik für Strahlentherapie UKSH Campus Lübeck, Lübeck, Germany, ³Klinik für Hals-, Nasen- und Ohrenheilkunde UKSH Campus Lübeck, Lübeck, Germany, ⁴Pathologie des Forschungszentrum Borstel, Leibniz Lungenzentrum, Borstel, Germany

Questions/Background

Patients with head and neck squamous cell carcinoma (HNSCC) continue to have a rather poor prognosis. Current therapies for HNSCC can have severe side effects such as dysphagia and tooth decay after radiotherapy or functional and visible impairments after surgery. Prognostic HNSCC biomarkers such as immune evasion have already been identified as pathological findings in tumor samples associated with poor prognosis. Nevertheless, additional HNSCC biomarkers can help predict the prognosis, i.e. the recurrence and progression of the tumor, and identify low-risk groups that would benefit from reduced treatment intensity.

Recently, tripartite motif containing-21 or TRIM21 was identified as a possible prognostic biomarker in HNSCC. TRIM21 is a cytosolic E3 ubiquitin ligase inducing ubiquitin-mediated proteasomal degradation of proteins. By binding antibody-virus complexes, TRIM21 leads to the degradation of the former and the upregulation of inflammatory signaling pathways. Here, we investigated the role of TRIM21 as a biomarker candidate for HNSCC in predicting tumor progression and patient survival.

Methods

TRIM21 expression and its association with clinical-pathological parameters in our HNSCC cohort was evaluated using immunohistochemistry. Our HNSCC cohort included samples from 419 patients consisting of primary tumors (n = 337), lymph node metastases (n = 156), recurrent tumors (n = 54), and distant metastases (n = 16).

Results

Increased cytoplasmic TRIM21 expression was associated with the infiltration of immune cells into primary tumors. In addition, TRIM21 expression was significantly higher in primary tumors compared to lymph node metastases. Increased TRIM21 expression correlated with shorter progression-free survival in HNSCC patients.

Conclusion

TRIM21 could serve as a new prognostic biomarker for disease progression in HNSCC patients.

AG10.05

CMTM6-Status in Head & Neck Squamous Cell Cancer Predicts Survival and Response to Radiochemotherapy

C. Kluge¹, A. Zimpfer¹, D. Strüder², A. Erbersdobler¹, C. Maletzki³, A.-S. Becker¹

¹Institut für Pathologie Universitätsmedizin Rostock, Rostock, Germany, ²Department of Otorhinolaryngology, Head and Neck Surgery "Otto Koerner", Rostock University Medical Center, Rostock, Germany, ³Department of Internal Medicine, Medical Clinic III Hematology, Oncology, Palliative Medicine, Rostock University Medical Center, Rostock, Rostock, Germany

Questions/Background

Head and neck squamous cell carcinoma (HNSCC) is the sixth most common cancer worldwide frequently presenting with locally advanced/ recurrent disease. Therapy standards are surgery, (radio-) chemotherapy (RCT), and immune checkpoint inhibitors. Therapeutic response and survival rates are affected by the mechanisms of carcinogenesis and the tumor microenvironment including the PD-L1 status. The CKLF Like MARVEL Transmembrane Domain Containing 6 (CMTM6) is known to stabilize PD-L1, thereby mediating prolonged responses to PD-L1 inhibitors in some tumors. In HNSCC, CMTM6 seems to drive Cisplatin resistance by the *Wnt* pathway. Here we examined the impact of CMTM6 protein status on survival and treatment response in HNSCC patients receiving RCT.

Methods

The combined positive score (CPS) of CMTM6 was examined on tumor and tumor-associated immune cells

via immunohistochemistry using tissue microarrays (TMAs) of RCT-treated HNSCC samples (n=183; inclusion period 2014-2020). Clinical data were obtained from patients' records. Based on previous findings including ROC analysis and median expression, the cut-off value for CMTM6 "high" was set at ≥ 10 . The status of p53, p21, AKT, phospho AKT, and PD-L1 were analyzed using immunohistochemistry.

Results

High expression of CMTM6 on either tumor and/or immune cells was found in 61% of all patients and associated with longer progression free (PFS) and overall survival (OS) (both $p < 0.05$; log-rank) compared to "CMTM6 low" cases irrespective of the anatomical site. Oropharyngeal cancers (55% p16^{INK4a} positive) showed the highest frequency of "CMTM6 high" cases (χ^2 test, $p = 0.04$). CMTM6 correlated significantly with PD-L1 (Spearman's $\rho = 0.23$), AKT (Spearman's $\rho = 0.26$) and phospho AKT (Spearman's $\rho = 0.22$; all $p < 0.01$). No association with p21 or p53 was detected.

Conclusion

CMTM6, if assessed analogously to the CPS used for PD-L1 in routine diagnostics, might predict OS and PFS in HNSCC patients. In our limited cohort CMTM6 protein expression correlates with PD-L1 positivity as well as molecules involved in the AKT axis. This hints towards CMTM6-initiated anabolic cell effects resulting in better sensitivity to chemotherapeutics but valid clinically relevant conclusions cannot be drawn due to missing molecular studies in this descriptive approach.

AG11 Dermatopathologie

AG11.01

Cutaneous B-cell infiltration: diagnostic algorithms, differential diagnosis and pitfalls.

I. Oschlies

Universitätsklinikum Schleswig-Holstein, Campus Kiel, Institut für Pathologie, Kiel, Germany

Der Übersichtsvortrag soll eine Hilfestellung zur diagnostischen Einordnung von lymphatischen, B-Zell-reichen Infiltraten in der Haut geben. Die diagnostischen Kriterien und biologischen Eigenschaften der häufigsten Subtypen der primär kutanen B-Zell-Lymphome der Haut werden vorgestellt. Die Abgrenzung gegenüber Pseudolymphomen, sekundären Infiltraten systemischer B-Zell-Lymphome/Leukämien sowie B-zellreichen T-Zell-Lymphoproliferationen werden erläutert. Diagnostische Immun-Algorithmen in Abhängigkeit vom Muster der B-Zellinfiltrate können eine gezielte Abklärung erleichtern. Diagnostische Fallstricke werden benannt und hilfreiche immunphänotypische und molekulare Methoden zur korrekten Befundung vorgestellt.

AG11.02

From digital workflow to AI assisted diagnosis

J. Schaller

MVZ Dermatopathologie Duisburg Essen GmbH, Duisburg, Germany

Dermatopathologische Institute stehen aufgrund immer höherer Anforderungen bei andererseits schwindenden Ressourcen vor zunehmenden Herausforderungen. Die Etablierung eines digitalen Laborworkflows ist eine Möglichkeit dies zu kompensieren und eröffnet neue Möglichkeiten für die Diagnostik und Qualitätssicherung. Gleichzeitig ist die Digitalisierung von Glasobjektträgern Grundlage für den Einsatz künstlicher Intelligenz (KI)-basierter Verfahren in der Dermatopathologie. Bislang haben diese Verfahren keinen Einzug in die Routinediagnostik gefunden. Ziel dieses Vortrags ist die Demonstration eines effektiven digitalen Laborworkflows der den Einsatz eines KI-basierten Modells zur automatisierten dermatopathologischen Diagnostik ermöglicht. Das Ausgangsmodell wurde mit Basalzellkarzinomen trainiert und etabliert. Im Routinebetrieb erzielte dieses Modell eine Sensitivität von 98,23 % und eine Spezifität von 98,51 %. Zusätzlich wurden eine automatisierte, KI-basierte Basalzellkarzinom-Subtypisierung und Tumordickenmessung etabliert. Darauf aufbauend können zahlreiche andere dermatopathologische Diagnosen mit diesem Modell erkannt und klassifiziert werden. Neben der KI gestützten automatisierten Erkennung und Klassifikation bestimmter Hautläsionen ermöglicht dieses System auch eine automatische Befunderstellung auf der Basis einer strukturellen Befundgenerierung. Zusammenfassend können KI-basierte Verfahren mit einer hohen Genauigkeit im Routinebetrieb

entsprechend trainierte Hauttumore erkennen und signifikant die Arbeit zeitlich als auch quantitativ unterstützen. Aktuell wird dies den Dermatopathologen nicht ersetzen, ihn aber unterstützen und damit neue Möglichkeiten in der Routinediagnostik, der Lösung schwieriger Fälle, aber auch der Weiterbildung und Forschung schaffen.

AG11.03

Loss BRCA-associated Protein 1 (BAP1) expression in uveal melanoma is associated with morphological features of dedifferentiation and adverse prognosis

A. Zimpfer¹, L. Dyballa¹, C. Brockmann²

¹Institut für Pathologie, Universitätsmedizin Rostock, Rostock, Germany, ²Klinik und Poliklinik für Augenheilkunde, Universitätsmedizin Rostock, Rostock, Germany

Questions/Background

Approximately 50% of patients with uveal melanoma (UM) develop metastatic disease, usually involving the liver. Metastatic disease is rarely apparent at the time of treatment for primary UM and may develop months to years after diagnosis. The development of metastatic disease correlates strongly with chromosomal abnormalities such as monosomy 3 and 8q gain. Previously, inactivating mutations in the BRCA-associated protein 1 (BAP1) gene on chromosome 3p21.1 were found to occur almost exclusively in metastatic UM class 2 with monosomy 3, and loss of nuclear BAP1 expression has been shown to be a good surrogate marker for both genetic alterations. Some immunohistochemical BAP1 studies have been performed in UM, but there are few data on the correlating morphologic findings. To fill this gap, we morphologically examined a larger UM collective and correlated the findings with BAP1 immunohistochemistry results.

Methods

A total of 139 UM were included in the retrospective study. BAP1 immunohistochemistry was evaluated for associations with clinical and various histological features, such as Callender classification, anaplasia, and mitoses. Additionally, survival analyses were performed.

Results

Uveal melanomas from 79 male and 60 female patients (median age 67 years, range 31-92 years) were included. Complete or incomplete nuclear loss of BAP1 expression was seen in 10.1% and 14.1% of cases, respectively. BAP1 loss was significantly associated with death, disease progression, and occurrence of anaplasia ($p < 0.05$). UM with loss of nuclear BAP1 expression showed a significant shorter overall survival ($p = 0.006$; Fig.), and a trend towards shorter progression-free survival ($p = 0.163$).

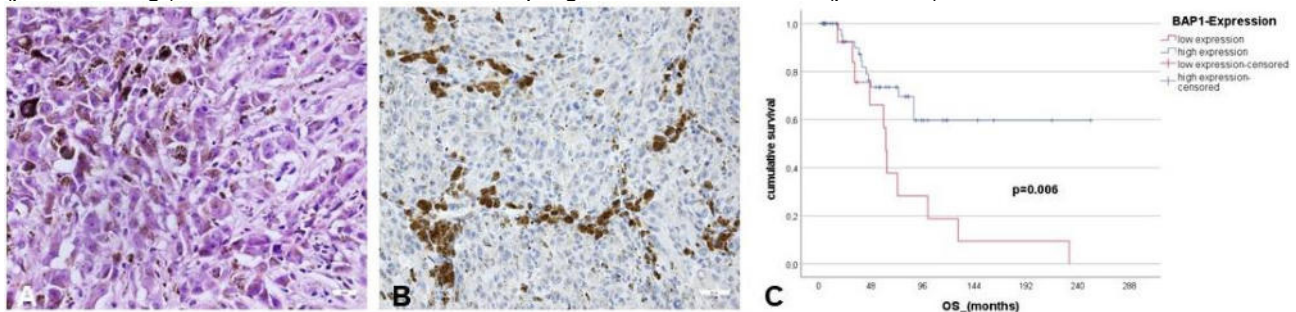


Figure legend: (A) Uveal melanoma with anaplastic features, and (B) complete loss of nuclear BAP1 expression. (C) In uveal melanomas with partial or complete loss of nuclear BAP1 expression, OS was significantly reduced.

Conclusion

We suggest that immunohistochemical screening for BAP1 should become routine in the histopathologic examination of uveal melanomas. The anaplastic phenotype correlates particularly with loss of BAP1. Furthermore, our results indicate that loss of BAP1 may play a special role in the progression of uveal melanoma to an aggressive, metastatic phenotype.

Expression of PRAME in Melanoma in situ versus dysplastic nevi: Immunohistochemical Study

M. Abbas¹, O. Bettendorf², J. de Jonge²

¹Universitätsklinikum Münster, Gerhard-Domagk-Institut für Pathologie, Münster, Germany, ²Institut für Pathologie und Zytologie, Schüttorf, Germany

Question/Background

PRAME (Preferentially expressed Antigen in Melanoma) is expressed frequently in malignant cutaneous melanocytic lesions but not common in normal or benign melanocytic lesions, which can be detected immunohistochemically. PRAME mRNA expression levels have been identified as an important biomarker for metastatic risk stratification of uveal Melanomas. Its expression was described by multiple authors and studies like Alomari et al., 2021 and Koh SS et al., 2022, who describe describe the wide expression of PRAME in Melanoma in situ and invasive Melanoma as well as in conjunctival Melanoma.

Methods

30 cases were retrospectively immunohistochemically examined after reaching the correct diagnosis either by local pathologist or after sending to reference pathology. 20 cases have been diagnosed as dysplastic nevi and 10 cases have been diagnosed as Melanoma in situ. The immunohistochemistry was done with antibody to PRAME (Abcam-219650) using automated Dakostainer. The staining results were recorded as the percentage of immunoreactive tumour cells with nuclear labelling per total number of tumour cells. Zero indicated no staining at all. Staining of 1-25% of tumour cells was scored as 1+. Labelling of 26-50% were scored as 2+. If the positive tumour cells were from 51-75%, then will be as 3+ scored. More than 75% of positive tumour cells will be scored 4+.

Results

PRAME-Expression in Melanoma in situ: 6 cases showed score 3+ (6/10=60%) and 4 cases showed score 1+ (4/10=40%). The total positive cases were 100%.

PRAME-Expression in dysplastic nevi: 6 cases showed score 1+ (6/20=30%) and the rest of the cases showed score 0 (14/20= 70%).

Conclusion

We suggest the immunohistochemical examination of PRAME as a marker to detect the actual spread of malignant melanocytes within the epidermis in cases of Melanoma in situ and to differentiate between these parts of Melanoma in situ from dysplastic nevi in combined melanocytic lesions to avoid inappropriate wide excision of these lesions especially in the face near the eye.

An immunohistochemical analysis of Basal Cell Carcinoma from 50 patients under the age of 40

V. Waller, M. Boeschen, M. Stiller, H. Bläker, M. von Laffert

Institute of Pathology, University of Leipzig, Leipzig, Germany

Questions/Background

Basal cell carcinoma (BCC) is the most common skin cancer, mainly occurring in the elderly. Thus, there is a plethora of studies encompassing aspects of cell cycle, epithelial mesenchymal transition (EMT) and immunogenity. BCC in younger patients is rare and studies reflecting the above-mentioned aspects are scarce.

Methods

We analysed 57 operative BCC-specimen of 50 patients (without Gorlin Goltz syndrom) with a median age of 35 years (range: 21-40). Besides localisation and conventional histology (growth pattern), we performed immunohistochemistry (IHC) focusing on cell cycle (p53, p16, Ki67, PPH3), and immunogenity (i.a. CD 3, CD4, CD8, CD20, PD-L1, PD1), as well as on Her2- expression, which was recently reported in BCC of the elderly.

Results

We found no correlation between the localisation (35x skin of other and unspecified parts of face, 7x ear, 6x eyelid, 3x lip, 3x hairy head, 2x trunk and 1x upper extremities) and the predominant histological subtype (32 nodular, 12 infiltrative, 6 superficial 7 mixed (3 nodular/morpheiform, 3 nodular/micronodular, 1 infiltrative/micronodular)). P53-alterations (overexpression, null staining) were found in 42% (24/57) and p16-

expression in 12% (7/57) samples. There was combined p16/p53 alteration in 7% (4/57) of the cases. The nodular subtype showed a lower p16-expression compared to the sclerodermiform type. P16-alteration lead to significantly higher expression of Cyclin E1. The scoring of Her2 had the following distribution: score 0: 26% (16/57); score 1: 60% (34/57); score 2: 12% (7/57). From the seven samples with a Her2-score=2, two had a p53 alteration and one a p16-alteration (no simultaneous p16/p53-alteration). The Her2-score 0 BCC showed significantly less expression of Ki67 and Cyclin E1 compared to Her2-score 1 and 2. In contrast, Her2-score 2 BCC showed significantly deeper infiltration, higher PPH3-expression and were more immunogenic with higher rates of T and B-lymphocytes in the stroma. These results were independent of the morphological subtype.

Conclusion

As already reported in the elderly, BCC of young patients also shows alterations of the cell cycle control (p16 and p53 interference). Moreover, Her2 expression can also be found. The latter seems to be a good discriminator for BCC in this patient cohort, as Her2 negative BCC are in line with slow growing BCC, whereas Her2 score=2 BCC correlate with a more immunogenic and aggressive subtype.

AG12 Geschichte und Ethik der Pathologie

AG12.01

Concept of disease and interdisciplinarity - are comparative sciences still reasonable?

T. Braunschweig¹, K. Schierle²

¹Institute of Pathology, University Hospital RWTH Aachen, Aachen, Germany, ²Institute of Pathology, SLK Kliniken Heilbronn, Heilbronn, Germany

Questions/Background

Der Krankheitsbegriff unterlag und unterliegt (noch) großen Veränderungen seit der „Gründung“ der modernen Pathologie im 19. Jahrhundert. Zu Beginn im 19. Jahrhundert waren auch vergleichende Wissenschaften wie die vergleichende Anatomie und vergleichende Pathologie bzw. Pathologische Physiologie von großer Bedeutung. Für die Pathologie im 20. Jahrhundert waren und sind neben neuen Interpretationen von histologischen Eigenschaften auch technische Errungenschaften in der Gewebeaufbereitung und neue diagnostische Verfahren maßgeblich

Methods

Zum einen wurden Verhandlungsbände in die Erarbeitung des Themas einbezogen wie auch Veröffentlichungen aus Zeitschriften, die seit dem 19. Jahrhundert/frühen 20. Jahrhundert im Bereich der Pathologie Artikel veröffentlichen und online zugänglich sind.

Results

Die vergleichende Anatomie und Pathologie sind im 19. Jahrhundert eine wichtige Quelle der Erkenntnis bezüglich der Vorgänge im menschlichen Körper. Dabei war die Pathologie in diesen Zeiten integraler Bestandteil der Krankenversorgung und auch von Internisten geleitet. Die Obduktion als Hauptinstrument stand für den aufkommenden „anatomischen Gedanken“ mit R. Virchow und für eine Pathologie als eigenständiges und teils isoliertes Fach. In der ersten Hälfte des 20. Jahrhunderts standen das Verständnis und der Aufbau der Erkrankungen und deren Ätiologie im Vordergrund. In der zweiten Hälfte des Jahrhunderts entwickelte sich ein interdisziplinärer Ansatz für das Verständnis und die Behandlung von Erkrankungen

Conclusion

Der Einfluss auf den Krankheitsbegriff ist vielfältig und besteht seit der Begründung des Fachbereichs der Pathologie. Für komplexe Zusammenhänge und die Erweiterung des Krankheitsbegriffs sowie der Behandlungsoptimierung spielte der interdisziplinäre Austausch innerhalb der Medizin eine Hauptrolle. Für die Zukunft werden sowohl diese Interdisziplinarität als auch die technischen Fortschritte der Computergestützten Datenverarbeitung und künstlichen Intelligenz (die man prinzipiell auch als vergleichende Wissenschaften interpretieren kann) maßgeblich für die Weiterentwicklung des Krankheitsbegriffes sein, wobei der (histo-)anatomische Gedanke nicht verloren gehen darf. Vergleichende Wissenschaften im ursprünglichen Sinne, z.B. im Zusammenschluss mit den Veterinärpathologen oder Biologen, spielen eine deutlich untergeordnete Rolle, hätten jedoch durchaus Potential in Hinsicht auf Spezies-übergreifende Infektionskrankheiten, wie zum Beispiel im Fall der Corona-Infektion.

Zoonosen bei einheimischen, wildlebenden Säugetieren

R. Ulrich

Institut für Veterinär-Pathologie, Universität Leipzig, Leipzig, Germany

Zoonosen sind Krankheiten und Infektionen, die auf natürliche Weise zwischen Tieren und Menschen übertragen werden können. Direkte und indirekte Kontakte von Menschen mit Wildtieren finden bei der Jagdausübung, beim Auffinden erkrankter Wildtiere und in gemeinsam genutzten Räumen in Feldern, Wäldern, Parks, Gärten und auch in Häusern statt. In diesem Vortrag werden einige Zoonosen vorgestellt, die aktuell in Deutschland bei wildlebenden Säugetieren vorkommen.

Mittels Literatursuche wurde die Prävalenz von Zoonosen bei einheimischen, wildlebenden Säugetieren ermittelt. Weiterhin wurden im Rahmen einer Totfundmonitoring-Studie 122 Eichhörnchen aus Aufzuchtstationen seziert und die häufigsten Erkrankungsursachen ermittelt.

Aktuell bei Wildtieren in Deutschland in hoher Prävalenz vorkommende virale Zoonoseerreger sind Lyssaviren, Hepatitis E Virus Genotyp 3 und Puumala Orthohantavirus. Die über typische Wund- und Lebensmittelinfektionserreger hinausgehenden bakteriellen Zoonoseerreger beinhalten *Brucella suis* Biovar 2, *Francisella tularensis* ssp. *holarctica*, *Mycobacterium caprae*, *Yersinia pseudotuberculosis* und *Leptospira interrogans sensu lato*. Bei Wildtieren häufige parasitäre Zoonoseerreger sind insbesondere *Echinococcus multilocularis*, *Alaria alata*, *Baylisascaris procyonis*, *Trichinella* spp. und *Sarcoptes scabiei*. Die wichtigsten Erkrankungskomplexe bei Eichhörnchen aus Aufzuchtstationen waren Aspirationspneumonien und Gastroenteritiden, wobei speziell eine hohe Prävalenz des parasitären Zoonoseerregers *Cryptosporidium parvum* nachweisbar war.

Zoonosen können nur bei ganzheitlicher Betrachtung von Ökosystem, Tierwelt und Mensch verstanden und bekämpft werden. Das in den letzten Jahren für einzelne Todesfälle bei Menschen in Sachsen-Anhalt verantwortliche Bunthörnchen Bornavirus 1 konnte in einheimischen Eichhörnchen nicht nachgewiesen werden. Eine aktive Zusammenarbeit von Human- und Tiermedizinerinnen kann helfen, neuartige Zoonosen frühzeitig zu erkennen, einzuschätzen und Gegenmaßnahmen zu entwickeln.

History of postgraduate specialisation

K. Schierle¹, T. Braunschweig²

¹SLK Kliniken Heilbronn, Klinikum am Gesundbrunnen, Institut für Pathologie, Heilbronn, Germany, ²Uniklinik RWTH Aachen, Institut für Pathologie, Aachen, Germany

Questions/Background

Die Weiterbildung zum Facharzt/ zur Fachärztin für Pathologie ist eine zentrale Grundlage unseres Fachgebietes und sichert die fachärztliche Versorgung. Den organisatorischen Rahmen tragen die Landesärztekammern.

Methods

Über Internet- und Literaturrecherche werden die Ergebnisse eingeordnet.

Results

Im Rahmen des Vortrags soll beleuchtet werden, seit wann es eine Form der organisierten Weiterbildung gibt und welche Veränderungen sie in der Zeit erfahren hat. Es wird auch ein spezieller Augenmerk darauf gelegt werden, welche unterschiedlichen Methoden in die Weiterbildungsordnung aufgenommen und wieder herausgenommen wurden.

Conclusion

Die Weiterbildung unterliegt dem Wandel der Zeit. Vom Beginn mit einzelnen Grundvoraussetzungen für die Weiterbildung in der Pathologie wurde die Weiterbildung immer komplexer. Die wechselnden Methoden, die gefordert werden und wurden spiegeln die aktuellen Entwicklungen in der Pathologie wider.

AG13 Informatik, digitale Pathologie und Biobanking I

AG13.02

Interactive AI training with minimal annotations

R. Kletzander¹, M. Benz¹, **V. Bruns¹**, P. Kuritcyn¹, D. Firmbach², C. Matek², C. I. Geppert², A. Hartmann², M. Eckstein²

¹Fraunhofer IIS, Digital Health Systems, Erlangen, Germany, ²Friedrich-Alexander-Universität Erlangen-Nürnberg, Institut für Pathologie, Erlangen, Germany

Questions/Background

Supervised AI training typically requires vast amounts of ground truth data. In the domain of histopathological image analysis, this means that experts need to create many precise annotations, which is a tedious and time-consuming task. However, especially in biomedical research, users by design seek to answer unique research questions, which would entail having to train many such custom AIs. How can this challenge be addressed?

Methods

“Few Shot Learning” denotes a set of methods that aim to train an AI on a new task using only a small set of training data. In our approach, we utilize a Prototypical Few Shot Network (ProtoNet) to realize an interactive graphical AI authoring system that enables medical researchers to adapt a pre-trained AI to their own data. We pre-trained a patch-wise classification ProtoNet on millions of histological image patches so that the model learns features that generalize well to other tasks rather than being optimal for the specific example use case. This is achieved by adding a component to the loss function that incentivizes the model to use features, which spread out in latent space. This backbone is then used to analyze the training annotations at runtime and compute one or more prototypical feature vectors for each tissue class. Subsequently, unknown patches can be classified by finding the class prototype with the smallest distance in latent space.

Results

Initially, our ProtoNet has been trained on a large annotated dataset of H&E stained colon resections. We evaluate its generalizability by adapting it to recognize “tumor”, “healthy” and “necrotic” areas in a heterogeneous dataset of urothelial carcinomas. The training set comprises only 18 “tumor” annotations (one per slide, 3 slides each for 6 subtypes), 12 “healthy” annotations (connective tissue, fat, muscle, inflammation in each 3 slides) and 3 “necrosis” annotations (from 3 slides). An F1 score of 0,91 (accuracy 92,9%) is achieved on a test set of >65.000 patches (50 µm² each) drawn from a disjoint set of N=39 whole-slide images (WSIs).

Conclusion

The presented system enables non-technical users to interactively teach an AI to segment histological WSIs into a set of user-defined classes merely by annotating a few stereotypical regions per class. The system can be used to segment WSIs, but it can also be regarded as an annotation assistance system, conceptually similar to Active Learning, where the AI produces base annotations that then only need to be corrected by the user where necessary.

AG13.03

Predicting simplified consensus molecular classes in muscle-invasive bladder cancer (MIBC) with deep learning (DL)

A. Stoll^{1,2}, F. Koll³, J. Triesch², H. Reis¹, M. Eckstein⁴, N. Flinkner^{1,2}, V. Da Silva Mourato Henriques⁵, P. J. Wild¹

¹Universitätsklinikum Frankfurt, Dr. Senckenbergisches Institut für Pathologie (SIP), Frankfurt am Main, Germany, ²Frankfurt Institute for Advanced Studies (FIAS), Frankfurt am Main, Germany, ³Universitätsklinikum Frankfurt, Klinik für Urologie, Frankfurt am Main, Germany, ⁴Uniklinikum Erlangen, Pathologisches Institut, Erlangen, Germany, ⁵Universitätsklinikum Heidelberg, Pathologisches Institut, Heidelberg, Germany

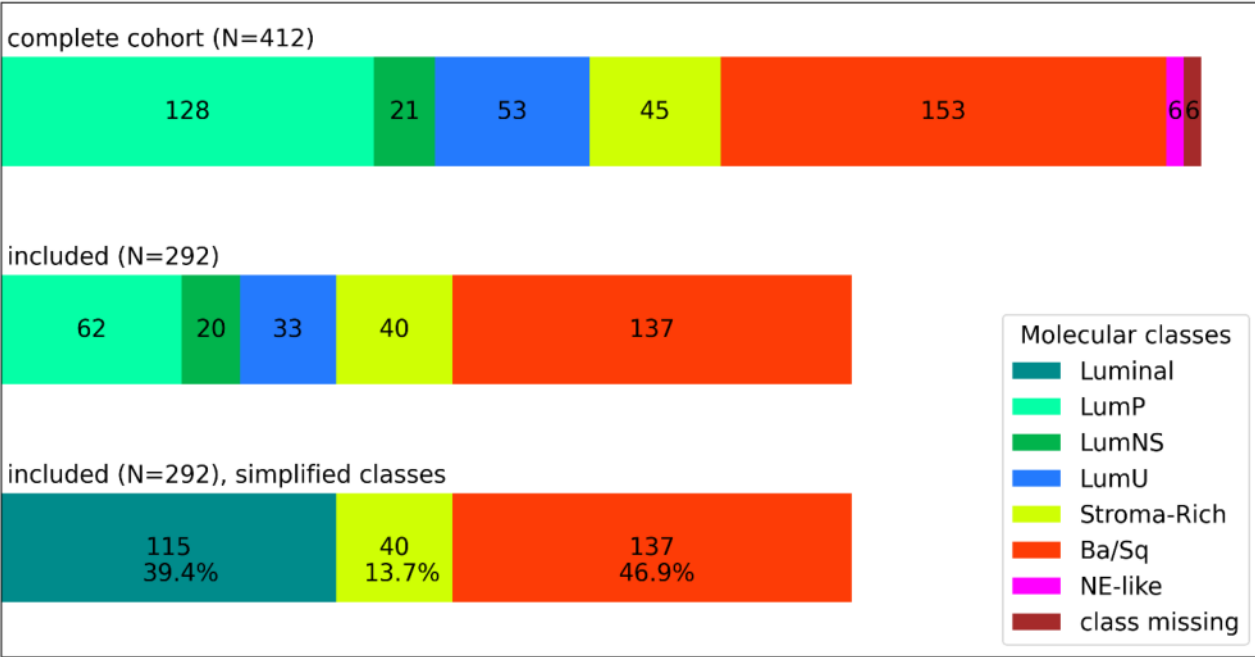
Questions/Background

Recently, a consensus molecular classification for muscle-invasive bladder cancer (MIBC) was established

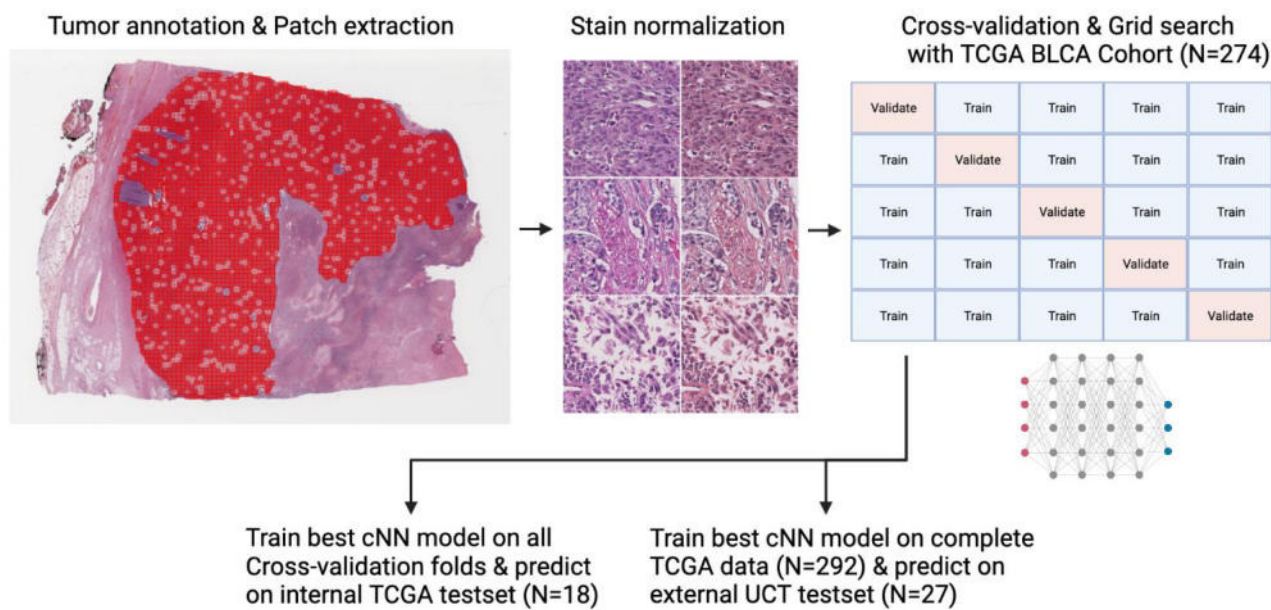
aligning earlier molecular classifications based on transcriptome profiling in MIBC [1]. We wondered if we could predict these molecular consensus subtypes based on morphology alone with deep learning (DL).

Methods

We reviewed and annotated whole slide images (WSIs) from MIBC cases from the publicly available TCGA BLCA Cohort (N=292) [2] and from the University Cancer Center Frankfurt (UCT) (N=27) [3]. RNA was extracted from the UCT Cohort and consensus molecular subtypes were assigned with a transcriptomic profiler from Kamoun et al. [1]. As there were both very few "Neuroendocrine-like" cases and few cases in two Luminal classes, we excluded the former cases while incorporating the Luminal cases in one common "Luminal" category. We predicted simplified consensus molecular subtypes (Luminal, Basal/Squamous and Stroma-rich) from WSIs alone in both the TCGA cohort and in cases from the UCT Cohort on the case level with convolutional neural networks (cNNs).



TCGA BLCA Cohort with respective molecular classes before and after inclusion criteria.



Workflow from annotations to final predictions with cNNs. Created with BioRender.com

Results

We reached an AUC of 74.2% in cross-validation experiments and an AUC of 85.1% for the internal TCGA

test set. For the external UCT test set, we reached an AUC of 73.7%.

Conclusion

While these prediction results are promising, our work also highlights the need for stringent inclusion criteria of MIBC cohorts for molecular subtyping to find its way into clinical practice.

Literaturangaben:

- [1] Kamoun, A. et al., (2020), A Consensus Molecular Classification of Muscle-invasive Bladder Cancer, *European Urology*, 420-433, Vol. 77 Issue 4, <https://www.sciencedirect.com/science/article/pii/S0302283819306955>, 2023-02-23, doi:10.1016/j.eururo.2019.09.006
- [2] Robertson, A. G. et al., (2017), Comprehensive Molecular Characterization of Muscle-Invasive Bladder Cancer, *Cell*, 540-556 e25, Volume 171, Issue 3, <https://pubmed.ncbi.nlm.nih.gov/28988769/>, 2023-02-23, 10.1016/j.cell.2017.09.007
- [3] Koll, F. J. et al., (2022), CK5/6 and GATA3 Defined Phenotypes of Muscle-Invasive Bladder Cancer: Impact in Adjuvant Chemotherapy and Molecular Subtyping of Negative Cases, *Frontiers in Medicine*, Volume 9, <https://www.ncbi.nlm.nih.gov/pubmed/35783619>, 2023-02-23, 10.3389/fmed.2022.875142

AG13.04

An Open Source Library for Anonymization of Whole Slide Images

T. Bisson¹, M. Franz¹, I. Dogan O¹, D. Romberg², C. Jansen¹, A. Homeyer², P. Hufnagel^{1,3}, N. Zerbe¹

¹Charité - Universitätsmedizin Berlin, Institut für Pathologie, Berlin, Germany, ²Fraunhofer MEVIS, Bremen, Germany, ³Hochschule für Technik und Wirtschaft Berlin, Centrum für Biomedizinische Bild- und Informationsverarbeitung, Berlin, Germany

Questions/Background

Whole Slide Images (WSI) are crucial for computational pathology research and education. Their transfer, whether within the same institution or between multiple institutions, often involves the use of public networks or cloud storage. To prevent the WSIs from being associated with patients, they must be anonymized prior to the exchange. However, common proprietary WSI file formats often contain sensitive information in multiple locations that cannot be easily removed, complicating their exchange. To address these issues, we analyzed all the information stored in WSIs and developed an open source tool that enables GDPR-compliant anonymization for a variety of different WSI file formats.

Methods

Existing solutions for anonymizing WSIs are not always sufficiently strong and are limited to only a few file formats. Therefore, we propose a policy to evaluate various degrees of anonymization and classify existing solutions accordingly. This policy is guided by the General Data Protection Regulation (GDPR) that has a strict interpretation of data privacy and thus is automatically compliant with the Health Insurance Portability and Accountability Act (HIPAA). Based on this policy, we developed an open source library for anonymization of major WSI formats beyond the requirements of GDPR and HIPAA.

Results

In our anonymization policy we have defined five different levels that specify different degrees of WSI anonymization. Although we already consider level III as GDPR compliant, our software library reaches level IV, where all associated images (e.g. label images) are completely removed from the WSIs and the potentially identifying metadata is deleted. The anonymization process runs offline and instantaneously. In addition, the library is designed to be easily extended to cover additional WSI formats or updates to existing versions. The library can be used as a standalone tool or may be integrated into other software systems using interfaces for common programming languages (including C, Python, JavaScript).

Conclusion

Using this policy, existing and future anonymization solutions can be classified regarding legal regulations. The modular structure of the introduced framework enables extensions towards both, additional WSI formats as well as variations of existing formats. With the open source library provided, sensitive information can be thoroughly removed from WSIs of common formats, which greatly facilitates data exchange.

AG13.05

Enhancing Accuracy and Transferability using CNN Ensembles

N. Flinner¹, R. Mayer², D. Savran², S. Gretser², P. Ziegler², P. J. Wild²

¹University Hospital Frankfurt, Dr. Senckenberg Institute of Pathology, Frankfurt, Germany, ²University Hospital Frankfurt, Dr. Senckenberg Institute of Pathology, Frankfurt, Germany

Questions/Background

Convolutional neural networks (CNN) frequently perform worse on external test datasets, which were collected at hospitals not used during CNN training. Here, we show that CNNs perform best on high quality

data, while the transferability depends strongly on the tissue quality used during training.

Methods

To improve the performance and transferability of trained CNN models, the ensemble technique was a promising approach, which is especially well suited for small data sets (~100 patients).

Results

We used bagging ensembles, where we randomly resample patients and patches during training to drastically improve the accuracy compared to individual CNNs or vanilla ensembles. Additional improvements could be achieved with the help of multi-head CNNs, where different labels (e.g. molecular subtypes and morphological features) are learned simultaneously and the addition of noise to the training could improve the transferability of learned models.

Conclusion

We have successfully applied our models to gastric, ovarian and bladder cancer.

AG13.06

Digital transformation of the histopathological routine laboratory - Do's & don'ts

C. Mogler, V. Iwuajoku, F. Stögbauer, A. Haas, K. Steiger, W. Weichert, **P. Schüffler**

Institut für Pathologie, Technische Universität München, München, Germany

Questions/Background

Die Digitalisierung hält Einzug in die deutschen Pathologien und wird die Arbeits- und Befundungsweise in den nächsten Jahren revolutionieren. Die digitale Transformation stellt die histopathologischen Routinelabore strukturell, personell als auch mental vor neue Herausforderungen.

Methods

Unser Ziel war es, den kompletten Routine-Eingang der TU München prospektiv ohne Zeitverzögerung der Turnaround time (TAT, Zeit zwischen Probeneingang und Befundausgang) zu digitalisieren. Mittels detaillierter Workflow-Analyse des histopathologischen Eingangslabors, Auswertung der Scan-Profile und der Scanner-Auslastung sowie regelmäßiger (Troubleshooting-) Besprechungen wird der Eingang des Pathologischen Instituts der TU München Schritt für Schritt digitalisiert. Dabei wurden Verzögerung durch die Digitalisierung erfasst, Laufzeiten erhoben und Problemstellen bei der Umsetzung detektiert.

Results

Die ersten Versuche, den kompletten histopathologischen Eingang zu digitalisieren, führte zu einer Verzögerung der TAT von rund 3 Stunden gegenüber der konventionellen Ausgabe von Glasschnitten. Der Hauptgrund hierfür vor allem war eine ungleichmäßige Beladung der Scanner, die am Nachmittag zu einer vollständigen Ausschöpfung der Scan-Kapazität führte. Durch schrittweise Umstellung der Arbeitsabläufe unter Einbindung des technischen Personals konnte die zeitliche Verzögerung schrittweise auf ein Minimum reduziert werden.

Conclusion

Die vollständige Umstellung auf digitale Pathologie stellt einen langen aber äußerst lohnenswerten Weg dar, der sich aber nur unter ganz bestimmten Voraussetzungen durchführen lässt. Wichtig ist neben einer entsprechenden Personalstärke auch eine maximale Optimierung der einzelnen Arbeitsabläufe in den Laboren, von Anfang an Einbeziehung des technischen Personals und detaillierter Dokumentation der entstehenden Probleme.

AG13 Informatik, digitale Pathologie und Biobanking II

AG13.09

How disruptive is Digital for (Continuing) Medical Education in Pathology

K. Mirza

Loyola Pathology and Laboratory Medicine, Department of Pathology and Laboratory Medicine, Maywood, United States of America

Digital technologies and social media have changed the way pathology pedagogy is deployed. This presentation will discuss the immense power of these platforms in educating about pathology in the UME, GME and CME space. Additionally, detailed description will be provided on the role of websites such as www.pathselective.com and www.hemereports.com and programs such as the Digital Communications Fellowship in Pathology, for promoting pathology education digitally.

AG13.10

Artificial Intelligence for pathology-based biomarkers in oncology

J. N. Kather

Technische Universität Dresden, Medizinische Klinik 1, Dresden, Germany

Precision oncology requires biomarkers to tailor treatment to individual patients. Artificial Intelligence enables us to extract quantitative information from tissue slides stained with hematoxylin and eosin. These histology-based biomarkers can be used to pre-screen patients for targeted genomic testing and can be combined with genomic tests to predict treatment response and clinical outcomes. This talk will summarize the state of the art of AI in histopathology for precision oncology biomarkers. It will cover the technical foundations, emerging use cases and established applications which are available for clinical use already.

AG13.11

A multi-center study: artificial intelligence assisted prediction of lymph node status in breast cancer

Y. Ding¹, F. Yang², M. Han¹, C. Li³, Y. Wang⁴, X. Xu⁵, M. Zhao⁶, M. Zhao¹, **M. Yue**¹, H. Deng¹, J. Yao², Y. Liu¹

¹The Fourth Hospital of Hebei Medical University, Department of Pathology, Shijiazhuang, China, ²Tencent, AI Lab, Shenzhen, China,

³Chengde Medical University Affiliated Hospital, Department of Pathology, Chengde, China, ⁴Affiliated Hospital of Hebei University, Department of Pathology, Baoding, China, ⁵Xingtai People's Hospital, Department of Pathology, Xingtai, China, ⁶First Hospital of Qinhuangdao, Department of Pathology, Qinhuangdao, China

Questions/Background

To develop a deep learning model based on clinicopathological data and digital pathological image of core needle biopsy specimens for predicting breast cancer lymph node metastasis.

Methods

We collected 3701 patients from the Fourth Hospital of Hebei Medical University and 190 patients from four medical centers in Hebei Province. Integrating clinicopathological data and image features build multi-modal and multi-instance (MMMI) deep learning model to obtain the final prediction.

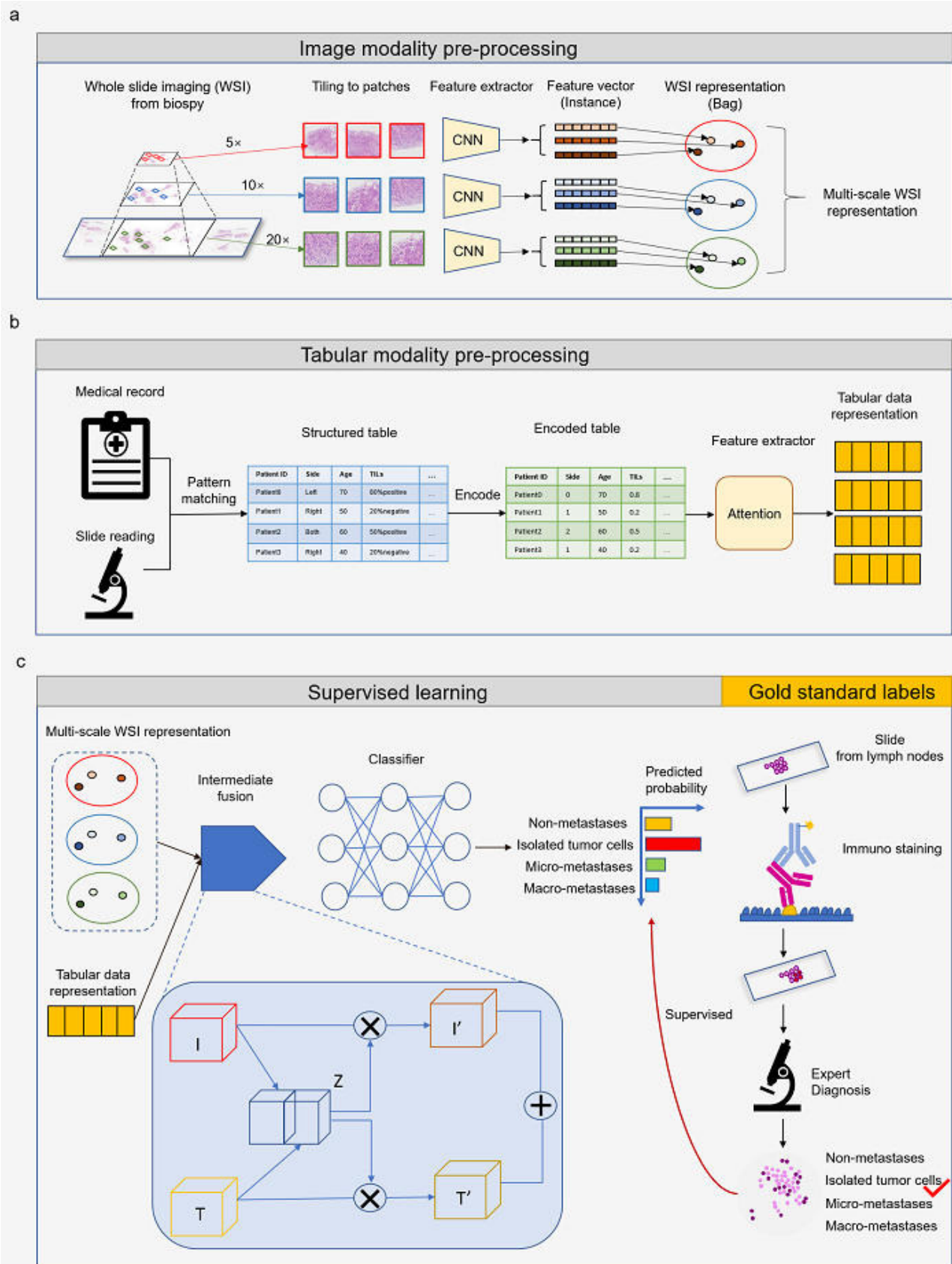


Figure 1. Model development overview. The model development can be categorized into three parts, the preprocessing of image modality data, the preprocessing of tabular data, and training of the classification model.

Results

1. For predicting with or without lymph node metastasis, the AUC was 0.770, 0.709, 0.809 based on the clinicopathological features, WSI and MMLI, respectively. 2. For predicting four classification of lymph node

status (no metastasis, isolated tumor cells (ITCs), micrometastasis, and macrometastasis), the prediction based on clinicopathological features, WSI and MMMI were compared. The AUC for no metastasis was 0.770, 0.709, 0.809, respectively; ITCs were 0.619, 0.531, 0.634, respectively; micrometastasis were 0.636, 0.617, 0.691, respectively; and macrometastasis were 0.748, 0.691, 0.758, respectively. The MMMI model achieved the highest prediction accuracy. 3. For prediction of different molecular types of breast cancer, MMMI demonstrated a better prediction accuracy for any type of lymph node status, especially in the molecular type of triple negative breast cancer (TNBC). 4. In the external validation sets, MMMI also showed better prediction accuracy in the four classification, with AUC of 0.725, 0.757, 0.525, and 0.708, respectively.

Class	Methods	AUC	ACC	SEN	SPE
negative	Tabular	0.770(0.737-	0.723(0.693-	0.791(0.662-	0.649(0.580-
		0.804)	0.752)	0.845)	0.769)
	MIL-WSI	0.709(0.672-	0.669(0.637-	0.593(0.458-	0.757(0.617-
		0.746)	0.703)	0.728)	0.874)
	MMMI	0.809(0.779-	0.751(0.720-	0.768(0.616-	0.734(0.637-
		0.840)	0.779)	0.855)	0.874)
ITCs	Tabular	0.619(0.501-	0.701(0.265-	0.600(0.240-	0.705(0.241-
		0.738)	0.938)	0.960)	0.962)
	MIL-WSI	0.531(0.424-	0.346(0.230-	0.880(0.200-	0.329(0.205-
		0.639)	0.938)	1.000)	0.964)
	MMMI	0.634(0.519-	0.746(0.392-	0.600(0.320-	0.751(0.375-
		0.749)	0.880)	0.960)	0.897)
micrometa stasis	Tabular	0.636(0.582-	0.538(0.351-	0.770(0.450-	0.508(0.261-
		0.690)	0.743)	0.960)	0.787)
	MIL-WSI	0.617(0.561-	0.490(0.380-	0.800(0.510-	0.440(0.302-
		0.673)	0.682)	0.930)	0.706)
	MMMI	0.691(0.638-	0.623(0.431-	0.710(0.450-	0.611(0.355-
		0.744)	0.773)	0.910)	0.818)
macromet astasis	Tabular	0.748(0.710-	0.723(0.638-	0.658(0.582-	0.757(0.568-
		0.785)	0.759)	0.827)	0.807)
	MIL-WSI	0.691(0.650-	0.616(0.552-	0.769(0.542-	0.544(0.415-
		0.731)	0.692)	0.871)	0.747)
	MMMI	0.758(0.721-	0.734(0.647-	0.653(0.556-	0.776(0.591-
		0.796)	0.773)	0.822)	0.844)

Table 1. Performance comparison of different models for predicting lymph node status

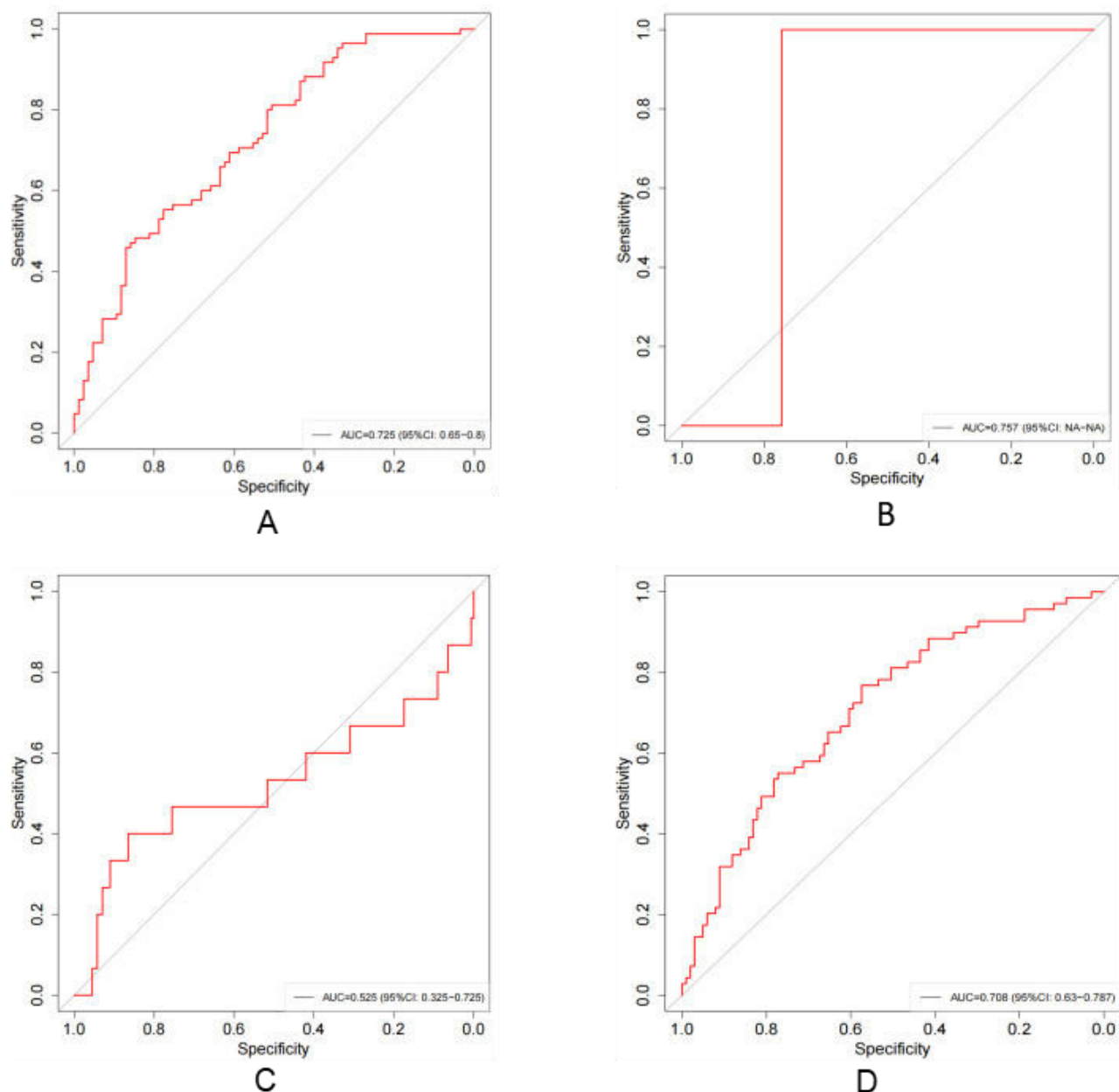


Figure 3. The ROC curve for external validation of lymph node metastatic status. MMMI was used to predict lymph node metastasis using external data. A: No metastasis B: ITCs C: micrometastasis D: macrometastasis.

Conclusion

We developed a breast cancer lymph node metastasis prediction model based on a MMMI model. Through all cases tests, the results showed that the overall prediction ability was high.

AG13.12

Knowledge Graphs in (Nephro-)pathology for decision tree extraction

M. Legnar¹, J.-H. H. Simoneit¹, P. Schirmacher¹, Z. Popovic², S. Porubsky³, C.-A. Weis¹

¹Pathologisches Institut Heidelberg, Abteilung Allgemeine Pathologie, Heidelberg, Germany, ²Pathologisches Institut Mannheim, Mannheim, Germany, ³Institut für Pathologie, Mainz, Germany

Questions/Background

Diagnostic expertise in pathology, typically stored in text form, is subject to continuous improvement. To overview this knowledge and to have a diagnostic algorithm for different diagnoses is beyond the capabilities

of a single pathologist.

Against this background, the question is if it is possible to automatically generate decision trees for pathologists based on text data alone.

In the project presented here, domain-specific knowledge (from nephropathology as a use case) is first stored in a knowledge graph, based on which diagnostic decision trees are generated using different approaches.

Methods

Nephropathology knowledge is stored from multiple sources in a Knowledge graph, initially based on the SnomedCT Ontology. It is enriched with information from textbooks and diagnostic texts.

For this purpose, the texts must first be decomposed into entities (as nodes) and their relationships (as edges) using Natural Language Processing methods. Each disease is represented by a node, and each case by a subgraph of the knowledge graph.

Then different node classification models are trained to predict the diagnoses of different cases to learn relevant relations between certain nephropathological features and diseases.

Finally, decision trees are extracted from the node classification model.

Results

Searching the relation between two entities in pathological texts failed in many cases due to the typical semantic style of such reports. Therefore we are to develop a custom relation extraction model based on the medspaCy-toolkit.

Training a MINDWALK-tree leads to comprehensible results since it can utilize the information of the knowledge graph more efficiently.

Conclusion

Converting a text classification task to a node classification task benefits from additional relation information stored within a knowledge graph.

AG 13 DACH-Symposium der AG Informatik, Digitale Pathologie und Biobanking

AG13.14

Digital Pathology in Austria

J. Haybäck

Neuropathologie & Molekularpathologie, Institut für Pathologie, Innsbruck, Austria

Viele Industriepartner sowie einige der Referenzzentren und manche Vereinigungen sind dabei, die Künstliche Intelligenz in Deutschland voranzutreiben, wobei ein Unternehmen, das Ökosystem mit Marktplatz für A.I.-Lösungen bereitstellt und Schnittstellen zur Interoperabilität bietet, sowie Wissen zur Thematik vermittelt. Schlagwörter, die in diesem Kontext fallen sind „Big Data und Artificial Intelligence“, „Automatisierung in der Pathologie“, „Praktische Implementierung“, „Boa_Image_Frames“, „Pathologie-Workflow in digitaler Medizin“ und „Digitales Pathologie-Institut“, zu denen Veranstaltungen beziehungsweise Kongresse stattfinden. K.I.-Projekte sind bereits initiiert worden.

Die Österreichische Gesellschaft für Pathologie (OEGPath) wird in Innsbruck die Herbsttagung der OEGPath zum Thema Digitale Pathologie und Mammopathologie abhalten. In Österreich sind mehrere Unternehmen, die mit Deep Learning-basierten Kernsegmentierungsalgorithmen eine Bildanalyse-Software anbieten aktiv. Von der Öffentlichen Hand werden finanzielle Mittel für die Digitale Pathologie bereitgestellt.

AG13.15

National digital pathology projects in Switzerland: an update

I. Zlobec

Universität Bern, Institut für Gewebemedizin und Pathologie, Bern, Switzerland

In this brief overview, the landscape of major developments in digital pathology in Switzerland will be outlined, most importantly the Swiss Digital Pathology Initiative (SDPI), which aims to develop a unified

national digital pathology network. Other impactful projects include the Swiss Clinical Guidelines for Digital Pathology and our national research project on computer-aided diagnostics, with results on pathologist-AI interactions.

AG13.17

Getting the most out of Digital Pathology for AI development

P. Regitnig

Medizinische Universität Graz, Diagnostik & Forschungsinstitut für Pathologie, Graz, Austria

To make the most of Digital Pathology for future AI developments, it is essential to introduce numerous conditions at an early stage. For the training of AI algorithms, large amounts of data, ideally from multiple institutions, are required.

The following main criteria have been identified for this purpose: a catalogue to find relevant cases and a trustworthy system that enables inter-institutional processing of large amounts of data.

Building a catalogue may sound trivial, yet the question arises why most institutions only manage to do this in a rudimentary way. The reasons for this are manifold, often due to unstructured data or lack of access to relevant clinical or follow-up data. Ideally several institutions contribute to build a catalogue to enable a later collaboration on these cases.

Nowadays, laboratory information systems offer at least partially structured reports, such as specific fields for TNM or ICD-O coding. Large parts of the report and content are still stored as free text. Large Language Models (LLMs) can extract research-relevant data in structured form from free texts. The alternative lies in the primary structuring of diagnostic content in pathology reports, as suggested, for example, by the ICCR or CAP. Structured reports, however, are disadvantageous in clinical practice due to their length and have therefore never become widely established since their invention. In comparison, LLMs do not offer a 100% correctness to extract specific features from free text reports, but are very efficient.

The catalogue contents should be oriented towards the typical search processes in pathology: by organ system, by diagnosis, by specific stains, immunohistochemistry, or also mutations related to cases. Also, slide or section-specific features should be automatically registered in a research database catalogue to enable an efficient search strategy.

To enable interinstitutional research in the field of AI development, data protection concerns often come to the fore and may prevent this. Approaches of multiparty computing allow the processing of large amounts of image data across different institutions without data transfer. The advantage here is the high control of property rights, governance, and compliance, as the data does not leave one's own institution.

Thus, the goal is to establish inter-institutional catalogues to quickly and efficiently select relevant cases and a trustworthy system for data processing for optimal AI development in pathology.

AG13.18

DIA / AI in Pathology Diagnostics – the Swiss view

S. Berezowska¹, G. Cathomas², R. Grobholz³, M. Henkel⁴, A. Janowczyk^{5,6}, W. Jochum⁷, V. H. Koelzer⁸, M. Kreutzfeldt⁹, K. D. Mertz¹⁰, M. Rössle¹¹, D. Soldini¹², I. Zlobec²

¹Institut Universitaire de Pathologie, Centre hospitalier universitaire vaudois (CHUV) et Université de Lausanne, Lausanne, Switzerland,

²Institute of Tissue Medicine and Pathology, Bern, Switzerland, ³Institute of Pathology Kantonsspital Aarau, Aarau, Switzerland,

⁴Research & Analytic Services University Hospital Basel, Basel, Switzerland, ⁵Precision Oncology Center, Centre hospitalier universitaire vaudois (CHUV) et Université de Lausanne, Lausanne, Switzerland, ⁶Department of Biomedical Engineering, Emory University, Atlanta, United States of America, ⁷Institute of Pathology, Cantonal Hospital St.Gallen, St. Gallen, Switzerland, ⁸Department of Pathology and Molecular Pathology, University and University Hospital of Zurich, Zürich, Switzerland, ⁹Department of Pathology and Immunology, University of Geneva, Geneva, Switzerland, ¹⁰Institute of Pathology, Cantonal Hospital Baselland, Liestal, Switzerland,

¹¹Pathologie Luzerner Kantonsspital, Luzern, Switzerland, ¹²Pathologie Zentrum Zürich medica, Zürich, Switzerland

Digital Pathology is increasingly entering routine clinical pathological diagnostics. As digitization of the routine caseload advances, implementation of digital image analysis algorithms and artificial intelligence tools becomes attainable and desirable in daily sign out. The Swiss Digital Pathology Consortium (SDiPath) has initiated a Delphi process to generate best-practice recommendations for various phases of the process of digitization in Pathology for the local Swiss environment, encompassing the 4 topics: (1) Scanners, Quality Assurance and Validation of Scans, (2) Integration of scanners and systems into the Pathology Laboratory Information System, (3) the Digital Workflow and (4) Digital Image analysis (DIA)/artificial intelligence (AI). The current presentation focuses on the DIA/AI related recommendations generated and agreed on by the

working group, and verified by the Delphi process among the members of the DiPath Consortium. Importantly, they include the view and the currently perceived needs of practicing pathologists from multiple academic and cantonal hospital and private practice, who comprised the majority of the participants.

AG13.20

How to harvest features from a pathologist viewing a WSI for development of AI-Algorithms

M. Plass

Medizinische Universität Graz, Diagnostik & Forschungsinstitut für Pathologie, Graz, Austria

The process of finding a diagnosis in the medical domain relies on a domain specific but also an implicit knowledge and the experience of a human expert.

The collection and understanding of this implicit knowledge can also support the development of robust AI algorithms in Digital Pathology focusing on the most relevant characteristics of a disease.

Currently, the collection of WSI-based metadata during routine diagnoses is limited. In some cases, annotations within the WSI viewers have been made, but this represents only a fraction of the potential metadata and by far is not complete to understand the relevant features of a WSI. To enhance this, software tools can be used to observe the pathologist's diagnostic process on a whole slide image (WSI).

There are two approaches for collecting this data: a) Active collection: Pathologists themselves can add additional metadata, such as annotations, during routine diagnoses on the WSI or, as it is done in most instances, afterwards on selected WSI following certain annotation rules based on the specific research question. It is obvious that such an approach is limited in several ways. b) Passive collection during WSI viewing: Software tools can collect additional data in the background without any further assistance from the pathologist. This can be achieved by recording the viewed area of a WSI and utilizing tools like eye tracking. Features that can be easily collected are for example the examined area, magnification and the duration of observation. Thereby, it is not only important which areas the pathologist examined, but also which regional or cellular parts were most intensively viewed.

The overall observation time is the accumulated time a region has been examined by a pathologist at a specific level of magnification. The time an observer is looking at an area is also an important indicator for the meaningfulness of a certain part of a WSI. Such a passive collection does not disturb a pathologist and therefore is able to collect a huge amount of data about the most important parts of a WSI in the diagnostic path.

In addition to facilitate the development of AI algorithms, this data can serve several other purposes, including pathologists' education, quality control, liability issues, and validation of AI algorithms.

AG13.21

MarrowQuant2.0, a move toward computational bone marrow pathology?

R. Sarkis

EPFL/UNIL Switzerland, --, Lausanne, Switzerland

Assessing bone marrow (BM) cellularity is a critical step in determining hematologic and nonhematologic disorders using BM trephine biopsies. Currently, hematopathologists use a semiquantitative method to visually estimate the hematopoietic and adipocytic components, but this approach doesn't provide quantitative data on other stromal compartments. To address this issue, we have developed MarrowQuant 2.0, a computational hematopathology workflow that is user-friendly and integrated within the QuPath software. MarrowQuant 2.0 quantifies five mutually exclusive compartments of BM (bone, hematopoietic, adipocytic, interstitial/microvasculature areas, and other) and calculates the cellularity of human BM trephine biopsies. We adapted the machine-learning algorithm StarDist for instance segmentation to identify individual adipocytes. We used this algorithm to analyze hematoxylin and eosin images of 250 bone specimens from control subjects and patients with acute myeloid leukemia or myelodysplastic syndrome at diagnosis and follow-up. We compared the MarrowQuant 2.0 cellularity estimates with the visual scores of four hematopathologists to assess its accuracy. The algorithm was able to accurately segment bone marrow compartments, with an average accuracy of 86%, and maximal accuracy for bone (99%), hematopoietic (92%), and adipocyte (98%) areas. We found a strong correlation between the MarrowQuant 2.0 cellularity score and hematopathologists' estimations ($R^2=0.92-0.98$, intraclass correlation coefficient [ICC]=0.98; interobserver ICC=0.96). Furthermore, our results quantitatively confirmed the hematopoietic and adipocytic compartments' reciprocity. We also evaluated the performance of MarrowQuant 2.0 on specimens collected during clinical routine diagnosis, we found similar results (R^2

=0.86, n=42). Thus, we conclude that these validation experiments establish MarrowQuant 2.0 as a reliable tool for BM cellularity assessment. Moreover, the use of MarrowQuant 2.0 allowed us to identify morphological changes in BM stroma, specifically bone marrow stromal edema, and we observed differences in the distribution of compartments at the same time point of BM trephine biopsies. We anticipate that this workflow will prove to be an invaluable clinical research tool for exploring new markers associated with BM stromal components and their corresponding changes over time. Furthermore, it may contribute to validating future digitalized diagnostic hematopathology workstreams.

AG14 Molekularpathologie I

AG14.01

MLH1 promotor methylation – comparison of different testing strategies and optimization of cut-off values for distinguishing hereditary and sporadic cancer origin

V. Welter¹, J. Siemanowski¹, B. Schömig-Markieka¹, N. Pfarr², E.-M. Mayr², R. Büttner¹, S. Merkelbach-Bruse¹, U. Siebolts¹

¹Institut für Pathologie, Universitätsklinikum Köln, Köln, Germany, ²Institut für Pathologie, Technische Universität München, München, Germany

Questions/Background

Genetic disorders can be of hereditary origin characterised by germline mutations or sporadic origin caused by somatic variants and methylation. Thus, for differentiation between microsatellite instability high and mismatch repair deficient sporadic or hereditary cancers further tests are necessary. The methylation status of the *MLH1* promotor, a mismatch repair gene, is a suitable, highly specific screening marker. Although methylation of the *MLH1* promotor can be present in both scenarios, a differentiation based on the methylation level is possible by quantitative methods. A high methylation level is present in sporadic cancers whereas hereditary cancers are characterised by low or no methylation.

The aim of this study was to optimize the analysis of the *MLH1* promotor methylation regarding the reliability and reproducibility of results. Different testing methods were compared in order to define cut-off values for distinguishing hereditary and sporadic tumours.

Methods

For the methylation detection several methods have been applied in different testing facilities: methylation specific restriction digestion and real-time qPCR, bisulfide conversion and subsequent pyrosequencing (PyroMark Q24 CpG *MLH1*) (Qiagen) and the Infinium EPIC DNA Methylation Array (850k) (Illumina). Furthermore, the influence of tumour purity and fluctuations in multiple determinations was determined.

Results

As the testing methods examine different DNA regions, results differ and have to be normalized for comparison. After evaluation of all methods, the restriction digestion and qPCR-based method seemed to be most suited for daily patient care. Due to the calculation formula fluctuations were observed regarding the reproducibility of the results. Thus, the threshold for positivity was expanded to a “marginal” state of 11-24% methylation around the predefined cut-off of 16.5% in colorectal cancer. A strong influence of the tumour purity could not be manifested. However, a threshold of ≥30% tumour purity is required for this method.

Conclusion

The study showed that there is a variety of methods to analyse the *MLH1* promotor methylation. For reliable and reproducible results the study defined a cut-off of 30% tumour purity for the analysis and a “marginal” area in which the classification of methylated or not methylated (sporadic or hereditary) is inconclusive in colorectal cancer. To transfer this method to other entities the cut-off value should be carefully validated.

AG14.02

A pilot study on the epigenomic profiling of homologous recombination deficient (HRD) high-grade serous carcinoma of the ovaries

T. Kraus, S. Assadi Kordlo, K. Sotlar

Uniklinikum Salzburg, Universitätsinstitut für Pathologie, Salzburg, Austria

Questions/Background

Ovarian cancer is a highly malignant tumour of the female reproductive system. Thereby, high-grade serous carcinoma (HGSC) of the ovaries accounts for approximately 70% of all primary ovarian HGSC. Within the last years, there was a tremendous progress in targeted treatment of ovarian HGSC. Analysis of homologous recombination deficiency (HRD) in ovarian cancer showed that patients with high HRD status show a favorable response to PARP inhibitor therapies. Thus, the identification of patients with high HRD scores is crucial for advanced patient care. The aim of this study was to perform an epigenomic profiling of ovarian HGSC with high and low HRD scores.

Methods

In this pilot study we performed epigenome-wide methylation analysis of 16 ovarian cancers with 8 ovarian HGSCs showing high HRD and 8 cancers showing low HRD status. Applying the Illumina Infinium EPIC bead chip array we were able to interrogate more than 850,000 methylation sensitive CpGs sites in parallel. Computational analyses were performed to identify significant differentially methylated genes. Gene ontology analysis was processed to reveal altered pathways.

Results

We found that ovarian HGSCs with high HRD showed 111 significantly differentially methylated gene regions compared with ovarian HGSCs with low HRD status. Thereby, 55 gene regions were hypermethylated and 56 gene regions were hypomethylated in HRD high ovarian HGSC compared with HRD low ovarian HGSC. Gene ontology (GO) analysis showed that DNA replication-dependent nucleosome assembly pathway was among top hypomethylated pathways.

Conclusion

In summary, in this pilot study, we found significant differences in DNA methylation profiles in ovarian HGSC depending on HRD status, possibly opening new targetable molecular pathways in HGSC therapy.

AG14.03

Deletions with Microhomologies - Patterns of DNA Double-Strand Break Repair - an in-silico Analysis of the Mutational Landscape of TCGA

S. Beck¹, E. Romanovsky¹, I. Ourailidis¹, K. Kluck¹, M. Menzel¹, P. Schirmacher², A. Stenzinger³, J. Budczies¹

¹Universitätsklinikum Heidelberg - Institut für Pathologie, Molekularpathologisches Zentrum - Medizinische Bioinformatik, Heidelberg, Germany, ²Universitätsklinikum Heidelberg - Institut für Pathologie, Allgemeine Pathologie, Heidelberg, Germany, ³Universitätsklinikum Heidelberg - Institut für Pathologie, Molekularpathologisches Zentrum, Heidelberg, Germany

Questions/Background

Double-strand breaks (DSB) of DNA can be induced by environmental factors or occur during cell cycle. Depending on break pattern and on cell cycle phase, different DNA repair mechanisms can be active. In cancer, if the primary error-free repair mechanism homologous recombination repair is defective or unavailable, other error-prone repair mechanisms take over, e.g. microhomology-mediated end joining (MMEJ). The study aims to detect specific mutational patterns of MMEJ and analyze its appearance in different cancer types.

Methods

We analyzed 112,167 somatic deletions in 7,228 tumors of TCGA and searched for deletions with flanking microhomology (MH). A classification scheme, based on length of deletion and MH, was conceived, separating MMEJ from other MH using repair mechanisms that introduce short deletions, i.e. non-homologous end-joining (NHEJ) and single-strand annealing (SSA).

Results

Analyses of MH-carrying deletions in pan-cancer showed that 16% could be assigned to MMEJ, 62% to NHEJ, and only 0.03% to SSA. In ovarian cancer (OV) MMEJ (42%) was the most frequent category, NHEJ could be assigned to 27% of deletions and a significant difference in the proportion of MMEJ between HRD-positive and HRD-negative tumors (47% vs. 19%, $p=2.6\cdot10^{-11}$) was detected.

In cancer entities with a high prevalence for defective DNA mismatch repair (MMR) like uterine corpus endometrial carcinoma, stomach, colon, and rectum adenocarcinomas, a higher proportion of deletions with MH were assigned to NHEJ (83%, 78%, 84%, and 68%) than to MMEJ (8%, 11%, 8%, and 14%).

Proportions of deletions assigned to MMEJ were significantly higher in MMR-proficient tumors compared to MMR-defective tumors (23% vs. 5%, $p=4.6\cdot10^{-51}$, 30% vs. 5%, $p=3.9\cdot10^{-80}$, 19% vs. 5%, $p=1.8\cdot10^{-21}$, and 20% vs. 5%, $p=0.00014$).

Conclusion

We analyzed the set of detected deletions in the TCGA pan-cancer cohort with respect to MH and assigned each of the deletions to one of the three repair mechanisms MMEJ, NHEJ, and SSA. The activity of the repair systems varied in different cancer types and between molecular subtypes, e.g. between HRD-positive

and HRD-negative OV, as well as between MMR-deficient and MMR-proficient tumors of various cancer types.

Analysis of MH in clinical cancer tissues can contribute to uncovering of the deficient and the active mechanisms of DNA repair in the cancer cells and thus to the ultimate goal of a comprehensive characterization of deficient DNA repair systems for optimal guidance of therapies based on synthetic lethality.

AG14.04

Comparison of five different assays for the detection and genotyping of human papillomavirus in cervical liquid-based cytology and formalin fixed paraffin embedded tissue

M. A. Ihle, M. Degenhardt, J. Fassunke, U. Siebolts, S. Merkelbach-Bruse
Universitätsklinikum Köln, Köln, Germany

Questions/Background

Due to the high standard of the General Safety And Performance Requirements of the In Vitro Diagnostic Regulation (IVDR) many companies stop the production of their assays. At the end of 2022 Chiprons' LCD-Array Kit HPV 3.5, that was established for the detection of human papillomavirus at our Institute, was no longer available. Therefore, we aimed at establishing a new assay for the detection of human papillomavirus that was comprehensive, fast and easy to perform and CE-IVD conform.

Methods

Cervical liquid-based cytology and formalin-fixed, paraffin-embedded samples were analyzed with four different assays: Anyplex™ II HPV28 Detection (Seegene), HPV DNA Array (AID), EUROArray HPV (EUROImmun) and VisionArray HPV Chip 1.0 (ZytoVision) compared to the results of the in-house established LCD-Array Kit HPV 3.5 from Chipron. To exclude pre-analytical divergences the same extracts were used for all analyses. The Anyplex™ II HPV28 Detection kit is a multiplex real-time PCR. All other assays use hybridization for the detection of HPV.

Results

The Anyplex™ II HPV28 Detection kit is fast and easy to perform for the detection and differentiation of 28 HPV types. For cervical liquid-based cytology 10 µl instead of 5 µl template DNA (as stated in the manual) was sufficient for a reliable detection of HPV. Furthermore, false positive results could be detected. The HPV DNA Array can be automated with the Croco 0204 to detect 29 different HPV types. In our study, we could detect cross-contaminations in the 96-well plate using the robot due to the open set-up on the desk of the robot. The automation of EUROArray HPV is coming soon and the assay is easy to perform even without an automation. It detects 30 different HPV types. However, it showed a high rate of false positive HPV 16 cases which is a high-risk HPV type. The VisionArray HPV Chip 1.0 was the assay with the highest amount of hands-on time and no automation is available. This array detects most types of HPV (41 different types) and showed the highest specificity.

Conclusion

Even if the VisionArray HPV Chip 1.0 showed drawbacks regarding hands-on time and automation, it had the highest specificity in our comparison study and can reliably detect and differentiate the highest number of HPV types.

AG14.05

Homologous recombination deficiency (HRD) assessment by targeted next generation sequencing using the OncoPrint Comprehensive Assay Plus and the determination of the Genomic Instability Metric (GIM) in ovarian cancer

I. Bonzheim¹, M. Grube², R. Rottscholl¹, A. Rau¹, F. Otto¹, F. Mihalik¹, T. Kopp¹, S. Brucker², F. Fend¹, S. Kommoss², A. Staebler¹

¹Institut für Pathologie und Neuropathologie, Universitätsklinikum Tübingen, Tübingen, Germany, ²Universitäts-Frauenklinik, Tübingen, Germany

Questions/Background

Poly ADP ribose polymerase inhibitors (PARPi) have significantly improved the management of high-grade ovarian cancers (HGO). Response to PARPi is based on homologous recombination deficiency (HRD)

present in tumor cells that have a defective DNA homologous recombination repair (HRR) pathway. Mutations in HRR genes, including *BRCA1/2*, may result in an HRD phenotype. Identifying HRD+ cancers allows the selection of patients likely to benefit from PARPi. Besides mutation analysis, which likely fails to identify all HRD+ cancers, different approaches are used to detect the “genomic scars” which occur in HRD cells. So far, the gold standard for HRD testing in HGOC is the MyChoice assay (Myriad Genetics). The aim of our study was to test the performance of the OncoPrint Comprehensive Assay Plus (OCAplus) (ThermoFisher Scientific) for HRD detection in comparison to the results of the MyChoice assay in cases which had been tested in routine diagnostics.

Methods

55 cases of HGOC, previously examined by Myriad MyChoice assay, were analyzed using OCAplus. The respective scores used to determine HRD status were compiled: Genomic Instability Score (GIS) (MyChoice assay) and Genomic Instability Metric (GIM) (OCAplus). In addition, the mutation status of *BRCA1/2* and relevant HRR genes was evaluated. Positive agreement between HRD status determined by score alone and inclusion of *BRCA* status was determined. Discrepant cases were evaluated in relation to available clinical data.

Results

GIS and GIM were determined in 49 of the 55 cases. Comparison of HRD status based on the score showed 82% concordance. With inclusion of *BRCA1/2* mutation status, positive agreement was 85% (18 cases HRD- and 28 cases HRD+ with both tests). 15% of cases showed discordance (one case GIS HRD+ GIM HRD-, one case with borderline scores with both analyses and six cases GIM HRD+ GIS HRD-). Clinical data were available for five of the six cases with positive HRD status by GIM and negative by GIS. Three patients received a PARPi. All five showed complete or partial remission at follow-up.

Conclusion

OCAplus can reliably detect HRD status in the high and low range. Since GIS and GIM are continuous variables, borderline cases may need additional workup. Discrepant cases with at least one test result HRD+ are most likely HRD+ as defined with response to PARPi and/or chemotherapy. Using the OCAplus GIM to define HRD may increase the group of patients who benefit from PARPi and would be missed with the current gold standard method.

AG14.06

QuIP EQA scheme for the molecular pathological detection of the HRD status in ovarian cancer 2023

M. Joosten¹, I. Braicu², M.-C. Demes³, W. Dietmaier⁴, F. Haller⁵, A. Hartmann⁵, D. Horst¹, M. Hummel¹, K. Ilm⁶, E.-M. Mayr⁷, S. Merkelbach-Bruse⁸, J. Siemanowski⁸, C. Vollbrecht¹, W. Weichert⁷, **N. Pfarr⁷**

¹Institut für Pathologie, Charité Berlin, Berlin, Germany, ²Tumor Bank Ovarian Cancer Network (TOC) and Biostatistics, Charité Berlin, Berlin, Germany, ³Institut für Pathologie, Universitätsklinikum Frankfurt, Frankfurt am Main, Germany, ⁴Institut für Pathologie, Universitätsklinikum Regensburg, Regensburg, Germany, ⁵Institut für Pathologie, Uniklinikum Erlangen, Erlangen, Germany, ⁶Qualitätssicherungs-Initiative Pathologie (QuIP GmbH), Berlin, Germany, ⁷Institut für Pathologie, Technische Universität München, München, Germany, ⁸Institut für Pathologie, Universitätsklinikum Köln, Köln, Germany

Angehts der Zulassung des PARP-Inhibitors Olaparib in Kombination mit Bevacizumab ist über die Analyse von Mutationen in den *BRCA1/2*-Genen hinaus der Homologe-Rekombinations-Defizienz (HRD)-Status für die Therapieentscheidung beim Ovarialkarzinom von Relevanz. Bei erwachsenen Patientinnen mit fortgeschrittenem *high-grade* epithelalem Ovarial-, Eileiter- oder primärem Peritonealkarzinom, die nach einer abgeschlossenen Platin-basierten Erstlinien-Chemotherapie in Kombination mit Bevacizumab ein Ansprechen (vollständig oder partiell) haben, ist für den Einsatz der Kombinationstherapie eine HRD-Testung erforderlich. Ein positiver HRD-Status ist gemäß der entsprechenden Fachinformation über entweder den Nachweis einer *BRCA1/2*-Mutation und/oder einer genomischen Instabilität definiert. Die QuIP GmbH hat daher 2023 den prototypischen Ringversuch zur molekulargenetischen Bestimmung des HRD-Status aufgesetzt.

Es handelte sich um einen methodenoffenen Ringversuch mit 10 Fällen bestehend aus genomischen DNA-Lösungen extrahiert aus Gewebeschnitten des Ovarialkarzinoms mit bekanntem MyChoice® CDx HRD-Score (Myriad Genetics).

Die meisten Teilnehmer*innen nutzten für die Bestimmung des HRD-Status Next Generation Sequencing (NGS) Panel von verschiedenen Herstellern sowie den OncoScan™ CNV FFPE Array (Affymetrix). Insgesamt haben 40 Institute aus 7 Ländern (weltweit) am Ringversuch teilgenommen. 32 von 40 Instituten (80 %) konnte eine erfolgreiche Teilnahme bescheinigt werden. Bezogen auf die DACH-Region haben 30 von 36 Instituten (83 %) erfolgreich teilgenommen. Die Mehrheit der teilnehmenden Einrichtungen ist in Deutschland ansässig (Bestehensquote 81,5 %; 22/27). Am häufigsten wurde für die NGS-basierte Detektion das AmoyDx® HRD Focus Panel (AmoyDx) und das QIAseq® targeted DNA HRD Panel (Qiagen)

verwendet. Insbesondere bei dem QIAseq® targeted DNA HRD Panel (Qiagen) war auffällig, dass die ermittelten Scores für die Bewertung einzelner Fälle eine große Streuung aufwiesen, wodurch die Teilnehmer*innen diese teilweise abweichend vom Sollwert bewerteten. Weiter hatten vier Einrichtungen Probleme bei der Interpretation der Ergebnisse bzw. der korrekten Anwendung der HRD-Definition. Der Ringversuch zeigte, dass die Versorgungslandschaft in Deutschland hinsichtlich der HRD-Testung gut aufgestellt ist, jedoch Herausforderungen bei der Bestimmung des HRD-Status und der Ergebnisinterpretation unter Anwendung unterschiedlicher, kommerziell verfügbarer Assays existieren.

AG14 Molekularpathologie II

AG14.07

Comprehensive transcriptomic analysis of prostate cancer lung metastases

A. Saraji¹, K. Hempel¹, J. Stegmann-Frehse¹, D. Kang¹, A. Offermann¹, D. Jonigk^{2,3}, M. P. Kuehnelt^{2,3}, J. Kirfel¹, S. Perner^{1,4}, V. Sailer¹

¹Institut of Pathology, University Hospital Schleswig-Holstein Campus Luebeck, Lübeck, Germany, ²Institute of Pathology, Hannover Medical School, Hannover, Germany, ³Biomedical Research in Endstage and Obstructive Lung Disease (BREATH), German Center for Lung Research, Hannover, Hannover, Germany, ⁴Research Center Borstel, Leibniz Lung Center, Borstel, Borstel, Germany

Questions/Background

Metastatic prostate cancer (mPCa) is a widespread disease with high mortality. Unraveling molecular mechanisms of disease progression is of utmost importance. The microenvironment in visceral organs and the skeletal system is of particular interest as a harbinger of metastatic spread. Therefore, we performed a comprehensive transcriptomic analysis of prostate cancer lung metastases with a special focus on differentially expressed genes attributable to the microenvironment.

Methods

Digital gene expression analysis using the NanoString nCounter analysis system was performed on formalin-fixed, paraffin-embedded (FFPE) tissue from prostate cancer (PCa) lung metastases (n=24). Data were compared to gene expression data from primary PCa and PCa bone metastases. Bioinformatic analysis was performed using several publicly available tools.

Results

In comparison to prostate cancer bone metastases, 209 genes were significantly upregulated, and 100 genes were significantly downregulated in prostate cancer lung metastases. Among the up-regulated genes, the top 10 genes with the most significant P-value were HLA-DPB1, PTPRC, ITGB7, C3, CCL21, CCL5, ITGAM, SERPINA1, MFAP4, ARAP2 and among the down-regulated genes, the top 10 genes with the most significant P-value were FOXC2, TWIST1, CDK14, CHAD, IBSP, EPN3, VIT, HAPLN1, SLC44A4, TBX1. In PCa lung metastases genes associated with immunogenic responses were upregulated while genes associated with epithelial-mesenchymal transition were down-regulated. We also showed that CXCR3/CXCL10 axis plays a significant role in prostate cancer lung metastases in comparison to bone metastases.

Conclusion

In this study, we comprehensively explored transcriptomic alterations in PCa lung metastases in comparison to primary PCa and PCa bone metastases. In PCa lung metastases genes associated with immunogenic responses are upregulated while genes associated with epithelial-mesenchymal transition are down-regulated. This points to a more immunogenic phenotype of PCa lung metastases thus potentially making patients more susceptible to immunotherapeutic approaches.

AG14.08

Aberrant fucosylation sustains the NOTCH and EGFR/NF-kB pathways and is a negative prognostic factor in human intrahepatic cholangiocarcinoma

C. E. Ament¹, **S. Steinmann**¹, K. Evert¹, G. M. Pes², S. Ribback³, H. Wang⁴, X. Chen^{4,5}, M. Evert¹, D. F. Calvisi¹

¹Institute of Pathology, University of Regensburg, Regensburg, Germany, ²University of Sassari, Department of Medicine, Surgery, and Pharmacy, Sassari, Italy, ³Institut für Pathologie, Greifswald, Germany, ⁴University of California, Department of Bioengineering and Therapeutic Sciences, San Francisco, United States of America, ⁵University of Hawaii Cancer Center, Honolulu, United States of America

Questions/Background

Aberrant protein glycosylation is a cancer hallmark associated with tumor development and progression. In the present study, we thoroughly investigated the role of fucosylation (a type of glycosylation) in intrahepatic cholangiocarcinoma (iCCA), a lethal malignancy with increasing incidence worldwide and limited therapeutic options.

Methods

Global protein fucosylation was determined using lectin histochemistry and Western blotting. The GDP-L-fucose synthetase (FX) and the GDP-fucose transmembrane transporter (SLC35C1), both prominent players of cellular fucosylation, were silenced via small interfering RNA. In addition, iCCA cell lines were treated with L-Fucose and 6-Alkynylfucose (6AF), a fucosylation inhibitor. The fucosylation effect on the NOTCH and NF- κ B pathway, two predominant cascades in cholangiocarcinogenesis and fucosylation targets, and the impact on proliferation and migration were investigated in these cells. Moreover, iCCA cell lines were treated with 6AF and used in the chick chorioallantoic membrane (CAM) assay.

Results

We discovered that levels of global fucosylation and members of the fucosylation pathway are ubiquitously upregulated in human iCCA tissues compared to non-tumorous surrounding livers and normal biliary cells. In addition, total fucosylation levels correlate with poor patients' prognosis. Furthermore, the fucosylation inhibitor 6-alkynylfucose (6AF) triggered a dose-dependent decrease in the proliferation and migration of iCCA cell lines that were annulled by adding fucose to the cell medium. At the molecular level, 6AF administration or small interfering RNA-mediated silencing of GDP-L-fucose synthetase (FX) and the GDP-fucose transmembrane transporter (SLC35C1) decreased NOTCH activity, NOTCH1/Jagged1 interaction, NOTCH receptors, and related target genes in iCCA cell lines. In the same cells, EGFR, NF- κ B p65, and Bcl-xL protein levels diminished, whereas I κ B α (a critical cellular NF- κ B inhibitor) increased after FX/SLC35C1 knockdown or 6AF administration. In the CAM assay, 6AF treatment profoundly suppressed the growth of iCCA cells.

Conclusion

In conclusion, elevated global fucosylation characterizes human iCCA, contributing to cell growth and migration via the upregulation of the NOTCH and EGFR/NF- κ B pathways *in vitro* and *in vivo*. Thus, aberrant fucosylation is a novel pathogenetic player and a potential therapeutic target for human iCCA.

AG14.09

eIF4A1 as an Actionable Target with Prognostic Value in Human Hepatocellular Carcinoma

S. Steinmann¹, A. Sánchez-Martín^{1,2}, E. Tanzer¹, A. Cigliano³, G. M. Pes³, M. M. Simile³, L. Desaubry⁴, J. J. G. Marín², M. Evert¹, D. F. Calvisi^{1,3}

¹Institute of Pathology, University of Regensburg, Regensburg, Germany, ²University of Salamanca, Experimental Hepatology and Drug Targeting Group, Salamanca, Spain, ³University of Sassari, Department of Medicine, Surgery, and Pharmacy, Sassari, Italy, ⁴University of Strasbourg, Laboratory for Therapeutic Innovation, Illkirch Cedex, France

Questions/Background

Hepatocellular carcinoma (HCC) is a primary liver tumor with high mortality and ever-increasing incidence worldwide. While tumor resection or liver transplantation is effective in the early stages of the disease, the therapeutic choices for advanced HCC remain limited with merely transient benefit. Thus, it is imperative to find novel therapeutic targets and more efficacious treatments against this deadly cancer. Frequently, mechanisms of the mRNA translation machinery are dysregulated in human malignancies. Elevated expression of the eukaryotic transcription initiation factor 4A1 (eIF4A1), a component of the translation initiating eIF4F complex which enzymatically catalyzes translation initiation, was reported in various cancers.

Methods

Herein, we investigated the pathogenetic role and therapeutic merit of eIF4A1 in HCC utilizing i.a. TCGA-based gene expression analysis, Western Blotting, classical immunohistochemistry and functional assays including cytotoxicity-, proliferation- and apoptosis assays.

Results

We observed consistent eIF4A1 upregulation in HCC lesions compared with non-tumorous surrounding liver tissues. eIF4A1 levels were negatively correlated with the prognosis of HCC patients. In HCC lines, the exposure to various eIF4A inhibitors provoked a remarkable decline in proliferation and augmented apoptosis, paralleled by the inhibition of several oncogenic pathways. Significantly, anti-growth effects of the eIF4A1 inhibitors were further increased by the simultaneous administration of Rapalink-1, a pan mTOR inhibitor.

Conclusion

In sum, our results highlight the pathogenetic relevance of eIF4A1 in HCC and suggest further assessment

of the potential usefulness of pharmacological combinations based on eIF4A and mTOR inhibitors for the treatment of this aggressive cancer.

AG14.10

Integrated epigenome-wide methylation analysis of EGFR amplified Glioblastoma

T. Kraus, D. Hölzl, C. Langwieder, K. Sotlar

Uniklinikum Salzburg, Universitätsinstitut für Pathologie, Salzburg, Austria

Questions/Background

Glioblastoma IDH Wildtype (CNS WHO Grade 4) is the most frequent primary brain tumour of adults having a very unfavourable outcome. Despite intensive research, there is still no curative therapy available. The aim of this study is to analyse differentially methylated pathways in *EGFR* amplified Glioblastoma to reveal novel candidate genes for molecular therapy.

Methods

We performed epigenome-wide methylation analysis of 50 cases (25 with *EGFR* amplification and 25 without *EGFR* amplification) using the Illumina Infinium EPIC bead chip array interrogating more than 850,000 methylation sensitive CpGs sites in parallel. Computational analysis was performed to identify significant differentially methylated genes. Gene ontology analysis was processed to reveal altered pathways.

Results

We found that *EGFR* amplified Glioblastomas show distinct alterations of the epigenomic landscape. Computational analysis revealed 9,849 significantly differentially methylated CpGs. Of these, 47% were hypermethylated and 53% were hypomethylated in *EGFR* amplified Glioblastoma. Analysis of genomic distribution showed that 21% of the loci were located in gene tiling regions, 1% in promoter regions, 1% in genes and 1% in CpG island regions. 76% were located in other genomic locations. Gene ontology analysis showed enrichment of genes being associated with DNA replication and packaging pathways.

Conclusion

In summary, we performed an integrated epigenome-wide analysis of *EGFR* amplified Glioblastoma and found distinct alterations in molecular pathways.

AG14.11

Single Nucleus RNA Sequencing of Gastric Normal and Tumor Tissue after Neoadjuvant Treatment enables the examination of tumoral heterogeneity

N. Jung, B. Grosser, A. Langer, B. Märkl, S. Dintner

Universitätsklinikum Augsburg, Institut für Pathologie und Molekulare Diagnostik, Augsburg, Germany

Question/Background

Single-cell transcriptomic profiles analysis has proposed new insights for understanding the behavior of human gastric cancer (GC). GC offers a unique model of intratumoral heterogeneity. However, the specific classes of cells involved in carcinogenetic passage, and the tumor microenvironment of stromal cells was poorly understood. Sample collection and conservation of fresh tissue by cryopreservation makes the examination of intact single cells difficult. Single-nucleus RNA-Seq (snRNA-Seq) is needed to profile such samples. It requires customization to different tissue and tumor types, posing a barrier to adoption. We have developed a method to isolate intact single cell nuclei from gastric carcinomas for successful snRNA-Seq. With that we characterized the heterogeneous cell population of normal and tumor lesions and gastric cancer after neoadjuvant treatment.

Methods

We successfully established a snRNA-Seq protocol on cryoconserved gastric tissue samples. Tissue samples of neoadjuvant treated gastric tumors were snap frozen in liquid nitrogen after surgery and stored at -80°C. Nuclei were resuspended in CST buffer and processed further to preserve intact single nuclei. After nuclei isolation, all of the protocols such as cell barcoding and library construction were performed according to the manufacturer's instructions for the 10× chromium single cell 5' v2 kit and sequenced with the Illumina NextSeq 550 Dx platform. For Single-cell quality control and data pre-processing SnRNA-seq data was analyzed using the 10× Genomics software package Cell Ranger version 2.1.1.

Results

We analyzed 17,000 nuclei from 8 samples, 3 normal tissues and 5 tumor tissues of gastric cancer lesions could thus be sequenced until now. A total of 13 cell types could be identified. Subtyping of T cells led to the identification of regulatory T cells, cytotoxic T cells, and T helper cells. Differences in cell type composition could be confirmed by corresponding HE and immunohistological staining, and the identified cell types could be correlated to the histological staining pattern in its corresponding tissue sections.

Conclusion

SnRNA-Seq decouples sample procurement from processing, recovers nuclei from hard-to-dissociate samples and allows multiplexing of samples accrued over time. The analysis of gastric normal and tumor tissue after neoadjuvant treatment may provide insights for understanding GC cell behavior, suggesting potential targets for the diagnosis and neoadjuvant treatment of GC.

AG14 Molekularpathologie III

AG14.12

A European newcomer's experience with NGS-based proficiency testing offered by College of American Pathologists

S. Lassmann^{1,2}, S. Kral^{1,2}, M. Kunz^{1,2}, X. Ungefug^{1,2}, M. Werner^{1,2,3}

¹Institute for Surgical Pathology, University Medical Center, Freiburg, Germany, ²Comprehensive Cancer Center Freiburg, University Medical Center, Freiburg, Germany, ³German Cancer Consortium (DKTK), partner site Freiburg, Freiburg, Germany

Questions/Background

NGS molecular pathology diagnostic testing requires continuous quality assurance for the entire work process (histology, pre-analytics, library preparation, sequencing, bioinformatics and reporting). So far, few external quality assurance programs covering all of these aspects are available. Here we report on our experiences with the College of American Pathologists (CAP, USA) NGS-based proficiency testing (PT) programs in 2022.

Methods

Enrollment was for five PT programs, with 3/5 starting from a DNA sample ("NGS-exome", "TMB", "CNV") and 2/5 from own/modified or provided Fastq files ("NGS-BV": exome, "NGSB": panel). PT programs were for certification (1/5 "NGS-exome") or for educational challenges (4/5). PT programs were in two phases (spring and autumn 2022). The laboratory processes included hybrid-capture NGS panel (TSO500, Illumina) and/or Whole Exome Sequencing (SureSelect All Human Exon V8; Agilent) and sequencing via NextSeq550Dx (Illumina). Diagnostic bioinformatics included commercial pipelines (TSO500 local app, Illumina; CLC Genomic Workbench, Qiagen) and/or custom in-house pipelines (WES).

Results

Administrative issues and sample processing were readily fulfilled. Interim result evaluation and program statistics were provided by CAP after the first phase: For the PT "NGS-exome" correct results were obtained in 92.5% and a specificity of 98.9%, resulting in a good overall assessment. For the "TMB" challenge (reference 7 mut/Mb) our results (9.5 and 9.6 mut/Mb by TSO500 and WES) and the other participants (n=50: 8.39±3.2 mut/Mb) were higher. For the "CNV" challenge, 10/14 alterations were correctly called (TSO500). For the "NGSB" challenge, all 16/16 alterations were correctly called (TSO500). For the "NGS-BV" challenge, data are still processed. Challenges experienced were 1) manual entering of detected variants into ELSS, 2) lack of hg19 and hg38 flexibility for all PTs and 3) in part provision of old-type fastq-files. Opportunities experienced were 1) availability of several comprehensive NGS PT programs, 2) twice a year PTs with few samples and 3) comprehensive results requested and evaluated (such as correct variant description).

Conclusion

NGS-based proficiency testing by the CAP is a highly valuable quality assurance resource also for European molecular pathology diagnostic laboratories for ensuring technical, bioinformatical and interpretational validity, worthwhile for investing in CAP PT costs and own laboratory capacities.

AG14.13

Specific T-cell receptor beta rearrangements of gluten-triggered circulating CD8⁺ T-cells are significantly enriched in duodenal celiac disease specimen

V. Seitz¹, K. Gennermann², S. Elezkurtaj¹, D. Groth³, S. Schaper², A. Dröge², N. Lachmann⁴, E. Berg¹, D. Lenze¹, A. Kühn⁵, C. Husemann¹, K. Kleo¹, V. Lennerz², S. Hennig², M. Schumann⁶, M. Hummel¹

¹Charité Universitätsmedizin Berlin, Institut für Pathologie, Berlin, Germany, ²HS Diagnostica GmbH, Berlin, Germany, ³Universität Potsdam, Institut für Informatik und Computational Science, Potsdam, Germany, ⁴Charité Universitätsmedizin Berlin, Institut für

Questions/Background

Celiac disease (CeD) is an autoimmune disorder in genetically susceptible subjects affecting the small intestine with gluten as disease trigger. While gluten-specific T-cell receptors (TCRs) from pathogenic CD4⁺ T-cells were broadly studied, only two studies analyzed TCRs from “gluten-triggered” CD8⁺ T-cells expressing the activation marker CD38 and gut homing receptors and being expanded in patients’ peripheral blood upon gluten challenge.

Although CD8⁺ T-cells play a central role in epithelial damage it was not evaluated yet, if TCRs derived from gluten-triggered circulating CD8⁺ T-cells are significantly enriched in duodenal CeD tissue samples and if the rearrangement frequencies of expanded TCR β -clonotypes are different in distinct CeD subgroups.

Methods

We compared 301 and 448 published TCR β -rearrangements derived from gluten-specific CD4⁺ T-cells and gluten-triggered circulating CD8⁺ T-cells respectively to our 309.579 TCR β -clonotypes derived from duodenal tissue specimens of 56 CeD patients and 22 control donors by TCR β -specific amplicon-based next generation sequencing.

Results

In addition to published data, we demonstrate that TCRs derived from circulating gluten-triggered CD8⁺ T-cells were significantly enriched in CeD patients’ duodenal tissue samples. TCR β -rearrangements of gluten-triggered CD8⁺ T-cells were more expanded than TCRs from gluten-specific CD4⁺ T-cells ($p < 0.0002$) being highest in refractory CeD. Sequence alignments with TCR-antigen databases suggest that a subgroup of these gluten-triggered TCRs recognize microbial, viral and autoantigens.

Conclusion

Our findings are in accordance with a model of CeD pathogenesis where gluten-specific CD4⁺ T-cells are central initiators of the celiac immune response and where CD8⁺ intraepithelial lymphocytes carrying $\alpha\beta$ TCRs, possibly being cross-reactive for viral and human antigens, elicit epithelial damage.

AG14.14

Analysis, interpretation and structured interactive reporting of a large NGS-panel and Whole Exome Sequencing in molecular pathology diagnostics

S. Kral^{1,2}, S. Wolter^{1,2}, U. Matysiak^{1,2}, M. Werner^{1,2,3}, S. Laßmann^{1,2}

¹Institute for Surgical Pathology, Medical Center, University of Freiburg, Freiburg, Germany, ²Comprehensive Cancer Center Freiburg, Medical Center, Freiburg, Germany, ³German Cancer Consortium (DKTK), partner site Freiburg, Freiburg, Germany

Questions/Background

Molecular pathology diagnostics encompasses increasingly complex technical laboratory workflows, associated quality controls, plausibility checks, automated bioinformatics pipelines and results communication in diagnostic reports for clinical decisions. Here, we present our molecular diagnostic approach of handling large NGS data sets post wet-lab processing for diagnostic reporting to requesting clinicians.

Methods

Formalin-fixed and paraffin-embedded tissue specimens are processed for NGS panel (TSO 500 HRD, Illumina) or Whole Exome Sequencing (Human All Exon V8, Agilent) analyses via NextSeq550(Dx) according to accredited/certified workflows.

Results

Sequencing data are processed by DRAGEN TSO 500 Analysis Software (Illumina) or by a custom, automated Snakemake WES bioinformatics pipeline. The latter includes: Quality control (fastQC), trimming (Agent Trimmer), mapping (BWA-mem), duplicate removal (Picard Tools), SNV/small indel calling (Manta+Strelka), CNV calling (Sequenza), annotation (Annovar), filtering (in-house scripts) and detection of the following complex biomarkers: TMB, MSI and HRD (in-house scripts, msisensor-pro, scarHRD). The DRAGEN TSO 500 Analysis Software additionally detects either RNA fusions or a Myriad Genetics-based Genomic Instability Score (GIS). Detected SNVs in both approaches are further filtered out, if VAF < 5 %, MAF > 1 % (gnomAD_exome_211), depth < 50 or if the variant is synonymous and non-exonic/non-splicing.

From this, an SNV table is automatically generated grouping actionable targets, ACMG and other genes providing gene name, coordinate, HGVS/p, VAF and external databases hyperlinks (e.g. dbSNP, ClinVar, REVEL, VICC, ClinTrials) as well as color-coded pathogenicity.

In the diagnostic report (PathoPro/IFSM) quality control parameters from nucleic acid to sequencing data (histological tumor cell content, nucleic acid, library and sequencing quality controls) are finally combined with all bioinformatic outputs as “one-pager” for key medical information with detailed molecular information as supplement. Prior to approval of the diagnostic report by the board certified pathologist, a plausibility check by bioinformaticians, medical scientists and pathologists is mandatory.

Conclusion

In conclusion, this approach enables a thorough and timely quality controlled analysis, interpretation and molecular pathology diagnostic reporting of currently up to 8-16 NGS cases biweekly for requesting clinicians in precision medicine.

AG14.15

Low-input WES using compromised tumor specimens – A challenge for routine molecular diagnostics

S. Wolter^{1,2}, S. Kral^{1,2}, U. Matysiak^{1,2}, M. Kunz¹, F. Beier¹, M. Werner^{1,2,3}, S. Laßmann^{1,2}

¹Institute for Surgical Pathology, Medical Center, University of Freiburg, Freiburg, Germany, ²Comprehensive Cancer Center Freiburg (CCCF), Medical Center, University of Freiburg, Freiburg, Germany, ³German Cancer Consortium (DKTK), partner site Freiburg, Freiburg, Germany

Questions/Background

Whole Exome Sequencing (WES) enables for comprehensive genomic profiling (including complex biomarkers TMB, MSI and HRD) but is not yet well-established in limited Formalin-fixed and Paraffin-embedded (FFPE) tissue specimens, especially with matched tumor/normal DNA derived from the same tissue block. Here, we present preliminary low-input WES results in compromised FFPE tissue specimens and discuss its applicability for routine molecular diagnostics.

Methods

This technical study included matched FFPE tumor/normal tissue specimens (n=12) of four cancer patients using DNA inputs of 100ng (n=4), 40ng (n=4) or 10ng (n=4), respectively. Library preparation (Human All Exon V8, Agilent) was performed with modifications of the manufacturer's protocol. WES libraries were sequenced (NextSeq550/550Dx, Illumina) and data was analyzed using an in-house pipeline. SNV/TMB/MSI status was correlated to previous analyses, if applicable. Additionally, input-sensitive intra-sample comparison was performed to control for sequencing performance and data quality.

Results

As expected from morphology and (tumor) cell content, DNA concentrations were quite variable (36±19ng/μl). Input amounts of 100ng, 40ng or 10ng DNA resulted in total amounts of 50-140ng, 218-443ng and 217-323ng WES library, respectively. Sequencing libraries generated from 100ng, 40ng and 10ng DNA yielded either 19-22MR, 19-24MR or 20-23MR passing filters. Total DNA input below 40ng significantly affected median target coverage (100ng: 114-200x, 40ng: 99-182x, 10ng: 52-106x). Accordingly, samples with a total DNA input of 10ng resulted in severe failure in calling of TMB-eligible variants/somatic MSI sites. Technically QC-valid and comparable TMB and MSI values were obtained in all four cases when 100ng and 40ng total input DNA was used, including one case with slight coverage drop-off in (TMB) target regions/MSI sites due to heavily compromised input DNA (DIN <3). Reported HRD scores were consistent in three cases across DNA input groups with a tendency of slight increase when using total DNA inputs of 10ng and an input-dependent decrease of HRD scores in one case.

Conclusion

This study demonstrates the feasibility of WES on matched compromised, routine diagnostic FFPE tumor/normal tissue specimens with quantitative (DNA yield) and/or qualitative limitations (DIN). DNA input amounts as low as 40ng may qualify for WES-based analysis of a tumor's mutation profile and determination of relevant complex biomarkers (TMB, MSI and HRD).

DGP07 Junges Forum I - How to do...

DGP07.02

How to: Bone Marrow Examination

H. M. Kvasnicka

Die moderne Knochenmarkdiagnostik ist ohne die breite Palette histologischer, immunhistochemischer Färbemethoden nicht mehr denkbar und erfordert daher eine entsprechende professionelle Aufarbeitung des Materials. Die Integration von Morphologie, Immunphänotyp, genetischen Merkmalen und klinischem Bild ist dabei wesentlich für die Diagnose verschiedener Entitäten. Dieser integrierte multiparametrische Ansatz bildet die Grundlage aller Klassifikationen und erlaubt prognostisch relevante Untergruppen zu definieren. Bei der Untersuchung des Knochenmarkes sollte stets ein strukturiertes Ablaufschema verfolgt werden, welches Zellularität, Topographie, Morphologie und Stroma nacheinander bewertet. In qualitativ guten Schnitten können die meisten differenzierten Zelltypen identifiziert werden: Granulozyten, erythroide Zellen, Megakaryozyten, Monozyten, Makrophagen, Mastzellen, Lymphozyten sowie Plasmazellen. Im Knochenmark findet, ausgehend von einem kleinen Pool sogenannter undeterminierter Stammzellen eine zelllinienspezifische Differenzierung, Reifung und Ausschleusung aller Zellen des peripheren Blutes sowie der Mastzellen und Zellen des Monozyten-Makrophagensystems statt. Die Knochenmarkszellularität ist altersabhängig und vermindert sich mit dem Lebensalter. Im normalen Knochenmark ist die Granulopoiese bevorzugt peritrabekulär und perivaskulär lokalisiert, wobei ausgehend von den frühen Vorläufern eine zunehmende Ausdifferenzierung stattfindet. Die Erythropoiese findet sich dabei in den perisinusoidalen Marksträngen lokalisiert, wobei unreife Vorläuferzellen wie Pro-Erythroblasten und phagozytierende Retikulumzellen die Funktionseinheit eines Erythrons bilden. Das Verhältnis zwischen Granulo- und Erythropoiese ist im gesunden adulten Knochenmark mit etwa 3:1 festzulegen, wobei Verschiebungen dieser Ratio sowohl im reaktiven als auch neoplastischen Kontext auftreten können. Megakaryozyten nehmen unter 2% der Zellen ein und sind bevorzugt perisinusoidal lokalisiert und zeigen im Rahmen der Ausdifferenzierung eine stetig zunehmende Größe sowie Kernlappung. Plasmazellen und reife B- und T-Lymphozyten können bis zu 10% der Zellen einnehmen. Die Indikationen für eine Knochenmarksbiopsie umfassen die Subklassifizierung aller hämatologischen Erkrankungen, auch wenn besonders bei akuten Leukämien die molekulare Einteilung die morphologische Gruppierung abgelöst hat. Eine Stärke der Histologie bleibt weiterhin die Beurteilung des Knochenmarkstromas.

DGP07.03

How to: Multiparametric tissue analysis

C. Schürch

Universitätsklinikum Tübingen, Institut für Pathologie, Tübingen, Germany

In recent years, tremendous developments in spatial biology technologies have enabled the identification and quantification of dozens to hundreds of proteins and RNAs at the subcellular level across millions of cells in intact tissue sections. These advances open new possibilities for many research fields, including oncology, immunology and pharmacology. The key for understanding biology often lies in the tissue itself, and unlocking its architecture, cellular composition, cell-cell interactions and cellular neighborhoods in health and disease will inform future diagnostics and therapies. In this presentation, I will give an overview of spatial proteomics technologies and provide tips and tricks on how to implement multiparametric tissue analysis in the laboratory. Patient cohort selection, antibody panel design, experimental execution, data processing and analysis, and costs are considered. Finally, I will briefly present our recently published results on how we used highly multiplexed tissue imaging to dissect cellular mechanisms of immunotherapy response in cutaneous T cell lymphoma.

P01 Postersitzung AG Hämatopathologie

P.01.01

Tissue-equivalents of lymphoid clonal haematopoiesis of indeterminate potential (L-CHIP): Potential precursor lesions of lymphoma

M. M. Brune, I. Bratic Hench, S. Dirnhofer, A. Tzankov

Institute of Medical Genetics and Pathology, Pathology, Basel, Switzerland

Question/Background

Clonal haematopoiesis of indeterminate potential (CHIP) is associated with the development of haematological malignancies. Depending on the underlying mutation, CHIP has recently been sub-classified into myeloid (M-CHIP) and lymphoid (L-CHIP) (PMID:34663986), the latter showing mutations in genes

encoding for epigenetic modifiers such as *KMT2D* and cell response regulators to DNA damage such as *ATM*. Most recently, the significance of L-CHIP as a predisposing condition to a variety of lymphomas has been highlighted (PMID:36599826). We presume that L-CHIP manifests in lymphoid tissues, fostering unexplained follicular hyperplasias (FH) and potentially representing an early precursor of lymphoma.

Methods

In our opinion, *L-CHIP tissue-equivalents* can be identified by histological, immunohistochemical and molecular testing based on high-throughput sequencing (HTS), as the following case series illustrates:

Results

1 – 30-years-old patient with FH of a lymph node and overexpression of H3K27m3 in the germinal centres. Molecular evaluation revealed 3 *KMT2D* variants of uncertain significance.

2 - 7-year-old child diagnosed with a massive atypical germinal centre reaction in the tonsil. HTS revealed a pathogenic *ATM* mutation.

3 - 64-year-old patient with an atypical follicular lymphoproliferation of the thyroid. Molecularly, an *ATM* mutation was present, as well as a non-productive BCR rearrangement.

4 - 68-year-old patient with an atypical nodal germinal centre reaction, H3K27m3 overexpression and loss of PTEN. Molecularly, a likely pathogenic *B2M* mutation and a non-productive BCR rearrangement were detected. 8 years later, the patient developed a follicular lymphoma, grade 3A, with the same BCR rearrangement.

5&6 - 79 and 53-year-old patients, respectively, with FH of the lung and follicular conjunctivitis, showing a loss of PTEN expression and the identical *PTEN* mutation. After almost 10 years, both are devoid of lymphoma.

Conclusion

All cases were morphologically suspect, without fulfilling the diagnostic criteria for lymphoma. Nevertheless, clonal populations with mutations in genes recurrently altered in lymphoid malignancies were present. In our opinion, these instances represent L-CHIP tissue-equivalents that provide a fertile ground for lymphomagenesis and give rise to autonomous lymphoproliferations with or without BCR rearrangements, depending on the time point of mutation emergence respecting IG rearrangement. Identification of such cases may help to detect patients at risk for lymphoma.

P.01.02

Case report: Follicular Dendritic Sarcoma in a cervical lymph node mimicking metastasis of anaplastic thyroid carcinoma.

A. Nettersheim, S. Abdullazade, C. Röcken

Institut für Pathologie, UKSH, Campus Kiel, Kiel, Germany

Question/Background

Follicular Dendritic Sarcoma (FDS) is an uncommon malign neoplasm that can develop in many locations, but most of all in cervical lymph nodes.[1] A manifestation in this region can easily be misinterpreted as metastasis of another entity if FDS is not kept in mind. Due to its rarity, an optimal treatment-regimen following surgery is not well defined.[2]

Methods

We present the case of a 65-year-old male who was admitted to our hospital with a cervical mass for which the initial biopsy was suggestive for anaplastic thyroid carcinoma. After thyroidectomy and resection of the cervico-lateral compartment containing the mass, the specimens were processed according to our standard protocols. Analyses on H&E and immunohistochemical (IHC) stained slides as well as various molecular analysis were performed and discussed by trained pathologists and biologists.

Results

Examination of the thyroid only revealed benign lesions, but within the cervico-lateral compartment a 7 cm large tumour resided within a lymph node. Extensive IHC staining allowed identification of FDS via positive staining for CD21, KI-M1P and CD23. Later a mass in the patient's liver was identified as metastasis of FDS via biopsy. Initial molecular testing did not reveal any therapeutic targets, but a conducted full exome sequencing showed a high tumour mutational burden that supported the use of pembrolizumab.[3]

Transcriptome analysis is still pending at the time of writing.

Conclusion

If manifested in lymph nodes, FDS might mimic metastasis of other neoplasms, but can be identified with relative ease via IHC staining for CD21, KI-M1P and CD23. Whole exome sequencing can provide

therapeutic rationales for this rare entity.

Literaturangaben:

- [1] Caner Saygin , Didem Uzunaslan, Mustafa Ozguroglu, Mustafa Senocak, Nukhet Tuzuner, (2013), Dendritic cell sarcoma: a pooled analysis including 462 cases with presentation of our case series, *Critical Reviews in Oncology/Hematology*, 253-271, Volume 88, Issue 2,, <https://doi.org/10.1016/j.critrevonc.2013.05.006>
- [2] Tiffany Chen, Purva Gopal, (2017), Follicular Dendritic Cell Sarcoma , *Archives of Pathology and Laboratory Medicine*, 596–599, Volume 141, Issue 4, <https://doi.org/10.5858/arpa.2016-0126-RS>
- [3] Aurélien Marabelle et al., (2020), Association of tumour mutational burden with outcomes in patients with advanced solid tumours treated with pembrolizumab: prospective biomarker analysis of the multicohort, open-label, phase 2 KEYNOTE-158 study, *The Lancet Oncology*, 1353-1365, Volume 21, Issue 10, [https://doi.org/10.1016/S1470-2045\(20\)30445-9](https://doi.org/10.1016/S1470-2045(20)30445-9)

P.01.03

Immune escape mechanisms in myeloid sarcomas

M. Bauer¹, A. Monecke², A. Wilfer¹, B. Seliger³, H. Bläker², C. Wickenhauser¹

¹University Hospital Halle (Saale), MLU, Institute of Pathology, Halle (Saale), Germany, ²University Hospital Leipzig, Institute of Pathology, Leipzig, Germany, ³Medical School Brandenburg, Institute of Translational Immunology, Brandenburg, Germany

Question/Background

Myeloid sarcomas (MS) comprise a heterogeneous group of extramedullary myeloid neoplasm, which are associated with poor patients' outcome. In recent years, the importance of immune escape mechanisms and the tumor microenvironment (TME) in tumor progression have been uncovered in many solid and hematopoietic tumor entities. However, little is known about the significance of immune evasion and the composition of the TME in MS.

Methods

In this study, the immune landscape of the TME with focus on T cell subpopulations as well as the expression of immune modulatory molecules on tumor cells was determined in 40 MS cases and matched bone marrow biopsies. The medullary and extramedullary samples were analyzed using histopathology, immunohistochemistry (IHC) and multispectral imaging (MSI).

Results

The number of infiltrating immune cells in the TME of extramedullary MS was generally low. In particular, the mean frequency of T cells was with 3.32% lower in MS when compared to bone marrow (8.14%). Interestingly, the amount of CD3⁺CD8⁺ T cells was slightly higher in MS, but the expression of Granzyme B was significantly lower. 50% of the neoplastic MS cells showed a significantly reduced expression of human leucocyte antigen (HLA) class I. This was accompanied in 40% of the samples analysed with a deficiency in antigen presenting machinery (APM) components, such as the transporter associated with antigen processing (TAP) 1 and 2 and tapasin. Furthermore, 25% of MS cases demonstrated surface expression of non-classical HLA-G, while almost 50% of samples with a functional HLA-I APM exhibited a strong expression of programmed cell death ligand 1 (PD-L1). Compared to bone marrow biopsies, the neoplastic cells showed a rather aberrant immune phenotype in the extramedullary lesions.

Conclusion

In this study, a high prevalence of different immune escape mechanisms in MS was shown including downregulation of HLA-I surface expression, deficient APM component expression and upregulation of non-classical HLA-G and PD-L1. Based on these data we suggest that MS employs different strategies to evade immune recognition, which are associated with the development of extramedullary disease manifestation.

P.01.04

Time dependent changes of the (immune-)phenotype upon JAK2 inhibition in JAK2 V617F mutated cell lines

M. Bauer¹, C. Vaxevanis², H. Hackl³, A. Wilfer¹, B. Seliger⁴, C. Wickenhauser¹

¹University Hospital Halle (Saale), MLU, Institute of Pathology, Halle (Saale), Germany, ²University Hospital Halle (Saale), MLU, Institute

Questions/Background

Mutations in *JAK2* are oncogenic drivers in the development of the myeloproliferative neoplasms (MPN) leading to a constitutive activation of the JAK/STAT signaling pathway. Upon JAK2 inhibition, most patients show a control of clinical symptoms, but the induction of a haematological remission is limited, which might be due to immunosuppressive properties. The aim of this study was to investigate therapy related changes of the (immune-)phenotype in the neoplastic cells.

Methods

The cell lines HEL and SET-2 were continuously treated with ruxolitinib. Phenotyping of CD34, CD33, MHC-I, PD-L1 expression and viability of the cells, as well as cytokine concentration in the cell supernatants was determined after 1, 2, 5, 10 and 15 weeks of treatment. Somatic mutations in naïve and 15 weeks treated cells were assessed with NGS including 75 genes. Changes in the transcriptional profile of untreated, 2 and 15 weeks treated cells was determined by RNA sequencing.

Results

Short-term ruxolitinib treatment of 2 weeks caused a decreased activation of JAK/STAT signaling with a simultaneous downregulation of MHC-I and PD-L1 expression, which was completely reversible after treatment stop. Continuous treatment over 15 weeks resulted in a resistant phenotype in HEL-cells, which persisted after treatment stop for 8 weeks, while the SET-cell phenotype was instable. No differences in the genome have been found after long-term treatment in both cell lines. Cells showed an increased IC₅₀ concentration after continuous treatment and displayed a time dependent change of the transcriptome profile during treatment. After 15 weeks ruxolitinib treatment 584 and 424 genes, respectively, were found to be significantly upregulated in HEL and SET cells, while 690 and 404 genes were downregulated. In both cell lines an upregulated expression of MYC- and E2F-target genes and a downregulation of inflammatory pathway genes were found, which were accompanied by a significant upregulation of the mitogen-activated protein kinase (MAPK) 4 and 1-phosphatidylinositol-4,5-bisphosphate phosphodiesterase epsilon (PLCE) -1.

Conclusion

JAK2 inhibition in *JAK2* V617F mutated cell lines showed reversible effects after short-term treatment, while continuous treatment caused a resistant phenotype of the neoplastic cells that was associated with a significant number of differentially expressed genes, including MAPK4 and PLCE1 known to be associated with treatment resistance and more aggressive biology in other diseases.

P.01.05

PTP1BΔ6 und PTP1BΔ2-4 – Functional analyses of the oncogenic variants of PTP1B

J. Wildfeuer, M. Zahn, R. Marienfeld, P. Möller

Universitätsklinikum Ulm, Pathologie, Ulm, Germany

Question/Background

Disregulated Janus kinase (JAK)/ Signal Transducer and Activator of Transcription (STAT) and NF-κB signaling is a hallmark of Hodgkin/Reed-Sternberg (HRS) cells, the malignant cells of the classical Hodgkin lymphoma (cHL). Although protein-tyrosine phosphatase 1B (PTP1B) is a negative regulator of the JAK/STAT signaling, studies of our group showed that PTP1B variants missing distinct exon sequences augment JAK/STAT signaling in cHL cell lines. Both oncogenic variants, the splice variant PTP1BΔ6 (lack of exon 6) and the mutant PTP1BΔ2-4 (lack of exons 2-4) increase cell proliferation and confer resistance against cytotoxic reagents. However, the molecular mechanisms underlying these positive effects are not fully understood. Thus, we performed protein interaction and expression analyses to get an insight into these molecular mechanisms.

Methods

For an insight into the impact of PTP1BΔ6 and PTP1BΔ2-4 on signaling, transcriptome analyses of stably transfected L428 and HEK-293T was performed. The modulation of NF-κB signaling was analyzed by luciferase reporter assay. Interactome studies of PTP1BΔ6 and PTP1BΔ2-4 was performed with stably transfected HEK-293T cells using the SILAC method with subsequent mass spectroscopy. Potential interactions were verified by co-immunoprecipitation.

Results

While both PTP1B variants activate JAK/STAT signaling, only PTP1BΔ2-4 augments NF-κB activity. To

determine the impact of these differential effects on signaling by the PTP1B variants, we are currently evaluating the results of RNA sequencing experiments. Interactome experiments revealed a higher number of PTP1BΔ6 interaction partners compared to wildtype PTP1B and PTP1BΔ2-4, including PTP1BΔ6-specific interactions, while PTP1BΔ2-4 showed the fewest interactions. We started to characterize the interaction of the PTP1B variants with the pyruvate kinase M2 (PKM2) and peroxiredoxin-1 (PRDX1), which might be a connection to the known redox regulation of PTP1B.

Conclusion

PTP1BΔ6 and PTP1BΔ2-4 are not functionally identical as shown by their different effects on NF-κB signaling. This functional diversity of PTP1BΔ6 and PTP1BΔ2-4 is reflected by the differential interactome observed for these PTP1B variants.

P.01.06

Supporting routine bone marrow diagnostics with NGS-based analyses

S. Cysar^{1,2}, I. Weber^{1,2}, A. Frey^{1,2}, S. Laßmann^{1,2}, M. Werner^{1,2,3}

¹Institute for Surgical Pathology, Medical Center Freiburg, Freiburg, Germany, ²Comprehensive Cancer Center Freiburg, Medical Center, Freiburg, Germany, ³German Cancer Consortium (DKTK), partner site Freiburg, Freiburg, Germany

Question/Background

Bone marrow biopsy (BMB) diagnostics increasingly more depends on the synopsis of morphology, immunohistochemistry and supportive molecular pathology analyses, as laid out in the current WHO classification. This not only secures classification of the disease, but also yields important information regarding prognosis and therapy. Here, we report on our experiences with NGS-based analyses of BMBs, illustrating the diagnostic benefit of molecular testing in three examples.

Methods

Formalin fixed and paraffin embedded (FFPE) BMBs of n= 32 cases were processed. BMBs and bone marrow aspiration smears were routinely processed, subjected to standard stains (e.g. Giemsa, NACE) and immunohistochemical stains (e.g. CD34, CD61, CD71, C-Kit) prior to histological evaluation. DNA-based NGS analyses were performed according to standard procedures using the QIAseq Targeted DNA Human Comprehensive Cancer Panel (CCP) with data analysis by the CLC genomic Workbench (Qiagen) or the TSO500 gene Panel with analysis by the TSO500 local app (Illumina). For NGS analyses gene sets were pre-defined for lymphoid and myeloid neoplasias.

Results

BMBs yielded enough and good quality DNA for NGS-based analyses. Case 1 with clinical “anemia and thrombocytosis, in peripheral blood no typical MPN associated mutations” the pathological evaluation defined MDS/MPN overlap syndrome with ring sideroblasts and thrombocytosis. Supportive TSO500 NGS-analysis yielded a typical variant in *SF3B1* (p.K700E, VAF 30%) and a variant in *CBL* (p.C404T, VAF 30%). The final diagnosis was “MDS/MPN with *SF3B1* mutation and thrombocytosis”. Case 2 with clinical information “anemia” presented histologically with hyperplastic erythropoiesis with ring sideroblasts and expanded megakaryopoiesis. QiaSeq CCP NGS-analysis again showed a typical variant in *SF3B1* (p.K700E, VAF 23%) resulting in the final diagnosis of “MDS with *SF3B1* mutation”. Finally, case 3 was clinically suspicious as “osteomyelosclerosis, anemia and thrombocytopenia” and histologically demonstrated multilinear dysplasia with erythroid hyperplasia. Here, TSO500 NGS-analysis yielded a variant in *TP53* (p.H179Y, VAF 91%) resulting in the final diagnosis of acute erythroid leukemia.

Conclusion

Gene-panel based NGS-analysis of bone marrow biopsies can be readily performed and provides important supplementary information for precise diagnostic pathology according to the WHO classification system, especially for myeloid neoplasms.

P.01.07

Digital pathology - workflow for quantification of bone marrow characteristics in reactive and neoplastic histological sections

A. Wilfer, M. Bauer, C. Wickenhauser

Question/Background

Various components of the bone marrow are microscopically examined and quantified with the aim to achieve the clearest possible diagnosis. Some of these characteristics are specified in percentages (fat marrow content and cellularity), while others are graduated (myelofibrosis). The aim of this study is to evaluate the use of digital image recognition in hematopathology and to compare the results with established methods.

Methods

In total 140 histological specimens of reactive and neoplastic bone marrow were analyzed using digital whole slide scans of Hematoxylin and Eosin (H&E) and Gomori's silver stained slides. All slides were analyzed with QuPath – an open sources software. Multiple bone marrow components were evaluated such as fat marrow content, numbers of megakaryocytes as well as their morphological features, and the amount of reticular and collagen fibrosis.

Results

The digital analysis of bone marrow biopsies showed good results in the quantification of the bone marrow cellularity and fat marrow content, while classifying artefacts is more challenging. Most important, well-prepared and evenly stained slides showed good results for the digital pattern and colour recognition of various slide scans. The recognition of megakaryocytes requires an intensive software training but showed reliable recognition for an exact morphometric characterization. Moreover, the ratio characterization of reticular to collagen fibrosis corresponds to the pathologist's visual graduation.

Conclusion

Various BM compartments could be successfully quantified with digital image recognition. There is an enormous potential for standardized evaluations both in experimental and clinical context.

P02 Postersitzung AG Gastroenteropathologie I

P.02.01

Morphological subtypes of low grade intraepithelial neoplasia in patients with and without ulcerative colitis: reproducibility, frequency and clinical relevance

C. Lang-Schwarz¹, M. Büttner-Herold^{2,3}, S. Burian¹, R. Erber², A. Hartmann², M. Jesinghaus⁴, K. Kamarádová⁵, C. A. Rubio⁶, W. Sterlacci¹, M. Vieth¹, S. Bertz^{2,7}

¹Klinikum Bayreuth GmbH, Friedrich-Alexander-Universität Erlangen-Nürnberg, Institut für Pathologie, Bayreuth, Germany,

²Universitätsklinikum Erlangen, Institut für Pathologie, Erlangen, Germany, ³Universitätsklinikum Erlangen, Institut für Nephropathologie, Erlangen, Germany, ⁴Universitätsklinikum Marburg, Institut für Pathologie, Marburg, Germany, ⁵Charles University Faculty of Medicine and University Hospital, The Fingerland Department of Pathology, Hradec Králové, Czech Republic, ⁶Karolinska Institute and University Hospital, Department of Pathology, Stockholm, Sweden, ⁷MVZ für Histologie, Zytologie und molekulare Diagnostik Düren GmbH, Pathologie, Düren, Germany

Question/Background

Special histomorphologic subtypes (SST) have recently been described and precisely defined in low grade intraepithelial neoplasia (LGIN) in patients with ulcerative colitis (UC) with variable risk of progression to colorectal cancer (CRC). However, those SSTs can also be seen in adenomas of patients without UC. The aim of this study was to analyze the frequency, reproducibility and potential prognostic impact of SSTs in patients with and without UC.

Methods

Six pathologists from three centers evaluated 500 slides of 5 randomized and anonymized cohorts à 100 cases of patients with colorectal LGIN. Cohort A: LGIN, UC-associated; Cohort B: LGIN in UC, sporadic; Cohort C: LGIN, no UC but CRC alio loco; Cohort D: LGIN, no UC, no CRC; Cohort E: LGIN, no UC, prospective. The following SSTs were assessed: hypermucinous, goblet cell deficient (GCD), paneth cell rich, crypt cell dysplasia, goblet cell rich and SST, not otherwise specified (SST-NOS). Correlation analyses and follow up analyses were performed.

Results

In 430 cases (84%) matching results were found in at least 4 of 6 pathologists. LGIN with SST was

diagnosed in 222 cases (44.4%), was significantly more frequent in patients with UC (n=104, 52%, p=0.005) and showed a trend for cohort C (0.056), indicating a UC-independent higher risk for CRC in patients with SST. In 26 cases (11.7%) more than one SST was found. Overall, SST-NOS (28.9%), goblet cell rich (24.4%), GCD (19.3%) and hypermucinous (15.2%) were most frequent. SSTs were found in 118 patients (39.3%) without UC and associated with lower tumour stages (p=0.035) and mismatch repair proficiency (p=0.039). In UC, SSTs were associated with higher frequency of LGIN and high grade intraepithelial neoplasia during follow up (p=0.019), non-polypoid lesions, additional risk factors, extended UC and male sex. SST-NOS and GCD were the most frequent SSTs in UC. Interestingly, 33 cases showed SSTs in cohort E, among them 10 SST-NOS or GCD. The SST-based classification was superior in predicting LGIN-relapse compared to a preceded expert-consented stratification based on various morphological and clinical criteria.

Conclusion

SSTs in colorectal LGIN are frequent with reproducible assessment, the malignant potential varying between SSTs. Our results indicate an increased risk for CRC in patients with SST in LGIN, probably independent of UC. We recommend to include SSTs in LGIN in routine pathology reports.

P.02.02

Morphological subtypes of low grade intraepithelial neoplasia in patients with ulcerative colitis: Frequency and prognostic value

S. Burian¹, A. Hartmann², M. Vieth¹, C. Lang-Schwarz¹

¹Klinikum Bayreuth GmbH, Friedrich-Alexander-Universität Erlangen-Nürnberg, Institut für Pathologie, Bayreuth, Germany,

²Universitätsklinikum Erlangen, Institut für Pathologie, Erlangen, Germany

Question/Background

Ulcerative colitis (UC) is a known premalignant condition with an increased risk for colorectal cancer (CRC) [1]. Diagnosing low grade intraepithelial neoplasia (LGIN) as precursor lesion is challenging and criteria for endoscopic and histomorphologic assessment are continuously updated. So far, diagnosis of LGIN was based on various morphological criteria in combination with second opinion by an independent expert. Recently, special histomorphological subtypes (SST) of LGIN in patients with UC have gained rising attention, distinguishing between conventional and non-conventional LGIN [2]. The aim of our study was to assess the reproducibility, frequency and prognostic impact of SSTs in patients with LGIN in UC and to compare their prognostic value with an established classification system.

Methods

381 cases of LGIN from 323 patients with UC, diagnosed 2009-2017 were included. All pseudonymized and randomized cases were independently analyzed by two observers (SB and CLS). LGIN was classified as conventional (no special type, NST) or non-conventional (SST) on base of the following SSTs: Hypermucinous, crypt cell dysplasia (CCD), goblet cell deficient (GCD), Paneth cell rich (DPD), serrated and - additionally - LGIN with increased goblet cells (GCR) and SST, not otherwise specified (SST-NOS). Statistical analyzes for frequency, correlation with clinical data and follow up were performed.

Results

Both observers showed high agreement (kappa 0.874, p<0.001). 220 lesions were classified as NST and 138 as SST. 30 cases showed >2 SSTs (21.7%). The GCD-SST was the most frequent, presenting either as pure or mixed in 61 lesions (44.2%). SST was significantly correlated with lesion size (p=0.002), extent of UC (p=0.021), additive risk factors (p=0.084), the development of high grade intraepithelial neoplasia (HGIN, p=0.011) and CRC (p=0.043), especially in GCD-LGIN. HGIN and CRC were not seen in patients with DPD. The SST-based LGIN-typing has equally prognostic value in predicting HGIN and LGIN compared to classical stratification and might be superior in predicting CRC, however the case number was low.

Conclusion

Assessment of SSTs in LGIN in UC is reliable. SSTs correlate with infavourable clinical parameters, especially the GCD-SST.

Literaturangaben:

[1] Eaden JA, Abrams KR, Mayberry JF. The risk of colorectal cancer in ulcerative colitis: a meta-analysis. Gut 2001;48:526-35.

[2] Choi WT, Yozu M, Miller GC, Shih AR, Kumarasinghe P, Misdradi J, Harpaz N, Lauwers GY. Nonconventional dysplasia in patients with inflammatory bowel disease and colorectal carcinoma: a multicenter clinicopathologic study. Mod Pathol. 2020 May;33(5):9

Microsatellite instability and sex-specific differences of survival in gastric cancer after neoadjuvant chemotherapy without and with taxane

T. Hiltner¹, M. Kohlruß¹, A.-L. Herz¹, S. Lorenzen², A. Novotny³, A. Hapfelmeier⁴, M. Jesinghaus¹, J. Slotta-Huspenina¹, K. Ott⁵, W. Weichert¹, L. Sisic⁶, M. Gaida⁷, **G. Keller¹**

¹Institute of Pathology, Technical University of Munich, Munich, Germany, ²III. Medizinische Klinik and Poliklinik, Technical University of Munich, Munich, Germany, ³Department of Surgery, Technical University of Munich, Munich, Germany, ⁴Institute of Medical Informatics, Statistics and Epidemiology, Technical University of Munich, Munich, Germany, ⁵Klinikum Rosenheim, Department of Surgery, Rosenheim, Germany, ⁶Department of General, Visceral and Transplantation Surgery, University Heidelberg, Heidelberg, Germany, ⁷University of Heidelberg, Institute of Pathology, Heidelberg, Germany

Question/Background

The aim of our study was to investigate the prognostic role of microsatellite instability (MSI) in association with sex of patients treated with platinum/fluoropyrimidine neoadjuvant chemotherapy (CTx) with or without a taxane-containing compound.

Methods

Of the 505 retrospectively analyzed patients with gastric or gastroesophageal adenocarcinoma, 411 patients were treated with platinum/fluoropyrimidine CTx without taxane and 94 patients with a taxane-containing compound. MSI was determined by PCR using DNA from formalin-fixed paraffin-embedded tissues. Five microsatellite markers (BAT25, BAT26, D2S123, D5S346, D17S250) were analyzed according to standard protocols. Tumors were classified as MSI-High (H) if at least 2 markers showed instability. Hazard ratios (HR) were calculated by Cox regression analysis.

Results

Females demonstrated a better overall survival (OS) than males in the non-taxane group (HR, 0.59; 95% CI 0.41-0.86; $p=0.005$), whereas no significant difference was found in the taxane group (HR 1.22; 95% CI 0.55-2.73, $p=0.630$).

MSI-H was found in 38 of 411 (9.2%) tumors in the non-taxane and in 10 of 94 (10.6%) tumors in the taxane group.

MSI-H was associated with a better prognosis in both groups (without taxane: HR 0.56; 95% CI 0.33-0.97; $p=0.038$; with taxane: HR 0.28; 95% CI 0.04-2.02, $p=0.204$).

In the non-taxane group, female MSI-H patients showed the best OS (HR 0.18, 95% CI 0.05-0.73; $p=0.016$), followed by the female microsatellite stable (MSS) (HR 0.67, 95% CI 0.46-0.98, $p=0.040$) and the male MSI-H group (HR 0.76; 95% CI 0.42-1.37, $p=0.760$) taken the male MSS group as reference.

In the taxane group, female and male MSI-H patients demonstrated the best OS (female MSI-H: HR 0.05, 95% CI 0.00-240.46; male MSI-H: HR 0.45, 95% CI 0.61-3.63, $p=0.438$), whereas the female MSS group showed a decreased OS (HR 1.39 95% CI 0.62-3.12, $p=0.420$) compared to male MSS patients.

Conclusion

OS in gastric/gastroesophageal cancer after CTx might depend on sex and MSI status and may differ between patients treated with or without a taxane compound in the chemotherapeutic regimen

Inflammatory pseudopolyps: a possible infrequent manifestation in neurofibromatosis type I

F. J. Farfán López¹, A. Maccagno¹, T. Schaller¹, F. Sommer², B. Märkl¹

¹Institut für Pathologie, Universität Augsburg, Augsburg, Deutschland, Augsburg, Germany, ²Klinik für Allgemein-, Viszeral- und Transplantationschirurgie, Augsburg, Germany

Question/Background

Neurofibromatosis type I (NF1) is caused by the loss of function of the gene NF1, whose coding protein is a tumor suppressor that counteracts the role of RAS. It is typically associated with neurofibromas, pheochromocytomas, optic nerve gangliogliomas, and hamartomas, as well as café-au-lait skin lesions.

Methods

We present the case of a 70-year-old patient with multiple café-au-lait spots, hyperpigmented axilla, a history of a wild-type GIST in the duodenum and several polypectomies and resection of the right colon with inflammatory pseudopolyps. A subsequent ileotransversostomy resection revealed anastomosisitis and polypous lesions with a glandular component without atypia, acute inflammation, and with the presence of

eosinophils and plasma cells. A spindle cell component was observed in some areas. The diagnosis of an inflammatory myofibroblastic tumor, a neurofibroma, a plasma cell-associated IgG4-lesion and Vanek's tumor were ruled out by immunohistochemistry (negative for: ALK, CD34, S100, IgG4). Finally, the NF1 mutation was detected.

Results

The presence of inflammatory juvenile-like mucosal polyps and inflammatory fibroid polyps have been described in right colon resections in the literature as a probably gastrointestinal lesion specific to NF1. It has also been reported that NF1 patients have an increased risk of developing GISTs.

Conclusion

The expressivity of the NF1 disease varies between individuals so we propose that these lesions may be an infrequent intestinal manifestation of the disease and reported it as a NF1-associated inflammatory pseudo polyp. There is no hint of the mechanistic background of such lesions that obviously can occur multiple.

P.02.05

Abdominal tuberculosis (Tbc) with perforation of the small intestine

M. Uhlig¹, V. Negrini¹, C. March², D. Jechorek³, R. S. Croner¹, F. Meyer¹

¹Dept. of General, Abdominal, Vascular and Transplant Surgery; Otto-von-Guericke University with University Hospital, Magdeburg, Germany, ²Dept. of Radiology and Nuclear Medicine; Otto-von-Guericke University with University Hospital, Magdeburg, Germany,

³Institute of Pathology, Otto-von-Guericke University with University Hospital, Magdeburg, Germany

Question/Background

The suspicion of an acute abdomen needs clarification of the diagnosis and in case of its confirmation, surgical intervention has to be derived in etiopathogenetically reasoned indication for surgical intervention despite eventually complicating factors.

Methods

Scientific case report

Results

CASE DESCRIPTION:

Medical Hx: - *Current*: 27-years old male patient (pat. – Pakistan-born student) with severe abdominal pain (VAS, 8/10), no stool excretion for 5-6 d, severe vomiting

- *Own*: Known intraperitoneal Tbc – convulsive complaints for 6 months + weight loss of 4 kg, ongoing tuberculostatic therapy for 2 months

Clinical findings: Pat. in reduced general status and stable but hypertonic blood circulation / abdomen, ubiquitary muscular defense

Diagnostic: - *Lab parameters* (SI): Venous pO₂ 19.6 mmHg, O₂ saturation 25.3%, Lactate 3.0 mmol/L, "L" 13.2 Gpt/L, CrP serum level 68.8 mg/L, neutrophils 81.9%

- *CT scan*: Hollow organ perforation with free air within the right upper abdomen, mechanic ileus of the small intestine in the right middle abdomen, additional signs of a fistula and abscess formation, no hint for pulmonary manifestation

Diagnosis: Suspicious perforation of the small intestine (jejunum) and abdominal Tbc manifestation

Decision-making: Implantation of a gastric tube, withdrawal of blood samples for microbiological investigation, initiation of i.v. broad spectrum antibiotics with Tazobac 3x4.5 g, infusion therapy, emergency explorative laparoscopy

Surgical management: Laparoscopy – segmental resection of the small intestine (20 cm) of the perforated bowel segment with side-to-side jejunojejunostomy, partial omentum resection, adhesiolysis of the small intestine and lavage, excision of several Tbc-typical nodes at the small intestine (according to the hygiene standard, use of an FFP3 mask)

Histology: Necrotizing granulomatous inflammation in the surgical specimen of the small intestine and the greater omentum according to Tbc infection

Proceeding: Gastric tube (due to intestinal atony), continuation of the calculated antibiotic administration, initiation of oral nutrition, nutritional advisement, continuing tuberculostatic therapy

Conclusion

This case can be considered the complication of an abdominal Tbc, which prompted to derive emergency surgical intervention despite a high complication potential in ongoing tuberculostatic therapy and further intraabdominal Tbc manifestations as well as simultaneous precautions for the surgical and anesthesiological personnel in (emergency) intervention.

Tumorbiological behaviour and metastatic spread in lower gastrointestinal tract cancer – correlation with gene expression patterns

E. Pretzsch¹, J. Neumann², H. Nieß¹, T. Kirchner², F. Klauschen², J. Werner¹, M. Angele¹, J. Kumbrink²

¹LMU Klinikum München, München, Germany, ²LMU München, München, Germany

Questions/Background

Epithelial-mesenchymal transition (EMT), angiogenesis, cell adhesion and extracellular matrix (ECM) interaction are essential for colorectal cancer (CRC) metastasis. Low grade mucinous neoplasia of the appendix (LAMN) and its advanced state low grade pseudomyxoma peritonei (IgPMP) show local aggressiveness with very limited metastatic potential as opposed to CRC. To better understand the underlying processes that foster or impede metastatic spread, we compared LAMN, IgPMP, and CRC with respect to their molecular profile with subsequent pathway analysis.

Methods

LAMN, IgPMP and (mucinous) CRC cases were subjected to transcriptomic analysis utilizing Poly(A) RNA sequencing. Successfully sequenced cases (LAMN n=10, 77%, IgPMP n=13, 100% and CRC n=8, 100%) were investigated using bioinformatic and statistical tests (differential expression analysis, hierarchical clustering, principal component analysis and gene set enrichment analysis).

Results

We identified a gene signature of 28 genes distinguishing LAMN, IgPMP and CRC neoplasias. Ontology analyses revealed that multiple pathways including EMT, ECM interaction and angiogenesis are differentially regulated. Fifty-three significantly differentially regulated gene sets were identified between IgPMP and CRC followed by CRC vs. LAMN (n=21) and IgPMP vs. LAMN (n=16). Unexpectedly, a substantial enrichment of the EMT gene set was observed in IgPMP vs. LAMN (FDR=0.011) and CRC (FDR=0.004). Typical EMT markers were significantly upregulated (Vimentin, TWIST1, N-Cadherin) or downregulated (E-Cadherin) in IgPMP. However, MMP1 and MMP3 levels, associated with EMT, ECM and metastasis, were considerably higher in CRC.

Conclusion

We show that the different tumorbiological behaviour and metastatic spread pattern of lower gastrointestinal tract malignancies is reflected in a different gene expression profile. We revealed a strong activation of the EMT program in non-metastasizing IgPMP vs. CRC. Hence, although EMT is considered a key step in hematogenous spread, successful EMT does not necessarily lead to hematogenous dissemination. This emphasizes the need for further pathway analyses and forms the basis for mechanistic and therapy-targeting research.

Coincidence of three carcinomas (Ca) of the gastrointestinal (GI) tract at different segments

L. Zaporozhchenko¹, C. March², R. Jänsch³, U. Vorwerk⁴, D. Medenwald⁵, D. Jechorek⁶, R. S. Croner¹, **F. Meyer**¹

¹Dept. of General, Abdominal, Vascular and Transplant Surgery; Otto-von-Guericke University with University Hospital, Magdeburg, Germany, ²Dept. of Radiology and Nuclear Medicine; Otto-von-Guericke University with University Hospital, Magdeburg, Germany,

³Dept. of Gastroenterology, Hepatology and Infectious Diseases; Otto-von-Guericke University with University Hospital, Magdeburg, Germany, ⁴Dept. of Otorhinolaryngology, Otto-von-Guericke University with University Hospital, Magdeburg, Germany, ⁵Dept. of

Radiation Therapy, Otto-von-Guericke University with University Hospital, Magdeburg, Germany, ⁶Institute of Pathology, Otto-von-Guericke University with University Hospital, Magdeburg, Germany

Question/Background

Coincidence of neoplastic lesions can be considered an extremely interesting subgroup of malignant tumor patients.

Methods

Scientific case report

Results

Case description:

- *Medical Hx:* * Current: Admittance of a 69-years old male patient because of colon Ca

* Own: **1)** Additional diagnoses (Dx) - status after early gastric Ca (intestinal type according to Lauren's classification at prepyloric site) pT1b(sm1)L1V0Pn0R0G1; MMRp status; HER2/new status, negative / - status after squamous cell Ca of the left oropharynx cT4cN2bcM0 w/ primary radiochemotherapy

2) Previous intervention - gastric endoscopic submucosal dissection (ESD)

- *Clinical findings:* Patient in age-related general & nutritional status
- *Diagnostic:* * Laboratory parameters: CrP, 172 mg/L / white blood cell count, within normal range
- * Colonoscopy/Histology (Bx), adeno-Ca of the sigmoid colon, 70x42x14 mm in size, lymphangiosis carcinomatosa
- *Dx:* Three Ca of the GI tract with a recently diagnosed adeno-Ca of the sigmoideo-rectal junction
- *Differential Dx:* Hemorrhoids, chronic inflammatory bowel disease, diverticulosis, diverticulitis, irritable bowel syndrome
- *Decision-making:* Indication for surgical intervention
- *Therapy:* Anteriore rectum resection with TME, lymphadenectomy & descendorectostomy + protective loop ileostoma
- *Histopathological investigation:* pT3pN1b(2/28)L1V0Pn0R0
- *Postop. course:* Intensive care for 24 h, peridural catheter-based pain therapy, wound & stoma care, peroral antimycotic treatment, nutritional advisement; on the 6th/12th postop. d: surgical re-intervention (anastomotic resection & new creation); thereafter, improvement of clinical finding & lab parameters
- *Complications:* Anastomotic insufficiency, wound seroma (with need for treatment)
- *Proceeding:* Antiseptic wound care (upper pole) in an outpatient clinic-setting, stoma care, postop. chemotherapy ("CAPOX") according to the recommendation of the tumor board conference, adequate follow up-investigations of the early gastric & oropharynx Ca
- *Long-term outcome:* Follow up-time periods of 45, 42 & 39 months, resp., depending on tumor Dx showing recurrent tumor growth of oropharynx Ca after 40 months w/ subsequent radiation

Conclusion

From the extremely rare case example of a three-fold tumor manifestation with Ca's at the same organ (GI tract), a substantial familial burden & a considerable individually increased risk constellation with regard to epithelial &/or GI tract-associated tumorigenesis (also carcinogenesis) can be derived.

P02 Postersitzung AG Gastroenteropathologie II

P.02.08

Squamous esophageal carcinoma of the young adult

E. Wolniczak¹, C. March², R. S. Croner¹, D. Medenwald³, F. Meyer¹

¹Dept. of General, Abdominal, Vascular and Transplant Surgery; Otto-von-Guericke University with University Hospital, Magdeburg, Germany, ²Dept. of Radiology and Nuclear Medicine; Otto-von-Guericke University with University Hospital, Magdeburg, Germany,

³Dept. of Radiation Therapy, Otto-von-Guericke University with University Hospital, Magdeburg, Germany

Question/Background

Squamous esophageal carcinoma of the young adult can be considered a rare tumor manifestation.

Aim: To illustrate the interesting and newsworthy case of a young female patient with squamous esophageal cancer as a rare tumor manifestation

Methods

Scientific case report

Results

CASE DESCRIPTION:

Medical Hx: - *Current:* Dysphagia

- *Social:* Lives with life partner, son – 3 years (yr) of age, secondary school certificate; profession, logistic manager; currently, reduced earning capacity pension

- *Family:* Maternal grandparents, diabetes mellitus type II, paternal grandmother, Parkinson's disease and Lupus

- *Premedication:* Cortison 4 mg 1-0-0, Pantoprazol 40 mg as needed

- No allergies

Diagnostic measures: - Esophagogastroduodenoscopy: tumor lesion extending from 22 to 38 cm from row of teeth

- Thoracic/Abdominal CT scan

Decision-making (tumor board conference): Neoadjuvant radiochemotherapy (derived from CROSS protocol with 41.4 Gy and 5 cycles of chemotherapy with Paclitaxel 50 mg/m² and Carboplatin AUC2 as well as subsequent resection within the 6-weeks interval

Diagnosis: Squamous esophageal carcinoma (ypT3 pN0 M0 L0 V0 R0 G1) of the middle and lower third (22-38 cm from row teeth)

Differential diagnosis: Adeno-carcinoma of the esophagus, achalasia

Secondary diagnosis: - Mixed collagenosis

- Liver hemangiomas within the segment III and the right hepatic lobe

Surgical intervention: Thoracoabdominal esophagus resection with thoracic transposition of the stomach and esophagogastronomy as well as pyloromyotomy (in a different hospital)

Course: - Leukopenia (approximately 2.6 [SI]) during radiochemotherapy

- 3-yr-interval: Lobectomy of the right upper lobe

- After 5 yr: i.v.-port explantation due to infection with recurrent fever attacks

Follow up: Adequate control investigations in a different hospital; currently, no hint for tumor recurrency

Conclusion

Despite the untypically young age, which does not exclude completely the manifestation of a squamous esophageal carcinoma, the same established treatment principles and modes are pursued (with limited experiences due to the rare manifestation), which resulted in a 7-yr-survival. A successively established minimally invasive and, subsequently, roboter-assisted surgical approach might provide a further step forward in managing the possibly postoperative functional alterations. The young age prompts to clarify the association with a HPV infection and a recommendable vaccination.

P.02.09

Immunohistochemical positivity of Nup153 is associated with neuroendocrine differentiation

K. Singer¹, E. Herpel², F. Bergmann^{2,3}, T. Muley⁴, M. Meister⁴, J. Lehmann-Koch⁵, B. Goeppert⁶, A. Warth⁷, P. Schirmacher³, K. Breuhahn³, F. Fend¹, S. Singer¹

¹Universitätsklinikum Tübingen, Institut für Pathologie, Tübingen, Germany, ²Klinikum Darmstadt, Klinische Pathologie, Darmstadt, Germany, ³Universitätsklinikum Heidelberg, Institut für Pathologie, Heidelberg, Germany, ⁴Universitätsklinikum Heidelberg, Thoraxklinik, Sektion translationale Forschung, Heidelberg, Germany, ⁵SLK-Kliniken Heilbronn, Institut für Pathologie, Heilbronn, Germany, ⁶RKH Klinikum Ludwigsburg, Institut für Pathologie und Neuropathologie, Ludwigsburg, Germany, ⁷ÜGP MVZ Institut für Pathologie, Dermatopathologie, Zytologie und Molekularpathologie GbR, Wetzlar, Germany

Question/Background

The nuclear pore complex (NPC), embedded in the nuclear envelope, is gateway for nucleocytoplasmic trafficking and consists of ~30 different nucleoporins (Nups). Over the last years, it became evident that Nups participate not only in nuclear transport, but also exert transport-independent functions (e.g. chromatin interaction). There is also some evidence for cell- or tissue-specific NPC alterations. In this project, we analyzed immunohistochemical staining patterns in human normal tissues and tumors of two functionally and structurally similar nucleoporins: Nup98 and Nup153 .

Methods

Using a pan-tissue microarray (TMA), various human tissues were stained with Nup98 and Nup153 antibodies. The immunoreactivity of Nup153 was further analyzed on additional TMAs containing more than 200 neuroendocrine neoplasias (NEN), such as medullary thyroid carcinomas, lung carcinoids, NEN of the gastrointestinal tract and pancreas as well as corresponding non-neuroendocrine tumors . The results were correlated with clinical and histomorphological data.

Results

Nup98 showed a strong nuclear/nuclear envelope positivity in all human tissues examined, whereas Nup153 showed not only organ-specific but also cell type-specific nuclear/nuclear envelope immunoreactivity. Nup153 positivity was particularly observed in cells of the diffuse neuroendocrine system such as the pancreatic islets of Langerhans or thyroid C cells. Moreover, neuroendocrine differentiated neoplasms (medullary thyroid carcinomas, lung carcinoids, NET of the gastrointestinal tract and pancreas) retained strong Nup153 immunoreactivity, whereas the corresponding non-neuroendocrine tumors were largely negative. In line with these findings patients with strong Nup153 positivity showed better survival compared to those with weak or negative Nup153 staining.

Conclusion

Our data indicate strikingly different staining patterns of Nup98 and Nup153 in normal tissues and tumors with the latter being surprisingly associated with neuroendocrine differentiation and patient survival.

P.02.10

Intratumoral heterogeneity in poorly cohesive gastric cancer correlates with clinicopathological features

N. Dabbagh¹, H.-M. Behrens², C. Röcken²

¹Städtisches MVZ Kiel, Institut für Pathologie, Kiel, Germany, ²University Hospital Schleswig-Holstein, Dept. of Pathology, Kiel, Germany

Question/Background

This study aimed to investigate intratumoral morphological heterogeneity of poorly cohesive gastric cancer (PC-GC) and the relationship between histological characteristics and clinicopathological features.

Methods

Clinicopathological data were collected prospectively from the archive of the Institute of Pathology, University Hospital Kiel. Resection specimens from 140 patients with poorly cohesive gastric adenocarcinoma of the stomach were included. Tumor cells were classified into four histologic subtypes: classic signet ring cells, small and histiocyte-like cells, undifferentiated cells (anaplastic), and cells forming minor tubular structures. The tumors were subsequently classified into 3 categories according to the International Gastric Cancer Association (IGCA):

PC-GC with > 90% poorly cohesive cells having signet ring cell morphology (SRC), PC-GC with SRC component < 90% but > 10% SRCs and with < 10% SRCs (PC non-SRC).

Results

There are differences in presentation and outcomes between the various histological phenotypes of PC-GC. A significant correlation was found between an undifferentiated component and UICC stage and T category ($p=0.001$), respectively, whereas SRC was observed significantly more often as the other subtypes in the small and mucosal tumors ($p<0.001$). Otherwise the undifferentiated phenotype showed the tendency of lymph node metastasis and lower survival rates, but these differences were not statistically significant ($p=0.004$). There was no significant association between other subtypes and tumor behaviours.

Conclusion

Tumors with an undifferentiated morphology were larger and associated with a poorer prognosis. An undifferentiated morphology can also be a risk factor for lymph node metastasis. SRC was observed more frequently on the tumor surface and might carry the risk of sampling errors.

P.02.11

Tumor area infiltration and absolute tumor cell numbers in endoscopic biopsies of therapy-naïve upper GI tract carcinomas – implications for predictive biomarker testing

A. Quaas

UKK, Institut für Pathologie, Köln, Germany

Questions/Background

Guidelines regulate how many (tumor-bearing) biopsies should be sampled to obtain representative results in predictive biomarker testing. Little is known about how well these guidelines are applied, and how many absolute tumor cells are captured by the biopsies.

Methods

Archival (H&E)-stained sections were digitized, and tumor areas were annotated. The tumor-bearing biopsy area and absolute carcinoma cell count per case were determined by image analysis

Results

Biopsies from 253 patients were analyzed. The following mean values were determined: a) tumor biopsy number: 6.5 (range: 1 – 25, standard deviation (SD)=3.33, b) number of tumor-bearing biopsies: 4.7 (1–20, SD=2.80), c) tumor infiltrated area: 7.5mm² (range: 0.18 – 59.46mm², SD=6.67mm²), d) absolute tumor cell count: 13,492 (range: 193–92,834, SD=14,185) e) tumor cell count in a surgical specimen (tumor size: 6.7 cm): 105,200,176.

The guideline-recommended biopsy-count of 10 was not achieved in 208 patients (82.2%), and the required tumor-bearing biopsy count of 5 was not achieved in 133 patients (52.6%).

Conclusion

To our knowledge, this is the first systematic study describing the relationships between biopsy number,

actual infiltrated tumor area, and carcinoma cell number. Digital pathology has the potential to objectively capture these parameters for documentation, quality assessment, and future clinical studies.

P.02.12

Significant tumor regression after neoadjuvant chemotherapy in gastric cancer, but poor survival of the patient? - Role of MHC class I alterations

T. Hiltner¹, N. Szörenyi¹, M. Kohlruß¹, A. Hapfelmeier², A.-L. Herz¹, J. Slotta-Huspenina¹, M. Jesinghaus¹, A. Novotny³, S. Lange⁴, K. Ott⁵, W. Weichert¹, **G. Keller¹**

¹Institute of Pathology, Technical University of Munich, Munich, Germany, ²Institute of Medical Informatics, Statistics and Epidemiology, Technical University of Munich, Munich, Germany, ³Department of Surgery, Technical University of Munich, Munich, Germany, ⁴II. Medizinische Klinik, Technical University of Munich, Munich, Germany, ⁵Klinikum Rosenheim, Department of Surgery, Rosenheim, Germany

Question/Background

The major histocompatibility complex (MHC) class I genes, encompassing the human leukocyte antigen (HLA) class I and the beta-2 microglobulin (B2M) genes, play a key role for neoantigen presentation to the immune system. We aimed to determine the clinical and prognostic relevance of allelic imbalance (AI) of the respective chromosomal regions in the context of neoadjuvant chemotherapy (CTx) for patients with adenocarcinoma of the stomach or gastroesophageal junction.

Methods

Biopsies of gastric/gastroesophageal adenocarcinomas before platinum/fluoropyrimidine CTx from 158 patients were analyzed. DNA was isolated from paired tumor and non-tumor formalin-fixed paraffin-embedded tissues. AI was determined by multiplex PCRs of four or five microsatellite markers spanning the HLA genes located on chromosome 6p21 and the B2M gene located on chromosome 15q21 as described (1). The response to CTx was histopathologically evaluated according to the classification of Becker (2). Patients with tumor regression grade (TRG) 1 were defined as responding and patients with TRG2 and 3 as non-responding patients. Hazard ratios (HR) were calculated by Cox regression analysis. AI was analyzed for an association with response and survival of the patients.

Results

AI with no marker was significantly associated with response or survival. However, subgroup analysis revealed differences. AI at marker D6S265, close to the HLA-A gene, was associated with a decreased survival only in responding (HR, 3.62; 95% CI, 0.96-13.68, p=0.058), but not in non-responding patients (HR, 0.92; 95% CI, 0.51-1.65, p=0.773). Markers D6S273 and D6S2872 showed similar results. The interaction between AI at D6S265 and response to CTx was significant in multivariable analysis (p=0.010). No associations were observed for B2M markers.

Conclusion

Our result underline the importance of intact neoantigen presentation specifically for responding patients and may help explain an unexpected poor survival of a patient despite significant tumour regression after neoadjuvant platinum/fluoropyrimidine CTx.

References:

1. Hiltner, Szörenyi et al. 2023. Cancers 15, 771.
2. Becker et al. 2011. Ann Surg 253 (5): 934-939.

P.02.13

Analysis of SH2D4A promoter activity reveals positive regulation by inflammatory cytokines via transcription factor KLF4.

J. Schreck¹, C. Ploeger¹, T. Huth¹, R. N. Sugiyanto¹, S. Pusch¹, K. Breuhahn¹, P. Schirmacher¹, B. Goeppert², S. Roessler¹

¹Institute of Pathology, Heidelberg University Hospital, Heidelberg, Germany, ²Institute of Pathology, RKH Hospital Ludwigsburg, Ludwigsburg, Germany

Question/Background

Hepatocellular carcinoma is typically preceded by chronic liver damage and inflammation. Cytokines associated with tumor initiation, invasion, and metastasis are often elevated in the tumor microenvironment. SH2D4A acts as a tumor suppressor in HCC, shows a reduced expression in tumor tissue and can be used

to predict survival[1]. In this study we aimed to explore the transcriptional regulation of SH2D4A expression in HCC.

Methods

HCC cells HepG2 and Hep3B were stimulated with cytokines IFN- γ and TGF β for different time periods and analysis of SH2D4A mRNA expression was done by qRT-PCR. Next, HepG2 and Hep3B cells were transfected with transcription factors YY1, FOXA1 and KLF4 previously predicted in-silico and change in endogenous SH2D4A mRNA expression and change in SH2D4A promoter activity were analysed by qRT-PCR and dual luciferase assay, respectively. The four most prominent KLF4 binding sites on the SH2D4A promoter were disrupted by site-directed mutagenesis. HepG2 and Hep3B cells were transfected with a plasmid for expression of KLF4 and a reporter plasmid containing a mutated SH2D4A promoter. Promoter activity was measured by dual luciferase assay. For gene expression analysis we used data obtained from TCGA dataset LIHC.

Results

We found that after stimulation with cytokines IFN- γ and TGF β , SH2D4A expression is significantly increased on mRNA level. Further studying the downstream regulators, the SH2D4A promoter emerged to be regulated by transcription factors FOXA1, YY1 and KLF4. Systemic study of KLF4 binding sites revealed two directly adjacent binding sites with significant impact on SH2D4A promoter activity in HepG2 cells. One binding site exhibited a direct positive effect on SH2D4A promoter activity when stimulated, the other binding site conveyed an increase in promoter activity by disinhibition. A decrease in SH2D4A promoter activity not associated with a specific binding site indicated a cooperative interaction in Hep3B cells. Gene expression data analysis demonstrated several differentially expressed KLF4 target genes associated to SH2D4A expression. Of those genes, PIK3R1 and CDC14B showed a significant positive association with overall survival.

Conclusion

We demonstrated an influence of cytokines on the endogenous SH2D4A expression activity and uncovered a regulatory interaction between KLF4 and the SH2D4A promoter. Understanding the regulation of SH2D4A is key to find new innovative therapeutic approaches targeting cancer cells.

Literaturangaben:

[1] Roessler, S., Long, E. L., Budhu, A., Chen, Y., Zhao, X., Ji, J., Walker, R., Jia, H. L., Ye, Q. H., Qin, L. X., Tang, Z. Y., He, P., Hunter, K. W., Thorgeirsson, S. S., Meltzer, P. S., & Wang, X. W., (2012), Integrative genomic identification of genes on 8p associated with hepatocellular carcinoma progression and patient survival., *Gastroenterology*, 142(4), 957–966.e12., <https://doi.org/10.1053/j.gastro.2011.12.039>

P.02.14

Does gastric cancer show gender-specific differences in the perioperative management, early postoperative and longterm oncosurgical outcome - results of a prospective multicentre observational study

P. Mahendran¹, R. Otto², R. S. Croner¹, H. Lippert², I. Gastinger², F. Meyer¹

¹Dept. of General, Abdominal, Vascular and Transplant Surgery; Otto-von-Guericke University with University Hospital, Magdeburg, Germany, ²Institute of Quality Assurance in Operative Medicine; Otto-von-Guericke University, Magdeburg, Germany

Question/Background

To investigate gender-specific differences of the **i)** perioperative management, **ii)** early postoperative & **iii)** long-term oncosurgical outcome by surgical treatment, in particular, by gastric Ca resection based on real-world data aiming at surgical quality assurance and a contribution to research on clinical care.

Methods

Systematic clinical prospective multicentre observational study (design)

Results

From 2007 to 2009, in total 2,897 consecutive patients were documented, 59.7% male and 40.3% female with a mean age of 67.4 vs. 70.3 years in men and women, respectively ($p < 0.001$). Significantly more often, men complained on dysphagia as symptom of admission ($p < 0.009$), had an intestinal type according to Laurén's classification in preoperative and definitive histopathological finding ($p < 0.001$) as well as showed ASA scoring III ($p < 0.017$). As risk factors, a significantly higher alcohol consumption ($p < 0.001$) and nicotine abuse ($p < 0.001$) was found. The esophagogastric junction was significantly more often diagnosed as tumor site in men ($p < 0.001$). Duration of surgery (202 vs. 184 min; $p < 0.001$) as well as hospital stay (20.99 vs. 20.68 d; $p < 0.024$) were significantly longer in men in addition to significantly more frequent pulmonary events postoperatively ($p < 0.001$).

In contrast, women had significantly more often pain in the upper abdomen and vomiting as first symptom as well as a diffuse and mixed type (Laurén's classification) in the pre- and postoperative histopathological

finding ($p < 0.001$). With regard to the risk profile, women were more obese and less susceptible for general complications postoperatively ($p < 0.001$).

Multivariable analysis (univariable analysis not shown) revealed higher ASA scoring, M1 status, longer duration of surgery and hospital stay as significant influencing factors for morbidity. With regard to mortality, men with mixed type (Laurén), R1/2 status, higher ASA scoring as well as complication in higher age indicated a significantly higher probability to die. In addition, male gender need to be considered a significantly negative influencing factor with regard to 5-years overall survival and disease-free survival (no gender-based impact onto 5-years local recurrence rate).

Conclusion

Taking into account the gender aspect, significant differences of the surgical therapy of gastric cancer were found in perioperative risk profile, tumor characteristics & in the early postoperative, operation-associated but also in tumor-, i.e., malignancy-related outcome.

P.02.15

Esophageal carcinomas with "fetal cell-like differentiation" - rare but therapeutically relevant

A. Quaas¹, T. Zander²

¹UKK, Institut für Pathologie, Köln, Germany, ²UKK, Innere 1 Onkologie, Köln, Germany

Question/Background

In the current WHO classification, carcinomas with fetal cell-like differentiation are described as rare subtypes in the stomach. This group subsumes a) AFP-producing carcinomas (other than hepatoid carcinomas) b) yolk sac-like carcinomas c) enteroblastic adenocarcinomas - often these subtypes co-exist within one tumor. A main immunohistochemical characteristic, besides AFP positivity, is the positivity of the carcinomas with proteins of fetal cell differentiation such as Glypican3, SALL4 and Claudin 6. There is no firm knowledge about the frequency, molecular as well as morphological characteristics of this tumor subtype in adenocarcinomas of the esophagus.

Methods

In this retrospective analysis, a total of 806 adenocarcinomas of the esophagus were analyzed. Tumors in which at least 50% of tumor cells showed dual expression with claudin 6 and glypican 3 or SALL4 were considered. These tumors were further analyzed by immunohistochemistry: Cytokeratin7 (CK7), SWI/SNF markers: BRM (SMARCA2), BRG1 (SMARCA4) and ARID1a, fetoprotein and β -HCG.

Results

Six carcinomas showed fulfilled the above criteria ($6/806 = 0.7\%$). The majority of patients were male (5/6), and the average age at diagnosis was 58 years (32-72). All tumors showed marked reduced expression or absence of CK7, all tumors showed alteration of at least one SWI/SNF marker (mostly SMARCA2), very different morphological growth patterns were found.

Conclusion

Carcinomas with fetal cell-like differentiation exist in the esophagus and are interpreted as "normal" adenocarcinomas of the esophagus based on their non-characteristic standard morphological findings. Due to their often very prominent claudin 6 positivity, CAR-T cell therapy using claudin 6 as a target protein may be considered as an individual therapeutic option. The detectable alteration of the SWI/SNF system in these tumors may be of therapeutic interest in the future. All carcinomas of the esophagus that are (nearly) CK7 negative (even tumors with highly differentiated papillary growth patterns) should be considered for this carcinoma subtype, among others.

P02 Postersitzung AG Gastroenteropathologie III

P.02.16

Impact of the underlying diagnosis comparing chronic pancreatitis ("Pan") vs. pancreatic head carcinoma ("Ca") onto the early postoperative outcome after pylorus-preserving pancreatic head resection (PPPHR) according to Traverso-Longmire

M. Grabowski¹, N. Scholz¹, R. Otto², D. Jechorek³, A. Perrakis¹, R. S. Croner¹, H. Ptak⁴, F. Meyer¹

¹Dept. of General, Abdominal, Vascular and Transplant Surgery; Otto-von-Guericke University with University Hospital, Magdeburg, Germany, ²Institute of Quality Assurance in Operative Medicine; Otto-von-Guericke University, Magdeburg, Germany, ³Institute of Pathology, Otto-von-Guericke University with University Hospital, Magdeburg, Germany, ⁴Dept. of General and Abdominal Surgery, Municipal Hospital ("Ernst-von-Bergmann-Klinikum"), Potsdam, Germany

Question/Background

To investigate the influence of different diagnoses (Pan vs. Ca) & interindividual differences like age & secondary diseases on the early postop. outcome in a comparable state of interventional invasiveness, surgical trauma & related SIRS.

Methods

Over a defined period of time, all consecutive patients (pats.) who had undergone PPPHR with Pan & Ca were recorded.

Results

From 2003-2015, in total 315 pats. were enrolled, of whom $n=290$ (sex ratio, m/w=178:112 [1.59:1]; median age, 59 [range: 20-82] years [yrs]) were evaluated. Out of them, 194 cases with Ca (66.9%) & 96 individuals with Pan (33.1%) were subclassified. Median age was significantly different: 68 (37-82) vs. 51 (20-62) yrs for Ca & Pan, resp. ($p<0.001$), with a trend for a different mean ASA score of 2.3 (Ca [1-4]) & 2.1 (Pan [1-4]; $p=0.084$). The median preop. hospital stay was 2 [0-17] d for both diseases; postoperatively, pats. were hospitalized for 18 (Ca [2-88]) & 15 (Pan [6-48]) d with a significant difference ($p=0.029$).

Surprising were the similar general & specific complication rates of 21.6% (Ca) vs. 15.6% (Pan) & 39.7% (Ca) vs. 42.7% (Pan) (resp.; $p=0.224$; $p=0.623$), & the corresponding 30-d mortalities of 2.6% (Ca) vs. 2.1% (Pan; $p=0.796$).

Of the potential factors influencing morbidity (general/specific/total) & mortality, gender, age, ASA scoring, secondary diagnoses, abuse habits (nicotine/alcohol), BMI, preop. CRP & white blood cell counts as well as the definitive diagnosis were tested using univariate analysis, with a significant impact of the ASA category & BMI onto the general complications ($p=0.013$ / $p=0.041$).

Multivariate analysis using logistic regression revealed that intraoperatively administered red cell packs showed a significant impact onto the general & specific complication rates ($p=0.004$ / $p=0.0001$) as well as mortality ($p=0.001$). Female pats. had a significantly lower microbial colonization postoperatively ($p=0.0004$), whereas the diagnosis (Pan vs. Ca) did not have any influence thereon ($p=0.305$). The postop. SOFA Score was higher in the Ca group, even though the complication rates were similar.

Conclusion

The influence of the cancer, which was previously considered to be disadvantageous (rather unfavorable soft pancreas, immunosuppressive phenomenon) in comparison to chronic inflammation, in spite of significant higher age & longer postop. hospitalization of the pats., cannot be clearly detected on the basis of the morbidity & mortality data mentioned above representing early postop. outcome.

P.02.17

Metastatic pancreatic ductal adenocarcinoma as a mimicker of lepidic non-small cell lung cancer – an exemplary case of a broad oncological autopsy program

R. Ihringer, I. Kleinlein, B. Märkl

Institut für Pathologie und Molekulare Diagnostik, Augsburg, Germany

Question/Background

At the university medical center of Augsburg, we are generating an extensive collection of neoplastic tissue samples from autopsies for investigating heterogeneity in metastasizing cancer. In 2022 we examined 200 autopsy cases, of which around 50 included metastasizing neoplasms.

Methods

Exemplary, we report here a case of an 81-year old female who died from fulminant pulmonary embolism. Clinically she had a suspicion for metastatic colorectal cancer with metastases in the lung, liver, and peritoneum.

Results

During autopsy, she showed, besides multiple tumors in both lungs, liver and peritoneum a 1,5 cm measuring tumor in the head of the pancreas. In the colon ascendens we found a 2 cm measuring, macroscopically not for sure infiltrating, polypous tumor.

Histologically the tumor of the pancreas turned out to be a ductal adenocarcinoma with extended perineural invasion, which expressed immunohistochemically CK7, CK20 and CA19.9, while being negative against SATB2, cdx-2 and NapsinA.

Remarkable was the histology of the lung tumors: In all of the lobes we saw disseminated foci of adenocarcinoma, which seemed to spread in a lepidic manner throughout the alveoli. The immunohistologically pattern was identical with the one in the pancreas: Expression of CK7, CK20 and CA19.9, while being negative against TTF-1, NapsinA, SATB2 and cdx-2.

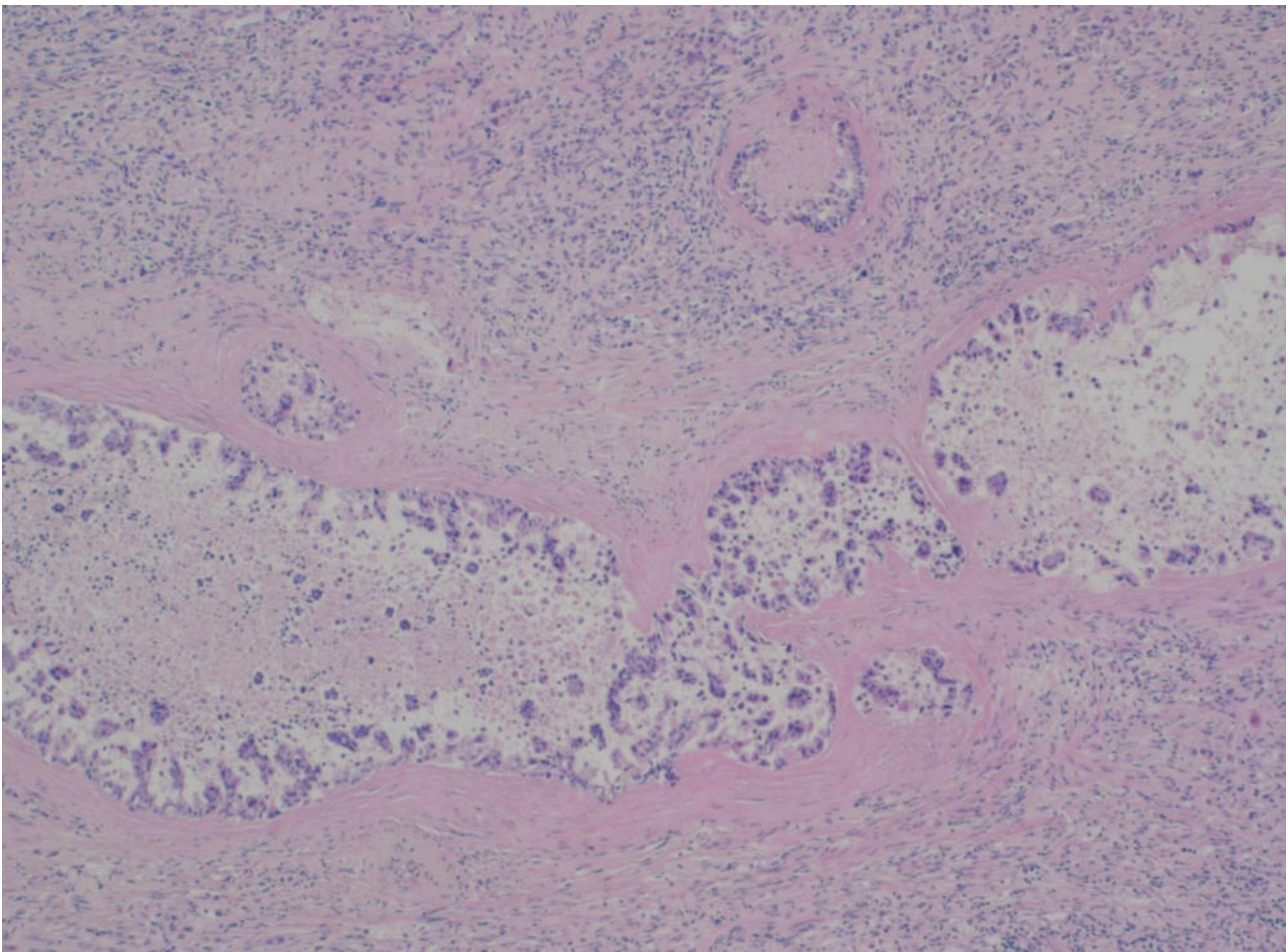
The metastases in the liver and peritoneum showed a different, more micropapillary architecture. The tumor in the colon ascendens turned out to be an initially infiltrating adenocarcinoma of colorectal type.

Conclusion

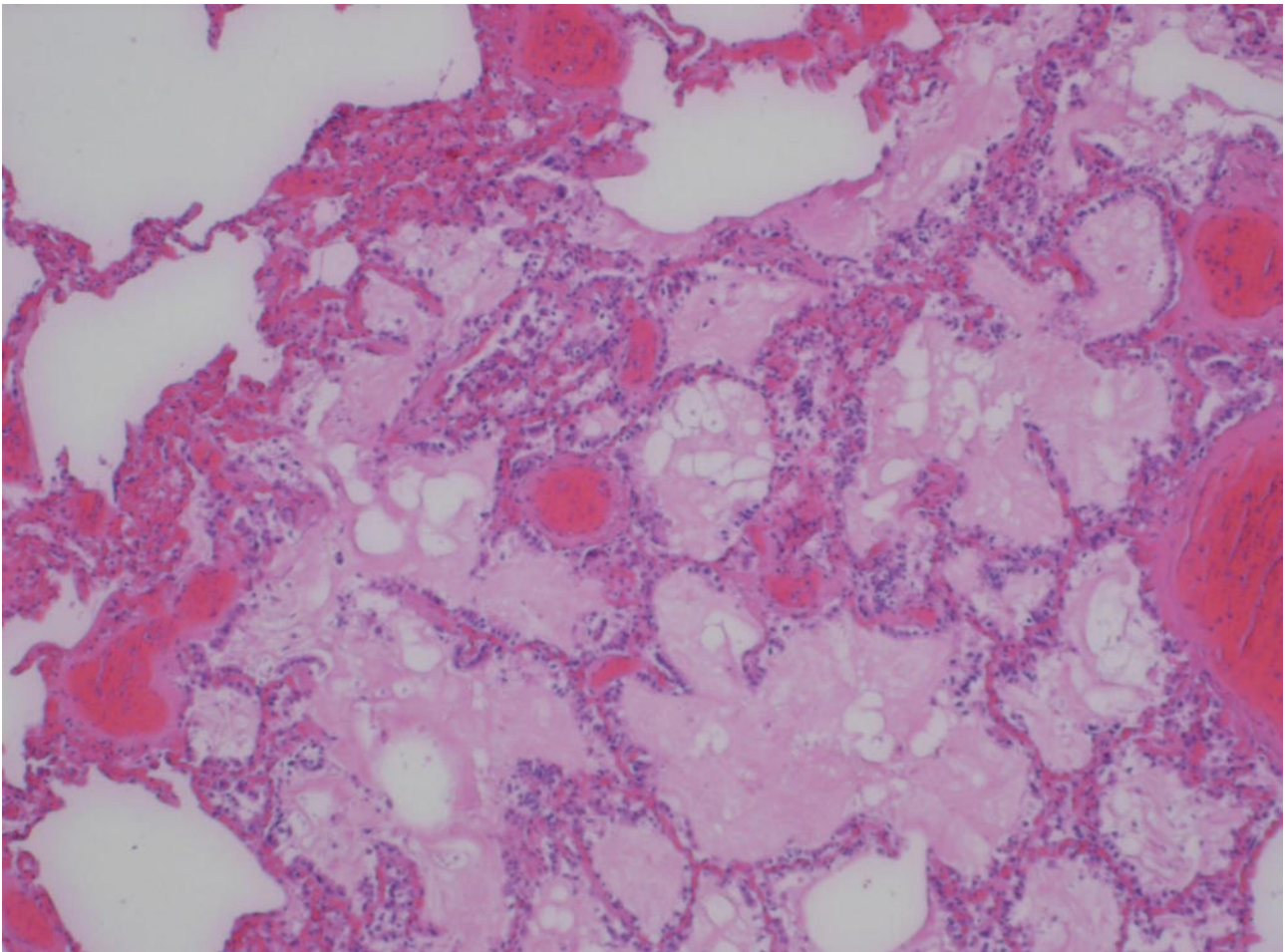
In this case the metastasis in the lung could have been easily confused with a non-small cell lung cancer of the lepidic type if seen in a biopsy (the more because the pancreatic cancer was not even suspected).

This is an example of how autopsies can improve the understanding of diseases and its correlations. Since autopsy rates are declining, it is the more important and relevant for the living to implement post-mortem examination.

Autopsies should be rendered systematically to achieve a better understanding of neoplastic diseases and their heterogeneity.



Ductal adenocarcinoma of the pancreas



Metastasis from an adenocarcinoma of the pancreas in the upper lobe of the left lung

P.02.18

Sarcoma as rare differential diagnosis of a pancreatic tumor lesion

C. Hellfors¹, F. Meyer¹, S. Acciuffi¹, C. March², D. Jechorek³, R. S. Croner¹, S. Al-Madhi¹

¹Dept. of General, Abdominal, Vascular and Transplant Surgery; Otto-von-Guericke University with University Hospital, Magdeburg, Germany, ²Dept. of Radiology and Nuclear Medicine; Otto-von-Guericke University with University Hospital, Magdeburg, Germany,

³Institute of Pathology, Otto-von-Guericke University with University Hospital, Magdeburg, Germany

Question/Background

Tumor(-like) lesions of the pancreas, in particular, those with solid characteristics show a broad differential diagnosis.

Aim: To describe the rarely described case of low-grade sarcoma as a rare tumor (Tu) entity of the pancreas

Methods

Scientific case report

Results

CASE DESCRIPTION:

A 52-years old female patient presented w/ a suspicious pancreatic Tu lesion as an intraop. finding by coincidence. Additional diagnoses are partial thrombosis of the thoracic aorta as well as left renal & hepatic arteries. Clin. characteristics comprised a reduced general & cachectic nutritional status (lab parameters, L/CRP increased; CA19-9/CEA within normal range). Thoracic/abdominal CT scan revealed inhomogeneous Tu lesion of the pancreatic tail & unclear Tu-suspicious lesions of the left pararenal gland + the 10th thoracic vertebra – in addition, pseudoaneurysm of the splenic artery, thrombus of the thoracic aorta & occlusion of the common hepatic artery. The Tu board recommended TEVAR & open resection of the pancreatic tail with splenectomy, which were performed w/o complications within a 4-d interval.

Postop. course was characterized by delayed GI passage & gastric atony (temporarily, approached w/ gastric tube & prokinetics) + therapy-resistant hypertension w/ need of a new medication. Postop. Tu board conference recommended radiation & adequate Tu-follow up due to the histopathologically investigated

diagnosis of a retroperitoneal, spindle-cell low-grade sarcoma. In case of the status CRM+ (< 1 mm; “R0 narrow” to the retroperit. vessels), histopathol. reference investigation was ordered in Muenster (Germany), which revealed an undifferentiated spindle-cell sarcoma – repeat Tu board confirmed need of additive radiation, which was postponed due to the delayed reconvalescence. The 3-months CT-scan follow-up detected peritoneal carcinomatosis, metastasis of the left pararenal gland as well as hepatic & bone metastases. Again, Tu board recommended systemic chemotherapy (1 application of doxorubicin mono – in addition, right thoracocentesis due to pleural effusion in case of suspicious “pleuritis carcinomatosa”) & radiation of the vertebral column (dosage, 40 Gy á 4 Gy) due to pain under palliative intention. Patient died from Tu disease 4 weeks after initiation of therapy.

Conclusion

This case demonstrates sarcoma as a rarely occurring Tu entity of the pancreas, which needs to be included basically into the spectrum of the differential diagnoses in case of unclear pancreatic Tu lesions.

P.02.19

Mid-term finding after pancreatic trauma mimics pancreatic tumor lesion

K. Dossow¹, F. Meyer¹, S. Acciuffi¹, C. March², A. Perrakis¹, R. S. Croner¹, S. Al-Madhi¹

¹Dept. of General, Abdominal, Vascular and Transplant Surgery; Otto-von-Guericke University with University Hospital, Magdeburg, Germany, ²Dept. of Radiology and Nuclear Medicine; Otto-von-Guericke University with University Hospital, Magdeburg, Germany

Question/Background

Pancreatic tumor lesion can be considered a demanding differential diagnosis.

Methods

Scientific case report

Results

CASE DESCRIPTION:

Medical Hx: - CURRENT: 57-years old male patient was presented with tumor(-like) lesion of the pancreas of unclear dignity in CT scan performed for staging purpose of a histologically diagnosed prostate cancer; no complaints or “B-symptomatology”

- OWN: Status after a fall with abdominal trauma and posttraumatic conservatively treated pancreatitis in 2020 (1.5 years ago)

Secondary diagnoses: Prostate cancer (first diagnosis, 06/2021) with open prostatectomy

Clinical finding: Good clinical and normosome nutritional as well as cardiopulmonarily compensated status; abdominal wall soft, no muscular defense, scar of a median laparotomy with no inflammatory signs

Diagnostic measures: - LABORATORY PARAMETERS: No elevated inflammatory parameters, liver parameters (such as GLDH) minimally elevated, cholestasis parameters and tumor markers not elevated (CA19-9: < 9 U/mL, CEA: 2.4 ng/mL)

- Thoracic/Abdominal CT scan (in a different hospital): Fluid formation within the pancreatic corpus, no clear tumor lesion, no cholestasis

- EUS: Semiliquid area within the isthmus, the remaining pancreas with no finding, transgastric puncture aspirating yellow-grey fluid for microbiological and histopathological investigation

Histopathological investigation: Pancreatic necrosis with hint for malignant tumor growth

Clinical course: After uncomplicated EUS-guided puncture, case was repeatedly presented in tumor board conference including polytrauma-related images with declining local finding

Diagnosis: Fluid formation within the pancreatic corpus after traumatic pancreatic contusion and posttraumatic pancreatitis

Differential diagnosis: Pseudocyst, cystic (serous-cystic, mucinous-cystic) pancreatic lesion

Therapy: Conservative approach

Proceeding: Control imaging using ultrasound after 3 months and clinical follow-up in an outpatient clinic setting, regular follow-up investigations of the prostate cancer according to guidelines, preventive colonoscopy, withdrawal from nicotine/alcohol

Conclusion

(Status after) Abdominal trauma is a not rarely occurring clinical finding in the emergency room with a broad spectrum of clinical aspects, which can be considered a challenge for the abdominal surgeon (during the early and long-term course) as in the presented case with a trauma-caused pancreatic lesion suspicious for pancreatic tumor growth in the differentialdiagnostic considerations.

N-cadherin helps discriminate primary liver carcinomas from liver metastases of an extrahepatic primary

T. S. Gerber¹, D. A. Ridder¹, A. Brobeil², B. Goeppert², P. Stenzel¹, S. Zimmer¹, E. Lippe¹, J. Jäkel¹, M. O. Metzigg¹, R. Schwab³, S. Z. Martin⁴, A. Kiss⁵, F. Bergmann², P. Schirmacher², P. R. Galle⁶, H. Lang⁷, W. Roth¹, B. K. Straub¹

¹University Medical Center Mainz, Institute of Pathology, Mainz, Germany, ²Heidelberg University Hospital, Institute of Pathology, Heidelberg, Germany, ³University Medical Center Mainz, Department of Obstetrics and Women's Health, Mainz, Germany, ⁴Charité - Universitätsmedizin Berlin, Institute of Pathology, Berlin, Germany, ⁵Semmelweis University Budapest, 2nd Institute of Pathology, Budapest, Hungary, ⁶University Medical Center Mainz, 1st Department of Internal Medicine, Gastroenterology and Hepatology, Mainz, Germany, ⁷University Medical Center Mainz, Department of General, Visceral and Transplant Surgery, Mainz, Germany

Question/Background

The differential diagnosis between the primary liver cancers (PLC) hepatocellular carcinoma (HCC) and intrahepatic cholangiocarcinoma (iCCA) from liver metastases of an extrahepatic primary is of crucial therapeutic importance but may be challenging. We previously identified E- and N-cadherin as constitutive transmembrane proteins of adherens junctions of hepatocytes and cholangiocytes of the normal liver that are also preserved in HCCs and iCCAs. N-cadherin is thereby not restricted to neural and mesenchymal cells as previously thought, although, besides liver, other epithelia were vastly negative. Therefore, we hypothesized that N-cadherin may distinguish between PLC and (metastatic) extrahepatic carcinomas.

Methods

We evaluated E- and N-cadherin in 2,489 different tumors using immunohistochemistry, and compared our results with previously published 882 cases of PLCs including 570 HCCs and 312 iCCAs.

Results

Irrespective of their origin, most carcinomas retained strong positivity for E-cadherin as in the respective normal epithelia. A strong staining reaction with antibodies against N-cadherin was detected in HCCs and iCCAs, yet also in some clear cell renal cell carcinomas (ccRCC, 23.6% of cases). N-cadherin was only rarely expressed in adenocarcinomas of the gastrointestinal tract (0-0.5%), lung (7.1%), pancreas (3.9%), gynecological organs (0-7.4%) and breast (2.2%) nor in urothelial (9.4%) or squamous cell carcinomas (0-5.6%). In other tumor entities, N-cadherin was in part detected in tumors of endocrine origin such as thyroid cancer (29.2%) and neuroendocrine tumors (25-75%), as well as in malignant melanoma (46.2%) and mesothelioma (41%).

Conclusion

In conclusion, N-cadherin is a useful marker for the distinction of PLC versus liver metastases of extrahepatic carcinomas ($p < 0.01$), with the exception of ccRCC, neuroectodermal tumors, and mesenchyme-derived tumors.

Expression of CDH6 in Cholangiocarcinogenesis and its Diagnostic Relevance in High-Grade Biliary Intraepithelial Neoplasia

F. Brinkmann^{1,2}, T. Albrecht^{1,2}, A. Charbel^{1,2}, B. Köhler^{2,3}, C. Springfield^{2,3}, M. N. Vogel⁴, M. W. Büchler⁵, A. Mehrabi^{2,6}, P. Schirmacher^{1,2}, S. Roessler^{1,2}, B. Goeppert⁷

¹Institute of Pathology, Heidelberg University Hospital, Heidelberg, Germany, ²Liver Cancer Center Heidelberg (LCCH), Heidelberg University Hospital, Heidelberg, Germany, ³National Center for Tumor Diseases (NCT), Heidelberg University Hospital, Heidelberg, Germany, ⁴Thoraxklinik at Heidelberg University Hospital, Diagnostic and Interventional Radiology, Heidelberg, Germany, ⁵Department of Surgery, Heidelberg University Hospital, Heidelberg, Germany, ⁶Department of General, Visceral and Transplantation Surgery, Heidelberg University Hospital, Heidelberg, Germany, ⁷Institute of Pathology and Neuropathology, RKH Klinikum Ludwigsburg, Ludwigsburg, Germany

Question/Background

Cholangiocarcinoma (CCA) is a heterogeneous, highly aggressive malignancy with poor prognosis. Surgical resection is currently the only curative therapy, however, reactive changes caused by inflammation may closely mimic biliary intraepithelial neoplasia (BilIN) precursor lesions hampering detection at a resectable stage. Several cadherins (CDH) have been linked to metastatic progression and downregulation of CDH6 has been reported in biliary carcinogenesis (Goeppert et al. Epigenetics, 2016). In this study, we focused on the role of CDH6 in early cholangiocarcinogenesis and aimed to assess its use as a diagnostic marker of early malignant transformation in bile ducts.

Methods

Tissue microarrays of CCA samples of a large and clinicopathologically well-characterized patient cohort, containing intrahepatic (iCCA, N=145), perihilar (pCCA, N=145) and distal CCA (dCCA, N=118) as well as high-grade BillIN (N=170) and adjacent non-neoplastic biliary tissue (N=144) were immunohistochemically analyzed for CDH6. The average staining intensity of invasive tumor, high-grade BillIN and non-neoplastic bile duct epithelium was assessed using the immunoreactive score (IRS). Furthermore, full slide specimen of a second control cohort, encompassing resection and brush cytology samples of CCA, high-grade BillIN, non-neoplastic atypic bile ducts and normal bile ducts were analyzed and assessed by CDH6 immunohistochemistry.

Results

CDH6 immunoreactivity was absent or reduced significantly in CCA (mean IRS: 2.7) and in high-grade BillIN (mean IRS: 2.5), whereas it was highly expressed in atypic and non-atypic, non-neoplastic bile duct epithelia (mean IRS: 10.4). Statistical analysis confirmed a significant CDH6 protein reduction in all CCA subtypes and in high-grade BillIN, compared to normal bile ducts (each $p < 0.001$). Furthermore, the comparison of non-neoplastic bile duct samples with their corresponding intraindividual CCA samples revealed a significant decrease of CDH6-expression in 99% of cases ($p < 0.001$). On full slide sections, BillIN and CCA could be clearly differentiated from adjacent non-neoplastic bile ducts due to reduced CDH6 signals (each $p = 0.004$), thus validating the tissue microarray data.

Conclusion

Our results show that reduced expression of CDH6 is indicative for early precursor lesions and invasive CCA and is easily detectable by immunohistochemistry. Thus, reduced CDH6 may serve as a diagnostic marker for discrimination of high-grade BillIN from reactive atypia in bile duct specimens.

P.02.22

Proteome-based characterization of Exportin-1 directed therapy in liver cancer

K. Singer¹, V. Hollfoth¹, P. Riemenschneider¹, D. Dauch², A. Ori³, M.-S. Schult⁴, Y. Bauer¹, F. Fend¹, S. Singer¹

¹Universitätsklinikum Tübingen, Institut für Pathologie, Tübingen, Germany, ²Universitätsklinikum Tübingen, Institut für Innere Medizin, Tübingen, Germany, ³Leibniz-Institut für Alternsforschung, Fritz-Lipmann-Institut, Jena, Germany, ⁴Universitätsmedizin Greifswald, Institut für Pathologie, Greifswald, Germany

Question/Background

Since nuclear transport is highly relevant for the activity of various cancer-related signaling pathways, selective inhibitors of nuclear export represent a promising approach for cancer treatment. The exportin-1 (XPO-1) inhibitor selinexor is already FDA approved for the treatment of a variety of hematological neoplasms, whereas its efficacy in solid tumors especially in liver cancer is poorly understood. Here, we aim to identify and characterize candidates potentially involved in selinexor treatment response and resistance mechanisms using quantitative mass spectrometry-based proteomics (LC-MS/MS)

Methods

A variety of human (HepG2, Hep3B, HLE and HLF) and murine liver cancer lines were treated with selinexor under several conditions. The cells were then analyzed by MTT viability assays and LC-MS/MS-based proteomics.

Results

Among the human liver cell lines HepG2 and Hep3B responded well to selinexor treatment (0.25 μ M, 72 h) showing a residual viability of 25 %, whereas HLE and HLF remained largely unaffected. The highest response (90% decrease in viability) among murine HCC cell line was detected in Nras^{G12V} p19Arf^{-/-} cells at 0.1 μ M and 72 h. Proteomic analysis of the emerging groups ('responders' and 'non-responders') revealed significantly higher abundance of Glutathione S transferase P (GSTP1), Myoferlin (MYOF) and Profilin 1 (PFN1) among others in the 'non-responders' before and/or after selinexor treatment. These candidates have previously been linked to the exosome, cytoskeleton and also drug resistance.

Conclusion

Our data so far suggest that selinexor resistance in liver cancer is linked to exosome formation and cytoskeleton remodeling. However, potential response- or resistance-related candidates require further validation by silencing and/or overexpression approaches currently being conducted.

P.02.23

IgG4-positive plasma cells in Echinococcus multilocularis affected liver tissue are significantly increased as compared to autoimmune hepatobiliary diseases

L. Zhang, J. Nell, P. Möller, T. F. E. Barth

Universitätsklinikum Ulm, Pathologie, Ulm, Germany

Questions/Background

Zoonotic infections of humans with the larval stage of the cestode *Echinococcus multilocularis* can give rise to alveolar echinococcosis (AE) – a lethal disease when left untreated. The parasitic lesions mostly manifest in the liver and are encircled by an inflammation zone with typical patterns.

Histopathological diagnosis of AE as compared to autoimmune hepatobiliary conditions can be challenging, since both are known to show increased IgG4 plasma cells. We aimed to analyze the expression of IgG4 in AE in comparison to primary biliary cholangitis (PBC), primary sclerosing cholangitis (PSC) and autoimmune hepatitis (AIH).

Methods

We immunohistochemically stained liver sections of 31 patients with alveolar echinococcosis using monoclonal antibodies against IgG4 as well as the plasma cell marker CD38. We evaluated the percentage of IgG4-positive cells in the inflammation border around the lesion and counted the maximum amount of IgG4-positive plasma cells per high power field (HPF) within the section.

We included 15 biopsies of patients with autoimmune hepatobiliary, including 8 PBC cases, 4 PSC cases, 1 AIH case and 2 cases with an overlap syndrome (PBC + AIH).

Results

All included sections of AE tissue showed presence of IgG4-positive cells within the lymphocyte infiltrates around the liver lesions in patients with AE. The density of IgG4-positive cells per HPF in each slide varied between a minimum of 2 and a maximum of 70 IgG4-positive plasma cells.

Out of 15 stainings from patients with PBC, PSC and/or AIH only 6 showed IgG4-positive cells which make up to a maximum of 1 % of the infiltrating cells in the inflammation area of the tissue section.

Conclusion

Our analysis shows that the percentage of IgG4-positive cells is significantly higher around AE lesions as compared to PSC, PBC and AIH. Regarding the severe course of disease in AE and the widely differing therapeutic consequences depending on the diagnostic result, elevated numbers of IgG4-positive plasma cells in liver sections should lead to consider AE in the differential diagnostic work up.

The different IgG4 levels in AE may point to different stages of activity of the disease.

P.02.24

The Value of fine needle aspiration cytology (FNAC) in determining the histogenesis of liver nodules

B. Soudah¹, M. Abbas²

¹Institut für Pathologie, Medizinische Hochschule Hannover, Pathologie, Hannover, Germany, ²Universitätsklinikum Münster, Gerhard-Domagk-Institut für Pathologie, Münster, Germany

Question/Background

FNA is a sensitive and specific method in characterising suspected liver lesions. It is appropriate to distinguish between primary and secondary liver tumours. The use of cell block preparations after processing the cytological specimens allows further investigations using immunocytochemical evaluation to determine the nature of the primary tumour.

Methods

In the Hannover medical School (MHH) 4.136 sonographically guided FNAs were performed for patients, who clinically and sonographically were diagnosed to have liver tumours. Successful FNAC provides cells and tissues that are extremely useful for the diagnosis. We have retrospectively analysed the sensitivity and specificity of this technique to reach the correct diagnosis of the clinically suspicious liver nodules.

Results

Cytological examination of 4.136 (FNAC) specimens revealed in about 39.6% of cases a malignant tumour, in about 57.5% of cases a benign tumour and 2.8% were with unclear morphology. Some of the specimens revealed inappropriate number of cells and these were 1.1% of the specimens. The diagnosis of malignant tumours in this collection was hepatocellular carcinoma in 40%, choangiocellular carcinoma (CCC) in 10.5% and metastasis from other organs like breast, colon and lung in 48.5%. The cytological diagnosis of these cases has been correlated with the histopathological diagnosis.

Conclusion

97.1% of the FNAC specimens were correctly diagnosed. The remaining of the cases were difficult to be diagnosed because of insufficient samples or inability to perform immunocytochemistry. We suggest this simple technique for the diagnosis of serious clinical conditions like liver tumours with little hazardous healthy conditions of the patients.

P03 Postersitzung Uropathologie I

P.03.02

EpCAM Tumor Specificity and Proteoform Patterns in Urothelial Cancer

F. F. Dreßler^{1,2}, S. Hinrichs², M. C. Roesch³, S. Perner^{2,4}

¹Charité - Universitätsmedizin Berlin, Institut für Pathologie, Berlin, Germany, ²Universität zu Lübeck und UKSH Campus Lübeck, Institut für Pathologie, Lübeck, Germany, ³Universität zu Lübeck und UKSH Campus Lübeck, Klinik für Urologie, Lübeck, Germany, ⁴Pathologie des Forschungszentrum Borstel, Leibniz Lungenzentrum, Borstel, Germany

Questions/Background

The role of the epithelial cell adhesion molecule (EpCAM) in cancer is still unclear. EpCAM cleavage through regulated intramembrane proteolysis results in fragments which interact with both oncogenic and tumor suppressive pathways, while glycosylation results in even more proteoforms. Also, the EpCAM molecule itself is used as a descriptive therapeutic target in urothelial cancer (UC), while data on its actual tumor specificity remains limited.

Methods

Samples from diagnostic formalin-fixed paraffin-embedded (FFPE) UC tissue and fresh-frozen UC cells were immunoblotted and used for qualitative characterization of five different EpCAM proteoforms. These expression patterns were quantified across a cohort of 76 samples with 52 UC and 24 normal urothelial samples and validated with liquid chromatography-coupled tandem mass spectrometric proteomic data. Cell viability effects of the extracellular EpEX fragment were assessed in the UC cell lines T24 and HT1376.

Results

The proteolytic EpCAM fragments could be identified in clinical FFPE tissue specimens. Neither overall nor proteoform-specific EpCAM expression showed relevant tumor specificity. EpEX and its deglycosylated variant showed an inverse relationship across healthy and tumor tissue with a decrease of deglycosylated EpEX in tumors. Amongst tumors, higher deglycosylated EpEX was favourably associated with longer overall survival. Adding extracellular EpEX, however, did not show a relevant effect *in vitro*.

Conclusion

EpCAM should not be regarded as tumor-specific in UC without patient-specific predictive testing. EpCAM proteoform patterns indicate cancer-specific changes and could be involved in its complex tumor-biological role.

P.03.03

Reverse transcriptases of endogenous retroviruses and LINE1 synthesize RNA:DNA hybrids induce inflammation in muscle invasive bladder cancer

S. A. Köhler¹, V. Mößler¹, L. Anheuser², A. Bauer², V. Bahlinger², P. L. Strissel³, M. Eckstein², A. Hartmann², M. W. Beckmann¹, R. Strick¹

¹Universitätsklinikum Erlangen, Frauenklinik, Erlangen, Germany, ²Universitätsklinikum Erlangen, Institut für Pathologie, Erlangen, Germany, ³Universitätsklinikum Erlangen, Institut für Pathologie, Erlangen, Germany

Question/Background

Endogenous retroviruses (ERVs) are epigenetically silenced and become activated in a variety of diseases. The role of ERVs in muscle invasive bladder cancer (MIBC) is unknown. We showed that ERVs induce an inflammatory response via double strand RNA (dsRNA). In addition, ERVs (ERV-K pol) and the retroposon LINE1 (ORF2) have enzymatic active reverse transcriptase (RT), which synthesize RNA:DNA hybrids. We want to investigate the influence of ERV and LINE1 derived RNA:DNA intermediates in MIBC for inflammatory processes and cell proliferation.

Methods

MIBC cells, RT112 (luminal), SCaBER (basal) and T24 were transfected with synthetic 60 nt long non-homopolymeric dsRNA and RNA:DNA structures. Expression of 66 cellular genes involved in immune response and inflammation, among others, was determined via qPCR. Cell proliferation was measured and visualized via live cell imaging. LINE1-ORF2 was transfected into RT112 for 20 hrs. RNA:DNA hybrids were shown by immunofluorescence using the specific S9.6 antibody. ERV-K103-pol mRNA was *in vitro* transcribed and transfected into RT112. A polyclonal antibody for ERV-K-pol was established to verify ERV-

K103-pol protein expression in cells.

Results

DsRNA and RNA:DNA induced a higher immune response in the luminal and basal cell lines, compared to T24. Especially *ZBP1*, interferons (*IFNA*, *IFNB1*) and cytokines (*CXCL8*, *IL-6*) showed a higher expression after transfection. This effect was more enhanced after dsRNA transfections. Live cell proliferation assays showed significantly reduced cell proliferation after transfection of dsRNA. Transfected MIBC cells with cloned LINE1-ORF2 showed significant higher levels of RNA:DNA hybrids using the S9.6 antibody, supporting a functional RT activity. Immunohistochemistry of ERV-K103-pol mRNA transfected RT112 with a novel ERV-K pol antibody verified protein expression *in vitro*.

Conclusion

ERV intermediates like dsRNA and RNA:DNA induce a high inflammatory response in cells. DsRNA showed an antitumor response by inhibiting cell proliferation. These findings, along with a better survival of MIBC patients with high ERV expression and inflammation signature, highlight the importance of ERVs in MIBC. Further investigations will address the molecular and cellular function of RNA:DNA hybrids derived from ERV-K103-pol and LINE1-ORF2. Additional RT activity and inhibitory assays will provide more information about the importance of ERV-K-pol and LINE1-ORF2 in MIBC tumorigenesis and inflammation.

P.03.01

TACSTD2 (Trop2) Expression on the urothelial Carcinoma (UC): Immunohistochemical Study

M. Abbas¹, C. Bernemann², M. Boegemann³, A. J. Schrader⁴, K. Schlack³, E. Wardelmann¹, B. Heitplatz⁵

¹Universitätsklinikum Münster, Gerhard-Domagk-Institut für Pathologie, Münster, Germany, ²Universitätskliniken Münster, Münster, Germany, ³Universitätskliniken Münster, Urologie, Münster, Germany, ⁴Universitätsklinikum Münster, Urologie, Münster, Germany,

⁵Gerhard-Domagk-Institut für Pathologie, Pathologie, Münster, Germany

Question/Background

In metastatic or locally advanced urothelial cancer, therapeutic options have been limited to chemotherapy and checkpoint inhibitors. Recently, new targets and medications like antibody drug conjugates have been developed with Enfortumab Vedotin targeting Nectin-4 and Sacituzumab Govitecan targeting Trop2 (a protein product of the TACSTD2 gene) being approved. We investigated the expression of Trop2 within urothelial and other carcinoma and within the tissue of different healthy organs to understand treatment response and toxicities.

Methods

We retrospectively analyzed the tissue of 66 patients including urothelial carcinoma in 42 tissue samples, other cancer types in 13 cases and normal tissue of 11 patients. Immunohistochemical staining of the Trop2 protein was performed on a VENTANA BenchMark ULTRA autostainer (Ventana) according to accredited staining protocols in a routine immunohistochemically accredited and certified facility.

Results

We observed different expression levels, the highest rate was observed in urothelial carcinoma, independent of the stage. However, normal urothelial cells had similar expression levels. Except ductal carcinoma in situ (DCIS), the expression was lower in other cancer types and very low in healthy tissue from other organs.

Conclusion

Given treatment response according to expression level of Trop2, we expect that Sacituzumab Govitecan will be effective in almost all cases of urothelial carcinoma. However, it will also have effect on the normal urothelium.

P.03.04

Surrogate Immune Marker Analysis for Simplified Molecular Classification in Upper Tract Urothelial Carcinoma

A. Löwl¹, J. Oldenburg², S. Kdimati¹, A. Erbersdobler¹, A. Zimpfer¹

¹Institut für Pathologie, Universitätsmedizin Rostock, Rostock, Germany, ²Institut für Implantattechnologie und Biomaterialien e.V., Universität Rostock, Rostock, Germany

Questions/Background

Upper tract urothelial carcinoma (UTUC) occurs in about 5% of all urothelial carcinomas (UCs). A recently published consensus classification divides muscle-invasive UC of the bladder (MIBC) into different molecular groups, including luminal, basal, and non-basal-non-luminal (NLNB) subtypes. So far, there are few investigations on whether the consensus classification and its prognostic value is applicable on UTUC. Our aim was to classify UTUC into basal, luminal, and NLNB subtypes according to consensus classification for

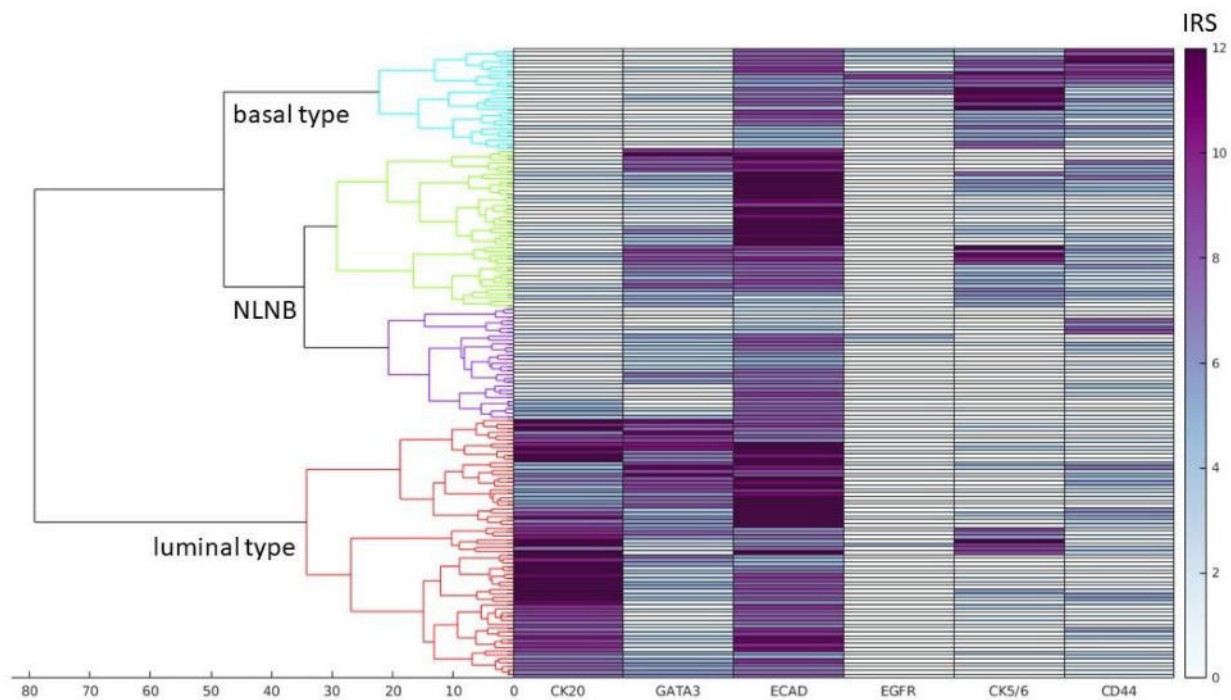
MIBC by evaluating the immunohistochemical expression of indicative proteins and to investigate the prognostic implications.

Methods

Using tissue microarrays (TMA), 224 UTUCs were immunohistochemically analyzed for the expression of six luminal/basal markers and two markers for neuroendocrine-like (NEL) UTUC. Except for CD56 and synaptophysin, which were considered positive when expressed >2% in tumor cells, the immunoreactive score (IRS) was applied to evaluate CK20, GATA3, CK5/6, CD44, ECAD, and EGFR. Hierarchical clustering of the IRS values of invasive UTUC was performed using Euclidean distance and ward-linkage clustering. Morphologic features including the presence of a distinct mesenchymal stroma as well as variant histology according to the updated WHO classification were determined on full tissue sections. Survival analyses evaluated the prognostic value of the molecular subgroups.

Results

All luminal or basal markers were evaluable in 163 invasive UTUC, which were clustered as follows: 67 luminal, 26 basal, 29 NLNB with both CK20 and CK5/6 negative, and 41 NLNB with both CK20 and CK5/6 positive (Fig.1).



Legend: Hierarchical cluster analysis of immunoreactive scores shows that the invasive cohort can be clustered into four groups with a silhouette value of 0.215.

Comparing to UTUCs of the other three subgroups, the patients with UTUC classified as luminal-like showed a significant shorter overall survival (OS) ($p=0.026$). Comparing to luminal type, NLNB being both CK20 and CK5/6 positive showed a significant longer OS ($p=0.004$). Correlation analyses revealed significant differences between the four UTUC clusters and conventional morphology ($p=0.027$), the presence of squamous differentiation ($p=0.015$), or variant histology ($p=0.010$).

Conclusion

UTUCs can be classified into four subgroups using a surrogate immune marker panel. UTUCs with dual expression of CK20 and CK5/6 characterize carcinomas with significantly longer OS.

P.03.05

The ETS transcription factor ELF3 regulates the matrisome of invasive bladder carcinoma via SERPINB2

C. Van Wymersch¹, M. Rogg¹, M. Werner¹, O. Schilling^{1,2}, C. Schell^{1,2}

¹Institute of Surgical Pathology, Faculty of Medicine, Medical Center - University of Freiburg, Freiburg, Germany, ²Freiburg Institute for Advanced Studies (FRIAS), University of Freiburg, Freiburg, Germany

Question/Background

Recent molecular classification systems have described ECM-rich subtypes in muscle invasive bladder cancer (MIBC) characterized by aggressive clinical disease course. The tumor microenvironment (TME) and in particular the matrisome can be assumed as a major defining factor for these ECM-rich cancer subtypes.

However, signaling pathways and transcriptional programs modulating matrisome features of MIBC are ill-defined.

Methods

TCGA, HPA and proteomic datasets of MIBC specimens were analyzed to characterize matrisome diversity and composition. Additional transcriptome analysis via RNASeq of bladder cancer cell lines was performed. Further functional analysis of identified transcription factors and candidate genes was completed employing a cohort of MIBC cases and genetic titration/knockdown approaches (including gap closure assays, western blot, immunofluorescence microscopy).

Results

MIBC specimens and cancer cell lines revealed large heterogeneity of synthesized ECM. The ETS transcription factor ELF3 was identified as a potential regulator of matrisome composition in BC. Loss of ELF3 is associated with mesenchymal cellular features, altered matrisome differentiation and decreased immune cell infiltration. Re-expression of ELF3 in T24 cancer cells reverted migratory features.

Mechanistically, ELF3 induced expression of prognostic beneficial matrisome components and suppressed expression of matrisome components associated with a negative prognosis like SERPINB2. Consequently, forced expression of SERPINB2 resulted in pro-migratory cellular phenotypes.

Conclusion

Our observations indicate a potential prognostic role of matrisome composition in MIBC. Moreover, identification of ELF3 demonstrated how cancer cell inherent features instruct the matrisome and TME. Further studies are required to examine additional functional consequences of ELF3 and SERPINB2 within the TME in vivo and in vitro. Finally, matrisome components like SERPINB2 might serve as novel biomarkers and therapeutic targets for invasive bladder cancer.

P.03.06

CKLF-like MARVEL Transmembrane Domain Containing Protein 6 and Programmed Cell Death Ligand 1 as Prognostic Biomarkers in Upper Tract Urothelial Carcinoma

S. Kdimati, C. Christoph, A. Erbersdobler, A. Zimpfer

Institut für Pathologie, Universitätsmedizin Rostock, Rostock, Germany

Question/Background

Upper tract urothelial carcinoma (UTUC) accounts for only 5-10% of all UC. Besides the conventional treatment, immunotherapy has been established for UCs due to their high immunogenicity. For platinum unfit UC patients the evidence supports atezolizumab (anti-Programmed Cell Death Ligand 1 (PD-L1)) and pembrolizumab (anti-PD-1). Even though immune checkpoint inhibitors have been reported to show durable responses and acceptable safety profiles, up to 80% of the patients may not respond to the new therapy. In several studies, chemokine-like MARVEL transmembrane domain-containing 6 (CMTM6) has been identified as a positive regulator of PD-L1. The evaluation of CMTM6 in UTUC cases could provide insights into the mechanisms of immune checkpoint therapy resistance. CMTM6 as well as PD-L1 may be used as predictive and prognostic markers for expected therapy response. Our aim was to investigate the impact of PD-L1 and CMTM6 protein status on the survival of UTUC patients.

Methods

In a retrospective study of 124 invasive UTUCs, the combined positive score (CPS) for PD-L1 was determined. The extent of CMTM6 expression in UTUC was represented by different scoring systems: by the immunoreactive score (IRS; ≥ 6 CMTM6 "high") the extent and expansion of PD-L1 expression in UTUC, furthermore CPS (threshold CPS ≥ 90 ; "high"), the immune cell score (ICS; threshold ICS ≥ 50 ; "high"), and the tumor proportion score (TPS; threshold TPS ≥ 60 ; "high"). Marker expressions were correlated with various morphological parameters such as the extent of chronic inflammation and desmoplastic stromal reaction as well as other clinicopathological parameters followed by survival analyses.

Results

High PD-L1 expressions (CPS ≥ 10) were detected in 29.3% of the cases, whereas high CMTM6 expression rates on the basis of IRS, ICS, TPS, and CPS were seen in 31.1%, 37.0%, 61.4%, and 58.0%, respectively. Multivariate analysis revealed a statistically significant association between high CMTM6 ICS and longer overall survival (OS) ($p=0.034$). In addition, positive correlations were found between high PD-L1-CPS and high CMTM6-CPS ($p=0.011$), higher chronic inflammation intensity ($p=0.003$), greater WHO grade ($p=0.041$), lack of angioinvasion ($p=0.033$), death ($p=0.009$), and disease progression ($p=0.025$). A high CMTM6 CPS score correlated with death ($p=0.034$) and disease progression ($p=0.034$).

Conclusion

This study reveals that PD-L1 and CMTM6 expression correlate with clinical outcome and may be useful as prognostic biomarkers in UTUCs.

P.03.07

Evaluation of immunohistochemical markers for neuroendocrine carcinomas of the bladder and prostate

E. Hammad¹, J. Möller¹, M. Rose¹, I. V. Samarska², D. Jonigk¹, N. T. Gaisa¹

¹RWTH Aachen University Hospital, Institute of Pathology, Aachen, Germany, ²GROW School for Oncology & Reproduction, Maastricht University, Medical Centre, Department of Pathology, Maastricht, The Netherlands

Question/Background

Neuroendocrine carcinomas of the bladder and prostate are rare malignomas. Histologically, most carcinomas show characteristic small cell carcinoma morphology, and the current WHO classification allows diagnosis even without expression of neuroendocrine markers in histomorphologically striking cases. However, immunohistochemical verification of neuroendocrine differentiation is recommended, and therefore we evaluated the performance of different immunohistochemical antibodies to detect neuroendocrine differentiation in bladder and prostate neuroendocrine carcinomas.

Methods

We used tissue microarrays of n=19 bladder and n=11 prostate neuroendocrine carcinomas to study immunohistochemical expression of synaptophysin, chromogranin A, ISL1, INSM1, CD56, NSE, TTF1, CK, Ki67 and p53 and evaluated expression by a modified immunoreactive score (IRS), proposed by Remmele and Stegner. Additionally, a molecular subtype consensus panel consisting of GATA3, FOXA1, CK5/6, CK14, and Vimentin was evaluated in bladder tumors.

Results

In neuroendocrine bladder carcinomas, the most predominant marker (IRS≥3) was synaptophysin showing expression in 16 out of 18 (88.9%) cases. Moreover, 9/18 tumors (50%) were characterized by strong synaptophysin expression (IRS 9-12). We also observed expression (IRS≥3) of INSM1 (73.7%), CD56 (52.6%), ISL1 (52.6%), and chromogranin A (31.6%). Both NSE and TTF1 were rarely expressed (2/19 cases). For p53 we found an aberrant expression (i.e. IRS =0 or IRS=12) in 13/18 of cases while 13/18 cases were positive for CK staining. All neuroendocrine bladder tumors showed a median Ki67 expression of 85%. Interestingly, a close correlation of synaptophysin and INSM1 expression was calculated (Spearman $r=0.89$, $p<0.001$). Surprisingly, when applying the molecular consensus markers, a basal or luminal phenotype was found in five tumors; two out of three basal phenotypes showed no neuroendocrine marker expression at all.

In prostate neuroendocrine carcinomas marker expression was comparable with an IRS≥3 of synaptophysin in 11/11 (100%), INSM1 9/11 (81.8%) and chromogranin A 8/11 (72.7%) cases. Median Ki67 expression was also 85%.

Conclusion

Synaptophysin and INSM1 were most promising to serve as qualified markers for neuroendocrine differentiation in bladder and prostate carcinomas. Thus, both markers will be further validated in larger cohorts to confirm their diagnostic impact.

P.03.08

ICAM-1 as a potential predictive marker for immune checkpoint inhibitor response in bladder cancer

A. Freude¹, E. Jüngel², M. Brandt², A. Haferkamp², S. Försch³, W. Roth³, D.-C. Wagner³

¹Universitätsmedizin Leipzig, Institut für Pathologie, Leipzig, Germany, ²Universitätsmedizin Mainz, Klinik für Urologie und Kinderurologie, Mainz, Germany, ³Universitätsmedizin Mainz, Institut für Pathologie, Mainz, Germany

Question/Background

Immune checkpoint inhibitors (ICI) have been approved for the treatment of locally advanced or metastasized muscle-invasive bladder cancer (MIBC), either in first-line or following cisplatin-based

chemotherapy. This first line therapeutic approach is biomarker-dependent, i.e. a minimal expression of PD-L1 on tumors cells and/or immune cells is necessary. However, a substantial number of MIBC patients fail to respond to ICI despite being PD-L1 positive. The adhesion molecule ICAM-1 is an integral component of the immunological synapse that is in turn essential for an adaptive anti-tumor immune response. We therefore hypothesized that the tumor expression of ICAM-1 could predict ICI response in MIBC.

Methods

We first determined PD-L1 and ICAM-1 expression as well as the density of CD8+ cytotoxic T cells (CTL) in tissue microarrays of 385 MIBC by means of immunohistochemistry and digital quantitative image analysis (QuPath). Optimal cut-off values to predict overall survival (OS) were evaluated using maximally selected rank statistics. This workflow was repeated in a second cohort of 22 MIBC patients that have been treated with ICI.

Results

The investigation of PD-L1 and ICAM-1 expression revealed three groups of patients: (1) PD-L1^{high}/ICAM-1^{high} (10,6%), (2) PD-L1^{high}/ICAM-1^{low} (45,9%) and (3) PD-L1^{low}/ICAM-1^{low} (43,2%). Double expression of PD-L1 and ICAM-1 was associated with significantly better OS and increased CTL density. In MIBC patients that received ICI, OS after therapy was significantly improved in patients with high ICAM-1 expression and high CTL density.

Conclusion

ICAM-1 expression is a favourable prognostic factor in PD-L1 positive MIBC and is associated with an increased adaptive anti-tumor immune response. Preliminary findings from a small treatment cohort suggest that ICAM-1 expression and CTL density could predict response to ICI therapy in MIBC.

P03 Postersitzung Uropathologie II

P03.09

The human telomerase reverse transcriptase (hTert) single nucleotide polymorphisms (SNPs) rs2736100 and rs2853669 are not associated to tumor characteristics in renal cell carcinoma (RCC).

C. Stöhr¹, R. Stöhr¹, S. Wach², H. Taubert², A. Hartmann¹

¹Institute of Pathology, University Hospital Erlangen-Nürnberg, Friedrich-Alexander-Universität Erlangen-Nürnberg, Erlangen, Germany,

²Department of Urology, University Hospital Erlangen-Nürnberg, Friedrich-Alexander-Universität Erlangen-Nürnberg, Erlangen, Germany

Question/Background

Compensating for telomere shortening upon proliferation is crucial for cancer cells to prevent genomic aberrations. In this context, conserving telomeres via activation of hTert expression is the mechanism best understood. Besides hotspot mutations in the hTERT promoter region, which create de novo binding motifs for ETS2 transcription factors, several SNPs are linked to susceptibility or prognosis in various cancer types. As rs2853669 putatively disrupts an ETS2 binding site in the hTERT promoter and rs736100 is located at intron 2 of hTert and was hypothesized to influence transcription, both might influence the clinical course of patients with renal cell carcinoma (RCC). Our aim was to determine the genotype distribution of both SNPs in a cohort of consecutive RCC patients.

Methods

We extracted DNA from 438 formalin-fixed paraffin-embedded (FFPE) tumors and adjacent normal kidney tissues from consecutive RCC patients of different subtypes (WHO 2016) with the Qiagen AllPrep DNA/RNA FFPE and genotyped the samples by pyrosequencing using the Qiagen PyroMark Gold Q24 system and reagents including custom primers and probes.

Genotype and allele distributions were tested for associations to tumor characteristics and survival with and without the inclusion of the previously determined hot spot promoter mutation statuses by two sided exact Chi² tests, log rank tests, Kaplan Meier estimates and multivariate Cox analysis using IBM SPSS Statistics Version 28.0.0.0.

Results

Genotype distributions were as follows: 58/431 (13.5%) C/C, 180/431 (41.8%) C/T, 193/431 (44.8%), T/T for rs2853669 and 112/429 (25.8%), 223/429 (51.4%), 94/429 (22.8%) for rs 2736100 in normal tissues. Genotypes or alleles of both SNP did not correspond with any tumor characteristics. Only presence of

rs2853669_C was associated to better DSS ($P = 0.029$), but not OS ($p = 0.051$). On inclusion of hotspot promoter mutation information, the association was only found in patients with wildtype promoters ($p = 0.038$). Upon multivariate Cox analysis also including tumor characteristics and hotspot promoter information, rs2853669 allele was not an independent predictor of DSS.

Conclusion

Although rs2853669_C may be protective in RCC regarding disease specific survival in patients with wildtype promoters, classical tumor characteristics outcompete this effect.

P03.11

Diagnostic and prognostic aspects of intratumoral morphological heterogeneity in clear cell renal cell carcinoma

P. Stenzel¹, S. Frees², K. Tagscherer¹, C. Justenhoven³, A. Haferkamp², S. Macher-Goeppinger¹, W. Roth¹, S. Porubsky¹

¹Institut für Pathologie, Universitätsmedizin Mainz, Mainz, Germany, ²Klinik für Urologie, Universitätsmedizin Mainz, Mainz, Germany,

³Krebsregister Rheinland-Pfalz, Mainz, Germany

Questions/Background

Clear cell renal cell carcinoma (ccRCC) displays a typical morphology in most cases. However, the correct classification of a renal neoplasm as ccRCC can be impaired through a marked heterogeneity in tumor architecture, cytomorphology and tumor microenvironment.

Methods

749 cases of ccRCC with corresponding clinicopathological information were collected and further used for construction of a tissue microarray (TMA). All cases were histologically reviewed and information on growth patterns, cytomorphology, tumor cell necrosis, fibrosis and amount of infiltrating immune cells was collected. The TMA was immunohistochemically stained against vimentin, CK7, CD10, RCC, racemase and CD117 and the expression semiquantitatively scored. The relationship between morphological and immunohistochemical results and the impact on patients' prognosis were examined.

Results

We identified three prognostic risk groups based on the morphological heterogeneity of ccRCC. The risk groups showed statistically significant differences in the immunohistochemical expression profiles. Moreover, the extent of vimentin and RCC expression in ccRCC tumors could further stratify the high risk group regarding disease specific survival, overall survival and progression free survival.

Conclusion

The correct classification of a renal neoplasm as ccRCC is usually straightforward in cases of typical morphology. However, we could show in this study, that ccRCC consists of a heterogeneous group of morphological patterns with impact on the expression of immunohistochemical markers and patients' prognosis. Knowledge on this issue can assist in finding the correct diagnosis in difficult cases and moreover provide valuable information for clinical surveillance and further therapy.

P03.12

No evidence for recurrent, functional mutations in exon 9 of the GPS1 gene in penile squamous cell carcinoma

R. Stöhr¹, O. Wendler², J. Giedl¹, N. Gaisa³, G. Richter⁴, V. Campean⁵, M. Burger⁶, B. Wullich⁷, S. Bertz¹, A. Hartmann¹, L. Tögel¹

¹Universitätsklinikum Erlangen, Institut für Pathologie, Erlangen, Germany, ²Universitätsklinikum Erlangen, Hals-Nasen-Ohren-Klinik –

Kopf- und Halschirurgie, Erlangen, Germany, ³Uniklinik RWTH Aachen, Institut für Pathologie, Aachen, Germany, ⁴Institut für Pathologie, Hameln, Germany, ⁵Institut für Pathologie, Ansbach, Germany, ⁶Universitätsklinikum Regensburg, Lehrstuhl für Urologie am Caritas-Krankenhaus St. Josef, Regensburg, Germany, ⁷Universitätsklinikum Erlangen, Urologische und Kinderurologische Klinik, Erlangen, Germany

Question/Background

Penile squamous cell carcinoma (SCC) is a rare, but biologically aggressive disease. The molecular alterations driving penile carcinogenesis in detail are still not clear and are therefore the focus of various research efforts. Recently, GPS1 (*G Protein Pathway Suppressor 1*, *COPS1*, *CSN1*) has been identified as frequently mutated gene in penile SCC (in 11% of all cases). GPS1 represents an essential component of the highly conserved COP9 signalosome complex (CSN). The CSN complex regulates the activity of E3

ubiquitin ligase complexes, and plays a critical role in the regulation of various cellular processes, including cell cycle control and DNA repair. Two of the reported, recurrent GPS1 mutations (p.D382H and p.M384I, located in exon 9) showed a functional relevance in *in vitro* studies (disruption of miRNA-mediated gene silencing in HeLa cells) suggesting these two mutations as oncogenic drivers for penile SCC. To date, no other study verified the presence of GPS1 p.D382H and p.M384I mutations in penile SCC. Therefore, we performed a sequence analysis of GPS1 exon 9 of an in-house penile SCC patient cohort to further validate the occurrence of these two mutations.

Methods

After microdissection, DNA was isolated from archival tumorous tissue of 106 penile SCC cases. Exon 9 of the GPS1 gene was analysed using Sanger sequencing. HPV detection in the SCC tissue was done utilizing GP5+/6+ primers followed by subtype-specific PCR.

Results

HPV analysis gave interpretable results for 104/106 cases. HPV DNA was detected in 38,5% of the penile SCC cases. Sanger sequencing of exon 9 of the GPS1 gene was successful in 104/106 cases. The reported, functional relevant GPS1 mutations p.D382H and p.M384I were not found in our cohort. However, two other GPS1 sequence alterations were detected in two cases: p.S372F (c.1115C>T) and p.A375D (c.1124C>A). In addition, the already described GPS1 SNP rs34689427 was detected with a MAF of 4,7% in our patient cohort which is in line with previously reported MAFs from several European population cohort studies.

Conclusion

The previously reported recurrent, functionally relevant GPS1 mutations were not detected in our large cohort of penile SCC arguing against their high prevalence in SCC. Nevertheless, GPS1 exon 9 sequence alterations are a feature of penile SCC but due to their low frequency and non-recurrent distribution, they do not seem to act as oncogenic drivers of the disease.

P03.13

Retrospective proteomics-analysis for the identification of tumour-resident protein markers for personalized risk and therapy stratification in prostate cancer patients

P. Bernhard^{1,2,3}, A. Chaves¹, K. Kurowski¹, P. Bronsert¹, C. Zamboglou⁴, A.-L. Grosu⁴, M. Werner¹, O. Schilling¹

¹Institute for Surgical Pathology, University Medical Center Freiburg, Freiburg, Germany, ²Spemann Graduate School of Biology and Medicine (SGBM), University of Freiburg, Freiburg, Germany, ³Faculty of Biology, University of Freiburg, Freiburg, Germany,

⁴Department of Radiation Oncology, University Medical Center Freiburg, Freiburg, Germany

Question/Background

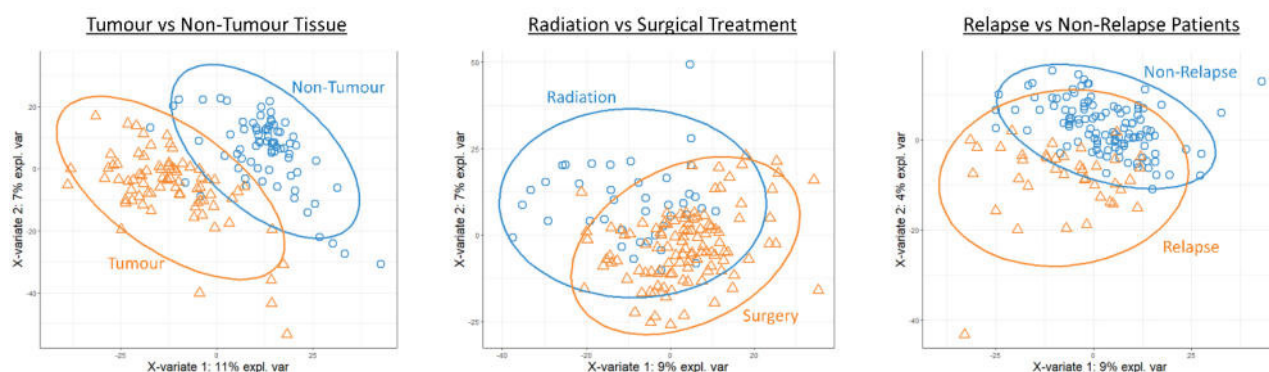
Prostate cancer (PCa) is the most frequently diagnosed neoplasm in men and represents the third leading cause of cancer mortality. Different therapy options are available for localized PCa including either radical prostatectomy, radiation therapy or active surveillance. However, all three therapy options may achieve almost comparable response rates [1]. This demonstrates that current diagnostic and prognostic tools are insufficient for a personalized treatment decision. Therefore, this project aims to find predictive protein profiles for each treatment group that correlate with treatment effectiveness (by means of biochemical relapse) and to enable the differentiation of aggressive from non-aggressive PCa.

Methods

A retrospective deep proteomics analysis is performed on a cohort including 117 patients, either undergoing radical prostatectomy or radiation therapy. Biopsy specimens of the primary, treatment-naïve tumour as well as normal adjacent tissue are available for each patient as formalin-fixed, paraffin-embedded specimens together with clinical-pathological data. Mass spectrometry is used for in-depth proteomics analysis.

Results

Tissue-specific protocol optimization and the application of cutting-edge mass spectrometry methods enabled the identification and quantification of > 4000 proteins per sample from smallest tissue amounts. Evaluation of the resulting dataset via Partial Least Squares Discriminant Analysis reveals clear differences in the proteomic profiles when comparing tumour and non-tumour tissue samples, radiation and surgical treatment or relapse and non-relapse patients.



Partial Least Squares Discriminant Analysis of acquired protein profiles comparing either tumour and non-tumour tissue samples, radiation or surgical treatment or relapse and non-relapse patients. X- and y-axis represent the percentage of explained variance of the respective component. Ellipses represent 95 % confidence intervals.

Further data processing and in-depth statistical analysis provides deeper insights to the proteomic differences of PCa patients and consequently enable their proper stratification.

Conclusion

The deep and unbiased feature extraction from proteomics data can pave the way for personalized therapy predicting models and risk-profiles in prostate cancer patients.

Literaturangaben:

[1] Hamdy FC, Donovan JL, Lane JA et al. , (2016), 10-Year Outcomes after Monitoring, Surgery, or Radiotherapy for Localized Prostate Cancer., The New England journal of medicine, 1415–1424, 375, <https://doi.org/10.1056/NEJMoa1606220>, 2023-02-23

P03.10

Recommendations of macroscopic examination after nephrectomy for cases with autosomal dominant polycystic kidney disease (ADPKD): Back to basics

M. Abbas¹, M. Pätzelt², A. Thurn³, O. Brinkmann², O. Bettendorf³

¹Universitätsklinikum Münster, Gerhard-Domagk-Institut für Pathologie, Münster, Germany, ²Bonifatius Hospital, Urologie, Lingen, Germany, ³Institut für Pathologie und Zytologie, Pathologie, Schüttorf, Germany

Question/Background

Autosomal dominant polycystic kidney disease (ADPKD) is one of the known genetic diseases. Almost 50% of patients will develop end-stage renal disease and the majority will be treated with renal transplantation. One possible complication is the development of papillary renal cell carcinoma in the native kidney, even many years after renal transplantation.

Methods

A 72-year-old patient, height 180 cm and weight 81 kg (BMI 25) with end-stage renal disease due to autosomal polycystic kidney disease (ADPKD), who received a living kidney graft. He has a family history of ADPKD. There was no medical indication for removal of the native kidneys at time of transplantation.

Results

After 8 years, he develops renal pain, weight loss and bad general condition. Ultrasonography showed bilateral polycystic kidneys and a normal transplanted kidney. Computer tomography showed multiple haemorrhagic cysts. There was a subsequent medical indication for removal of the native kidney. In the gross pathology and due to careful examination, we detected a tumor measuring 4 cm in diameter in the removed kidney. Macroscopic examination revealed it was a papillary renal cell carcinoma.

Conclusion

There is an urgent need for medical screening of patients with ADPKD including urine analysis, ultrasonography and computer tomography in order to avoid missing cases with tumours. After nephrectomy, a careful macroscopic examination should be performed and we suggest cutting the specimen in 5-10 mm thick slices to avoid mishandling and missing serious complication like papillary renal cell carcinoma.

P03.16

Diagnostic pitfall of a urogenital condition with simple solution by conventional histopathological techniques and ultrastructure: Old is gold

M. Abbas¹, A. J. Schrader², E. Wardelmann¹, M. Janssen², P. Barth¹

Question/Background

Background:

Some of urinary bladder diseases, which causes dysuria and microhaematuria because of possible ulcerations of the urothelium of the urinary bladder, may be misdiagnosed from clinicians as neoplastic diseases, as it occurs in most cases in older age. After cystoscopy and clinical examination, there is still doubt, as it appears as a hard yellow plaque with ulcerated surface with associated signs of inflammation, which disables the right clinical diagnosis. The way of the right diagnosis is still in the hand of a pathologist.

Methods

An 87-year old man with recurrent symptoms of urinary bladder infection. He suffers from dysuria and microhaematuria. In 2001 he had a prostatectomy because of prostate carcinoma. He has been staged as pT3a without metastasis, but with Gleason-score of 4+4. In 1970 he had an orchidectomy because of Teratoma. The laboratory analysis revealed an E.coli-infection in urine analysis. In the cystoscopy, the urinary bladder showed multiple small foci and tumour-like yellow areas with ulcerations. Multiple biopsies were taken and sent to histopathology.

Results

In the microscopic examination, there were subepithelial accumulations of macrophages and histiocytes with some intracytoplasmic whorls of calcifications. There were no atypical changes in the rest of the urothelium. We have performed some special stains like Prussian blue iron stain and modified Von Kossa stain, Alcian blue stain, which revealed the presence of intracytoplasmic calcific bodies which called Michaelis-Gutmann bodies. To be sure, we have processed the sample to be investigated with Electron Microscope. After careful examination, we have detected the Michaelis-Gutmann bodies.

Conclusion

After detecting the Michaelis-Gutmann bodies in the cytoplasm of the histiocytes, we were sure, that the condition is only a rare disease of urinary bladder, which affects humans and animals. In humans, there is a wide affection of women and misdiagnosed as a tumour. After histopathological and ultrastructure examination, we will be sure that is a malakoplakia.

P03.14

TROP2 is a possible target but not a prognostic biomarker in prostate cancer

M. Bernhardt¹, P. Krausewitz², J. Ellinger², M. Ritter², G. Kristiansen¹

¹Universitätsklinikum Bonn, Institut für Pathologie, Bonn, Germany, ²Universitätsklinikum Bonn, Klinik und Poliklinik für Urologie und Kinderurologie, Bonn, Germany

Question/Background

Prostate cancer is the most common malignancy in men in the western world and ranks amongst the leading cause of death.

TROP2 is a cell surface protein involved in embryonic and fetal development. In cancer tissue it plays a role in cell renewal and proliferation. TROP2 has been shown to be upregulated in several cancers including breast, ovarian, pancreatic and prostate cancer.

Antibody drug conjugates are a novel kind of drugs that enable direct targeting of cancer cells by attaching a cytotoxic drug directly to an antibody. Antibodies used in the approach are raised against structures on cancer cells but not healthy tissue, thereby reducing treatment side effects. TROP2 is a promising target for ADCs as it is not strongly expressed in most healthy tissues.

Methods

TROP2 expression was tested by immunohistochemistry in a large cohort of primary prostate cancers (n=197) using a TMA based approach.

Results

TROP2 expression was scored semiquantitatively (Score 0, 1+, 2+, 3+) and could be detected in 97.5 % of prostate cancers, with most cancers showing a moderate (2+) expression. There was no significant association between intensity of expression and progression free survival, ISUP grade, pT- or pN-Stage. There was a tendency towards a strong expression of TROP2 and loss of androgenreceptor.

Conclusion

TROP2 does not serve as a prognostic biomarker but is strongly expressed in most primary prostate cancers

regardless of differentiation.

P03.15

BRD9 inhibition as potential treatment option for testicular germ cell tumors

A. Hansen, K. Funke, L. Arévalo, H. Schorle

Institut für Pathologie, Universitätsklinikum Bonn, Entwicklungspathologie, Bonn, Germany

Questions/Background

Testicular germ cell tumors (TGCT) represent the most common tumor in young men [1]. While curation rates are high, 15-20 % of patients with metastatic non-seminomas develop resistance to chemotherapy [2,3]. In prostate cancer, glioblastoma and breast cancer using inhibitors of BET proteins (BRDT, BRD2, BRD3 and BRD4) interfering with the epigenetic landscape was already shown to be effective [2]. The bromodomain protein BRD9 is an epigenetic reader modulating gene expression by recruiting transcription factors [4]. BRD9, a member of the SWI/SNF chromatin remodeling complex, showed significantly increased protein levels in acute myeloid leukemia (AML) cells, overexpression in cervical cancer and high expression in malignant rhabdoid tumor (MRT) cells [5]. Therefore, we addressed the question whether BRD9 is also overexpressed in TGCTs and if inhibition of BRD9 by the inhibitor I-BRD9 impacts viability, cell cycle distribution and apoptosis rate in TGCT cell lines. Further, we investigated the impact of BRD9 inhibition on changes of global gene expression. The most important goal was to investigate whether I-BRD9 could be a possible alternative treatment option for TGCTs.

Methods

BRD9 expression in TGCT cell lines was determined by meta-analysis of microarray data and on protein level by Western Blot. XTT-assay was performed to evaluate the impact of I-BRD9 treatment on viability of cells. Cell cycle arrest as well as apoptosis rate were analyzed by FACS after treatment with I-BRD9. 3'mRNA-sequencing was performed after I-BRD9 treatment to determine differentially expressed genes caused by inhibition of BRD9.

Results

TGCT cell lines showed strong decrease in viability after treatment with I-BRD9 whereas the control cell line was hardly affected. FACS analysis revealed increased apoptosis and cell cycle arrest in G1-phase in TGCT cells treated with I-BRD9. Analysis of 3'mRNA-sequencing data showed downregulation of pluripotency markers such as NANOG and KLF4 in TGCT cell lines after I-BRD9 treatment. Inhibition of BRD9 led to exit of pluripotency and upregulation of genes associated with neuronal differentiation.

Conclusion

I-BRD9 strongly reduces viability, initiates cell cycle arrest and apoptosis in TGCT cells while control cells remain mostly unaffected. Further, transcriptomic data indicate exit of pluripotency and differentiation towards the neuronal fate. The data suggest I-BRD9 as an effective treatment option for TGCTs, especially in the situation of cisplatin resistance.

Literaturangaben:

- [1] Balk C, Witjes JA, (2004), Advances in the management of testicular cancer, Expert Rev Anticancer Ther, 669-77, 4(4), doi:10.1586/14737140.4.4.669, 2023-03-03
- [2] Jostes S, Nettersheim D, Schorle H, (2019), Epigenetic drugs and their molecular targets in testicular germ cell tumours, Nat Rev Urol, 245-259, 16(4), doi:10.1038/s41585-019-0154-x., 2023-03-03
- [3] Singh R, Fazal Z, Freemantle SJ, Spinella MJ, (2019), Mechanisms of cisplatin sensitivity and resistance in testicular germ cell tumors, Cancer Drug Resist, 580-594, 2(3), doi: 10.20517/cdr.2019.19, 2023-03-03
- [4] Ali MM, Naz S, Ashraf S, Knapp S, Ul-Haq Z, (2023), Epigenetic modulation by targeting bromodomain containing protein 9 (BRD9): Its therapeutic potential and selective inhibition, Int J Biol Macromol, 123428, 230, doi: 10.1016/j.ijbiomac.2023.123428, 2023-03-03
- [5] Zhu X, Liao Y, Tang L, (2020), Targeting BRD9 for Cancer Treatment: A New Strategy, Onco Targets Ther, 13191-13200, 13, doi: 10.2147/OTT.S286867, 2023-03-03

P04 Postersitzung AG Gynäkopathologie und Mammopathologie

P.04.06

HPV-genotyping versus conventional cervical cytology as a screening method to detect dysplastic cervical epithelial changes

M. Abbas¹, J. de Jonge², O. Bettendorf²

¹Universitätsklinikum Münster, Gerhard-Domagk-Institut für Pathologie, Münster, Germany, ²Institut für Pathologie und Zytologie, Schüttorf, Germany

Question/Background

Cytology-based screening has been for decades the conventional method of screening. Ancillary techniques like immunocytochemistry (P16/Ki67) were added to deliver the best results of diagnosis. In Germany, at the beginning of 2020, a Co-test-based screening program was applied for each woman above 35 years old. This study will analyze, which HPV-subtypes are common and when they will appear and which age groups are susceptible to produce dysplasia under HPV infection. It will show the distribution of these HPV-subtypes in the different age groups.

Methods

In the Institute for Pathology and Cytology-Schüttorf-Leer-Germany 210.510 samples of women in the screening program were investigated between the beginning of January 2020 until the beginning of January 2021. The samples were processed for both conventional cytological technique and molecular detection and subtyping of HPV according to the advice and measurements of BD-manufacture.

Results

Under the age of 35 years, there were 0.037% of the cases with HPV 56/59/66, followed by 0.03% with HPV16 and then 35/39/69, 51 with frequency of 0.017%. In the age-group 35–40 years old, there were HPV16 in 1.23%, then HPV56/59/66 in 0.93% followed by HPV35/39/68 and HPV31 with incidence of 0.76%. In the age-group 41–50 years old, there were HPV 56/59/66 in 1.1%, HPV 16 in 1%, HPV 35/39/68 in 0.87% and HPV 31 in 0.66%. In the age-group 51–60 years old, there were HPV 56/59/66 in 0.99%, HPV 16 in 0.7%, HPV 35/39/68 in 0.58%, HPV 31 in 0.42% and HPV 52 in 0.3%. In the age-group over 60 years, there were HPV 16 in 0.67%, HPV 56/59/66 in 0.66%, HPV 35/39/68 in 0.42% and HPV31 in 0.28%.

Conclusion

There are too many HPV-positive cases, which have been psychologically impaired with higher costs, although they have no cervical epithelial changes during the HPV-infection. There are too many HPV-negative cases, which develop cervical cancer. We are of the opinion and are convinced that the screening should be both morphologically via cytological examination and may be with adding immunocytochemistry and the HPV-Genotyping as an automated fast method, but the results of both should be respectively analyzed and both clinicians and patients should be accordingly advised.

P.04.01

Molecular subtyping of breast cancer by Ki67 in the era of artificial intelligence

C. Connolly, Q. Simon, R. Masser, B. Padberg Sgier, S. Hauptmann, J. Friemel, E. Karamitopoulou, B. Bode, M. Tinguely
Pathologie Institut Enge, Zurich, Switzerland

Questions/Background

Oncotype DX, a 21-gene molecular test, has become a gold standard for guiding therapeutic decisions in ER+/HER2- early breast cancers, and has led to a dramatic reduction in adjuvant chemotherapy usage without adversely affecting clinical outcomes. However, Ki67 continues to be used and endorsed as a surrogate marker, alongside ER, PR and HER2, for determining luminal subtypes despite ongoing controversy on the optimal cut-off value. The purpose of this study was to compare the performance of IHC-based luminal subtyping against results of Oncotype DX in our institution, and to investigate a CE-certified artificial intelligence (AI) pathological image Ki67 analysis program for improving subtyping accuracy.

Methods

We evaluated all breast biopsies with B5b-diagnoses at our institute from 2019-2021 (n=1309), and identified 65 cases which were tested with Oncotype DX according to clinician-led requests. We performed a retrospective analysis comparing the accuracy of our IHC-based luminal subtyping against the results of Oncotype DX. Furthermore, we investigated the impacts of VMscope's Ki67 Quantifier (Berlin, Germany) and consensus pathologist Ki67 scoring on concordance rates.

Results

10.5% of the eligible ER+ HER2- patient population underwent clinician-requested multigene testing. We observed consistently higher average Ki67 values in luminal B compared to luminal A tumours (difference 8.2%, $p < 0.01$) and the accuracy of our IHC-based subtyping was 68.9%. A *moderate* correlation was noted between Ki67 and Oncotype DX recurrence score (Spearman's coefficient 0.45, $p < 0.01$). Biopsy Ki67 slides were independently re-scored by 3 breast pathologists and digitalised for assessment by AI. The optimal Ki67 cut-offs for luminal subtyping, as calculated using ROC curve analyses, were 18% (using original reported value), 20% (using AI assessment) and 23% (using consensus pathologist scoring).

Conclusion

Our data provides a snapshot of real-world allocation of Oncotype DX testing by clinicians and supports other studies in highlighting the discrepancy between IHC-based and gene test-based luminal subtyping, which is not readily harmonised by implementing AI for Ki67 assessment.

P.04.02

Sclerosing stromal tumor of the ovary: clinicopathological and immunohistochemical characteristics of eight cases

J. Müller¹, M. Stanik², R. Schatz², F. Noack³, G. Teichmann⁴, A. Dannenmann⁵, G. G. R. Hiller⁶, A. K. Höhn⁶, I. Krücken¹, L.-C. Horn⁶

¹University Hospital Leipzig, Institute of Pathology, Leipzig, Germany, ²Südharz Klinikum Nordhausen, Institute of Pathology, Nordhausen, Germany, ³Institute of Pathology Berlin-Grünwald, Berlin, Germany, ⁴Heinrich-Braun-Klinikum, Department of Gynecology and Obstetrics, Zwickau, Germany, ⁵Sana Kliniken Leipziger Land, Department of Gynecology and Obstetrics, Borna, Germany, ⁶University Hospital Leipzig, Institute of Pathology, Division of Gynecologic, Breast and Perinatal Pathology, Leipzig, Germany

Question/Background

Sclerosing stromal tumor (SST) is a very rare subtype within the group of ovarian sex-cord stromal tumors, occurring mostly in young patients in the 2nd to 3rd decade with benign biological behavior. The tumor is diagnosed on distinct histological features with a recently suggested FHL2-GLI2 fusion as oncogenic driver. The aim of the study is to provide further information on SST, especially the immunohistochemical profile, by analysis of eight cases.

Methods

Clinicopathologic analyses and detailed immunohistochemical examination of the cases.

Results

The patients age ranged from 16 to 68 years (mean = 44 years), with 5/8 being postmenopausal, one showing marked elevated serum CA 125 and one post-menopausal woman showing non-atypical endometrial hyperplasia. Tumor size ranged from 3 to 22 cm (mean = 8 cm). Nearly all tumors had solid white grey yellow cut surface, few with cystic degeneration, one predominantly cystic. On histological examination, pseudobubulation was well formed in 5/8 cases with admixed majorly spindle and luteinized cells as well as ectatic, partly branching vessels. The stroma was typically collagenous, partly with oedematous areas. The mitotic rate with a range of 0 - 1 mitoses/10 HPF. On immunohistochemical analysis, almost all neoplasms expressed calretinin (partly positive 7/8), CD99 (8/8), estrogen/ progesterone receptor (7/8), SMA (spindle cells 7/7). Few expressed desmin (focal positivity of spindle cells 3/7) and WT1 (3/7). Overall no expression of CD10, STAT 6 and CD34. Antibodies against CD34 and WT1 highlighted a dense, delicate vessel network apart from ectatic vessels.

Conclusion

SST generally occurs in the young, although cases in the elderly are reported. Few cases with elevated serum CA 125 and evidence of hormonal manifestation are noted. Common gross and histomorphological features are evident in our cases. Experience on immunohistochemical phenotype is little with low case numbers in literature referring to positivity of calretinin, inhibin, melan-A, vimentin, estrogen/ progesterone receptor, SMA, CD10, WT1 and occasionally desmin and negativity of CD34, S100, caldesmon and cytokeratin. Our study furthermore showed positivity for CD99 and negativity for CD10 and STAT 6. More cases for further understanding of SST are needed to minimize misleading or complicating clinical features

(elevated serum CA 125, large tumor size or hormonal functionality).

P.04.03

p16^{INK4a} immunohistochemistry as a diagnostic marker in endometrial stromal sarcomas

L.-M. Mar¹, C. Kölsche¹, A. von Deimling², P. Schirmacher¹, P. Sinn¹, F. Kommoss¹

¹Institute of Pathology, Heidelberg University Hospital, Heidelberg, Germany, ²Institute of Neuropathology, Heidelberg University Hospital, Heidelberg, Germany

Question/Background

Endometrial stromal sarcomas (ESS) are malignant uterine tumors, which are classified into low-grade ESS (LGESS) and high-grade ESS (HGEES) based on recurrent genomic alterations. Recently co-occurring *CDKN2A* alterations have been described in a subset of HGEES. However, results from larger cohorts of ESS are currently missing. In this study, we investigated *CDKN2A* alterations and p16^{INK4a} (p16) expression in a large cohort of LGESS and HGEES.

Methods

We collected a multicenter cohort of LGESS and HGEES (including *YWHAE*- and *BCOR*-rearranged tumors). Samples were analyzed for copy number of *CDKN2A* using array-based DNA methylation analysis (EPIC). p16 immunohistochemistry was performed using a tissue microarray. Both nuclear and cytoplasmic staining of the tumor cells were evaluated. Staining was considered to be absent if there was a complete lack of cytoplasmic and nuclear staining.

Results

11 LGESS and 12 HGEES samples were available for copy number analysis. While LGESS showed disomy for *CDKN2A* in all tumors, HGEES showed a heterozygous or homozygous deletion of *CDKN2A* in 3/12 (25%) and 4/12 (33%) of tumors, respectively. P16 immunohistochemistry was performed on an extended cohort of 43 LGESS and 17 HGEES. LGESS were negative (21/43, 49%) or showed a weak and only focal p16 expression (22/43, 51%). Most HGEES showed a strong and diffuse positivity for p16 (11/17, 65%). The remaining HGEES exhibited either complete absence of p16 staining (4/17, 24%) or only weak and focal positivity (2/17, 12%). Complete absence of p16 staining in HGEES was highly associated with homozygous deletion of *CDKN2A* in HGEES (4/4).

Conclusion

In contrast to LGESS, most HGEES in our study showed a strong and diffuse p16 expression indicating p16 immunohistochemistry as a novel diagnostic marker in ESS. Furthermore, our study confirms *CDKN2A* deletion with consecutive loss of p16 expression as an oncogenic mechanism in a subset of HGEES, which may represent a novel therapeutic target.

P.04.04

Giant cell tumor of the uterus

T. Tsvetkov¹, J. Meinel¹, E. Piriyev², T. Römer³, D. Schmidt⁴, R. Büttner¹, A. Quaas¹

¹University of Cologne, Institute of Pathology, Cologne, Germany, ²University Witten-Herdecke, Department of Obstetrics and Gynecology Academic Hospital Cologne Weyertal University of Cologne, Cologne, Germany, ³University of Cologne, Department of Obstetrics and Gynecology Academic Hospital Cologne Weyertal University of Cologne, Cologne, Germany, ⁴MVZ of Pathology, Cytology and Molecular Diagnostics, Trier, Germany

Question/Background

CASE REPORT

The tumor was detected in a 61-year-old asymptomatic female patient during a routine gynecologic examination via transvaginal sonography. It was resected in the follow-up hysteroscopy and referred for pathological investigation.

Methods

We report on the uncommon finding of a giant cell tumor in the uterine corpus of a 61-year-old female patient.

Results

Gross Findings

After formalin-fixation, the small tissue fragments with a reconstructed maximal dimension of approximately 6

cm appeared gray to brownish and had a substantial amount of blood clots. They were processed according to specific institutional standards and embedded in paraffin.

Microscopic Findings

Based on H&E-stainings, the lesion consisted of a mixture of round to oval mononuclear cells (at some locations, mononuclear cells with spindle-cell cytology) and osteoclast-like giant cells (OLGC) (Fig.1). Mononuclear cells showed mild focal atypia with a slight variance in nuclear size. While some areas showed predominately round nuclei, there were also regions with increased cell density, spindled nuclei showing occasionally inconspicuous nucleoli. OLGCs did not show any significant cytological atypia. The mitotic activity was restricted to mononuclear cells with up to 5 regular mitotic figures per 10 high-power-fields (HPF). Focal aggregates of foamy histiocytes and larger regression areas with bleeding, hyalinization and cholesterol clefts could be seen. (Fig.1). Multifocally, metaplastic cartilaginous or bony areas without any cytological atypia were evident. Areas of necrosis were not found.

Immunohistochemically, CD68 positivity was present in both OLGCs and mononuclear cells (Fig. 2). Only OLGCs were Cyclin D1 positive, and only mononuclear cells were CD163 positive. Some of the mononuclear cells were focally p63 positive, and some expressed SATB2, especially in areas of bone formation. CD10 positivity was seen focally. Tumor cells were uniformly negative for pan-cytokeratin (AE1/AE3), estrogen receptor, and SOX10. There was no evidence of TP53 alteration ("wild-type" expression pattern of p53). Staining with G34W-antibody yielded a negative reaction in all tumor cells. The Ki67 proliferation index was 10-15% in hotspots, while most areas were under 5% (Fig. 3).

DIAGNOSIS

Giant cell tumor of the uterus

Conclusion

In conclusion, we report on a very rare case of uterine giant cell tumor - a tumor entity with potential aggressive biological behavior reported only in isolated cases so far.

P.04.05

HPV test improves CIN 3 detection in the 2020 launched German cervical cancer screening programme

L. Jung¹, B. Bier², E. Eltze^{1,2}

¹Institute of Pathology, Saarland University, Homburg, Germany, ²Institute of Pathology Saarbrücken Rastpfuhl, Saarbrücken, Germany

Question/Background

In 2020, Germany implemented its revised cervical cancer early detection programme. One of the most important changes is the introduction of the HPV test. The primary objective was to examine the role of the HPV test.

Methods

Data from 15841 patients were gathered from the start of the new screening programme up to a three-year follow-up period and compared with the findings of the years 2015-2019. A spreadsheet in Excel was used to evaluate the data.

Results

At baseline, 9309 (59%) women received an HPV test using the BD Onclarity™ HPV test, of which 781 (8%) tested positive. Regardless of age and HPV test result, 222 (1.4%) abnormal findings regressed during the three-year follow-up period, whereas progression of the initial finding was observed in 110 (0.7%) cases. Regarding these 110 women who showed progression of the initial finding, 59 (54%) were between 35 and 49 years old, 34 (31%) were over 50 years old, 11 (10%) belonged to the 30 to 34 year old group, and only 6 (5%) were under 30 years old. 105 (95.5%) of the 110 women had a positive HPV test result. 75 (71%) of the 105 patients developed cervical intraepithelial neoplasia (CIN1-3), and 34 (45%) of these CIN 3. According to the work-up algorithm, three (2.7%) of the 110 women who showed progression were not tested for HPV because of their young age. Two (1.8%) of the 110 women who demonstrated progression of the initial findings lacked HPV. One of the two women developed a CIN 3 four months after the initial checkup and the other woman developed a Pap IIID2, 20 months after initial Pap IIID1. A total of 42 (0.26% of 15841) women were detected with CIN 2 or higher only because of an initial positive HPV test. Compared to the previous screening programme, 26 (0.16%) women with CIN 3 were detected and treated earlier due to a positive HPV test despite of a negative Pap smear.

Conclusion

In addition to the Pap smear the HPV test for cervical cancer screening exhibits great sensitivity, providing a better opportunity to target follow-up in order to enable early detection.

Molecular classification of vulval cancer: Comparing pre-surgical biopsy and surgical specimen of radical vulvectomy from the same patients

M. Forberger¹, G. G. R. Hiller¹, A.-K. Höhn¹, I. Krücken¹, E. F. Thompson², L. Hoang³, A. Palicelli⁴, K. L. Talia⁵, N. Tchakian⁶, J. Senz², A. Jamieson³, J. Huvila², J. N. McAlpine³, B. Gilks³, M. Höckel⁷, N. Singh⁶, L.-C. Horn¹

¹Institut für Pathologie, Universitätsklinikum Leipzig, Leipzig, Germany, ²Department of Molecular Oncology, BC Cancer Research Centre, Vancouver, Canada, ³Vancouver General Hospital and the University of British Columbia, Vancouver, Canada, ⁴Azienda Unita Sanitaria Locale- IRCCS di Reggio Emilia, Reggio Emilia, Italy, ⁵Royal Women's Hospital and VCS Foundation, Melbourne, Australia, ⁶Barts Health NHS Trust, London, United Kingdom, ⁷Leipzig School of Radical Pelvic Surgery, Division of Gynecologic Oncology, Universitätsklinikum Leipzig, Leipzig, Germany

Question/Background

Classification of vulvar carcinoma (VCX) into one of the three molecular subtypes has significant prognostic and therapeutic impact. An HPV-associated lesion that is p16 positive and p53 wild type represents improved prognosis compared to other subtypes. HPV-independent VCX, mostly associated with lichen sclerosus is characterized by *TP53*-alteration (i.e. aberrant p53-expression) and p16 non-aberrant staining. A third (minor) subtype is characterized by normal staining for both markers. It has been shown that patients with p53-aberrant tumors may benefit from more radical surgical approach. Contrary, HPV-high risk associated VCA (with p16-block positivity) represent better response to chemoradiation. The aim of this study was to determine the concordance of molecular subtyping on diagnostic biopsy compared to the surgical resection specimen.

Methods

56 matched pairs of VCA diagnostic biopsies (Bx) and its surgical resection specimens (vulvectomies) were immunohistochemically evaluated for the immunoexpression of p16 and p53 using the criteria recommended by the International Society of Gynecological Pathologists (ISGyP), the British Association of Gynecological Pathologists and the LAST-Project. Doubtful immunohistochemical staining results were molecularly analysed for HPV-DNA and/or *TP53*-mutation. The molecular results of the resection specimens were used as "gold standard". The examination of the Bx were blinded to the findings within the resection specimen.

Results

Matched pair analysis represented a high agreement for molecular subtyping of VCX comparing diagnostic Bx and the surgical resection specimen: 93.7% (16/17 cases) for the p16+/p53^{wt} cases; 94.4% (34/36) for p16-/p53^{mut}. Within the p16-/p53^{wt} VCX there was a lower concordance (50%; 2/4 cases).

Conclusion

There is a high concordance rate (~94%) between diagnostic Bx and surgical resection specimen for the two major types within the molecular classification of VCX using immunoexpression of p53 (as a surrogate marker for *TP53*-alterations) and p16 (as a surrogate marker for HPV high-risk infection).

These results may represent a valuable finding within the clinical setting for treatment decisions. By accurate subtyping of the VCX before curative treatment, the prognostically best treatment approach can be chosen for the patients.

So, molecular subtyping of VCX within diagnostic biopsies represents a robust tool to tailor the treatment approach of patients with VCX.

TROP-2 expression in vulval carcinoma - as a possible target for the treatment approach with antibody drug conjugates (ADC)

A. K. Höhn¹, M. Forberger¹, G. G. R. Hiller¹, E. Thompson², B. Gilks³, M. Höckel⁴, N. Singh⁵, C. E. Brambs⁶, L.-C. Horn¹

¹Institut für Pathologie, Arbeitsgruppe Gynäko-, Mamma- & Perinatalpathologie, Leipzig, Germany, ²BC Cancer Research Center, Department of Molecular Oncology, Vancouver, Canada, ³Vancouver General Hospital of the University of British Columbia, Columbia, Canada, ⁴University Hospital, Leipzig School of Radical Pelvic Surgery, Division of Gynecologic Oncology, Leipzig, Germany, ⁵Barts Health NHS Trust and Queen Mary University, London, United Kingdom, ⁶Kantonsspital Luzern, Department of Gynecologic Oncology, Luzern, Switzerland

Question/Background

The Trophoblast Cell Surface Antigen 2 (TROP-2) is associated with invasiveness and tumor progression in several malignancies. Strong TROP-2-expression is associated with poor prognosis in cervical carcinoma. Recently, TROP-2 was identified as a target protein for treatment of solid tumors using antibody-drug conjugates (ADC). There are no details about the expression profiles of TROP-2 in vulval cancer (VCX).

Methods

55 cases of squamous cell carcinomas of the vulva were immunohistochemically analysed for TROP-2 expression using a H-score. The staining intensity (SI) was scored as negative (0), weak (1), moderate (2) and strong (3). The percentage of positive stained tumor cells was calculated as 0 (complete negative staining of tumor cells), 1 (1-10% positive stained tumor cells), 2 (11-50%) and 3 (51-100%). Overall staining results were calculated by SI x percentage staining score as follows: negative (score 0), + (scores 1;2;3), ++ (scores 4-6) and +++ (score 7-9) as previously described. Overall staining scores were compared to the molecular subtypes of vulval carcinoma, defining p16⁺/p53^{wt}, p16⁻/p53^{mut} and p16⁻/p53^{wt} VCX. Staining evaluation of TROP-2 was blinded to the molecular subtype.

Results

All 55 cases were immunohistochemically positive for TROP2. 7 cases (13%) showed weak reactivity (+), 31 cases (56%) represented moderate reactivity (++) and 17 cases (31%) strong positivity (+++). There were no significant differences within the median h-score values when the different molecular subtypes of vulvar cancer were compared (9 in p16⁺/p53^{wt} versus 6 in p16⁻/p53^{mut} versus 4 in p16⁻/p53^{wt}; p=0.079).

Conclusion

It has been shown that the antibody drug conjugate (ADC) topoisomerase-1-inhibitor irinotecan, coupled via a linker to a humanised IgG-1 antibody hRS7 binding to TROP-2 (i.e. sacituzumab) represents an effective treatment approach to several carcinoma types. Virtually all examined VCX showed at least weak staining for TROP-2 within the tumor cells. So, TROP-2 may represent a potential target for ADC in vulval cancer. There are no differences of TROP-2 expression within the different molecular subtypes of VCX.

P05 Gemischte Postersitzung II

P.05/11.01

Mogamulizumab-associated rash (MAR) of the scalp in a patient with follicular Mycosis fungoides

A. Menz¹, N. Booken², S. Schneider², C. von Bahren¹

¹Universitätsklinikum Hamburg-Eppendorf, Institut für Pathologie, Hamburg, Germany, ²Universitätsklinikum Hamburg-Eppendorf, Klinik für Dermatologie, Hamburg, Germany

Question/Background

Mogamulizumab is a CCR4 antibody used as a second line treatment in patients with advanced mycosis fungoides and Sezary Syndrome. 24% of patients develop a mogamulizumab associated rash (MAR), mostly affecting head and neck, which clinically may mimic a relapse of mycosis fungoides /Sezary syndrome. Histopathologically, spongiotic/psoriasiform, lichenoid/interface and granulomatous patterns may occur, with mixed patterns being possible. We present a 71-year old patient with tumor stage follicular MF, who developed scaly plaques of the scalp in the late course of treatment with Mogamulizumab after the 38th infusion.

Methods

A biopsy was taken and immunohistochemical stainings (CD4, CD8 and CD7) and molecular studies (T-cell-clonality) were applied.

Results

The biopsy showed a mainly granulomatous pattern with a normalized CD4/CD8 ratio. Clonal persistence was demonstrated by molecular studies. A relapse of mycosis fungoides was ruled out by conventional and immunohistochemical studies. The molecular evidence of a clonal expansion was interpreted as being non dominant. After evaluation of the biopsy in correlation with the clinical presentation, treatment with mogamulizumab was continued. Lesions on the scalp were successfully treated by local steroids. The patient showed no progress of the disease.

Conclusion

It is important to know about the cutaneous side effect of this novel treatment modality in which a biopsy is mandatory for evaluation. An inflammatory pattern with a reversed or normal CD4/CD8 ratio and retained expression of CD7 is helpful in pointing to the reactive origin. On a molecular basis, a finding of clonality should not automatically lead to a diagnosis of a tumoral relapse. A careful clinical evaluation of the symptoms should be established to avoid unnecessary cessation of the therapy. This is a relevant example for clinical pathological correlation.

P.05/11.02

Hypoxia and Ezrin Expression in Primary Melanoma Have High Prognostic Relevance

U. Maccio¹, A. Mihic², D. Lenggenhager¹, I. Kolm³, C. Mittmann¹, M. Heikenwälder⁴, A. Lorentzen⁵, D. Mihic-Probst¹

¹Universitätsspital Zürich, Institut für Pathologie, Zürich, Switzerland, ²Bavarian State Office for Health and Food Safety, Oberschleissheim, Germany, ³Universitätsspital Zürich, Dermatologische Klinik, Zürich, Switzerland, ⁴German Cancer Research Center, Divisione Chronic Inflammation and Cancer, Heidelberg, Germany, ⁵Aarhus University, Institute of Biomedicine, Institute of Molecular Biology and Genetics, Aarhus, Denmark

Questions/Background

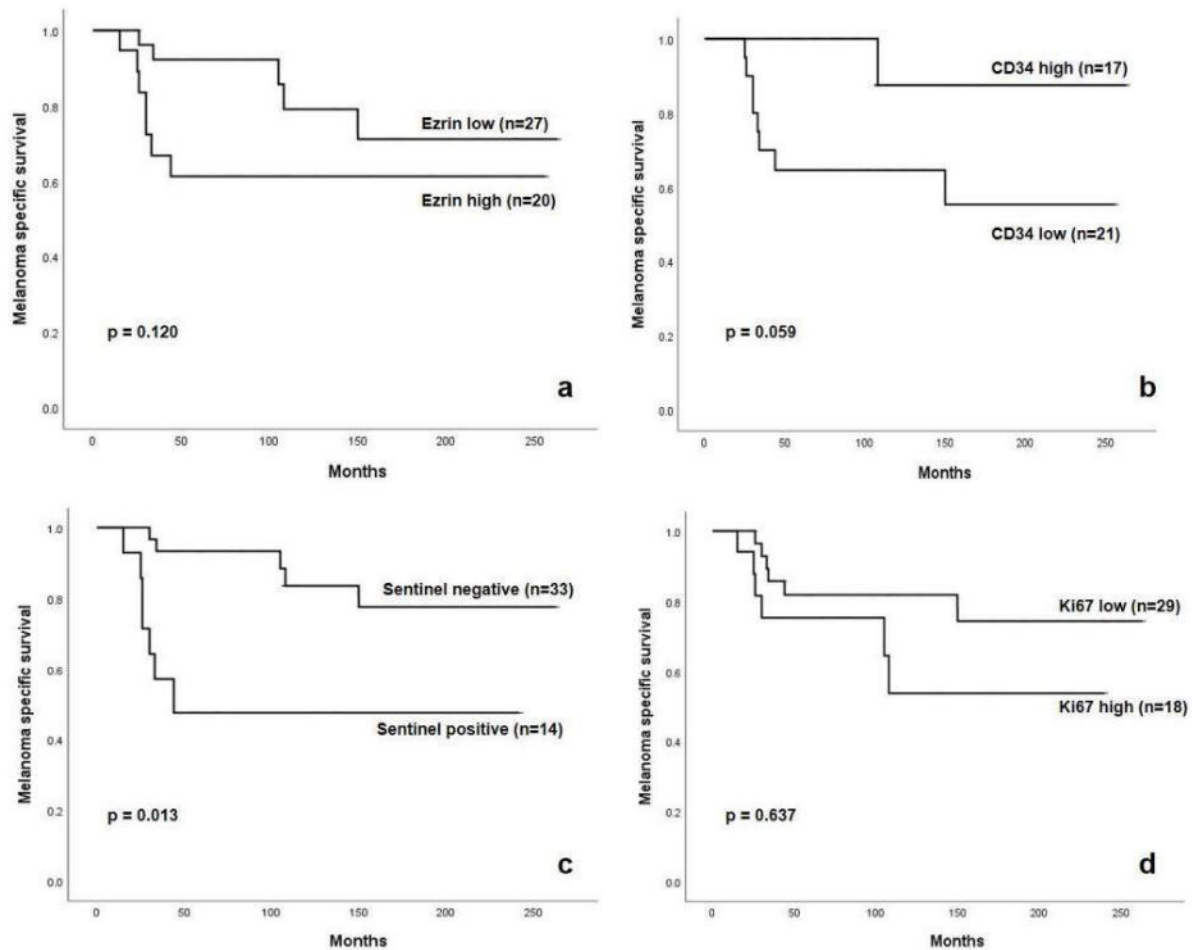
Hypoxia affects tumor aggressiveness and activates pathways associated with epithelial mesenchymal transition (EMT), which are crucial for tumor progress. In this study, the correlation of hypoxia and EMT with sentinel lymph node status and tumor-specific survival was investigated in primary melanomas.

Methods

CD34 for capillary count and Hypoxia inducible factor-1 α (HIF-1 α) as hypoxia indicators as well as Ezrin and L1-Cell Adhesion Molecule (L1CAM), both critical proteins contributing to EMT, were analyzed using immunohistochemistry in 49 melanoma patients with long follow-up (F/U, mean 110 months; range 12–263 months).

Results

We found a significant correlation between Breslow tumor thickness and Ezrin expression ($p = 0.018$). L1CAM expression in primary melanoma was significantly associated with HIF-1 α expression ($p < 0.0001$) and sentinel lymph node metastasis ($p = 0.011$). Furthermore, low capillary count, reflecting hypoxic condition, was significantly associated with Ezrin expression ($p = 0.047$) and decreased tumor-specific survival ($p = 0.035$). In addition, patients with high Ezrin expression in their primary melanomas had a dramatic loss of life early in their F/U period (mean survival time 29 months; range 15–44 month).



Melanoma specific survival

Conclusion

Our results highlight the relevance of Ezrin, L1CAM and HIF-1 α as prognostic markers in melanoma patients. Additionally, we demonstrate that hypoxia in primary melanoma affects EMT and is at least partly responsible for early metastatic dissemination.

P.05/11.04

Acute myocardial infarction caused by anomalous left coronary artery in a 3-year-old boy with repaired tetracuspid truncus arteriosus communis

M. A. Pantea¹, S. Huber-Schumacher¹, F. A. Kari², M. Czerny², M. Werner¹

¹Center of Pathology, Medical Center University of Freiburg, Freiburg, Germany, ²Department of Cardiovascular Surgery, University Heart Center Freiburg - Bad Krozingen, Bad Krozingen, Germany

Question/Background

In truncus arteriosus communis (TAC) the coronary arteries may show an increased anatomic variability and myocardial infarction or sudden death have been described in association with anomalous coronary arteries.^[1-3]

Methods

[Case report]

Results

We present a case of a 3 years old boy with neonatally repaired tetracuspid Truncus arteriosus communis type A1 with a slit-like left coronary ostium who died of acute myocardial infarction. The patient presented with 1-day fever followed by chest pain, paleness, loss of consciousness and respiratory arrest. After prolonged reanimation and best intensive care the patient developed hypoxemic encephalopathy followed by cerebral death 4 days after onset of symptoms. The solely autopsy of the heart (as requested by the parents)

showed marked cardiac hypertrophy, especially of the left ventricle. Extensive areas of acute infarction with incipient granulocytic demarcation were observed in right and left myocardial muscle and in one papillary muscle. The left coronary artery showed an acute angle takeoff with a slit-like left coronary ostium opening with subsequent formation of an ostial ridge. The autopsy report concluded a functional stenosis caused by the coronary ostial particularities and followed by myocardial infarction and acute cardiac insufficiency as the cause of death.

Conclusion

Coronary artery anomalies can be found in patients with TAC. Pathologic autopsy findings and thoroughly examinations of the coronary ostia may be of great importance in explaining the cause of death in case of congenital heart disease or sudden cardiac death.

Literaturangaben:

[1] de la Cruz MV, Cayre R, Angelini P, Noriega-Ramos N, Sadowinski S. Coronary arteries in truncus arteriosus. *Am J Cardiol.* 1990 Dec 15;66(20):1482-6.

[2] Virmani R, Chun PK, Goldstein RE, Robinowitz M, McAllister HA. Acute takeoffs of the coronary arteries along the aortic wall and congenital coronary ostial valve-like ridges: association with sudden death. *J Am Coll Cardiol.* 1984 Mar;3(3):766-71.

[3] Bonilla-Ramirez C et al. Coronary Artery Anomalies Are Associated With Increased Mortality After Truncus Arteriosus Repair. *Ann Thorac Surg.* 2021 Dec;112(6):2005-2011.

P.05/11.05

Congenital infantile fibrosarcoma with fatal perinatal complications - a case report

P. Grochowski¹, S. Dintner¹, M. Franitza², W. Schenk³, B. Märkl¹, T. Schaller¹

¹Institut für Pathologie und molekulare Diagnostik, Universitätsklinikum Augsburg, Augsburg, Germany, ²Klinik für Frauenheilkunde und Geburtshilfe, Universitätsklinikum Augsburg, Augsburg, Germany, ³Pädiatrische Intensivmedizin, Klinik für Kinder- und Jugendmedizin, Universitätsklinikum Augsburg, Augsburg, Germany

Question/Background

Congenital infantile fibrosarcoma (CIF) is a rare malignant soft tissue tumor characterized by a *ETV6-NTRK3*-gene fusion, with a predominantly favorable outcome with local infiltrative growth but low metastatic risk. Typically localized on extremities or trunk, it can be successfully surgically removed and/or treated with *NTRK*-inhibitors. However CIF can rarely lead to a fatal outcome. We present a case of an infant born in 33 WG with a post mortal diagnosed cervical CIF.

Methods

A 23 years old patient in 33 +0 WG presented in the Clinic for Gynaecology and Obstetrics of University Medical Center of Augsburg due to premature labour onset, without known abnormalities in prenatal diagnostic. In the course of labor, a left-side cervical tumour mass was identified in the infant. Shortly, a tumor haemorrhage occurred and led to hypovolemic shock. Moreover, distinctly changed anatomy of the cervical region posed an insurmountable obstacle to endotracheal intubation. Despite resuscitation the infant died. An autopsy was performed.

Results

The autopsy revealed a eutrophic female infant with a cervical tumour mass of 7 x 4 x 3,5 cm, which spread between the hypopharyngeal region and the larynx, causing a shift of cervical structures to the contralateral side. The mucosal surface of mouth and pharynx showed significant fibrosis and scarring with obstruction of the upper airways. Examining the cervical region, we observed a tumor infiltration in the larynx and tracheal wall as well as in surrounding soft tissue. The histological examination showed a slightly fibrotic encapsulated, locally haemorrhaged and regressively alternated malignant lesion consisting of spindle cells with prominent nuclear atypia and rather sparse cytoplasm. Immunohistochemically, the tumor cells were positive for panTRK, the Ki67-index was 30%. NGS and FISH revealed a characteristic gene fusion *ETV6-NTRK3* (exon 5/15) in 84% of the tumor cells. Finally, due to morphological appearance, immunohistochemical profile and *NTRK*-gene fusion, a congenital infantile fibrosarcoma was diagnosed. No other abnormalities were identified.

Conclusion

Although CIF can be successfully treated surgically or with *NTRK*-inhibitors, early and proper diagnosis is crucial for patients' survival. In most cases, assuming favourable location, life of the children with this malignancy is not threatened. Unfortunately, fatal outcomes are not ruled out. The substantial conclusion of this case is a need of early diagnostic of CIF including prenatal screening.

P.05/11.06

An exceptionally rare case of Fetal Lung Interstitial Tumor (FLIT)?

M. Allgäuer¹, M. Eichhorn², T. Loukanov³, P. Schirmacher¹, A. Stenzinger¹

¹Institut für Pathologie, Universitätsklinikum Heidelberg, Heidelberg, Germany, ²Thoraxklinik, Universitätsklinikum Heidelberg, Heidelberg, Germany, ³Herzchirurgie, Universitätsklinikum Heidelberg, Heidelberg, Germany

Question/Background

Lobectomy specimen of an infant considered to have a congenital malformation/tumor. Features did not fit congenital pulmonary airway malformation, type 3 (CPAM). Could this be a rare case of Fetal Lung Interstitial Tumor (FLIT)?

Methods

Comprehensive morphological, immunohistological, and molecular analysis.

Results

Macroscopy: Lobectomy specimen of 7.5 x 4.5 x 3.5 cm, almost entirely occupied by a grey, solid and microcystic (up to 0.4 cm) lesion with incomplete fibrous capsule.

Histology: Microcystic architecture resembling fetal airspaces lined by cuboidal, non-ciliated epithelium. Occasional structures with ciliated cells and smooth muscle bundles reminiscent of bronchioles. The underlying stroma expanded by a rather homogenous population of mesenchymal cells with distinct borders, cytoplasmic glycogen (PAS), and bland round-oval nuclei. Focally mild subepithelial condensation but no blastemal layer with hyperchromasia, atypia, or increased mitotic activity. Some chondro-myxoid, partly nodular areas.

Immunohistochemistry: TTF1- and AE1/3-positive cuboidal cells with nuclear beta-catenin. Interstitial cells with homogenous, strong expression of vimentin. Desmin expressed in 50% of interstitium, mostly pan-septal but also subepithelial. ASMA positive in smooth muscle bundles. Myogenin negative. Protein S100 stains focal islands of chondroid matrix. No ALK-expression. P53 wild-type expression. Ki-67 at 15 %.

Molecular: Comprehensive targeted DNA (> 500 genes) and RNA sequencing without driver mutations (e.g. KRAS, EGFR, DICER1) or rearrangement (e.g. ALK, ROS1). Possible low-level amplification of ARID1A.

Conclusion

Fetal Lung Interstitial Tumor (FLIT) constitutes a very rare entity of congenital mesenchymal lung tumors described in 2010 with fewer than 20 reported cases to date. In contrast, pleuropulmonary blastoma type I presents as single or multiple cysts. There are areas of subepithelial condensation with atypical, primitive mesenchymal cells. Usually, a DICER1 mutation is identified. Another consideration is CPAM type III which is microcystic but has no fibrous capsule and occupies mostly an entire lobe. Also, there would be ciliated, bronchiolar-type respiratory epithelium. Pathogenesis and classification, maldevelopment vs. neoplasia, is unclear. No known association with other childhood tumors or a tumor predisposition. Surgical resection is therapy of choice, with no role for chemotherapy. Close follow-up is recommended. Diagnostic separation from aggressive PPB is essential.

P.05/11.07

Late pregnancy infection with *Listeria monocytogenes* with fatal fetal outcome

M. E. E. Liebetrau¹, L.-C. Horn¹, P. Kuzman², J. Kern³, G. G. R. Hiller¹

¹Universitätsklinikum Leipzig, Pathologie, Leipzig, Germany, ²Universitätsklinikum Leipzig, Neuropathologie, Leipzig, Germany,

³Universitätsklinikum Leipzig, Geburtsmedizin, Leipzig, Germany

Question/Background

Infection with *Listeria* most often occurs due to the consumption of contaminated food. Although the infection is rare with a prevalence of 0.7 per 100,000 in Germany, pregnant women are at a 10-20 times higher risk to be affected than the general population. Listeriosis often shows only mild clinical symptoms or can be even asymptomatic in the pregnant women, while fetal effects can be severe including systemic infection, miscarriage, and preterm birth. Overall, listeriosis has a high fetal and neonatal mortality rate up to 20-40%.

Methods

We report the case of a pregnancy-associated listeriosis at 39 weeks of gestation with fatal fetal outcome.

Results

A 30-year-old firstgravida nullipara with no clinical symptoms presented with intense labor pain at 38+4

weeks of gestation and revealed green amniotic fluid after rupture of membranes on the way to the hospital. Fetal assessment showed fetal bradycardia of 90 bpm and a pathological cardiotocography. An emergency cesarean section was performed and a stillborn male neonate was delivered, Apgar score 0/0/0 despite intense reanimation. Microbiological assessment confirmed *L. monocytogenes* in swabs of maternal uterus, fetal skin and fetal oral/nasal mucosa. Histology of the placenta showed intervillous hypoxia and acute villitis and intervillitis with abscesses, the autopsy and histological examination of the fetus revealed multiple abscesses in the liver as well as the meninges and brain. Gram-staining revealed positive bacteria in all of these locations.

Conclusion

Although listeriosis in general is rare, pregnancy-associated listeriosis should always be considered in case of maternal gastrointestinal or flu-like symptoms, even when mild, or abnormal fetal heart rate to start an appropriate antibiotic therapy promptly and to prevent adverse fetal outcome.

P06 Postersitzung Thoraxpathologie

P.06.01

“Super Survivor” after Lung Transplantation – Protective Role of Macrophages?

E. K. Plucinski¹, J.-C. Kamp², J. Gottlieb², T. Welte², M. Höper², H.-H. Kreipe¹, D. Jonigk³, L. Neubert¹, M. P. Kuehn¹

¹Medizinische Hochschule Hannover, Institut für Pathologie, Hannover, Germany, ²Medizinische Hochschule Hannover, Klinik für Pneumologie, Hannover, Germany, ³Uniklinik RWTH Aachen, Institut für Pathologie, Aachen, Germany

Question/Background

Eine Lungentransplantation (LTx) ist oft die letzte verbleibende therapeutische Option für Patienten mit Lungenerkrankungen im Endstadium, wie idiopathischer Lungenfibrose, chronisch obstruktiver Lungenerkrankung oder pulmonaler Hypertonie. Trotz zahlreicher Fortschritte auf dem Gebiet der Transplantationschirurgie und postoperativer Nachsorge, ist das Transplantatüberleben nach LTx auf etwa sieben Jahre begrenzt. Kliniker und Patienten sind nach wie vor mit unterschiedlichen Komplikationen, wie zellulärer oder humoraler Abstoßung, konfrontiert. Dennoch konnten wir eine Gruppe von Lungenempfängern identifizieren, die jahrelang ohne jegliche Komplikation leben und daher als "Supersurvivor" bezeichnet werden. Histologisch zeichnet sich diese Gruppe durch eine hohe Anzahl von Alveolarmakrophagen aus, ohne Anzeichen einer Infektion oder eines Gewebeumbaus.

Methods

Um die Rolle des angeborenen Immunsystems mit Makrophagen als Hauptakteuren bei der Transplantattoleranz zu untersuchen, analysierten wir Alveolarmakrophagen aus transbronchialen Biopsien von Supersurvivoren (n=16) und gesunden Kontrollpersonen (n=12) mit der neuartigen Nanostring GeoMx Spatial Transcriptomics Technologie.

Results

Wir identifizierten ein spezifisches Genexpressionsmuster der Alveolarmakrophagen der Supersurvivor, das sich vom klassischen M1-M2-Schema unterscheidet.

Conclusion

Wir fanden Alveolarmakrophagen, die im Zusammenhang mit dem Langzeitüberleben nach LTx Merkmale von anti-inflammatorischen und anti-arteriosklerotischen Makrophagen aufweisen und vermuten, dass diese Makrophagen eine schützende Wirkung auf das Allotransplantat haben.

P.06.02

miR-338-3p and miR-126-3p expression is associated with tumour differentiation in primary squamous cell carcinomas of the lung

J. Hohnneck¹, E. Ebert¹, N. Ludwig², E. Meese², R. M. Bohle¹

¹Department of Pathology, Saarland University Hospital, Homburg, Germany, ²Institute of Human Genetics, Medical School, Saarland University, Homburg, Germany

Question/Background

MicroRNAs have been shown to be involved in cancer initiation and progression in many carcinomas [1], including non-small cell lung cancer [2]. Additionally, for pulmonary adenocarcinomas an association between dysregulated microRNA expression and tumour differentiation has been demonstrated [3]. The aim of my here, briefly summarized dissertation was to check whether a similar association could be shown for primary squamous cell carcinomas of the lung.

Methods

In 45 patients the tumour differentiation of resected primary squamous cell carcinomas of the lung was evaluated using two different grading schemes: Besides a commonly used grading scheme [4], a newer scheme was also used, which assesses the tumour growth pattern at the invasion front by quantifying the phenomena of “*tumour budding*” and “*tumour nesting*” [5]. After RNA extraction from paired tumour and lung tissue, microRNA expression was analysed by microarray analysis (Agilent SurePrint v21) and polymerase chain reaction.

Results

In the microarray analysis, a total of 79 differentially expressed microRNAs could be detected. In the subsequent polymerase chain reaction, for two of the most dysregulated microRNAs (miR-338-3p and miR-126-3p) a significant correlation between their downregulation and a lower tumour differentiation was found for the new grading system (see Figure 1). For the older grading scheme no significant correlation with microRNA expression could be demonstrated.

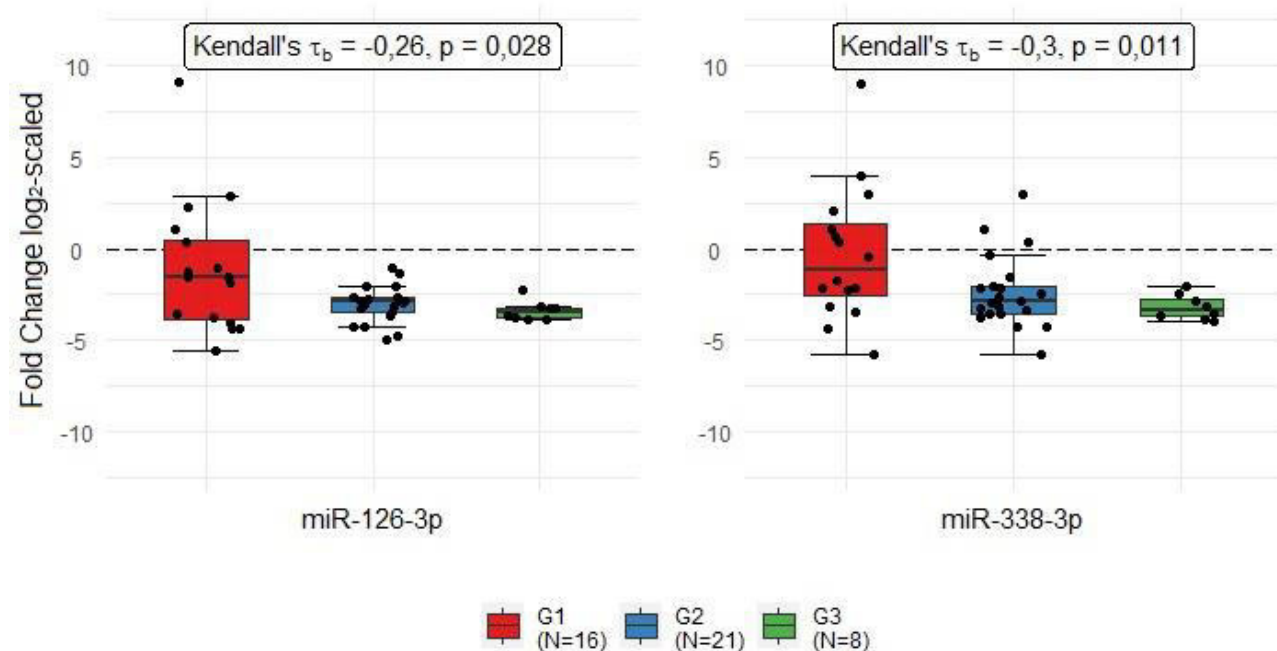


Figure 1: Fold Change of miR-126-3p and miR-338-3p between squamous cell carcinomas of the lung and paired tumour free lung tissue in relation to the newer histological grading. X-Axis: Subgroups depending upon the tumour grade. Y-Axis: Fold Change, log2-scaled. Abbreviations: τ_b : rank correlation coefficient Kendall's τ_b , p: p-value

Conclusion

The most important function of miR-126-3p and miR-338-3p is inhibition of cell migration and invasion [6][7]. The results of the presented study show that the downregulation of miR-338-3p and miR-126-3p is associated with a poorer tumour grade of primary squamous cell carcinomas of the lung. Hence, downregulation may influence the manner of tumour invasion, indicating poor prognosis in these cancer cases. In situ microenvironmental effects of microRNA downregulation will be studied in the near future.

Literaturangaben:

- [1] Van Roosbroeck K, Calin GA, (2017), Cancer Hallmarks and MicroRNAs: The Therapeutic Connection, Adv Cancer Res, 135:119-149, doi: 10.1016/bs.acr.2017.06.002.
- [2] Leidinger P, Keller A, Meese E, (2012), MicroRNAs - Important Molecules in Lung Cancer Research, Front Genet, Jan 23;2:104, doi: 10.3389/fgene.2011.00104
- [3] Nadal E, Zhong J, Lin J, Reddy RM, Ramnath N, Orringer MB, Chang AC, Beer DG, Chen G, (2014), A microRNA cluster at 14q32 drives aggressive lung adenocarcinoma, Clin Cancer Res, Jun 15;20(12):3107 - 3117, doi: 10.1158/1078-0432.CCR-13-3348
- [4] Rao N, Moran C, Suster S, (2007), Tumors of the Lungs and Pleura, Damjanov I, Fan F, Cancer Grading Manual, Springer Heidelberg New York Dordrecht London, pp 31 - 41, doi: 10.1007/978-3-642-34516-6

- [5] Weichert W, Kossakowski C, Harms A, Schirmacher P, Muley T, Dienemann H, Warth A, (2006), Proposal of a prognostically relevant grading scheme for pulmonary squamous cell carcinoma, *Eur Respir J*, Mar;47(3):938-46, doi: 10.1183/13993003.00937-2015
- [6] Ebrahimi F, Gopalan V, Smith RA, Lam AK, (2014), MiR-126 in human cancers: Clinical roles and current perspectives, *Exp Mol Pathol*, Feb;96(1):98-107, doi: 10.1016/j.yexmp.2013.12.004
- [7] Li Y, Chen P, Zu L, Liu B, Wang M, Zhou Q, (2016), MicroRNA-338-3p suppresses metastasis of lung cancer cells by targeting the EMT regulator Sox4, *Am J Cancer Res*, Jan 15;6(2):127-40, URL: <https://pubmed.ncbi.nlm.nih.gov/27508100/>

P.06.03

Tumor microenvironment patterns in pulmonary carcinoids

A. Ziehnert, B. V. Sinn, D. Horst, **P. Bischoff**

Charité - Universitätsmedizin Berlin, Institut für Pathologie, Berlin, Germany

Question/Background

The lung is the second most common anatomic origin of neuroendocrine tumors, behind the gastrointestinal tract. While typical carcinoids (NET G1) have a good prognosis, atypical carcinoids (NET G2) present with lymph node metastasis at the time of diagnosis in 10 % of cases and have a 5-year survival of approximately 70 %. In a metastasized setting, there is no consensus on standardized systemic treatment. Targeted therapies, such as somatostatin analogues, have demonstrated clinical benefit, whereas conventional chemotherapy has limited effects. The benefit of therapies targeting the tumor microenvironment, such as immune checkpoint inhibitors or angiogenesis inhibitors, still needs to be evaluated.

Methods

We studied a retrospective cohort of 59 pulmonary carcinoid tumors, comprising 43 typical and 16 atypical carcinoids. The tumor microenvironment at the invasive front and in the tumor center was characterized by immunohistochemical (IHC) staining of CD3, CD4, CD8, CD20, CD68, FCN1, SMA, PDGFR β and ERG. The fraction of positive cells was quantified using QuPath.

Results

We found that the invasive front of typical and atypical carcinoids was enriched in CD4+ and CD8+ T lymphocytes compared to the tumor center. T lymphocytes at the invasive front were increased in atypical carcinoids and correlated with the occurrence of lymph node metastasis. B lymphocytes, macrophages and monocytes were more evenly distributed throughout the invasive front and tumor center in atypical carcinoids, while being enriched at the invasive front and depleted in the tumor center in typical carcinoids. The density of vascularization was similar in typical and atypical carcinoids.

Conclusion

We observed different patterns of cellular composition of the tumor microenvironment in typical and atypical pulmonary carcinoids, which might represent different mechanisms of tumor immune escape and can therefore be important in evaluation of immunotherapies in pulmonary carcinoids.

P.06.04

Indolyl-chalcone derivatives induce pleural mesothelioma cell apoptosis through aberrant tubulin polymerization and deregulation of microtubule-associated proteins

S. Steinlein^{1,2,3}, F. Essmann⁴, L. Sun⁵, H. Horn^{1,2,3}, J. Schüler⁶, A. Hausser⁷, G. Ott¹, C. Kalla^{1,2,3}

¹Department of Clinical Pathology, Robert-Bosch-Krankenhaus, Stuttgart, Germany, ²Dr. Margarete Fischer-Bosch Institute of Clinical Pharmacology, Stuttgart, Germany, ³University of Tuebingen, Tuebingen, Germany, ⁴Robert Bosch Center for Tumor Diseases, Stuttgart, Germany, ⁵Harvard Medical School, Beth Israel Deaconess Medical Center, Boston, United States of America, ⁶Charles River Discovery Research Services Germany GmbH, Freiburg, Germany, ⁷Institute of Cell Biology and Immunology and Stuttgart Research Center Systems Biology, University of Stuttgart, Stuttgart, Germany

Question/Background

Malignant pleural mesothelioma (MPM) is a neoplasm with dismal prognosis and notorious resistance to the standard therapeutics cisplatin/pemetrexed. We investigated the efficacy of two novel indolyl-chalcones (CITs) to inhibit growth and viability of MPM cells and defined the mechanism by which the compounds induce cell death.

Methods

The effects of CIT-026 and CIT-223 were analyzed in five MPM cell lines, using viability, immunofluorescence, real-time cell death monitoring, and tubulin polymerization assays, along with siRNA knockdown. Phospho-kinase arrays and immunoblotting were used to identify signaling molecules that contribute to cell death.

Results

CIT-026 and CIT-223 were toxic in all five MPM cell lines at sub-micromolar concentrations, in particular in three cell lines resistant to cisplatin and/or pemetrexed. Both CITs targeted tubulin polymerization via (1) direct interaction with tubulin and (2) phosphorylation of microtubule regulators STMN1, CRMP2 and WNK1. Formation of aberrant tubulin fibers caused abnormal spindle morphology, mitotic arrest and apoptosis. CIT activity was not reduced in CRMP2-negative and STMN1-silenced MPM cells, indicating that direct tubulin targeting is sufficient for toxic effects of CITs. Viability of normal cells, fibroblasts, was not affected at a drug concentration that reduced viability in all five cancer cell lines.

Conclusion

CIT-026 and CIT-223 are highly effective inducers of MPM cell apoptosis by disrupting microtubule assembly. CITs are potent anti-tumor agents against MPM cells, in particular cells resistant to standard therapeutics, with only modest side effects on normal cells, which warrant further evaluation as potential small-molecule therapeutics in MPM.

P.06.05

Genomic profiling of histomorphologic subtypes reveals distinct molecular patterns in NSCLC

T. Kolb¹, T. F. Barth², P. Möller², R. Marienfeld³

¹Universitätsklinikum Ulm, Pathologie, Ulm, Germany, ²Institut für Pathologie, Universitätsklinikum Ulm, Ulm, Germany, ³Pathologie Universitätsklinikum Ulm, Ulm, Germany

Question/Background

Lung carcinoma ranks first among the deadliest cancers worldwide, with an approximate survival rate of 15% within 5 years. While molecular profiling of driver mutations guides targeted therapy, assessment of cytotoxic T-lymphocyte associated protein 4 (CTLA-4) and programmed death ligand one (PD-L1) are used to predict response to immune checkpoint inhibitory (ICI) therapy. Tumor mutational burden (TMB) and micro satellite instability (MSI) are other biomarkers, used to identify eligible patients for immune therapy. Although these biomarkers have led to an improvement in survival rates, only about 20 % of patients benefit from ICI therapy, as resistance mechanisms remain complex and in parts undiscovered. To get an insight into novel potential mechanisms affecting ICI or targeted therapy we focused on tumor heterogeneity with respect to the different growth patterns seen in pulmonary adenocarcinomas. These are divided into five different histological growth patterns according to the 2004 WHO classification: lepidic, acinar, papillary, micropapillary, and solid. Here, we investigated the relationship between these growth patterns by genomic profiling to shed light on the complexity of tumor heterogeneity.

Methods

Targeted sequencing (TSO500), fusion transcript detection (TST170) and RNASeq-analyses was performed to characterize the molecular profiles of the different growth pattern areas.

Results

Although no significant differences in TMB and MSI levels between the growth patterns were detected, we observed an intratumoral heterogeneity regarding genomic alterations such as SNVs, CNVs, indels, and fusions. In addition, RNASeq revealed overlapping and specific expression profiles of the growth patterns. Further differences in affected signalling pathways and cellular functions of lepidic versus acinar and solid growth patterns were observed.

Conclusion

While TMB and MSI did not reveal growth pattern specific differences, intratumor heterogeneity still remains a challenge for the prediction of targeted or ICI therapy due intratumoral variability of genetic alterations and TMB values.

P.06.06

Hepatoid differentiated Adenocarcinoma in the Lung: Primary or Metastasis? – Two examples of a rare differential diagnosis.

A. Maccagno¹, I. Kleinlein¹, T. Schaller¹, M. Trepel², H. Messmann³, B. Märkl¹

¹Universitätsklinikum Augsburg, Pathologie und Molekulare Diagnostik, Augsburg, Germany, ²Universitätsklinikum Augsburg, II. Medizinische Klinik, Augsburg, Germany, ³Universitätsklinikum Augsburg, III Medizinische Klinik, Augsburg, Germany

Question/Background

Hepatoid carcinoma of the lung (HAL) has a rare incidence (2.3%) compared to hepatoid differentiated

carcinomas in other locations and shows a poor prognosis. It is characterized by immunohistological positivity to typical hepatic markers such as Hep-Par-1, Arginase and Glypican as well as nuclear negativity for TTF-1. This subtype of carcinoma typically shows a lack of expression for SMARCA43.

Methods

Here we present two cases that were clinically suspicious for a primary cancer in the lung.

Results

Patient 1: 61-year-old man with 4,5 cm lung lesion. Microscopically, a lesion with epithelioid morphology and evident nuclear pleomorphism with prominent nucleoli is observed. The cells show strong reactivity for staining with Hep-Par-1 Arginase and Glypican, but no reactivity for TTF-1, PAX8 and p40. No reactivity is also observed for staining with SMARCA4. These results led to the diagnose of hepatoid carcinoma of the lung with SMARCA4-deficiency.

Patient 2: A 85-year-old man with a suspected metastasis in the left shoulder of a lesion in the lung. Also in this case the tumor shows microscopically an epithelioid morphology with positivity for liver markers. In this case, however, the reaction for SMARCA4 is preserved. On staining with TTF-1 an exclusively cytoplasmic reactivity is observed. These results led to the diagnose of hepatocellular carcinoma of the liver with metastases in the soft tissues of the shoulder and lung. After that a primary hepatic tumor could be confirmed by radiological imaging.

Conclusion

HAL is a very insidious subtype of carcinoma that can easily lead to a misdiagnosis. In the presence of extrapulmonary carcinoma with hepatoid morphology a metastasis of a HAL should be always excluded with immunohistological stain for SMARCA4. It is also important to remember that while a nuclear positivity for TTF-1 is characteristic for carcinomas of lung origin, a cytoplasmic positivity has often been described in hepatocytes and hepatocellular carcinomas

P.06.07

Inhibition of paracrine signaling by cancer-associated fibroblasts leads to depletion of malignant pleural mesothelioma cells in vitro.

M. Wessolly^{1,2}, D. Kreidt¹, L. Hammerschmidt¹, Y. Krause^{1,3}, A. Mathilakathu¹, S. Borchert^{1,2,3}, F. Mairinger^{1,2,3}

¹Universitätsklinikum Essen, Institut für Pathologie, Essen, Germany, ²Deutsches Konsortium für Translationale Krebsforschung (DKTK), Partnerstandorte Universitätsklinken Essen und Düsseldorf, Essen und Düsseldorf, Germany, ³Ruhrlandklinik, Westdeutsches Lungenzentrum, Institut für Pathologie, Essen, Germany

Question/Background

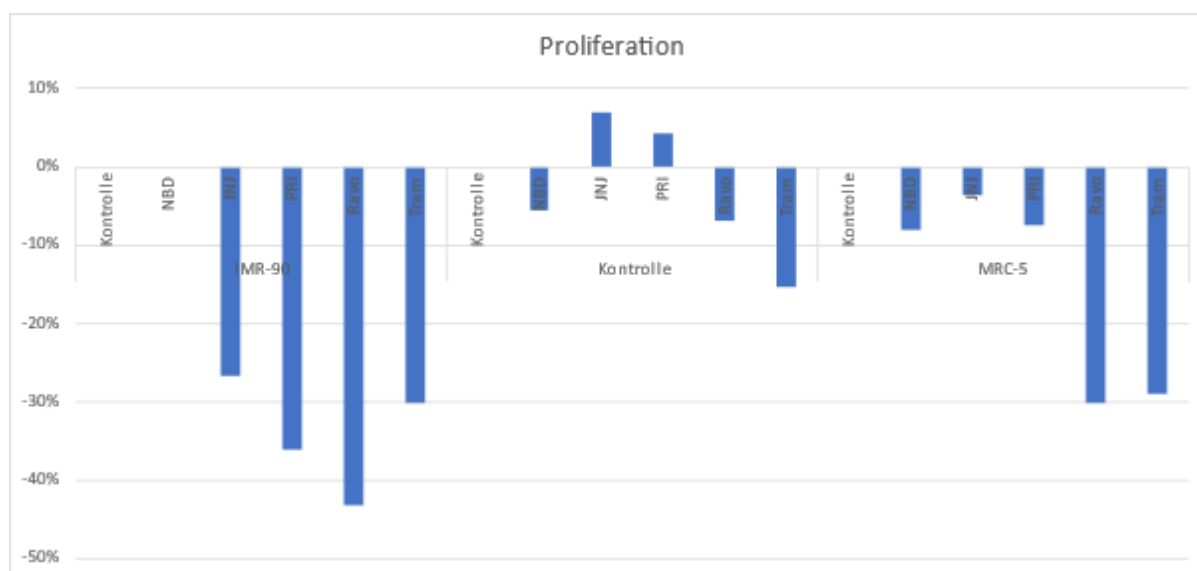
Cancer-associated fibroblasts (CAFs) are key players in the tumour microenvironment, essentially contributing to tumour progression. In previous studies, we analysed CAF-mediated effects on behavior and activity of malignant pleural mesothelioma (MPM) cells. In this aggressive malignancy, long time therapy responses are barely durable. We identified five promising targets for modern treatment and now want to evaluate the activity of those in this study.

Methods

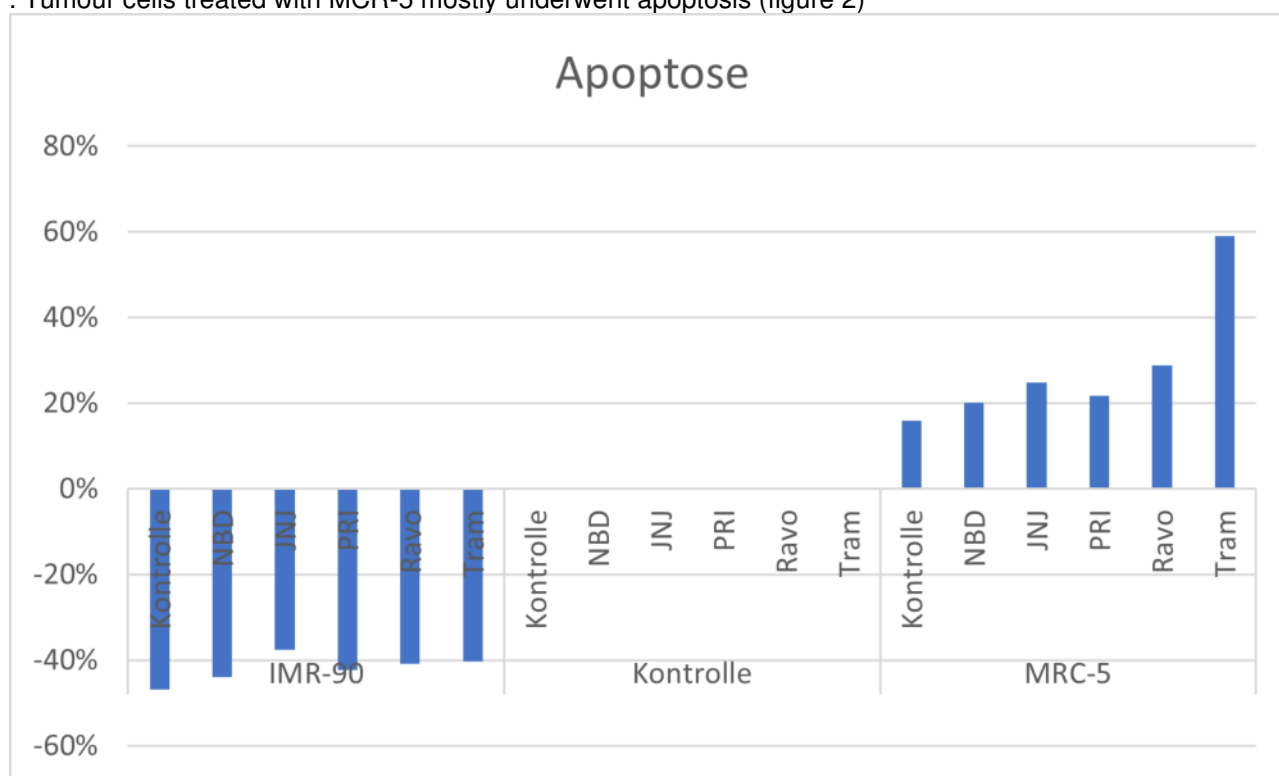
MPM cell lines were activated with conditioned medium (CM), derived from myofibroblast cell lines as previously described (IMR-90 and MRC-5). Cell viability, necrosis, and apoptosis rates were examined in an enzyme activity-based approach. Cell motility was assessed by cell migration and invasion assays. Inhibitors targeted IKK (NBD Peptide), CDK1/2 (JNJ-7706621), β -catenin /CBP (PRI-724), ERK1/2 (Ravoxertinib) as well as MEK1/2 (Trametinib).

Results

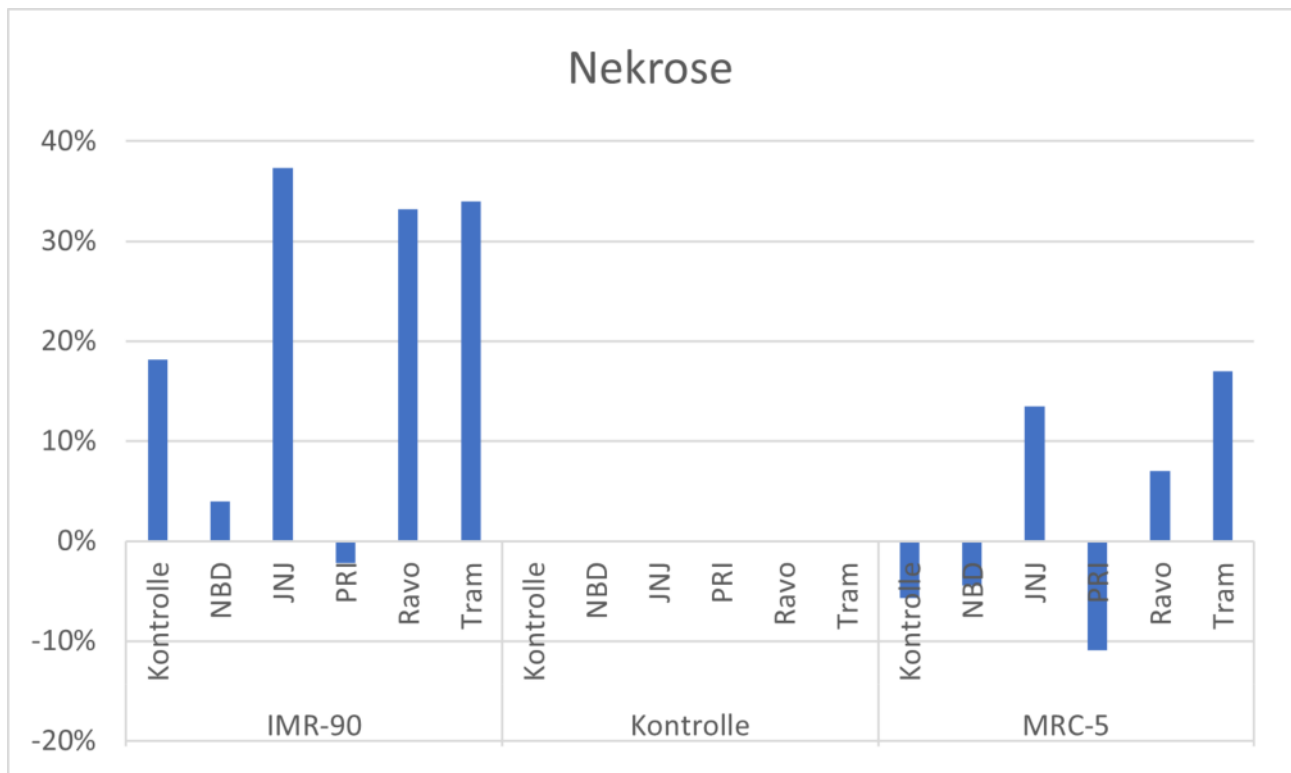
Mesothelioma cells, treated with fibroblast-derived CM displayed increased cell viability, proliferation, and migration. We saw strong effects of CDK1/2 inhibition in MPM cell activated by IMR-90, ERK and MEK inhibition show a strong reduction of cell count after activation with MRC-5 as well as with IMR-90 (figure 1)



Proliferation and cell count of mesothelioma cell lines treated with fibroblast-conditioned medium (IMR-90 and MRC-5). After incubating tumour cells with conditioned medium, various inhibitors targeting IKK, CDK1/2, beta-catenin, ERK1/2 as well as MEK1/2 were applied. . Tumour cells treated with MCR-5 mostly underwent apoptosis (figure 2)



Necrosis rate measured in mesothelioma cell lines treated with fibroblast-conditioned medium (IMR-90 and MRC-5). Apoptosis was examined using the ApoTox-Glo Triplex assay (enzyme activity-based). After incubating tumour cells with conditioned medium, various inhibitors targeting IKK, CDK1/2, beta-catenin, ERK1/2 as well as MEK1/2 were applied. , whereas tumour cells treated with IMR-90 more likely underwent necrosis (figure 3)



Necrosis rate measured in mesothelioma cell lines treated with fibroblast-conditioned medium (IMR-90 and MRC-5). Necrosis was examined using the ApoTox-Glo Triplex assay (enzyme activity-based). After incubating tumour cells with conditioned medium, various inhibitors targeting IKK, CDK1/2, beta-catenin, ERK1/2 as well as MEK1/2 were applied.

Conclusion

Our results underline the potential tumour-supportive effect of CAFs in mesothelioma. Our work reveals the specific role of CAFs in mesothelioma development, providing potential new therapeutic targets addressing the tumour microenvironment.

P07 Gemischte Postersitzung I

P.07/08/10.01

Lasso-based feature selection identifies active relaxation as the most informative left ventricular parameter for proteomic perturbations during myocardial remodeling and reverse-remodeling

B. A. Barta^{1,2}, M. Ruppert², N. Pinter¹, E. Brombacher³, C. Kreutz³, S. Korkmaz-Icöz⁴, A. Olah², A. A. Sayour², S. Spiesshofer², G. B. Szabó⁵, B. Merkely², T. Radovits², O. Schilling¹

¹University of Freiburg Medical Center, Faculty of Medicine, Institute of Surgical Pathology, Translational Proteomics Laboratory, Freiburg, Germany, ²Semmelweis University, Faculty of Medicine, Heart and Vascular Center, Scientific Research Laboratory, Budapest, Hungary, ³University of Freiburg Medical Center, Faculty of Medicine, Institute of Medical Biometry and Statistics, Freiburg, Germany, ⁴University of Heidelberg, Department of Cardiac Surgery, Heidelberg, Germany, ⁵University Hospital Halle, Department of Cardiac Surgery, Halle (Saale), Germany

Question/Background

Pressure overload (PO) leads to myocardial remodeling to the detriment of left ventricular (LV) function, while the effective use of pressure unloading therapies may induce reverse-remodeling and recovery of LV dynamics. We set out to identify parameters of LV function, that show the closest relation to alterations of the myocardial proteome in various stages of myocardial remodeling and reverse-remodeling.

Methods

LV-PO was induced in male and female rats by aortic banding (AB, n=12). Sham-operated animals served as controls (Co, n=5). Pressure unloading was performed by debanding of the aorta at week 6 in some of the once AB rats (DB, n=5). Morphologic and functional aspects of LV remodeling were detected by echocardiography and pressure-volume analysis at week 6 and week 12. LV samples were prepared for high

throughput LC-MS/MS explorative proteomics. Bioinformatic feature selection based on Lasso regularization was applied to find LV parameters closely related to the myocardial proteome.

Results

Among the 3343 proteins identified and quantified in our study, 416 proteins have shown significant association with changes in Tau (parameter of LV active relaxation) due to myocardial remodeling in the AB and to reverse-remodeling in the DB groups. Gene ontology biological process (GO:BP) analysis of above 416 proteins has indicated the role of epigenetic, post-transcriptional and post-translational regulatory processes. The altered regulation of protein expression affected processes related to cardiac structure and function, such as “regulation of cation channel activity” and “regulation of ion transmembrane transporter activity”, “cardiac muscle tissue development”.

Conclusion

We propose that parameters of LV active relaxation may be the best measures to assess the extent of myocardial reverse-remodeling after pressure unloading in experimental as well as clinical studies.

P.07/08/10.02

Comparative analysis of the mitochondrial population surrounding the intercalated discs in heart diseases – an ultrastructural study

R. Schönmehl¹, D. Mendelsohn^{2,3}, L. Winter³, S. Pabel⁴, S. Sossalla^{4,5}, C. Brochhausen^{1,3}

¹University Medical Centre Mannheim, Institute of Pathology, Mannheim, Germany, ²University Hospital Regensburg, Department for Trauma Surgery, Regensburg, Germany, ³University of Regensburg, Institute of Pathology, Regensburg, Germany, ⁴University Hospital Regensburg, Department of Internal Medicine II, Regensburg, Germany, ⁵Georg-August University Göttingen, Clinic for Cardiology and Pneumology and German Center for Cardiovascular Research, Göttingen, Germany

Question/Background

Mitochondria morphology plays a crucial role in keeping up with the fluctuating energy demand in several heart diseases. Recent studies identified a mitochondrial enrichment in proximity to the intercalated discs of individuals suffering from tachycardia-induced cardiomyopathy. The present study aimed to compare human heart tissue samples from patients with sinus rhythm (SR), arterial fibrillation (AF), dilated cardiomyopathy (DCM) and ischemic cardiomyopathy (ICM) to analyze the mitochondrial population adjacent to the intercalated discs.

Methods

Transmission Electron Microscopy (TEM) was performed on 36 patient samples (SR/AF/ICM/DCM n= 9/10/8/9) to analyze mitochondria near the intercalated discs (0-3,5µm, 3,5-7µm distance). Besides mean size, count and the percental mitochondrial area in the measuring field, bloated and otherwise defect mitochondria were quantified. Furthermore mitochondrial accumulation was analyzed by assigning a conglomeration score (CS, 0-100). Kruskal-Wallis tests were performed to identify differences between the analyzed heart damages, and a Spearman correlation to investigate the relation between the given parameters.

Results

Patients with AF expressed a high count of small mitochondria, that showed only low amounts of swelling or other defects. Overall, this group was very similar to the control group (SR) but had slightly more mitochondria that tended to be smaller. The groups DCM and ICM showed similar results, as they had fewer but larger mitochondria, that were often swollen compared to their AF counterparts. All groups expressed a similar rate of accumulated mitochondria, as well as percental mitochondrial area in the measuring field.

Conclusion

In this study no notable increase of accumulated mitochondria could be found. All patients seemed to have similar percental mitochondrial area in the measuring field as well. An increase in AF and a decrease in DCM and ICM mitochondria count could be observed in addition to a change in mitochondrial health, as DCM and ICM mitochondria were often swollen or otherwise defect. The pathophysiological meaning of these results are yet unclear and require further investigations.

P.07/08/10.03

Post-mortem diagnosis of lethal microscopic polyangiitis in a 41-year-old male with arthralgia and hemoptysis. A case report.

S. K. Hauck¹, C. Mitteldorf², A.-K. Gersmann¹, S. Hakrrouch^{1,3}, P. Ströbel¹

¹Institut für Pathologie Universitätsmedizin Göttingen, Göttingen, Germany, ²Klinik für Dermatologie, Venerologie und Allergologie,

Question/Background

Microscopic polyangiitis is a rare vasculitis initially presenting with insidious symptoms (e.g. fatigue, myalgia, arterial hypertension).[1] We report a fatal case of a patient with a clinical diagnosis of community acquired pneumonia, acute renal failure and a positive COVID-19-test, which turned out to be microscopic polyangiitis on autopsy.

Methods

A 41-year-old male patient presented at the hospital with a history of fatigue, depression, arterial hypertension, obesity (BMI 35 kg/m²), myalgia, arthralgia, a positive test for COVID-19, hemoptysis and acute renal failure. Laboratory findings showed high CRP values and an obscured right lower lobe of the lung on chest x-ray. The clinical diagnosis was community-acquired pneumonia, and treatment with ampicillin/sulbactam and azithromycin was started. After initial clinical improvement of the patients' condition and decreasing CRP values, the patient suddenly developed acute respiratory failure and died. Autopsy revealed purpuric exanthemas on both legs, severe non-granulomatous crescentic glomerulonephritis (GN) in both kidneys, and massive generalized pulmonary hemorrhagic edema, but without evidence of COVID-19 pneumonia. Immunohistochemistry was hampered due to autolysis, but did not show immune globulin or complement deposits, compatible with pauci-immune GN. Together, these findings were considered diagnostic of microscopic polyangiitis.

Results

Untreated and severe microscopic polyangiitis has an extremely high mortality rate of about 80 %.[2] Death is usually due to fulminant renal and/or pulmonary failure.[1] However, remission can be achieved with appropriate treatment in >75% of patients, making early diagnosis an utmost necessity.[2] The disease onset can be insidious[1] and may resemble other diseases such as viral flue, pneumonia, or even depression. In retrospective, myalgia and arthralgia, which were also present in this patient, are typical. Together with sudden onset of arterial hypertension and purpuric skin lesions, they are alarming symptoms and should prompt laboratory testing for proteinuria and elevated ANCA.

Conclusion

This case highlights the important contribution of autopsy in the post-mortem diagnosis of a rare disease causing the hitherto unexplained death of a young patient.

Literaturangaben:

[1] Villiger PM, Guillevin L, (2010), Microscopic polyangiitis: Clinical presentation, Autoimmun Rev. , 812-819, 9

[2] Mukhtyar C, Flossmann O, Hellmich B, Bacon P, Cid M, Cohen-Tervaert JW, Gross WL, Guillevin L, Jayne D, Mahr A, Merkel PA, Raspe H, Scott D, Witter J, Yazici H, Luqmani RA, (2008), Outcomes from studies of antineutrophil cytoplasm antibody associated vasculitis: a systematic review by the European League Against Rheumatism systemic vasculitis task force, Ann Rheum Dis. , 1004-10, 67

P.07/08/10.04

Interstitial vasculitis associates with severe kidney injury independent of ANCA-associated glomerulonephritis

I. Kluge¹, P. Ströbel¹, B. Tampe², S. Hakrrouch^{1,3}

¹Universitätsmedizin Göttingen, Institut für Pathologie, Göttingen, Germany, ²Universitätsmedizin Göttingen, Klinik für Nephrologie und Rheumatologie, Göttingen, Germany, ³SYNLAB Medizinisches Versorgungszentrum Pathologie Hannover GmbH, Pathologie, Hannover, Germany

Question/Background

Hintergrund:

Die Antineutrophile Zytoplasma-Antikörper (ANCA), assoziierte Vaskulitis (AAV) stellt eine Pathologie der kleinen Gefäße dar, welche diverse Organsysteme, einschließlich der Niere, betrifft.

Zielsetzungen:

Das aktuelle Verständnis bezüglich interstitieller Vaskulitis bei ANCA GN soll mittels systematischer histologischer Auswertung von Gefäßläsionen analog zu Banff erweitert werden.

Methods

Retrospektiv wurden 49 Nierenbiopsien mit nachgewiesener Nierenbeteiligung bei AAV an der Universitätsmedizin Göttingen eingeschlossen. Die Biopsien wurden gegenüber der klinischen Datenerfassung und Datenanalyse verblindet bewertet.

Results

Interstitielle Vaskulitis, welche sich als peritubuläre Kapillaritis (ptc, $p=0,0002$) und Arteriitis (v, $p=0,0069$) widerspiegelt, zeigte eine Korrelation zu schwerer Nierenschädigung, die eine Nierenersatztherapie (RRT) erforderlich machte. Es zeigte sich kein Zusammenhang zwischen interstitieller Vaskulitis und einer glomerulären Läsion bei ANCA GN, was nahelegt, dass interstitielle Vaskulitis unabhängig von ANCA GN zur schweren Nierenschädigung beiträgt.

Conclusion

Durch Verwendung des Banff- Scoring-Systems konnten wir zeigen, dass peritubuläre Kapillaritis und Arteriitis wichtige histologische Veränderungen darstellen, die bei einer substantiellen Untergruppe von AAV mit schweren Nierenschädigungen einhergehen. Die Merkmale der verschiedenen Vaskulitis-Manifestationen sind unabhängig voneinander und könnten unser Verständnis der Mechanismen, die zur Nierenschädigung führen, verbessern. Diese Beobachtungen lassen darüber hinaus die Annahme zu, dass interstitielle Vaskulitis bei AAV auch die Langzeitprognose beeinflussen kann, was weitere Untersuchungen erfordert.

P.07/08/10.05

The role of Insulin-like Growth Factor-1 and Bone Morphogenetic Protein-7 in the pathophysiology of non-unions – an in vitro study on the differentiation of human mesenchymal stem cells and possible therapeutic perspectives

B. Reible¹, F. Westhauser², L. Winter¹, T. Niedermair³, M. Rupp⁴, A. Moghaddam⁵, C. Brochhausen¹

¹Ruprecht-Karls-University Heidelberg, University Medical Centre Mannheim, Institute of Pathology, Mannheim, Germany, ²Heidelberg University Hospital, Center for Orthopaedics, Trauma Surgery and Spinal Cord Injury, Heidelberg, Germany, ³University of Regensburg, Institute of Pathology, Regensburg, Germany, ⁴University Hospital Regensburg, Department for Trauma Surgery, Regensburg, Germany, ⁵Private Medical Center Aschaffenburg, Aschaffenburg, Germany

Question/Background

The pathophysiology of non-infectious non-unions is not fully understood. Different signal molecules, growth factors, progenitor, or stem cells are involved in physiological fracture healing. Bone Morphogenetic Protein-7 (BMP-7) promotes the differentiation of mesenchymal stem cells (MSC) into osteoblasts and was used in clinical settings to treat complex non-unions. Fracture healing is associated with higher serum levels of Insulin-like Growth Factor-1 (IGF-1) compared to non-unions. We compared the osteoinductive potential of IGF-1 and BMP-7 on human mesenchymal stem cells from iliac crest bone marrow (BMSC) and reaming debris (RMSC) gained from use of the reamer-irrigator-aspirator system.

Methods

BMSC and RMSC of 6 donor patients were induced into osteogenic differentiation and stimulated with addition of increasing concentrations of IGF-1 or BMP-7 to the growth medium (100, 200, 400, 800, 1600, and 6400 ng/ml). Extracellular calcium deposition as a correlate of osteogenic differentiation was measured on days 7 and 14 by alizarin red staining and photometric extinction.

Results

BMSC reacted more sensitively to stimulation with IGF-1 than RMSC; significant differences in extracellular calcium deposition compared to the unstimulated control group were measured on day 7 starting at concentrations of 100 ng/ml, compared to 400 ng/ml for RMSC. In contrast, when stimulated with BMP-7, BMSC only showed a significantly higher calcium deposition than the control group at concentrations of 6400 ng/ml; RMSC showed a significant difference at a concentration of 400 ng/ml. In comparison, BMSC stimulated with IGF-1 showed a significantly higher calcium deposition than those stimulated with BMP-7 on day 7 for concentrations of 400 and 800 ng/ml and on day 14 for 200, 400, 800, and 1600 ng/ml.

Conclusion

IGF-1 in low to moderate doses stimulates the osteogenic differentiation of MSC *in vitro* significantly better than BMP-7. Furthermore, the results point towards a difference in the sensitivity to stimulation for MSC depending on their origin – BMSC reacted more sensitively to IGF-1, whereas RMSC reacted more sensitively to BMP-7. Our results indicated a potential role of IGF-1 in the pathophysiologic mechanism of non-unions, which should be analyzed further.

P.07/08/10.06

Rare case of an isolated Echinococcus cyst within the iliopsoas muscle

T. Oksentyuk Polyakova¹, F. Meyer¹, M. S. Hinnerichs², A. Surov², W. Obst³, D. Jechorek⁴, M. Petersen¹, R. S. Croner¹

¹Dept. of General, Abdominal, Vascular and Transplant Surgery; Otto-von-Guericke University with University Hospital, Magdeburg, Germany, ²Dept. of Radiology and Nuclear Medicine; Otto-von-Guericke University with University Hospital, Magdeburg, Germany,

Question/Background

Echinococcus cysts may occur at various locations of the human body.

Methods

Illustration of a rare case of a primary isolated muscular *Echinococcus* cyst

Results

Case presentation:

A 18-years old male patient with a medical history significant for chronic hepatitis B presented with pain extending from lumbar column down to the right infrapatellar site for months associated with a slight reduction of muscular strength within the right leg. After initial symptomatic treatment, magnet resonance imaging (MRI) of the lumbar column was performed in a regional hospital, which revealed a celled cystic formation of 3.8 x 4.0 x 9.0 cm in size within the right iliopsoas muscle affecting nerve root L4. *Echinococcus* serology was negative. Therefore, patient was transferred for further care to our department.

Ultrasound as well as contrast-media-enhanced MRI of abdomen and pelvis showed the same lesion as described before (plain film of the thorax, no additional findings). Repeat *Echinococcus* serology was negative. Electrophysiological investigation revealed no noticeable problems.

According to the therapeutic decision-making of an interdisciplinary tumor board conference, open resection *in toto* under strict avoidance of cystic lesion was performed. Intraoperatively, there was no adherence of neural structures. Histopathological investigation described suspicious diagnosis of an *Echinococcus* cyst (*E. multilocularis*) with vital "Protosolices" and complete resection of the lesion. The postoperative CT scan of head and pelvis revealed only reactively changed lymph nodes within the surrounding tissue of the former surgical site.

Postoperatively, there was a rapid reconvalescence after temporary increase of the reduced muscular strength, hyp- and dysesthesia of the right leg. An anti-infective treatment with Albendazol was initiated. After a follow-up time period of approximately 18 months, clinical and, in particular, neurological status is normal.

Conclusion

In industrial nations with high standards of hygiene, infections with *Echinococcus multilocularis* are rare. Due to the long latency extending from infection to making a diagnosis and growing international migration, German physicians are confronted more frequently with echinococcosis. Mostly, liver is affected w/ or w/o other organs. In contrast, an isolated manifestation of the soft tissue occurs rarely and, therefore, needs a specific differential diagnostic consideration. Surgical resection *in toto* can be considered therapy of choice.

P.07/08/10.08

Nectin-4 is widely expressed in Head and Neck Squamous Cell Carcinoma

C. Sanders¹, J.-F. Lau¹, D. Dietrich², S. Strieth², P. Brossart³, G. Kristiansen¹

¹Institut für Pathologie, Universitätsklinikum Bonn, Bonn, Germany, ²Hals-Nasen-Ohren-Klinik, Universitätsklinikum Bonn, Bonn, Germany, ³Hämatonkologie/ medizinische Klinik III, Universitätsklinikum Bonn, Bonn, Germany

Question/Background

Nectin-4 wurde erfolgreich als Zielmolekül bei lokal fortgeschrittenem und metastasiertem Blasenkrebs etabliert. Ein Antikörper-Wirkstoff-Konjugat (Enfortumab-Vedotin), das gegen Nectin-4 gerichtet ist, hat bei dieser Tumorart, die für eine hohe Expressionsrate von Nectin-4 bekannt ist, deutliche Tumorremissionsraten gezeigt. Da Plattenepithelkarzinom des Kopf-Hals-Bereichs und Urothelkarzinome morphologische und molekulare Ähnlichkeiten aufweisen, untersuchten wir die Expression von Nectin-4 in Plattenepithelkarzinomen des Kopf-Hals-Bereichs (HNSCC).

Methods

Die Expression von Nectin-4 wurde immunhistochemisch in einer HNSCC-Kohorte (n=159) und mit klinisch-pathologischen Daten korreliert.

Results

Eine Nectin-4-Expression wurde in 86,2 % der HNSCC gefunden, wobei in 32,7 % der Fälle eine mittlere/hohe Expression festgestellt wurde. Tumorproben von Nichtrauchern und p16-positive HNSCC wiesen eine höhere Expression von Nectin-4 auf (p<0,005). Es gab keine Korrelation von Nectin-4 mit dem Grading oder dem Tumorstadium. Nectin-4-positive Tumoren zeigten eine signifikant bessere Überlebensrate (log rank p=0,006).

Conclusion

Ähnlich wie beim Urothelkarzinom wird Nectin-4 in der Mehrzahl der HNSCC-Tumoren exprimiert.

Darüber hinaus wird die Expression von Nectin-4 mit einer HPV-Infektion in Verbindung gebracht und könnte als prognostischer Marker bei HNSCC dienen.

P13 Postersitzung AG Informatik, digitale Pathologie und Biobanking I

P.13.01

Segmentation of renal microvasculature and detection of cell types in glomeruli using convolutional neural networks (CNNs)

H. P. Brandt¹, D. Christensen^{1,2}, J. Schmitz¹, L. Müller¹, J. H. Bräsen¹

¹Hannover Medical School (MHH), Institute of Pathology, Nephropathology Unit, Hannover, Germany, ²MetaSystems Hard and Software GmbH, Altlussheim, Germany

Question/Background

In renal biopsies, quantitative scoring of glomerulitis is critical for the diagnosis of humoral graft rejection according to the Banff classification. However, visual scoring is not well reproducible between different diagnosticians, labor- and time-intensive and requires experienced nephropathologists. Automated CNN-based classification of whole slide images may provide a valuable diagnostic addition. The main objective of this study was to train a fully automatic CNN for detection of glomerular microvasculature.

Methods

We trained a CNN to semantically segment glomerular structures, in particular capillary lumina, as well as to classify glomerular cell types and to detect and classify intracapillary cells in glomeruli. A total of 45 kidney biopsies and 21 nephrectomies was used. Consecutive immunofluorescent and brightfield stains (CD3, CD10, CD34, CD45, CD68, Hemalum, H&E, Jones' H&E and PAS) of identical sections were prepared and digitized with the Metafer Scanning Platform. The structures were annotated using QuPath. 12,813 Capillary lumina and Bowman's capsules of 213 glomeruli were manually annotated according to strictly predefined rules. Endothelial cells, podocytes, mesangial cells, epithelial cells of the Bowman's capsule and leukocytes were manually classified in hemalum stain based on additional immunophenotyping (n=19,646 cells). Automated capillary detection was subsequently developed using a modified VGG U-Net and utilized to quantify intracapillary cells in hemalum staining.

Results

Detection of glomerular capillary lumina and Bowman's capsule achieved a pixel-based hit rate of 96.32%. Within the semantic detection of capillaries 88.39% of all intracapillary cells were correctly allocated. For glomerular cell classification in hemalum staining, a cell-based hit rate of 60.96% was archived, with wide variations between cell types (accuracy for parietal epithelial cells: 97.80%; podocytes: 91.05%; mesangial cells: 80.82%; leukocytes: 77.88%; endothelial cells 74.37%).

Conclusion

Our CNNs for capillary detection and intraluminal cell detection are promising examples of the great potential of CNNs in histopathological structure recognition. Automated capillary detection can provide a basis for quantification of intracapillary immunohistochemically stained cells. However, automatized detection of intracapillary immune cells in hemalum remains a challenge due to high morphological variability and similarity to endothelial cells.

P.13.02

Automated segmentation of tubuli and peritubular capillaries in kidney tissue using Convolutional Neural Networks (CNNs)

D. Christensen^{1,2}, F. Größler², T. Zachrau², J. Schmitz², L. Müller², L. Neugeboren², J. H. Bräsen²

¹MetaSystems Hard- & Software GmbH, Softwaredevelopment, Altlussheim, Germany, ²Hannover Medical School, Nephropathology Unit, Institute of Pathology, Hannover, Germany

Questions/Background

Histopathological assessment of biopsies is gold standard for kidney transplant diagnosis. We aimed to study whether Artificial Intelligence can reliably detect tubuli and peritubular capillaries (PTCs) in kidney tissues in order to assist nephropathological work.

Methods

Tissue was digitized with Metafer slide-scanning system (MetaSystems Hard & Software GmbH) and

imported in QuPath [Ref01]. Six different stainings of the identical sections were used to generate training data. In 115 whole slide images, 41,209 tubuli and 70,265 PTCs were annotated manually, immunofluorescence (CD34) served to identify ground truth for capillary detection. An overall area of 184.64mm² (Hemalum: 53.85mm², Jones-HE: 68.65 mm², HE-Elastica: 31.07 mm², PAS: 31.07 mm²) was annotated. A multi-class semantic CNN was trained with the classes tubulus, PTCs, tubular membranes and interstitium. Evaluation of the CNN was done on 10 hemalum stained slides of new samples by comparison of the CNN prediction with manually annotated regions as ground truth.

Results

Evaluation on 10 slides resulted in an overall pixel hit rate of 97.48% with intersection-over-union vales of 0.983 for tubuli, 0.897 for tubular membranes, 0.889 for peritubular capillaries and 0.915 for interstitium. Further pixel related results are listed in TABLE01.

	interstitium	tubule	tubular membrane	peritubular capillary
Sensitivity	95.67%	98.74%	96.72%	91.87%
Specificity	99.01%	99.33%	98.51%	99.79%
Accuracy	98.42%	98.98%	98.22%	99.34%
Prevalence	17.89%	60.42%	15.94%	5.74%
Precision	95.49%	99.56%	92.47%	96.44%
Intersection over union	0.9154	0.9832	0.8966	0.8886
Dice coefficient	95.58%	99.15%	94.55%	94.10%

TABLE01: Detailed statistics across 10 hemalum-stained evaluation slides for pixel-wise evaluation.

The evaluation slides contained 1,003 tubuli of which 994 were successfully detected. 30 tubuli were falsely connected with neighbouring tubuli. Nine or 0.9% tubuli (mainly Henle-loop) were not found: 3 in cortex, 6 in medulla. 16 or 1.6% false positive tubuli were either on PTCs or small spots in the interstitium: 9 in cortex, 7 in medulla.

The slides contained 1,393 PTCs (749 in cortex). Sensitivity was 79.9% (cortex: 83.0%, medulla: 76.2%). Precision was 83.2% (cortex: 84.97%, medulla: 81.02%).

Conclusion

Automated structure segmentation by CNNs works reliably and can be used in future as an additional tool in nephropathological diagnostics and research.

Classes with low prevalence result in lower pixel hit rates. Mixing different stains in training data seems to be beneficial concerning robust performance across different biopsies. Currently, cell and immune cell allocation within the tissue compartments are evaluated and investigated for their diagnostic value.

Literaturangaben:

[Ref01] Bankhead, P., Loughrey, M.B., Fernández, J.A. et al, (2017), Open source software for digital pathology image analysis., Scientific Reports, 7, Article number: 16878 (2017) , <https://doi.org/10.1038/s41598-017-17204-5>, 2023-03-04

P.13.03

Polarized light scanner for digital pathology

D. Al Sheikhyaqoob¹, A. Oliveira¹, M. Fella¹, D. Laferty², G. Niedobitek¹

¹Sana Klinikum Lichtenberg, Institut für Pathologie, Berlin, Germany, ²Objective Imaging Ltd., Kansasville, United States of America

Question/Background

Virtual microscopy is being increasingly used for routine diagnostic purposes. Several studies have demonstrated that histopathological analysis of H&E stained sections using virtual microscopy is comparable to conventional diagnostic procedures using microscopes and can be safely applied to diagnosis. However, as yet, analysis of scanned digital histopathological images has certain technical limitations. Notably, application of polarised light microscopy is currently not possible.

Methods

75 cases previously diagnosed as containing birefringent materials were retrieved from the archives of the

Department of Pathology Sana Klinikum Lichtenberg, Berlin, including 16 cases of amyloidosis, 21 periprosthetic membranes, 17 cases of foreign body granulomas, mainly suture granulomas, 8 cases of gout, 6 cases of pseudogout, 3 cases with calcium oxalate crystals in breast tissue, and 4 cases of nodular sclerosing Hodgkin lymphoma. H&E- and where appropriate Kongo red stained sections were examined using an Olympus BX53 light microscope and images were captured using an Olympus digital camera and a 20x objective. Subsequently, all slides were captured digitally using a Glissando POL Brightfield Polarized Light Scanner with a 20x objective. Three representative areas were identified from all cases and corresponding images were recorded from these sites with both methodologies for comparison.

Results

For all cases examined, standard polarised light microscopy revealed birefringent materials and images recorded the Glissando POL Brightfield Polarized Light Scanner yielded comparable results showing birefringent materials with identical distribution.

Conclusion

We show that images acquired using a commercially available polarised light scanner are comparable to those obtained using a conventional light microscope equipped with polarizer and analyzer. Thus, the Glissando POL Brightfield Polarized Light Scanner represents a further step towards establishing a fully digital workflow in histopathology.

P.13.04

Separate classification of central and peripheral regions of HE-stained colorectal carcinomas for clinical outcome

D. Rusche¹, M. Runz^{2,3}, T. Gaiser^{2,4}, S. Hetjens⁵, C.-A. Weis¹

¹Institute of Pathology, University Medical Centre Heidelberg, Heidelberg University, Heidelberg, Germany, ²Institute of Pathology, University Medical Centre Mannheim, Heidelberg University, Mannheim, Germany, ³Mannheim Institute for Intelligent Systems in Medicine (MIISM), Medical Faculty Mannheim, Heidelberg University, Mannheim, Germany, ⁴Institute of Applied Pathology, Speyer, Germany, ⁵Institute for Medical Statistics, University Medical Centre Mannheim, Heidelberg University, Mannheim, Germany

Question/Background

Tumor budding is a well-established risk factor for colorectal carcinoma (CRC). Many works describe its assessment based on counting tumor buds [BUD1], [BUD2]. Against this background we asked the following question: Can the budding status and progress in CRC be predicted singularly by a convolutional neural network (CNN) on central or peripheral tumor areas (CT/PT)?

Methods

This study includes 400 clinically annotated CRC cases. Tiled whole slide images (WSIs) are segmented with a U-Net [UNet] and sorted based on their content into groups: CT (40,686 tiles) and PT (104,210 tiles), respectively.

Color normalization with a generative adversarial network (GAN) is performed to prevent case recognition instead of the real study goal [GAN].

A standard, pre-trained residual neural network (ResNet152) is trained to predict nodal status (pN0-2), budding status (Bd. 0-4) and progress (P0-1) on each group, respectively [RNet].

To determine the tiles' areas with a high impact on the classification outcome, we compute class activation maps (CAMs) [CAM].

Results

The ResNet152 model predicts the prognostic factors with good accuracy (0.86 - 0.93). The classification performs significantly ($p < 0.0001$) better for CT based predictions than for PT based predictions.

An almost perfect agreement between clinical data and ResNet152 prediction is achieved for budding status predictions based on CT (Cohen's Kappa 0.8716, 95% CI [0.8519; 0.8914]).

The prediction of budding status based on PT results in substantial agreement with the clinical data with a Kappa value of 0.6684 (95% CI [0.6505; 0.6862]).

CAMs from the classification task central tumor areas to nodal status highlight different tile areas as relevant for the ResNet's prediction than CAMs from the classification task central tumor areas to case-ID.

Conclusion

CNN classification tasks performed on CT show a significantly higher predictive power compared to those tasks working on PT, which are interestingly usually used for budding evaluation.

Literaturangaben:

[BUD1] Koelzer VH, Zlobec I, Lugli A., (2016), Tumor budding in colorectal cancer-- ready for diagnostic practice?, Hum Pathol, 47:4-19

[BUD2] Lee VWK, Chan KF., (2018), Tumor budding and poorly-differentiated cluster in prognostication in Stage II colon cancer., Pathol Res Pract, 214:402-407

[CAM] Ian Pointer, Class Activation Mapping In PyTorch, <http://www.snappishproductions.com/blog/2018/01/03/class-activation->

mapping-in-pytorch.html.html, 2023-02-20

[GAN] Runz, M.; Rusche, D.; Schmidt, S.; Weihrauch, M.R.; Hesser, J.; Weis, C.A., (2021), Normalization of HE-stained histological images using cycle consistent generative adversarial networks., *Diagnostic Pathology*, 16/1-10

[RNet] Cleo-Aron Weis, (2021), Assessment of glomerular morphological patterns by deep learning, <https://github.com/catweis/Assessment-of-glomerular-morphological-patterns-by-deep-learning>, 2023-02-21

[UNet] Janowczyk, A., (2021), PytorchDigitalPathology: segmentation epistroma unet, https://github.com/choosehappy/PytorchDigitalPathology/tree/master/segmentation_epistroma_unet, 2023-02-20

P.13.05

Spatial distribution and determinants of *Helicobacter pylori* cases in the Rhine-Main area - A spatial ecological study.

S. Strobl¹, M. Kloth¹, R. Müller¹, W. Roth¹, G. Moirano²

¹Institut für Pathologie der Universitätsmedizin Mainz, Mainz, Germany, ²Department of Medical Sciences, University of Turin and CPO-Piemonte, Torino, Italy

Question/Background

In pathological routine diagnostics, a vast amount of patient data is collected on a daily basis which is usually not spatially analyzed, even though information on the address of patients is available. However, spatial epidemiology is a scientific discipline providing valuable insights into the distribution and determinants of diseases encompassing several dimensions next to disease mapping, such as risk assessment (1), geographic correlation (2), and disease cluster identification (3).

Hence, we initialized a disease mapping project intended to use the data collected within the course of pathological routine diagnostics at the Institute of Pathology of the University Medical Center Mainz to map specific diagnoses for cluster detection and analysis. Specifically, we aimed at answering the research question how *H. pylori* was distributed in the Rhine-Main region and which determinants influenced this distribution.

Methods

Reports of gastric biopsies collected in pathological routine diagnostics were automatically data-mined for patients having received a stomach biopsy together with the *H. pylori* status. These patients were then mapped geographically according to the GPS-coordinates of their residential address. Further, statistical models were established to draw conclusions with regard to other relevant risk factors of *H. pylori* infection, such as the socioeconomic status (SES), and variables potentially influencing the likelihood of biopsy collection, such as the distance to the study site.

Results

This study identified densely populated urban areas as well as the SES, both on an individual and a municipal level, to critically influence the likelihood of *H. pylori* diagnosis. Further, it provided vital insights into the geographical distribution of populations especially at risk of infection.

Conclusion

In summary, this study generated reliable data on the distribution and determinants of *H. pylori* infection in the Rhine-Main region. Further, spatial methods for the systematic analysis of data originating from pathological routine diagnostics were established. By means of these methods, it will not only be possible to analyze the distribution of certain diseases but also their relationship to associated risk and environmental factors.

P.13.06

Prediction of molecular subtypes in muscle invasive bladder cancer (MIBC) based on histopathological images

I. Frøberg Mathisen, N. Flinner

Dr. Senckenberg Institute of Pathology, Frankfurt am Main, Germany

Question/Background

Bladder cancer is the ninth most commonly diagnosed cancer worldwide. Muscle invasive bladder cancer (MIBC) represents 25% of bladder cancers and is associated with high mortality. Distinct molecular subtypes of MIBC have been identified and research suggests they are predictive of patient treatment response.

Methods

Recently a neural network (CNN) model was reported to exceed the accuracy of human experts in classifying tumour samples based on histopathological images.

Results

However high levels of intra-tumour heterogeneity leads to challenges in training robust neural networks due to label noise. Large parts of the images are given a potentially wrong label, as only a small part is experimentally examined and the remaining tissue may differ due to the intra-tumour heterogeneity.

Conclusion

We aim to improve upon prediction of MICB molecular subclasses from histopathological images using CNNs through addressing the issue of noisy labelling.

P.13.07

Deep learning-based classification of pancreatobiliary differentiated carcinomas in the liver

A. Ewert¹, B. Goeppert^{1,2,3}, S. Roessler¹, P. Schirmacher¹, A. Brobeil¹, T. Albrecht¹, C.-A. Weis¹

¹Universitätsklinikum Heidelberg, Institut für Pathologie, Heidelberg, Germany, ²RKH Klinikum Ludwigsburg, Institut für Pathologie und Neuropathologie, Ludwigsburg, Germany, ³Kantonsspital Baselland, Institut für Pathologie, Liestal, Switzerland

Question/Background

Für die Differenzierung eines intrahepatischen Cholangiokarzinoms von einer hepatischen Pankreasmetastase existieren gegenwärtig keine objektivierten diagnostischen Kriterien. Auch der Immunphänotyp beider Entitäten ist identisch. Dieses Projekt soll klären, ob a) eine morphologische Differenzierung von Cholangiokarzinomen und hepatischen Pankreasmetastasen anhand H&E-gefärbter Slides mittels künstlicher Intelligenz möglich ist und b) ggf. morphologische Charakteristika zur Abgrenzung beider Entitäten identifizieren.

Methods

Grundlage für das Projekt ist ein Patientenkollektiv aus dem Archiv des Pathologischen Instituts Heidelberg mit histologisch gesicherten Diagnosen eines intrahepatischen Cholangiokarzinoms oder einer hepatischen Metastase durch ein Adenokarzinom des Pankreas. Die Objektträger werden hierfür hochauflösend digitalisiert und zunächst annotiert. Als Modell soll zum einen ein Tile-basiertes, klassisches CNN (TensorFlow) und ein Multiple-Instance-basierter Ansatz (PyTorch) zum Einsatz kommen. Zur besseren Reproduzierbarkeit wird eine skalierbare Pipeline auf einer Serverinstitution etabliert.

Results

Jeweils 320 Patienten mit einem histopathologisch gesicherten intrahepatischen Cholangiokarzinom oder einer Lebermetastase durch ein pankreatisches Adenokarzinom konnten identifiziert werden. Das Kollektiv wurde im Anschluss in ein Training (70%), Validation (10%) und Test-Set (20%) aufgeteilt. Die informatische Pipeline wurde implementiert und an wenigen Fällen erfolgreich getestet. Derzeit laufen die ersten Berechnungen an der Gesamtkohorte.

Conclusion

Die Klassifikation pankreatobiliärer Karzinome in der Leber mittels künstlicher Intelligenz könnte einen Beitrag zur Verbesserung der Routinediagnostik leisten und histologische Kriterien entschlüsseln, die dem Pathologen bei der morphologischen Abgrenzung pankreatobiliärer Entitäten unterstützen.

P13 Postersitzung AG Informatik, digitale Pathologie und Biobanking II

P.13.09

Quality Control: a Closer Look at How Training and Test Data Influence CNN Performance

R. Mayer, S. Gretser, P. Wild, N. Flinner

Universitätsklinikum Frankfurt, Dr. Senckenbergisches Institut für Pathologie, Frankfurt am Main, Germany

Question/Background

Whole Slide Images (WSI) are high resolution histopathological images of tissue. To train CNNs (convolutional neural networks), smaller tiles are usually extracted to make training computationally feasible. However, there are no fixed quality standards to decide which WSI and which regions/tiles should be used for training in order to reach optimal performance.

Methods

We trained CNNs on the TCGA-OV dataset to classify tiles into cancerous and non cancerous tissue. Here,

we showed that during testing there were higher performing and lower performing WSIs. Interestingly, these subsets are strongly connected to the institution from which the slides were obtained.

Results

We then asked the question whether training with exclusively one sites WSIs influences transferability of CNNs. Training on site A WSIs resulted in a high accuracy (97%) for site A WSIs and a low accuracy (82%) for site B WSIs. On the other hand, training with site B WSIs resulted in consistently high performance (accuracy site A: 96%; site B: 93%). Both approaches reach a good performance on inter dataset transferability to external UKF data with accuracy of ~90%, with the site B trained CNNs slightly outperforming the site A CNNs.

To see whether the differences in performance could be due to image quality we asked a pathologist to score WSI quality based on subjective non fixed parameters. Although tissue quality correlates with WSI performance, the use of quality control tools such as HistoQC¹ and PathProfiler² has failed to increase accuracy.

Therefore, we looked for another measure to increase the intra dataset transferability of site A to site B during the application phase. Therefore, we introduced label noise to enforce stronger variability within a CNN ensemble, leading to an improved transferability.

Conclusion

By monitoring ensemble confidence we could see that dropping tiles of lower ensemble confidence further improved the ensembles accuracies for WSIs of all data sets.

P.13.10

Prediction of progression free survival in non muscle invasive bladder cancer (NMIBC) based on histopathological images

H. Lecomte^{1,2,3}, S. Bultmann⁴, J. Köllermann¹, S. Braun⁴, P. Wild¹, N. Flinner¹

¹Dr. Senckenbergisches Institut für Pathologie, Frankfurt am Main, Germany, ²University Hospital Frankfurt, Frankfurt am Main, Germany, ³TU Darmstadt, Künstl.Intelligenz u.Maschinelles Lernen, Darmstadt, Germany, ⁴Institut für Pathologie, Sana Klinikum Offenbach, Offenbach, Germany

Question/Background

With an estimated 573,278 new cases worldwide, bladder cancer is the tenth most common cancer. Superficially invasive, nonmuscle infiltrating urothelial carcinoma represents a prognostically heterogeneous group of patients. Classically, bladder-preserving therapy is the goal in these patients. However, some of these patients suffer from disease progression or even lethal outcome. In these patients, surgical removal of the urinary bladder may be the first choice. However, the safe and early identification of this subgroup of patients is still uncertain.

Methods

Recent technological developments in machine learning may pave the way for a better understanding of this disease, its progression and recurrence.

Results

Using a cohort of 259 NMIBC patients for whom we have histological slides of tumor tissue harvested by TURBT, we aim to develop a binary classifier capable of predicting progression-free survival after 5 years. To this end, we plan to use convolutional neural networks, automated segmentation by deep learning, and other imaging techniques. In a second step, we would like to look for ways to make more accurate predictions about the timing of disease.

Conclusion

If successful, this work could lay the basis of a diagnostic tool that could help improve healthcare provided to the patients.

P.13.11

ProteoGenDB: A Fast Proteogenomic Pipeline for Identifying Sequence Variants in Proteomics Data

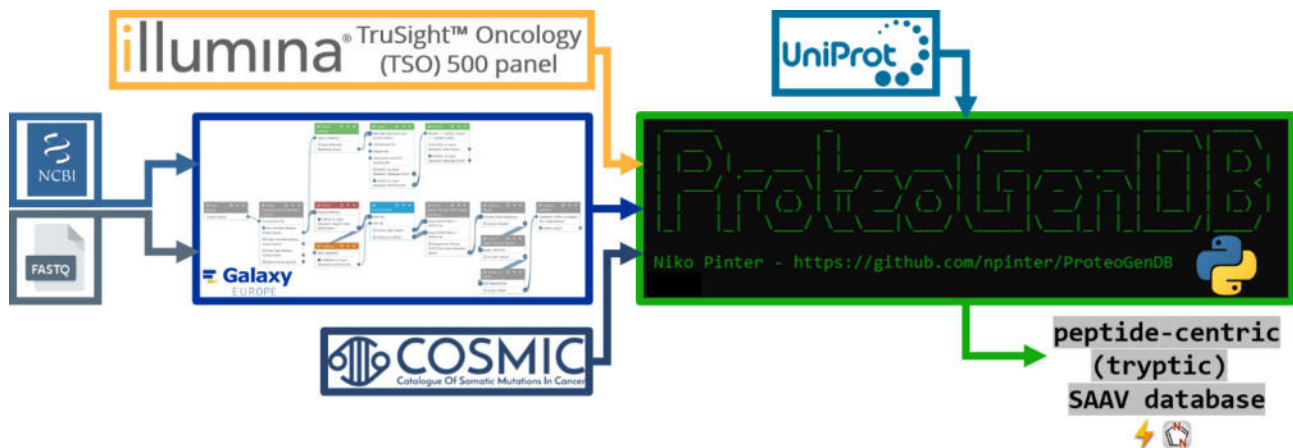
N. Pinter¹, M. Cosenza-Contreras^{1,2,3}, J. Werner^{1,4}, P. Bernhard^{1,2,5}, M. Fahrner¹, M. Werner^{1,6}, O. Schilling^{1,6}

¹University of Freiburg, Institute for Surgical Pathology, Faculty of Medicine, Freiburg i. Br., Germany, ²University of Freiburg, Faculty of Biology, Freiburg i. Br., Germany, ³University of Freiburg, MelnBio Graduate School, Freiburg i. Br., Germany, ⁴University of Heidelberg, Surgical Clinic of Mannheim, Heidelberg, Germany, ⁵University of Freiburg, Spemann Graduate School of Biology and Medicine (SGBM), Freiburg i. Br., Germany, ⁶German Cancer Consortium and German Cancer Research Center, Heidelberg, Germany

Question/Background

Identification and characterization of protein variants and isoforms remains a major challenge in modern proteomics since they are often difficult to detect using traditional proteomics methods. These variants can have important functional and clinical implications, and they can provide insight into the underlying genetic alterations that drive cancer development and progression.

Methods



We developed ProteoGenDB, a bioinformatic tool that creates a peptide-centric FASTA database of single amino acid variants (SAAVs), and addresses this problem by providing a powerful approach to generate unique and tryptic variant peptides. The tool can take input data from various sources, including processed RNAseq data of a custom Galaxy workflow, variant information of the COSMIC database, and Illumina's TruSight Oncology 500 gene panel output. By cross-referencing processed peptide variants with the UniProt database, the resulting database enables identification of variants previously reported to be associated with disease or other clinically relevant conditions. Subsequently, the peptide variants can be filtered against a list of proteins previously identified in the dataset of interest. Using this list of proteins, the tool pipeline can also generate a subsetting reference proteome that can be used to further filter peptide variants. This approach reduces the filter penalty of peptide variants, as the targeted proteome contains only identified proteins.

Results

We identified sequence variants of KRAS and ANKHD1 in formalin-fixed paraffin-embedded (FFPE) tissues of a pancreatic ductal adenocarcinoma (PDAC) and chronic pancreatitis (CP) cohort. The proteogenomic analysis identified 112 PDAC-specific and 32 CP-specific single amino acid variants and showed a tendency for higher mutational burden in PDAC using the ProteoGenDB pipeline [1].

Conclusion

ProteoGenDB is a fast and powerful proteogenomic pipeline that allows for the identification and characterization of protein variants in proteomics data. Our findings highlight the importance of protein variant detection in understanding cancer biology.

Literaturangaben:

[1] J. Werner & P. Bernhard et. al, (2022), Targeted and explorative profiling of kallikrein proteases and global proteome biology of pancreatic ductal adenocarcinoma, chronic pancreatitis, and normal pancreas highlights disease-specific proteome remodelling, Elsevier, Neoplasia, Volume 36, <https://doi.org/10.1016/j.neo.2022.100871>, 2023-02-27

P.13.12

Explainable artificial intelligence providing better comprehensibility for artificial intelligence using the example of prostate cancer – Preliminary results

L. Rentschler^{1,2}, J. Bäcker², S. Cramer², R. Manz², P. Meyer², D. Müller^{2,3}, C. Wengenmeyer², B. Märkl¹, R. Huss^{1,2}, J. Raffler², I. Soto Rey²

¹University of Augsburg, Medical Faculty, Pathology, Augsburg, Germany, ²University Hospital Augsburg, Digital Medicine, Augsburg, Germany, ³University of Augsburg, IT-Infrastructure for Translational Medical Research, Augsburg, Germany

Question/Background

Artificial intelligence (AI) tools can aid pathologists in their diagnostic decision-making processes. However,

the acceptance of AI in clinical practice depends on offering a transparent rationale together with the AI's assessment of the tissue. One approach to make the rationale behind the automated image evaluation more transparent is to include explainable AI (XAI) tools. In the project presented here, we developed a deep-learning algorithm capable of grading prostate cancer according to the Gleason Grading System based on image data from prostate biopsies. Subsequently, pathologists will evaluate different XAI approaches in terms of comprehensibility and usefulness for clinical routine applications.

Methods

We digitized a total of 620 hematoxylin and eosin stained (H&E) slides of prostate needle biopsies. 375 whole slide images were annotated by a pathology resident, marking regions with either inconspicuous tissue or tissue corresponding to prostate carcinoma with a Gleason score of 3, 4 or 5 as well as artifacts such as air pockets or creases in the tissue. Using these annotations, we trained a deep learning model using the AUCMEDI software [1]. We included various XAI algorithms (GradCam, Guided Backpropagation and Saliency Maps) into the AUCMEDI software and developed a web-based user interface to visualize and evaluate the results. We developed a structured questionnaire to assess the usefulness and comprehensibility of the XAI algorithms. Board certified and resident pathologists will review this questionnaire.

Results

The AUCMEDI-AI showed an overall good performance in assessing prostate cancer in H&E slides. Preliminary results indicate a good usability of the user interface and enhanced comprehensibility of the AI assessment through XAI-heat maps.

Conclusion

The developed AI pipeline can be easily modified and potentially used in various automated image analyzing tools. XAI algorithms have the potential to improve the comprehensibility and acceptance of AI tools for pathologists, although further evaluations and possibly refinements are needed.

Literaturangaben:

[1] Müller, D., Mayer, S., Hartmann, D., Schneider, P., Soto-Rey, I., & Kramer, F. , (2022), AUCMEDI: a framework for Automated Classification of Medical Images, [Computer software], Augsburg, GitHub repository. <https://github.com/frankkramer-lab/aucmedi>

P.13.13

Neural Network Assisted Pathology for Labeling Tumors in Whole-Slide-Images of Glioblastoma

D. Hieber^{1,2}, G. Prokop³, M. Karthan², B. Märkl¹, J. Schobel², F. Liesche-Starnecker¹

¹University Augsburg, Pathology, Medical Faculty, Augsburg, Germany, ²Neu-Ulm University of Applied Sciences, Institute DigiHealth, Neu-Ulm, Germany, ³Technical University of Munich, Department of Neuropathology, Institute of Pathology, Munich, Germany

Question/Background

Introduction:

Most segmentation models that are based on Machine Learning (ML) focus on lower-resolution MRI images rather than high-resolution histopathological images, especially for brain tumors [1]. The main reason for this is the reduced labeling effort required to train models for lower-resolution imaging.

Objective:

To utilize the large data available in pathology, we trained an ML model to handle the segmentation of glioblastoma in hematoxylin and eosin (HE) slides. The trained model is then capable to conduct labeling of histopathological images without the need for manual annotation by domain experts.

Methods

Methods:

We used 103 hematoxylin and eosin-stained high-resolution Whole-Slide-Images (WSI) of 56 patients whose tumor-containing regions had been annotated by a neuropathologist. The images were tiled into processable chunks of 1024x1024 pixels and rescaled to 512x512 pixels. We used the „Segmentation Models“-framework [2], a simple-to-use tool for image segmentation and classification in PyTorch [3], to conduct the segmentation.

Results

Results:

The tumor tiles were segmented with an Intersection-over-Union (IoU) of 84.5% after only 7 training epochs. Better preprocessing algorithms (e.g., removing small errors in the labels) can further increase the IoU and are scope of future research. Moreover, a generic segmentation model was used, that was not specifically tailored to our application scenario. With specific fine-tuning, the accuracy may also be increased.

Conclusion

Conclusion:

Based on a dataset of labeled, HE-stained WSIs, we could segment these into tumor-containing and non-neoplastic tissue with an IoU of 84.5% using a preconfigured ML model. Utilizing this initial manual labeling of 103 WSIs, future labeling tasks can be handled automatically via ML. While the current segmentation score is not sufficient for daily routine diagnostic, it can already be used for preprocessing tasks (e.g., selecting relevant tissue for future analysis). Adjustments in the applied algorithms will increase the accuracy, allowing a broader use.

The prototype shows the enormous potential in histopathological data, allowing accurate analysis with ML models with rather small effort. While the presented model was trained using glioblastoma WSIs, the applicability for other tumors is easily achievable with a few dozen labeled WSIs.

Literaturangaben:

- [1] Ranjbarzadeh, R., Bagherian Kasgari, A., Jafarzadeh Ghouschi, S., Anari, S., Naseri, M., & Bendeache, M. , (2021), Brain tumor segmentation based on deep learning and an attention mechanism using MRI multi-modalities brain images, Springer, Scientific Reports, 1-17, <https://pubmed.ncbi.nlm.nih.gov/34035406/>, 2023-03-03
- [2] Pavel Iakubovskii, (2019), Segmentation Models Pytorch, GitHub repository, https://github.com/qubvel/segmentation_models.pytorch, 2023-03-03
- [3] Paszke, A., Gross, S., Massa, F., Lerer, A., Bradbury, J., Chanan, G., Killeen, T., Lin, Z., Gimelshein, N., Antiga, L., Desmaison, A., Kopf, A., Yang, E., DeVito, Z., Raison, M., Tejani, A., Chilamkurthy, S., Steiner, B., Fang, L., Bai, J., & Chintala, S. , (2019), PyTorch: An Imperative Style, High-Performance Deep Learning Library , Advances in neural information processing systems, <https://doi.org/10.48550/arXiv.1912.0170>, 2023-03-03

P.13.14

Optimization of workflows in pathological diagnostics through the interlink of AutoHotkey with a laboratory information system

S. Timme, L. Bergmann, M. Werner, S. Walter, **P. Bronsert**

Institute for Surgical Pathology, Freiburg im Breisgau, Germany

Questions/Background

In the field of pathological reporting, accuracy and efficiency go hand in hand. The standardization of the repetitive ordering of immunohistochemical and molecular pathology test and the resulting reports strongly supports this process. AutoHotkey (AHK) is a free and open-source automation scripting language for Windows. By creating nearly any script that automates any task on a computer, AHK allows users (in our field technicians, scientists and pathologists) the automation of the afore mentioned repetitive tasks. Here we describe the potential benefits of interlinking AHK with a laboratory information system (LIS).

Methods

The study involved the implementation of AutoHotkey scripts in the reporting process of a LIS (PathoPro) within a Windows 10. Scripts automating repetitive tasks included test ordering for lung-, gynecological- and gastrointestinal cancers.

Results

The implementation of AutoHotkey scripts led to a significant personalization of ordering processes. Herby time for ordering and reporting decreased by an average of over 40%, leading to an increase in the laboratory's efficiency and productivity. Of note, development cost and time for the personalized AHK-based LIS modifications are not worth mentioning.

Conclusion

Free automation software like AHK allows pathologists to continuously create, customize and share optimized / personalized workflows, which is directly reflected by increased efficiency and productivity rates. The easy to learn and use language of AHK also small pathology laboratories generating own customized scripts without dedicated human IT resources and incurring additional costs.

P.13.15

Artificial intelligence-based assessment of Ki67 concordance and prognosis in breast cancer: Update from the automated Ki67 scoring guideline of the International Ki67 Working Group

L. Cai, **Y. Liu**

The Fourth Hospital of Hebei Medical University, Department of Pathology, Shijiazhuang, China

Questions/Background

Ki67 has predictive value for the prognosis of breast cancer. Therefore, IKWG released the consensus

update to improve the consistency of Ki67 assessment.

Methods

Here we reported a new deep learning algorithm (DLA) and a whole-slide artificial intelligence (AI-W) method to improve the Ki67 scoring in terms of consistency and accuracy. Then we evaluated the prognostic significance of 3 categories of Ki67 expressions.

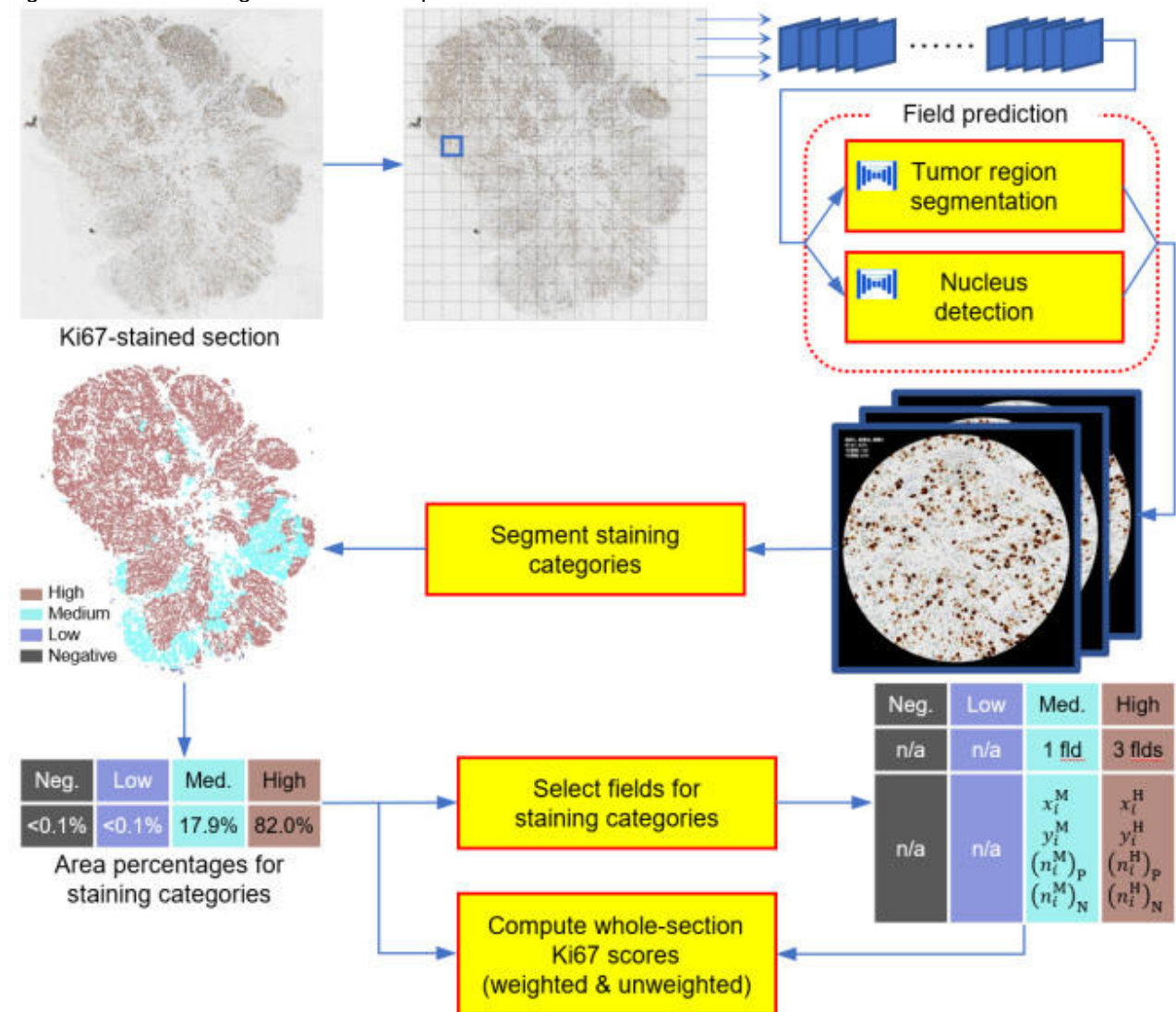


Figure 1. System diagram of the AI-empowered whole-section assessment algorithm for Ki67.

Results

15 pathologists from 3 laboratories conducted Ki67 scoring on 150 screened cases from a large number of patients in ring studies and for prognosis prediction. 18 chips of the IKWG public cases were obtained to analyze the accuracy of our DLA interpretations against the reference scores (with intra-class correlation (ICC=0.982)). We performed 3 rounds of ring studies to analyze the visual assessment (VA), count assessment (CA), and an AI-empowered microscope (AIM) based interpretation. By using CA, VA and AIM, the consistencies of all pathologists were 0.914, 0.790 and 0.950, respectively, which demonstrated that CA and AIM were generally more objective than VA. In the accuracy analysis, the AI-W method achieved 0.912 in ICC (95%CI:0.770-0.959), while VA only obtained ICCs of 0.693(95% CI: 0.716-0.763) and 0.729(95%CI:0.658-0.794) for the weighted and unweighted global assessments, respectively. Moreover, the consistency between the weighted and unweighted global AI-W scores was very high, namely 0.981. Then, we categorized Ki67 scores into the low, moderate and high expressions by employing a median value of 28% and a fluctuation of $\pm 10\%$ from a previous work. Survival results showed that 3 categories of Ki67 expressions enjoyed significant correlation with the DFS.

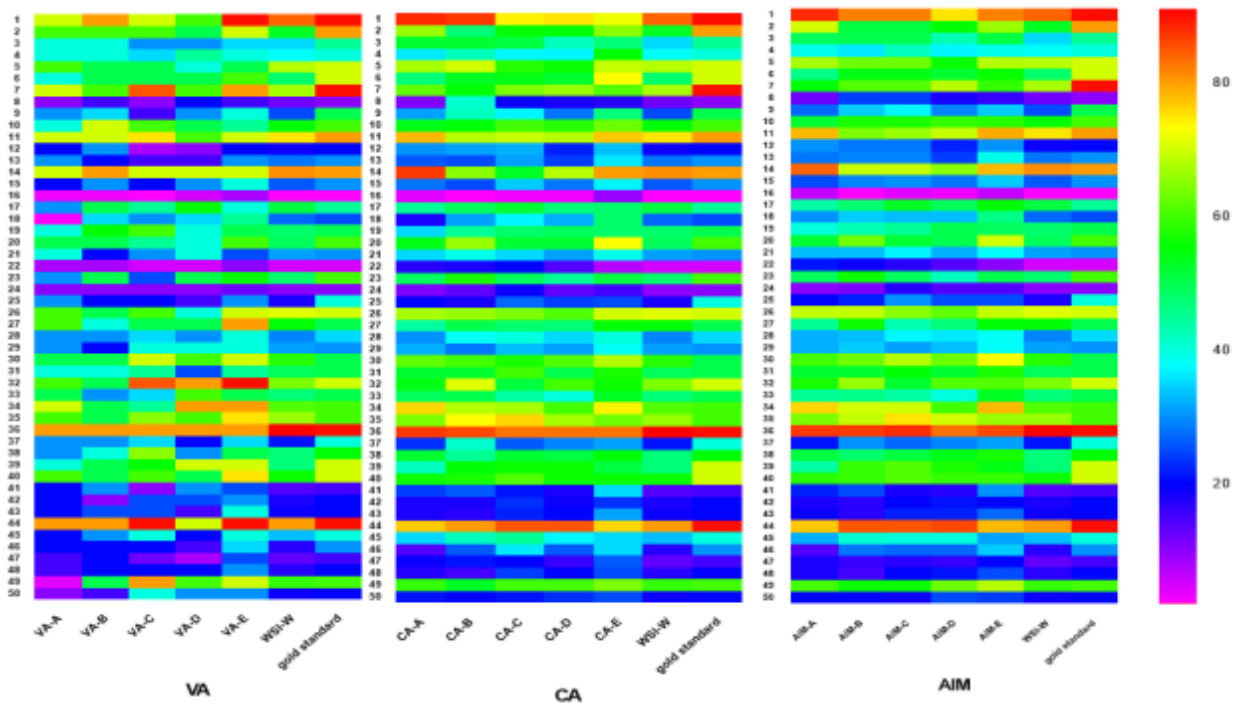


Figure 2. Ki67 scoring of 50 cases by 5 pathologists in three rounds of ring studies.

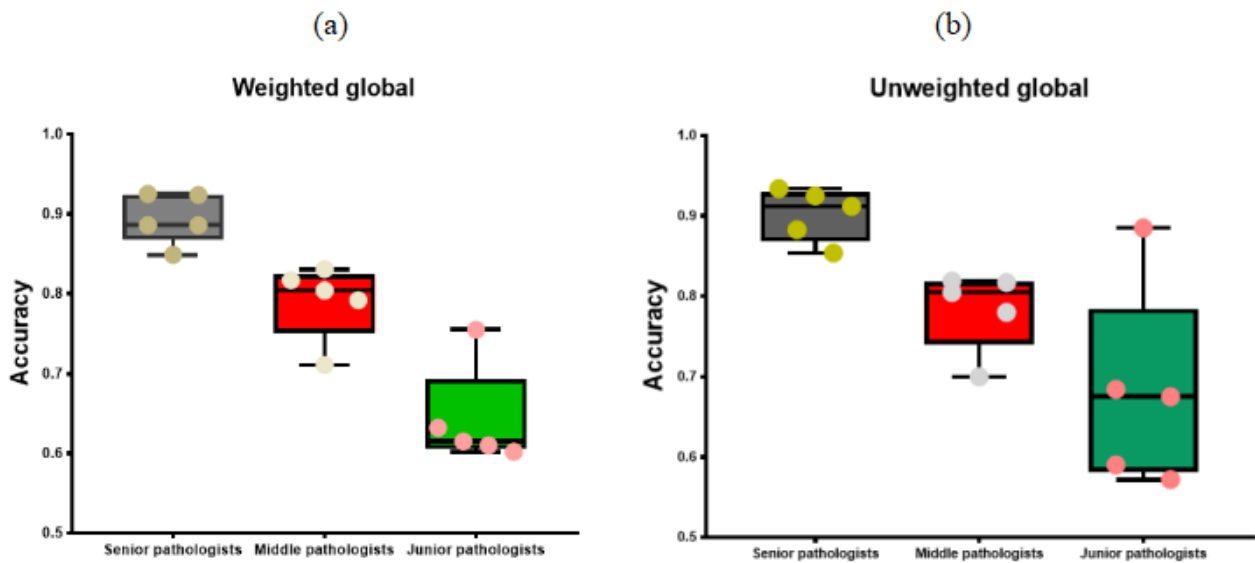


Figure 3. The accuracy between the Ki67 assessment of pathologists with different seniority and the gold standard.

Conclusion

Our study showed that the AI could be effective in bringing consistency and accuracy to clinical diagnosis. The global scoring using AI-W method demonstrated adequate reproducibility and accuracy.

Comparative analysis of morphological parameters of breast cancer NST with immunophenotypical parameters using Artificial Intelligence (AI).

I. A. Montes Mojarro¹, M. Granai¹, T. Schotte¹, D. Silimon¹, L. M. Serna Higuaita², L. L. Volmer³, A. Staebler¹, F. Fend¹

¹University Hospital Tübingen, Eberhard-Karls-University, Institute of Pathology and Neuropathology and Comprehensive Cancer Center Tübingen, Tübingen, Germany, ²University Hospital Tübingen, Eberhard-Karls-University, Department of Clinical Epidemiology and Applied Biostatistics, Tübingen, Germany, ³University Hospital Tübingen, Eberhard-Karls-University, Department for Womens' Health, Tübingen, Germany

Questions/Background

Histologic grading reflects the biological behavior of solid tumors and provides valuable prognostic information. In breast cancer, the Elston & Ellis score is the gold standard. However, the inter- and intra-observer reproducibility of this score varies, especially for the mitotic count. More recently, molecular classification, including hormone receptors, the proliferation marker Ki67 and multigene expression signatures have improved the risk stratification. But diagnostic challenges remain, especially in early hormone-receptor positive, HER2 negative breast carcinomas of no special type (NST) with intermediate differentiation.

Methods

To further improve the accuracy of the classification of invasive breast carcinoma, no special type (IBC-NST), we propose a multiparametric approach, including the quantification of the mitotic marker pHH3 and Ki67. In addition to visual assessment by pathologists, we used the digital analysis tool QuPath. Agreement evaluation was performed by intraclass correlation (ICC) with a 95% confidence interval. Our study comprises a discovery cohort of 72 core biopsies of IBC-NST and a validation cohort of 120 cases including core biopsies and resections with > 10 years of follow-up.

Results

According to histologic grading, the discovery cohort consisted of 12 cases grade 1 (16.7%), 16 grade 2 (22.2%), and 44 cases grade 3 (61.1%). However, counting mitosis score based on p-HH3 staining would have reallocated the majority of cases to a higher grade, documenting a higher sensitivity of mitosis detection with immunohistochemistry. Comparing mitotic count in HE (visual assessment) and proliferation index by Ki67 staining, a moderate agreement (ICC 0.58) was observed, with higher accuracy when using digital analysis (ICC 0.74). A strong correlation was observed between visual and digital counting of pHH3 in the three grades (ICC: G1: 0.95, G2: 0.76, G3: 0.88). Based on Ki67 and mitotic counts, a K-medoids cluster analysis was performed, grouping the data points into three homogeneous clusters. The clinical relevance of this stratification is being evaluated in the validation cohort and these data will be presented.

Conclusion

Mitotic count and proliferation index are crucial for IBC grading and prognosis, but their reproducibility varies. Therefore, digital image analysis can provide an additional resource with distinct advantages in time efficiency, accuracy, and likely reproducibility of cancer stratification. This study was supported by the DFG (GRK 2543).

P14 Postersitzung Molekularpathologie I

Biomarker analysis from Phase 1/2 study of tusamitamab ravtansine (SAR408701) in patients with advanced non-small cell lung cancer (NSCLC)

A. Gazzah¹, J. S. Lee², P. Wild³, E. Wang², N. Ternès⁴, H. Wang², E. Boitier⁴, A. Lartigau⁴, M. Chadjaa⁴, C. Dib⁴, G. Muzard⁴, S. Longuemaux-Valence⁴, A. Remaury⁴, C. Palu⁵, A.-L. Bauchet⁴

¹Drug Development Department, Gustave Roussy, Villejuif, France, ²Sanofi, Cambridge, MA, United States of America, ³University Hospital Frankfurt, Frankfurt, Germany, ⁴Sanofi, Paris, France, ⁵Sanofi, Cambridge, United Kingdom

Question/Background

Tusamitamab ravtansine is an antibody-drug conjugate of a humanized carcinoembryonic antigen (CEA)-related cell adhesion molecule 5 (CEACAM5)-specific monoclonal antibody linked to DM4. A Phase 1/2 study (NCT02187848) showed tusamitamab ravtansine antitumor activity in pretreated patients (pts) with advanced nonsquamous NSCLC and high CEACAM5 expression. Here, we explore biomarker associations with tumor CEACAM5 expression by immunohistochemistry (IHC), and whether biomarkers predict objective

response rate (ORR).

Methods

We assessed CEACAM5 expression by IHC, RNA sequencing, and whole exome sequencing (WES) on latest archival tumor samples; and circulating CEACAM5 (cCEACAM5) and CEA (cCEA). We enrolled 2 cohorts of pts with IHC CEACAM5 membrane expression at $\geq 2+$ intensity: in $\geq 50\%$ of tumor cells (high expressors, HEs, n = 64); and in $\geq 1\%$ to $< 50\%$ of tumor cells (moderate expressors, MEs, n = 28). Pts received tusamitamab ravtansine 100mg/m² IV every 2 weeks.

Results

cCEA and cCEACAM5 were strongly associated (Spearman rho, 0.9), with weak associations between IHC CEACAM5 and cCEA or cCEACAM5 (Spearman rho, 0.3 and 0.4, respectively). Higher levels of CEACAM5 mRNA were observed in CEACAM5 HEs vs MEs (P=0.0027). EGFR and KRAS genetic alterations by WES were present in 44.8% and 65.5% of CEACAM5 HEs, respectively, and 21.4% and 78.6% of CEACAM5 MEs, respectively. Confirmed partial responses were seen in 13/64 HEs (ORR 20.3%) and 2/28 MEs (ORR 7.1%). In CEACAM5 HEs with available baseline (BL) cCEA data, 25/62 (40.3%) had a cCEA level ≥ 100 µg/L, with a median value of 71.6 µg/L (range 1–8809); corresponding values in CEACAM5 MEs were 7/28 (25.0%) and 12.4 µg/L (range 0.5–684). In response evaluable CEACAM5 HEs with available BL cCEA data (n = 61), ORR was 10/24 (41.7%) in pts with high cCEA (≥ 100 µg/L) and 3/37 (8.1%) in pts with low cCEA (< 100 µg/L); corresponding ORRs in CEACAM5 MEs were 0/7 and 2/21 (9.5%).

Conclusion

In CEACAM5 HEs, high cCEA was associated with numerically greater ORR vs low cCEA (41.7% vs 8.1%). Associations were also observed between: cCEA and cCEACAM5; IHC CEACAM5, cCEA, and cCEACAM5; and IHC CEACAM5 and CEACAM5 tumor mRNA levels, but not between IHC CEACAM5 and actionable oncogenic drivers.

P.14.02

Prognostic Relevance Of Q787Q EGFR Polymorphism In Adenocarcinomas Of The Lung

M. N. Haffner¹, E. Ebert¹, G. Wagenpfeil², M. Becker³, B. Holleczer⁴, C. Stegmaier⁴, R. M. Bohle¹

¹Universitätsklinikum des Saarlandes, Institut für Allgemeine und Spezielle Pathologie, Homburg, Germany, ²Universitätsklinikum des Saarlandes, Institut für Medizinische Biometrie, Epidemiologie und Medizinische Informatik, Homburg, Germany, ³Justus-Liebig-Universität, Medizinische Klinik IV Organonkologie, Gießen, Germany, ⁴Krebsregister Saarland, Saarbrücken, Germany

Question/Background

Mutations in the *EGFR* and *KRAS* genes play an important role in the development of NSCLC. They may be instrumental in determining the therapeutic options. Currently, there are only few reported studies about the common synonymous variant Q787Q in EGFR exon 20. We sought to identify the clinical relevance of the Q787Q SNP using a qualitative and a semiquantitative approach.

Methods

We conducted a retrospective study of histologically confirmed cases of pulmonary adenocarcinomas from 2007 to 2017 (N=387). Variant status of *EGFR* and *KRAS* including mutation burden, clinical-histopathological standard parameters and survival were analyzed. The mutation status was assessed by sanger sequencing. Groups were formed on the basis of relative Q787Q-burden and compared among each other.

Results

In a comparison of Q787Q SNP versus wild type patients, overall survival was better in (ex)smokers (median 496 d versus 433 d, p=0.03), especially in (ex)smokers younger than 65 years (median 523 d versus 318 d, p=0.02), but disease specific survival of patients older than 65 years was worse (median 324 d versus 633 d, p=0.01). Survival rates did not differ significantly either in (ex)smokers ≥ 65 years or in patient subgroups formed on the basis of sex, tumor grading, TNM status, UICC8 stage. High Q787Q burden was significantly associated with longer overall survival in (ex)smoker patients (median of patients with high Q787Q burden=523-642 d versus median of patients with Q787Q wild type=433 d, p=0.01-0.03) and frequently coincided with „M1“ status (percentage of patients with „M1“ in the groups with high Q787Q burden=66-70 % versus percentage of patients with „M1“ in the groups with lower Q787Q burden=47-57 %, p=0.03-0.33). The Q787Q SNP and Q787Q burden did not correlate with median age of disease onset, sex, smoking history, tumor grading, TN status, UICC8 stage, *KRAS* mutation status including *KRAS* mutation burden and other *EGFR* mutations or *EGFR* mutation burden.

Conclusion

The prognostic value of the Q787Q SNP in pulmonary adenocarcinoma was discordant among different patient subgroups, indicating better prognosis in (ex)smokers but worse in patients ≥ 65 years regardless of smoking history. A high Q787Q SNP burden was correlated with better survival in (ex)smokers despite being

found more often in patients with „M1“ status. Multivariate survival analyses taking into consideration the chosen therapy would provide a more definitive evaluation of the prognostic value of the Q787Q SNP and its burden.

P.14.03

Comparative bioinformatic analysis of KRAS, STK11 and KEAP1 (co-)mutations in Non-Small Cell Lung Cancer with a special focus on KRAS G12C

M. Boeschen¹, C. Kuhn², H. Wirtz³, H.-J. Seyfarth³, A. Frille³, F. Lordick⁴, U. T. Hacker⁴, U. Obeck¹, M. Stiller¹, H. Bläker¹, M. von Laffert¹

¹University of Leipzig Medical Center, Institute of Pathology, Leipzig, Germany, ²Medical Faculty, University of Leipzig, Rudolf Schönheimer Institute of Biochemistry, Leipzig, Germany, ³University Hospital Leipzig, Department of Respiratory Medicine, Leipzig, Germany, ⁴Leipzig University Medical Center, Department of Medicine II, University Cancer Center Leipzig (UCCL), Leipzig, Germany

Question/Background

Mutations in *STK11* (*STK11*^{MUT}) and *KEAP1* (*KEAP1*^{MUT}) occur frequently in non-small cell lung cancer (NSCLC) and are often co-mutated with *KRAS* (*KRAS*^{MUT}). Several studies linked the co-occurrence of *KRAS*^{MUT}+*STK11*^{MUT}, as well as of *KRAS*^{MUT}+*KEAP1*^{MUT} to a negative impact on survival and response to immune checkpoint inhibitors (ICI). Data focusing *STK11*+*KEAP1* co-mutations or the triple mutation (*KRAS*+*STK11*+*KEAP1*) are scarce. The recent availability of *KRAS*-G12C inhibitors increases the relevance of this topic.

Methods

We present a comprehensive bioinformatic analysis encompassing six datasets with 6.046 mainly advanced NSCLC-patients retrieved from cBioPortal. We investigate the influence of *KRAS*^{MUT}, *STK11*^{MUT} and *KEAP1*^{MUT} co-occurrences on overall survival (OS) as well as the association with PD-L1 expression and tumor mutational burden (TMB) across different treatment lines including ICI. We analyze the influence of these mutations on metastatic behavior in patient's data and on the drug response in pan-cancer cell lines. We put a special focus on *KRAS* G12C.

Results

Across treatments, triple mutations, *KRAS*^{MUT}+*KEAP1*^{MUT} or *STK11*^{MUT}+*KEAP1*^{MUT} were significantly associated with a reduced OS. OS of patients with a *KRAS* G12C triple mutation was significantly reduced compared to patients with *KRAS* G12C-only. Under ICI-therapy, patients with the triple mutation or with *STK11*^{MUT}+*KEAP1*^{MUT} were significantly associated with a reduced overall survival. There was no significant difference in OS between patients harboring the *KRAS* G12C-only and patients with the *KRAS* G12C triple mutation, but a significant difference between patients harboring *KRAS* non-G12C and *KRAS* non-G12C triple mutations. This seems not to be reflected by means of a reduced PD-L1 expression or a higher TMB. Triple mutated primary tumors showed a significantly increased frequency of distant metastases in bone and in adrenal gland compared to *KRAS*-only mutated tumors. Additionally, our drug response analysis in cancer cell lines harboring the triple mutations revealed the WNT pathway inhibitor XAV-939 as a potential future drug candidate for this mutational situation.

Conclusion

The *KRAS*+*STK11*+*KEAP1* co-mutation status may serve as a negative prognostic and predictive factor across treatments compared to *KRAS*^{MUT}-only. This consideration is also true for *KRAS* G12C. *KRAS* G12C alone is a negative prognostic factor in patients under ICI therapy. In perspective, it appears promising to explore combinations of *KRAS* inhibition and ICI.

P.14.04

Acyl-coA synthetase long chain 5 (ACSL5) inhibits tumor cell growth and serves as a diagnostic marker in non-small cell lung cancer

Y. Ma, D. Schröder, M. Nenkov, A. Berndt, Y. Chen, N. Gassler

Institute of Forensic Medicine, Jena University Hospital, Friedrich Schiller University Jena, Section Pathology, Jena, Germany

Question/Background

Aberrant genetic alteration of metabolic enzymes or oncogene activation reprogramming the lipid metabolism through regulation of acyl-coA synthetase long chain (ACSL) metabolites is one of remarkable features of cancer. ACSL isoenzymes have different effects on driver mutant non-small cell lung cancer (NSCLC). ACSL3 and ACSL4 are essential for maintaining mutant *KRAS* and EGFR-TKI resistant lung cancer, respectively; however, the role of ACSL5 in lung cancer is not yet clear.

Methods

'Gain and Loss of Function' cell models were established and cell-based functional assays and underlying

molecular mechanism were analyzed. Immunohistochemistry was performed in normal lung and primary lung tumors.

Results

We found ACSL isoenzymes were differentially expressed in normal lung tissue, particularly in alveolar type II cells. ACSL1 and ACSL4 were universally expressed in all lung cancer cell lines, while ACSL3 and ACSL5 were widely absent; interestingly ACSL5 was highly expressed in two adenocarcinoma (ADC) cell lines harbouring EGFR mutations.

Lines of evidence show that ACSL5 four isoforms have distinct functions. Transfection of three ACSL5 isoforms (a, b and xl), respectively, led to decreased tumor cell proliferation, migration and invasion, and cell cycle arrest, along with reduced phosphorylated level of ERK1/2 and AKT, and dysregulated cyclin-dependent kinases: cyclin D and cyclin B, compared to control cells, suggesting ACSL5 has a tumor inhibitory behaviour. However, transfection of different isoforms exhibits different ectopic expression levels of ACSL5 accompanied by different ACSL activities, and exerts different levels of tumor suppressive function. It is worth to mention that transfection of ACSL5-iso.xl remarkable enhanced gemcitabine-induced apoptosis and activity of caspase 3. Knockdown of ACSL5 resulted in an increased migratory and invasive ability of tumor cells, as well as an elevated activity of ERK1/2 and AKT.

In primary lung tumors, ACSL5, ACSL1 and ACSL4 are potential diagnostic markers in lung ADC and higher ACSL5 expression was significantly correlated with a lower grade in lung ADC. Moreover, higher expression of ACSL1 was correlated with a lower grade, while higher expression of ACSL4 was correlated with higher grade.

Conclusion

In conclusion, our data suggest that ACSL5, ACSL1 and ACSL4 are potential diagnostic markers in lung ADC. ACSL5 plays a tumor suppressive role in NSCLC, however, three ACSL5 isoforms exert different levels of tumor suppressive function.

P.14.05

Investigating the role of oncogenic mutation BRAF-V600E in the diet-associated ChREBP knock-out mice Hepatocarcinoma development.

M. Yasser, M. Karim, F. Dombrowski, S. Ribback

Universitätsmedizin Greifswald, Institut für Pathologie, Greifswald, Germany

Question/Background

BRAF belongs to the RAF family of serine/threonine protein kinases, and acts as a crucial component of MAPK/ERK signalling pathways [1,2]. It also regulates wide range of cellular processes, including apoptosis, stress response, proliferation & differentiation [3]. Multiple studies have shown as BRAF and MEK pathways playing central role in the HCC (hepatocellular carcinoma) development [4,5,6]. The most common BRAF-V600E gene mutation, is reported to cause high kinase activation, proliferation and resistance to apoptosis [7,8,9]. Its functionality has not been reported in NAFLD (non-alcoholic fatty liver disease) associated HCC development or with the emerging central metabolic-regulator, ChREBP (carbohydrate responsive element binding protein) [10].

Methods

After 3, 6 & 12 months of control & high-fat diet administration to liver-specific ChREBP-KO & C57Bl/6J wild type mice (n=2-3/group). They were humanly anesthetized & abdominally perfused. The liver/tumor tissues were collected, histologically examined and DNA was extracted.

BRAF-V600E mutation analysis & allele frequency quantification was carried out by QIAcuity-digital-PCR (Qiagen, 26k nanoplate format). Briefly, digested template-DNA (ECORI) assayed with dPCR-LNA-mutation-assay (Qiagen, duplex-format, WT-HEX, mutation-FAM) for 1799 site. Positive control for BRAF-mutation included from: "therascreen-BRAF-V600E-RGQ-PCR-Kit" (Qiagen) & analysed by QIAcuity-software-suite.

Results

The dPCR mutant fraction (%) limits were detected in the range of 0.01 - 25%. Concordance of ~100% was observed for BRAF-V600E positive control and ~50% for WT & mutated DNA-sample mix (1:1), as expected. Mutant frequency in range of 0.1% detected for the mice HFD-tumor (12 months), whereas it was lower in the non-tumor sample from the same mice. Interestingly, a much higher mutant-allele frequency (0.3 - 25%) was detected in the pre-neoplastic liver-lesions from the patient samples, that were also added for the reference. There were no false positives detected and the values were consistent in duplicate runs.

Conclusion

The data demonstrate the potential of the assay to specifically detect & quantify BRAF-V600E mutant DNA in liver samples. However, efforts are ongoing in designing the BRAF-multiplex assay, to accurately quantify

various BRAF-V600 mutations with the QIAcuity-multiplex system in the mice samples to have a more integrated analysis.

Literaturangaben:

- [1] Hindley, Alison, and Walter Kolch., (2002), Extracellular signal regulated kinase (ERK)/mitogen activated protein kinase (MAPK)-independent functions of Raf kinases., Journal of cell science, 1575-1581
- [2] Śmiech, M., Leszczyński, P., Wardell, C., Poznański, P., Pierzchała, M. and Taniguchi, H., (2022), Oncogenic Mutation BRAF V600E Changes Phenotypic Behavior of THLE-2 Liver Cells through Alteration of Gene Expression, International Journal of Molecular Sciences, 23(3), p.1548.
- [3] Guo, Y. J., Pan, W. W., Liu, S. B., Shen, Z. F., Xu, Y., & Hu, L. L., (2020), ERK/MAPK signalling pathway and tumorigenesis, Experimental and therapeutic medicine , 19(3), pp.1997-2007
- [4] Ito, Y., Sasaki, Y., Horimoto, M., Wada, S., Tanaka, Y., Kasahara, A., Ueki, T., Hirano, T., Yamamoto, H., Fujimoto, J. and Okamoto, E., (1998), Activation of mitogen-activated protein kinases/extracellular signal-regulated kinases in human hepatocellular carcinoma., Hepatology , 27(4), pp.951-958.
- [5] Hoffmann, K., Shibo, L., Xiao, Z., Longerich, T., Büchler, M.W. and Schemmer, P., (2011), Correlation of gene expression of ATP-binding cassette protein and tyrosine kinase signaling pathway in patients with hepatocellular carcinoma, Anticancer research, 31(11), pp.3883-3890.
- [6] Zuo, Q., Huang, H., Shi, M., Zhang, F., Sun, J., Bin, J., Liao, Y. and Liao, W. (2012), Multivariate analysis of several molecular markers and clinicopathological features in postoperative prognosis of hepatocellular carcinoma, The Anatomical Record: Advances in Integrative Anatomy and Evolutionary Biology , 295(3), pp.423-431.
- [7] Cantwell-Dorris, E.R., O'Leary, J.J. and Sheils, O.M., (2011), BRAFV600E: implications for carcinogenesis and molecular therapy., Molecular cancer therapeutics, 10(3), pp.385-394.
- [8] Śmiech, M., Leszczyński, P., Kono, H., Wardell, C. and Taniguchi, H., (2020), Emerging BRAF Mutations in Cancer Progression and Their Possible Effects on Transcriptional Networks, Genes, 11(11), p.1342.
- [9] Loo, E., Khalili, P., Beuhler, K., Siddiqi, I. and Vasef, M.A. (2018), BRAF V600E mutation across multiple tumor types: correlation between DNA-based sequencing and mutation-specific immunohistochemistry, Applied Immunohistochemistry & Molecular Morphology, 26(10), pp.709-713
- [10] Nuernberger, V., Mortoga, S., Metzendorf, C., Burkert, C., Ehrlicke, K., Knuth, E., Zimmer, J., Singer, S., Nath, N., Karim, M. and Yasser, M.et.al, (2021), Hormonally Induced Hepatocellular Carcinoma in Diabetic Wild Type and Carbohydrate Responsive Element Binding Protein Knockout Mice, Cells, 10(10), p.2787

P.14.06

Genetic alterations with potential impact on PD-(L)1 targeted treatment in various cancer entities – Biobank research project of the INFINITY registry

L. E. Hillebrand¹, C. Vannier¹, P. M. Jermann², M. Matter², H. Läubli³, S. Grebhardt¹, P. R. Wright¹, S. M. Woerner¹, B. Kansenda³, N. Marschner¹, K. Potthoff¹

¹iOMEDICO AG, Medical Department, Freiburg, Germany, ²University Hospital Basel, Institute of Pathology and Medical Genetics, Basel, Switzerland, ³University Hospital Basel, Medical Oncology Department, Basel, Switzerland

Question/Background

The multicenter INFINITY registry investigates biomarker-driven treatment and management of patients with advanced malignancies not eligible for standard therapy options within routine clinical care in Germany. PD-(L)1 antibodies are frequently used in different tumor types and several biomarkers have been proposed to identify patients most likely to benefit. However, there is still a great need to further understand mechanisms of resistance to these immunotherapies. This research project was designed to analyze the genomic tumor profile of patients with clinical benefit from PD-(L)1 antibody treatment compared to those without.

Methods

All patients who received PD-(L)1 antibodies as monotherapy were identified from the INFINITY clinical database. A case-control design (clinical benefit vs. no-clinical benefit) was used based on predefined criteria: clinical benefit was defined as treatment duration >182 days and no clinical benefit was defined as treatment duration 22-63 days. The aim was to retrieve 24 tissue samples from the INFINITY biobank, 12 samples each from patients with and without clinical benefit. Next generation sequencing (NGS) was performed at a central molecular pathology laboratory (University Hospital Basel) using the OncoPrint™ Comprehensive Assay Plus panel (Thermo Fisher).

Results

Following sample selection and preparation, quality checks and NGS, ultimately 19 samples were available for interpretation in the full analysis set (FAS), thereof 11 samples of patients with clinical benefit and 8 samples of patients without clinical benefit from PD-(L)-1 antibody monotherapy. Patient and disease characteristics including clinical outcome data (best overall response and progression free survival), as well

as in depth data on genomic profiling comparing patients with vs. without clinical benefit will be presented.

Conclusion

Although sample numbers were too small to detect a clinically meaningful signal for clinical benefit from PD-(L)1 inhibitor therapy or not, the biobank research project of the INFINITY registry shows the feasibility of combining comprehensive clinical and genomic real-world data within a multidisciplinary team to address important clinical questions. The INFINITY registry provides a real-world dataset to address data gaps and generate new hypotheses on clinical questions that are otherwise difficult to investigate in prospective studies.

P.14.07

Immune cell profiles in solid tumors and correlation to PD-L1 and tumor mutational burden

S. Cysar^{1,2}, S. Laßmann^{1,2}, M. Werner^{1,2,3}

¹Institute for Surgical Pathology, Medical Center Freiburg, Freiburg, Germany, ²Comprehensive Cancer Center Freiburg, Medical Center, Freiburg, Germany, ³German Cancer Consortium (DKTK), partner site Freiburg, Freiburg, Germany

Question/Background

Our goal was to examine tumor infiltrating lymphocytes (TILs) including their subtypes (CD8+ and CD4+ subtypes) in primary or metastatic solid tumors and correlate this to PD-L1 expression as well as tumor mutational burden (TMB).

Methods

A total of 32 formalin fixed and paraffin embedded (FFPE) tissue specimens of primary tumors (n=9) and metastatic tumors (n=22) were assessed. For this, ovarian carcinoma (n=13), breast carcinoma (n=4), colorectal carcinoma (n=11), stomach carcinoma (n=3) and squamous cell carcinoma (n=1) were stained for HE as well as for PD-L1, CD4 and CD8. The TILs were analyzed with subgrouping of CD4- and CD8-positive cells in stromal (sTILs) /intraepithelial (ieTILs) areas per HPF, 400x magnification. Data of tumor mutational burden (TMB) was available from NGS-based panel diagnostics (TSO500, Illumina).

Results

Lymphocytes were predominantly seen in the stroma (sTILs: mean 18%, range 1%-70%) as compared to intraepithelial areas (ieTILs: mean 5%, range 1%-30%). Whilst CD4- and CD8-positive TILs were similar distributed in the stroma (absolute counts CD4: 75 +/- 61; CD8: 59 +/- 50), CD8-positive TILs were more frequent in intraepithelial areas (absolute counts: CD4: 4 +/- 7; CD8: 14 +/- 28). PD-L1 expression showed a wide range (TPS <1% to 65%, CPS <1 to 70, IC 0 to 2). Similarly, a broad range of TMB was observed (1.6 to 29.1 Mut/Mb). As expected, this biomarker diversity was due to the different tumor entities and stage. However, ovarian carcinomas appeared with higher number of CD8-positive ieTILs as compared to colorectal carcinomas (absolute counts: 28+/-41 versus 7+/-11). This was associated with increased PD-L1 positivity (TPS: 14+/-20, CPS 17+/-19 versus TPS 3+/-2, CPS 12+/-9), but not TMB (6.0+/-7.5 versus 6.1+/-2.9 Mut/Mb) respectively. In individual cases, high numbers of TILs were associated with high PD-L1 scoring. In contrast, a higher TMB was not associated with higher TILs and/or PD-L1 expression.

Conclusion

This small case series exemplifies the case-specific biomarker profiles, although a predominance of CD8-positive ieTILs in ovarian carcinomas was identified. Thereby, a high TMB did not necessarily lead to increased infiltration of lymphocytes and /or associated PD-L1 levels.

P.14.08

Analytic validation of EasyPGX ready NTRK Fusion – A CE-IVD approved one step real-time multiplex RT-PCR assay for the fast track detection of clinically relevant NTRK1,2,3 genetic rearrangements

A. Soiron^{1,2}, K. Falkenberg², L. Braun², A.-C. Puller², L. Heinst^{1,2}, R. Berthold^{1,2}, I. Isfort^{1,2}, M. Abbas², E. Wardelmann², W. Hartmann^{1,2}, M. Trautmann^{1,2}

¹Division of Translational Pathology, Gerhard-Domagk-Institute of Pathology, Münster University Hospital, Münster, Germany, ²Gerhard-Domagk-Institute of Pathology, Münster University Hospital, Münster, Germany

Question/Background

This retrospective validation study was designed to evaluate the fast track performance of Diatech's *in vitro*

diagnostic (CE-IVD) approved EasyPGX ready NTRK fusion one step real-time multiplex RT-PCR assay (ref. RT035) in a cohort of FFPE tumor specimens previously profiled for therapeutically actionable *NTRK1,2,3* genetic rearrangements by RNASeq (Illumina TruSight RNA Fusion Panel), pan-TRK IHC, and/or FISH. According to Diatech Pharmacogenetics, the limit of detection (LOD) and analytical sensitivity has been defined as the lowest input RNA quantity (2.5 ng/reaction), used for the RT-PCR amplification, that generates the correct results on covered *NTRK1,2,3* genetic rearrangements with a turnaround time from tissue to result in less than 3 hours with only 10 minutes of hands-on time.

Methods

Available formalin-fixed, paraffin-embedded (FFPE) tumor specimens previously profiled for *NTRK1,2,3* genetic rearrangements were selected from the archive of the Gerhard-Domagk-Institute of Pathology (Münster University Hospital, Germany). In total, >30 FFPE tissue specimens comprising a set of clinically relevant cancer types and various *NTRK1,2,3* fusion genes were included to assess analytical accuracy, sensitivity, and precision. In addition, the cell line-derived (I) Pan-Cancer 6-Fusion Panel FFPE RNA Reference Boa_Image_Frame (HD834, Horizon) and (II) Sereq FFPE NTRK Fusion RNA Reference Material (0710-1031, Seracare) were used as commercial quality-controlled material to monitor nucleic acid extraction, and *NTRK1,2,3* fusion RNA detection under Diatech's bioinformatics pipeline parameters.

Results

In this initial validation study, the EasyPGX ready NTRK fusion kit showed high analytic concordance, sensitivity and specificity potentials, consistent with requirements allowing the implementation of this CE-IVD assay for routine clinical fast track application.

Conclusion

Our results suggest that Diatech's EasyPGX ready NTRK fusion kit holds the potential as viable fast track solution for robust testing of covered therapeutically actionable *NTRK1,2,3* genetic rearrangements when time efficiency is crucial and/or comprehensive NGS capacity is not available. The integrated software suite allows for efficient interpretation with robust analytical performance.

P.14.09

Analytic validation of EasyPGX ready PIK3CA – A CE-IVD approved one step real-time multiplex RT-PCR assay for the fast track detection of PIK3CA mutations

L. Heinst^{1,2}, A. Soiron^{1,2}, S. Wosnig^{1,2}, K. Falkenberg², L. Braun², A.-C. Puller², R. Berthold^{1,2}, I. Isfort^{1,2}, M. Abbas², E. Wardelmann², W. Hartmann^{1,2}, M. Trautmann^{1,2}

¹Division of Translational Pathology, Gerhard-Domagk-Institute of Pathology, Münster University Hospital, Münster, Germany, ²Gerhard-Domagk-Institute of Pathology, Münster University Hospital, Münster, Germany

Question/Background

This retrospective validation study was designed to evaluate the fast track performance of Diatech's *in vitro* diagnostic (CE-IVD) approved EasyPGX ready PIK3CA one step real-time multiplex RT-PCR assay (ref. RT036) in a cohort of tumor specimens previously profiled for genetic alterations of the *PIK3CA* oncogene by NGS. Based on the Cosmic Database, approximately 90% of all *PIK3CA* mutations (in exon 4, 7, 9 and 20) described in breast and colorectal cancer are covered by this assay. According to Diatech Pharmacogenetics, the limit of detection (LOD) has been defined as the lowest amount of mutant DNA (0.5-2%) in a background of wild-type DNA at which a mutant sample will provide correct mutation-positive results on *PIK3CA* mutational status of covered variants in at least 95% of tests (medium input DNA concentration 12.5 ng/reaction) with a turnaround time from tissue to result in less than 3 hours with only 10 minutes of hands-on time.

Methods

Available formalin-fixed, paraffin-embedded (FFPE) tumor specimens previously profiled by NGS for genetic alterations of the *PIK3CA* oncogene were selected from the archive of the Gerhard-Domagk-Institute of Pathology (Münster University Hospital, Germany). In total, >60 FFPE tissue specimens (neoplastic content down to 30%) comprising a set of clinically relevant cancer types and various *PIK3CA* mutations (4-57% allelic frequency) were included to assess analytical accuracy, sensitivity, and precision. In addition, the cell line-derived Quantitative Multiplex FFPE Reference Boa_Image_Frame (HD200, Horizon) was used as commercial quality-controlled material to monitor mutated *PIK3CA* DNA detection under Diatech's bioinformatics pipeline parameters.

Results

In this initial validation study, the EasyPGX ready PIK3CA kit showed high analytic concordance, sensitivity and specificity, consistent with requirements allowing the implementation of this CE-IVD assay for routine clinical fast track application. External quality assessment and proficiency testing for *PIK3CA* mutation status (QulP, 10x HR+/HER2-negative breast cancer tissue samples) was successfully completed.

Conclusion

Our results suggest that Diatech's EasyPGX ready PIK3CA kit holds the potential as viable fast track

solution for robust testing for covered genetic alterations of the *PIK3CA* oncogene when time efficiency is crucial and/or comprehensive NGS capacity is not available. The integrated software suite allows for efficient interpretation with robust analytical performance.

P.14.10

Analytic validation of EasyPGX ready ALK/ROS1/RET/MET – A CE-IVD approved one step real-time multiplex RT-PCR assay for the fast track detection of clinically relevant ALK, ROS1, RET, MET genetic rearrangements

A. Soiron^{1,2}, K. Falkenberg², L. Braun², A.-C. Puller², L. Heinst^{1,2}, R. Berthold^{1,2}, I. Isfort^{1,2}, M. Abbas², E. Wardelmann², W. Hartmann^{1,2}, M. Trautmann^{1,2}

¹Division of Translational Pathology, Gerhard-Domagk-Institute of Pathology, Münster University Hospital, Münster, Germany, ²Gerhard-Domagk-Institute of Pathology, Münster University Hospital, Münster, Germany

Question/Background

This retrospective validation study was designed to evaluate the fast track performance of Diatech's *in vitro* diagnostic (CE-IVD) approved EasyPGX ready ALK/ROS1/RET/MET one step real-time multiplex RT-PCR assay (ref. RT025) in a cohort of FFPE tumor specimens previously profiled for therapeutically actionable *ALK*, *ROS1*, *RET*, *MET* genetic rearrangements by NGS, IHC, and/or FISH. According to Diatech Pharmacogenetics, the limit of detection (LOD) and analytical sensitivity has been defined as the lowest input RNA quantity (2.5 ng/reaction), used for the RT-PCR amplification, that generates the correct results on covered *ALK*, *ROS1*, *RET*, *MET* genetic rearrangements with a turnaround time from tissue to result in less than 3 hours with only 10 minutes of hands-on time.

Methods

Available formalin-fixed, paraffin-embedded (FFPE) tumor specimens previously profiled for *ALK*, *ROS1*, *RET*, *MET* genetic rearrangements were selected from the archive of the Gerhard-Domagk-Institute of Pathology (Münster University Hospital, Germany). In total, >45 FFPE tissue specimens comprising a set of clinically relevant cancer types and various *ALK*, *ROS1*, *RET*, *MET* genetic alterations were included to assess analytical accuracy, sensitivity, and precision. In addition, the cell line-derived Pan-Cancer 6-Fusion Panel FFPE RNA Reference Boa_Image_Frame (HD834, Horizon) was used as commercial quality-controlled material to monitor nucleic acid extraction, and *ALK*, *ROS1*, *RET* fusion RNA detection under Diatech's bioinformatics pipeline parameters.

Results

In this initial validation study, the EasyPGX ready ALK/ROS1/RET/MET kit showed analytic concordance, sensitivity and specificity potentials, consistent with requirements allowing the implementation of this CE-IVD assay for routine clinical fast track application.

Conclusion

Our results suggest that Diatech's EasyPGX ready ALK/ROS1/RET/MET kit holds the potential as viable fast track solution for testing of covered therapeutically actionable *ALK*, *ROS1*, *RET*, *MET* genetic rearrangements when time efficiency is crucial and/or comprehensive NGS capacity is not available. The integrated software suite allows for efficient interpretation with robust analytical performance.

P14 Postersitzung Molekularpathologie II

P.14.11

Clonal and „intrinsic“ heterogeneity of somatic variants in microsatellite-stable colorectal carcinomas and their metastases

M. Hühns¹, N. Ameziane², C. Holzmann³, R. Al-Ali², F. Prall⁴

¹Universitätsmedizin Rostock, Institut für Pathologie/Molekularpathologie, Rostock, Germany, ²Centogene AG, Rostock, Germany,

³Universitätsmedizin Rostock, Institut für Medizinische Genetik, Rostock, Germany, ⁴Universitätsmedizin Rostock, Institut für Pathologie, Rostock, Germany

Questions/Background

This study was designed to explore the heterogeneity of somatic genomic aberrations in colorectal carcinomas. Specifically, we set out to test if the heterogeneity patterns thus delineated would be consistent with Darwinian-type tumour evolution or rather suggest a different genesis.

Methods

We selected six treatment-naïve microsatellite-stable colorectal standard-type adenocarcinomas and their synchronous lymph node and liver metastasis. Genomic variants were identified by whole exome sequencing of large tumour fragments from the primaries and one liver metastasis each and used to design targeted resequencing NGS panels, one per case. Gross genomic aberrations were tested for by OncoScan array analyses.

Results

Targeted resequencing (mean coverage 2725/median 2222) was done with DNA from punch samples (1 mm tissue microarrayer needles) obtained from different regions of the primaries and their metastases. In total, 255 genomic variants were interrogated for heterogeneity in 108 punch samples. Notably, clonal heterogeneity was infrequent: in fact, a pattern of clonal heterogeneity consistent with a role in metastasis formation was seen but in a single instance (p.Asp604Tyr of the PTPRT gene). However, when comparing variant allele frequencies of genomic variants in adjacent positions on chromosomes ("matched genomic variant loci") across punch samples, there were seen differences that exceeded 2 standard deviation of the NGS assays' variations (*ad hoc* dubbed as VAF dysbalance) in 7.1% of the samples (2.6% to 12.0% per case). Additional OncoScan studies on a subset of the punch samples (31 in total) showed concomitant gross genomic aberrations in 39.2% of the matched genomic variant loci with VAF dysbalance.

Conclusion

Our study provides a fairly direct (statistical model-free) view into the genomic states of microsatellite-stable colorectal carcinomas and their metastases and suggests that, at least in a pre-chemotherapy setting, Darwinian-type tumour evolution is not the key pathway to metastasizing disease; instead, we recorded an intrinsic genomic heterogeneity which may echo an initial Big Bang-like event.

P.14.12

The role of mitochondrial DNA alterations and mTOR signalling in pancreatic neuroendocrine tumors (panNETs)

J. Buchwaldt, D.-C. Wagner, K. E. Tagscherer, W. Roth, N. Hartmann
Institute of Pathology, Mainz, Germany

Question/Background

Since a considerable percentage of pancreatic neuroendocrine tumors (panNETs) exhibit high mTOR activity, the current therapy for advanced panNETs includes inhibitors of the mTOR pathway. In addition to regulating cellular proliferation, mTOR signaling affects both mitochondrial activity and the expression of nuclear-encoded mitochondria-related genes. Therefore, in recent years it has been discussed whether the combined treatment with inhibitors of cellular metabolism could be beneficial for patients. However, little is known about the interaction between mTOR and mitochondria, particularly in panNETs. Thus, the aim of this study was to identify proteins that link these two systems.

Methods

For this purpose, we established a well-characterized cohort of 157 panNETs and determined the activity of the mTOR pathway for all cases by expression analysis of the phosphorylated ribosomal protein S6 in a tissue micro array (TMA). Somatic mutations in the mitochondrial DNA of panNETs were identified by Next Generation Sequencing (NGS) and gene expression of various mTOR and mitochondria related genes were measured by real-time PCR analysis.

Results

In total 34 cases of panNETs (22 %) showed activation of mTOR signaling. Mutational analysis of the entire mitochondrial genome identified numerous somatic mutations in the mitochondrial DNA of panNETs with and without mTOR activation suggesting mitochondrial DNA mutations are independent of the mTOR activity status. However, analysis of gene expression showed that the transcriptional co-activator PGC1 α seems to be activated by mTOR signaling. This is evidenced by the observation that the expression of PGC1 α is upregulated by up to 50 % in cases with activated mTOR pathway in comparison to cases with no activation.

Conclusion

Taken together, our results suggest that the master regulator of mitochondrial biogenesis PGC1 α could be a new possible linker between mTOR signaling and mitochondria activity.

P.14.13

Whole-exome sequencing of five mixed neuroendocrine-non-neuroendocrine neoplasms of the gastrointestinal tract

F. Kellers¹, A. Fährlich², N. Reimer², S. Fliedner^{3,4,5}, L. Bastian⁵, V. Stoll¹, K. Heß¹, H. Busch², C. Röcken¹, M. Jesinghaus⁶, B. Konukiewitz¹

¹University Medical Center Schleswig-Holstein, Campus Kiel, Department of Pathology, Kiel, Germany, ²University Medical Center Schleswig-Holstein, Campus Lübeck, Institute of Experimental Dermatology, Division Medical Systems Biology, Lübeck, Germany, ³University Cancer Center Schleswig-Holstein, Kiel & Lübeck, Germany, ⁴University Medical Center Schleswig-Holstein, Campus Lübeck, Department of Hematology and Oncology, Lübeck, Germany, ⁵University Medical Center Schleswig-Holstein, Campus Kiel, Department of Hematology and Oncology, Kiel, Germany, ⁶Universitätsklinikum Gießen und Marburg, Institut für Pathologie, Marburg, Germany

Question/Background

Most mixed neuroendocrine-non-neuroendocrine neoplasms (MiNENs) of the digestive system comprise a neuroendocrine carcinoma component combined with an adenocarcinoma component. These neoplasms are rare but correlate with a poor prognosis. Their genetic profile is incompletely understood. Most of them share genetic alterations with site-specific conventional adenocarcinomas. This study aims to explore the diagnostic potential and relevance of whole-exome sequencing of both components in order to decipher their clonal relation.

Methods

Five MiNENs (stomach n=2, colorectum n=3) were analysed. Histological and immunohistochemical classification and identification of glandular and solid differentiated tumor areas were conducted. DNA was extracted after microdissection. Whole-exome sequencing was performed on both tumor components. Two pure rectal neuroendocrine carcinomas served as control cases. Data analysis was conducted through MIRACUM Pipe. Variants with VAF ≥ 0.05 were analysed.

Results

We performed phenotypic and immunohistochemical analysis and whole-exome sequencing on five MiNENs of the colorectum and stomach and two colorectal NECs. All tumours were microsatellite stable. Whole-exome sequencing revealed the same oncogenic TP53 mutations in one gastric MiNEN in both tumour components. Two colonic MiNEN either showed an oncogenic KRAS or NRAS mutation only in the glandular component. In two colonic MiNENs likely oncogenic APC variants were found, either with the same variant in both components or only in the solid component.

Conclusion

The finding of identical putative driver mutations in both the solid and glandular components points to a shared clonal background. However, the occurrence of distinct mutations not shared in both components is evidence of separate tumor evolution and demands further investigation.

P.14.14

Analysis of miRNA Expression in Dedifferentiated Chondrosarcoma

F. S. Karras¹, J. Schreier¹, K. Körber-Ferl², S. R. Ullmann¹, S. Franke¹, A. Roessner¹, D. Jechorek¹

¹Institute of Pathology, Otto-von-Guericke University Magdeburg, Magdeburg, Germany, ²Institute of Human Genetics, Martin-Luther University Halle, Halle, Germany

Questions/Background

Dedifferentiated chondrosarcoma (DDCS) is a rare malignant subtype of cartilage tumors arising out of a conventional chondrosarcoma [1]. The histological appearance is typically characterized by two distinct areas, a well-differentiated low-grade tumor component and a mesenchymal high-grade sarcoma component [1]. Despite the obvious histological differences of both components, the underlying genetic mechanisms are widely unknown [2]. MiRNAs are able to regulate processes like differentiation by silencing gene expression on RNA level [3][4][5]. Therefore, we investigated differences in miRNA expression in the different components of DDCS.

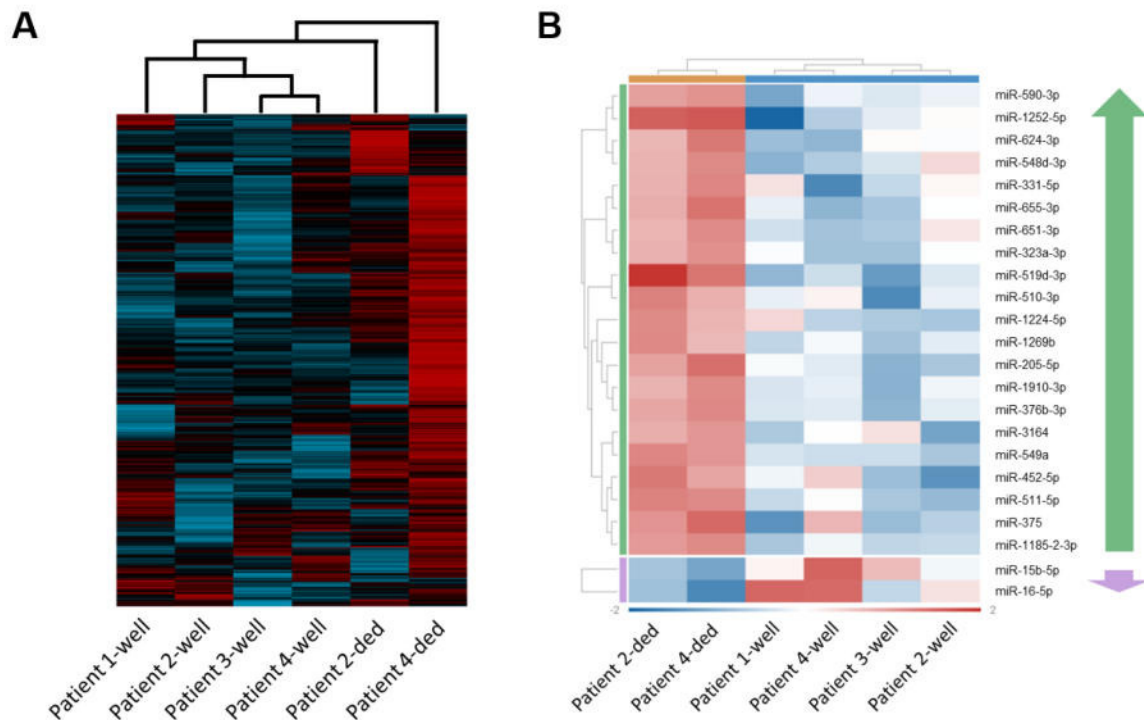
Methods

We analyzed the miRNA expression in both components of four DDCS using the miRNA panel for the nCounter® MAX Analysis System (NanoString Technologies). RNA was isolated from formalin-fixed,

paraffin-embedded tissue samples. Expression data was analyzed with nSolver (NanoString Technologies) and the bioinformatics platform ROSALIND® (OnRamp Bioinformatics). After quality control, four well-differentiated and two dedifferentiated samples were included in the final analysis. Data normalization was performed in two steps: positive control normalization and codeset normalization on the top 100 reference probes regarding average counts.

Results

Unsupervised clustering analysis revealed a correlation between the well-differentiated components and a tendency towards miRNA upregulation in the dedifferentiated components (Fig. 1A). We identified 21 upregulated and 2 downregulated miRNAs in the dedifferentiated components by differential expression analysis influencing signaling pathways like PI3K/Akt, NF- κ B, Wnt/ β -Catenin and the cell cycle (Fig. 1B).



miRNA profile of the well-differentiated and dedifferentiated components of DDCS. Heat maps of unsupervised clustering analysis of 797 miRNAs in the well-differentiated and dedifferentiated components (A) and the significantly deregulated miRNAs in the dedifferentiated components (B) of DDCS (red – upregulation, blue – downregulation, $p \leq 0.05$).

Conclusion

To our knowledge, we are the first to analyze the differential expression of miRNAs in the different components of DDCS. This study is a preliminary analysis due to a small number of samples. However, the identified deregulated miRNAs are a new indication of underlying mechanisms of the dedifferentiation process of conventional chondrosarcoma.

Literaturangaben:

- [1] WHO, (2020), Soft tissue and bone tumours, World Health Organization; International Agency for Research on Cancer, Geneva; Lyon, vol. 3, 5th edition
- [2] Lucas, C-HG.; Grenert, JP.; Horvai, A, (2021), Targeted Next-Generation Sequencing Identifies Molecular and Genetic Events in Dedifferentiated Chondrosarcoma, Arch. Pathol. Lab. Med., 1009–1017, 145(8)
- [3] Parafioriti, A; Cifola, I; Gissi, C; Pinatel, E; Vilardo, L; Armiraglio, E; Di Bernardo, A; Daolio, PA, (2020), Expression profiling of microRNAs and isomiRs in conventional central chondrosarcoma, Cell Death Discov., 46, 6
- [4] Zhang, L; Yang, M; Mayer, T; Johnstone, B; Les, C; Frisch, N; Parsons, T; Mi, Q-S; Gibson, G, (2017), Use of MicroRNA biomarkers to distinguish enchondroma from low-grade chondrosarcoma, Connect. Tissue Res., 155-161, 58(2)
- [5] Yoshitaka, T; Kawai, A; Miyaki, S; Numoto, K; Kikuta, K; Ozaki, T; Lotz, M; Asahara, H, (2013), Analysis of microRNAs expressions in chondrosarcoma, J. Orthop. Res., 1992-1998, 31(12)

Proteogenomic landscape of non-small cell lung cancer

A. Seredynska^{1,2}, R. Fiestas Cueto¹, L. Goncharenko¹, A. E. Cabrita Figueiredo¹, K. Konrad Kurowski¹, P. Westermann³, C. Messner³, K. Baerenfaller³, M. Werner¹, O. Schilling¹

¹Institute for Surgical Pathology, University Hospital Freiburg, Freiburg im Breisgau, Germany, ²German Cancer Consortium (DKTK) and German Cancer Research Center (DKFZ), Heidelberg, Germany, ³Swiss Institute of Allergy and Asthma Research (SIAF), University of Zurich, Davos, Switzerland

Question/Background

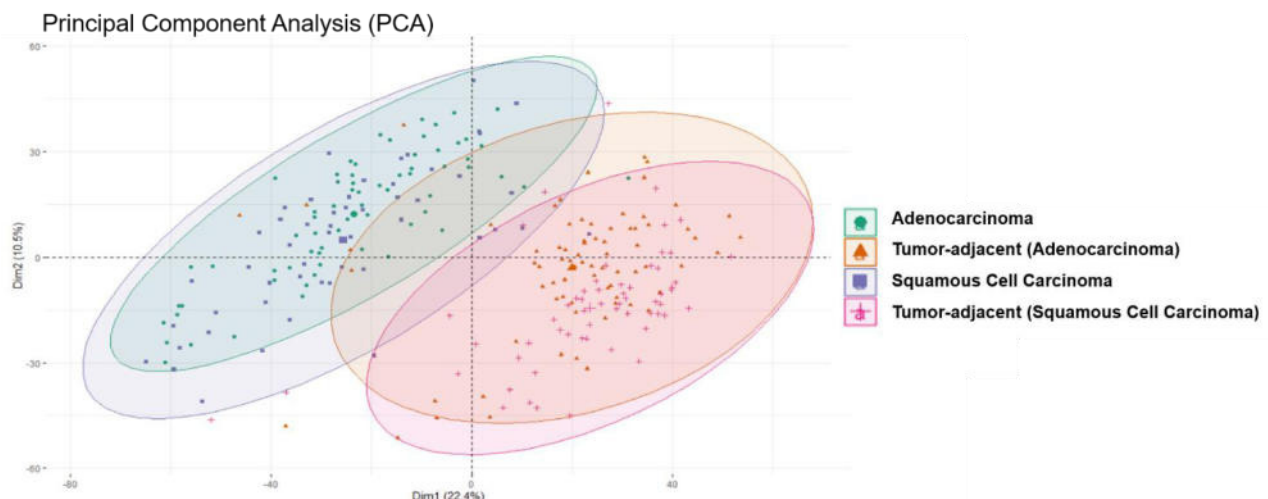
Non-small cell lung carcinoma (NSCLC) is the most common type of lung cancer, with adenocarcinoma (LUAD) and squamous cell carcinoma (LUSC) being the most prevailing histological subtypes with distinct biological signatures. Correct classification and accurate molecular profiling are essential for effective therapeutic guidance. Therefore, a correct distinction between LUAD and LUSC and deeper understanding of the molecular alterations on the genetic and protein level are required in order to detect biologically relevant biomarkers.

In this study, we aim to perform an in-depth mass spectrometry (MS)-based proteogenomic study of a large patient cohort representing the two aforementioned subtypes of NSCLC. The MS-based profiling of the LUAD and LUSC and their primary types revealed the proteogenomic alterations that might determine their clinical behaviour. High-coverage proteome analysis should also unravel the mechanisms of immune evasion in NSCLC. Moreover, a follow up immunopeptidomics study should reveal the tumor-associated antigens, which are pivotal for the development of epitope-specific cancer immunotherapies.

Methods

Patient-derived samples were processed with optimized, semi-automated single-pot, solid phase enhanced sample preparation (SP3-beads) workflow utilizing a pipetting BRAVO robot. Thereby, extracted proteins were digested and the resulting peptides were analyzed via liquid-chromatography tandem-mass spectrometry (LC-MS/MS).

Results



Principal Component Analysis of Non Small Cell Lung Carcinoma (NSCL)

The MS-analysis of the patient cohort (consisting of $n = 153$ tumor and $n = 138$ normal tissue) resulted in high proteome coverage of a total of 6951 proteins. Initial statistical analysis shows significant differences between LUAD and LUSC and suggest a possible distinction of proteome profiles based on patient's gender.

Conclusion

Deep proteomic coverage enables us to gain deeper insight into fundamental molecular biology of LUAD and LUSC. Ongoing proteomic analysis will also unravel their key differences.

P.14.16

N-Glycan in-situ Characterization of Small Blue Round Cell Tumors

J. P. L. Goncalves, C. Bollwein, W. Weichert, K. Schwamborn
TU München, Institut für Pathologie, München, Germany

Question/Background

orphological characterization of small blue round-cell tumors (neuroblastoma, rhabdomyosarcoma, lymphoma, and Ewing sarcoma) is challenging, and routine immunohistochemistry (IHC) is often insufficient to define the tumor.

Glycosyltransferases enzymatic activity and gene expression are altered in various pathophysiological situations, namely in tumor development. In this study, we have characterized the *N*-Glycan content of the tumors utilizing matrix-assisted laser desorption/ionization (MALDI) mass spectrometry imaging (MSI) to better comprehend the molecular signatures of each tumor type.

Methods

Samples from small blue round-cell tumors (SBRCT, n = 26) were assembled in a tissue microarray: Ewing sarcoma (EWS, n = 5), rhabdomyosarcoma (RMS, n = 5), neuroendocrine carcinoma (NEC, n = 5), acute lymphoblastic leukemia (ALL, n = 5), nephroblastoma (NEPB, n = 3), and neuroblastoma (NEUB n = 3). The specimens were subjected to on-tissue enzymatic digestion, utilizing *N*-glycosidase F, followed by matrix application (α -cyano-4-hydroxycinnamic acid). Samples were analyzed utilizing MALDI-TOF mass spectrometry. Subsequently, the matrix was removed, the section was stained by hematoxylin and eosin for meticulous histopathological annotation. Data analysis was performed using SCI²S Lab (Bruker) and statistical analysis was performed on R.

Results

MSI data was employed for the training and validation of classification algorithms. Random forest classification yielded over 96% accuracy. From the analysis of feature extraction, it was possible to establish correlation between some molecular features and tumor types (Hex4dHex1HexNAc5, could be associated with NEPB, while Hex3dHex1HexNAc5 is overexpressed in NEPB and NEUB). From the receiver operating characteristic – area under the curve (ROC-AUC) analysis we found that Hex5HexNAc4 was a discriminating feature between EWS and RMS; and Hex4dHex1HexNAc5 and Hex3dHex1HexNAc6, were found to be differently expressed between NEPB and NEUB subtypes.

Conclusion

In this study, we show that *N*-Glycan imaging is an auspicious methodology to assist in the stratification of different small blue round-cell tumors.

P.14.17

Gene Expression Profiling of Uveal Melanoma revealed Immunogenic Phenotypes in Primary Tumors as well as in Metastases

S. Borchert¹, K. Al-Ghazzawi², Y. Krause¹, M. Wessolly¹, S. Ting³, N. Bechrakis², F. D. Mairinger¹

¹Institut für Pathologie am Universitätsklinikum Essen, Translationale Tumorforschung, Essen, Germany, ²Klinik für Augenheilkunde, Universitätsklinikum Duisburg-Essen, Essen, Germany, ³Institut für Pathologie Nordhessen, Kassel, Germany

Question/Background

Uveal melanoma (UM) is known as melanoma of the choroid, ciliary body, and iris of the eye. Among ocular melanomas, 83% arise from the uvea. UM could be divided into two molecular classes, predicting metastatic death: class 1 UM with low metastatic risk and class 2 UM with high metastatic risk, that are characterized by monosomy of chromosome 3.

Therapy options of metastatic UM are limited in patients. Therefore, prediction of localization of distant metastases would be a helpful tool for management of the disease.

The aim of this study was to investigate gene expression of UM primary tumors and their respective metastases. By the comparison of gene expression patterns, we aimed to find predefined gene expression patterns in primary tumors that potentially predict localization of metastases. These predefined molecular patterns could enhance clinical outcome of this severe disease.

Methods

We investigated 24 formalin-fixed, paraffin-embedded (FFPE) specimens of uveal melanoma and metastases by using the oncology biomarker panel (HTG Molecular). 14 samples were primary tumors and 10 samples represented metastases of the liver (n= 8), the bone (n= 1), and the lymph node (n= 1). The wing probes of the OBP panel hybridized to the target RNA in an extraction-free technology by HTG. Hybridized wing probes were tagged with sequence adapters in an additional PCR step and the subsequent library was sequenced on an Illumina Next Seq 500/550 platform. Sequencing data were parsed by the HTG parser and the results were analyzed by using the R environment.

Results

We were not able to identify a predefined expression pattern in primary tumors, predicting localization of distant metastases. However, gene set enrichment analysis (GSEA) revealed in both primary tumors and metastases an immunogenic phenotype that has been associated with enhanced response to immune checkpoint blockade (ICB).

Conclusion

The gene expression pattern of primary tumors do not indicate the localization of metastases. We could observe different biological phenotypes in our cohort. Especially, we found an immunogenic phenotype in both primary tumors and metastases. These patients seem to show enhanced response to immunotherapy. There was no association to clinical markers like involvement of the ciliary body, the iris or the size stage. The present data may improve the understanding of underlying cellular mechanisms and open new possibilities for enhanced management of therapeutic approaches for this severe disease.

P.14.18

Analysis and annotation of next generation sequencing data with the database Cancer Genome Interpreter-Clinics

J. Fassunke¹, N. Ortiz-Brüchle², A. Maurer², C. Jonas¹, M. Kirschner³, S. Merkelbach-Bruse¹, M. Ihle¹

¹Uniklinik Köln, Institut für Pathologie, Köln, Germany, ²Uniklinik Aachen, Institut für Pathologie, Aachen, Germany, ³Uniklinik Aachen, Klinik für Hämatologie, Onkologie, Hämostaseologie und Stammzelltransplantation, Aachen, Germany

Questions/Background

Interpretation of data is a bottleneck for the full deployment and broad accessibility of Next Generation Sequencing (NGS) for personalized medicine in cancer management. Cancer Genome Interpreter-Clinics (CGI-Clinics) is a 5-year €10 million European research initiative initiated by Dr. Nuria Lopez-Bigas and her team at the Institute for Research in Biomedicine, Barcelona, and focuses on a database for interpreting gene mutations in a biological and clinical context. CGI Clinics brings together 17 project partners from four countries, including with the University Hospitals of Cologne and Aachen also two sites from Germany.

Methods

The current challenge for the interpretation of variants from comprehensive sequencing is the lack of standardization and consolidation of the different platforms and databases. As a result, a particularly large amount of time is required to interpret the variants. Another challenge is the huge number of variants with unknown significance, meaning their impact for the patients is unknown. CGI-Clinics is a community-driven project that aims to improve personalised medicine in oncology by optimising genomic data interpretation by using a systematic approach, dealing with a majority of variants of unknown significance and patient empowerment.

Results

CGI-Clinics identifies the likely driver alterations in cancer genes in the tumor type in question using computational methods (BoostDM and OncodriveMut). Alterations that constitute biomarkers of response to anti-cancer drugs are identified according to several databases (CIViC, OncoKB and the Cancer Biomarkers database). The special feature of the project is the increased focus on patients. The data and results will be more accessible to patients. CGI-Clinics will develop a virtual molecular tumor board as well as an app for patients during the course of the project.

Conclusion

Overcoming the challenges of data interpretation the CGI Clinics platform will be a huge benefit for cancer management and personalized medicine. Patients will have the opportunity to gain a better understanding of their disease and will be encouraged to make their data available for research purposes. Data maintenance will remain a challenge as science evolves and new biomarkers are identified. Therefore, an important focus of CGI clinics is flexibility for new candidate genes and keeping data as current as possible. This project received funding from the EU Horizon program HORIZON-HLTH-2021-CARE-05-02 under grant agreement No. 101057509.

Integrating proteomics into diagnostic molecular pathology reports for molecular tumor board decisions

M. Fahrner^{1,2}, U. Matysiak^{1,3}, J. Thiery¹, N. Pinter¹, S. Cysar¹, U. Wlokka¹, S. Laßmann^{1,3}, M. Werner^{1,2,3}, O. Schilling^{1,2}

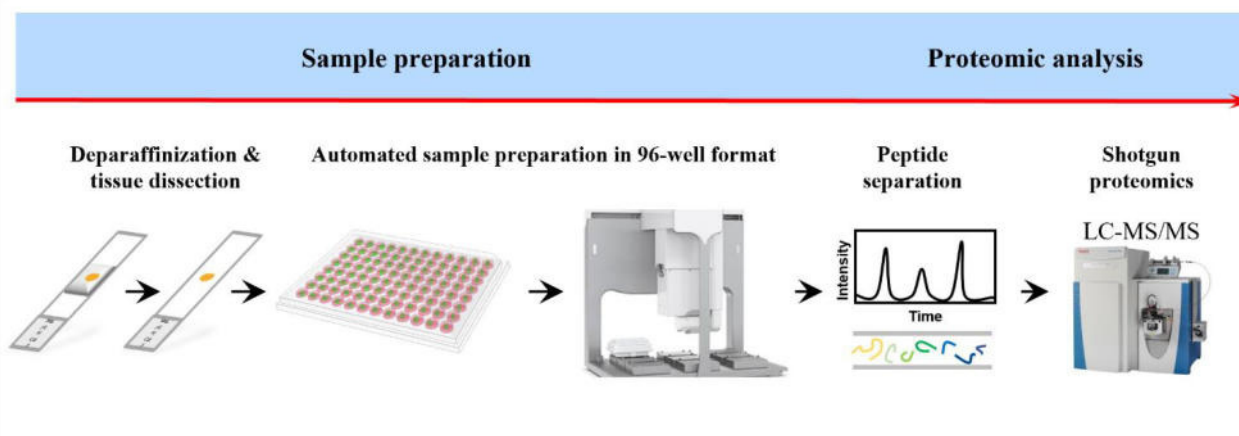
¹Institute for Surgical Pathology, Medical Center – University of Freiburg, Faculty of Medicine, University of Freiburg, Freiburg, Germany, ²German Cancer Consortium (DKTK) and Cancer Research Center (DKFZ), Freiburg, Germany, ³Comprehensive Cancer Center Freiburg, Medical Center, Freiburg, Germany, Freiburg, Germany

Question/Background

Molecular pathology largely relies on genomic and transcriptomic approaches for comprehensive and sensitive molecular diagnostics. Continuous instrument and method development in quantitative mass spectrometry (MS)-based proteomics enable reproducible in-depth proteome investigations in various patient-derived samples, including body fluids and tissue specimens. Thus, we set out to integrate clinical proteomics into molecular diagnostics, complementing and expanding the existing molecular diagnostic routine and providing another layer of biological information.

Methods

We applied automated MS-based quantitative proteomic workflows to perform reproducible and robust in-depth proteomics of formalin-fixed paraffin-embedded (FFPE) tissue from patients that were included in the molecular tumor board.



Automated sample preparation for quantitative mass spectrometry-based proteomics using patient-derived tissue specimens.

All patients also received molecular diagnostic routines including Gene-Panel sequencing and RNA Fusion analysis.

Results

With our robust, reproducible, and automated sample preparation approach, we identified and quantified reliably more than 4000 proteins in over 50 MTB-derived samples. In 26 cases the proteomic analysis has contributed to the molecular pathology reports, providing additional insights into the underlying molecular mechanisms in the respective malignancies.

In addition to the full proteome approach, we established a phosphoproteomic approach, which has yielded functional insights regarding the activity of pathways of interest in selected MTB cases.

Furthermore, we established a proteogenomic analysis workflow that enables the integration of proteomics and genomics.

Exemplary contribution of proteomics includes the detection of CDK4 and CDK6 in cases with a CDKN2A loss-of-function mutation, supporting the efficiency of a CDK inhibition treatment, as well as the detection of ERK signaling in a patient with a BRAF-KIAA1549 fusion, providing a rationale for MEK inhibition.

Conclusion

We demonstrate the added value and potential of such integrated analysis in the molecular characterization

of particularly rare and challenging tumors that are investigated and discussed in the interdisciplinary molecular tumor board.

P.14.20

Analytic validation of OncoDEEP – A comprehensive genomic profiling NGS panel for mutational and clinical biomarker analysis in routine cancer patient diagnostics

K. Falkenberg¹, L. Braun¹, A.-C. Puller¹, L. Heinst^{1,2}, R. Berthold^{1,2}, I. Isfort^{1,2}, M. Abbas¹, E. Wardelmann¹, W. Hartmann^{1,2}, M. Trautmann^{1,2}

¹Gerhard-Domagk-Institute of Pathology, Münster University Hospital, Münster, Germany, ²Division of Translational Pathology, Gerhard-Domagk-Institute of Pathology, Münster University Hospital, Münster, Germany

Questions/Background

Comprehensive genomic profiling (CGP) and reliable molecular characterization of solid tumors using next-generation sequencing (NGS) technology has become a key tool to facilitate treatment decisions and the clinical management of cancer patients. With a broad spectrum of targeted therapies already approved or in clinical trials, rapid and scalable detection of an increasing number of therapeutically relevant genomic alterations and cancer molecular signatures is required. OncoDNA's OncoDEEP workflow integrates both, a comprehensive cancer NGS panel powered by Twist Bioscience hybrid capture enrichment and library preparation technology in combination with OncoDNA's cloud-based bioinformatic data analysis and clinical interpretation software suite (OncoKDM and MERCURY) resulting in an integrated theranostic report of a patient's tumor molecular profile. The CE-IVD approved assay covers single-nucleotide variants (SNVs), copy number variants (CNVs), deletions and insertions (indels) in 638 genes relevant to solid tumors while also determining key complex immuno-oncology biomarkers such as homologous recombination deficiency (HRD), tumor mutational burden (TMB), or microsatellite instability (MSI).

Methods

Extensive validation of OncoDNA's OncoDEEP workflow was performed on DNA from >250 clinical cancer tissue specimens (neoplastic content down to 20%) in combination with commercially available reference materials with known genomic profile to assess analytical accuracy, sensitivity, and precision. DNA was extracted from formalin-fixed and paraffine-embedded (FFPE) material and sequenced on a NextSeq 550 system (Illumina).

Results

In this initial validation study, the OncoDEEP workflow facilitated robust sample preparation and exhibited high analytic concordance, sensitivity and specificity consistent with requirements allowing the implementation of this CE-IVD assay for routine clinical application.

Conclusion

Our results demonstrate that OncoDNA's OncoDEEP workflow provides a complete and powerful solution for accurate comprehensive genomic profiling of cancer DNA samples not only for clinical actionability but also for differential diagnostics to guide personalized treatment decisions. The integrated software suite allows for efficient interpretation and clinical reporting of patient's tumor molecular profile with robust analytical performance.

P.InterPath. Postersitzung Pathologie und Interdisziplinarität

P.InterPath.01

Pathology Cancer Dashboard: Development of a pathology-centered online application for epidemiologically guided differential diagnosis

T. S. Gerber, S. Strobl, M. Kloth, S. Porubsky, W. Roth, B. K. Straub
University Medical Center Mainz, Institute of Pathology, Mainz, Germany

Question/Background

The histopathological diagnosis of rare malignant tumors may be challenging. Especially among non-specialized and young pathologists, the diagnosis of rare entities is inherently laborious and may carry a high

risk of both temporal delays and relevant misdiagnosis as not all relevant differential diagnoses may be taken into account. The knowledge of epidemiologic data may be inherently important, yet not comprehensively available. To give pathologists diagnostic tools in these challenges, the Pathology Cancer Dashboard project was developed.

Methods

The National Cancer Institute's Surveillance, Epidemiology, and End Results (SEER) data provide information on cancer statistics among the United States population. These data were obtained from the SEER Research Limited-Field Data, 22 Registries, Nov 2021 Sub (2000-2019; SEER 22) using SEER*Stat software (version 8.4.0.1). The German data were retrieved from the Centre for Cancer Registry Data (Zentrum für Krebsregisterdaten, ZfKD).

Results

We have created an application using more than 25 million individual data from SEER and ZfKD cancer registries. In addition to age and gender, information on tumor localization and entity can be extracted (each coded according to the ICD-O-3 classification). The user can define search criteria such as localization and lineage differentiation i.e. mesenchymal, epithelial, and neuroendocrine progeny. According to the criteria selection, aggregated data is generated, including a ranking with the respective frequency and percentage of each entity as well as age and sex distributions.

Conclusion

With the help of this online application, basic epidemiological information may be retrieved at any time, sorted by line differentiation and localization. This powerful diagnostic ancillary tool allows a fast and reliable estimation of the entities, which, from an epidemiological point of view, could be considered for differential diagnosis and could thus significantly facilitate the differential diagnosis of tumors.

P.InterPath.02

Shortage of vascular surgery specialists as of other medical specialists in Germany - alarming aspects and a possible multidisciplinary effective approach for its improvement

U. Barth¹, Z. Halloul², F. Meyer³

¹Dept. of General, Vascular and Abdominal Surgery; Municipal Hospital ("Helios Klinik Jerichower Land"), Division of Vascular Surgery, Burg, Germany, ²Dept. of General, Abdominal, Vascular and Transplant Surgery; Otto-von-Guericke University with University Hospital, Division of Vascular Surgery, Magdeburg, Germany, ³Dept. of General, Abdominal, Vascular and Transplant Surgery; Otto-von-Guericke University with University Hospital, Magdeburg, Germany

Question/Background

The shortage of specialists has also arrived in vascular surgery.

Methods

Compact narrative review based on selective references of the current medical-scientific literature & own experiences from daily practice

Results

A research report commissioned by the "Deutsche Krankenhausgesellschaft" (DKG, "German Hospital Association") in 2010 predicted a replacement demand for physicians of a good 108,000 by 2019 & an additional demand of almost 31,000 physicians. While 14.6 to 27.2% of those employed in 2008 will retire by 2020, between 45.6 & 68.5% will retire by 2030.

The following recommendations for action emerged from the expert reports were derived: Relief from administrative tasks & documentation obligations, professional personnel planning & development, reduction of the "drop-out" rates in medical studies & increase of study capacities in human medicine, family-oriented measures, overcoming of double care through strict separation of outpatient & inpatient treatment, the reorganisation of medical tasks through delegation & a promoted immigration of foreign doctors.

Although the emerging trend has been known for years, the hesitant attempts of politicians & professional societies have not led to a decisive turnaround. Practical solutions at country level could be:

- Bringing vascular diseases more into the public focus,
- Stronger/more accentuated organisation & unification of vascular surgeons at regional level,
- The creation of a chair for vascular surgery (vascular medicine) at one of the universities,
- More regional-level continuing education for young residents,
- Creation of a platform for young vascular surgeons (&)
- State-wide networking forms for day-to-day problems such as bed, intensive care &/or

surgical intervention capacities (as well as)

- Central organisational coordination as well as coordinated & fair revenue generation + subsequent reimbursement for outpatient clinic & day surgery in vascular medicine.

Conclusion

The current situation & the expected worsening of it should give reason to address the problems with practical solutions & initiatives beyond the particular interests of the hospital operators **as it seems to be also the case in several other medical disciplines**. A turnaround can only be achieved with the cooperation of all vascular surgeons & vascular surgery departments or future clinics in the state with concrete proposals & demands to state policy & clinic operators. As leading institution & coordinator, university hospitals should act.

P.InterPath.03

Joining Forces for Better Treatment: The Power of Multidisciplinary Limb Board Meetings with Live Microscopy

L. Winter¹, D. H. Mendelsohn^{1,2}, N. Walter², A. Mamilos¹, T. Niedermair¹, V. Alt², M. Rupp², C. Brochhausen^{1,3}

¹University Regensburg, Institute of Pathology, Regensburg, Germany, ²University Hospital Regensburg, Department for Trauma Surgery, Regensburg, Germany, ³Ruprecht-Karls-University Heidelberg, University Medical Centre Mannheim, Institute of Pathology, Mannheim, Germany

Question/Background

Multidisciplinary team (MDT) meetings have emerged as a promising approach for the treatment of cancer patients. Although MDT meetings are well established in oncology, they play a minor role in other diseases. Recent evidence suggests that implementing MDT meetings can improve patient outcomes in musculoskeletal infections [1]. The pathologist's input may be particularly valuable in clarifying diagnoses, leading to optimal patient treatment strategies.

Methods

We described the set-up of the multidisciplinary limb board, including live microscopy, with a special focus on the pathologist's role. Furthermore, the patient characteristics and relevant findings were extracted from the electronic medical records of our institute. We investigated the impact of the pathologist's assessment on the patient's diagnosis, including whether it was confirmed or rejected.

Results

Our multidisciplinary limb board team meets regularly to discuss imaging data, laboratory chemistry data, intraoperative observations, and histopathological findings utilizing live microscopy for enhanced visualization. From May 2020 to December 2022, the pathologies for a total of 66 patients were demonstrated to our multidisciplinary limb board by live microscopy using 124 histopathological findings and 181 histochemical stainings. The most frequently discussed pathologies included periprosthetic joint infection (24.2%), osteomyelitis (22.7%), and fracture-related infections (18.2%). In 85.5% of the findings, the pathologist specified the suspected diagnosis of the requesting physician. A total of 14.5% of the suspected diagnoses were rejected.

Conclusion

Our results demonstrate that MDT meetings including live microscopy in patients with musculoskeletal infections holds potential benefits for patient care. Thus, the pathologist plays a relevant role in clarifying the diagnosis, leading to an optimal treatment plan for each patient. However, potential challenges, such as organizational effort and technical prerequisites should be considered. Finally, the interdisciplinary limb board improves communication, and scientific collaboration and raises clinicians' awareness of relevant histopathology findings, which is crucial in the current concept of minimal bone resection.

Literaturangaben:

[1] Walter N, Rupp M, Baertl S, Ziarko TP, Hitztenbichler F, Geis S, Brochhausen C, Alt V., (2022), Periprosthetic joint infection : patients benefit from a multidisciplinary team approach, Bone Joint Res., 2023-02-16

P.InterPath.04

αvβ6-integrin expression in different cancer entities: new insights for theranostics

T. Groll¹, S. Ballke¹, M. Jesinghaus², W. Weichert¹, J. Notni³, K. Steiger¹

¹Institut für Pathologie, Technische Universität München, Comparative Experimental Pathology, München, Germany, ²Institut für Pathologie, Universitätsklinikum Gießen und Marburg, Marburg, Germany, ³Targeted Radiopharmaceuticals In Molecular Theranostics (TRIMT) GmbH, Radeberg, Germany

Question/Background

$\alpha\beta 6$ -integrin belongs to a class of 24 transmembrane cell adhesion receptors. It is solely expressed by epithelial cells and upregulated in a variety of carcinomas. It promotes cancer invasion and is linked to poor prognosis, making it a promising target for theranostics. The successful application of the novel, improved ^{68}Ga -labeled trimerized $\alpha\beta 6$ -integrin selective nonapeptide ^{68}Ga -Trivehexin for imaging of human carcinomas has been reported [1]. The aim of this study was to evaluate the expression of $\alpha\beta 6$ -integrin in Non-small cell lung cancer (NSCLC) and Colorectal cancer (CRC) to test for eligibility as diagnostic imaging and/or therapeutic target. Comparative evaluation of $\alpha\beta 6$ -integrin expression by immunohistochemistry (IHC) in NSCLC and CRC has not been performed so far.

Methods

Two Tissue Microarray (TMA) cohorts consisting of 71 NSCLC cases (1-3 TMA cores per case; 188 cores in total) and 152 CRC cases (1-2 TMA cores per case; 260 cores in total) were evaluated. Samples were fixed in 10% neutral-buffered formalin and routinely processed for histology. Tissue was examined by using anti-human $\beta 6$ -Integrin antibody [clone 442.5C4] (#407317, dilution 1:100, Merck Millipore, Burlington, Massachusetts, USA). Slides were digitalized and evaluated by using Aperio ImageScope (Leica Biosystems). A modified score [2] including intensity and frequency of membranous $\alpha\beta 6$ -integrin expression was applied.

Results

The majority of NSCLC (77,5 %) showed strong (49,3 %) or moderate (28,2 %) positivity for membranous $\beta 6$ -integrin expression. Most of the evaluated CRC cases (69,1 %) were negative (31,6 %) or revealed low (37,5 %) $\beta 6$ -integrin expression. Thus, NSCLC generally displayed a higher membranous $\beta 6$ -integrin expression score than CRC.

Conclusion

Based on our findings, $\alpha\beta 6$ -integrin seems to be a promising target for radiopharmaceuticals in NSCLC. Targeting $\alpha\beta 6$ -integrin may facilitate the assessment of carcinoma margins and/or invasiveness and may also allow therapeutic intervention with radioligands at critical locations [3]. For CRC, we could show an overall lower $\alpha\beta 6$ -integrin expression compared to NSCLC on protein level. IHC screening for membranous $\alpha\beta 6$ -integrin expression may be a helpful tool before moving on to clinical application, as the cell membrane is the crucial site for binding integrin selective radiopharmaceuticals.

Literaturangaben:

- [1] Quigley, N.G., et al., (2022), PET/CT imaging of head-and-neck and pancreatic cancer in humans by targeting the "Cancer Integrin" $\alpha\text{v}\beta 6$ with Ga-68 -Trivehexin., *Eur J Nucl Med Mol Imaging*, p. 1136-1147, 49(4), PubMed
- [2] Sipos, B., et al., (2004), Immunohistochemical screening for $\beta 6$ -integrin subunit expression in adenocarcinomas using a novel monoclonal antibody reveals strong up-regulation in pancreatic ductal adenocarcinomas in vivo and in vitro., *Histopathology*, p. 226-36., 45(3), PubMed
- [3] Steiger, K., et al., (2021), There is a world beyond $\alpha\text{v}\beta 3$ -integrin: Multimeric ligands for imaging of the integrin subtypes $\alpha\text{v}\beta 6$, $\alpha\text{v}\beta 8$, $\alpha\text{v}\beta 3$, and $\alpha 5\beta 1$ by positron emission tomography., *EJNMMI Res*, p. 106, 11(1), PubMed

P.InterPath.05

Correlation of pathological and microbiological findings in non-neoplastic vitrectomy specimens: a single-center retrospective study

M. Sulyok¹, K. Schmauder², S. Peter², I. Bonzheim¹, D. Süsskind³, K. U. Bartz-Schmidt³, F. Fend¹

¹Eberhard Karls University of Tübingen, Department of Pathology and Neuropathology, Tübingen, Germany, ²Eberhard Karls University of Tübingen, Institute of Medical Microbiology and Hygiene, Tübingen, Germany, ³Eberhard Karls University of Tübingen, Klinik für Augenheilkunde, Tübingen, Germany

Question/Background

German data about the etiology of non-neoplastic uveitis and endophthalmitis are scarce. Thus, we aimed to provide descriptive statistics in this large retrospective single-center epidemiological study from a tertiary care university hospital. As a secondary endpoint, we aimed to characterize the concordance between microbiological and pathological diagnosis in the subgroup of acute endophthalmitis.

Methods

We have searched cases using "Glaskörperpunktat" as material type in the electronic case record system (PAS-NET) of the Institute for Pathology and Neuropathology, University of Tuebingen on 10JAN2023. Cases with a diagnosis of vitreoretinal lymphoma or other malignancy were excluded. Diagnosis and basic demographic parameters were extracted. Data with regard to microbiological diagnoses were also added. Descriptive statistics were performed in R (version 4.0.3).

Results

Altogether, 374 non-neoplastic vitreous fluid samples from 342 patients were analyzed (from 01JAN2010 to 10JAN2023), consisting of 279 lymphocytic uveitis, 66 acute endophthalmitis, 5 candida endophthalmitis, 2 intraocular HSV infection, 5 toxoplasmosis, 2 Tropheryma infection, 1 intraocular Leishmaniasis, and 13 other causes according to cytological findings. According to the microbiological diagnosis, 15 *S. epidermidis*, 3 *S. aureus*, 6 *C. albicans*, 13 *T. gondii*, 2 *S. pneumoniae*, 2 *T. whippelii*, 1 *S. oralis*, 1 *S. dysgalactiae*, 1 *K. pneumoniae* and 1 *Prevotella* spp were detected in the 181 microbiologically analyzed samples. 135 samples were microbiologically negative. The presence of neutrophils had a 0.81 (95% CI: 0.73-0.86) accuracy, 0.51 Kappa, 0.87 sensitivity, 0.79 specificity, 0.49 positive predictive value and 0.96 negative predictive value for a positive bacteriological or fungal result. As expected, no infectious agent was found in most cases of lymphocytic uveitis. Within this subgroup, 98 of 112 microbiologically analyzed samples were negative; in the remaining cases, 10 *Toxoplasma*, 1 *Tropheryma*, 1 *Prevotella*, 1 *S. epidermidis* and 1 *C. albicans* were identified.

Conclusion

The absence of neutrophils precluded a microbiologically identifiable organism with a high negative predictive value. Although most cases of lymphocytic uveitis lack an infectious etiology, rare cases with an underlying infection could be identified. Combined pathological and microbiological examination of vitreous aspirates is a valuable tool for diagnosing intraocular infection.

P.InterPath.06

Individualized targeted treatment in a case of a rare TFG-ROS1 fusion positive inflammatory myofibroblastic tumor (IMT)

M. Schmutz¹, S. Sommer¹, M. Trepel^{1,2}, S. Dintner³, B. Märkl^{2,3}, R. Claus^{1,2,3}, B. Heinrich⁴

¹University of Augsburg Medical Center, Medical Faculty, Hematology and Oncology, Augsburg, Germany, ²University of Augsburg Medical Center, Comprehensive Cancer Center Augsburg (CCCA), Augsburg, Germany, ³University of Augsburg Medical Center, General Pathology and Molecular Diagnostics, Augsburg, Germany, ⁴Hematology-Oncology Practice Augsburg, Augsburg, Germany, Augsburg, Germany

Question/Background

IMTs are rare mesenchymal neoplasms with slow growth. Resection is considered the therapeutic standard, with chemotherapy being insufficiently effective in advanced disease. *ALK* translocations are present in 50% of cases, and *ROS1* fusions (*YWHAE-ROS1*, *TFG-ROS1*) have been described. Here, we present a case of *TFG-ROS1* fusion that provides a treatment option, and we highlight the significance of MTBs in routine clinical precision oncology for successful post-last-line therapy.

Methods

NGS using the AmpliSeq Focus panel (52 genes, 23 RNA fusions) was applied to FFPE specimens of an IMT manifestation in the posterior abdomen. Treatment recommendation at the MTB of the Comprehensive Cancer Center Augsburg (CCCA) involved oncologists, (molecular) pathologists, and geneticists, evidence levels were assigned according to NCT guidelines.

Results

A 32-year-old woman presented to the CCCA with IMT diagnosed at age 27 for biopsy and evaluation of treatment options. Previous treatments included three sequential resections and systemic therapy with vinblastine, cyclophosphamide, and methotrexate. The CT scan showed extensive tumor infiltration of the psoas muscles and the posterior abdomen.

NGS revealed an actionable *ROS1*-fusion (*TFG::ROS1*, 26794 reads; ref, 33654reads) with breakpoints at exon4/35 including the kinase domain and activating the *RAS*-pathway. *TFG*, the *Trk*-fused gene exerts functions such as intracellular trafficking and exhibits high sequence homology between species.

The treatment recommendation was based on 6 single reports of IMTs in various locations harboring *TFG-ROS1*-fusion with responses up to >3 years. The patient was started on Crizotinib, an ATP-competitive small molecule C-Met, *ALK* and *ROS1*-inhibitor on 250 mg bid. Due to nausea and muscle spasms, the dose was reduced to 250 mg od.

A CT scan 5 months after start of therapy showed profound regression of the tumor justifying treatment continuation. After 9 months of therapy, the patient had no adverse events and a good quality of life.

Conclusion

This case highlights the uniqueness of a rare, disease-defining genotype that makes an otherwise difficult-to-treat disease targetable. NGS and interdisciplinarity in precision oncology are key for adding benefit to individual patient trajectories. Increased availability of genomic profiling for patients in last-line stages, more elaborate workflows and large-scale patient data collection to support cohort selection and generation of evidence are needed.

Literaturangaben:

- [1] Gleason, B. C. & Hornick, J. L., (2008), Inflammatory myofibroblastic tumours: where are we now?, J Clin Pathol
- [2] Coffin, C. M., Watterson, J., Priest, J. R. & Dehner, L. P., (1995), xtrapulmonary inflammatory myofibroblastic tumor (inflammatory pseudotumor). A clinicopathologic and immunohistochemical study of 84 cases., Am J Surg Pathol

P.InterPath.07

Thrombospondin 3 affects lineage commitment in primary liver cancer

N. Ganjian¹, Z. Abadi¹, O. Trompak², R. Geffers³, L. Zender², R. Pellegrino¹, T. Longerich¹

¹Institute of Pathology, Heidelberg University Hospital, Heidelberg, Germany, ²Innere Medizin VIII University Hospital Tübingen, Tübingen, Germany, ³Helmholtz Centre for Infection Research (HZI), Braunschweig, Germany

Question/Background

The main types of primary liver cancer are hepatocellular carcinoma (HCC), cholangiocarcinoma (CCA), and combined hepatocellular cholangiocarcinoma (cHCC-CCA). Lineage-tracing experiments in mice demonstrated that both CCA and HCC may develop either from hepatocytes or ductular cells highlighting the plasticity of epithelial liver cells. We aimed at the identification of mechanisms leading to the formation of human cHCC-CCA.

Methods

Comparative exome and transcriptome sequencing of microdissected CCA and HCC components of 13 human cHCC-CCA was performed. An *in vivo* RNAi screen in transposon-based mosaic mouse models of CCA (mutant kras, p19-deficient) and HCC (MYC-AKT) induced by hydrodynamic tail vein injection was used for validation. After tumor development, individual tumor nodules were dissected and tumor typing was performed by histology and immunohistochemistry (Hnf4alpha, keratin 19). Isogenic cell lines were derived from the respective mouse models and were used for functional analyses *in vitro*.

Results

Overall, 54 differentially expressed and/or mutated candidate genes were detected by comparative exome and transcriptome sequencing of the two components of cHCC-CCA. Thrombospondin 3 (THBS3) was mutated in the HCC compartment of human cHCC-CCA. Both, knockdown of THBS3 and expression of the synonymous mutation resulted in the formation of primary liver cancer with a cHCC-CCA phenotype in the murine CCA model. Overexpression of mutant THBS3 in isogenic cell lines increased AFP and decreased SOX9 mRNA expression in CCA cells, while overexpression of the wildtype protein decreased albumin expression in HCC cells. shRNA-mediated knockdown of THBS3 in CCA cells phenocopied this functional effect *in vitro*.

Conclusion

In conclusion, THBS3 affects lineage commitment in primary liver cancer.

P.InterPath.08

Diagnostic challenge on liver biopsy: AFP-positive carcinoma of the esophagogastric junction with MET Exon 14 Skipping mutation

B. Huang¹, L. Füzesi¹, M. Trepel², T. Kröncke³, B. Märkl¹

¹Faculty of Medicine, Pathology, Augsburg, Germany, ²Faculty of Medicine, Hematology and Oncology, Augsburg, Germany, ³Faculty of Medicine, Radiology, Augsburg, Germany

Question/Background

A liver biopsy with a tumor on histopathological examination presents a challenging diagnostic scenario. The differential diagnosis for a liver tumor is broad and includes both primary and secondary malignancies, as well as benign lesions. Hepatocellular Carcinoma (HCC) is the most common primary liver malignancy and accounts for up to 90% of liver tumors. Metastatic tumors are more common than primary liver tumors and

can originate from various primary sites, including the lung, colon, breast, and pancreas. The most common metastatic liver tumor is adenocarcinoma. Accurate diagnosis is essential for appropriate management and prognosis.

Methods

We report a case of a 69-year-old female patient who presented with persist abdominal pain. The patient had a history of H.p.-positive Gastritis with eradication therapy. CT-Abdomen revealed disseminated liver metastasis and a gastric cardiac thickening.

Blood tests showed elevated levels of alpha-fetoprotein (AFP) (17000 ng/mL; normal range: <10 ng/mL) and carcinoembryonic antigen (CEA) (1400 ng/mL; normal range: <5 ng/mL). A computed tomography (CT) scan of the abdomen revealed disseminated liver metastasis and a gastric cardiac thickening and multiple perigastric lymph nodes.

Results

Liver biopsy showed adenocarcinoma with trabecular and glandular formation. The tumor cells displayed irregular, vesicular nuclei and eosinophilic cytoplasm with some intracytoplasmic droplets. Immunohistochemical staining showed strong positivity for CDX2 and unicellular positivity for AFP, as well as negative for HepPar-1, Glypican, Arginase. The patient was diagnosed with AFP-positive gastric carcinoma, microsatellite stable. Molecular pathological investigation detected MET Exon 14 skipping mutation.

Despite two chemotherapy schemata suffered the patient after six months massive tumor progression and quickly cholestasis with a bilirubin value of 18 mg/dl (normal range: <1.2 mg/dl) as well as peritoneal carcinosis. Finally died she after 8 days of hospitalization.

Conclusion

AFP-positive gastric carcinoma is a rare aggressive tumor with early metastasis, poor prognosis and histologically similar with HCC. AFP-positive tumor in liver biopsy should be interpreted cautiously. The therapy of this tumor is not standardized, MET-selective tyrosine kinase inhibitors (TKIs) (capmatinib, tepotinib, and savolitinib) may role as a therapeutic target. However, further studies are needed to determine the clinical significance of AFP expression in gastric carcinoma.

P. InterPath.09

Correlation of imaging and (histo)pathological evaluation in the diagnosis of hepatocellular carcinoma in liver explants

S. Wucherpfennig¹, F. De Beukelaer², D. Jonigk¹, C. Kuhl², P. Bruners², N. T. Gaisa¹

¹Institute of Pathology, University Hospital RWTH Aachen, Aachen, Germany, ²Department of Diagnostic and Interventional Radiology, University Hospital RWTH Aachen, Aachen, Germany

Question/Background

Liver transplantation (LTx) is a treatment option for patients with cirrhosis and/or hepatocellular carcinoma (HCC) meeting the Milan criteria. While HCCs are being identified with imaging techniques with steadily increasing diagnostic confidence, the diagnosis of small HCCs (< 2 cm) is still challenging. Also macroscopically, differentiation of HCCs from premalignant lesions and regenerative nodules is difficult. To improve the diagnostic precision of imaging and macroscopy, we correlated the results of imaging before and after explantation with macroscopic and histopathological finding results.

Methods

In this prospective, institutional review board-approved study, the cirrhotic liver explants of 38 patients, who gave written informed consent, were examined. The explants were fixed with 4% formalin, scanned in a defined axis by CT and MRI imaging, and then sliced into 4-mm-thick slices in identical orientation. Ex vivo images were acquired in a 1.5 T MR imager with a head coil using high spatial resolution sequences. All macropathological and radiologically conspicuous nodules were described, photodocumented, and finally histologized. Histologic sections were stained with hematoxylin eosin and a reticulin fiber staining. In diagnostically inconclusive cases, immunohistochemical staining was performed with antibodies against Glypican-3 (1G12), Glutamine Synthetase (GS-6), Heat Shock Protein 70 (W27) and CD34 (QBEnd-10). Knowing the histological results, the macroscopic impression and the radiological imaging before and after explantation were compared and reevaluated.

Results

In all cases in where HCC was not suspected by preoperative imaging, none could be diagnosed after histopathological examination. In 13 of 14 patients, the imaging diagnosis of HCC was confirmed histopathologically. However, in 8 of these patients, additional previously unknown HCCs were discovered after histopathological workup. These were between 0.4 and 2 cm in size. Macropathologically, especially large nodules with inhomogeneous cut surfaces were correctly classified as HCC. In contrast, especially nodules with a size below 1 cm and sharp border at the same time were misinterpreted as benign.

Conclusion

The negative and positive predictive value of imaging in detecting HCCs is very good. However, small HCCs are not yet reliably detected. Therefore, and due to the frequent multifocal occurrence in cirrhotic livers, accurate (histo)pathological examination of cirrhotic livers is required for proper staging.

P.InterPath.10

Theranostic Imaging of SSTR expression in iodine-refractory thyroid carcinoma

J. Enke¹, N. G. Reitsam², B. Märkl², C. Lapa¹, A. Dierks¹

¹Nuclear Medicine, Faculty of Medicine, University of Augsburg, Augsburg, Germany, ²Pathology, Faculty of Medicine, University of Augsburg, Augsburg, Germany

Question/Background

While differentiated thyroid cancer is characterized by excellent therapy responses to surgical and ablative radioiodine therapy concepts, iodine-refractory thyroid cancer still poses a major clinical challenge. Tyrosine kinase inhibitors and tropomyosin kinase inhibitors can be part of therapy regimens, and redifferentiation attempts or somatostatin receptor directed peptide receptor radionuclide therapies are gaining in clinical relevance.

Methods

We report on a 59 year old patient, who presented with tumor recurrence. Ten years prior he was diagnosed with papillary thyroid carcinoma and underwent surgery and ablative radioiodine therapy. [¹⁸F]F-FDG-positron emission tomography/computed tomography (PET/CT) showed extended local recurrence, multiple lymph nodes and lung and pleural metastases. Only minimal iodine uptake of the local recurrence could be detected on whole-body scintigraphy with I-131.

Results

Histopathological workup of the cervical lesion was most consistent with oncocytic carcinoma (Hurtle cell carcinoma). As not all thyroid carcinomas express somatostatin receptors (SSTR), we immunostained for SSTR and could identify a strong but heterogenous (more than 50% of tumor cells) SSTR expression (score 3+) on biopsy tissue. This finding could be visualized by [⁶⁸Ga]Ga-DOTATOC-PET/CT, a SSTR-agonist, which showed intermediate to intense tracer uptake of all tumor lesions. Furthermore a PET/CT using [⁶⁸Ga]Ga-SS0120, a SSTR-antagonist, was performed, yielding even better tumor-to-background-ratio in all tumor lesions. Based on these findings, the patient underwent SSTR-directed PRRT.

Conclusion

As SSTR antagonists have more binding sites on cell surface combined with longer residence times, SSTR antagonists could pose major advantages in SSTR-directed diagnostics and therapy. Further studies on the theranostic use of SSTR antagonist throughout different SSTR expressing carcinomas, such as differentiated, undifferentiated and medullary thyroid cancer, as well as small cell lung cancers should be performed. Potentially, SSTR antagonists could serve as tumor-agnostic theranostic strategies in carcinomas with SSTR expression.

P.InterPath.11

Proteomic signatures of recurrent and non-recurrent primary tumors in the head and neck area to differentiate patient conditions highlighting age and smoking specific alterations

A. Langner¹, T. Halstenbach¹, T. Feilen¹, K. Kurowski¹, S. Nahles², K. Nelson¹, C. Doll², M. Heiland², M. Werner^{1,3}, J. Wüster², O. Schilling^{1,3}

¹University of Freiburg, Faculty of Medicine, Institute for Surgical Pathology, Freiburg, Germany, ²Charité-Universitätsmedizin, Department of Oral and Maxillofacial Surgery, Berlin, Germany, ³German Cancer Consortium and German Cancer Research Center, Heidelberg, Germany

Question/Background

Oral squamous cell carcinoma (oSCC) is only barely studied on the proteomic level with regard to the impact of tobacco and age. Recent data of the DEBRA-study shows that the number of adolescents aged 14 to 17 who smoke on a regular basis redoubled in the past year[1]. Considering that tobacco is the most significant risk factor, current diagnostic tools are insufficient for a personalized treatment and highlight the need for new marker candidates, particularly in connection with smokers.

This experimental project aims find proteins associated with each patient group (young – old, male – female,

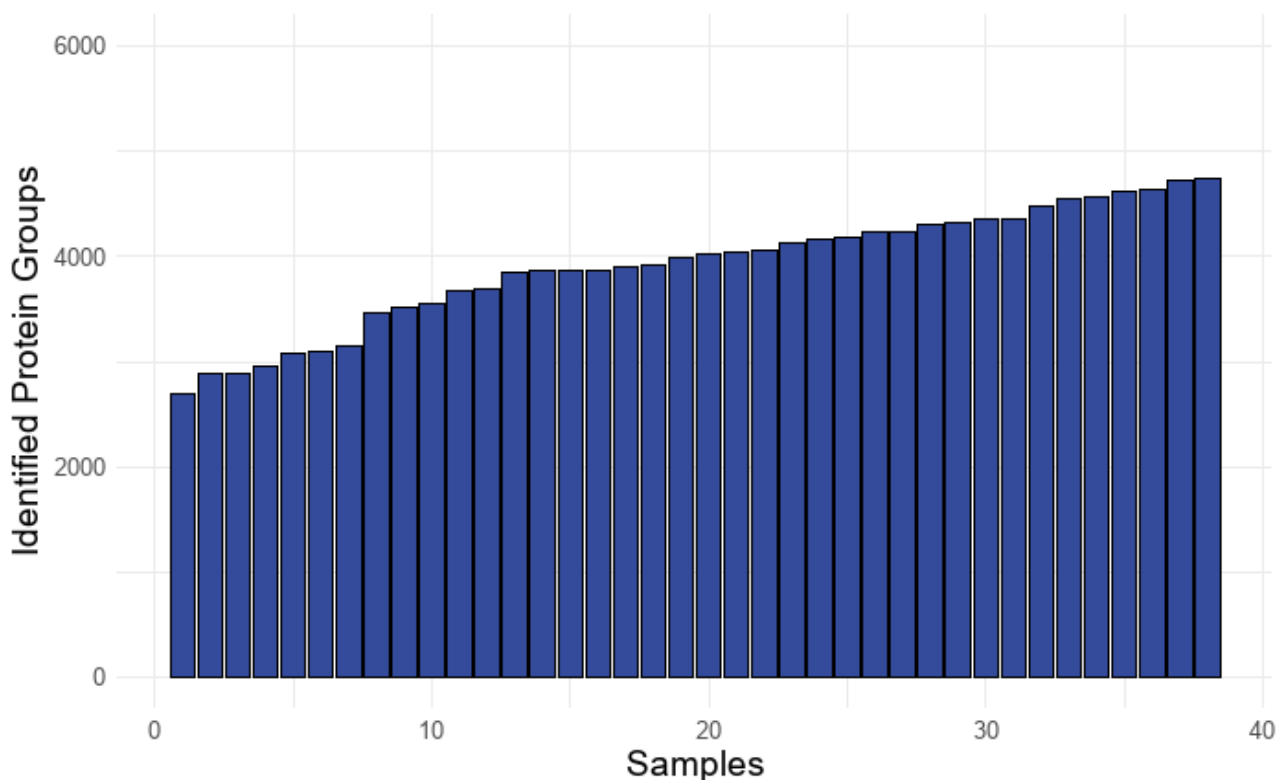
smoking – non-smoking) and thus, enables the differentiation in treatment options among all patients with oSCC.

Methods

After optimizing a tissue-specific protocol, formalin-fixed paraffin-embedded (FFPE) specimens are processed using the single-pot, solid-phase-enhanced sample preparation[2]. Proteins are extracted and digested into peptides which are then analyzed via data-independent acquisition in liquid chromatography-tandem mass spectrometry.

Results

Retrospective deep proteomics analysis was performed on a cohort including 38 patients using clinical-pathological data. High proteome coverage of more than 4500 proteins per sample and accurate protein quantification provide the basis of our study.



Identified Proteingroups

Conclusion

Ongoing statistical analysis suggests the possibility of proteomic stratification of different patient groups such as smokers and non-smokers.

Literaturangaben:

[1] Sabrina Kastaun, (2022), Mental Health Symptoms and Associations with Tobacco Smoking, Dependence, Motivation, and Attempts to Quit: Findings from a Population Survey in Germany (DEBRA Study), European Addiction Research, 2023-02-27

[2] Christopher S. Hughes, (2019), Single-pot, solid-phase-enhanced sample preparation for proteomics experiments, Nature Publishing Group, Nature Protocols, <https://www.nature.com/articles/s41596-018-0082-x>, 2023-02-27

P.Multipar. Postersitzung Multiparametrische Zell- und Gewebeanalyse

P.Multipar.01

Comprehensive characterization of virus and inflammation distribution in human Borna virus encephalitis

N. Jungbäck¹, E. Sipos¹, Y. Vollmuth², T. Mögele¹, T. Schaller¹, B. Märkl¹, D. Tappe³, F. Liesche-Starnecker¹

¹Pathology, Medical Faculty, University of Augsburg, Augsburg, Germany, ²Institute of Pathology, School of Medicine, Technical University of Munich, Munich, Germany, ³Bernhard Nocht Institute for Tropical Medicine, National Reference Centre for Tropical Pathogens, Hamburg, Germany

Question/Background

The Borna disease virus 1 (BoDV-1) is a highly neurotropic virus and a model disease for neurotropic viruses in general. Although it has been known to cause severe infections in mammals like horses and sheep for over a century, it was just recently shown that BoDV-1 can also lead to predominantly fatal encephalitis in humans [1]. As newly proven zoonotic virus, only little is known about the pathogenesis of the human infection. In a previous study, we characterized the typical histomorphology as lymphocytic panencephalitis with pronounced astrogliosis, formation of microglial nodules and detection of intranuclear eosinophilic inclusion bodies. Interestingly, we demonstrated an accentuation of virus and inflammation in the basal ganglia [2], which was later confirmed by our multicenter analysis of magnet resonance imaging data of patients with Borna virus encephalitis [3].

Methods

In a current study viral distribution pattern was further analyzed. We embedded a complete coronary cross section of an autopsic retrieved brain of a deceased with borna virus encephalitis. The cross section was divided into 34 formalin-fixed and paraffin-embedded blocks, which were all stained for hematoxylin and eosin, as well immunohistochemically for GFAP as markers for astrocytes, Iba-1 for microglial cells, CD3 for T-lymphocytes, CD20 for B-lymphocytes and the nucleoprotein of BoDV-1 using the antibody Bo18. Furthermore, RNA in situ hybridization using the RNAscope technology was conducted and with quantitative PCR, virus concentration in each block was evaluated. For the analysis, all slides were digitized using the Panoramic scanner 2.2.0 provided by 3DHISTECH Ltd. Afterwards, the total cross sections for each stain were digitally reconstructed. Masks were drawn on immunohistochemically positive areas resulting in a detailed imaging of the virus and inflammation distribution.

Results

Results of immunohistochemistry and RNA in situ hybridization were then compared to the results of PCR. Interestingly, distinct tracts showed a strong virus affection while directly adjacent areas remained BoDV-1-negative, which weighs against a direct spread per continuitatem and indicates an initially strict axonal transmission.

Conclusion

With this detailed and comprehensive distribution analysis, further insight into the human disease with potential to understand the pathogenetic processes can be made.

Literaturangaben:

[1] Schlottau K., et al., (2018), Fatal Encephalitic Borna Disease Virus 1 in Solid-Organ Transplant Recipients, N Engl J Med, 1377 - 1379, 379 (14), doi: 10.1056/NEJMc1803115

[2] Liesche F., et al., (2019), The neuropathology of fatal encephalomyelitis in human Borna virus infection, Acta Neuropathol, 653 - 665, 138 (4), doi: 10.1007/s00401-019-02047-3

[3] Finck T., et al., (2020), Bornavirus Encephalitis Shows a Characteristic Magnetic Resonance Phenotype in Humans, Ann Neurol, 723 - 735, 88 (4), doi: 10.1002/ana.25873

P.Multipar.02

Influence of vaccination status and virus variant on the immunological events in fatal SARS-CoV-2 infections

N. Jungbäck¹, L. Müller², T. Mögele¹, L. Rentschler¹, B. Grosser¹, E. Sipos¹, S. Dintner¹, T. Schaller¹, B. Märkl¹, F. Liesche-Starnecker¹

¹Pathology, Medical Faculty, University of Augsburg, Augsburg, Germany, ²Department of Cardiothoracic Surgery, Augsburg University Hospital, Augsburg, Germany

Question/Background

The systematic performance of autopsies of COVID-19 deceased at the Institute of Pathology and Molecular Diagnostics of the University Hospital Augsburg has created the basis for a comprehensive scientific reappraisal, especially with regard to the morphological and immunological processes of a SARS-CoV-2 infection. Besides pre-existing conditions, the immunopathological components are one of the crucial factors of the clinical course.

In the present study, we addressed the question to what extent SARS-CoV-2 vaccination status and virus variant impact the immunological processes as part of the pathogenesis. We included samples from 111 autopsy cases. Among these, 105 were found to have COVID-19, and the remaining 6 served as control group and as baseline for expression patterns. Of the COVID-19 deceased, 39 were completely immunized and 58 not vaccinated. The remaining patients had an incomplete vaccination status (n=10) or vaccination status was unknown (n=4).

Methods

For RNA analysis, the *nCounter* technology provided by *Nanostring*[®] was used. After RNA extraction, the expression levels of over 500 genes that are relevant for immunological processes were investigated using the *Immunology V2 Panel*. The analyses were performed on fresh frozen lung tissue retrieved during autopsy beforehand and preserved in Trizol at – 80 °C to guarantee virus inactivation and RNA preservation. Results of 101 patients met quality criteria and were further analyzed using the *nSolver Analysis Software 4.0* with the addition of the *nCounter Advanced Analysis* program.

Results

Our results show that the group of non-immunized patients had higher signatures for both, the innate and the adaptive immune system compared to the fully vaccinated patients. Furthermore, a higher relative frequency of T-cells and neutrophils was observed in the vaccinated patients. When subdividing the cohort, based on virus variants, clear different expression levels of the included immunologically relevant genes could be identified. Particularly striking was the similarity of the immunological profile of patients infected with the delta variant to the non-infected control group.

Conclusion

It can be concluded that we were able to confirm that both, vaccination status and virus variant have high impact on the immunopathological processes in COVID-19 patients.

P.Multipar.03

Development of novel oligonucleotide sequences to increase the multiplexing capacity of the CODEX platform

A. Rochwarger, C. Schürch

University Hospital and Comprehensive Cancer Center Tübingen, Department of Pathology and Neuropathology, Tübingen, Germany

Question/Background

High-multiplex imaging is a driving force for biological discoveries and the development of personalized cancer therapies. The CO-Detection by indEXing (CODEX) platform enables high-multiplex imaging on both fresh-frozen and formalin-fixed, paraffin-embedded tissue. CODEX is based on DNA oligonucleotide-labeled antibodies that are cyclically imaged by the addition and removal of complementary fluorophore-labeled oligonucleotides. We evaluated a new set of candidate DNA sequences for the expansion of our antibody panels, which are currently limited to 57 markers.

Methods

After evaluating different strategies for antibody-DNA linkage, results were verified using flow cytometry, manual staining of cell suspensions and subsequent fluorescence microscopy. Multiple combinations of cells and antibodies were evaluated on the CODEX platform. Peripheral blood mononuclear cells were stained with anti-CD47 antibodies linked individually to both existing and new unique DNA sequences. Multicycle experiments were run on the CODEX platform to validate the applicability of candidate oligonucleotides and to exclude cross-reactivity of candidate DNA sequences with each other and priorly established DNA sequences. Data processing and cell segmentation were followed by unsupervised clustering.

Results

While many strategies for antibody-DNA linkage and signal amplification, including secondary antibody staining and utilizing biotin/streptavidin conjugates, worked in flow cytometry and manual cell stainings for fluorescence microscopy, they performed poorly in the multicycle reactions necessary to identify unique sequences. Therefore, antibody-DNA linkage was performed using the maleimide reaction. We identified 22 new oligonucleotide sequences that showed unique clusters in the unsupervised analysis. 26 of the candidate sequences were excluded due to cross-reactivity or insufficient performance on the CODEX platform.

Conclusion

We present an exemplary workflow for the validation of new DNA sequences and antibody-DNA linkage strategies for the CODEX platform. Our results provide a new unique set of DNA sequences that can be

used in combination with the already existing DNA sequences to increase the CODEX multiplexing capacity.

P.Multipar.04

Diagnosis of a sialidosis case using tissue-based liquid chromatography-tandem mass spectrometry (LC-MS/MS)

A. Rochwarger¹, V. Hollfoth², S. Mattern², P. Riemenschneider², M. Franz-Wachtel³, E. Sturm⁴, C. Schürch⁵, F. Fend¹, S. Singer²

¹Universitätsklinikum Tübingen, Institut für Pathologie, Tübingen, Germany, ²Universitätsklinikum Tübingen, Institut für Pathologie, AG Singer, Tübingen, Germany, ³Universität Tübingen, Proteome Center Tuebingen, Tübingen, Germany, ⁴Universitätsklinikum Tübingen, Kindergastroenterologie/-hepatologie, Tübingen, Germany, ⁵University Hospital and Comprehensive Cancer Center Tübingen, Department of Pathology and Neuropathology, Tübingen, Germany

Question/Background

Sialidosis is a very rare, autosomal recessive, lysosomal storage disease caused by impairment of α -N-acetyl neuraminidase (also referred to as sialidase) due to mutations in the NEU1 gene. Impairment of sialidase leads to accumulation of sialyloligosaccharides and over-sialylated LAMP1 protein. LAMP1 protein was shown to be essential for exocytosis of lysosomal content and exhibits increased half-time when over-sialylated. Consequently, loss of NEU1 function leads to excessive LAMP1-mediated excretion of lysosomal content. The various clinical manifestations of sialidosis as a systemic disease involving the nervous system, bone, muscle and visceral organs have in part been linked to this mechanism. Here, we report a case of a female patient with prenatally abnormal facial features and (shortly after birth) acute respiratory distress, systemic inflammation with abdominal focus, and splenomegaly. Heart failure developed within the first months of life.

Methods

Liver and duodenal biopsies were obtained for routine pathological assessment with the clinical question: “storage disease?”. In addition to conventional histology LC-MS/MS was performed for identification and quantification of several thousand proteins. Enrichment analysis was performed by means of the STRING database.

Results

Histological evaluation of the liver biopsy revealed vacuolated Kupffer cells and hepatocytes, while the duodenal biopsy was largely inconspicuous. LC-MS/MS data indicated distinct changes in relative intensities of proteins including high abundance of LAMP1. Enrichment analysis in the STRING database revealed the following terms: “lysosomal storage disease” and “extracellular exosome”, among others. Together with the clinical presentation and detection of increased sialyloligosaccharides in urine the diagnosis of sialidosis could be made (and was genetically confirmed).

Conclusion

This case report exemplifies the great potential of LC-MS/MS in the tissue-based diagnosis of rare storage diseases. Moreover, the resulting proteomic data will improve our understanding of the molecular disease mechanisms with potential impact on therapeutic intervention.

P.Multipar.05

Digital Spatial Profiling: Pre-analytical effect of EDTA and target sequence annotation.

A. Oszwald¹, C. Kaltenecker¹, L. Zisser², E. Compérat¹, A. Rees¹, R. Kain¹

¹Medical University of Vienna, Department of Pathology, Vienna, Austria, ²Medical University of Vienna, Department of Biomedical Imaging and Image-guided Therapy, Division of Nuclear Medicine, Wien, Austria

Question/Background

Digital Spatial Profiling (DSP, Nanostring “GeoMx” Platform) can obtain transcriptomic expression profiles from regions of intact tissue sections, but pre-analytical variables need to be characterized to fully utilize these methods. For instance, it is unknown how tissue decalcification with ethylenediaminetetraacetic acid (EDTA) affects DSP probe counts. Probes may be more or less affected depending on their length, sequence, or other properties. Although some information on the DSP assay is available, the full probe sequences are not disclosed.

Methods

Samples from 24 formalin-fixed specimens were divided into four pieces and processed immediately or first incubated in EDTA solution for one, three, and seven days. Whole-transcriptome DSP (Nanostring) was performed according to manufacturer protocols. Regions of interest were designated with equal histological content between different EDTA conditions. Full target sequences of the assay probes were retrieved using the assay configuration file, R Statistics (genomicFeatures and BSGenome packages), and RefSeq

GrCh38.p13 annotations.

Results

EDTA treatment reduced probe counts and their signal-to-noise ratio, but not the number of probes above the level of quantitation. Samples retained their tissue-specific expression despite increased discrepancies detected starting with three days of EDTA treatment. Quantile normalisation was more stringent in reducing these discrepancies than other methods, and best preserved the original probe profile. Batch-effect adjustment across all samples further reduced discrepancies, but substantially altered the expression profiles. Specific probes were particularly sensitive to EDTA treatment, sufficient to translate into misleading interpretations using gene set enrichment analysis. We assigned full-length target sequences to ~98% of the target probes and obtained an updated list of target transcripts using BlastN, confirming most of the gene targets. Surprisingly, target-promiscuity of probes was a greater predictor of sensitivity to EDTA than probe length.

Conclusion

EDTA treatment reduces the magnitude of DSP probe counts. Specific probes are particularly sensitive to EDTA, affecting similarity between EDTA-treated and untreated paired samples. Quantile normalisation is most effective at partially countering the effect of EDTA treatment. The previously undisclosed probe sequences allow re-assessment of probe specificity.

P.Multipar.06

Multivariate modelling of mid-infrared spectra of colorectal cancer

E. Kontsek¹, B. Borkovits², A. Pesti¹, S. Gergely³, I. Csabai², A. Kiss¹, P. Pollner⁴

¹Semmelweis University, Department of Pathology, Forensic and Insurance Medicine, Budapest, Hungary, ²Eötvös Lorand University, Department of Physics of Complex System, Budapest, Hungary, ³Budapest University of Technology and Economics, Department of Applied Biotechnology and Food Science, Budapest, Hungary, ⁴Hungarian Academy of Sciences, MTA-ELTE Statistical and Biological Physics Research Group, Budapest, Hungary

Questions/Background

The applicability of techniques based on spectroscopy outside the visible light range is increasingly being investigated. The mid-infrared technique is non-invasive and non-destructive, which is one of its main advantages over the use of ionizing radiation. In addition, it can provide sufficient chemical information to effectively predict whether a patient has cancer using appropriate machine learning methods.

Methods

Sections of tissue microarrays of formalin-fixed tissue samples embedded in paraffin-embedded tissue were selected and analysed. Spectra were acquired using a Fourier transformation mid-infrared Perkin Elmer Spotlight microscope. Conventional H&E stained sections were digitized using a 3DHitech P1000 scanner. The 32 cores are containing intact colon mucosas (NC) and primary colorectal carcinomas (CRC). A digital database was created to organize and assemble data from different modalities. Both unsupervised (PCA) and supervised methods (Random Forest, Linear Discriminant Analysis, Support Vector Machine, XGBoost, U-Net) were used to process the data.

Results

7744 spectra were collected from each core. Point clouds visualized for the first two principal components of PCA show some mixing of tumor versus normal spectra. The Random Forest algorithm resulted in a model accuracy of 0.575, Linear Discriminant Analysis 0.644, Support Vector Machine 0.593, XGBoost 0.592 and the U-Net 0.532. Linear Discriminant Analysis produced the highest sensitivity of 0.885.

Conclusion

The accuracies were poor in the discrimination of normal colon mucosa from colorectal cancer on the non-filtered spectra. Therefore, data preprocessing is suggested to be performed on larger cohort after spectral background filtration.

P.Multipar.07

Shotgun proteomics of breast carcinoma pathological subtypes

A. Cabrita Figueiredo¹, A. Seredynska¹, K. Kurowski¹, P. Bronsert¹, P. Bronsert¹, M. Werner^{1,2}, O. Schilling^{1,2}

¹Institute for Surgical Pathology, Freiburg im Breisgau, Germany, ²German Cancer Consortium and German Cancer Research Center, Heidelberg, Germany

Question/Background

Relevance:

Breast cancer (BC) is the most common and often fatal cancer affecting women worldwide. BC has many subtypes that display distinctive biological characteristics and different response patterns to existing treatments. Despite the established benefits of subtyping breast cancer, significant knowledge gaps persist in understanding the biological variations within each subtype. New developments using proteomic approaches have yielded results such as the improved separation between subgroups in luminal subtypes with prognostic significance[1], or the identification of new groups and potential biomarkers for triple-negative tumors[2]. This type of research is of great importance for improving our understanding of cancer pathology and enhancing modern cancer diagnostics.

Aim:

The aim of this project is to continue the progress of characterization of BC subtypes through exploratory proteomic analysis.

Methods

We conducted a retrospective deep proteomic analysis of 128 tumor samples from patients with multiple breast cancer subtypes. The available specimens consisted of archival formalin-fixed, paraffin-embedded (FFPE) tumour and tumour-adjacent tissue combined with pathological data. The analysis involved robot-assisted sample preparation, single-pot, solid-phase-enhanced sample preparation[3], liquid chromatography–tandem mass spectrometry and data-independent acquisition.

Results

On average, each sample yielded the identification of 4173 unique proteins. The in-progress data processing and in-depth statistical analysis will provide deeper insights into the proteomic differences of BC patients. Preliminary results show a differentiation between the subgroups at the proteome level.

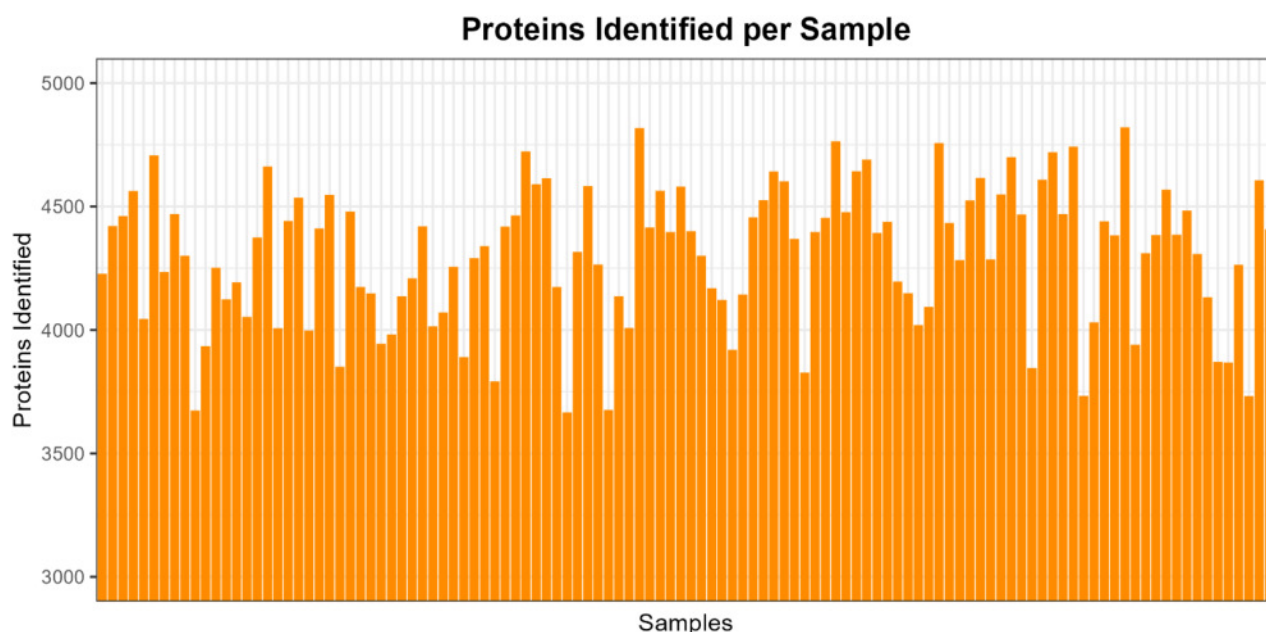
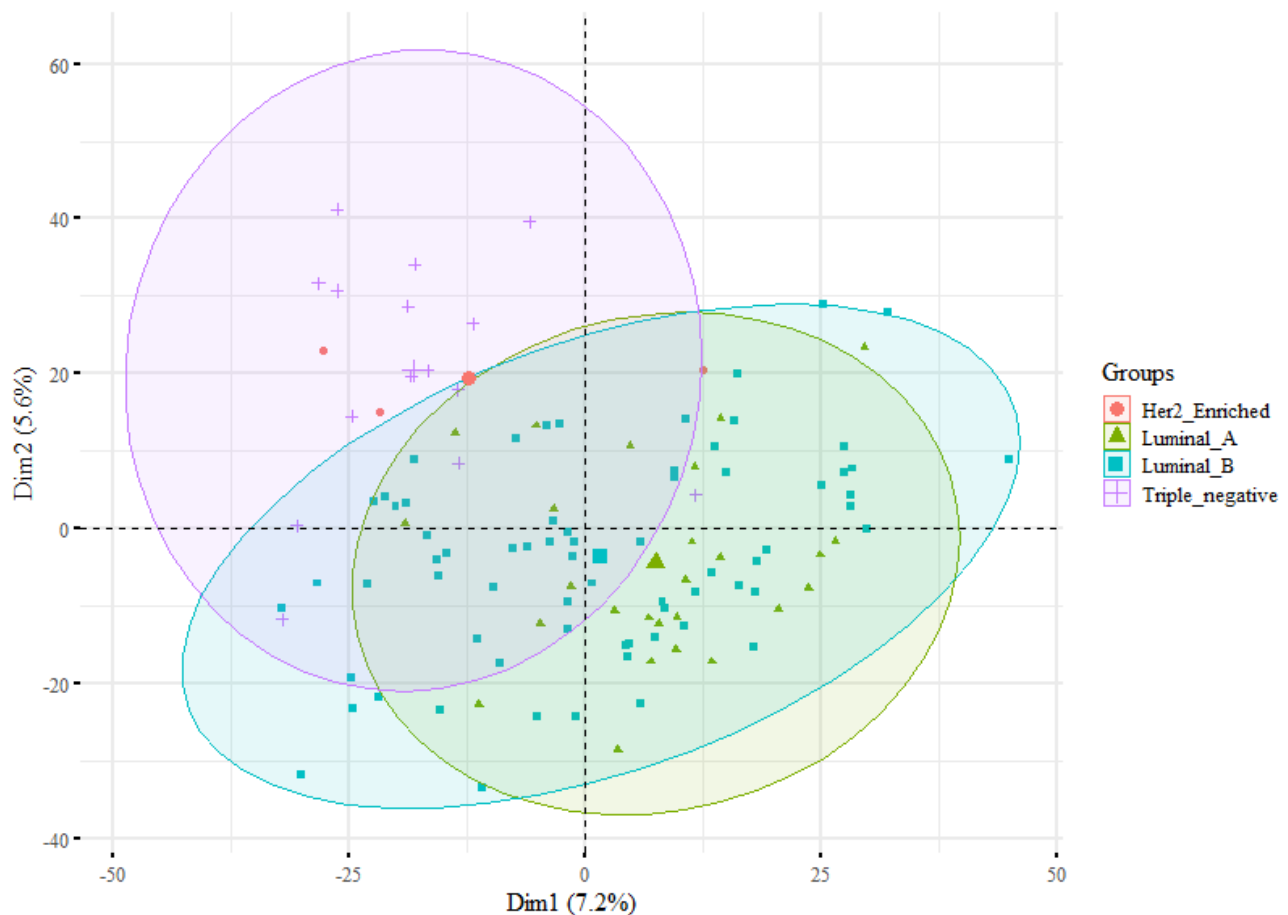


Fig.1: The initial exploratory analysis revealed a high number of proteins identified per tumor sample.



Principal Component Analysis of tumor samples demonstrates the expected differentiation between immunohistochemically defined BC tumor subtypes.

Conclusion

Proteomic analysis of FFPE breast cancer samples highlight differences between BC subtypes by presenting a thorough characterization of the proteome.

Literaturangaben:

- [1] Krug K, Jaehnig EJ, Satpathy S, et al. , (2020), Proteogenomic Landscape of Breast Cancer Tumorigenesis and Targeted Therapy, Cell, 1436-1456.e31, 183(5), doi:10.1016/j.cell.2020.10.036, 2022-01-01
- [2] Asleh K, Negri GL, Spencer Miko SE, et al., (2022), Proteomic analysis of archival breast cancer clinical specimens identifies biological subtypes with distinct survival outcomes. , Nat Commun, 896, 13(1), doi:10.1038/s41467-022-28524-0, 2022-01-01
- [3] Hughes CS, Moggridge S, Müller T et al., (2019), Single-pot, solid-phase-enhanced sample preparation for proteomics experiments., Nat Protoc. , 68-85, 14(1), doi:10.1038/s41596-018-0082-x, 2022-01-01

Autorenindex

(fett = Erstautor*innen)

Abadi, Z.	P.InterPath.07
Abbas, M.	AG11.04 , DGP13.08, P.02.24, P.03.01 , P.04.06 , P.14.08, P.14.09, P.14.10, P.14.20, P03.10 , P03.16
Abdullazade, S.	P.01.02
Abedpour, N.	AG03.09
Acciuffi, S.	P.02.18, P.02.19
Adam, P.	DGP13.08
Agaimy, A.	AG04.01
Al Kallaa, M.	DGP23.09
Al Sheikhyaqoob, D.	P.13.03
Al-Ali, R.	P.14.11
Al-Ghazzawi, K.	P.14.17
Al-Madhi, S.	P.02.18, P.02.19
Alakus, H.	AG02.01
Alber, M.	DGP12.04
Albers, P.	AG03.01
Alborelli, I.	DGP03.02
Albrecht, J.	DGP13.08
Albrecht, T.	DGP06.04, P.02.21, P.13.07
Allgäuer, M.	P.05/11.06
Alt, V.	P.InterPath.03
Altendorf-Hofmann, A.	AG08.05
Amanzada, A.	AG02.15
Ament, C. E.	AG14.08
Ameziane, N.	P.14.11
Amin, M.	AG03.05
Anagnostopoulos, I.	DGP03.01
Angele, M.	P.02.06
Angeloni, M.	DGP13.09
Anheuser, L.	P.03.03
Arévalo, L.	P03.15
Arndt, S.	AG08.04
Arnold, A.	AG06.02
Assadi Kordlo, S.	AG14.02
Asskali, M.	DGP06.06
Auber, B.	DGP14.04
Aubert, O.	AG06.02
Austgen, J.	AG02.02
Baart, V. M.	AG02.04
Babendererde, N.	DGP04.05
Bäcker, J.	P.13.12
Baerenfaller, K.	P.14.15
Bahlinger, V.	DGP13.09 , P.03.03
Ballke, S.	P.InterPath.04
Balogh, A. M.	DGP04.06
Barreiros, A. P.	AG07.05
Barrionuevo, C.	DGP18.07
Barta, B. A.	DGP15.04, DGP23.03, P.07/08/10.01
Barth, P.	P03.16
Barth, T. F. E.	AG01.04, AG08.03, P.02.23, AG01.06, P.06.05, AG08.04, AG02.06, DGP18.04
Barth, U.	P.InterPath.02
Bartkuhn, M.	DGP14.03
Bartz-Schmidt, K. U.	P.InterPath.05
Baschun, K.	AG03.02
Bastian, L.	P.14.13
Bauchet, A.-L.	P.14.01
Bauer, A.	P.03.03
Bauer, M.	P.01.03 , P.01.04 , P.01.07
Bauer, Y.	P.02.22
Baumhoer, D.	AG08.04
Bechrakis, N.	P.14.17
Bechstein, W. O.	AG07.05
Beck, J.	DGP22.03

Beck, S.	AG14.03
Becker, A.-S.	AG10.03 , AG10.05
Becker, M.	P.14.02
Beckmann, M. W.	AG04.04, P.03.03
Bedőházi, Z.	DGP04.06
Behrens, H.-M.	P.02.10
Beier, F.	AG14.15
Beiske, K.	DGP18.03
Below, E.	DGP13.08
Bemis, K. A.	DGP04.03
Ben Cheikh, B.	DGP23.01
Benz, M.	AG13.02
Berclaz, L. M.	AG08.05
Berg, E.	AG14.13
Bergmann, A. K.	DGP14.04
Bergmann, F.	P.02.09, P.02.20
Bergmann, L.	AG03.06, P.13.14
Berking, A.-C.	DGP14.04
Bernard, V.	DGP01.03
Bernd, H.-W.	AG01.06, DGP18.03
Berndt, A.	P.14.04
Bernemann, C.	P.03.01
Berner, F.	DGP15.03
Bernhard, P.	P.13.11, P03.13
Bernhardt, M.	P03.14
Berthold, R.	P.14.08, P.14.09, P.14.10, P.14.20
Bertz, S.	AG03.05, P.02.01, P03.12
Beschorner, C.	AG04.02
Bettendorf, O.	AG11.04, P.04.06, P03.10
Bier, B.	P.04.05
Biricz, A.	DGP04.06
Bischoff, P.	P.06.03
Bisson, T.	AG13.04, DGP17.05
Bittner, G.	AG02.15
Bläker, H.	AG06.02, AG11.05, P.01.03, P.14.03
Blasberg, C.	AG04.11
Bobe, S.	DGP13.05
Böck, S.	AG02.12, AG02.13
Bode, B.	P.04.01
Boegemann, M.	P.03.01
Boeschen, M.	AG06.02, AG11.05, P.14.03
Bohle, R. M.	P.06.02, P.14.02
Böhm, C.	DGP12.04
Bohnenberger, H.	AG02.04, AG02.04, AG02.15, AG03.01, AG06.01
Boitier, E.	P.14.01
Bojunga, J.	AG07.05
Bolenz, C.	DGP13.08
Bollwein, C.	P.14.16
Bomze, D.	DGP15.03
Bonham, T. A.	DGP12.03
Bonzheim, I.	AG14.05 , DGP01.04, DGP13.07, DGP18.07, DGP18.08, P.InterPath.05
Booken, N.	P.05/11.01
Borchert, S.	DGP06.06, P.06.07, P.14.17
Borkovits, B.	P.Multipar.06
Boschung, K.	DGP12.04
Bösherz, M.-S.	DGP24.02
Bösmüller, H.	DGP13.07
Bottner, J.	DGP24.03
Bovier, A.	AG03.09
Bozek, K.	DGP12.05
Brambs, C. E.	P.04.08
Brandt, H. P.	P.13.01
Brandt, M.	P.03.08
Branz, A.	DGP13.09
Bräsen, J. H.	P.13.01, P.13.02
Bratic Hench, I.	P.01.01
Bratic-Hench, I.	DGP03.02
Braubach, O.	DGP23.01
Braun, L.	AG08.07, P.14.08, P.14.09, P.14.10, P.14.20

Braun, L.	AG03.06
Braun, R.	DGP01.04
Braun, S.	P.13.10
Braun, Y.	AG05.04
Bräuninger, A.	DGP14.03, DGP18.02
Braunschweig, T.	AG12.01 , AG12.03
Bremer, S.	AG02.15
Bremmer, F.	AG03.01, DGP24.05
Breuhahn, K.	P.02.09, P.02.13
Breyer, J.	DGP13.08
Brinkmann, F.	P.02.21
Brinkmann, O.	P03.10
Brobeil, A.	P.02.20, P.13.07
Brochhausen, C.	P.07/08/10.02, P.07/08/10.05, P.InterPath.03
Brockmann, C.	AG11.03
Brombacher, E.	AG03.06, P.07/08/10.01
Bronsert, P.	AG02.16, AG03.06, AG04.10 , DGP04.03, DGP09.05, DGP15.04, DGP22.03, DGP23.03, P.13.14, P.Multipar.07, P.Multipar.07, P03.13
Brossart, P.	P.07/08/10.08
Brown, R.	DGP12.07
Bruchhage, K.-L.	AG10.04
Brucker, S.	AG04.02, AG14.05
Bruckman, K. C.	DGP12.03
Brune, M. M.	P.01.01
Bruners, P.	P.InterPath.09
Bruns, C.	AG02.01, DGP04.07
Bruns, V.	AG13.02
Büchler, M. W.	P.02.21
Buchwaldt, J.	P.14.12
Budau, K. L.	DGP09.05
Budczies, J.	AG14.03
Bultmann, S.	P.13.10
Buness, A.	AG03.02
Burger, M.	P03.12
Burian, S.	P.02.01, P.02.02
Burkert, C.	AG03.03
Busch, H.	AG06.03, DGP01.03, DGP18.06, P.14.13
Büttner, R.	AG02.01, AG03.09, AG14.01, DGP04.05, DGP04.07, DGP04.08, DGP12.04, P.04.04
Büttner, T.	DGP13.08
Büttner-Herold, M.	P.02.01
Bychkov, A.	DGP04.05, DGP04.08
Cabrita Figueiredo, A.	P.Multipar.07
Cabrita Figueiredo, A. E.	P.14.15
Cai, L.	P.13.15
Calin, G. A.	DGP06.04
Calina, T. G.	DGP06.04
Caliskan, F.	AG02.14
Calvisi, D. F.	AG14.08, AG14.09
Campean, V.	P03.12
Capper, D.	DGP06.02, DGP06.04
Carvalho, R.	DGP17.05
Casavilca Zambrano, S.	DGP18.07
Castven, D.	AG02.07
Ceribas, Y.	DGP06.03
Chadjaa, M.	P.14.01
Chai, T.	DGP12.07
Charbel, A.	P.02.21
Chaves, A.	P03.13
Che, Y.	AG03.01
Chen, J.	DGP23.09
Chen, X.	AG14.08
Chen, Y.	AG06.05, DGP10.06, P.14.04
Cheng, L.	AG03.05
Chirica, M.	AG06.02
Chon, S.-H.	AG02.01
Chott, A.	DGP01.04
Christensen, D.	P.13.01, P.13.02
Christoph, C.	P.03.06
Chun, F.	DGP24.04

Chung, L.	DGP12.07
Cigliano, A.	AG14.09
Claus, R.	P.InterPath.06
Cogliatti, S.	DGP01.04
Colecchia, M.	AG03.05
Comp��rat, E.	AG03.05, P.Multipar.05
Connolly, C.	P.04.01
Cordes, L.	AG06.01
Cosenza-Contreras, M.	DGP09.05, AG03.06, DGP23.03, P.13.11
Cramer, S.	P.13.12
Croner, R. S.	P.02.05, P.02.07, P.02.08, P.02.14, P.02.16, P.02.18, P.02.19, P.07/08/10.06
Csabai, I.	DGP20.04, P.Multipar.06
Cseh, �.	DGP04.06
Cualco, G.	DGP18.07
Cui, L.	DGP12.07, DGP13.02
Cupovic, J.	DGP15.03
Cysar, S.	P.01.06, P.14.07 , P.14.19
Czerny, M.	P.05/11.04
Da Silva Mourato Henriques, V.	AG13.03
Dabbagh, N.	P.02.10
Damanakis, A.	DGP04.07
Dang, T. H.	DGP18.02
Dannenmann, A.	P.04.02
Darr, C.	DGP13.08
Dauch, D.	P.02.22
Davies, J.	AG01.02
De Beukelaer, F.	P.InterPath.09
de Jonge, J.	AG11.04, P.04.06
Degenhardt, M.	AG14.04
Delgado, J.	DGP18.07
Deng, H.	AG13.11
Denkert, C.	AG02.03, AG02.09, AG04.11, DGP10.07
Derben, J.	AG04.11
Dernbach, G.	DGP12.04
Desaubry, L.	AG14.09
Dib, C.	P.14.01
Dickemann, A.	DGP09.06
Dickson, B.	AG04.01
Diedrichs, F.	DGP09.04
Diehl, L.	DGP13.09
Dierks, A.	P.InterPath.10
Dietrich, D.	P.07/08/10.08
Ding, Y.	AG13.11
Dingendorf, E.	AG06.04, DGP13.02 , DGP23.07
Dinh, T.-L. J.	AG03.06
Dinter, H.	AG02.15
Dintner, S.	AG14.11, P.05/11.05, P.InterPath.06, P.Multipar.02
Diop, M.	DGP12.03
Dirnhofer, S.	AG01.02, DGP01.04, DGP03.02, P.01.01
Dogan O, I.	AG13.04, DGP17.05
Doll, C.	P.InterPath.11
Dombrowski, F.	AG03.03, P.14.05
D��ring, C.	DGP24.04
D��rrbecker, M.	DGP14.03
Dossow, K.	P.02.19
Dragomir, M.	DGP12.04
Dragomir, M. P.	DGP06.04
Dreher, E. C.	AG02.07
Dre��ler, F. F.	DGP09.04, DGP23.02, DGP23.08, P.03.02
Dreyling, K.	AG04.10
Dr��ge, A.	AG14.13
D��rr, H. R.	AG08.05
Dyballa, L.	AG11.03
Ebert, E.	P.06.02, P.14.02
Eckstein, M.	AG03.05 , AG04.04, AG13.02, AG13.03, DGP10.07, DGP13.08, DGP13.09, P.03.03
Eich, M.-L.	AG03.09, DGP04.05, DGP04.07, DGP04.08
Eichhorn, M.	P.05/11.06
Einhaus, J.	DGP12.03

Eiteneuer, E.	AG02.07
Elakad, O.	AG02.15
Elboudwarej, E.	DGP13.09
Elezkurtaj, S.	AG14.13, DGP17.05
Elges, S.	AG08.07
Ellenrieder, V.	AG02.04, AG02.15
Ellenson, L.	AG04.03
Ellinger, J.	AG03.02, DGP13.08, P03.14
Eltze, E.	P.04.05
Engel, J.	AG02.09, AG02.12, AG02.13, DGP10.07
Engeler, M.	AG03.03
Engelhard, M.	DGP18.03
Enke, J.	P.InterPath.10
Erben, P.	DGP13.08
Erber, R.	AG04.04, P.02.01
Erbersdobler, A.	AG10.05, P.03.04, P.03.06
Erdmann, T.	DGP03.01
Erlmeier, F.	DGP13.08
Erne, E.	DGP13.08
Espadas, G.	AG03.06
Esposito, I.	AG02.14, DGP23.05
Esser, L. K.	AG03.02
Essmann, F.	P.06.04
Evert, K.	AG14.08
Evert, M.	AG14.08, AG14.09
Ewert, A.	P.13.07
Fährnrich, A.	AG06.03, DGP18.06, P.14.13
Fahrenschon, F.	AG03.04
Fahrner, M.	P.13.11, P.14.19
Falkenberg, K.	AG08.07, P.14.08, P.14.09, P.14.10, P.14.20
Farfán López, F. J.	P.02.04
Fasching, P. A.	AG04.04
Fassunke, J.	AG14.04, P.14.18
Fausser, J.	DGP01.06
Feilen, T.	P.InterPath.11
Fella, M.	DGP17.04, P.13.03
Feller, A.	DGP01.03, DGP01.04, DGP18.06, AG01.06, DGP18.03
Fend, F.	AG04.02, AG14.05, DGP01.04, DGP03.01, DGP09.06, DGP13.07, DGP18.07, DGP18.08, P.02.09, P.02.22, P.13.16, P.InterPath.05, P.Multipar.04
Fernandez, A.	AG02.08, AG10.01
Ferrazzi, F.	DGP13.09
Ferreira, L.	DGP12.03
Feyaerts, D.	DGP12.03
Fichtner-Feigl, S.	DGP15.04
Fiestas Cueto, R.	P.14.15
Firnbach, D.	AG13.02
Fischer, A.	AG04.02
Flatz, L.	DGP15.03
Fliedner, S.	P.14.13
Flinner, N.	AG13.03, AG13.05 , P.13.06, P.13.09, P.13.10
Florian, S.	AG04.07, DGP12.05
Föll, M.	DGP04.03, DGP15.04 , DGP23.03
Forberger, M.	P.04.07
Forberger, M.	P.04.08
Forchhammer, S.	DGP01.04
Försch, S.	AG02.08, AG02.09, AG10.01, DGP10.07 , P.03.08
Franitza, M.	P.05/11.05
Franke, S.	DGP06.05, P.14.14
Franz, M.	AG13.04
Franz-Wachtel, M.	DGP09.06, P.Multipar.04
Frees, S.	P03.11
Freiberger, S. N.	AG10.02
Freiherr von Hammerstein-Equord, A.	AG02.15
Freude, A.	P.03.08
Frey, A.	P.01.06
Frickel, N.	DGP10.07
Friedrich, C.	DGP12.04
Friedrich-Rust, M.	AG07.05
Friemel, J.	P.04.01

Frille, A.	P.14.03
Fritz, R.	DGP12.04
Fritzsche, H.	AG08.04
Frontzek, F.	DGP03.01
Frosina, D.	AG04.03
Frost, N.	DGP12.04
Frøberg Mathisen, I.	P.13.06
Fuchs, F.	AG02.04
Fuchs, K.	AG03.02
Fuchs, M.	DGP04.05, DGP04.07
Fuhr, N.	DGP18.02
Fukuoka, J.	DGP04.05, DGP04.08
Füllgraf, H.	DGP15.04
Funke, K.	P03.15
Fusco, S.	DGP09.06
Füzesi, L.	P.InterPath.08
Gaedcke, J.	AG02.04, AG02.15
Gaida, M.	P.02.03, AG02.03
Gaisa, N. T.	DGP24.02, P.InterPath.09, P.03.07, P03.12
Gaiser, T.	DGP06.03, P.13.04
Gaitzsch, E.	DGP18.03
Galle, P. R.	P.02.20
Ganio, E. A.	DGP12.03
Ganjan, N.	P.InterPath.07
García Rivello, H.	DGP18.07
Gaßler, N.	AG06.05, DGP10.06
Gass, P.	AG04.04
Gassler, N.	P.14.04
Gastinger, I.	P.02.14
Gattenlöhner, S.	DGP14.03, DGP18.02
Gaudilliere, B.	DGP12.03
Gaudilliere, D.	DGP12.03
Gazzah, A.	P.14.01
Gebauer, F.	DGP04.07
Gebauer, N.	DGP01.03, DGP18.06
Gebbers, J.-O.	AG04.10
Geffers, R.	P.InterPath.07
Geisenberger, C.	DGP06.02
Gennermann, K.	AG14.13
Geppert, C.	DGP10.07, DGP13.09, AG03.05, AG13.02
Geppert, J.-P.	DGP01.04
Gerber, T. S.	AG06.06, P.02.20, P.InterPath.01
Gergely, S.	P.Multipar.06
Gersmann, A.-K.	P.07/08/10.03
Ghosh, S.	DGP12.04
Giedl, J.	P03.12
Gil, L.	AG02.13
Gilks, B.	P.04.07, P.04.08
Glasner, C.	AG10.01
Glavinsky, I.	AG03.06
Gleitsmann, M.	DGP10.07
Gloßner, L.	AG04.04
Goeppert, B.	DGP06.04, P.02.09, P.02.13, P.02.20, P.02.21, P.13.07
Goldmann, T.	AG06.03
Goltsev, Y.	DGP12.06
Goncalves, J. P. L.	P.14.16
Goncharenko, L.	P.14.15
Göring, W.	DGP23.05
Gottlieb, J.	P.06.01
Grabbert, M.	AG03.06, DGP13.04
Grabowski, M.	P.02.16
Grabowsky, J.	AG06.01
Gradhand, E.	AG05.03, AG05.04, DGP14.04
Gräfe, D.	AG06.02
Granai, M.	DGP13.07, P.13.16
Grass, A.	AG02.03, DGP10.07
Grau, M.	DGP03.01, DGP18.03
Gräwe, K.	DGP13.04
Grebhardt, S.	P.14.06

Greif, K.	AG04.02
Greten, F. R.	DGP10.04
Gretser, S.	AG05.03, AG05.04 , AG07.05, AG13.05, P.13.09
Griem, J.	DGP04.05
Grimm, J.	AG02.06
Grochowski, P.	P.05/11.05
Groll, T.	DGP10.07, P.InterPath.04
Größler, F.	P.13.02
Grosser, B.	AG02.02 , AG14.11, DGP10.02, P.Multipar.02
Grosu, A.-L.	AG04.10, P03.13
Groth, D.	AG14.13
Grube, M.	AG04.02, AG14.05
Grünwald, V.	DGP13.08
Gschwend, J.	DGP13.08
Guerrero, M.	DGP18.07
Günther, M.	AG02.10, AG02.12 , AG02.13 , AG03.04
Haag, J.	AG01.03
Haas, A.	AG13.06
Haas, M.	AG02.12
Häberle, L.	AG02.14, DGP23.05
Hacker, U. T.	P.14.03
Hackl, H.	P.01.04
Haferkamp, A.	P.03.08, P03.11
Haffner, M. N.	P.14.02
Hagedorn, F.	DGP18.02
Hahn, O.	DGP13.08
Hailfinger, S.	DGP03.01
Hakroush, S.	P.07/08/10.03, P.07/08/10.04
Halfter, K.	AG02.09
Halloul, Z.	P.InterPath.02
Halstenbach, T.	P.InterPath.11
Hammad, E.	P.03.07
Hammerschmidt, L.	P.06.07
Han, M.	AG13.11
Han, X.	DGP12.03
Hansen, A.	P03.15
Hansen, K.	AG03.03
Hansmann, M.-L.	AG01.06, DGP18.03
Hapfelmeier, A.	AG02.03, P.02.03, P.02.12
Harbecke, A.	DGP23.09
Harter, P.	AG05.04
Hartmann, A.	AG03.05, AG04.04, AG13.02, DGP13.08, DGP13.09, P.02.01, P.02.02, P.03.03, P03.09, P03.12
Hartmann, F.	DGP15.03
Hartmann, N.	AG10.01, P.14.12
Hartmann, S.	DGP18.03
Hartmann, W.	AG08.04, AG08.07, DGP03.01, P.14.08, P.14.09, P.14.10, P.14.20
Hassas, S.	DGP13.07
Hattesohl, A.	AG04.11
Hauck, S. K.	P.07/08/10.03
Hauptmann, K.	AG06.02
Hauptmann, S.	P.04.01
Hause, F.	AG03.06, DGP09.05
Hauser, A.	AG02.02
Hausser, A.	P.06.04
Hedou, J.	DGP12.03
Heemann, U.	DGP17.06
Heidel, C.	AG06.03
Heikenwälder, M.	P.05/11.02
Heiland, M.	P.InterPath.11
Heinemann, V.	AG02.12, AG02.13
Heinrich, B.	P.InterPath.06
Heinst, L.	P.14.08, P.14.09 , P.14.10, P.14.20
Heintz, A.	AG02.08
Heitkötter, B.	AG08.07
Heitplatz, B.	P.03.01
Hekmat, K.	DGP12.04
Held, U.	AG10.02
Heldwein, M.	DGP12.04

Hellfors, C.	P.02.18
Hempel, K.	AG14.07
Henes, J.	DGP09.06
Hennig, M.	DGP09.04
Hennig, S.	AG14.13
Heramvand, N.	AG02.01
Herfarth, K.	DGP18.03
Hernandez, E.	AG04.03
Herpel, E.	P.02.09
Herz, A.-L.	AG02.03, P.02.03, P.02.12
Heß, K.	P.14.13
Heselmeyer-Haddad, K.	DGP06.03
Hetjens, S.	P.13.04
Heusinger-Heß, V.	DGP23.09
Heyer, C. M.	AG02.02
Hieber, D.	P.13.13
Hillebrand, L. E.	P.14.06
Hiller, G. G. R.	P.04.02, P.04.07, P.04.08, P.05/11.07
Hillmer, A. M.	AG02.01
Hiltner, T.	P.02.03, P.02.12
Hinnerichs, M. S.	P.07/08/10.06
Hinrichs, S.	DGP09.04, DGP23.02, P.03.02
Hintertaner, M.	AG06.01
Hirsch, D.	DGP06.03
Hirsch, F. W.	AG06.02
Hoang, L.	P.04.07
Höckel, M.	P.04.07, P.04.08
Höhn, A. K.	P.04.02, P.04.08 , P.04.07
Hohneck, J.	P.06.02
Holleczeck, B.	P.14.02
Hollfoth, V.	DGP09.06, P.02.22, P.Multipar.04
Holm, M.	AG10.03
Holte, H.	DGP18.03
Hölzel, M.	AG03.02, DGP13.08
Hölzl, D.	AG01.05, AG14.10, DGP03.04
Hölzl, M.	DGP13.09
Holzmann, C.	P.14.11
Holzmann, D.	AG10.02
Holzner, P.	DGP15.04
Homeyer, A.	AG13.04
Hönscheid, P.	DGP15.04
Höper, M.	P.06.01
Hoppe, S.	AG02.01
Horn, H.	AG01.06, DGP03.01, DGP18.03, P.06.04
Horn, L.-C.	P.04.02, P.04.07, P.04.08, P.05/11.07
Horn, T.	DGP13.08
Horst, D.	AG03.04, AG04.07, AG06.02, DGP06.04, DGP12.04, DGP12.05, P.06.03
Horvath, L.	DGP01.06
Hoster, E.	DGP18.03
Howitt, B.	AG04.01
Huang, B.	P.InterPath.08
Huber, O.	AG06.05, DGP10.06
Huber, R.	DGP22.04
Huber-Schumacher, S.	P.05/11.04
Hufnagl, P.	AG13.04
Hughes, B.	DGP23.01
Hühns, M.	P.14.11
Hulla, W.	DGP04.05, DGP04.07, DGP04.08
Hummel, M.	AG14.13
Hundt, J.	DGP22.04
Husemann, C.	AG14.13
Huss, R.	P.13.12
Huth, T.	AG02.07, P.02.13
Huvila, J.	P.04.07
Huynh, A.	AG03.06
Ibberson, D.	AG02.07
Idel, C.	AG10.04
Ihle, M. A.	AG14.04 , P.14.18
Ihringer, R.	P.02.17

Ikonomi, N.	DGP03.03
Imberg, F.	AG03.06
Isfort, I.	P.14.08, P.14.09, P.14.10, P.14.20
Ivanova, V.-S.	AG01.02
Ivison, G.	DGP12.06
Iwuajoku, V.	AG13.06
Jagomast, T.	AG10.04
Jahveri, N.	DGP23.01
Jäkel, J.	P.02.20
Jamieson, A.	P.04.07
Jank, P.	AG02.09, DGP10.07
Jänsch, R.	P.02.07
Jansen, C.	AG13.04
Janssen, M.	P03.16
Jechorek, D.	DGP06.05, P.02.05, P.02.07, P.02.16, P.02.18, P.07/08/10.06, P.14.14
Jelonnek, T. S.	AG04.10
Jermann, P. M.	P.14.06
Jesinghaus, M.	AG02.03 , AG02.08, AG02.09, DGP10.07, P.02.01, P.02.03, P.02.12, P.14.13, P.InterPath.04
Jeske, S.	DGP17.06
Jin, L.	AG06.05
Jokic, M.	AG06.03
Jonas, C.	AG02.01 , P.14.18
Jonigk, D.	DGP24.02, AG14.07, P.03.07, P.06.01, P.InterPath.09
Jox, T.	DGP14.03
Jud, A.	DGP15.04
Jundt, G.	AG08.04
Jung, L.	P.04.05
Jung, M.	DGP24.02
Jung, N.	AG14.11
Jungbäck, N.	P.Multipar.01, P.Multipar.02
Jungbluth, A.	AG04.03
Jüngel, E.	P.03.08
Junker, K.	AG03.05
Jürgensmeier, J. M.	DGP13.09
Jurinovici, V.	DGP18.03
Jurmeister, P.	DGP06.02
Justenhoven, C.	P03.11
Kain, R.	P.Multipar.05
Kalder, M.	AG04.11
Kalla, C.	P.06.04
Kalmbach, S.	DGP18.03
Kaltenecker, C.	P.Multipar.05
Kamarádová, K.	P.02.01
Kamp, J.-C.	P.06.01
Kang, D.	AG14.07
Kansenda, B.	P.14.06
Karamitopoulou, E.	P.04.01
Kari, F. A.	P.05/11.04
Karim, M.	P.14.05
Karpf, S.	DGP22.04
Karras, F.	DGP06.05
Karras, F. S.	P.14.14
Karthan, M.	P.13.13
Kather, J. N.	AG10.01, AG13.10 , DGP10.02
Kdimati, S.	P.03.04, P.03.06
Keck, T.	AG02.16
Keilholz, U.	DGP12.04
Keller, G.	AG02.03, P.02.03, P.02.12
Kellers, F.	AG02.08, P.14.13
Kelly, M.	DGP06.03
Kern, J.	P.05/11.07
Kestler, H. A.	DGP03.03
Ketzer, J.	DGP18.06
Kiefer, F.	DGP13.05
Kinzler, M. N.	AG07.05
Kirchner, M.	AG08.06
Kirchner, T.	P.02.06

Kirfel, J.	AG06.03, AG10.04, DGP24.03, AG14.07
Kirschner, M.	P.14.18
Kiss, A.	DGP04.06, DGP20.04 , DGP23.03, P.02.20, P.Multipar.06
Kittel, D.	AG06.04, DGP13.02, DGP23.07
Kitz, J.	AG02.04
Klapper, L.	AG10.04
Klapper, W.	AG01.03, AG01.06, DGP01.04, DGP03.01, DGP18.03
Klauschen, F.	AG06.02, AG08.05, DGP06.02, DGP12.04, P.02.06
Klein, S.	DGP04.05, DGP04.07
Kleinlein, I.	P.02.17, P.06.06
Kleo, K.	AG14.13
Kletzander, R.	AG13.02
Klintschar, M.	DGP14.04
Kloth, M.	P.13.05, P.InterPath.01
Kluck, K.	AG14.03
Kluge, C.	AG10.05
Kluge, I.	P.07/08/10.04
Kluge, J.	AG04.07 , DGP12.05
Klümper, N.	AG03.02, DGP13.08 , DGP13.09
Knemöller, L.	AG01.03
Knösel, T.	AG08.05
Koch, I.	AG04.07, DGP06.04, DGP12.04, DGP12.05
Koch, K.	AG01.03
Kocsmár, É.	DGP04.06, DGP23.03
Kocsmár, I.	DGP23.03
Köhler, B.	P.02.21
Kohler, E.	DGP01.04
Köhler, S. A.	P.03.03
Kohlruss, M.	AG02.03, P.02.03, P.02.12
Kolb, J. P.	DGP22.04
Kolb, T.	P.06.05
Kolin, D.	AG04.01
Koll, F.	AG13.03, DGP24.04
Köllermann, J.	DGP17.04, DGP24.04, P.13.10
Kollmeier, J.	DGP06.06
Kolm, I.	P.05/11.02
Kölsche, C.	P.04.03
Kommoss, F.	AG04.01 , P.04.03, AG08.06
Kommoss, S.	AG04.02, AG14.05
König, A.	AG02.15
Konrad Kurowski, K.	P.14.15
Kontsek, E.	DGP04.06, DGP20.04, P.Multipar.06
Konukiewitz, B.	AG02.08, AG02.09, DGP10.07, P.14.13
Kopp, T.	AG14.05
Körber-Ferl, K.	P.14.14
Körholz, D.	DGP14.03
Korkmaz-Icöz, S.	P.07/08/10.01
Kössinger, A.	DGP13.04
Kovalenko, M.	DGP13.09
Kral, S.	AG14.12, AG14.14 , AG14.15
Kraus, T.	AG01.05, AG04.08, AG14.02, AG14.10, DGP03.04
Krause, Y.	P.06.07, P.14.17
Krausewitz, P.	P03.14
Kreidt, D.	P.06.07
Kreipe, H.-H.	P.06.01
Kresbach, C.	AG03.01
Kreten, F.	AG03.09
Kreutz, C.	AG03.06, P.07/08/10.01
Kreuz, M.	AG01.06
Krey, L.	DGP23.03
Krisp, C.	DGP09.04, DGP23.02
Kristiansen, G.	AG03.02, AG06.04, DGP13.02, DGP13.08, DGP23.07, P.07/08/10.08, P03.14
Kröncke, T.	P.InterPath.08
Krönke, J.	DGP18.04
Krowicki, E. A.	DGP18.07
Krücken, I.	P.04.02, P.04.07
Kuehnel, M. P.	AG14.07, P.06.01
Küffer, S.	AG02.04, AG03.01, AG06.01
Kühl, A.	AG14.13

Kuhl, C.	P.InterPath.09
Kuhn, C.	P.14.03
Kulasinghe, A.	DGP23.01
Kull, M.	DGP18.04
Kumbrink, J.	P.02.06
Kümpers, C.	AG06.03 , DGP22.04
Künstner, A.	DGP01.03, DGP18.06
Kuntze, A.	AG08.07
Kunz, M.	AG14.12, AG14.15
Kuritsyn, P.	AG13.02
Kurowski, K.	AG03.06, DGP09.05, DGP22.03, P.InterPath.11, P.Multipar.07, P03.13
Kurz, K.	DGP03.01, DGP01.04, DGP18.03, AG01.06
Kuzman, P.	P.05/11.07
Lacher, M.	AG06.02
Lachmann, N.	AG14.13
Laferty, D.	P.13.03
Lahmer, T.	DGP17.06
Lakkimsetty, S. S.	DGP04.03
Lang, C.	AG02.09
Lang, H.	P.02.20
Lang-Schwarz, C.	DGP10.07, P.02.01 , P.02.02
Lange, F.	DGP13.09
Lange, S.	AG02.03, DGP10.07, P.02.12
Langer, A.	AG14.11
Langner, A.	P.InterPath.11
Langwieder, C.	AG14.10
Lapa, C.	P.InterPath.10
Lartigau, A.	P.14.01
Laßmann, S.	AG14.14, AG14.15, P.14.19, AG14.12 , P.01.06, P.14.07
Lau, J.-F.	P.07/08/10.08
Läubli, H.	P.14.06
Lauterbach, H.	DGP15.03
Laycock, A.	DGP10.04
Lazarev, P.	DGP04.08
Lecomte, H.	P.13.10
Lee, C.-H.	AG04.01
Lee, J.-C.	AG04.01
Lee, J. S.	P.14.01
Legnar, M.	AG13.12
Lehmann, J.	AG03.05
Lehmann-Koch, J.	P.02.09
Leich, E.	DGP18.03
Leichtle, A.	AG10.04
Leinauer, B.	AG08.04
Lemke, S.	AG02.07
Lemster, A.-L.	DGP24.03
Lenggenhager, D.	P.05/11.02
Lennerz, V.	AG14.13
Lenz, G.	DGP03.01, DGP18.03
Lenz, P.	DGP03.01
Lenze, D.	AG14.13
Lerbs, T.	AG06.04, DGP12.07 , DGP13.02, DGP23.07
Li, C.	AG13.11
Li, J.	DGP04.04
Li, L.	DGP12.06
Li, M.	AG03.06
Li, Y.	AG02.04
Lieberich, J.	DGP06.03
Liebetrau, M. E. E.	P.05/11.07
Liesche-Starnecker, F.	P.13.13, P.Multipar.01, P.Multipar.02
Liese, J.	AG10.03
Lindner, L. H.	AG08.05
Lippe, E.	P.02.20
Lippert, H.	P.02.14
Litmeyer, A.-S.	DGP10.07
Liu, Y.	AG04.09, AG13.11, DGP04.04, P.13.15
Loeffler, M.	AG01.06
Löffler, C. M. L.	DGP10.02
Lohneis, P.	DGP01.03 , DGP18.06

Lome Maldonado, C.	DGP18.07
Longerich, T.	DGP13.01, P.InterPath.07
Longuemaux-Valence, S.	P.14.01
Lopez-Beltran, A.	AG03.05
Lordick, F.	P.14.03
Lorentzen, A.	P.05/11.02
Lorenzen, S.	P.02.03
Lotz, G.	DGP04.06, DGP23.03
Loukanov, T.	P.05/11.06
Löwl, A.	P.03.04
Lubk, L.	DGP24.05
Lüchtenborg, A. M.	AG04.10
Ludewig, B.	DGP15.03
Ludwig, N.	P.06.02
Luibrand, J.	DGP09.06
Lutteri, G.	AG08.03
Ma, N.	DGP23.01
Ma, Y.	AG06.05 , DGP10.06, P.14.04
Maccagno, A.	P.02.04, P.06.06
Maccio, U.	P.05/11.02
Macek, B.	DGP09.06
Macher-Goeppinger, S.	P03.11
Mackedanz, P.	DGP09.04, DGP23.02
Mahendran, P.	P.02.14
Maier, J. I.	DGP13.06
Maier, J.	DGP03.03
Mairinger, F.	DGP06.06, P.06.07, P.14.17
Mairinger, T.	DGP06.06
Makky, A.	DGP15.03
Malek, N.	DGP09.06
Maletzki, C.	AG10.05
Màlyi, A.	AG02.16
Mamilos, A.	P.InterPath.03
Mankel, B.	DGP18.08
Manseck, A.	DGP13.08
Manz, R.	P.13.12
Manzo, M.	DGP03.02
Mar, L.-M.	P.04.03
March, C.	P.02.05, P.02.07, P.02.08, P.02.18, P.02.19
Marienfeld, R.	DGP03.03, P.01.05, P.06.05
Marín, J. J. G.	AG14.09
Marinkova, R.	AG06.05
Marion, I.	AG10.01
Märkl, B.	AG02.02, AG14.11, DGP10.02, P.02.04, P.02.17, P.05/11.05, P.06.06, P.13.12, P.13.13, P.InterPath.06, P.InterPath.08, P.InterPath.10, P.Multipar.01, P.Multipar.02
Marquardt, J. U.	AG02.07
Marr, C.	DGP01.05
Marschner, N.	P.14.06
Martin, S. Z.	P.02.20
Marwitz, S.	AG06.03
Marx, A.	AG06.01, AG06.06
Masser, R.	P.04.01
Matek, C.	AG03.05, AG13.02, DGP01.05
Mathilakathu, A.	P.06.07
Matter, M.	P.14.06
Mattern, S.	DGP09.06 , P.Multipar.04
Matysiak, U.	AG14.14, AG14.15, P.14.19
Maurer, A.	P.14.18
Mauthe, T.	AG10.02
Mauz-Körholz, C.	DGP14.03
Mayer, A.	DGP12.06
Mayer, R.	AG13.05, P.13.09
Mayerle, J.	AG02.13
Mayr, E.-M.	AG14.01
McAlpine, J. N.	P.04.07
McNally, J.	AG05.04
Mecktersheimer, G.	AG08.06
Medenwald, D.	P.02.07, P.02.08

Medinger, M.	DGP01.06
Meerwein, C. M.	AG10.02
Meese, E.	P.06.02
Mehrabi, A.	P.02.21
Meier, N.	DGP15.04
Meinel, J.	P.04.04
Meister, M.	P.02.09
Mellert, K.	AG08.03, AG08.04
Mendelsohn, D.	P.07/08/10.02, P.InterPath.03
Menter, T.	AG01.02, AG07.03 , DGP01.06 , DGP03.02
Menz, A.	P.05/11.01
Menzel, M.	AG14.03
Merg, N.	DGP22.04
Merkelbach-Bruse, S.	AG02.01, AG14.01, AG14.04, DGP12.04, P.14.18
Merkely, B.	P.07/08/10.01
Merle, U.	DGP13.01
Merz, A.	DGP24.06
Merz, H.	DGP01.03, DGP18.06
Messmann, H.	P.06.06
Messner, C.	P.14.15
Metrebian, M. F.	DGP18.07
Metzger, M.	DGP22.03
Metzig, M. O.	P.02.20
Meyer, F.	P.02.05, P.02.07, P.02.08, P.02.14, P.02.16, P.02.18, P.02.19, P.07/08/10.06,
P.InterPath.02	
Meyer, L.	DGP15.04
Meyer, P.	P.13.12
Micci, F.	DGP18.03
Michael, B.	DGP09.04, DGP23.02
Miernik, A.	DGP09.04
Mihalik, F.	AG14.05, DGP01.04
Mihic, A.	P.05/11.02
Mihic-Probst, D.	P.05/11.02
Mitteldorf, C.	P.07/08/10.03
Mittmann, C.	P.05/11.02
Mock, A.	DGP06.02
Mögele, T.	P.Multipar.01, P.Multipar.02
Moghaddam, A.	P.07/08/10.05
Mogler, C.	AG08.04, AG13.06
Moirano, G.	P.13.05
Möller, J.	P.03.07
Möller, P.	AG01.04, AG01.06, AG02.06, AG08.03, AG08.04, DGP03.03, DGP18.04, P.01.05,
	P.02.23, P.06.05
Monecke, A.	P.01.03
Monkman, J.	DGP23.01
Montes Mojarro, I. A.	DGP13.07 , DGP18.07 , P.13.16
Montironi, R.	AG03.05
Moritz, L.	DGP15.04
Moser, S.	DGP23.09
Mößler, V.	P.03.03
Mottok, A.	DGP18.02
Mueller, C.	AG10.01
Mukhopadhyay, A.	DGP04.05, DGP04.07
Muley, T.	P.02.09
Müller, D.	AG06.01
Müller, D.	P.13.12
Müller, F.	AG08.07
Müller, J.	P.04.02
Müller, L.	P.13.01, P.13.02
Müller, L.	P.Multipar.02
Müller, R.	P.13.05
Munkhdelger, J.	DGP04.05
Murga Penas, E. M.	DGP01.03
Murrieta-Coxca, J. M.	DGP10.06
Muscat, C.	DGP12.07
Musholt, T. J.	AG10.01
Mustea, A.	DGP13.08
Muti, H. S.	DGP10.02
Muzard, G.	P.14.01

Nagtegaal, I.	DGP10.07
Nagy, D.	DGP13.08
Nahles, S.	P.InterPath.11
Nahnsen, S.	AG02.07
Nann, D.	DGP01.04
Narbaitz, M.	DGP18.07
Nawroth, R.	AG03.04
Neesse, A.	AG02.04
Negrini, V.	P.02.05
Neiß, S.	AG02.01
Nell, J.	AG02.06, AG08.03, P.02.23
Nelson, K.	P.InterPath.11
Nenkov, M.	AG06.05, DGP10.06 , P.14.04
Nettersheim, A.	P.01.02
Nettersheim, D.	AG03.01, DGP24.05
Netto, G.	DGP04.08, AG03.05
Neubert, L.	P.06.01
Neudeck, N.	AG04.02
Neuer, M.	AG03.06
Neugeboren, L.	P.13.02
Neumann, J.	AG02.10, P.02.06
Niedermair, T.	P.07/08/10.05, P.InterPath.03
Niedobitek, G.	DGP17.04 , P.13.03
Nieß, H.	P.02.06
Noack, F.	P.04.02
Nolan, G.	DGP12.06
Notni, J.	P.InterPath.04
Novotny, A.	AG02.03, P.02.03, P.02.12
Nucci, M.	AG04.01
Obeck, U.	AG06.02, P.14.03
Obst, W.	P.07/08/10.06
Offermann, A.	AG03.08 , AG10.04, AG14.07, DGP24.03
Okada, S.	AG06.01
Oksentyuk Polyakova, T.	P.07/08/10.06
Olah, A.	P.07/08/10.01
Olar, A.	DGP20.04
Olchers, T.	AG06.03
Oldenburg, J.	P.03.04
Oliveira, A.	DGP17.04, P.13.03
Opitz, F.	AG02.14, DGP23.05
Ori, A.	P.02.22
Orlinger, K.	DGP15.03
Ormanns, S.	AG02.10, AG02.12, AG02.13, AG03.04
Ortega, M. V.	DGP18.07
Ortiz-Brüchle, N.	P.14.18
Örüm, M.	AG04.11
Oschlies, I.	AG01.03, DGP01.04
Oszwald, A.	P.Multipar.05
Ott, G.	AG01.06, DGP01.04, DGP03.01, DGP18.03, P.06.04
Ott, K.	AG02.03, P.02.03, P.02.12
Otto, F.	AG14.05, DGP01.04, DGP18.08
Otto, R.	P.02.14, P.02.16
Ourailidis, I.	AG14.03
Ozawa, M. G.	DGP12.03
O'Byrne, K.	DGP23.01
Pabel, S.	P.07/08/10.02
Pablik, J.	AG08.04
Padberg Sgier, B.	P.04.01
Palicelli, A.	P.04.07
Palm, M. A.	AG02.13
Palmowski, Y. A.	DGP15.03
Palu, C.	P.14.01
Pantea, M. A.	P.05/11.04
Paolini, A.	DGP24.06
Papić, D.	AG04.07, DGP12.05
Parra-Herran, C.	AG04.01
Passerini, V.	DGP18.03
Pasternak, J.	AG04.02
Pätzelt, M.	P03.10

Pauli, L.	AG03.06
Pauls, S.	AG03.01
Paulsen, F.-O.	AG06.03
Pawlowski, B.	DGP23.05
Peca, N.	AG06.05
Peifer, M.	AG02.01, AG03.09
Pellegrino, R.	P.InterPath.07
Peng, L.	AG02.04
Perez, E.	DGP06.04
Perner, S.	AG06.03, AG10.04, AG14.07, DGP09.04, DGP22.04, DGP23.02, DGP24.03, P.03.02
Perrakis, A.	P.02.16, P.02.19
Pes, G. M.	AG14.08, AG14.09
Pesti, A.	DGP04.06, DGP20.04, P.Multipar.06
Peter, S.	P.InterPath.05
Petersen, M.	P.07/08/10.06
Petrovay-Cselényi, K.	DGP04.06
Pfarr, N.	AG02.09, AG14.01
Pikki, N.	DGP12.05
Pinter, N.	AG03.06, DGP09.05, P.07/08/10.01, P.13.11 , P.14.19
Pircher, A.	DGP01.06
Piriyev, E.	P.04.04
Ploeger, C.	P.02.13
Plucinski, E. K.	P.06.01
Pollner, P.	DGP04.06, DGP20.04, P.Multipar.06
Pongratanakul, P.	AG03.01
Popovic, Z.	AG13.12
Porubsky, S.	AG06.06, AG13.12, DGP17.06, P.InterPath.01, P03.11
Posch, B.	DGP01.06
Pöschke, P.	AG04.04
Potthoff, K.	P.14.06
Poxleitner, P.	DGP22.03
Prall, F.	P.14.11
Pretzsch, E.	P.02.06
Pries, R.	AG10.04
Probst, A.	AG02.02
Prokop, G.	P.13.13
Protzer, U.	DGP17.06
Pryalukhin, A.	DGP04.05, DGP04.07, DGP04.08
Ptok, H.	P.02.16
Puller, A.-C.	AG08.07, P.14.08, P.14.09, P.14.10, P.14.20
Purde, M.-T.	DGP15.03
Pusch, S.	AG02.07, P.02.13
Quaas, A.	DGP04.05, DGP04.07, DGP04.08, DGP12.04, P.02.11 , P.02.15 , P.04.04, AG02.01
Quintanilla-Martinez, L.	DGP18.07, DGP03.01, DGP01.04
Rácz, G.	DGP23.03
Rades, D.	AG10.04
Radovits, T.	P.07/08/10.01
Raffler, J.	P.13.12
Ralser, D.	DGP13.08
Ramirez-Ibarguen, A. F.	DGP18.07
Randerath, W.	DGP12.04
Rasch, S.	DGP17.06
Rau, A.	AG14.05, DGP01.04, DGP18.07
Rausch, S.	DGP13.08
Reck, M.	AG06.03
Rees, A.	P.Multipar.05
Reible, B.	P.07/08/10.05
Reimer, N.	P.14.13
Reis, H.	AG07.05, AG13.03, DGP24.04
Reitsam, N. G.	DGP10.02 , AG02.02, P.InterPath.10
Reitz, A.	AG05.03 , AG07.05, DGP14.04
Remaury, A.	P.14.01
Rentschler, L.	P.13.12 , P.Multipar.02
Reuss, D.	AG08.06
Reuter-Jessen, K.	AG03.01
Ribback, S.	AG03.03, AG14.08, P.14.05
Ribbat-Idel, J.	AG10.04
Richter, A.	AG03.01
Richter, G.	P03.12

Richter, J.	AG01.03 , DGP03.01
Richter, M.	DGP14.04
Ridder, D. A.	P.02.20
Ried, T.	DGP06.03
Riedel, J.	DGP18.06
Rieger, K.	DGP12.07
Riemenschneider, P.	DGP09.06, P.02.22, P.Multipar.04
Ring, S. S.	DGP15.03
Ripperger, T.	DGP14.04
Ritter, M.	AG03.02, DGP13.08, P03.14
Rochwarger, A.	DGP15.03, P.Multipar.03 , P.Multipar.04
Röcken, C.	P.01.02, P.02.10, P.14.13
Roesch, M. C.	P.03.02
Roessler, S.	DGP06.04, P.02.13, P.02.21, P.13.07
Roessner, A.	DGP06.05, P.14.14
Rogg, M.	DGP13.04, DGP13.06 , DGP24.06, P.03.05
Roghmman, F.	DGP13.08
Rojas Mena, B.	DGP18.07
Rókusz, A.	AG08.04
Rolle, U.	AG05.04
Romanovsky, E.	AG14.03
Romberg, D.	AG13.04
Römer, T.	P.04.04
Rose, C.	DGP22.04
Rose, M.	DGP24.02, P.03.07
Rosenfeldt, M. T.	DGP23.06
Rosenwald, A.	AG01.06, DGP01.04, DGP03.01, DGP18.03, DGP23.06
Roßner, F.	DGP06.04
Rössler, S.	AG02.07
Roth, W.	AG02.08, AG06.06, AG10.01, DGP10.07, P.02.20, P.03.08, P.13.05, P.14.12,
P.InterPath.01, P03.11	
Rottscholl, R.	AG14.05
Ruane, S.	DGP12.04
Rubio, C. A.	P.02.01
Rückert, J.-C.	DGP12.04
Ruebner, M.	AG04.04
Ruff, L.	DGP12.04
Ruh, P.	AG04.03
Rummel, M.	DGP18.02
Runz, M.	P.13.04
Rupp, M.	P.07/08/10.05, P.InterPath.03
Rupp, N. J.	AG10.02
Ruppert, M.	P.07/08/10.01
Rusche, D.	P.13.04
Sabido, E.	AG03.06
Sabtan, D.	DGP09.04
Sahu, A.	AG03.02
Sailer, V.	AG10.04, AG14.07, DGP24.03
Samarska, I. V.	P.03.07
Sammarco, A.	DGP13.04, DGP13.06, DGP24.06
Sánchez-Martín, A.	AG14.09
Sander, P.	DGP01.04
Sanders, C.	P.07/08/10.08
Sanner, A.	DGP04.05
Santino, J. P.	DGP18.07
Saraji, A.	AG14.07
Sato, M.	DGP12.03
Sauer, C.	AG06.01
Savran, D.	AG13.05
Sayour, A. A.	P.07/08/10.01
Schad, A.	AG10.01
Schade, T.-C.	DGP01.04
Schallenberg, S.	DGP04.05, DGP04.07, DGP04.08, DGP06.04, DGP12.04
Schaller, T.	P.02.04, P.05/11.05, P.06.06, P.Multipar.01, P.Multipar.02
Schanze, D.	DGP06.05
Schaper, S.	AG14.13
Schatz, R.	P.04.02
Schell, C.	AG03.06, DGP13.04, DGP13.06, DGP24.06, P.03.05
Schenk, W.	P.05/11.05

Schickтанz, F.	DGP10.07
Schierle, K.	AG12.01, AG12.03
Schilling, O.	AG03.06, DGP09.05, DGP13.04, DGP13.06, DGP15.04, DGP23.03, P.03.05, P.07/08/10.01, P.13.11, P.14.15, P.14.19, P.InterPath.11, P.Multipar.07, P03.13
Schindeldecker, M.	AG02.08
Schirmacher, P.	AG02.07, AG13.12, AG14.03, DGP13.01, P.02.09, P.02.13, P.02.20, P.02.21, P.04.03, P.05/11.06, P.13.07
Schlachtenberger, G.	DGP12.04
Schlack, K.	DGP13.08, P.03.01
Schlesner, M.	AG02.02
Schlößer, H.	AG02.01
Schlotfeldt, M.	DGP09.04, DGP23.02
Schlüter, H.	DGP09.04, DGP23.02
Schmauder, K.	P.InterPath.05
Schmelzeisen, R.	DGP22.03
Schmid, K. W.	DGP24.04
Schmid, M.	AG03.06, DGP23.03
Schmid, R.	DGP17.06
Schmidt, D.	P.04.04
Schmidt, M.	DGP10.06
Schmidt, S.	DGP15.03
Schmidt, T.	AG02.03
Schmitt, M.	AG02.09 , DGP10.07
Schmitz, G.	DGP17.04
Schmitz, J.	P.13.01, P.13.02
Schmitz, N.	AG01.06
Schmitz, R.	DGP18.02
Schmutz, M.	P.InterPath.06
Schneider, S.	P.05/11.01
Schnitzbauer, A. A.	AG07.05
Schöb, D.	DGP09.04
Schobel, J.	P.13.13
Schöckel, L.	AG02.10
Scholz, N.	P.02.16
Schömig-Markiefka, B.	AG14.01, DGP04.05, DGP04.07
Schönmehl, R.	P.07/08/10.02
Schorle, H.	P03.15
Schotte, T.	P.13.16
Schrader, A. J.	P.03.01, P03.16
Schreck, J.	P.02.13
Schreiber, L.	AG02.06
Schreier, J.	DGP06.05 , P.14.14
Schröder, D.	P.14.04
Schröder, W.	AG02.01, DGP04.07
Schöffler, P.	AG13.06
Schüler, J.	AG03.06, DGP09.05, P.06.04
Schüller, U.	AG03.01
Schult, M.-S.	P.02.22, AG08.07
Schultheiss, M.	AG08.04
Schulz, G. B.	AG03.04
Schulz, S.	AG10.01
Schulze, F.	AG07.05
Schumann, M.	AG14.13
Schürch, C.	DGP12.03, DGP15.03, DGP12.06, P.Multipar.03, P.Multipar.04
Schustetter, C.	DGP17.06
Schwab, C.	DGP13.01 , DGP13.08
Schwab, J.	DGP03.03
Schwab, R.	P.02.20
Schwaibold, L.	DGP13.07
Schwaiger, J.	AG04.08
Schwamborn, K.	DGP13.08, P.14.16
Schwarting, J.	DGP01.03
Schweitzer, S.	AG06.02
Seidel, S.	DGP23.01
Seidl, M.	DGP23.09
Seitz, V.	AG14.13
Seliger, B.	P.01.03, P.01.04
Senz, J.	P.04.07
Seper, A.	DGP04.05, DGP04.08

Seredynska, A.	P.14.15 , P.Multipar.07
Serna Higuita, L. M.	DGP13.07, P.13.16
Sers, C.	DGP06.04
Seyfarth, H.-J.	P.14.03
Shibata, T.	DGP12.07
Shmorhun, O.	AG07.05
Siebolts, U.	AG14.01, AG14.04
Siemanowski, J.	AG14.01
Sier, C. F.	AG02.04
Sigel, C.	DGP09.05
Sikic, D.	AG03.05, DGP13.08, DGP13.09
Silimon, D.	P.13.16
Silva, M.	AG02.03, AG02.09
Simile, M. M.	AG14.09
Simon, Q.	P.04.01
Simoneit, J.-H. H.	AG13.12
Singer, K.	DGP09.06, P.02.09 , P.02.22
Singer, S.	DGP09.06, P.02.09, P.02.22, P.Multipar.04
Singh, N.	P.04.07, P.04.08
Sinn, B. V.	P.06.03
Sinn, P.	P.04.03
Sipos, E.	AG02.02, P.Multipar.01, P.Multipar.02
Sisic, L.	P.02.03
Sitova, M.	DGP04.08
Skowron, M.	AG03.01
Slotta-Huspenina, J.	DGP01.04, DGP17.06, P.02.03, P.02.12
Smirnov, M.	DGP04.08
Soiron, A.	P.14.08 , P.14.09, P.14.10
Sojka, N.	AG06.01
Solass, W.	AG04.05
Sommer, F.	P.02.04
Sommer, S.	P.InterPath.06
Sonnemann, J.	AG06.05
Sopper, S.	DGP01.06
Sossalla, S.	P.07/08/10.02
Sotlar, K.	AG01.05, AG04.08, AG14.02, AG14.10, DGP03.04
Soto Rey, I.	P.13.12
Soudah, B.	P.02.24
Spada, F.	AG01.04
Spiesshofer, S.	P.07/08/10.01
Springfeld, C.	P.02.21
Staebler, A.	AG04.02, AG14.05, P.13.16
Staehle, S.	DGP13.07
Staiger, A.	DGP03.01, DGP18.03, AG01.06
Standvoss, K.	DGP12.04
Stanik, M.	P.04.02
Staubitz, J. I.	AG10.01
Stegmaier, C.	P.14.02
Stegmann-Frehse, J.	AG14.07
Stehl, V.	DGP23.09
Steiger, K.	AG02.09, AG13.06, P.InterPath.04
Stein, H.	AG01.06, DGP01.04, DGP18.03
Steinhart, J.	DGP18.04
Steinlein, S.	P.06.04
Steinmann, S.	AG14.08, AG14.09
Stelzer, I. A.	DGP12.03
Stenzel, P.	P.02.20, P03.11
Stenzinger, A.	AG08.06, AG14.03, P.05/11.06
Stenzl, A.	DGP13.07
Stephan-Falkenau, S.	DGP06.06
Sterlacci, W.	P.02.01
Steybe, D.	DGP22.03
Stieber, J.	DGP04.05
Stief, C.	AG03.04
Stilgenbauer, S.	DGP03.03
Stiller, M.	AG06.02, AG11.05, P.14.03
Stillger, M.	DGP15.04
Stock, K.	DGP17.06
Stöckle, M.	AG03.05

Stoffel, M.	AG06.04, DGP13.02, DGP23.07
Stögbauer, F.	AG13.06
Stöhr, C.	P03.09
Stöhr, R.	P03.09, P03.12
Stoll, A.	AG13.03
Stoll, V.	P.14.13
Stölting, S.	DGP01.03
Strähle, J.	DGP22.03
Straub, B. K.	P.02.20, P.InterPath.01
Strauch, M.	DGP22.04
Strick, R.	DGP13.09, P.03.03
Strieth, S.	P.07/08/10.08
Strissel, P. L.	DGP13.09, P.03.03
Ströbel, P.	AG02.04, AG02.15, AG03.01, AG06.01, DGP24.05, P.07/08/10.03, P.07/08/10.04
Strobl, S.	AG06.06, AG10.01, P.13.05 , P.InterPath.01
Strüder, D.	AG10.05
Stühler, K.	AG03.01
Sturm, E.	P.Multipar.04
Sugiyanto, R. N.	P.02.13
Sulyok, B.	DGP20.04
Sulyok, M.	P.InterPath.05
Sun, L.	P.06.04
Surendran, S.	AG02.12, AG02.13
Surov, A.	P.07/08/10.06
Süsskind, D.	P.InterPath.05
Szabó, G. B.	P.07/08/10.01
Szarvas, T.	DGP24.04
Szendrői, M.	AG08.04
Szörenyi, N.	P.02.12
Tagscherer, K.	AG02.08, P03.11, P.14.12
Takács, F.	DGP15.04
Talia, K. L.	P.04.07
Talsania, K.	DGP06.03
Tampe, B.	P.07/08/10.04
Tang, L.	DGP09.05
Tanzer, E.	AG14.09
Tappe, D.	P.Multipar.01
Taube, C.	DGP06.06
Taubert, H.	AG03.05, DGP13.09, P03.09
Tchrakian, N.	P.04.07
Teichmann, G.	P.04.02
Ternès, N.	P.14.01
Thalwaththe Gedara, M.	DGP23.09
Theunissen, J.	DGP17.04
Thiery, J.	DGP15.04, P.14.19
Thompson, E.	P.04.08, P.04.07
Thomsen, A. R.	AG04.10
Thurn, A.	P03.10
Timme, S.	AG02.16, DGP22.03, P.13.14
Timme-Bronsert, S.	AG04.10
Ting, S.	P.14.17
Tinguely, M.	P.04.01
Tögel, L.	P03.12
Tolkach, Y.	AG03.09 , DGP04.05, DGP04.07 , DGP04.08
Toma, M.	DGP13.08, AG03.02
Trautmann, M.	AG08.07, DGP03.01, P.14.08, P.14.09, P.14.10, P.14.20
Trebo, M.	DGP01.06
Trepel, M.	P.06.06, P.InterPath.06, P.InterPath.08
Triesch, J.	AG13.03
Trompak, O.	P.InterPath.07
Trümper, L.	AG01.06
Tsai, A. S.	DGP12.03
Tschurtschenthaler, M.	AG02.09, DGP10.07
Tsvetkov, T.	DGP04.05, P.04.04
Tzankov, A.	AG01.02, DGP01.06, DGP03.02, P.01.01
Ugliano, S.	DGP12.05
Uhlig, M.	P.02.05
Ullmann, S. R.	DGP06.05, P.14.14
Ungefug, X.	AG14.12

Vakeel, P.	AG03.03
van der Kwast, T.	AG03.05
van Rhijn, B. W. G.	AG03.05
Van Wymersch, C.	AG03.06, DGP13.06, P.03.05
Vannier, C.	P.14.06
Vasaturo, A.	DGP12.04
Vaupel, P.	AG04.10
Vaxevanis, C.	P.01.04
Vecsler, M.	DGP17.04
Végyvári, Á.	DGP09.04, DGP23.02
Vieth, M.	DGP10.07, P.02.01, P.02.02
Vijnovich-Barón, A.	DGP18.07
Vitek, O.	DGP04.03
Vlasenko, D.	AG02.02
Vlasic, I.	AG06.03
Vogel, M. N.	P.02.21
Vogelsberg, A.	DGP18.08
Vollmer-Kary, B.	DGP15.04
Vollmuth, Y.	P.Multipar.01
Volmer, L. L.	P.13.16
von Baer, A.	AG08.04
von Bargaen, C.	P.05/11.01
von Bergwelt-Baildon, M.	AG02.12, AG02.13
von Bernuth, A.	AG10.04
von Bubnoff, N.	DGP01.03, DGP18.06
von Deimling, A.	AG04.01, AG08.06, P.04.03
von Hahn, X.	AG06.01
von Hammerstein-Equord, A.	AG06.01
von Laffert, M.	AG06.02 , AG11.05, P.14.03
Vorwerk, U.	P.02.07
Voss, P.	DGP22.03
Wach, S.	AG03.05, DGP13.09, P03.09
Wagenpfeil, G.	P.14.02
Wagner, D.-C.	AG10.01, P.03.08, P.14.12
Wagner, P.	AG04.04
Waller, V.	AG11.05
Wallwiener, D.	AG04.02
Walter, N.	P.InterPath.03
Walter, S.	P.13.14
Walz, G.	DGP24.06
Walz, S.	DGP13.07
Wang, E.	P.14.01
Wang, H.	AG14.08
Wang, H.	P.14.01
Wang, X.	DGP04.04
Wang, Y.	AG13.11
Wardelmann, E.	AG08.07 , P.03.01, P.14.08, P.14.09, P.14.10, P.14.20, P03.16
Warth, A.	P.02.09
Weber, A.	DGP04.03, DGP15.04
Weber, I.	P.01.06
Weber, K.	AG05.04
Weber, T.	DGP18.02
Weers, L.	DGP24.04
Wehkamp, U.	AG01.03
Weichert, W.	AG02.03, AG02.09, AG13.06, DGP10.07, DGP13.08, DGP17.06, P.02.03, P.02.12, P.14.16, P.InterPath.04
Weigert, A.	DGP24.04
Weigert, O.	DGP18.03
Weingart, A.	DGP24.03
Weirich, G.	DGP17.06
Weis, C.-A.	AG13.12, P.13.04, P.13.07
Weller, J.	DGP01.04
Wellner, U.	AG02.16
Welte, T.	P.06.01
Welter, S.	AG06.01
Welter, V.	AG14.01
Wendler, O.	P03.12
Wengenmeyer, C.	P.13.12
Werle, S. D.	DGP03.03

Werner, J.	P.13.11
Werner, J.	AG02.12, AG02.13, P.02.06
Werner, M.	AG02.16, AG03.06, AG14.12, AG14.14, AG14.15, DGP04.03, DGP09.05, DGP13.04, DGP13.06, DGP15.04, DGP22.03, DGP23.03, DGP24.06, P.01.06, P.03.05, P.05/11.04, P.13.11, P.13.14, P.14.07, P.14.15, P.14.19, P.InterPath.11, P.Multipar.07, P03.13
Werner, T.	AG03.06, DGP09.05
Wernig, G.	AG06.04, DGP12.07, DGP13.02
Wess, M.	DGP13.04 , DGP24.06
Wessolly, M.	DGP06.06 , P.06.07 , P.14.17
Westermann, P.	P.14.15
Westhauser, F.	P.07/08/10.05
Westhoff, C. C.	DGP10.07, AG04.11
Wetterauer, U.	DGP09.04
Wickenhauser, C.	P.01.03, P.01.04, P.01.07
Wieczorek, M.	DGP23.09
Wiesweg, M.	DGP06.06
Wild, P.	AG03.05, DGP24.04, P.13.09, P.13.10, P.14.01, AG07.05, AG13.03, AG13.05,
DGP10.0	
Wildfeuer, J.	P.01.05
Wilfer, A.	P.01.03, P.01.04, P.01.07
Wilhelm, D.	AG02.09, DGP10.07
Wilhelmi, A.-L.	DGP18.08
Winter, L.	P.07/08/10.02, P.07/08/10.05, P.InterPath.03
Wirtz, H.	P.14.03
Wirtz, R.	DGP13.08
Witte, H. M.	DGP01.03, DGP18.06
Wlokka, U.	P.14.19
Wobser, M.	AG01.03
Woerner, S. M.	P.14.06
Wohlschläger, J.	DGP06.06
Woischke, C.	AG02.10
Wolf, D.	DGP01.06
Wolf, P.	DGP09.04, DGP23.02
Wolgast, L. M.	DGP04.07
Wolkenstein, P.	DGP06.04
Wolniczak, E.	P.02.08
Wolter, S.	AG14.14, AG14.15
Wosnig, S.	P.14.09
Wright, P. R.	P.14.06
Wucherpennig, S.	P.InterPath.09
Wullenkord, R.	DGP03.01
Wullich, B.	AG03.05, DGP13.08, DGP13.09, P03.12
Wüster, J.	P.InterPath.11
Xu, X.	AG13.11
Yang, F.	AG13.11
Yang, T.-P.	AG02.01
Yao, J.	AG13.11
Yao, S.	AG02.04
Yasser, M.	AG03.03, P.14.05
Yavas, A.	AG02.14, DGP23.05
Ying, J.	AG04.09, DGP04.04
Youssef, A.	DGP23.06
Yue, M.	AG13.11
Zachrau, T.	P.13.02
Zahn, M.	P.01.05
Zamboglou, C.	P03.13
Zamo, A.	DGP01.04
Zander, T.	P.02.15
Zaporozhchenko, L.	P.02.07
Zapukhlyak, M.	DGP18.03
Zapuklyak, M.	DGP03.01
Zayats, V.	DGP04.05
Zeller, M.	AG02.07
Zender, L.	P.InterPath.07
Zengerling, F.	DGP13.08
Zerbe, N.	AG13.04, DGP17.05
Zeuzem, S.	AG07.05
Zhang, L.	AG02.06, P.02.23

Zhao, M.	AG04.09 , AG13.11
Zhao, M.	AG13.11
Zhao, Y.	DGP06.03
Zhao, Y.	AG02.01
Zhdanovich, Y.	DGP06.02
Ziegler, P.	AG07.05, AG13.05
Ziegler, P. K.	DGP10.04
Ziehnert, A.	P.06.03
Ziepert, M.	AG01.06
Zimmer, S.	P.02.20
Zimpfer, A.	AG10.03, AG10.05, AG11.03 , P.03.04, P.03.06
Zirngibl, M.	AG03.06
Zisser, L.	P.Multipar.05
Zschäbitz, S.	DGP13.08
Zubarev, R.	DGP09.04, DGP23.02